Room Temperature Chemoselective Phosphine Oxide Reduction and Mechanism-Based Inhibitors of BioA

A THESIS
SUBMITTED TO THE FACULTY OF
UNIVERSITY OF MINNESOTA
BY

Carter G. Eiden

IN PARTIAL FULFILLMENT OF THE REQUIREMENTS
FOR THE DEGREE OF
DOCTOR OF PHILOSOPHY

Advisor: Courtney C. Aldrich

May, 2017

Acknowledgements

I thank Malcolm Cole, John Schultz, Scott Brody, Dr. Kishore Viswanathan, Dr. Curtis Engelhart, Dr. Anja Meissner, Dr. Kathy Nelson, Dr. Shuhei Kawamura, Dr. Ben Duckworth, Dr. William Fiers, Dr. Yang Li, and Matthew Bockman for making the lab an enjoyable place to spend five years

I thank Enoch You, Dr. Kimberly Maize, Daniel Wilson, and Kathleen Wang for the excellent work they put in towards the success of my projects

Erick Carlson, Chris Seiler, Emily Boldry, Matthew Bockman, Cody Lensing, and Andi Wisniewski were excellent TA partners, classmates, made me laugh, and helped with a lot of assignments those first two years

Dr. Zheng Liu was a fantastic help when it came to basically any part of synthetic chemistry.

I thank Dr. Melanie Rogers and Dr. Brent Rivard for the extra time that each of them took to help me design and work-up experiments as well as to ensure I was using the stopped-flow correctly.

Evan Alexander helped me a little with a great number of things. I thank him for his great attitude when it came to taking time for me to assist with anything I needed.

I thank Dr. Elizabeth Ambrose and Dr. Natalia Tretyakova for taking the time to be a part of my committee, listening to what must have been a riveting oral proposal, and glancing over this monstrous document.

I thank Dr. Surendra Dawadi for his fantastic willingness to help on almost any topic and specifically for his assistance in setting up mass spec experiments

I thank Dr. David Ferguson for his professional mentorship, making me laugh, and insulting me every chance he got. I will miss him.

I thank Dr. John Lipscomb for teaching me transient kinetics and for making me take that test I didn't have to take. I also thank him for his mentorship, his sponsorship of me, and his guidance in a wide range of topics relating to kinetics.

Looking back, I have to thank my parents, Glen and Darla Eiden, for providing opportunities for me to thrive in school from a young age. There is absolutely no way I would be here without the doors they shoved open.

Dr. Ce Shi was my first mentor in graduate school. I don't know if he saw much synthetic chemist potential in me, but he was extremely patient, taught me tons of organic synthesis from the very basics, gave me excellent professional advice, and deserves the most credit for ensuring I survived 5 years of graduate school.

I thank my wife, Miranda Eiden, for being by my side during the long and crazy hours, the tough first couple of years, and the much better last two. You loved me, and it was wonderful. I also thank her for her continued encouragement that I did have what it takes to get a Ph. D.

I owe quite a bit to my comrade-in-arms, Joe Buonomo, as he is the main reason I ended up thriving in graduate school. I thank him for his endless stream of ideas, for challenging my ideas, for his passion for discovery on our project together, and for sharing the thoughts of his brilliant mind. I especially thank him for trying to work with me on various projects, and for being a wonderful friend. I will miss him.

Finally, I thank my advisor, Dr. Courtney Aldrich. Courtney gave me the tools to succeed in multiple areas, from insisting that I attend transient kinetics lectures, to designing a project that fit my skillset, to being the driving force in my selection for a traineeship. He demonstrated large degrees of patience with me in several areas, including my initially pitiful synthetic skills, my distaste for medicinal chemistry seminar, and my poor scientific writing. Additionally, I deeply appreciate his willingness to let me explore personal project ideas, as without it I would not have ended up thriving.

Abstract

The reduction of phosphine oxides with silanes occurs with high specificity and fidelity and represents one of the most useful methods for synthesis of phosphines. The chemoselectivity of this process also allows for *in situ* recycling of phosphine oxide by-products to afford catalytic versions of the Wittig, Staudinger, and Mitsunobu reactions, among others. However, silane-mediated reduction of phosphine oxides generally requires both elevated temperatures (80–120 °C) and additives, substantially limiting substrate scope.

Abnormal patterns in the reduction rates of phosphetane oxides by phenylsilane were noted, causing initiation of a comprehensive investigation of silane-mediated phosphine oxide reduction which revealed widespread misunderstandings of the reduction process. This led to characterization of a required pre-activation step for all commercially available silane reductants as well as a key 6-membered transition state that explains reactivity trends. Such insight fueled rational reagent design, furnishing 1,3-diphenyldisiloxane (**DPDS**), a superior disiloxane reducing agent. **DPDS** allowed for development of room temperature phosphine recycling Wittig, Staudinger, and Appel methodologies and is broadly applicable in phosphine synthesis, reducing acyclic phosphine oxides either additive-free at 110 °C or in combination with an additive under ambient conditions.

Mechanism-based inhibitors (MBIs) are widely employed in chemistry, biology, and medicine due to their exquisite specificity and sustained duration of inhibition. The global kinetic parameters k_{inact} and K_I have been used to characterize MBIs, but derivation reveals they provide far less information than is commonly assumed. A more rigorous approach is determination of the individual microscopic rate constants of inactivation, which is demonstrated in the optimization of MBI **1**.

1 inactivates tubercular BioA through a four-step mechanism, and kinetic analysis revealed the rate-limiting step is the removal of the α-proton of **1**. This knowledge was subsequently applied to rationally design dihydro-4-pyranone **42**, dihydro-4-pyridone **43** and dihydro-4-thiopyranone **51**. A unified synthetic strategy was employed for heterocycle construction featuring α-amino ynone generation followed by 6-*endo-dig* cyclization. However, competitive 5-*exo-dig* cyclization, β-elimination of the ynone, and dimerization of the resultant α-amino carbonyls had to be overcome through Teoc and Boc-MOM protection amino groups. Dihydro-4-pyridone **3** possessed an improved k_{inact} value against BioA, validating the pK_a–based design strategy.

Table of Contents

List of Schemes

List of Tables

List of Figures

Chapter 1

How Phosphine Reduction by Silanes Actually Works and Applications to Phosphine Recycling and Phosphine Synthesis

Adapted with permission from:

Eiden, C. G.; Buonomo, J. A.; Aldrich, C. C. Phosphine Reduction Mechanism Paper. *J. Am. Chem. Soc.* **2017**, *unknown*, unknown

And

Buonomo, J. A.; Eiden, C. G.; Aldrich, C. C. Phosphine Synthesis Paper. *J. Am. Chem. Soc.* **2017**, *unknown*, unknown

And

Buonomo, J. A.; Eiden, C. G.; Aldrich, C. C. Scalable Synthesis of Disiloxanes from Silanes: A One-Pot Preparation of 1,3-Diphenyl-Disiloxane from Phenylsilane. *Synthesis* **2017**, *unknown*, unknown

This work was done in collaboration with Joseph A. Buonomo and Dr. Courtney C. Aldrich. Credit is due as follows:

J.A.B designed and synthesized the phosphine precatalysts. He also performed the initial Mitsunobu silane and phosphine screen, the initial NMR studies with **TMPPO** (Section 1.3.3, 1.3.4), the functional group compatibility studies with **DPDS**, the ball-milling synthesis of disiloxanes, the phosphine recycling reactions, and the non-NMR based reductions of acyclic phosphines with **DPDS**.

C.G.E designed and synthesized the silane reductants. He also designed and coded MassNMRProcessing. He performed all of the rest of the NMR studies, the kinetic analysis of the progress curves, the mathematical proofs, the reaction modeling, and the failed room temperature catalytic Mitsunobu reactions with **DPDS** (Section 1.10.1).

1.1 Introduction

Phosphorous(III) compounds are nearly ubiquitous throughout the synthetic organic literature, serving as ligands in transition metal-catalyzed transformations and as essential reagents in classical reactions such as the Wittig[1], Mitsunobu[2], Staudinger[3] (ligation and reduction), and Appel[4]. The reduction of phosphorous(V) oxides is a high-value process, as the final step of phosphine synthesis is commonly reduction of the corresponding phosphine oxide,[5] and each of the aforementioned venerable reactions generate a stoichiometric equivalent of phosphine oxide. Whether used for phosphine recycling or construction, a simple, chemoselective, and facile method for the reduction of phosphine oxides is necessary, and many investigations have aimed at the development of such conditions.

Speaking specifically towards phosphine recycling, there are multiple strategies one could pursue. The most straightforward and "brute-force" method involves regeneration of the phosphine in an additional step following purification and isolation of the phosphine oxide from the initial reaction. An alternative, and many would suggest superior, option involves using only a catalytic amount of phosphine and reducing its oxide continually *in situ*. The first method uses stoichiometric amounts of the phosphine, requires multiple purifications (including purification of a phosphine oxide, which can be extremely difficult) and a subsequent reaction. This would lead to the loss of substantial amounts of phosphine materials as well as being far less atom-economical than the second option, which uses catalytic amounts of phosphine and only requires a single, much simpler (phosphines are much easier to separate) purification. There is a third approach, the use of redox neutral catalysis, but it appears to have very limited reaction breadth as well as substrate scope.[6] So far, the most generalizable[7] method necessitates the *in situ* generation of chlorophosphonium species, requiring harsh reagents,[8][9][10] and there is no clear path to facilitate redox neutral versions of many phosphine-dependent reactions.

For both phosphine synthesis and in situ phosphine recycling, extreme levels of chemoselectivity and stability of the reducing agent to alternative functional groups is necessary. The ideal catalytic-in-phosphine Wittig, Mitsunobu, Staudinger, or Appel reaction would have the substrate scope of the non-catalytic versions, and novel phosphines often contain reducible or reactive groups to tune the reactivity of the transition metals effectively. The remaining portion of the introduction describes the development of methods for phosphine oxide reduction, their application to both phosphine construction and in situ recycling, and the proposed mechanisms of such processes.

The first example of reducing of a phosphine oxide to a phosphine was described by Hein and coworkers, utilizing lithium aluminum hydride and calcium aluminum hydride in 1,4-dioxane to reduce phosphine oxides.[11] Lithium aluminum hydride was found to be the superior reagent, producing yields of trialkylphosphines in the 70% range, while calcium aluminum hydride produced yields around 40%. However, when triphenylphosphine oxide (**TPPO**) was added to $LiAlH_4$, they found that only about 20% of the desired product was formed, while the byproduct diphenylphosphoric acid was formed in about a 30% yield.[12] This diphenylphosphoric acid was suggested to be formed following reduction of **TPPO** to diphenylphosphine, which then oxidized upon contact with atmospheric oxygen. Subsequent investigations by Issleib and Grams about the choice of solvent revealed that this side reactivity was substantial in both THF and dioxane, but was greatly hampered in non-cyclic ethers, as diethyl-, dipropyl-, and dibutyl-ether all furnished only trace amounts of diphenylphosphoric acid.[13] The problem of phosphorous-carbon bond breakage was thus alleviated, but substantial problems remained for application of this reduction to phosphorous recycling.

These problems revolve around the complete lack of chemoselectivity of this reduction system. Campbell and Way found that 6-7 hours of heating to 80 °C with $LiAlH_4$ in di-n-butyl ether was necessary to complete reduction of a phosphine oxide,[14] which is subjecting the

phosphine oxide to extremely harsh conditions for an extended period of time. As is well known, $LiAlH_4$ rapidly reduces aldehydes, carboxylic acids, esters, and amides in a relatively short amount of time at 0 °C, so the conditions necessary for phosphine oxide reduction have no functional group tolerance. In fact, heating to 80 °C with $LiAlH_4$ for multiple hours is harsh enough that the attempted regeneration of triphenylphosphine (TPP) immobilized on a polymeric surface using such conditions is believed to result in degradation of the polymer.

Multiple groups have also developed non-chemoselective reductions of phosphine oxides.[15] The reduction of **TPPO** using hydrogen gas proceeds smoothly using high pressure and high temperature (98 bar, 160 °C) or with heterogeneous metal catalysts at extreme temperature (500 °C).[16] Electrochemical methods have also been used in combination with a silylating agent (TMSCl, TMSOTf) or alkylating agent (MeOTf).[17] Additionally, metal hydrides other than $LiAlH_4$ also demonstrated proficiency, including boranes at 120 °C[18], sodium borohydride with or without alkylating agents, DIBAL, and Aluminum hydride. Clearly, each of these reactions suffer from very low functional group tolerance, and as such none will be sufficient for general reduction of phosphine oxides.

Currently, the best reagents for phosphine oxide reduction are silanes, displaying moderate reductive potential in combination with moderate to high functional group tolerance depending on the system used. The first silane-mediated reduction of phosphine oxides was reported by Fritszche and coworkers in 1964, using Polymethylhydrosiloxane (**PMHS**), phenylsilane, diphenylsilane, and triphenylsilane to reduce a variety of both acyclic phosphine oxides and phospholane oxides.[19] The same group followed this up with an additional manuscript that described the use of trichlorosilane in place of the other silanes.[20] Most of the reduction conditions were solvent-free, though they did report highly concentrated reactions with trichlorosilane in benzene.

Fritzsche and coworkers determined conditions for the reduction of **TPPO** in under three hours, and successfully obtained good yields (80–95%) with all silanes in this time frame. The real test for the effectiveness of each of the different silanes was the degree of heating required to achieve the reported conversion, which drastically differed between the silanes. Phenylsilane and diphenylsilane were far most facile reductants of **TPPO** than **PMHS** and triphenylsilane, as only 120 °C was necessary for the former compared to 280 °C and 300 °C for **PMHS** and triphenylsilane, respectively.[21] Trichlorosilane was the most powerful of them all, achieving reduction at only 80 °C.[22] Of the silanes used, **PMHS** is the most desirable from a sustainability standpoint, as it is an inexpensive industrial byproduct, but the intense heat necessary has limited its usefulness. Trichlorosilane was the most potent reductant; however, it is unpleasant to work with in a laboratory setting due to its corrosive nature, high flammability, and boiling point of 31 °C, necessitating pressurized vessels. It also displays limited functional group tolerance. Phenylsilane and diphenylsilane have thus been widely perceived as the best reducing agents for generalized phosphine oxide reduction.

One final discovery that Fritzsche and coworkers made was that the nature of the phosphine greatly influenced its ease of reduction. Multiple dihydrophospholes were reduced to the corresponding phosphines by heating phenylsilane to only 80 °C for 2 hours. A decade later, Marsi thoroughly investigated the use of phenylsilane for the reduction of 5-membered phosphorous heterocycles and found that phospholanes could also be reduced by phenylsilane at 80 °C. It appeared that most 5-membered phosphorous heterocycles were reduced in a more facile manner than their acyclic coutnerparts, which was a key finding for the development of *in situ* phosphine oxide reduction.

The first silane-mediated catalytic-in-phosphine reaction was reported by O'Brien and coworkers as they developed the first catalytic Wittig reaction.[23] Instead of initializing the reaction with the addition of a phosphine, O'Brien and coworkers used phosphine oxide

precatalysts to take advantage of the latter's significantly greater stability. They chose 3-methyl-1-phenylphospholane-1-oxide (M**1PPO**), one of the phosphine oxides reported by Marsi that gets reduced at a lower temperature, as their precatalyst and used diphenylsilane as the preferred reductant. With a model system of benzaldehyde, methyl bromoacetate, sodium carbonate, and precatalyst at 100 °C for 24 hours, they tested phenylsilane, trimethoxysilane, and triphenylsilane, and found that the first two furnished lower yields of product than diphenylsilane, while triphenylsilane afforded no product at all. These trends in silane reactivity are consistent with the aforementioned results of Fritzsche and coworkers.[24]

O'Brien and coworkers also reported varying the temperature of the reaction to empirically determine its effect.[25] They found lowering the temperature from 100 to 80 °C did not compromise the reaction yield, but any additional decrease, to 70 °C or 60 °C, was detrimental to turnover. However, reducing the temperature to 80 °C reduced the *E*/*Z* ratio from >95:5 to 67:33, which suggested the enhanced stereoselectivity was due to post-olefination isomerization of the *Z* alkene to the more stable *E* isomer. Consequently, the preferred temperature was 100 °C. Evaluating the substrate scope, they found their methodology produced *E*–olefins from a wide range of aldehydes. The success of para-nitrobenzaldehyde and 4-cyanobenzaldehyde with labile cyano and nitro groups demonstrated the high chemoselectivity of diphenylsilane. O'Brien and coworkers also employed both bromo and chloro compounds as ylide precursors. This pioneering work by O'Brien and coworkers showed that phosphine recycling is feasible with impressive chemoselectivity with the proper selection of phosphine and silane reagents. This seminal finding inspired others to further advance this recycling methodology in other phosphine-dependent reactions.

Two years later, van Delft and coworkers reported the development of a catalytic Appel reaction that used similar methods to implement phosphine recycling.[26] Recognizing the large gap in reducibility with different phosphines, they synthesized many potential phosphine oxide

precatalysts and investigated the effect of ring-strain and electronics on reduction rate. Through GC and NMR studies, they monitored the reaction rate of 5-membered, 6-membered, and 7-membered phosphorous heterocycles when combined with diphenylsilane at 100 °C in 1,4-dioxane. They found that that ring size is extremely important in determining the potential for precatalyst reduction by diphenylsilane. The 5-membered phospholanes are reduced much more quickly than the 6-membered phosphine oxides, and the 7-membered phosphepanes are barely reduced at all. They also showed that removal of the methyl group on M**1PPO** did not impact reactivity.

With the trend in ring size established, they next explored replacing the aliphatic 5-membered phosphine oxides with aromatic dibenzophospholes. Phospholes have additional ring strain when compared to phospholanes, which O'Brien and coworkers proposed was the reason for the ease of reduction of M**1PPO** in comparison to acyclic phosphine oxides. Phospholes also have the additional benefit of being easily tuned to have different electronic properties through incorporation of substituents on the dibenzophosphole core. However, when testing the aromatic phospholes, they found that diphenylsilane reduced the entire class of compounds slower, with the best compound reacting at approximately one-seventh the rate of the phenylphospholanes under otherwise identical conditions. When tuning the electronics of the dibenzophosphole, they found that adding electron withdrawing trifluoromethyl substituents provided a two-fold decrease in the rate of reduction, while electron donating methoxy substituents caused only a small increase in rate. Dibenzophospholes are much more electron deficient than phospholanes, which in combination with the diminished reduction rate observed with trifluoromethyl substituents, suggests electronic factors heavily influence the ease of reduction. On the other hand, clearly some ring strain is necessary, but whether or not additional ring strain helps the rate of reduction was inconclusive.

In terms of the actual development of the catalytic Appel reaction, van Delft and coworkers first tested for the stability of the phospholanes and dibenzophospholes with (2-bromoethyl)benzene.[27] They found that 3-methyl-1-phenylphospholane (M1PP) reacted with the bromo compound, while no alkylation occurred in the presence of the dibenzophosphole. Therefore, despite the substantially slower reduction of dibenzophospholes when compared to phospholanes, they selected phenyldibenzophosphole as their catalyst of choice for further optimization. Another major concern was finding a bromonium donor stable to diphenylsilane at 100 °C. They thus tested tetrabromomethane, *N*-bromosaccarine, bromine, *N*-bromosuccinimide, *N*-bromoacetamide, 2,4,4,6-tetrabromocyclohexa-2,5-dienone, and diethyl bromomalonate (DEBM) for their reactivity with diphenylsilane, and found that DEBM was the most stable. Van Delft and coworkers then tested the reaction of 2-phenylethanol with DEBM, diphenylsilane, and a catalytic amount of phenyldibenzophosphole in multiple solvents, finding that the reaction to form 2-bromoethylbenzene proceeded best in MeCN. Switching silanes to either trimethoxylsilane or triethylsilane gave yields under 10%, while a switch of the phosphine catalyst to a substituted dibenzophosphole had no effect. However, this methodology was extremely limited when it came to both substrate scope and yield. For the synthesis of primary bromides, the highest yield determined by GC was only 80%, and isolated yields hovered between 50 and 75%. For secondary bromides, they were able to achieve good yields with a specialized cholesterol, but simple bromocyclohexane was produced from the corresponding alcohol in only 20% yield, and other secondary alcohols were unreactive towards the reported conditions. They were also unable to obtain similar results with a chloronium donor. Overall, this methodology is very important in terms of the careful study of the dependence of the rate of reduction on the identity of the precatalyst as well as demonstrating that alkyl bromides and alcohols are rather stable towards silanes at 80 °C, but not particularly useful for generalized Appel reactions.

In 2012, an unrelated publication by Beller and coworkers reported that using the esoteric silane diethoxymethylsilane with bis-phenolic phosphoric acid additives allows reduction of acyclic phosphine oxides at 110 °C.[28] This system also worked with phenylsilane replacing diethoxymethylsilane, though they did not choose to further explore phenylsilane. A screen of bis-phenolic phosphoric acids was performed and found that the addition of electron withdrawing groups on the phenols increased reductive activity, while replacing the phenyls with benzyl or alkyl groups had the opposite effect. Electron withdrawing groups decrease the pK_a of the phosphoric acid proton, while benzyl and alkyl groups would increase it, making the pK_a of this proton likely responsible for the changes in rate, though this concept is not elaborated on. Their best additive from the screen, bis-(4-nitrophenyl)-phosphoric acid (**BNPA**), facilitated the reduction of a wide variety of acyclic phosphines in 48 hours at 110 °C using 4 equivalents of silane. Therefore, if a given phosphine-dependent reaction can handle high temperature with a strong phosphoric acid, using **BNPA**, diethoxymethylsilane, and relatively cheap **TPPO** could be an alternative to the use of non-commercially available cyclic phosphines, even if the usage of 4 equivalents is certainly not atom-economical.

Beller's system was indeed put to use in multiple publications. Mecinovic and coworkers reported a triphenylphosphine and carbon tetrachloride mediated amide bond formation that they successfully made catalytic in phosphine through the addition of bis-(4-nitrophenyl)-phosphoric acid and diethoxymethylsilane at 110 °C.[29] They successfully applied this methodology to both primary and secondary amines. Fourmy and Voituriez also reported making the cyclization of diazodicarboxylates with α-ketoesters catalytic in phosphine using bis-(4-nitrophenyl)-phosphoric acid, phenylsilane, and phenyl dibenzophosphole at 90 °C.[30] The use of **TPPO** as the phosphine catalyst did furnish product, but they found that switching to a cyclic phosphine facilitated much more turnover, likely due to a reduction of the temperature from 110 °C in Beller's original conditions to 90 °C. These reactions demonstrate the effectiveness of the

diethoxymethylsilane/**BNPA** system in promoting catalytic-in-phosphine reactions with the inexpensive reagent **TPPO**, but requiring such a high temperature is certainly not ideal and hampers substrate scope.

Beller's system using catalytic **BNPA** is the first organo-catalyzed reduction of phosphine oxides by silanes, but metallic additives were also previously explored. Seeking to utilize cheaper but less reactive silanes such as **PMHS** or 1,1,3,3-tetramethyldisiloxane (**TMDSO**), Lemaire and coworkers reported a $Ti(O^iPr)_4$ catalyzed system that reduced phosphine oxides while heating to 100 °C.[31] Using **TMDSO** with 7.5-15% $Ti(O^iPr)_4$ facilitated 100% conversion of acyclic phosphines including **TPPO** within 10 hours. They also reported the use of **PMHS** with the titanium additive, but conversion to TPP from **TPPO** was lessened. They were able to reduce both alkyl and aryl phosphines, but included very few functional groups as ethers, ketones, esters, amides, and many other functional groups are known to not be stable to such conditions.[32] In another report by Beller's group, they obtained 96% conversion of **TPPO** to TPP with 10 mol% copper(II) triflate and three equivalents of **TMDSO** at 100 °C.[33] They also demonstrate that at least among copper salts, copper(II) triflate is uniquely active, as it facilitated at least 3x more phosphine reduction than copper(II) fluoride, chloride, or bromide, and copper(I) iodide demonstrated no activity at all. The copper triflate/**TMDSO** system was then used to reduce a range of acyclic phosphine oxides to the corresponding phosphines in reasonable yields. Based on the scope of substrates compared to Beller's organocatalytic system, it is safe to say that Cu(II) triflate/**TMDSO** is likely much less chemoselective.

The first and only room temperature silane-mediated catalytic-in-phosphine reaction was reported by O'Brien and coworkers in 2013.[34] They studied the isolated reduction of 1-phenylphospholane-1-oxide (**1PPO**) in the presence of 14 equivalents of silane and DIPEA as well as a single equivalent of benzoic acid. These conditions were very similar to their previous Wittig reaction conditions but with a small amount of benzoic acid added. They found that with

diphenylsilane, they were able to correlate the yield of phosphine with the pK_a of the benzoic acid additive, where substituents were added to the benzoic acid to adjust the pK_a. The addition of electron withdrawing groups to lower the pK_a furnished higher yields of phosphine, while electron donating groups had the opposite effect. The key result, however, was that switching the silane to phenylsilane while keeping the rest of the system the same caused a huge spike in the rate of reduction, reaching upwards of 70% conversion in just two minutes at room temperature.

O'Brien and coworkers also decided to change the non-cyclic substituent on the phosphine for the first time, replacing the phenyl with a butyl to make 1-butylphospholane-1-oxide (**1BPO**). The increased electron density on the phosphine of **1BPO** as opposed to **1PPO** likely contributed to its increased rate of reduction, as 85% conversion was achieved in just 2 minutes.[35] Satisfied, they explored a range of aprotic solvents and found that the system worked quite well in THF as well as the more environmentally friendly EtOAc and cyclopentylmethyl ether (CPME). Using EtOAc as the solvent, they explored adding their **1BPO** recycling system with the 4-nitrobenzoic acid additive to a range of aldehydes and primary or secondary bromides and successfully formed the Wittig products with most yields between 60 and 80%. These results validated this approach to room temperature recycling in the Wittig reaction, the first of its kind.

O'Brien and coworkers also explored applying the DIPEA/phenylsilane/4-nitrobenzoic acid to acyclic phosphine oxides.[36] By increasing the temperature to 100 °C with toluene as the solvent, they were able to achieve competent reduction with tri-*n*-octylphosphine oxide (TOPO), and successfully synthesized a range of Wittig products from the corresponding aldehydes and alkyl bromides. Naturally, they were interested in using the inexpensive phosphine oxide **TPPO** as well, but they found that their yields decreased unless *para*-trifluoromethylphenylsilane was used in place of phenylsilane, indicating that this electron-deficient silane reduced **TPPO** more rapidly. They did successfully synthesize a few alkenes using **TPPO** and *p*-trifluoromethylphenylsilane in the presence of 4-nitrobenzoic acid at 100 °C. Through the use of

phenylsilane and addition of *p*-nitrobenzoic acid to the previous catalytic Wittig conditions, O'Brien and coworkers created the most ideal reduction system to date.

Unfortunately, this system could not be applied to other common phosphine-dependent reactions as benzoic acids act as nucleophiles in the Mitsunobu, Appel, and Staudinger reactions. It also is not able to be applied universally to Wittig reactions, as O'Brien and coworkers reported a catalytic Wittig reaction that uses a masked strong base and a phosphine specifically designed to lower the pK_a of its ylides.[37] This report does not include the use of the room temperature recycling system with a benzoic acid, presumably because the addition of an acid to a reaction mixture that needs to be strongly basic interferes with the basicity. Therefore, while O'Brien's room temperature recycling conditions were indeed an important stepping stone towards generalized room temperature catalytic-in-phosphine reactions, their scope is limited both across the class of phosphine-dependent reactions as well as within Wittig reactions themselves.

The application of *in situ* phosphine recycling to other reactions continued with the development of a "traceless" catalytic Staudinger ligation by Ashfeld and coworkers.[38] They mixed benzyl azide, a benzoic acid, TPP, and phenylsilane in a single pot at 60 °C to make benzyl benzoyl amides in high yields. Some notable features of this system include the fact that 1.2 equivalents of azide is necessary for optimal yields, and increasing the phenylsilane equivalents to 1.5 drastically decreases the amount of product obtained. Additionally, diphenylsilane furnished product, though in much lower yield, but other silanes such as trichlorosilane, diethoxymethylsilane, and trimethoxysilane did not. This methodology is highly effective with benzyl azide and benzoic acids, but yields dip into the 60–80% range when benzyl azide is replaced with alkyl or allylic azides, or when the benzoic acid is replaced by an alkyl carboxylic acid.

A year later, Van Delft and coworkers reported a Staudinger/aza-Wittig sequence using esters of 2-azidophenol, 10 mol% phenyldibenzophosphole, and diphenylsilane.[39] The phosphine reacts

with the azide to form a phosphine imine, which is primed for an aza-Wittg reaction with the ester. This aza-Wittig reaction produces a benzoxazole and a molecule of phosphine oxide, which is then be recycled by the diphenylsilane. They were concerned with the competing reaction where the intermediate phosphine imine is reduced to form an amine while regenerating the phosphine, so they tested both phenylsilane and diphenylsilane in their initial benzoxazole forming reaction, and found that much higher yields were obtained with the less potent reducing agent diphenylsilane. Using the 2-azidophenolic esters primed for benzoxazole formation, they were able run this reaction successfully with a variety of esters at 101 °C in dioxane. The reactions also succeeded with azidophenol analogues, but yields dropped to the 55–65% range. They also synthesized azido esters that could form benzodiazepinones through the Staudinger/aza-Wittig sequence, and were able to form select products successfully with reduction of the phosphine imine predominating in the other cases. Ashfeld's and van Delft's reports clearly demonstrate that silane-based recycling of phosphine reagents is a successful strategy in Staudinger-like processes, though it is interesting that Ashfeld was able to use TPP at only 60 °C, while van Delft used a dibenzophosphole and had to increase the temperature to 101 °C. Room temperature Staudinger processes remain elusive.

A catalytic-in-phosphine methodology for the Mitsunobu reaction was reported by Buonomo and Aldrich in 2015, completing the set of classical phosphine-dependent reactions.[40] They reported good yields on a Mitsunobu reaction at 80 °C using phenylsilane, **1PPO**, diisopropylazodicarboxylate (DIAD), benzyl alcohol, and 4-nitrobenzoic acid as their pronucleophile. Originally phenyldibenzophosphole was used as the precatalyst, but they found that **1PPO** gave superior yields, presumably due to the increased rate of reduction. Diphenylsilane was also tried, but was less effective. The benzyl alcohol could be replaced with aliphatic alcohols with no decrease in yield, indicating a wide substrate scope for the alcohol, but replacing 4-nitrobenzoic acid with phenols and aliphatic esters was more problematic, reducing

the yields to 50–65%. This system demonstrated that phenylsilane was compatible with DIAD at elevated temperature, providing a further illustration of the chemoselectivity of phenylsilane. It is interesting as well to note that high temperatures were required for turnover of the catalyst, as benzoic acid, which facilitated room temperature recycling of **1PPO** in the catalytic Wittig reaction, is present in the Mitsunobu reaction. Other components combined with the benzoic acid must be what renders that reduction facile at room temperature.

We want to note at this point that the previously discussed reports are certainly not a comprehensive list; other manuscripts describe the use of silanes to make phosphine-dependent reactions catalytic, but these have narrow utility and do not include developments in reduction conditions.[41,42,43,44,45] Consequently, we have elected not to highlight them.

We have quite thoroughly discussed the state-of-the-art reduction conditions as well as the drawbacks inherent in each system. In order to provide further improvements, it is vital to fully understand how phosphine oxides are reduced via silanes, with or without additives. Several mechanistic suggestions have been made, beginning with Fritzche and coworkers in their seminal work on the reduction of phosphine oxides with trichlorosilane.[46] They proposed the bimolecular reaction of phosphine oxide with trichlorosilane to form a reduced phosphine and trichlorosilanol (Scheme 1.1). They propose that trichlorosilanol condenses into silyl-oxy polymers, releasing HCl, which then reacts with another molecule of trichlorosilane to form hydrogen and silicon tetrachloride (Scheme 1.1). The suggested steps that took place post-phosphine oxide reduction steps were made based on the observation that without additives, two equivalents of trichlorosilane were necessary to reduce a single equivalent of phosphine oxide to completion, but if a full equivalent of amine base was added, only one equivalent of trichlorosilane was necessary.

Horner and Balzer added to this proposal by suggesting that the phosphine oxide and trichlorosilane react via 4-membered transition state to form a phosphonium silanolate ion pair

(Figure 1.1), ultimately producing the reduced phosphine and trichlorosilanol.[47] The phosphonium-silanolate ion pair is predicted to be transient, and following the generation of trichlorosilanol, they propose it condenses into silyl-oxy polymers. 4-Membered transition states, while certainly not unheard of, are not particularly common in organic chemistry. It is likely that Horner and Balzer put for such a suggestion due to the fact that the transition state for the Wittig reaction, which contains a phosphorous center, is predicted to be 4-membered.[48]

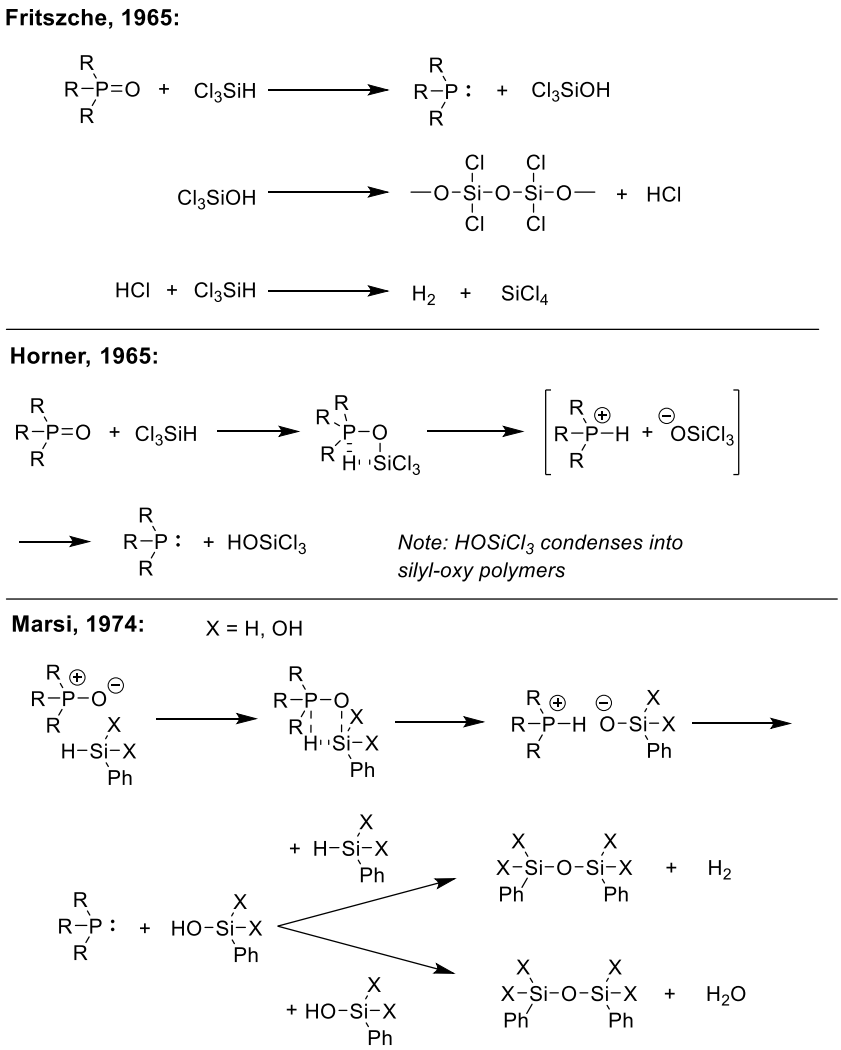

Scheme 1.1. Proposed Mechanisms for Additive-free Reduction of Phosphine Oxides by Phenylsilane and Trichlorosilane

A decade later, Marsi proposed the first mechanism of reduction of phosphine oxides by phenylsilane.[49] Drawing from the mechanistic proposals with trichlorosilane, Marsi also suggested a phosphine oxide and phenylsilane come together in a 4-membered transition state and dissociate to from a transient ion pair. A proton is exchanged to form the phosphine and a silanol, after which Marsi proposes two additional reactions to account for the observed formation of hydrogen gas and water. The first is a reaction of the silanol with another silyl-hydride to form a disiloxane bond and hydrogen gas, and the second is a combination of two silanols to form a disiloxane and water. Interestingly, without explicitly discussing the potential differences between phenylsilane, phenylsilanol, and phenylsilanediol, Marsi suggests that phenylsilanol and/or phenylsilanediol are also active reductants. This is due to a previous observation by Fritzsche and coworkers that full conversion to the phosphine was achievable with only 0.7 equivalents of phenylsilane.

Horner and Marsi's 4-membered transition state for additive-free silane-mediate reduction of phosphine oxides appears to be widely accepted as multiple groups refer to it. Computational studies have much more recently been performed on the mechanisms of phosphine oxide reduction by both trichlorosilane[50] and phenylsilane[51], seeking to ascertain the theoretical energy barriers towards transition state formation. Using quantum mechanical calculations with the SCS-MP2 method, Krenske reports that trichlorosilane and trimethylphosphine oxide would need 27.1 kcal/mol to undergo the 4-membered transition state towards reduction. Phenylsilane, when reacting with the admittedly more sterically hindered tri-n-butylphosphine oxide, is reported to need a shocking 43-45 kcal/mol to enter the transition state. This is using B3LYP calculations of the silane and phosphine oxide in solution, so the results for trichlorosilane and phenylsilane are not directly comparable. Both results, but particularly the ones with phenylsilane, suggest a very high activation barrier towards reduction, so much so if the calculations are accurate, the observed rates of reduction should be much slower.

Lemaire and coworkers propose a much different mechanism for their reduction of phosphine oxides using **TMDSO** and Ti(O^{i}Pr)$_4$. They suggest the mechanism shown in Scheme 1.2 based on observation of the reduction with EPR and ^{29}Si NMR.[52] The EPR revealed the presence of Ti(III) and small amounts of an Si-Si species, so they propose that the Ti(IV) abstracts an electron from **TMDSO** to form a Ti(III) species and a silicon radical. This silicon radical can either go through an unproductive dimerization to form the Si-Si species, or it can react with the double bond of a phosphine oxide to produce a phosphorous-centered radical with a single bond between the phosphorous and oxygen. This then breaks apart to form reduced phosphine and a silyl-oxy radical, which they propose oxidizes the TI(III) back to Ti(IV). Lemaire and coworkers thus proposed that phosphine oxides are reduced in their system via single-electron transfer, a unique and interesting mechanistic proposal.

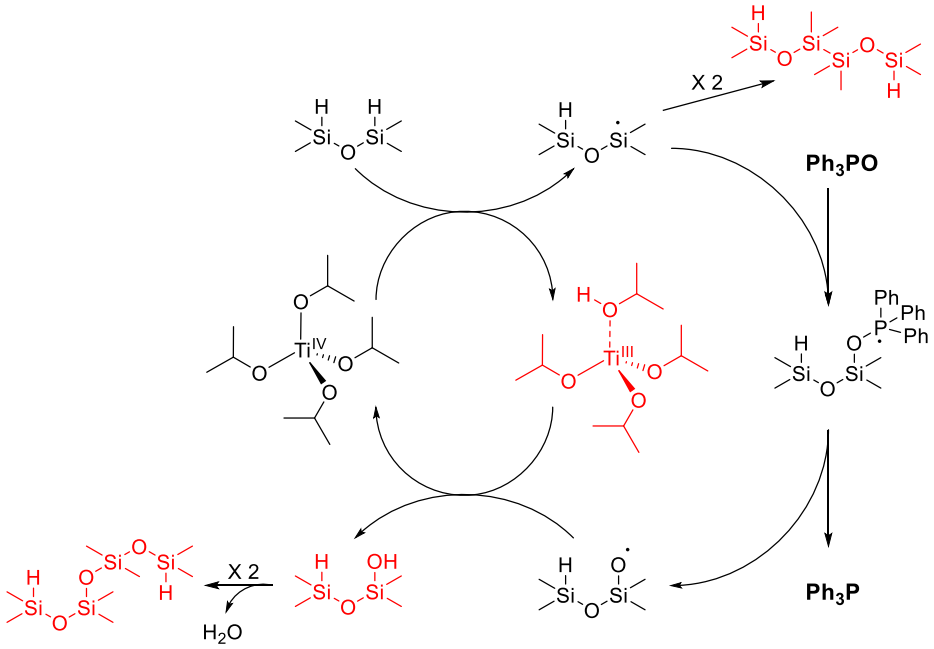

Scheme 1.2. Proposed Mechanism for the Reduction of Phosphine Oxides by **TMDSO**/Ti(O^{i}Pr)$_4$. Entries in red are intermediates observed by either EPR or ^{29}Si NMR studies.

Substantial progress has clearly been made in developing catalytic methodologies for phosphine dependent redox reactions, with phenylsilane and diphenylsilane appearing to be

excellent chemoselective reagents for the recycling of cyclic phosphines at 80-100 °C.[53,54,55] With reactions and substrates that are compatible with the Bronsted acid **BNPA** at 110 °C, one can even use commercially available and cheap **TPPO** as the precatalyst, though four equivalents of the silane are required.[56] The catalytic Wittig reaction can even be run at room temperature with the addition of a catalytic amount of benzoic acid to the reaction mixture, as long as the conditions require only a low degree of basicity.[57] However, there are clearly multiple areas that these methodologies could be improved. An ideal system would be completely chemoselective for phosphine oxides and reduce them at room temperature in the absence of non-silane additives. This would greatly aid both phosphine recycling and phosphine ligand synthesis. Finally, it would also be ideal to have a better understanding of why additives such as PNBA or **BNPA** can affect the reaction rate so drastically. The remainder of this chapter describes our attempts and progress towards these goals, with the initial intention of improving the catalytic Mitsunobu described by Buonomo and Aldrich.[58]

1.2 Towards a Room Temperature Catalytic Mitsunobu: Phosphine and Silane Screen

1.2.1 The Design and Synthesis of Phosphine Precatalysts

As mentioned previously, the Mitsunobu reaction is a widely used reaction in organic synthesis today, as its combination of broad applicability and substrate scope with exquisite stereocontrol are extremely attractive features to chemists.[59] Stoichiometric Mitsunobu reactions are regularly run at room temperature, but when Buonomo and Aldrich developed the catalytic-in-phosphine Mitsunobu reaction, they required heating to 80 °C in THF.[60] This temperature is above the boiling point of THF, necessitating a sealed pressure vessel to accommodate those conditions, which is certainly not ideal. As expected, the rate-limiting step in the catalytic Mitsunobu was found to be reduction of the phosphine oxide back to the phosphine, with the

increased temperature required to obtain a reasonable rate of phosphine generation. Unfortunately, they reported multiple undesired side reactions that were likely caused by the addition of heat, and such temperatures provide general limitations to the substrate scope of this catalytic modification to the Mitsunobu reaction. We thus began an investigation to obtain facile room temperature reduction of phosphine oxides, preferably additive-free, but at least in such a way that the conditions would be compatible with a catalytic-in-phosphine Mitsunobu reaction.

We first sought to redesign the phosphine precatalyst, attempting to achieve room temperature reduction in combination with either phenylsilane or diphenylsilane. To find inspiration, we first noted that O'Brien and Chass[61] suggest that the reason cyclic phospholane oxides are reduced at much lower temperatures than acyclic phosphine oxides is the relief of ring strain that is granted in the 5-coordinate trigonal bipyramidal state immediately following transfer of the hydride. Van Delft attempted to increase the ring strain through the design of phenyldibenzophospholes, but these were found to have less reductive potential when paired with silanes.[62] The reason for this was not thoroughly examined, but van Delft and coworkers varied the electronics on their dibenzophospholes and found that increasing electron density on the phenyl rings correlated with faster reduction. We hypothesized that the differences in reactivity between the dibenzophosphole and phospholane scaffolds were due to electronics, as the dibenzophosphole scaffold certainly has less electron density on the phosphine oxide than an alkyl phospholane oxide due to the more electron withdrawing nature of an sp^2 carbon compared to sp^3. Also, when O'Brien and coworkers replaced the phenyl ring on **1PPO** with a less electron withdrawing butyl substituent (**1BPO**), they found that **1BPO** had a superior rate of reduction.[63] From these reports, there appears to be a consistent pattern where increased electron density on the phosphine oxide increases the reductive potential of the precatalyst. It is less clear exactly what role ring strain plays in reductive potential, as van Delft and coworkers demonstrated that 5-

membered cyclic phosphine oxides are superior to larger ring sizes, but were unable to fully characterize effects of ring strain on reactivity.[64]

As no evidence appeared to contradict such an assumption, we hypothesized that increasing the ring strain through the use of 4-membered cyclic phosphetanesn would lead to faster reduction. Substituted 2,2,3-trimethylphosphetane oxides, 2,2,3,3-tetramethylphosphetane oxides, and 2,2,3,4,4-pentamethylphosphetane oxides can easily be synthesized[65] from the corresponding phosphinic dichlorides via McBride synthesis.[66] Radosevich and coworkers have used the trimethyl and pentamethyl variants in catalytic-in-phosphine reactions with phenylsilane as the reductant,[67] demonstrating the efficacy of both scaffolds. We chose to use the 2,2,3-trimethylphosphetane scaffold due to its presumed lower level of steric bulk around the P=O bond when compared to the tetramethyl or pentamethyl variants. Utilizing a phenyl substituent on the phosphorous atom would provide a direct comparison to **1PPO**, potentially allowing for the isolation of ring strain effects, but more electron donating substituents were likely to increase the rate of reduction further. We chose to make P-butyl and P-pyrrolidinyl phosphetanes, with butyl being a safe option;[68] it is less electron withdrawing than phenyl and should therefore increase the electron density on both the phosphorous and oxygen atoms of the precatalyst. On the other hand, a pyrrolidinyl substituent should decrease the electron density on the phosphorous atom due to the increased electronegativity of nitrogen, but it should substantially increase the electron density on the oxygen atom of the precatalyst through resonance. Based on the mechanism proposed by Marsi,[69] where phosphine oxide and silane are predicted to come together with an attack of the oxygen atom on the silicon center, it appeared much more likely that increased electron density on the oxygen atom, not the phosphorous atom, is what facilitates faster reduction. Phosphinic amides had previously been synthesized but never evaluated for their isolated rate of reduction, so we chose to be the first to test one. Our belief was that the use of a highly-strained phosphetane

with an electron donating P-substituent would increase the rate of reduction enough to facilitate a room temperature catalytic Mitsunobu reaction.

2,2,3-trimethyl-1-phenylphosphetane oxide (**TMPPO**) was synthesized in quite poor yield from the combination of phenylphosphonous dichloride and 3,3-dimethyl-1-butene (Scheme 1.3).[70] Beginning with the known compound 2,2,3-trimethyl-1-chlorophosphetane oxide,[71] the addition of butyl magnesium bromide afforded 2,2,3-trimethyl-1-butylphosphetane oxide (**TMBPO**) as a white crystalline solid. Similarly, submitting the chlorophosphetane precursor to a mixture of pyrrolidine and triethylamine at 60 °C produced 2,2,3-trimethyl-1-pyrrolidinylphosphetane oxide (**TMPyrPO**) in good yield. For stability purposes, all three phosphine oxide precatalysts were stored at -20 °C under the exclusion of light.

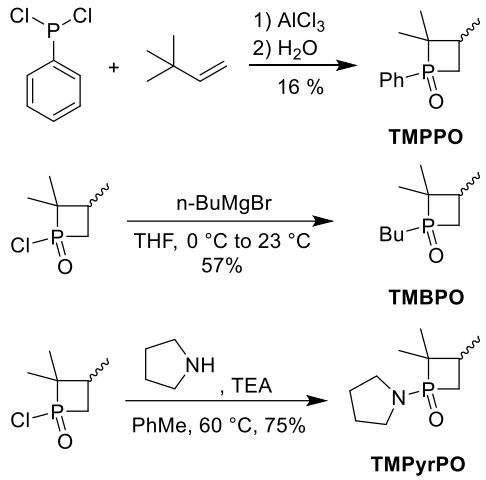

Scheme 1.3. Synthesis of Phosphetane Precatalysts **TMPPO**, **TMBPO**, and **TMPyrPO**

1.2.2 Phosphine and Silane Screen

With the precatalysts in hand, we performed an empirical screen of their effectiveness by testing each of them in the catalytic Mitsunobu reaction at 80 °C (Table 1.1) using the previously optimized conditions by Buonomo and Aldrich for **1PPO**.[72] While doing this, we noted that O'Brien and coworkers had evaluated a few silyl hydrides as potential reductants,[73] but a more thorough list was necessary to determine whether any previously unreported silanes had reductive

activity. We thus selected a list of silanes, and evaluated each one with each of our precatalysts. Using a very basic Mitsunobu reaction with benzyl alcohol and *p*-nitrobenzoic acid (PNBA) combining to form benzyl *p*-nitrobenzoate, we examined each combination of precatalyst and silane. The results are shown in Table 1.1

Table 1.1. Screening Phosphine Precatalysts and Silanes for Effectiveness in the Catalytic Mitsunobu Reaction

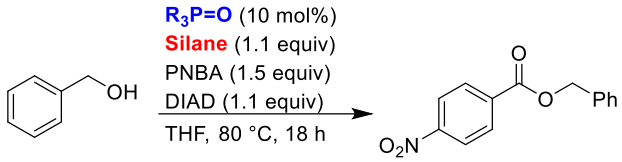

Entry	$R_3P=O$	Silane	Yield (%)
1	**1PPO**	$PhSiH_3$	77[74]
2	**TMPPO**	$PhSiH_3$	65
3	**TMBPO**	$PhSiH_3$	44
4	**TMPyrPO**	$PhSiH_3$	0
5	**1PPO**	Ph_2SiH_2	42[75]
6	**TMPPO**	Ph_2SiH_2	42
7	**TMBPO**	Ph_2SiH_2	15
8	**TMPyrPO**	Ph_2SiH_2	0
9	**1PPO**	Ph_3SiH	0
10	**TMPPO**	Ph_3SiH	0
11	**TMBPO**	Ph_3SiH	0
12	**TMPyrPO**	Ph_3SiH	0
13	**1PPO**	**PMHS**	0
14	**TMPPO**	**PMHS**	0
15	**TMBPO**	**PMHS**	0
16	**TMPyrPO**	**PMHS**	0
17	**1PPO**	**TMDSO**	0
18	**TMPPO**	**TMDSO**	0
19	**TMBPO**	**TMDSO**	0
20	**TMPyrPO**	**TMDSO**	0
21	**1PPO**	Et_3SiH	0
22	**TMPPO**	Et_3SiH	0
23	**TMBPO**	Et_3SiH	0
24	**TMPyrPO**	Et_3SiH	0
25	**1PPO**	$^{i}Pr_3SiH$	0
26	**TMPPO**	$^{i}Pr_3SiH$	0
27	**TMBPO**	$^{i}Pr_3SiH$	0
28	**TMPyrPO**	$^{i}Pr_3SiH$	0
29	**1PPO**	$(TMS)_3SiH$	28
30	**TMPPO**	$(TMS)_3SiH$	26
31	**TMBPO**	$(TMS)_3SiH$	<5
32	**TMPyrPO**	$(TMS)_3SiH$	0

These results were discouraging, as the silane screen revealed that the conditions used by Buonomo and Aldrich in terms of phosphine and silane identity were still the highest yielding set discovered. Looking exclusively at the silanes, most resulted in the formation of no product, and TLC analysis allowed us to infer this was due to zero precatalyst reduction. Diphenylsilane and tris-TMSsilane were the only silanes besides phenylsilane to furnish product. Based on previous results, phenylsilane performed as expected, it afforded product, but less than phenylsilane. On the other hand, tris-TMSsilane being successful was more surprising, though TLCs of each of the reaction mixtures revealed quite a smattering of UV-active products, suggesting that many side reactions are also occurring. This can be explained by the fact that tris-TMSsilane is often used as a radical initiator due to the ease of homolytic fragmentation of its Si-H bond. Therefore, the side reactions are likely radical-mediated, which is certainly undesirable, and caused us to remove this silane from further consideration with any precatalyst.

As for trends with the phosphines, **1PPO**>**TMPPO**>**TMBPO**>**TMPyrPO**, with the phosphinic amide affording no product with any silane. As the system was optimized with **1PPO**, it was likely that adjusting the conditions would allow us to obtain similar yields with **TMPPO**, which is okay, but does not move the project forward. The yields with **TMBPO** were consistently and significantly below the P-phenyl phosphines. Taken together, we observed the exact opposite trend that we hypothesized during the design process, though this was only an empirical screen. We decided to investigate each of the phosphetane precatalysts further, choosing to perform isolated reduction studies with each of **TMPPO**, **TMBPO**, and **TMPyrPO** with phenylsilane.

1.3 Isolated Reductions of Precatalysts

1.3.1 Reduction of TMPyrPO

To begin, we chose to investigate **TMPyrPO**, attempting to see if we could uncover the reason that it produced zero product in the catalytic Mitsunobu reaction. Isolated reduction studies were performed by adding **TMPyrPO**, $PhSiH_3$, and solvent to a sealed NMR tube, heating it for a predetermined amount of time, cooling, and evaluating the percentage reduction by obtaining a ^{31}P NMR spectrum of the resulting mixture (integrating ^{31}P NMR peaks accurately reveals relative species amounts). This method produces a time course of the percentages of reduced and unreduced precatalyst that can be displayed as a reaction progress curve. Our isolated reduction studies were also performed using a large excess of silane so that the reduction proceeded under pseudo-first order conditions with respect to phosphine oxide. Pseudo-first order conditions allow for easy calculation of the rate constant of reduction, which can be used to directly compare catalysts as well as provide a quantitative number for the activation energy through Arrhenius analysis. However, when we mixed **TMPyrPO** and $PhSiH_3$ in THF and heated the mixture to 80 °C for only 5 minutes, the subsequent ^{31}P NMR revealed no peaks. This result demonstrated that **TMPyrPO** degrades in THF when reacted with $PhSiH_3$ and heat, which would explain the lack of product formed in the catalytic Mitsunobu reaction. Radosevich and coworkers had previously used 2,2,3,4,4-pentamethyl-1-pyrrolidinyl-phosphetane oxide in a phosphine redox reaction with phenylsilane in CH_2Cl_2, suggesting that the choice of solvent could be important when using **TMPyrPO**.

To explore this possibility, we reacted **TMPyrPO** with $PhSiH_3$ under pseudo-first order conditions in CH_2Cl_2, toluene, and 25% THF in CH_2Cl_2. 25% THF in CH_2Cl_2 was chosen because PNBA, BnOH, and DIAD were all soluble in this mixture, meaning if this solvent allowed for reduction without degradation of **TMPyrPO**, a catalytic Mitsunobu using the phosphinic amide was still a possibility. Unfortunately this was not the case, as no ^{31}P peaks were visible after 30 minutes, meaning the degradation was slowed, but still far too fast to be competent in reactions. The other solvent choices were substantially more successful. **TMPyrPO** was found to be fully

reduced within 90 minutes in both CH_2Cl_2 and toluene, with ^{31}P product peaks visible in both cases.

Further investigation of this reduction, however, revealed that a lot more was going on than removal of the P=O bond. According to the spectra provided by Radosevich and coworkers, the reduced phosphinic amide should have a chemical shift around 100-120 ppm.[76] We did observe the presence of such peaks, however, they were short-lived. Most of the final reduction product had a chemical shift around 10 ppm. Due to the intense degradation observed, we proposed that **TMPyrPO** was reduced all the way to the secondary phosphetane, which are known to be unstable. With such results, it was extremely unlikely that **TMPyrPO** could serve as an effective catalyst with $PhSiH_3$ as the reductant, though possible if a reduced temperature blocked over-reduction to the secondary phosphetane.

1.3.2 Reduction of TMBPO

Isolated reduction studies with **TMBPO** revealed a different problem, as before any silane was added, multiple ^{31}P NMR peaks were visible regardless of the solvent used. The catalyst was thus unstable and had undergone substantial degradation despite being stored in the freezer under exclusion of light. Upon addition of phenylsilane, **TMBPO** reduced quite quickly, finishing in a 90 minute period, but additional degradation peaks were observed. Even though the degradation peaks only accounted for ~15% of the total post-reduction phosphine peaks when beginning with a purified sample, we believed that the observed degradation was the reason for **TMBPO** halving the yield of the catalytic Mitsunobu. Any of the unidentified phosphorous species could cause side reactions within the Mitsunobu, and the catalyst must undergo multiple redox cycles over an 18 hour period, which would undoubtedly prompt further degradation. This degradation was also visible regardless of whether the solvent was THF, CH_2Cl_2, or toluene. **TMBPO** was thus unlikely to be a successful precatalyst in a redox recycling phosphine depedent reaction.

1.3.3 Reduction of TMPPO

TMPPO was the most successful of the three phosphetane precatalysts synthesized in the catalytic Mitsunobu reaction, so we did not expect to observe any obvious issues in isolated reduction studies. This was indeed the case, as **TMPPO** reductions proceeded smoothly with phenylsilane with minimal or no appearance of other phosphorous containing by-products. Reduction of **TMPPO** by phenylsilane also was successful in THF, CH_2Cl_2, and toluene, with each solvent producing slight but insignificant differences in the reduction rate. To directly compare the reductive potential of **TMPPO** and **1PPO**, we decided to do Arrhenius analysis on the reduction of **TMPPO** by phenylsilane in THF (**1PPO** has already been reported[77]), which revealed two interesting features about this reaction.

Both diasteromers of **TMPPO** have the same ^{31}P NMR signal in THF, but the peaks for the corresponding reduced phosphine diasteromers are separated by several ppm. Close examination revealed the presence of a fourth ^{31}P peak that appears after only 5 minutes of heating. It accounts for about 10% of the total phosphorous in this time point, and then decreases over time. We were very excited about this, as we thought the fourth peak could potentially represent an intermediate in the reduction of **TMPPO** by phenylsilane. A similar peak was not observed with either **1PPO** or **TMBPO**. However, further investigation revealed that this peak was in equilibrium with the main **TMPPO** peak, as heating **TMPPO** in THF without phenylsilane for 5 minutes caused the fourth peak to appear, again accounting for about 10% of the total ^{31}P NMR signal. Further heating did not increase this percentage, indicating that it was not the product of an irreversible reaction. Additionally, careful monitoring of the reduction time courses revealed that the fourth peak was always about 10% of the size of the main **TMPPO** peak. We thus discarded this peak as meaningful, and still are not certain what it represents.

Our other observation proved much more important. Figure 1.1 shows a reaction progress curve for the reduction of **TMPPO** by $PhSiH_3$. As you can see, the reduction appears to start off more slowly, then speed up between the 30 and 45 minute mark. The reason that the observation is important is that such behavior is contrary to both our expectation and the presumed mechanism presented by Marsi. That mechanism would predict the concentration of phosphine oxide would decay in a single-exponential fashion as occurs with single-step mechanisms. Instead, Figure 1.1 strongly suggests that we are observing some kind of a multi-step process, which was very exciting, as no one has ever suggested that the reduction of phosphine oxides by phenylsilane occurs via a multi-step process.

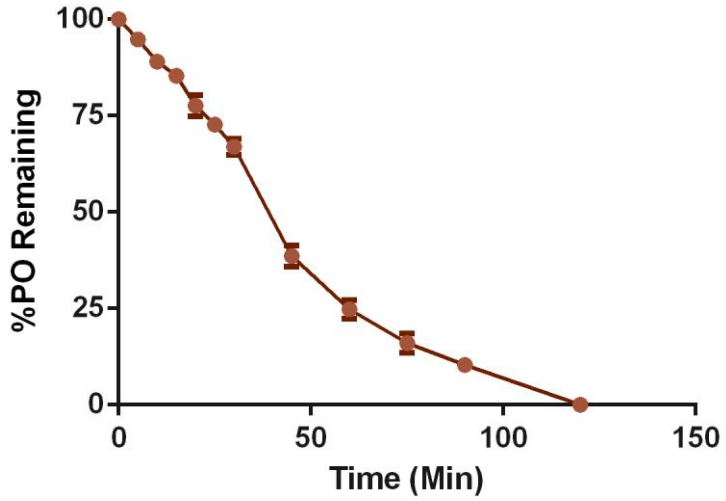

Figure 1.1. Reaction Progress Curve for the Reduction of **TMPPO** by Phenylsilane. [$PhSiH_3$] = 0.4 M & [**TMPPO**] = 0.04 M

1.3.4 Evaluating Potential Kinetic Mechanisms

We sought to determine what was the cause of the multi-step behavior of the curve in Figure 1.1, and thus listed every potential cause that we considered feasible for the reduction process occurring. The four ideas that we settled on were that the reduction process itself could be multi-step, the silane could be undergoing pre-activation, the phosphine could be undergoing pre-

activation, and phenylsilanol and/or phenylsilanediol could be substantially more rapid reductants than phenylsilane (Figure 1.2). It could also be due to any combination of these, but we designed experiments to evaluate each one of these potential causes individually.

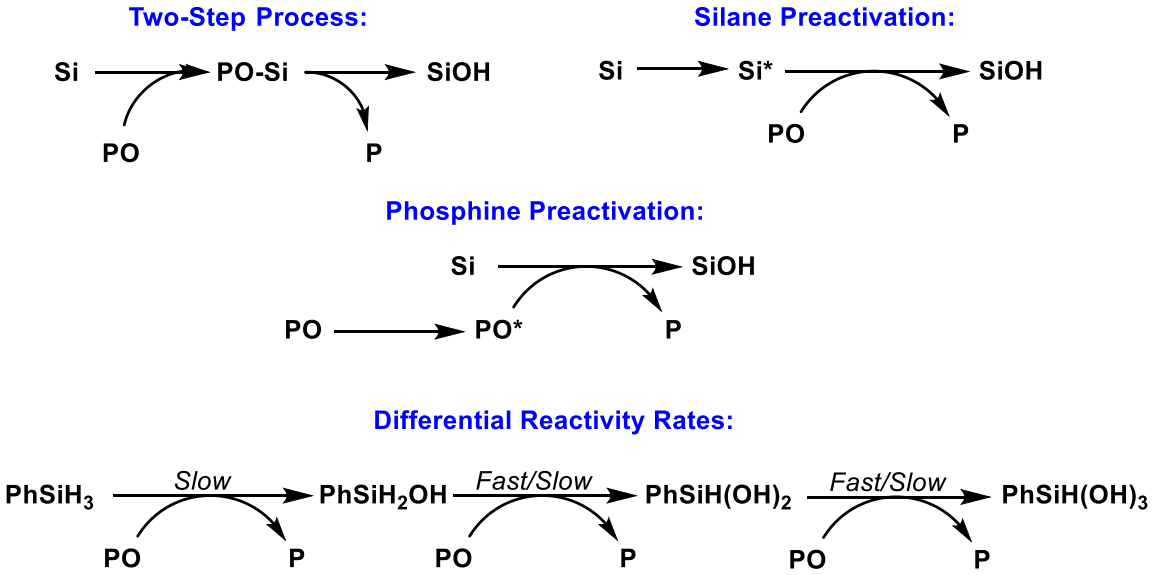

Figure 1.2. Potential Kinetic Mechanisms that Would Cause an Increase in the Rate of Reactivity Following Initiaition of the Reaction. PO = Phosphine Oxide. P = Reduced Phosphine. Si = A silyl hydride species. SiOH = Si with a hydride replaced by a hydroxyl. The * symbol denotes a potential unknown intermediate.

We decided to begin by testing whether pre-activation of silane or phosphine was occurring during the reduction process. We did not consider phosphine pre-activation likely to yield any results, as there are no obvious pre-activation pathways, but due to the ease of testing it was still deemed worth doing. Pre-activation of the silane appeared much more plausible, as phenylsilane could react with water to form phenylsilanol, which is almost certain to have some reductive potential (This theory is a combination of the silane pre-activation/differential reactivity rates mechanisms). Alternatively, phenylsilane could homocouple to form a silylsilane that could also theoretically reduce phosphine oxides faster than itself. To perform the actual tests, we heated **TMPPO** and phenylsilane separately in THF at 80 °C for one hour before addition of the other component. Figure 1.3 shows the resulting time courses following initiation of the reaction, as

well as their comparison to a no preincubation control. The phosphine preincubation curve appears to have a slightly less sigmoidal trajectory when compared to the control, but this could be just experimental error, and the difference between the two curves in terms of rate of reduction is likely insignificant. Fitting the phosphine preincubation curve to a single exponential still fits quite poorly (Figure 1.4), making it unlikely that there is an important phosphine oxide pre-activation preceding reduction. Silane preincubation, on the other hand, appears to cause a slightly faster reduction, but the curve still fits very poorly to a single exponential (Figure 1.5). The data was thus inconclusive, as silane preincubation does not appear to remove the multi-step nature of the reaction, but did appear to improve the rate of the reaction.

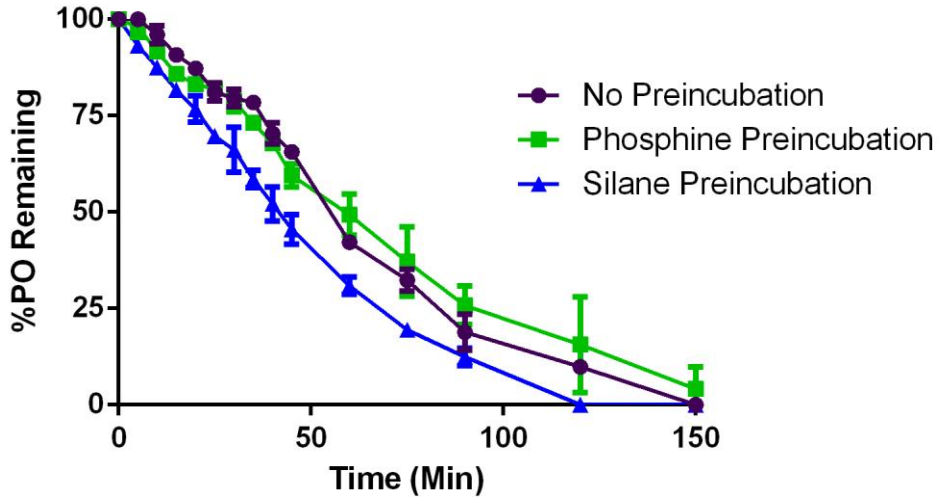

Figure 1.3. Comparison of Reduction Rates when **TMPPO** or $PhSiH_3$ is Pre-incubated in Heated THF. [$PhSiH_3$] = 0.2 M & [**TMPPO**] = 0.04 M

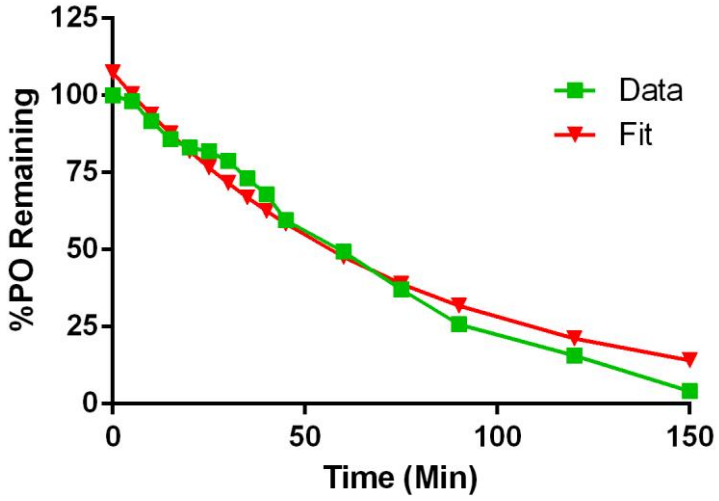

Figure 1.4. Fitting the Phosphine Pre-incubation Curve to a Single Exponential. [$PhSiH_3$] = 0.2 M & [**TMPPO**] = 0.04 M

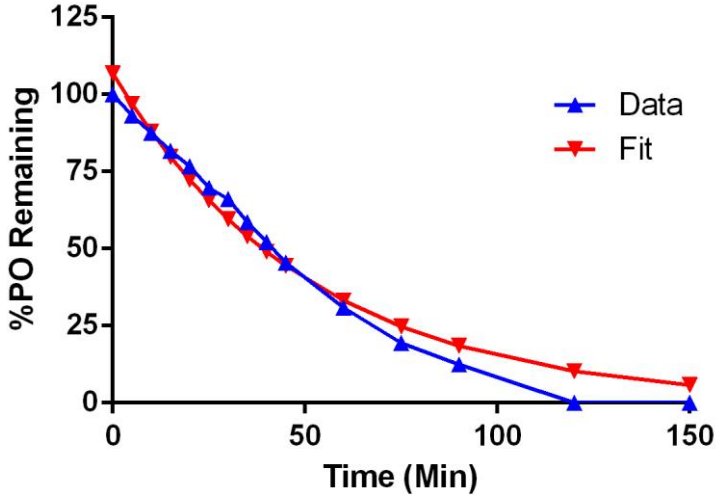

Figure 1.5. Fitting the Silane Pre-incubation Curve to a Single Exponential. [$PhSiH_3$] = 0.2 M & [**TMPPO**] = 0.04 M

We were able to obtain strong evidence that the reduction of **TMPPO** by phenylsilane is not a multi-step process. A multi-step process of reduction should involve one or more intermediates, which would have distinct ^{31}P NMR signatures. With such a substantial increase observed in the rates of reduction at earlier time points compared to what single-exponential decay would

provide, a significant buildup of the intermediate should be seen. Even when increasing the concentration of **TMPPO** to 0.10 M to obtain a greater signal-to-noise ratio, we observed no peaks that could credibly be intermediates in the reduction process (there was still that 4th peak mentioned earlier). We thus ruled out a multi-step reduction process contributing in any significant way to the sigmoidal nature of the reduction curves.

One more interesting result was obtained from varying the concentration of **TMPPO** (as previously mentioned) or silane while holding the other constant and maintaining pseudo-first order conditions with respect to the phosphine oxide. Increasing concentrations of silane correlated with increases in the rate of reduction, which was unsurprising (Compare Figure 1.4 to Figure 1.3). Higher concentrations of silane also appeared to decrease the sigmoidal nature of the curves, though they still fit to a single exponential somewhat poorly. On the other hand, increasing the concentration of phosphine oxide appeared to cause a corresponding increase in the rate of reduction when measured by the percentage of total phosphine (Figure 1.6). Unfortunately, the data was again inconclusive, as reduction with the concentration of **TMPPO** being 0.10 M was slower than with 0.07 M, but still faster than 0.04 M. This result was important because if the initial concentration of phosphine influences the percentage rate of reduction of phosphine oxide even with a large excess of silane, we are not actually succeeding in making the reaction first-order with respect to phosphine. (See section 1.14).

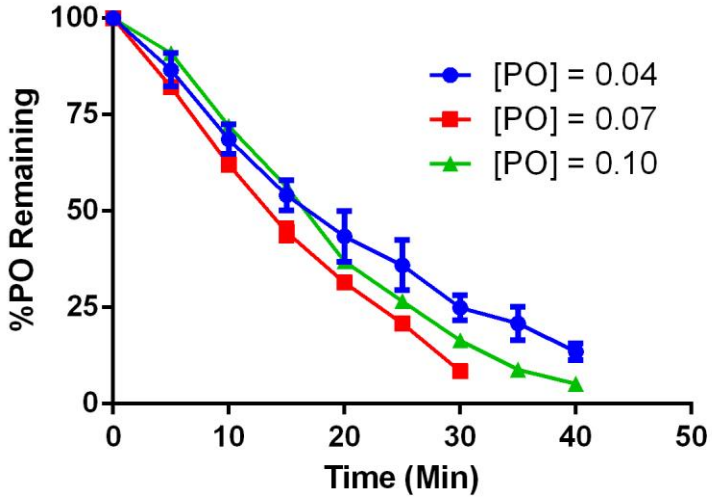

Figure 1.6. The Effect of the Concentration of **TMPPO** on the Reduction Rate. [$PhSiH_3$] = 0.75 M

Throughout this process, we became frustrated that our reaction progress curves contained so much error, especially in the silane preincubation and phosphine concentration dependence studies. With more accurate results, we could have conclusively ruled out explanations for why an increase in the rate of reduction of **TMPPO** with phenylsilane is observed after initiation. Even with running each of our reactions in triplicate (while removing curves that strayed too far from the norm), we were unable to obtain data that was sufficient for our purposes. With these frustrations in mind, we decided to pursue using variable temperature (VT) NMR. The idea was that by starting the reaction (in an NMR tube) and then submitting it to the NMR, we could continually obtain FID files at intervals of our choosing as the tube would be heated to the desired temperature, which would accomplish what we had been doing with an oil bath. This method would reduce sources of error such as the time between when a timer signaled that an NMR was to be taken and the actual cooling of the NMR tube, as well as the time spent waiting in the NMR queue or the NMR itself at room temperature, during which the reaction is likely proceeding at a slower rate. We were particularly interested in obtaining multiple FIDs in the initial portion of the

reduction for accuracy in assessing the increase in the rate of reduction during that time. This would require the time of collection for each FID to be quite short, resulting in numerous FIDs. Standard processing of each FID is time consuming, so we decided to write a program that automates processing of our FIDs.

1.4 MassNMRProcessing

1.4.1 Introduction and Outlining

In order to write the program, which we termed MassNMRProcessing, we first had to outline exactly what we expected it to accomplish, included proposing inputs and outputs. The basic idea for this program was that a set of NMR data and instructions on which peaks should be integrated will be submitted to MassNMRProcessing, which will then sort, process, and integrate the spectra, ultimately providing the numbers obtained from integration. With such a framework, the main output should be a list of the integrated values for each peak in table format, with each column a peak and each row an individual FID, with the rows sorted by the order in which the experiments were performed. As an additional output, we wanted to display up to twelve of the integrated spectra. This would provide quality control for the program to make sure the spectra were being processed and phased correctly, as well as quality control for the experiment to see if anything unexpected happened.

Concerning the inputs, one has to be the ppm of each peak that is to be integrated. Another should be the ppm of a peak that will serve as the standard to orient the spectra, much like the residual solvent peak is used in typical ^{1}H or ^{13}C NMR. To allow for different substances to serve as the standard, it is easiest to just have the chemical shift of the chosen standard submitted to MassNMRProcessing. The final input would need to tell the program where to obtain the experimental data. In order to ascertain how this should be input, we had to choose how we were going to set up our NMR time courses. We eventually settled on submitting several experiments

in a single queue as opposed to using an arrayed experiment. The reason for this is that arrayed experiments generate a single file containing all of the individual spectra, and there was no information available on how to successfully extract each of the spectra from this file, likely for proprietary reasons. An ideal final input would thus be the location and name of the overarching folder containing all of the data-filled folders generated from each experiment. The program should be able to take this input and extract the raw data.

1.4.2 Processing Spectra

With these basic inputs and outputs established, we began working on writing functional NMR processing code. We decided to write this program in Matlab, as though the use of such a high level language may decrease the speed of our program, there are several presets relating to mathematical functions and input/output that we would be able to use and not have to write/find ourselves. As we had easy access to both Varian and Bruker instruments, we also decided that we wanted MassNMRProcessing to be able to input both Varian and Bruker data.

Moving on to actual coding, there are several parts involved in processing a FID, as it is often apodized, zerofilled, fourier transformed, and phased before integration occurs. Apodization is the process of multiplying the FID by a decaying function, usually a Lorentzian or Gaussian function. The choice of apodization function can either improve the signal to noise ratio or the resolution of the NMR spectra, which are each useful under differing circumstances. Zerofilling is the process of adding zeros to the end of the FID, which increases the apparent digital resolution of the spectrum. This improves the cosmetic appearance of the spectrum without actually generating any new data, which would be useful when visualizing the output spectra through MassNMRProcessing. Taking the Fourier Transform of the FID is what actually generates the NMR spectrum that all organic chemists know and love, and phasing the spectrum is essential, as otherwise the peaks cannot be accurately integrated due to poor peak shapes. We

decided that we wanted our program to implement user-friendly controls for changeable parameters for all of these features.

The first task was to input the data from an FID. This is easily accomplished with a Matlab preset function, and the data was placed in a Matlab array. From there, it was again trivial to multiply this array with an apodization function and perform zerofilling. Doing a Fast Fourier Transform is another preset function in Matlab, which resulted in a spectrum 2X the width of a typical spectrum with the left half being a mirror image of the right half. Removal of the left half brought about an unphased NMR spectrum. Unfortunately, phasing proved quite difficult, for two reasons. The first is that we were finding it difficult to write an area minimization function for the spectrum that would properly phase it (likely due to our inexperience, not the difficulty of the task).[78] The second was specific to Bruker data, as we discovered that Bruker includes a digital filter at the beginning of the FID which must be placed at the end of the spectrum after apodization and zerofilling. Leaving the filter data at the beginning results in extremely "wiggly" NMR spectrum[79] that are completely unusable. Therefore, it must be removed and appended to the end of the spectrum, though this requires knowing the precise number of time points at the beginning of the FID in order to have a spectrum with an accurate baseline. Even with the correct number of points moved, certain apodization and zerofilling procedures result in a spectrum with baseline artifacts that either increase (smiles) or decrease (frowns) at each end of the spectrum.[80] Avoiding smiles and frowns is even more difficult, with the information and algorithms necessary to do so not easily obtained.

After several attempts to bypass these issues, we decided to take a different approach to writing MassNMRProcessing. Instead of coding *de novo*, we would attempt to build our program out of NMR processing programs already written in Matlab. We found two programs, MatlabNMR and MatNMR 3.9, that uploaded their code to the internet and licensced it for open use/modification. When testing them, we found that MatlabNMR no longer ran due to the

changes in Matlab syntax over the last few years. MatNMR, however, was a fully functional NMR processing program, similar to ACDlabs or the default Varian or Bruker NMR workup packages. Because MatNMR was functional, we chose to use its code as our starting point for MassNMRProcessing. Through performing several processes on FIDs loaded into MatNMR, we discovered MatNMR created an object that contained most the information about the FID that we would need, including the FID, the folder it was stored in, whether the data was Bruker or Varian, and many other important variables. It also contained much more information that was mostly related to how the spectrum was supposed to be visualized, which was not useful as we were not interested in using the MatNMR visual interface, but rather in creating automated code behind the scenes. Following creation of the main spectrum-containing object, that were separate functions that MatNMR used to perform modifications to it. Again, most of these concerned the visual appearance/orientation of the spectrum, and thus were not useful. However, we found that the functions “apodize1d”, “regelsize1d”, “four1d”, and “setphase1d” apodized, zerofilled, fourier transformed, and autophased the actual FID/spectrum, respectively. These functions served as our main initial development tools.

MatNMR used the function matNMRReadBinaryFID to bring the FID and related acquisition parameters into the main spectrum-containing object. It needed to be fed both the file name of the FID (including the directory) and whether the spectra was obtained on a Bruker or Varian instrument, so we would have to write code that provided those inputs to the function later. With placeholders pointing to a spectrum we were using for testing, we were able to use this input function by removing all of the code that had to do with initialization or adjustment of the matNMR visual interface, as these lines caused bugs since the interface was non-existent. We envisioned writing a for loop over all of the spectra intended to be processed each time MassNMRProcessing was run. Following removal of any lines of code adjusting the visual interface in apodize1d and regelsize1d, we successfully were able to apodize and zerofill the FID.

However, this was by again using placeholders for the inputs. apodize1d needed to be fed three inputs: the type of function used, and one or more parameters defining that function. regelsize1d only needed a single one, the desired size of the spectrum in number of data points. To provide control to the user of MassNMRProcessing, we would want to obtain the inputs for these functions as inputs when the program is initialized. For the sake of user-friendliness, we decided to modify regelsize1d further, changing its input instead to a number that would define the number of zeros to be added as a multiplier of the original size of the spectrum. Using "1" would leave the spectrum as is, "2" would double the size of the spectrum through the addition of the same number of zeros as the length of the spectrum, "4" would quadruple the size of the spectrum, and so on. This made it so when the user input this number, he or she would not need to know the typical number of points in an FID, which can change depending on the instrument.

Before performing the Fourier Transform, we had to remove the dreaded Bruker digital filter for Bruker spectra. The function regelBrukerdig (with the typical modifications) did an admirable job of this, which we found out after performing the Fourier Transform with four1d. There were very few to no "smiles" or "frowns" on our tested spectra, which was excellent. setphase1d (with the typical modifications) successfully phased our spectra as well once we discovered we had to set a flag to allow for autophasing, providing us with spectra that were visually indistinguishable from one processed using a conventional NMR processor.

The next step was to create the x-axis for the spectra, as previously the pseudo-x-axis went from 0 to the post-zerofilling number of points in the FID. This had to be performed differently for Varian and Bruker data, as each company records the important parameters in different files: procpar for Varian and acqus for Bruker. Justin Gardner at Stanford University developed a Matlab file called readprocpar that reads the information from the procpar file into a Matlab object. After a couple of trials, we were able to pinpoint the procpar parameters from this file that described the starting frequency, the reference frequency, and the acquisition frequency width,

allowing for reconstruction of the axis. For Bruker files, MatlabNMR contained a function that created an array of every data point from the original axis. Through extraction of the original start and end points, we could build a new axis that contained the appropriate number of points according to the degree of zerofilling.

With the axis completed, now all we had to do was perform an automated shift based on the ppm of whatever compound was used as the standard, which is from an input value. Since the standard peak should be near the ppm input, we told our function to test a symmetrical range of data points on each side of the inputted ppm for the maximum value, which would correspond to the top of the reference peak. In determining the size of the range of data points, we wanted this value to be in terms of ppm, not raw data points, so that zerofilling does not affect the ppm distance searched. We settled on searching within 2 ppm for ^{19}F and ^{31}P spectra, and 0.2 ppm for ^{1}H spectra. This distinction between nuclei seemed quite important, though this did necessitate one more input on what atom type was being magnetized. Following determination of the top of the peak, the x-axis would shift accordingly.

With the spectra being evaluated by MassNMRProcessing now phased and referenced, it was time to integrate. Integration was performed by creating a "bin" for each range specified by the inputs that contained all of the data points within that range of ppm values. To perform integration in the most simplistic way possible, the y-values of each data point within an individual "bin" were summed. The summed values for an individual "bin" were then divided by the sum total from all "bins" and multiplied by 100 to provide normalized integration values. These were then placed in a matrix, with the value from each bin in a different column, which completed the goal of taking in a raw set of data and producing integrated values based on provided ranges. This completed the processing and integration phase, and looping over the process for multiple spectra would provide all of the information that we wanted.

1.4.3 Inputs

The central portion of the program was thus complete (Figure 1.11), with inputting and the final QC check remaining. Through development of the middle of the program, we had identified all of the inputs that we would need. One of the Matlab preset functions that would be ideal for inputting information was inputdlg, which automatically opened a window with a specified number of fields for data entry, sized the window appropriately, and allowed for the addition of text in the title of the window and above each entry field. We decided that we would first prompt the user for the desired ranges for integration. This is done through the window shown in Figure 1.7.

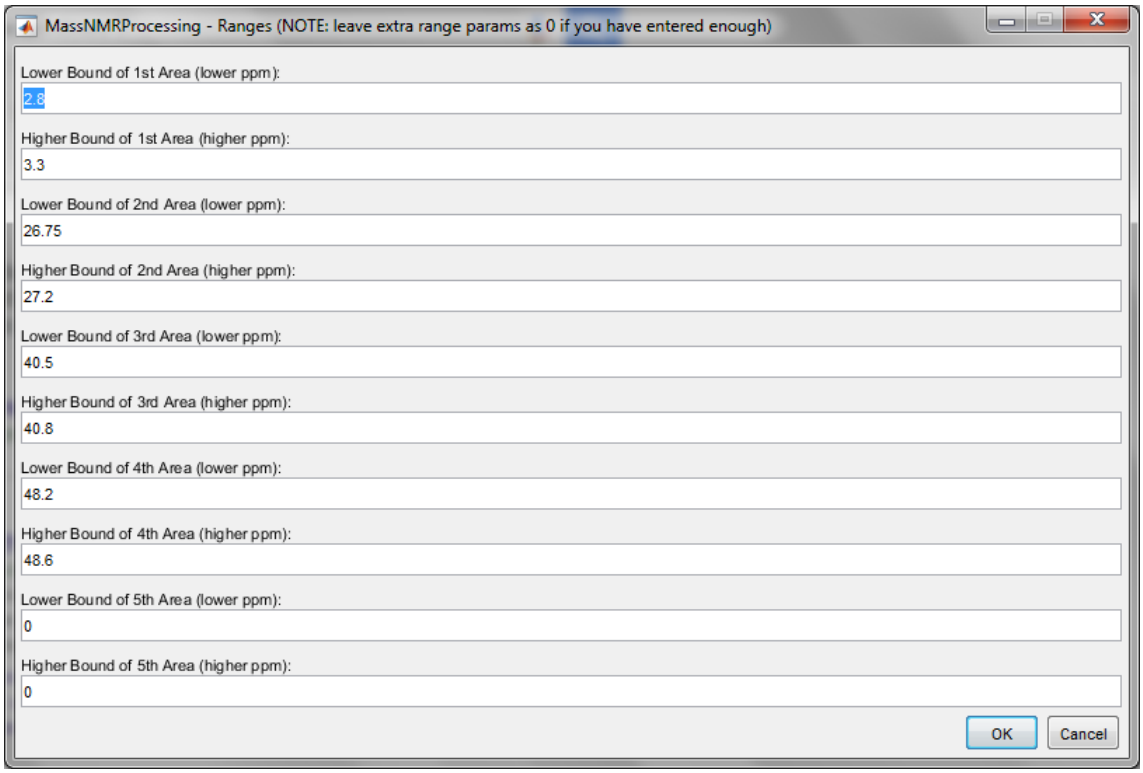

Figure 1.7. The First Input Window for MassNMRProcessing. This window asks the user for the desired ranges of integration.

Clicking the OK button at the bottom sends the data to MassNMRProcessing. We then have the program bring a second prompt (Figure 1.8) which contains all of the extra inputs we learned

we needed when writing the main loop of the program, including the identity of the nuclei, the ppm of the standard, the zerofilling multiplier, and the apodization information.

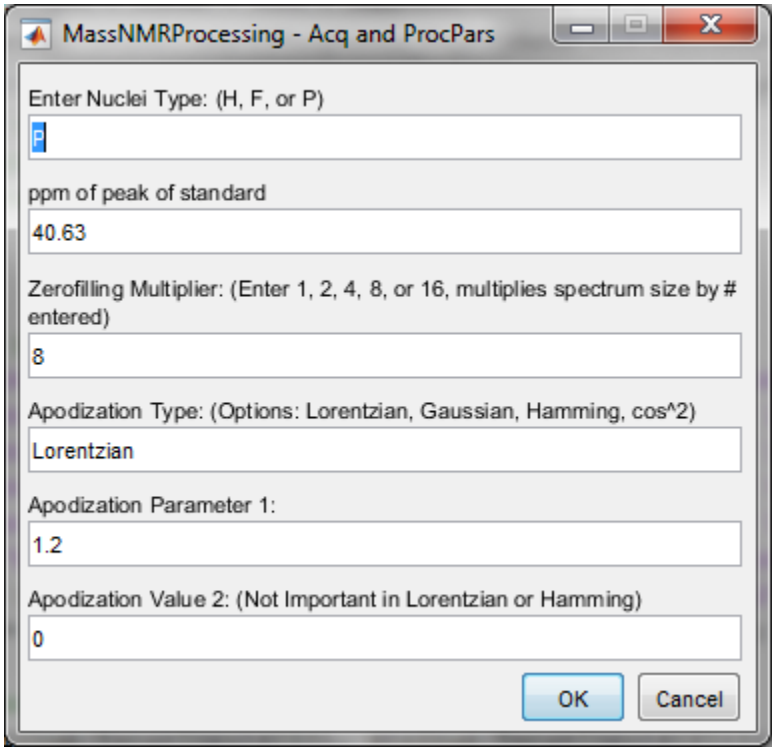

Figure 1.8. The Second Input Window for MassNMRProcessing. This window asks the user for parameters regarding spectrum processing.

Most of these inputs are fairly straightforward and unlikely to cause bugs/problems, with the lone exception being the zerofilling multiplier, as large numbers would drastically decrease the performance of MassNMRProcessing and all numbers below 1 would cause it to crash. Therefore, we added a failsafe that states if 1, 2, 4, 8, or 16 is not entered, the program will set the zerofilling value to 2. The only remaining input that was necessary was the identity and location of the overarching folder. Matlab contains an extremely convenient prompt for this purpose, uigetdir, which opens a window that allows the user to select a folder and input its path into the program. The selection window is shown in Figure 1.9.

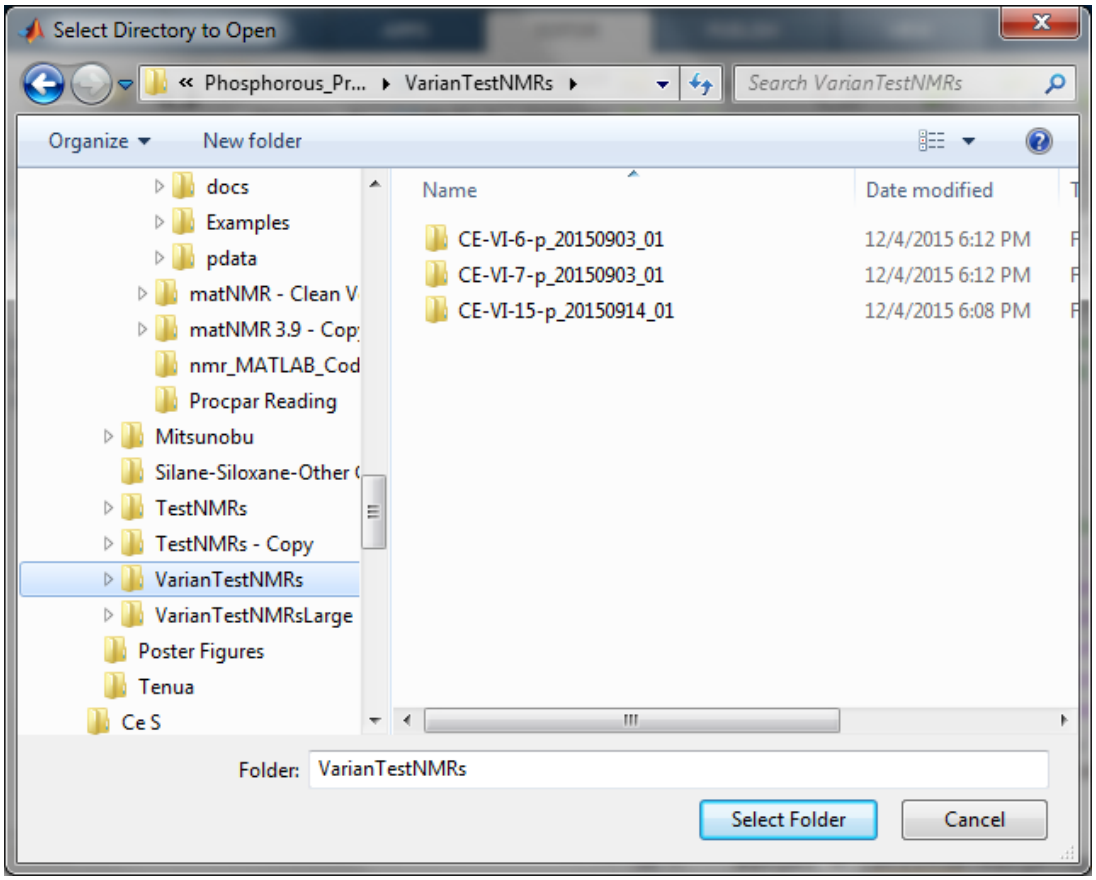

Figure 1.9. The Third Input Window for MassNMRProcessing. This window asks the user for the folder containing the NMR data.

Once the path of the desired overarching folder was obtained by the program, we needed to use it to acquire the path of the folder that directly contained the fid and the procpar or acqus parameter file. Since both Bruker and Varian name the filter directly containing the data by the title of the experiment, we decided that we would require these titles to contain an underscore. The program would then search the contents of the overarching folder to find those folders that had an underscore and sort them according to name. This was necessary to avoid the inclusion of hidden folders/files that appear to be present in every Windows folder but have nothing to do with our experiments. Then, the program checks to see if the first folder (from the above sorting) has ".fid" in its name. If it does, MassNMRProcessing recognizes that this is Varian data, and sets a flag accordingly. If not, it sets the flag to tell the program the current session is processing Bruker

data. This completed the input section, as MassNMRProcessing now had all of the required information to facilitate the processing of spectra.

1.4.4 Outputs and QC

The only remaining unwritten piece of the program was the QC part. We wanted to ensure that the spectra were being processed correctly, with the main concerns being correct identification of the standard and phasing of the spectrum. At the end the loop, the data for the spectrum that had just been processed was added to a structure for future use. Once the program had looped over every data-containing folder, we had MassNMRProcessing display the spectra in a window using the standard Matlab "plot" function (Figure 1.10).

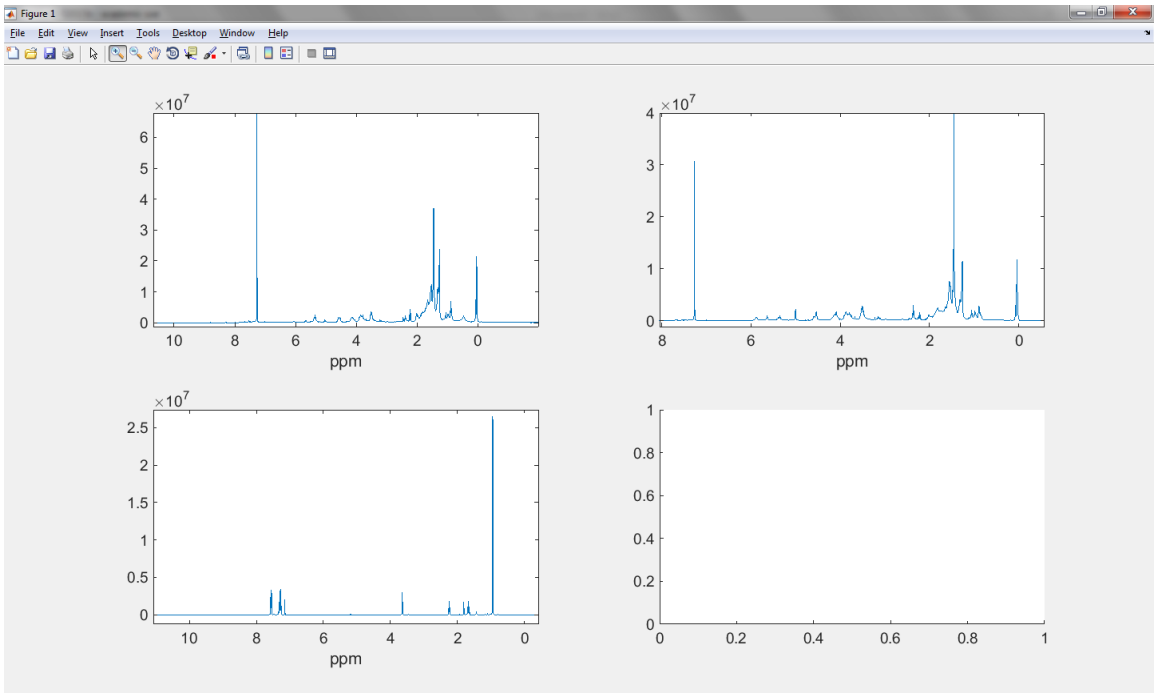

Figure 1.10. A sample set of QC data from MassNMRProcessing.

Zoom is possible for each of these spectra for evaluation of the phasing and the correct positioning of the x-axis. For jobs submitted to MassNMRProcessing that included less than 12 spectra, we had the program display all of them. They are displayed in a 1x1 format for a single spectrum, in a 1x2 if the job contains 2 spectra, in a 2x2 for 3 or 4, up to a 3x4 format for 10, 11,

or 12 spectra. If the job contains more than 12 spectra, MassNMRProcessing displays the first spectrum and 11 more representative examples evenly spaced throughout the list that was submitted to it. That way, one can view how the spectra look while the reaction proceeds.

With the implementation of the final output, we completed this program. A flowchart of MassNMRProcessing is shown in Figure 1.11, showing the inputs, outputs, and the loop in the middle where the processing takes place. With this layout, the program could process a spectrum every 3-4 seconds on our personal lab computer. The only parameter that dramatically changed the processing speed was degree of zerofilling. 8x zerofilling caused a dramatic increase in processing time, increasing it to around 15 seconds per spectrum. We were able to trace this to a substantial slowing of phasing, which was already the most time intensive aspect of MassNMRProcessing, taking nearly two seconds per spectra with no zerofilling. Regardless, we were satisfied with the speed of processing, as it would greatly improve productivity since all the user had to do was enter the correct inputs.

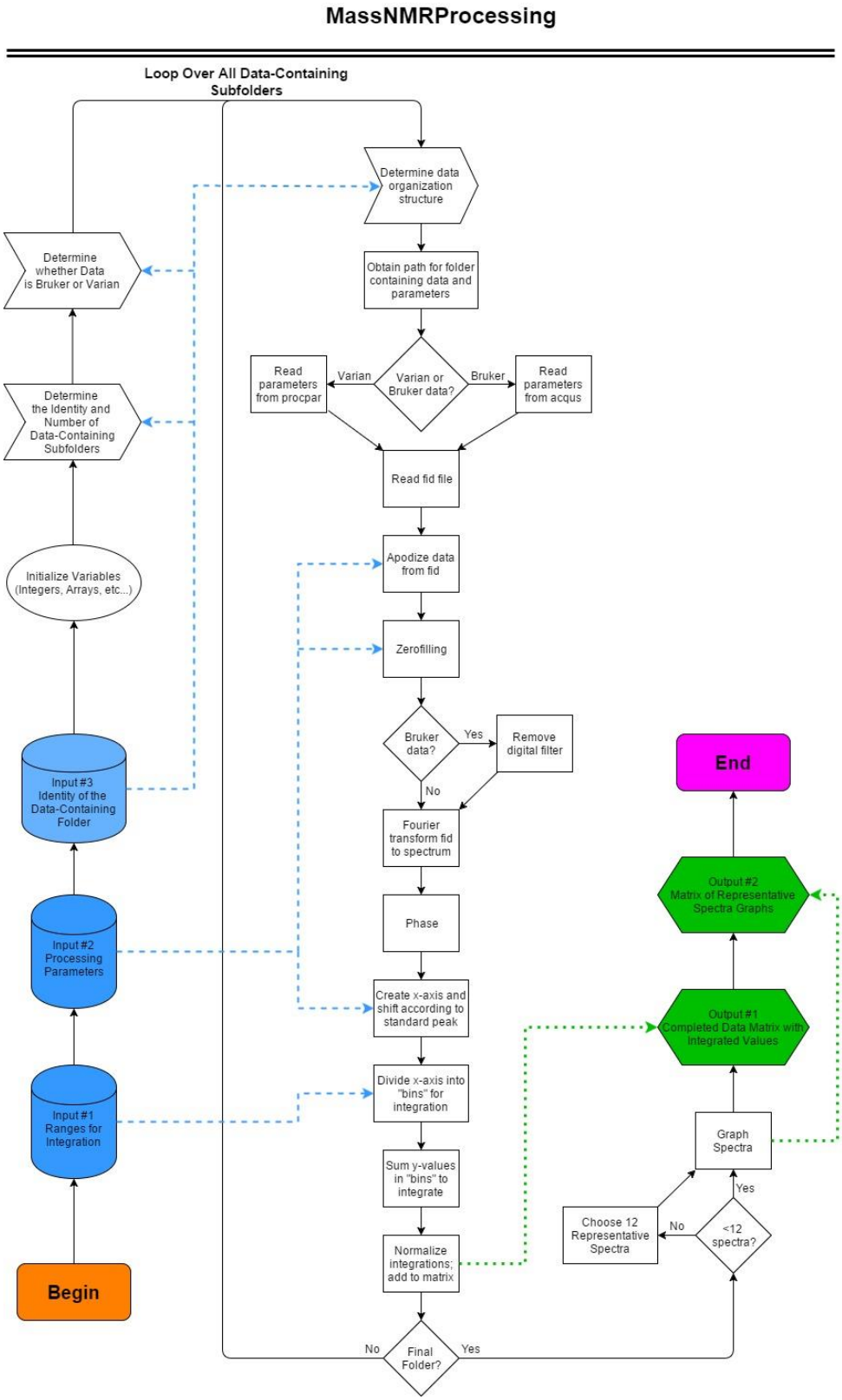

Figure 1.11. Flowchart Describing the Actions of MassNMRProcessing.

1.4.5 Improving the Phasing Algorithm

Unfortunately, continued testing of MassNMRProcessing with a variety of NMR spectra revealed that the algorithm from MatNMR only phased the spectrum correctly about two-thirds of the time, far below our desired threshold of 95%. We thus investigated other phasing algorithms, specifically looking for ones that were already written or simple to implement, and selected one described by Liu and coworkers as a two-step method for NMR phasing, beginning with "coarse tuning" and finishing with "fine tuning".[81] Their "coarse tuning" method is based on baseline recognition and minimization of the height difference at the edges of peaks, while "fine tuning" proceeds via minimization of negative area. They specifically note the excellent performance of their algorithm in phasing spectra with a very low signal-to-noise (S/N) ratio, which was essential for our usage of ^{31}P NMR with low concentrations of the phosphorous containing compound. Finally, they published their algorithm online using Matlab code, which was wonderful.

Through the usual changing of various names and addition or removal of flags, we were able to replace the old phasing algorithm with this new two-step one. Initial testing of the Liu algorithm was not promising, but this was expected, as they intended for the method to be able to phase DEPT spectra and others that had intentionally negative peaks. Following the "coarse tuning" process, their algorithm classifies peaks as either positive, negative, or distorted. The second round of tuning attempts to minimize negative area within a positive peak, positive area within a negative peak, and ignores distorted peaks. Through removal of the ability for the algorithm to classify peaks as negative or distorted, we achieved an excellent rate of success in properly phasing spectra. We tested MassNMRProcessor with over 100 spectra from different sources and deemed (subjectively) that greater than 90% were excellently phased and the rest were merely satisfactory. The switch in algorithms did come at a processing speed cost, as the phasing time increased about 4 seconds to 6-7 per spectrum, but this was still an acceptable speed

since the only user input required was at the beginning. Basically, through modification of the algorithm reported by Liu and coworkers and implementation in MassNMRProcessing, we removed the last barrier to large-scale processing of NMR spectra, and could proceed in our original desire to study detailed reaction time courses.

1.4.6 Future Directions for MassNMRProcessing

As will be demonstrated in following sections of this chapter, MassNMRProcessing is a useful and functional NMR processing and integrating program. There are certain aspects, however, that could be modified to improve both the process and scope of its usage. The main reason that we developed MassNMRProcessor was to allow us to perform other experiments while our NMRs were processing, saving valuable time that would otherwise be spent manually processing the spectra. With that in mind, we were satisfied with a processing speed of 10 seconds per spectrum. For time courses that included many spectra, this could take up to half an hour, or much longer if large amounts of zerofilling was necessary. As mentioned previously, we deemed this acceptable, but less time would certainly be preferred. We are certain that the time for processing each spectrum could be reduced by complete removal of all lines of code that performed unimportant processes in every function, particularly the functions that were originally from MatNMR, as these were meant to be used in a much different manner. This would be time consuming, but not difficult, and we did not choose to undertake it. It is also likely that the algorithms we obtained from the internet were not properly optimized for performance. With our level of programming expertise, it would be very difficult to upgrade these algorithms to improve performance, but another could probably develop improved code.

While trying to make a program that needed as little input as possible, we realized early on that the input structure necessitated substantial prior knowledge of the system being investigated. In order to know what ranges to input, one needed to know how the peaks drifted over time, and

how broad the peaks were. This knowledge could usually be obtained by observing the first spectrum and one near the end of the time course in a conventional NMR processor. We observed that the first peak often contained the broadest peaks, and peak drift was usually in a single direction, so looking at just two spectra provided all of the necessary information. However, it would be preferred if this was not necessary, if this information could be obtained by MassNMRProcessing without user inputs. We thus propose two changes/additions that would assist the program and the user during this process. These could be used either in combination or alone.

The first change that we could make would require minimal changes to the input and no change to the overall structure of the program, and as such would be easiest to implement. Currently, following creation of the x-axis, MassNMRProcessing takes the ranges that are submitted in the first input window and divides the spectrum that is being processed at that moment into bins for integration purposes. This could be changed so that the inputs were ppm values that stated a location near where each peak should be found, rather than describing the lower and upper bounds of the bins to be created. The program would then have a preset value that showed how far to look on each side of the inputs for a peak maximum. The highest point would be declared the top of the peak, and MassNMRProcessing would divide the spectrum into bins again with the center point of the bin the location of peak maximum. The width of the bin would also be preset in MassNMRProcessing, but in one of the input boxes the user would be allowed to change this value. This would eliminate needing to look at each reaction time course, and would probably be slightly more accurate as the bins could be smaller. With a knowledge of where the peaks generally are, the program would find the peak and then create a symmetrical bin around it for integration. We believe that this would result in significant improvement to the program without being hard to implement.

Another change that could really increase the applicability of MassNMRProcessing would be to reorder the structure of the program so as to let the user see the phased spectra first and then submit either ranges for integration or a ppm value to tell the program where to search for the peak. This would remove the need to use another NMR processing program to observe the location of the peaks, which is currently one of the largest drawbacks of using MassNMRProcessing. This could be accomplished by letting the user submit the second window of inputs (Figure 1.8) and the overarching folder (Figure 1.9) first. The structure of the program would then be changed so that MassNMRProcessing would process and store the data but not integrate it. The program would then pause and display the phased spectra just like it does right now as the second output (Figure 1.10). After the user perused through the spectra and recorded both peak location as well as whether the peaks drift, a second set of inputs would be required. Here this could be combined with the first change, as these inputs could be the ppm values of the peaks or the edges of the to-be-formed integration bins, whichever is preferred. In addition, if the inputs were set to be those that were described in the first change, then we could add another input describing how far to the sides of each input the program should look for the peak, giving even more control to the user. Implementing this new program structure would require a reordering of the program, the breaking up of the main loop, and a few other substantial changes. However, it would allow for MassNMRProcessing to be the only program used when integrating long series of NMR, and could provide the user with additional control over this process, both of which are worthy goals for this program.

1.5 DPDS and a Six-Membered Transition State for the Reduction of Phosphine Oxides

1.5.1 Initial NMR Studies

With MassNMRProcessing complete, we began to run detailed NMR time courses on the reduction of our phosphine precatalysts with phenylsilane. We used variable temperature NMR, setting the NMR to the desired temperature before reaction initiation. All of the components were then mixed at room temperature in an NMR tube which was loaded into the NMR spectrometer, where the reaction was monitored in 2-4 minute increments. We fixed the concentration of precatalyst to 0.04 M and the concentration of phenylsilane to 0.4 M for our precatalyst comparison. Setting the temperature of the NMR to 80 °C, we monitored the reduction of **1PPO**, **TMPPO**, **TMBPO**, and **TMPyrPO** in d^8-toluene, with **TPPO** as a control (Figure 1.12)

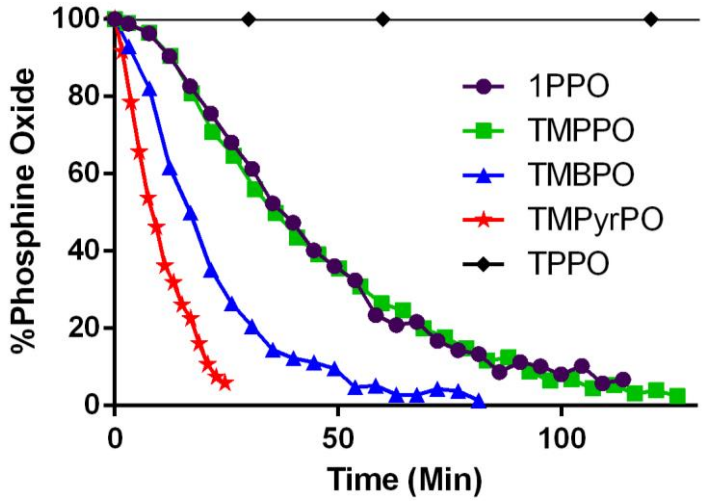

Figure 1.12. Reaction Progress Curves for the Reduction of Phosphine Precatalysts by $PhSiH_3$ at 80 °C in Toluene. [PO] = 0.04 M. [$PhSiH_3$] = 0.4 M.

The data obtained by this method appears much more precise than the data without VT-NMR (Figures 1.3-1.6), with the shapes of each of the curves quite clear. Near the end of the time courses, accuracy does appear to decrease, but we are far more interested in studying the initial part of the reaction. During the early time points, it is now clear the reduction rate of each of the precatalysts increases, which confirms what we were observing earlier in Figure 1.3. With this observation in the reaction progress curves for four separate precatalysts, we can now state with near certainty that the conventional understanding of how the reduction of phosphine oxides by

silanes proceeds is incorrect. It is also noteworthy that we observe substantial differences in the reduction rate between the precatalysts, with **TMPyrPO** being the fastest and **1PPO** probably the slowest. As expected, **TPPO** displays no reduction during the time scale monitored.

To quantify these observations, we first fit each of the curves in Figure 1.12 to either a single exponential or the difference of two exponentials (double exponential fitting) by minimizing the variance over the entire curve. Graphical overlays of the fitting with each individual curve are shown in Figure 1.13. As one would expect, it seems clear that from a visual standpoint double exponential fitting is far better than single exponential fitting. To quantify the degree of superiority, we calculated the variance per data point for both single and double exponential fitting, which is shown in Table 1.2. We are using this in place of the Pearson correlation coefficient, as the coefficient is not as informative for non-linear fitting. The numerical data confirms the visual observations, as double exponential fitting is 4 to 12 fold superior by the chosen metric

Table 1.2. Numerical Comparison of the Quality of Fitting between Using a Single Exponential or Two Exponentials

Entry	Variance (%PO Reduced)^2	# Data Points	Variance Per Data Point
1PPO-Single	612.79	26	23.57
1PPO-Double	60.93	26	2.34
TMPPO-Single	468.99	28	16.74
TMPPO-Double	37.93	28	1.35
TMBPO-Single	215.23	16	13.45
TMBPO-Double	35.14	16	2.20
TMPyrPO-Single	133.23	14	9.52
TMPyrPO-Double	37.09	14	2.65

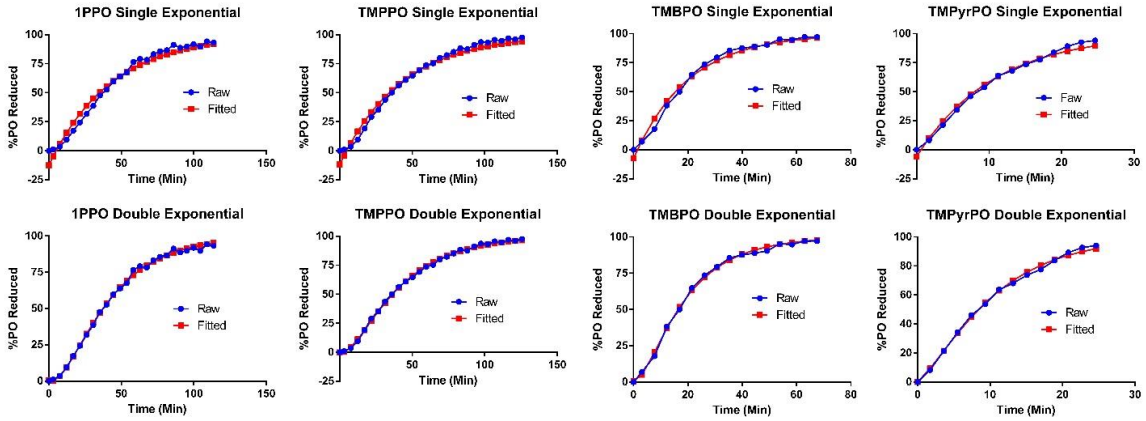

Figure 1.13. Graphical Comparison of the Quality of Fitting between Using a Single Exponential or Two Exponentials

Next, we wanted to quantify the differences in rate between the phosphine oxide precatalysts. From the single exponential fitting, we obtained the rate constant (*k*) for the exponential for each of the precatalysts, which is shown in Table 1.3. While this affords a convenient single-number comparison, we wanted to use additional metrics due to the inaccuracy of the single exponential fitting (Table 1.2). As such, we also include the time each reduction takes to become 50 and 90% finished (Table 1.3) using the double exponential fitting rather than the raw data to avoid noise-induced errors. Taken together, these results suggest that **TMBPO** is about 2X faster than **1PPO** and **TMPPO**, which are reduced at similar rates. **TMPyrPO** is the fastest of the four, with a reduction rate about 4X faster than **1PPO** and **TMPPO**.

Table 1.3. Numerical Comparison of the Rates of Reduction of the Precatalysts by $PhSiH_3$. *k* is from single-exponential fitting, while $t_{50\%}$ and $t_{90\%}$ are from obtaining the equation describing the double exponential fitting and setting it to 50 and 90 percent, respectively. [PO] = 0.04 M. [$PhSiH_3$] = 0.4 M

Precatalyst	k (min)$^{-1}$	$t_{50\%}$ (min)	$t_{90\%}$ (min)
1PPO	0.028	37.3	91
TMPPO	0.027	36.5	92
TMBPO	0.054	16.4	48
TMPyrPO	0.103	8.4	21
TPPO	ND	ND	ND

1PPO and **TMPPO** being reduced at the same rate established that our original hypothesis that increasing the ring strain of the phosphorous catalyst through switching from a 5-membered phospholane to a 4-membered trimethylphosphetane would improve the rate of reduction was incorrect. The trimethylphosphetane, however, is more sterically hindered than a phospholane ring, which could also impact the rate of reduction. Therefore, it is premature to state that there can be no benefit obtained from additional ring strain, it is possible that the removal of the methyls would improve the rate of reduction to be faster than **TMPPO**. Sadly, this theory is not testable, as phosphetanes with less than three substituents on the phosphetane ring cannot be synthesized using current methods.

The fact that **TMPyrPO** > **TMBPO** > **TMPPO** in reduction rate actually validates our hypothesis that increased electron density on the oxygen of the phosphine oxide, and not the phosphorous, is what facilitates reduction with phenylsilane. The slight increase in reduction rate of **TMBPO** as compared to **TMPPO** is roughly what we anticipated based on the results from O'Brien and coworkers.[82] However, we projected that the resonance donation from the amine would result in a greater degree of enhancement than what was observed. We decided to test whether or not **TMPyrPO** reduces at a reasonable rate at room temperature and whether this eliminates its aforementioned over-reduction.

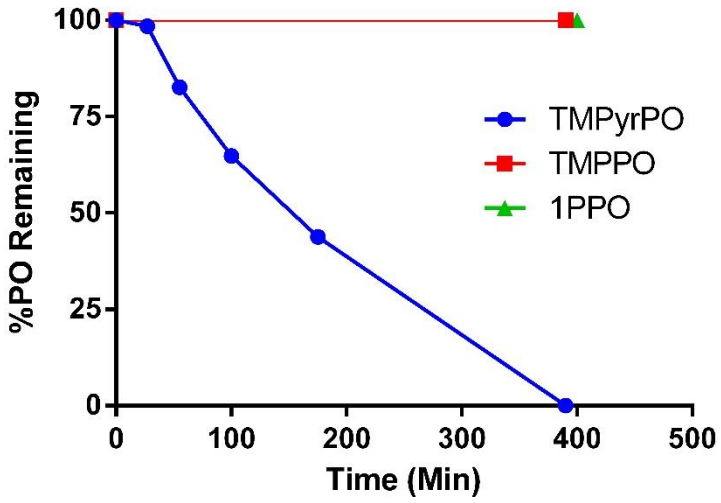

Figure 1.14. The Observed Rates of Reduction of **1PPO**, **TMPPO**, and **TMPyrPO** with $PhSiH_3$ at 23 °C. [PO] = 0.04 M. [$PhSiH_3$] = 0.4 M

Figure 1.14 demonstrates that reduction of **TMPyrPO** does complete after six-and-a-half hours. Based on previous reports, the observed rate is fast enough for a catalytic-in-phosphine reaction to complete within 24 hours using 10-15 mol% of precatalyst. Unfortunately, we still observed significant degradation to the secondary phosphetane. Therefore our initial hypothesis in the design of **TMPyrPO** did furnish a precatalyst that undergoes facile reduction at room temperature, but its lack of stability limits its usefulness.

Given the superior data acquired with the new method (Figure 1.12), we wanted to retest our results that indicated a dependence of the rate on the concentration of phosphine oxide. Testing similar concentrations of **TMPPO** and phenylsilane as were previously chosen (Figure 1.7), we obtained the data shown in Figure 1.15A. With this data, it is clear that increasing the concentration of **TMPPO** does in fact increase the percentage rate of its reduction. We set out to determine the origin of this increase in combination with the observed "lag phase" in every single reduction progress curve with $PhSiH_3$.

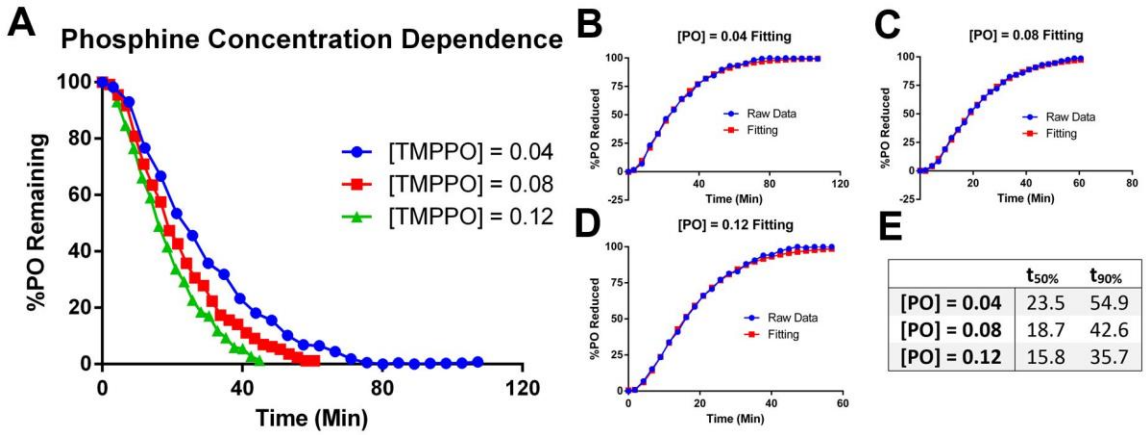

Figure 1.15. The Reduction Rate Dependence on the Concentration of **TMPPO**. All reductions were run with phenylsilane = 0.8 M in toluene at 80 °C. (A) Graphical comparison of the rates of reduction with differing concentrations of **TMPPO**. (B-D) Fitting the curves from part A. (E) Numerical comparison of the rates of reduction from B-D.

1.5.2 DPDS

As previously mentioned, we had ruled out the possibilities of phosphine pre-activation or a multi-step mechanism being responsible for the observed increase in precatalyst reduction rate over the first few minutes using phenylsilane. Silane preincubation without any additives provided a minimal increase in rate at most (Figure 1.4) and did not change the curve shape to a single exponential, so it was unlikely that silane pre-activation in such a manner was responsible for the "lag phase". We thus hypothesized that phenylsilanol and/or phenylsilanediol were substantially more rapid reductants than phenylsilane, as it was the only other explanation we could conceive which could explain the observed behavior.

Phenylsilanol is known to equilibrate with diphenyldisiloxane (**DPDS**), with the equilibrium favoring the disiloxane in organic solvents. **DPDS** was synthesized in a single step from phenyl(chloro)silane in good yield (Scheme 1.3), and tested for its activity in reducing phosphine oxides. We were excited to find that **DPDS** completely reduced both **1PPO** and **TMPPO** within 5 minutes at 80 °C. When tested at room temperature, we found **DPDS** competently reduced

1PPO and **TMPPO** in under three hours. To monitor this reaction more closely, we obtained reduction progress curves of the reductions of our suite of precatalysts with **DPDS** at room temperature, which are shown in Figure 1.16. **TPPO** is again shown as a control.

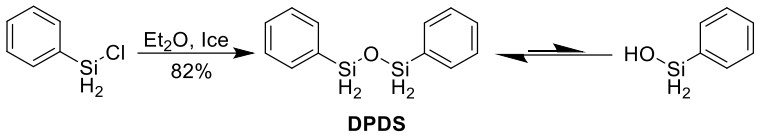

Scheme 1.4. The Synthesis of **DPDS** and its Equilibration with Phenylsilanol

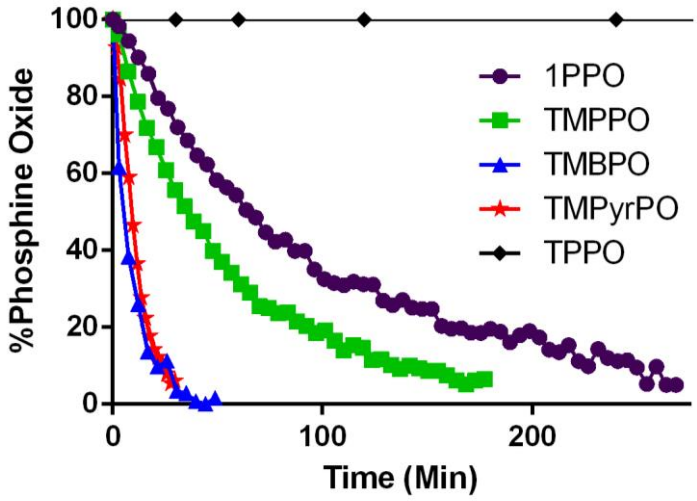

Figure 1.16. Reaction Progress Curves for the Reduction of Phosphine Precatalysts by **DPDS** at 23 °C in Toluene. [PO] = 0.04 M. [**DPDS**] = 0.3 M.

Clearly, **DPDS** is a remarkably potent reductant for the phosphorous heterocycles we synthesized. Both **TMBPO** and **TMPyrPO** are reduced to completion in 30 minutes. **TMPPO** and **1PPO**, while slower, are reduced on a time scale that would certainly facilitate room temperature catalytic-in-phosphine reactions. These reactions represent the first reported example of additive-free room temperature reduction of phosphine oxides using silane reagents. The curves in Figure 1.16 also show a high degree of single-exponential character, with no visible "lag phase", validating our hypothesis of phenylsilanol being responsible for the "lag phase" via it having a higher reductive potency than commercially available phenylsilane.

An obvious next step was to test the rate of reduction of **TPPO** with **DPDS** at elevated temperature. Monitoring this reaction with ^{31}P NMR (Figure 1.17), we found that **TPPO** is completely reduced at 110 °C in 5 hours, again with single-step kinetics. This is the fastest known reducing system for triphenylphosphine oxide at 110 °C,[83,84] which will be further elaborated on later in this document.

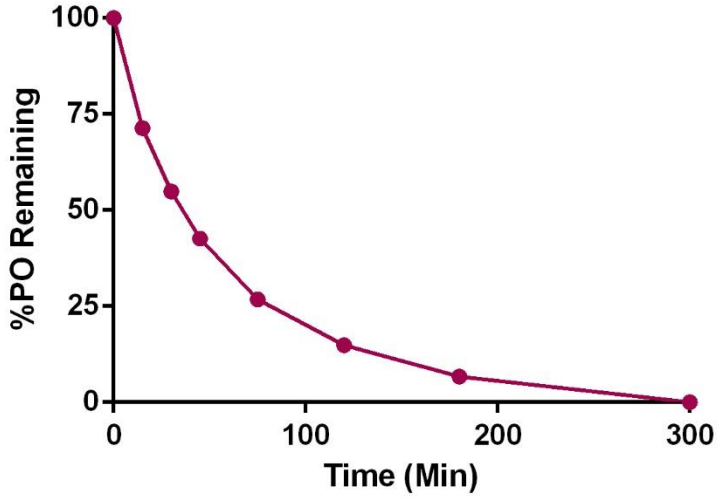

Figure 1.17. A Reaction Progress Curve for the Reduction of **TPPO** by **DPDS** at 110 °C in Toluene. [**TPPO**] = 0.04 M. [**DPDS**] = 0.5 M.

1.5.3 Other Silanes

The impressive gains in reductive activity that we obtained by substituting **DPDS** for phenylsilane suggested a more thorough investigation of silane materials would be valuable. Previously, we performed a silane screen with commonly utilized silanes, but we wanted to specifically try silicon hydride compounds that would represent different classes. Examining what was commercially available, we purchased two compounds that fulfilled the desired criteria, *n*-hexylsilane and 1,1,3,3-tetramethyldisilazane (**TMDSA**).

n-Hexylsilane was of interest because it was a tri-hydrido alkyl silane, and to our knowledge a member of that class had not been tested for its reductive potency against phosphine oxides.

Unfortunately, in isolated reduction studies in THF, DCM, and toluene at 80 °C, it was notably slower than phenylsilane at reducing each of our phosphine precatalysts.

The other silane we chose, **TMDSA**, is a member of the hydrido-disilazane class of compounds, of which none had been previously evaluated. Addition of **TMDSA** to **1PPO** in THF furnished no reduction, but using the same combination in DCM produced 61% of the reduced phosphine in 30 minutes at 80 °C (Figure 1.18), which is quite fast. However, the reaction was heated for 5.5 more hours, and no further reduction was observed. At this point, the reaction (which had taken place in an NMR tube) was cooled to ambient temperature and opened. Notably, substantial pressure had built up, even after cooling, and the released gas reeked of ammonia. Several reports on the synthesis of amino-silanes suggest that they are very unstable,[85] so we thought perhaps **TMDSA** was converted to **TMDSO** by the small amount of water that is present in the NMR tube. **TMDSO** does not reduce **1PPO** at 80 °C (Table 1.1, Figure 1.18), so such a conversion would explain the lack of reduction after 30 minutes, as well as why re-opened bottles of **TMDSA** (which smell strongly of ammonia) were inactive.

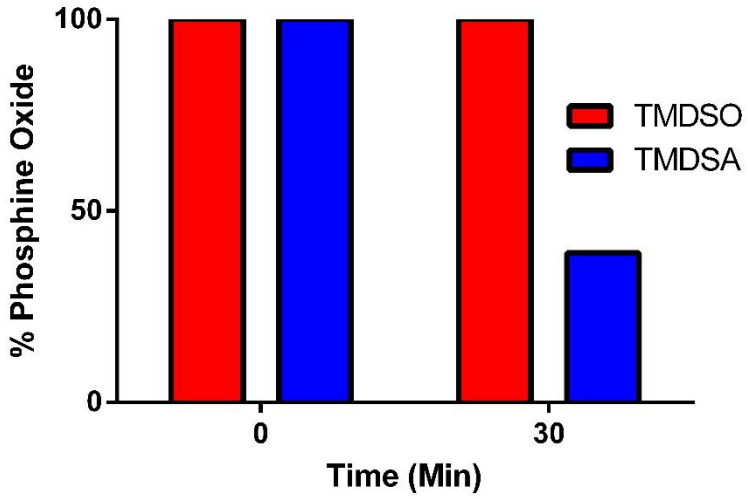

Figure 1.18. The Reduction of **1PPO** by **TMDSO** and **TMDSA** at 80 °C in CH_2Cl_2. [**1PPO**] = 0.04 M. [**TMDSA**] = 0.4 M. [**TMDSO**] = 0.6 M

1.5.4 A Six-Membered Transition State

The striking difference in activity between **TMDSO** and **TMDSA** was perplexing as the only difference between the two silanes is the identity of the heteroatom, and based on precedent, greater electron-deficiency on the silicon center correlated with faster reduction.[86] Even if they were switched, and **TMDSO** was the active one, it appeared rather unlikely that the rather small difference of electron density on the silicon atoms could explain the gulf in reactivity. We thus looked for alternative ways to explain the result in Figure 1.18.

The only justification that appeared to contain any merit was the proposal of TS-2, a 6-membered transition state for the reduction of phosphine oxides by silanes. In TS-2, the hydride is delivered directly to phosphorous following formation of a hydrogen bond between the silane and the oxygen atom of the phosphine oxide. TS-1, the 4-transition state that has long been postulated for this reduction,[87] is known to be quite high in energy,[88] so it appeared quite possible that the 6-membered nature of TS-2 makes it a lower-energy alternative. The difference in reactivity is thus explained by the fact that **TMDSA** contains a hydrogen bond donating moiety, and could thus access TS-2. **TMDSO**, on the other hand, is known to be a particularly stable disiloxane, even in an aqueous environment, and thus cannot form the key hydrogen bond.[89]

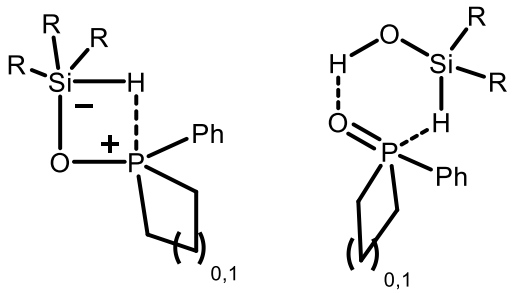

TS-1 **TS-2**

Figure 1.19. Marsi's 4-Membered Transition State (TS-1) and Our Proposed 6-Membered Transition State (TS-2) for the Low-Temperature Reduction of Phosphine Oxides by Silanes

With further examination, we realized that TS-2 could explain the observed difference in reactivity between phenylsilane and phenylsilanol (in equilibrium with **DPDS**). Phenylsilanol can form the hydrogen bond, whereas reduction with phenylsilane necessitates going through TS-1. Even more notable is the fact that the three most commonly employed silanes (phenylsilane, diphenylsilane, and trimethoxysilane) can form hydrido-silanols by reacting with water, whereas the inactive (except at 300 °C) mono-hydrido silanes (triethyl-, triphenyl-, tris(trimethylsilyl)-, etc.) cannot form hydrogen-bond donating species and thus could only reduce phosphine oxides through TS-1.

The addition of acids and bases to a solution containing disiloxanes is known to shift the disiloxane-silanol equilibrium towards the silanol side. We thus reasoned that addition of acids or bases should facilitate phosphine oxide reduction with **TMDSO**. This was tested through the catalytic addition of protic acids, Lewis acids, and potassium t-butoxide to solutions of **TMDSO** and **1PPO**. Potassium t-butoxide caused complete degradation of the phosphorous precatalyst, but use of both protic and Lewis acids facilitated reduction (Figure 1.20, 1.21). Just as one would expect if the equilibrium is responsible for the reductive activity, the strongest of the protic and Lewis acids promoted the most reduction. Reaction mixtures including TFA went much faster than those using AcOH, and usage of $ZnCl_2$ was better than $MgCl_2$ which in turn was superior to LiCl, which follows the presumed trend of Lewis acidity. These results strongly suggest that TS-2 is indeed a valid transition state and is much lower energy than TS-1. At this point, we noted that we had no direct evidence for TS-1 occurring in any of our reaction mixutes, and thus questioned whether TS-1 was even a valid transition state for this reaction at 110 °C or below (i.e. triphenylsilane does reduce phosphine oxides when heated to 300 °C, so TS-1 is certainly valid at intense temperatures[90]).

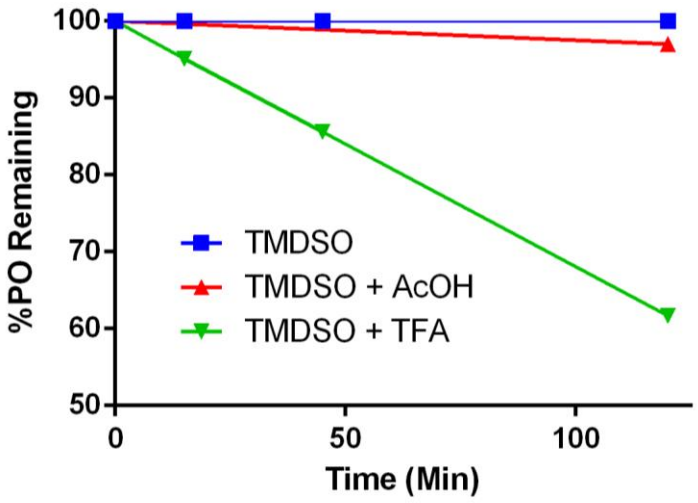

Figure 1.20. The Reduction of **1PPO** by **TMDSO** and either AcOH or TFA at 80 °C in THF. [**1PPO**] = 0.04 M. [**TMDSO**] = 0.6 M. [Acid] = 0.2 M

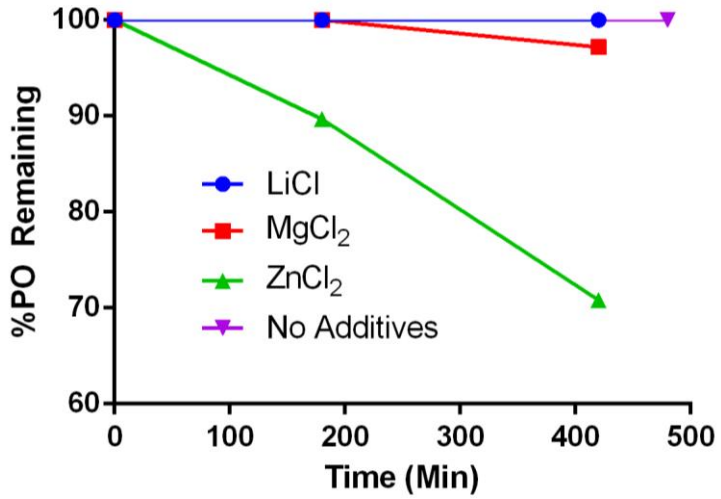

Figure 1.21. The Reduction of **1PPO** by **TMDSO** and a Lewis Acid at 80 °C in THF. [**1PPO**] = 0.04 M. [**TMDSO**] = 0.6 M. [Lewis Acid] = 0.2 M

1.6 Proof that Only the 6-Membered Transition State Occurs at Reasonable Temperatures

1.6.1 The Trajectory of Reaction Progress Curves of Phenylsilane-Mediated Reduction

If TS-1 is not a valid transition state at 80 °C, then phenylsilane cannot be an actual reductant, but must instead react with water to form phenylsilanol, the active reagent. Proof of such a mechanism would thus lend strong evidence towards the hypothesis that low temperature phosphine oxide reduction must proceed through TS-2. If phenylsilane itself is a competent reductant, concentrations of phenylsilanol and phenylsilanediol will either reach or remain below equilibrium concentrations following initiation of the reaction, which would limit the magnitude of the increase in reduction rate. This is shown below, comparing the initial rate to the rate when 50% of the phosphine oxide has already been reduced.

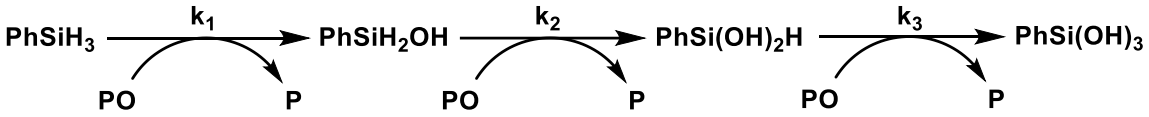

Figure 1.22. Kinetic Schematic of the Reduction of Phosphine Oxides by Phenylsilane Assuming Phenylsilane itself is Competent

Figure 1.22 shows the mechanism of phosphine oxide reduction by phenylsilane while assuming that phenylsilane itself is a capable reductant, where PO refers to unreduced phosphine oxide and P the reduced phosphine. Inferring that this mechanism is correct, we can write the rate of reduction as the change in [PO] with respect to time:

$$\frac{d[PO]}{dt} = k_1[PhSiH_3][PO] + k_2[PhSiH_2OH][PO] + k_3[PhSi(OH)_2H][PO]$$

Due to the fact that we are operating in pseudo-first order conditions with an excess of phenylsilane:

$$[PhSiH_3] = [PhSiH_3]_i$$

Now, at time $t = 0$, it is also known that:

$$[PhSiH_2OH]_i = [PhSi(OH)_2H]_i = 0$$

The initial rate of phosphine formation is thus:

$$Rate_i = k_1[PhSiH_3]_i[PO]_i$$

To prove that the maximum rate at 50% PO reduced is 3/2 the initial rate of reduction, we first write the rate of reduction where half the PO has already been reduced.

$$\frac{d[PO]}{dt} = \frac{k_1[PhSiH_3]_i[PO]_i}{2} + \frac{k_2[PhSiH_2OH][PO]_i}{2} + \frac{k_3[PhSi(OH)_2H][PO]_i}{2}$$

Evaluating the above equation term by term, it is clear that the first term is equal to half of the initial rate. To evaluate the second term, we note that this term would be at a maximum when the concentration of phenylsilanol is at a maximum. From the proposed mechanism, the concentration of phenylsilanol will reach a maximum at the time its rate of formation equals its rate of consumption, or where the derivative of the concentration of phenylsilanol is zero. We then write the derivative of the concentration of phenylsilanol with respect to time at 50% PO reduced.

$$\frac{d[PhSiH_2OH]}{dt} = \frac{k_1[PhSiH_3]_i[PO]_i}{2} - \frac{k_2[PhSiH_2OH][PO]_i}{2}$$

Setting that derivative to 0, we obtain:

$$\frac{k_1[PhSiH_3]_i[PO]_i}{2} = \frac{k_2[PhSiH_2OH][PO]_i}{2}$$

This means the second term can, at a maximum, be equal to half the initial rate.

We can apply the same strategy to the third term. The concentration of phenylsilanediol will also be at a maximum when its rate of formation equals its rate of consumption. The derivative of the concentration of phenylsilanediol at 50% PO reduced is:

$$\frac{d[PhSi(OH)_2H]}{dt} = \frac{k_2[PhSiH_2OH][PO]_i}{2} - \frac{k_3[PhSi(OH)_2H][PO]_i}{2}$$

Setting this derivative to 0:

$$\frac{k_2[PhSiH_2OH][PO]_i}{2} = \frac{k_3[PhSi(OH)_2H][PO]_i}{2}$$

Now, we have already shown that the maximum the term on the left could be is half the initial rate. If this is the maximum that the term on the right could be, we have now shown that the maximum all three terms can be is just half the initial rate. Adding up all of them, we find that the maximum rate of phosphine oxide reduction following this mechanism at 50% PO reduced is just 3/2 the initial rate.

$$\frac{d[PO]}{dt} = \frac{k_1[PhSiH_3]_i[PO]_i}{2} + \frac{k_2[PhSiH_2OH][PO]_i}{2} + \frac{k_3[PhSi(OH)_2H][PO]_i}{2}$$
$$= \frac{3}{2}Rate_i$$

Now, it is worth stating explicitly that this derivation of the maximum fold rate increase assumes that the concentrations of both phenylsilanol and phenylsilanediol have reached equilibrium. It is entirely possible, perhaps even likely, that this is not the case, which would lower the maximum fold rate increase.

With the maximum fold increase at 50% reduction established, we now need to determine whether the curves in Figure 1.12 provide values under that maximum. To do this, we used the double-exponential fitting from Figure 1.13 to obtain an equation for a smooth curve that closely follows the raw data. This equation provides an excellent estimate of the actual time to 50% reduction and allows for the calculation of the derivative at each time point. The **TMPyrPO** reduction curve is removed from this analysis since the resulting phosphine is further reduced with cleavage of the P-N bond during the reaction. We also found that when we just took the derivative of the fitted double exponential equation, a fitting artifact caused us to obtain negative derivatives for the very early time points. Therefore, the initial rate was calculated from the slope of the line between the initial point and the first time point or the initial time point and the second time point. This practice of listing the average rate observed over the first 1–5 minutes as the initial rate almost certainly overestimates it. Using these methods, we calculated the rate fold

increase at 50% reduction. The double exponential fitting and the derivative curves used to calculate the rate fold increase are shown in Figure 1.23.

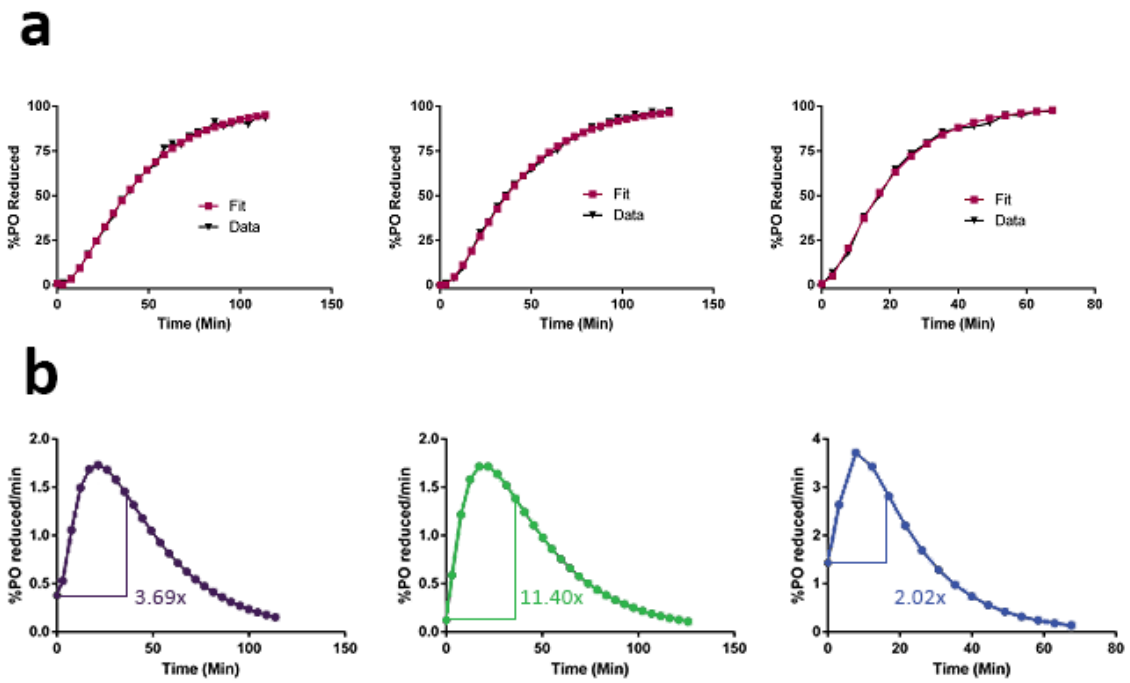

Figure 1.23. Derivative Curves and Double Exponential Fitting of Reaction Progress Curves from Precatalyst Reduction by Phenylsilane. (a) Comparison between raw data (from Figure 1.12) and double exponential fit for the reduction of **1PPO** (left), **TMPPO** (center), and **TMBPO** (right) by phenylsilane at 80 °C. (b) Derivative curves of the fit from part (a) with the fold increase in reduction rate at 50% conversion indicated.

With all three of our phosphorous precatalysts, more than a 1.5X increase in reduction rate is observed at 50% reduction. It is thus quite likely that phenylsilane requires a pre-activation by reacting with water to form phenylsilanol, which is then the active species, reducing phosphine oxides by proceeding through TS-2.

1.6.2 Diphenylsilane Series

While the kinetic evidence for phenylsilane reduction of phosphine oxides only proceeding through **TS-2** is quite strong, we wanted further experimental evidence. We thus designed a series of Si, Si-diphenylsilanes that are quite similar in structure, but should have dramatically different reactivities if our hypothesis is correct. The three that were tested are 1,1,3,3-

tetraphenyldisiloxane (**TPDS**), diphenylsilane, and methyldiphenylsilane (**MDPS**). **TPDS** should equilibrate with diphenylsilanol, the presumed active species, and should thus be a more rapid reductant than diphenylsilane due to the pre-activation already being complete. **MDPS**, on the other hand, cannot form a hydrido-silanol species to reduce phosphine oxides through TS-2, so it should be completely inactive. We synthesized **TPDS** from diphenylchlorosilane in good yield (Scheme 1.5), and compared the three Si, Si-diphenylsilanes for their reductive capacities against **TMPPO** (Figure 1.24).

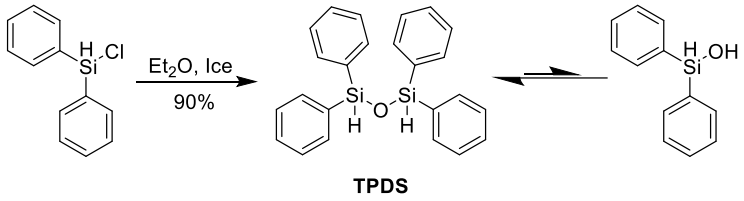

Scheme 1.5. Synthesis of **TPDS** and its Equilibration with Diphenylsilanol

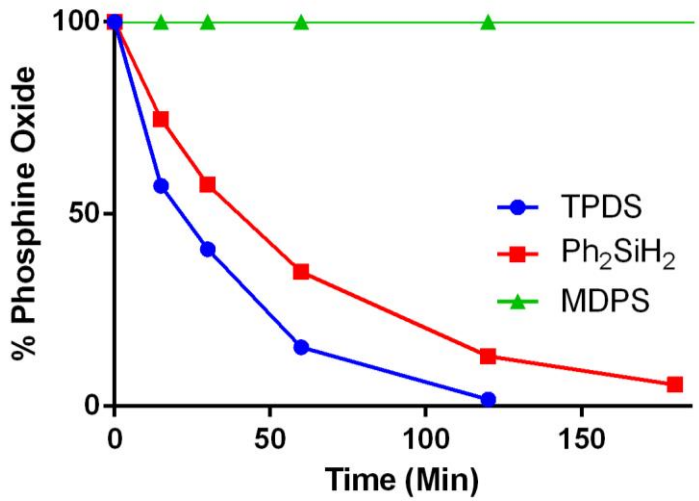

Figure 1.24. Reaction Progress Curves of the Reduction of **TMPPO** by the Diphenylsilane Series. [**TMPPO**] = 0.04 M, [**TPDS**] = 0.3 M, [Ph_2SiH_2] = 0.4 M, [**MDPS**] = 0.6 M

The reactivity of the three silane reagents was precisely in line with our expectations. **TPDS** was faster than diphenylsilane, and **MDPS** was inactive under the reaction conditions for 7 hours.

These results provide further support for our proposed mechanism of silanol-mediated reduction of phosphine oxides and argue against reduction through non-silanols.

1.6.3. Additional Evidence

We were also able to find additional evidence from the literature that supports the hypothesis that phenylsilane and diphenylsilane require preactivation to a hydrido-silanol to furnish the reduced phosphine. In their seminal work on the reduction of phosphine oxides with silanes, Fritzsche and coworkers used 0.67 equivalents of phenylsilane to reduce a full equivalent of phosphine oxide.[91] Marsi then reported the same substoichiometric usage of phenylsilane for reduction ten years later.[92] However, no one has ever reported the substoichiometric usage of diphenylsilane to reduce a full equivalent of a phosphine oxide.[9394] All known procedures use at least 1.1 equivalents of diphenylsilane, which should not be necessary if both diphenylsilane and diphenylsilanol were competent reductants. Similarly, if phenylsilane could reduce a phosphine oxide three times (via phenylsilanol and phenylsilanediol generated following the initial reduction), then we should observe its usage at around 0.4-0.5 equivalents, which has never been reported.

Another interesting piece of evidence is from a procedure for the reduction of phosphine oxides written by Marsi.[95] Under the heading “Typical Reaction of Phenylsilane with Phosphine Oxides.”, he writes: “The phosphine oxide (10 mmol) and 6.7 mmol of freshly distilled phenylsilane are added together in a 10-ml pear-shaped flask fitted with a small condenser. … If the reaction does not commence spontaneously, the mixture is heated carefully with an oil bath. Heating is especially necessary if the oxide is a solid to effect solution of the oxide with phenylsilane. Initial slow evolution of hydrogen signals the onset of the reaction.” This means that despite Marsi’s proposed mechanism (Scheme 1.1) where he proposes the production of hydrogen post-reduction, he observes hydrogen formation at the beginning of the reaction. This is

exactly the sort of behavior we would expect if our proposed mechanism is correct. The "onset of the reaction" is signaled by the "initial slow evolution of hydrogen", which is occurring because phenylsilane is reacting with water to form phenylsilanol.

Taken together, we believe that the pieces of evidence presented in the end of section 1.5 and the entirety of section 1.6 point very strongly towards our theory that all reduction of phosphine oxides below 120 °C or so proceeds through TS-2.

1.7 Completing the Mechanism of Phenylsilane-Mediated Reduction of Phosphine Oxides

1.7.1 Benzoate as a Catalyst for Rapid Reduction with Phenylsilane

Despite our acceptance that silanes reduce phosphine oxides through TS-2, a few questions remained about smaller mechanistic details, specifically in regards to phenylsilane. The first of these is: how does phenylsilane react with water to form phenylsilanol? In Figure 1.4 we showed that heated preincubation of phenylsilane in THF produced an insignificant increase in the rate of reduction. Clearly, phenylsilanol was not formed during this preincubation, as the rate increase would have been much more pronounced, so another explanation is necessary for how to explain the *in situ* formation of phenylsilanol.

The answer came through the results of an investigation of the mechanism of the room temperature catalytic Wittig reaction reported by O'Brien and coworkers. The addition of benzoic acid, DIPEA, and phenylsilane facilitated room temperature reduction of **1PPO** and another phospholane precatalyst. It has been shown that DIPEA and benzoic acid individually provide almost no improvement in the rate of phenylsilane reductions, so we wanted to investigate whether the drastic rate improvement was due to the combination of the two, or whether a proton exchange between them was producing a single active species.

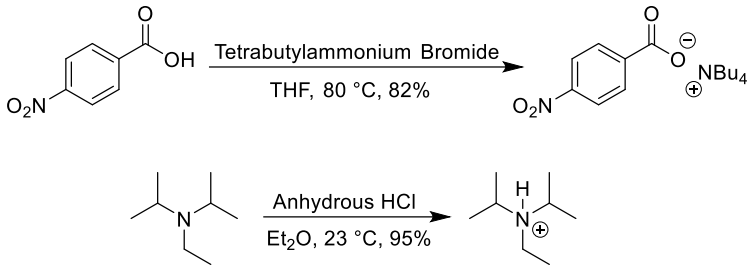

Scheme 1.6. Synthesis of DIPEA-HCl and Tetrabutylammonium *p*-nitrobenzoate

Diisopropylethylamine (DIPEA)•HCl and Tetrabutylammonium *p*-nitrobenzoate were synthesized as shown in Scheme 1.6, and each were added to phenylsilane reductions of **TMPPO**. The benzoate caused vigorous production of gases in the NMR tube upon addition, and formed substantial amounts of the reduced product at room temperature. DIPEA•HCl was added without a physically observable effect, though upon heating to 80 °C, the reduction rate was improved compared to the control, finishing within 15 minutes of initiation. Therefore, the observed improvement in the catalytic Wittig reaction is due to both components, but mostly from *in situ* carboxylate formation. Further testing with the benzoate demonstrated that vigorous bubbling initiated upon addition to a solution of phenylsilane regardless of whether the phosphine oxide was present. Given the rapid reduction with the benzoate, we concluded that the gas is likely hydrogen produced from the reaction of phenylsilane with water to form phenylsilanol.

1.7.2 An Oxyanionic Catalyst is Necessary for Phenylsilanol Formation

At this point, we proposed that phenylsilane requires a Lewis base to activate it to phenylsilanol, likely through the mechanism shown in Scheme 1.7. In this mechanism, the Lewis base donates electrons density to the electron-poor silicon atom of phenylsilane, forming a transient pentacoordinate silicon species. We advocate that the hydride is donated from this species to water, forming hydrogen gas and hydroxide ion, which displaces the Lewis base as a ligand on the silicon atom to afford phenylsilanol. Phosphine oxide, which has substantial Lewis basic character, is hypothesized to be the activating agent during additive-free phenylsilane

reductions. This proposed mechanism is also consistent with our preincubation trials, and can also account for the increased rate observed with DIPEA-HCl by projecting that the increased acidity of the solution facilitates more rapid hydride donation.

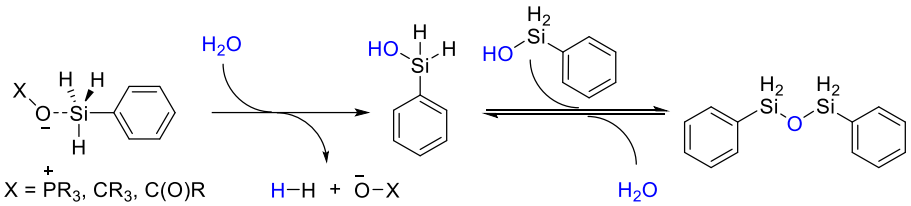

Scheme 1.7. Proposed mechanism for Lewis-Basic Activation of Phenylsilane to React with Water. The Lewis Base with oxyanionic character donates electron density into the silicon atom, allowing for hydride donation from phenylsilane to form phenylsilanol and hydrogen gas.

To test whether or not phosphine oxides are acting as Lewis-basic catalysts in the formation of phenylsilanol, we decided to add Lewis acids to reaction mixtures to potentially block the activation of phenylsilane. Specifically, we chose to add the same Lewis acids that were tested for competency with **TMDSO** in Figure 1.21. The results, which are shown in Figure 1.25, are striking. Zinc chloride, which was the strongest promoter of reduction with **TMDSO**, completely abolishes all of the reductive activity of phenylsilane. The fact that absolutely zero reduction is observed with zinc chloride, combined with it promoting reduction using **TMDSO**, strongly suggests that the Lewis acid is inhibiting the formation of phenylsilanol, and not the subsequent reduction. Lithium chloride, which was presumably not a strong enough Lewis Acid to induce dimethylsilanol formation from **TMDSO**, also substantially inhibits the reaction, though it does not completely stop it. The observed trend in reactivity is the exact opposite of that observed when using **TMDSO**, providing strong evidence for our hypothesis of phosphine oxide acting as a Lewis-basic catalyst for the reaction of phenylsilane with water.

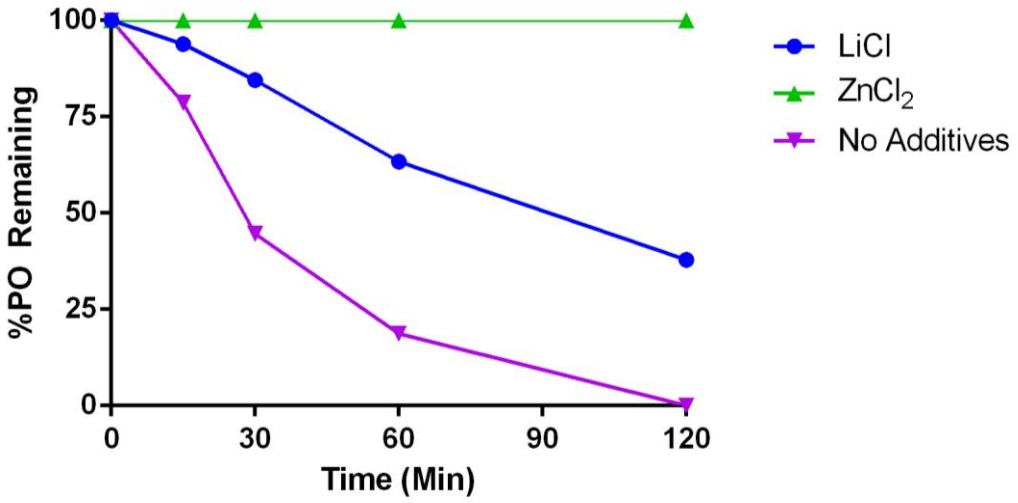

Figure 1.25. Reaction Progress Curves of the Reduction of **1PPO** by Phenylsilane with or without Lewis Acid Additives. [**1PPO**] = 0.04 M, [$PhSiH_3$] = 0.4 M, [LiCl] = 0.2 M, [$ZnCl_2$] = 0.1 M

Next, we wanted to test additional Lewis-basic compounds for their competency in phenylsilanol formation. DIPEA, highly electron donating tributylphosphine, and sterically unencumbered n-propylamine were added to phenylsilane-mediated reductions of **1PPO**. To our surprise, none of these additives significantly affected the rate of formation of the reduced product. Since these are nitrogen and phosphorous-based Lewis acids, we surmised that perhaps the Lewis-base needed to have oxy-anionic character. When previously tested, potassium tert-butoxide produced large amounts of hydrogen gas. The observed trend could be due to the naturally strong affinity between oxygen and silicon, and the considerably lower affinity that silicon has for nitrogen or phosphorous, though we have not thoroughly examined this. Regardless, it does appear that only oxygen-based Lewis basic compounds promote activation of phenylsilane to phenylsilanol.

1.7.3 Comparing Rates of Precatalyst Activation of Phenylsilane

We desired to test additional oxy-anionic additives to test whether stronger oxy-anionic character promoted faster activation of phenylsilane. However, most compounds considered were

either too weak (ketones, aldehydes, carboxylic acids, amides) or too strong (alkoxides). We could have tested a series of carboxylates with different pKa values, or perhaps tried ureas or sulfoxides, as these compounds are probably in the "sweet spot" for reactivity. That would certainly be useful in the future, but we decided to model our existing data of phenylsilane reduction of our precatalysts, as this would show whether or not our proposed mechanism of reduction could provide a reasonable fit to the data in addition to answering the desired question. We already know the electronic trend, as **TMPyrPO** has the most oxyanionic character of the synthesized precatalysts, followed by **TMBPO** and then **TMPPO** and **1PPO** in an unknown order. We also know that the overall reduction rate follows the trend **TMPyrPO** > **TMBPO** > **TMPPO** ≈ **1PPO**, so the challenge is to tease out the rates of the individual steps from the overall data.

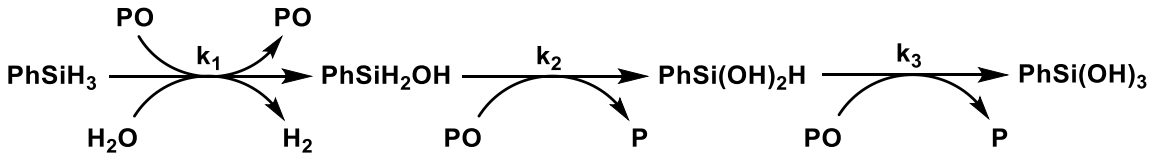

Figure 1.26. Kinetic Schematic of the Reduction of Phosphine Oxides by Phenylsilane Including Phosphine Oxide Catalyzing the Initial Reaction of Phenylsilane with Water

We used the scheme shown in Figure 1.26 as the presumed mechanism for reduction of each of the phosphine oxides. As the concentrations of phosphine oxide and reduced phosphine are known at each data point, along with the initial concentration of phenylsilane, the goal was to obtain specific values of k_1, k_2, and k_3 through fitting the data. Each phosphine oxide is treated as a catalyst in the initial activation, which is important as that means the concentration of phosphine oxide will affect the rate of this step. We also considered taking into account the concentration of water, but decided against this, as it will be constantly changing according the many disiloxane-silanol equilibra present in the reaction mixture, each with an individual and unknown equilibrium constant.

First, we obtained the following equations for the derivatives of the concentrations of each of the components with respect to time.

$$\frac{d[PhSiH_3]}{dt} = -k_1[PO][PhSiH_3]$$

$$\frac{d[PhSiH_2OH]}{dt} = k_1[PO][PhSiH_3] - k_2[PO][PhSiH_2OH]$$

$$\frac{d[PhSi(OH)_2H]}{dt} = k_2[PO][PhSiH_2OH] - k_3[PO][PhSi(OH)_2H]$$

$$\frac{d[PhSi(OH)_3]}{dt} = k_3[PO][PhSi(OH)_2H]$$

$$\frac{d[PO]}{dt} = -k_2[PO][PhSiH_2OH] - k_3[PO][PhSi(OH)_2H]$$

$$\frac{d[P]}{dt} = k_2[PO][PhSiH_2OH] + k_3[PO][PhSi(OH)_2H]$$

Then, the process was initiated by setting the initial concentration of phosphine oxide to 0.04 M, the initial concentration of phenylsilane to 0.4 M, and the initial concentrations of the other components to 0. Guesses were selected for the values of each of the rate constants, and the concentrations of each of the components were calculated using Excel in an iterative process to create simulated reduction progress curves using the equations above. The time scale was set to 0.1 seconds per iteration, so the derivative was recalculated and the concentrations adjusted every 0.1 seconds along the curve. The calculated concentration curves of phosphine oxide were overlaid with the curves from Figure 1.12, and iterations were continued until the data suggested that 95% of the phosphine oxide had been reduced (at this point the data was known to be less accurate).

We then utilized Excel Solver to solve for the rate constants. This was done by minimization of the sum of the variance between the experimental concentration of phosphine oxide at each data point and the simulated concentration of phosphine oxide at the closest time point calculated.

The rate constants were allowed to float, however, we were forced to choose k_3 to be a fixed multiple of k_2 in order to obtain a finite number of solutions. Each fixed multiple pairing produced two solutions of k_1 and k_2/k_3 that fit each precatalyst reduction curve, however, each time we were able to rule one out, as one solution would describe a system where almost all of the phenylsilane gets converted to phenylsilanol, and the other a system where most of the phenylsilane remains at the end of the reaction. When monitoring the reaction by ^{1}H NMR, it is clear that most of the phenylsilane remains following completion, so we chose the appropriate set of rate constants.

First, we chose to confirm that the proposed mechanism and rate constant combinations did in fact result in adept fitting of our experimental reduction curves (Figure 1.27). We wanted to limit the number of analyses as the relationship between k_2 and k_3 had to be manually defined, and thus decided to run the simulation with $k_3 = k_2$, $k_3 = 10k_2$, and $k_3 = \infty$. These were chosen because a wide range of ratios was desired and, at least at the time, it seemed unlikely that k_3 would be slower than k_2 due to the decreased electron density on silicon of phenylsilanediol as opposed to phenylsilanol. Eliminating all of the solutions that had k_1 fast and k_2 slow, we successfully obtained a single pair of rate constants for each ratio of k_2 and k_3/phosphine oxide combination, which are shown in Table 1.4. A graphical comparison each of the simulations with the data modeled is shown in Figure 1.27.

Table 1.4. Rate Constants Obtained through Simulation of Reaction Progress Curves for the Reduction of Phosphine Oxides by Phenylsilane. All rate constants are in ($M^{-1}s^{-1}$)

	$k_3 = k_2$		$k_3 = 10k_2$		$k_3 = \infty$	
	k_1	k_2	k_1	k_2	k_1	k_2
1PPO	0.049	1.83	0.051	1.14	0.058	0.87
TMPPO	0.038	3.01	0.039	1.90	0.040	1.67
TMBPO	0.077	8.23	0.078	5.46	0.079	5.02
TMPyrPO	0.133	25.0	0.134	16.7	0.135	15.4

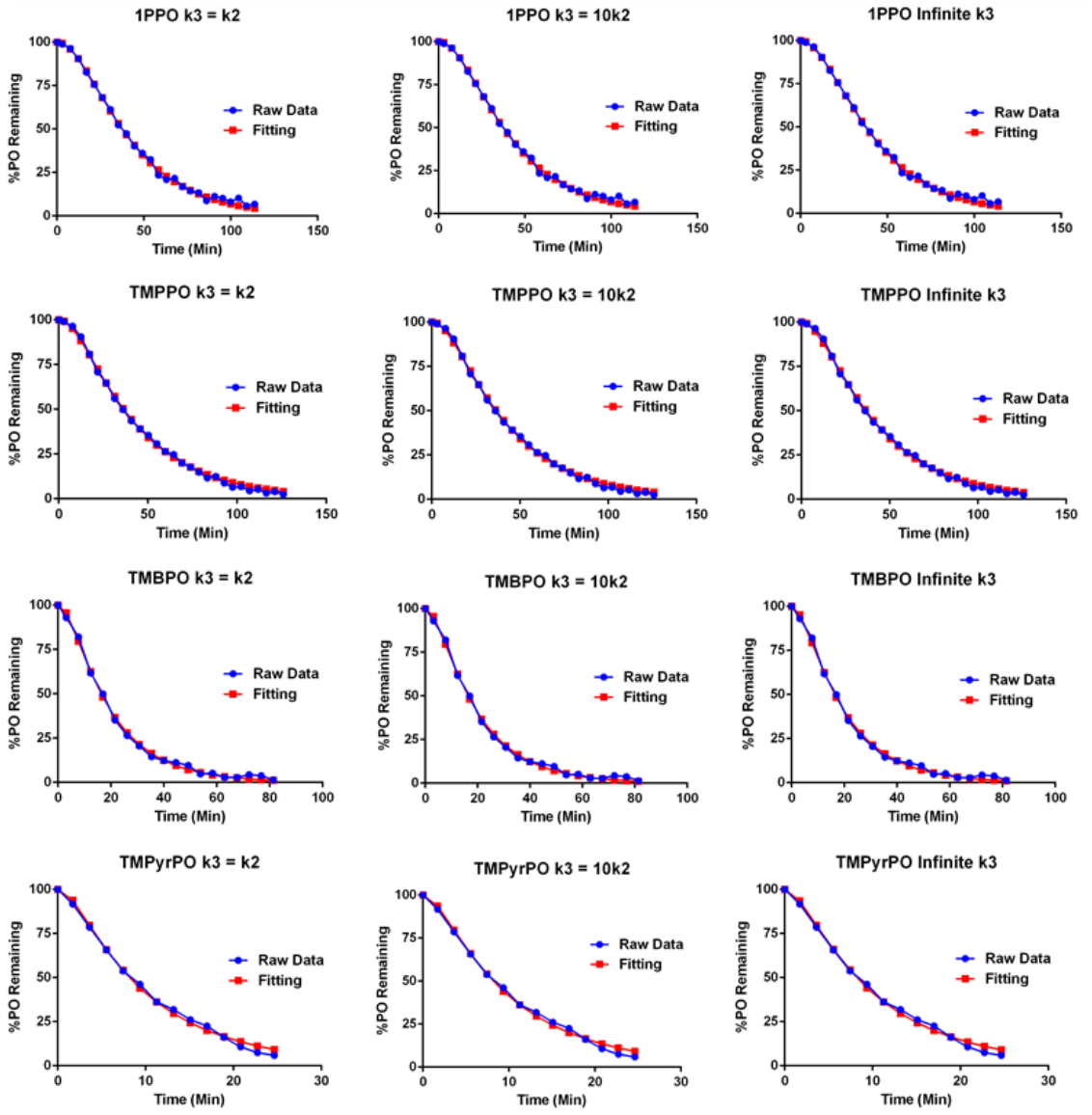

Figure 1.27. Graphical Comparison of Reaction Progress Curves of the Reduction of Phosphine Oxides by Phenylsilane and the Fit Obtained by the Indicated Ratio Between k_2 and k_3. k_2 and k_3 are from Figure 1.26

The simulation curves mirror the actual data quite nicely. The proposed mechanism for phenylsilane reduction certainly could produce the data in Figure 1.12, which was pleasing to confirm as so many other mechanisms were able to be ruled out simply because they could not produce the obtained data.

The other goal of this analysis was to allow for a comparison of which phosphine oxides activate phenylsilane to phenylsilanol the fastest (as well as which are reduced the fastest by phenylsilanol/phenylsilanediol). Clearly, with our method of analysis, we cannot differentiate between k_3 and k_2, nor use the absolute values of the rate constants, as they change based on the relationship chosen between k_3 and k_2. However, the data in Table 1.4 can still be used quite effectively, as the relative rates of the different phosphine oxides can be compared since the trends stay the same regardless of the relationship between k_3 and k_2. The key findings can be summarized in two points.

1. **1PPO** activates phenylsilane to phenylsilanol faster than **TMPPO** but is reduced by the produced silanols slower than the phosphetane.

2. The phosphetanes follow a clear trend demonstrating adding electron density to the phosphine oxide causes both faster activation of phenylsilanol and faster reduction by silanols

The first point confirms the expected differences in reactivity between **1PPO** and **TMPPO** based on the reduction curves in Figure 1.12 and Figure 1.16. The two phosphine oxides are reduced at similar rates in Figure 1.12, while in Figure 1.16, **TMPPO** is reduced nearly twice as fast as **1PPO**. The difference in Figure 1.16 suggests silanols reduce **TMPPO** faster than **1PPO** (based on the Arrhenius equation, which is an oversimplification), indicating that the similar rates observed in Figure 1.12 would be a result of faster phenylsilane activation by **1PPO**. This is interesting because **1PPO** and **TMPPO** likely have fairly similar amounts of electron density on the phosphine oxide, making it likely that the differences in ring strain/steric hindrance are causing the differing rates of the steps.

The second point, that adding electron density to the phosphine oxide causes both faster activation and reduction, provides further support for our theory that oxygen-based Lewis basicity is necessary for phenylsilanol formation. It appears that the greater the degree of oxyanionic

character, the more facile the activation of phenylsilane. It is important to note, for future phosphine design, that greater electron density on the phosphine oxide does in fact causes faster reduction with silanols, and not just faster pre-activation of the reductant.

1.7.4 The Water Cycle

At this point, we had concluded that phenylsilane itself has no reducing capacity towards phosphorous precatalysts, but requires phosphine oxide to catalyze a reaction between it and water, forming hydrogen gas and phenylsilanol, the active reductant. Though this interpretation of the data made sense, we were concerned about the quantity of water that would be required to be present to react with the required amount of phenylsilane. It has been shown that the disiloxane-silanol equilibrium heavily favors disiloxane bond formation, especially with silanediols or silanetriols.[96] Therefore, only a small amount of water is necessary at the beginning of the reaction, as the water that reacts with phenylsilane at the beginning is regenerated following condensation of phenylsilanetriol into silyl-oxy polymers (Scheme 1.8). Specifically, 3/2 of an equivalent of water is generated following condensation for each molecule of phenylsilane that requires activation, which explains Marsi's observation that water is generated over the course of the reaction.[97] This regeneration creates a "water cycle" that is occurring during phosphine formation, which is shown in Scheme 1.8.

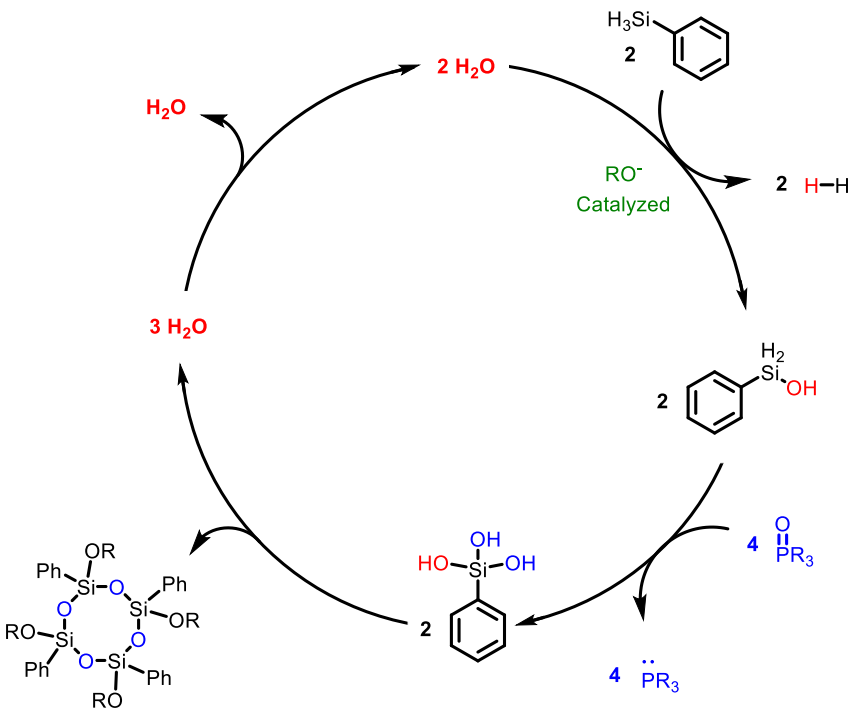

Scheme 1.8. The Reaction of Water with Phenylsilane and Generation of Water Following Condensation of Phenylsilanetriol to form the "Water Cycle". Phenylsilanetriol is certainly not the only silanol that condenses to form disiloxane linkages, but it is illustrated as such in this cycle to show that 3/2 of an equivalent of water is generated for each molecule of water that react with phenylsilane.

1.8 Reinterpretation of Previous Reports

1.8.1 Ashfeld's Traceless Staudinger Ligation

A natural result of overturning postulates that have held for the last 40 years is that many results that were previously considered strange now make sense, and explanations built off of the incorrect postulates need to be revised. We set out to do just that, with the first mystery already unraveled when we demonstrated why addition of benzoic acid to a basic catalytic Wittig solution facilitates room temperature recycling.[98]

Ashfeld and coworkers reported a catalytic-in-phosphine Staudinger ligation, which we were particularly interested in investigating as the conditions reported appeared inconsistent with our results.[99] Specifically, the reaction is purported to involve reduction of **TPPO** with phenylsilane

while heating to only 60 °C. The overall reaction scheme and the proposed mechanism are shown in Scheme 1.9.

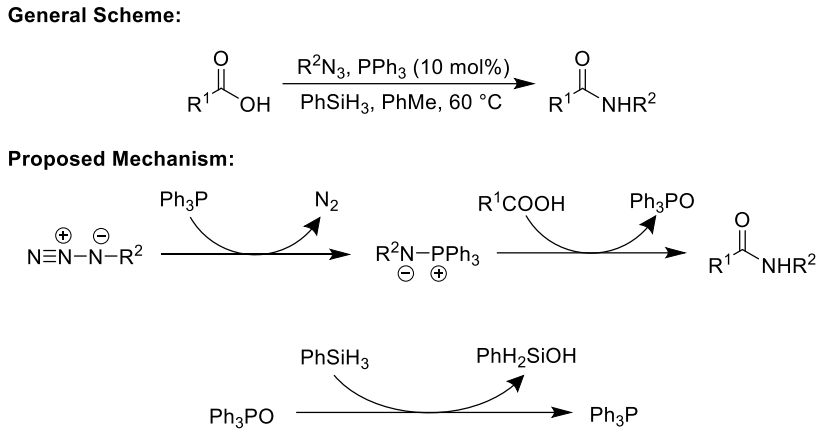

Scheme 1.9. General Scheme for Ashfeld's "Traceless Staudinger Ligation" and the Reported Mechanism of the Reaction.

As we found that **TPPO** could be reduced by **DPDS** in a reasonable time frame at 110 °C (Figure 1.17), we were skeptical that a reaction that used phenylsilane and required 10 turnovers of phosphine could proceed at 60 °C. Therefore, we decided to test the validity of such a reduction under the reported conditions. While planning the experiments, we realized that if some of the aza-ylide is hydrolyzed, it will form triphenylphosphine oxide and an amine. The amine would then interact with the carboxylic acid that is already present to form carboxylate, which would in turn form phenylsilanol from phenylsilane. All of this could occur without any loss in yield, as 1.2 equivalents of azide were reported to be the optimal conditions. Therefore, we decided to test the reduction of **TPPO** under what we viewed as the best possible reducing conditions achievable with the reported chemicals. We added phenylsilane (1.0 equiv.), PNBA (1.2 equiv.), and N-benzylmethylamine (1.0 equiv.) to **TPPO** (0.1 equiv.) and heated this to 60 °C for 16 hours (the amount of time reported for these reactions). Taking phosphorous NMR, we found that 49% of the **TPPO** was reduced, so the half-life of reduction under these "ideal" conditions was almost exactly 16 hours. Even if these unrealistically favorable reduction

conditions were achieved, the reaction could not have proceeded under the mechanism proposed, as the half-life of this reduction would have to be in the 2-3 hour range.

Next, we decided to probe the reaction conditions, partially due to the suspicious lack of a reported stoichiometric trial without silane during the initial optimization. We exchanged 4-trifluoromethylbenzoic acid out for PNBA, but otherwise utilized the exact optimized conditions reported, and obtained a 62% yield (Entry 1 in Table 1.5). Switching the phosphine from TPP to **TPPO** greatly decreased the yield to 23% even with an increased reaction time of 24 h (Entry 2 in Table 1.5). This only further confirmed our doubts about the actual mechanism of the reaction, as this yield is much more in line with what could occur based on our isolated reduction study. Next, we tested the effects of increasing the temperature to 110 °C, a much more typical temperature for these catalytic-in-phosphine reactions, and found that it had an insignificant effect on the yield (Entry 3 in Table 1.5).

Table 1.5. Catalytic and Stoichiometric Staudinger Ligation Reactions. Entry 4 furnished 16% of benzylamine, while Entry 5 afforded a quantitative yield of benzylamine

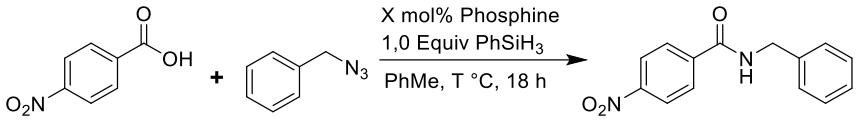

Entry	Phosphine	Phosphine Loading	Silane	Temperature (°C)	Isolated Yield
1	TPP	17 mol%	Yes	60	62
2	**TPPO**	17 mol%	Yes	60	23
3	TPP	17 mol%	Yes	110	65
4	TPP	17 mol%	No	60	0
5	TPP	110 mol%	No	23	0
6	TPP	110 mol%	No	60	0
7	TPP	110 mol%	No	110	0

Finally, we ran the stoichiometric trial that should have been present in Ashfeld's report. The conditions remained exactly the same except that the silane was removed and we used an excess of TPP. Regardless of temperature (Entries 5-7 in Table 1.5), we found that no product was

formed. Instead, we isolated a quantitative yield of benzylamine post-workup, the Staudinger reduction product. To be thorough, we also tested removal of the silane while using a catalytic amount of TPP, and again isolated no product.

We were now 100% certain that the proposed mechanism was incorrect, as the failed stoichiometric runs proved that the amide coupling was silane-mediated. While seeking to determine an alternative mechanism that could explain the formation of the product while remaining concurrent with our reduction experiment, we found a report by Ruan and coworkers that used phenylsilane as an amide coupling reagent.[100] Their conditions were remarkably simple, with no heat or additives required, just carboxylic acid, amine, and silane. Denton and coworkers later used this reaction to do an amidation/reduction combination reaction.[101] With the results in Table 1.5, it is extremely likely that this phenylsilane-mediated amide coupling is the actual mechanism for product formation in Ashfeld's reaction.

Then, all we had to do was explain how the amine was formed in quantitative yield with a catalytic amount of phosphine. We propose that following Staudinger reduction to form the phosphine imine, it is reduced by phenylsilanol, giving the amine and recycling the TPP. It is quite possible that this P=N bond reduction could occur at 60 °C, as at least in certain cases (*vide infra*), the P=N bond is much more rapidly reduced than the P=O bond. With our investigation complete, we propose the mechanism shown in Scheme 1.10, a catalytic-in-phosphine Staudinger reduction combined with phenylsilane-mediated amide coupling, as what is actually occurring under Ashfeld's conditions.

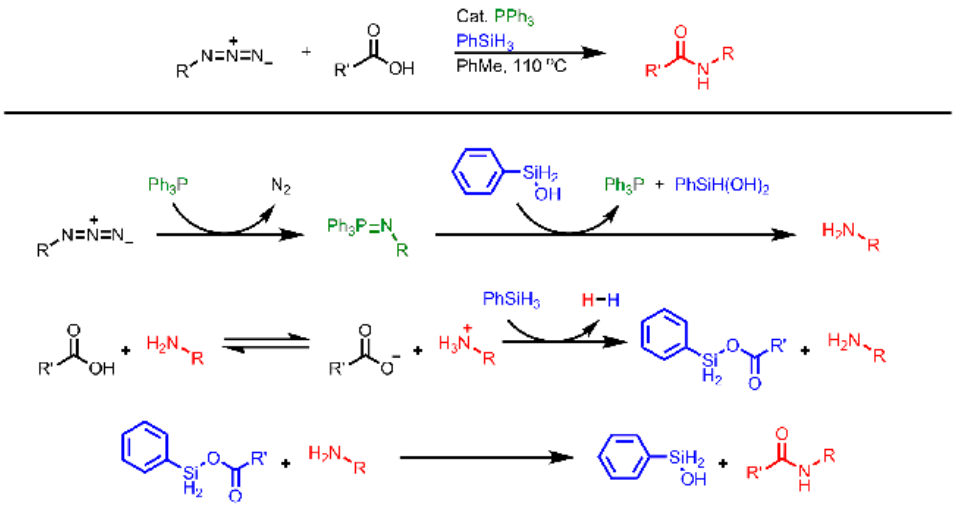

Scheme 1.10. Our Proposed Mechanism for Ashfeld's "Traceless Staudinger Ligation".

1.8.2 Lemaire's Reduction using Ti(O^{i}Pr)$_4$/TMDSO

The final set of reports that we wanted to investigate were those of Lemaire and coworkers, who published multiple papers on Ti(O^{i}Pr)$_4$ catalyzed reduction of phosphine oxides with **TMDSO**.[102103104] As mentioned previously, they performed ^{29}Si NMR studies and electron paramagnetic resonance (EPR) spectroscopy to obtain information about the nature of the intermediates and products of the reduction.[105] Based on this information, they proposed the mechanism shown in Scheme 1.2, which, if true, would be quite interesting as it is quite different from any other known silane-mediated reduction of phosphine oxides.

The proposed phosphine radical was of particular interest to us, as it would represent a non-hydride based mechanism of reduction. To begin our investigation, we designed the phosphine oxide TMCypPO (Scheme 1.11), which would be able to facilitate a so-called "radical clock" experiment where a cyclopropyl ring is adjacent to the location of the proposed radical center.

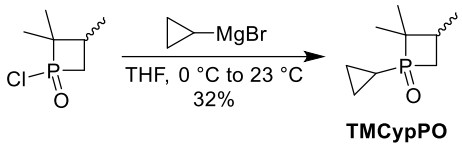

Scheme 1.11. Synthesis of TMCypPO.

TMCypPO was synthesized in poor yield through the addition of cyclopropyl magnesium bromide to 2,2,3-trimethyl-1-chlorophosphetane oxide. Since cyclopropyl represents the fastest known "radical clock", if a phosphorous-centered radical is generated during reduction of TMCypPO under Lemaire's conditions, we should observe the presence of 1-*n*-propyl-2,2,3-trimethylphosphetane following completion of the reaction. This occurs through generation of a phosphonium ylide, which is known[106] to react with water to form the corresponding phosphine oxide, 1-*n*-propyl-2,2,3-trimethylphosphetane oxide in our specific case. As an excess of silane reductant is used, the *n*-propyl phosphine oxide will also be reduced (Scheme 1.12)

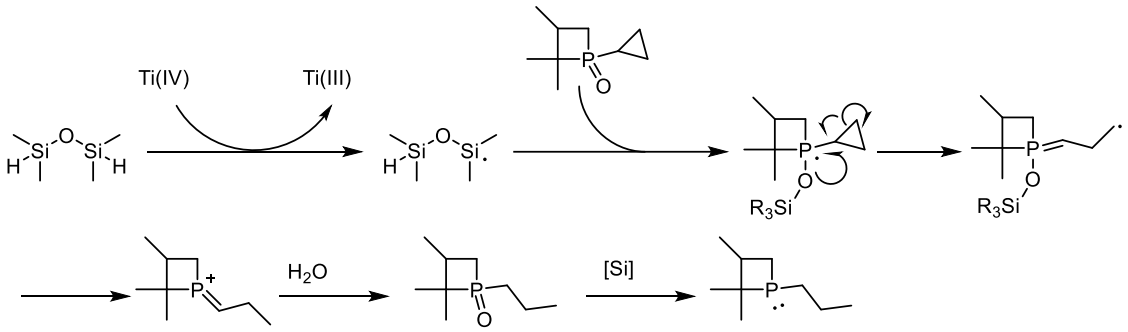

Scheme 1.12. Formation of 1-*n*-Propyl-2,2,3-trimethylphosphetane through Phosphine-Centered Radical Formation

In our actual test, we submitted TMCypPO to the conditions reported by Lemaire and coworkers, and compared the results to a reduction of TMCypPO with **DPDS** at room temperature. Initially we wanted to use ^{1}H NMR to watch for formation of peaks with shifts that would correspond to an *n*-propyl group, but those experiments were inconclusive. Instead, we used LC-MS analysis, watching for the formation of both reduced TMCypPO [M] and [M+2], which would be the reduced *n*-propyl compound. With both **DPDS** and Lemaire's conditions, a

[M+2] peak was observed (Section 1.15), but its intensity was approximately 0.01% of the [M] peak, which is the expected amount of [M+2] that would be observed from just the presence of [M] with natural isotopic abundance. This indicates that a phosphorous-centered radical is not an intermediate that occurs under Lemaire's conditions.

Therefore, a new mechanism had to be proposed that could account for the lack of a phosphine radical as well as all of the NMR and EPR studies.[107] A report by Samuel and coworkers describes the disproportionation of **TMDSO** by bis-cyclopentadienyl titanium (III) complexes, including characterization of additional reaction products by X-ray crystallography, NMR, IR, and GC studies.[108] This work is slightly different from the Lemaire reports, as no phosphine oxide is added to the reaction mixture, but it both adds to and confirms the proposed intermediates from Lemaire, including the formation of a titanium (III) hydride species. In particular, the key result from Samuel and coworkers that drives our proposed mechanism (Scheme 1.13) is the combination of a titanium hydride and a silyl-titanium species to form a bimetallic intermediate which dissociates to form a hydridosilyloxy-titanium (III) compound and a dimethylsilyl-titanium (III) species. The hydridosilyloxy-titanium species, in the presence of phosphine oxide, is perfectly positioned to undergo reduction via the 6-membered transition state with the Ti(III) acting like a gigantic proton (Scheme 1.13).

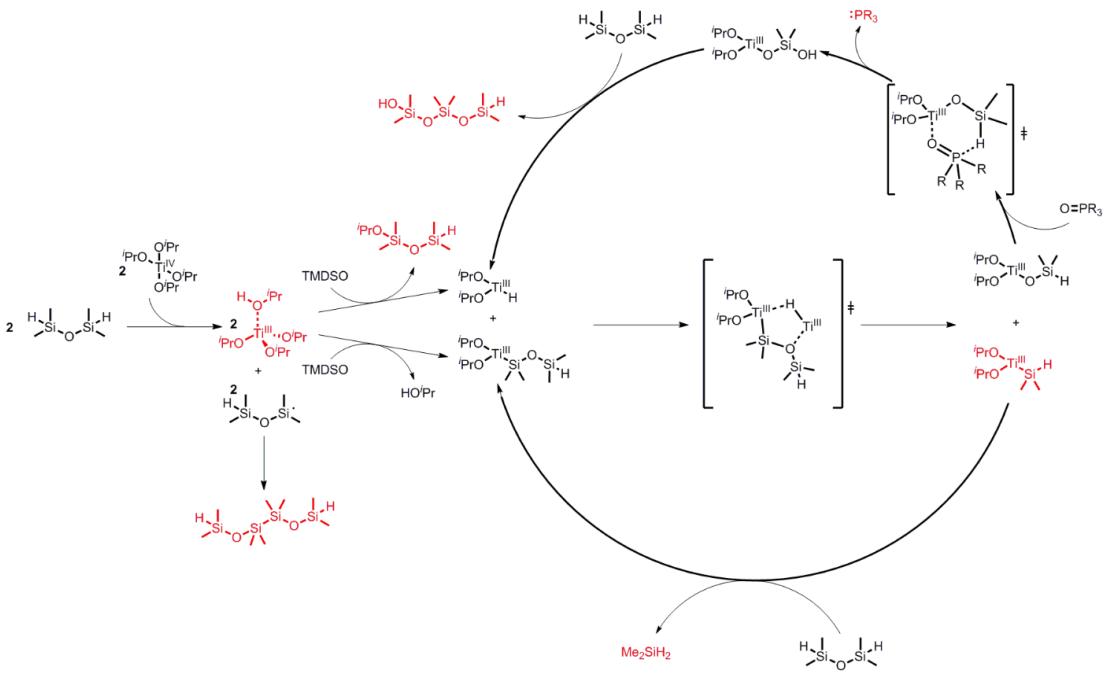
TMDSO
TMDSO
HO^{i}Pr
^{i}PrO
^{i}PrO
^{i}PrO

transformation. The only area that our proposed mechanism is incongruent with the results reported by Lemaire and coworkers is that they specifically note not observing a titanium(III) hydride species by EPR. However, these EPR studies were conducted at titanium concentrations that are 32-fold less than the catalytically-relevant system, and Samuel indicates that the proposed titanium hydride may be short-lived or exist as a dinuclear titanium complex with high valency. This high valency complex is actually supported by the data from Lemaire's EPR studies.

Therefore, our new mechanism for the $Ti(^{i}OPr)_4$-catalyzed reduction of phosphine oxides by **TMDSO** takes into account observations of titanium-catalyzed disproportionation of **TMDSO**, the ^{29}Si NMR studies, the EPR studies, and the lack of a phosphorous-centered radical. This mechanism does suggest that two equivalents of silylhydride are required to reduce a single equivalent of phosphine oxide, and that some **TMDSO** is require for suicide activation, which confers nicely with Lemaire's usage of no less than 1.25 equivalents of **TMDSO**. Finally, the new mechanism utilizes the Ti(III) as if it were essentially a giant proton for reduction through the 6-membered transition state.

1.9 Disiloxane Synthesis and Testing

1.9.1 DMDPDS Synthesis and Testing

We now desired to return to the original goal of improving phosphorous recycling and phosphine synthesis. Currently, only three disiloxanes had been tested for their reductive potential: **DPDS**, **TPDS**, and **TMDSO**, each with drastically different reactivities. Since disiloxanes only require equilibration with water to form a silanol, we wanted to pursue the synthesis of additional disiloxane materials. With our previous method of purchasing a commercially available chlorohydridosilane, dissolving it in diethyl ether, and pouring this over ice, we were able to make one more disiloxane for testing: 1,3-dimethyl-1,3-diphenyldisiloxane (**DMDPDS**) (Scheme 1.14). We then tested its effectiveness in reducing **TMPPO**. It was found

to be much slower than even **TPDS**, much less **DPDS**; however, we got a very interesting result when testing its reductive potential in THF versus toluene (Figure 1.28).

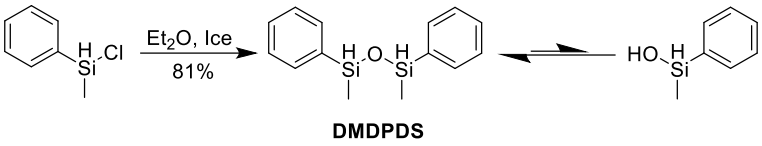

Scheme 1.14. Synthesis of **DMDPDS** and its Equilibrium with Methylphenylsilanol

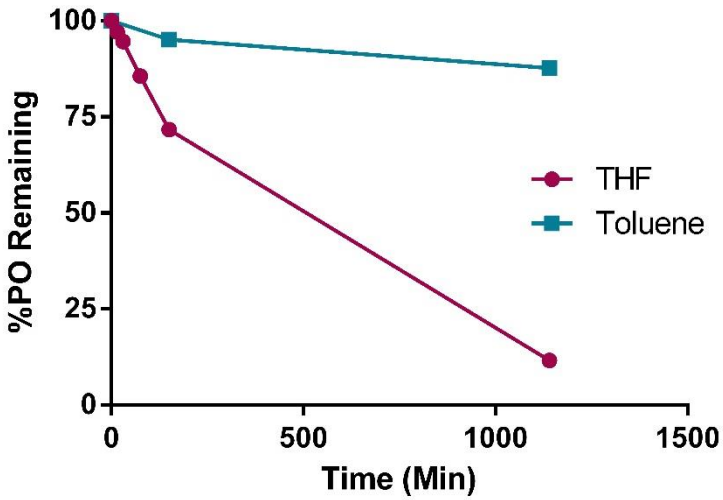

Figure 1.28. Reaction Progress Curves for the Reduction of **TMPPO** with **DMDPDS** at 80 °C. [**TMPPO**] = 0.04 M, [**DMDPDS**] = 0.3 M

DMDPDS reduces **TMPPO** much faster in THF than it does in toluene. In fact, fitting the data in Figure 1.28 to single-exponential curves reveals that the rate of reduction is almost exactly 20-fold higher in THF than it is in toluene. With most conditions we have observed a minimal difference in reduction rate between solvents, provided solubility of all of the reagents is not in question. However, observing the difference in reduction rate between **TPDS** and **TMDSO**, and knowing that **TMDSO** is a particularly stable disiloxane,[111] we propose that phenyl substituents on a disiloxane greatly assist in driving the disiloxane-silanol equilibrium towards the silanol when compared to methyl groups. A reasonable explanation for this would be the fact that a phenyl group could help stabilize (through resonance) a negatively-charged pentavalent silicon

species that could be an intermediate in the reaction of a disiloxane with water. It could also be due to methyl being less electron withdrawing than phenyl, making **DPDS** have less electron density on the silicon than **TMDSO**, opening it up for more nucleophilic attack. With this theory, we attribute this massive difference in the reactivity of **DMDPDS** in THF and toluene to the two solvents' differential affinity for water, as there is likely much more water in THF than there is in toluene.

Now, we have not commonly observed large differences in the rate of reduction when switching solvents, which does call into question the suppositions above. However, I believe that the lack of differences in rate between solvents despite substantially differing in the amount of water available to form silanols can be rationalized quite well. In the case of THF vs toluene, THF has a lot more water, and thus with it as the solvent, more silanol should be present in a **DPDS**-facilitated reduction of a precatalyst. However, THF is a hydrogen-bond acceptor, and the additional water is both a hydrogen-bond acceptor and donor. Reductions in THF could thus be predicted to undergo TS-2 substantially less, as forming the hydrogen-bond between the silanol and the phosphine oxide will be more intermittent, and when this bond does form, it will be weaker. We propose that this difference in reactivity balances out the greater amount of silanol that is present in THF in most cases. There may be incidents where this balance does not even out, and since there are relatively few other explanations that rationalize the difference in Figure 1.28, it appears likely that **DMDPDS** is one of them.

1.9.2 Ball-Milling Synthesis of Disiloxanes

Now that we had established that hydrido-disiloxanes bypass the pre-activation step necessary when using hydrido-silanes to reduce phosphine oxides, we sought to synthesize such disiloxanes via a more cost-effective method in order to obtain significant amounts of these compounds for use in chemical reactions. Synthesis of disiloxanes from the corresponding

chloro-silanes requires a very simple procedure that is high yielding. However, synthesizing chlorohydridosilanes has been shown to be challenging. The best general scheme known for generation of such silanes appeared to be a copper-based synthesis that utilized "ceramic spheres" to break apart the reaction. As the methods for synthesis of symmetrical disiloxanes from chlorohydridosilanes appeared to be rather robust, we designed a simple, 1-pot procedure to obtain these disiloxanes from the corresponding silane (Scheme 1.15).

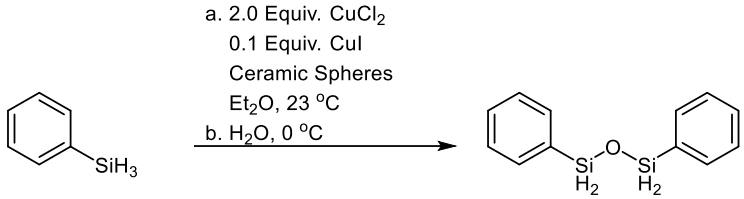

Scheme 1.15. One-pot Procedure to Synthesize Symmetrical Disiloxanes from the Corresponding Silane. **DPDS** and phenylsilane are shown as representative examples in the scheme

The synthesis of **DPDS** begins with the complexation of $CuCl_2$ and catalytic CuI in diethyl ether for 30 min in the presence of either chrome or ceramic spheres. Phenylsilane is then added and the reaction is ball-milled at 350 rpm at ambient temperature under air with an overhead stirrer for 1.5 h until 100% conversion has been noted by ^1H NMR to afford the intermediate chlorophenylsilane. The reaction mixture is filtered directly onto ice chips and extracted with diethyl ether to afford **DPDS** in 93% percent yield and approximately 95% purity, which is sufficient for most applications. Distillation under high-vacuum can be performed to provide **DPDS** in >99% purity and 88% overall yield in cases where higher purity is required (Table 1.6, Entry 1). The reaction is scalable and does not require increased reaction times to obtain purified product. For example, **DPDS** is obtained in an 88% yield on a 10 gram scale in less than three hours.

We were particularly interested in synthesizing large amounts of **DPDS** via a reasonably cost-efficient method, but wanted the scope of this reaction to be quite general so that novel

disiloxanes could be created. We found that the reaction conditions could easily be extended to secondary arylsilanes as well as alkylsilanes, as diphenylsilane and *n*-hexylsilane were readily converted to **TPDS** and 1,3-di-*n*-hexyl-disiloxane (**DHDS**) in 90% and 85% yield, respectively (Table 1.6, Entries 2-3).

Table 1.6. Synthesis of **DPDS**, **TPDS**, and **DHDS** via the One-Pot Copper-Based Procedure

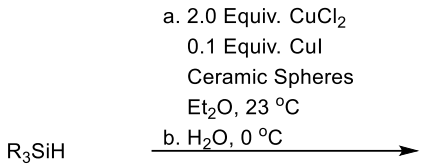

Entry	Product	Yield (%)
1	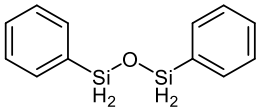	88
2	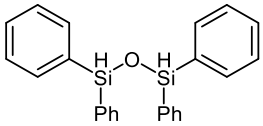	90
3	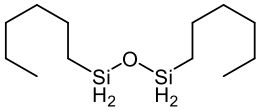	85

1.9.3 DHDS Synthesis and Testing

With a medium-scale (10 g), single-step synthesis of disiloxanes from silanes ironed out, we decided to test **DHDS**, the last unique disiloxanes that could both be synthesized from a commercially available silane and would likely have reductive activity against phosphine oxides. **DHDS** was evaluated for its reductive capacity against **1PPO** at elevated temperature. **DHDS** showed moderate activity against **1PPO** at 80 °C, certainly enough to facilitate a catalytic-in-phosphine reaction at that temperature. However, the rate was still far too slow for **DHDS** to be used as a reasonable alternative to **DPDS**. We therefore set **DHDS** aside and concluded the

synthesis of new disiloxanes, choosing to move forward into reactions with our most promising reducing agent, **DPDS**.

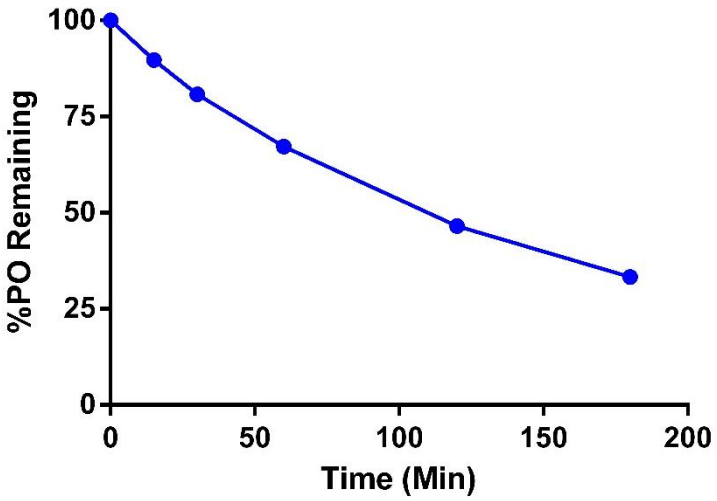

Figure 1.29. Reaction Progress Curve of the Reduction of **1PPO** by **DHDS** at 80 °C in THF. [**1PPO**] = 0.04 M, [**DHDS**] = 0.3 M

1.9.4 Evaluation of DPDS

With a convenient, large-scale synthesis of **DPDS** secure, we wanted to test it for its stability and functional group compatibility before taking it into reactions. **DPDS** exhibited exquisite benchtop stability with virtually no degradation occurring after 2 weeks, and less than 2% degradation over a 6 month period. Satisfied, we tested it for its functional group compatibility. At room temperature, **DPDS** displayed no reactivity with alcohols, aldehydes, carboxylic acids, cyano groups, and nitro groups for up to 16 hours. At 80 °C, **DPDS** still displayed no reactivity with aldehydes, cyano groups, and nitro groups, but displayed minimal reactivity with carboxylic acids (Figure 1.30) and substantial reactivity with alcohols (Figure 1.31 & Table 1.7). Alcohol reactivity at elevated temperature was expected given the projected ease of substituent replacement on the silicon between a silanol and an alcohol. Following isolation of the products through column chromatography, we recovered the alcohol in 97% yield with a basic workup, suggesting that **DPDS** forms an extremely weak silyl “protecting group” that is unstable. This

reactivity could be problematic if **DPDS** is used at high temperature in a reaction that necessitates an alcohol taking place in the reaction, but otherwise appears quite benign since the silyl group cleaves during a workup. We noted that the reactivity of **DPDS** with alcohols at elevated temperature is increased when a benzoic acid is included in the reaction mixture (Table 1.7, entries 7 & 8), which makes sense as acids are known to facilitate ligand exchange at silicon. The reactivity of **DPDS** with carboxylic acids at 80 °C was minimal for up to 17.5 hours, though it did become substantial after multiple days (Figure 1.30). We were very satisfied with this overall functional group compatibility profile, and decided to move on to using **DPDS** in reactions.

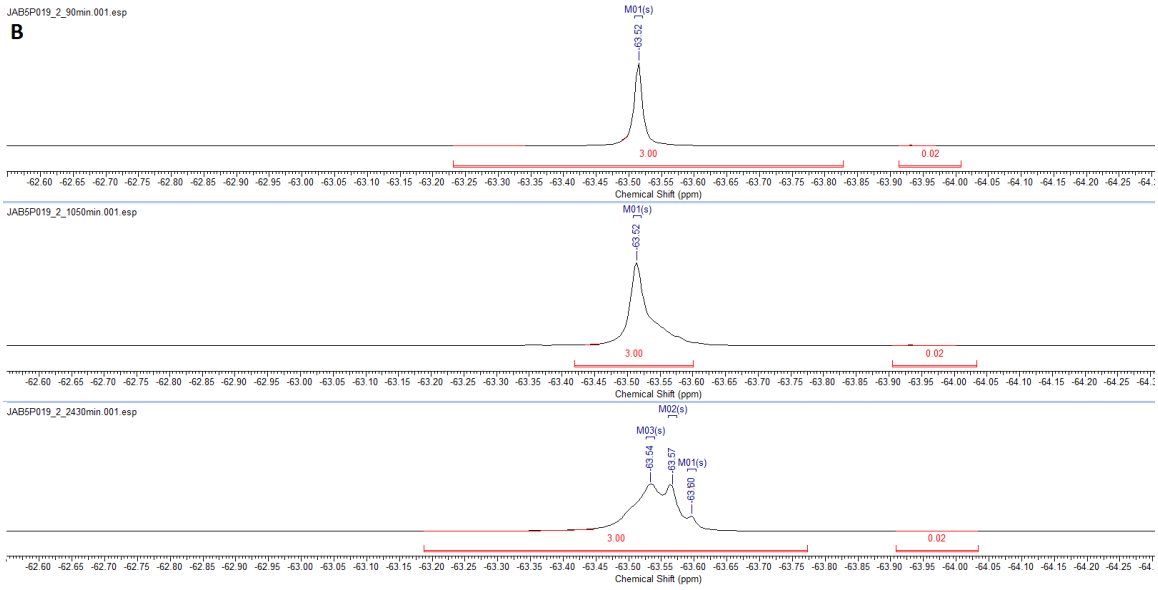

Figure 1.30. Evaluation of the Reactivity of **DPDS** with 3-(Trifluoromethyl)-Benzoic Acid at 80 °C. Reactivity is not noted at 1.5 h (top) and appears minimal at 17.5 h (middle), but grows to be substantial by 40.5 h (bottom)

Table 1.7. The reaction of 4-(trifluoromethyl)benzyl alcohol and **DPDS** with or without benzoic acid additives.

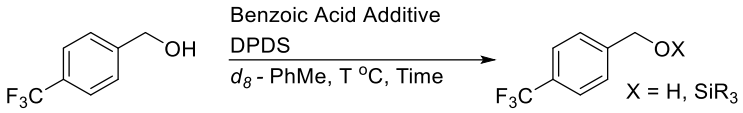

Entry	Benzoic Acid	T (°C)	Time (Min)	% Alcohol Remaining
1	None	23	1080	>95
2	None	23	2520	>95
3	*p*-Nitrobenzoic acid	23	1080	>95
4	*p*-Nitrobenzoic acid	23	2520	>95
5	None	80	1050	57
6	None	80	2430	16
7	3-(Trifluoromethyl)-benzoic acid	80	1050	25
8	3-(Trifluoromethyl)-benzoic acid	80	2430	0

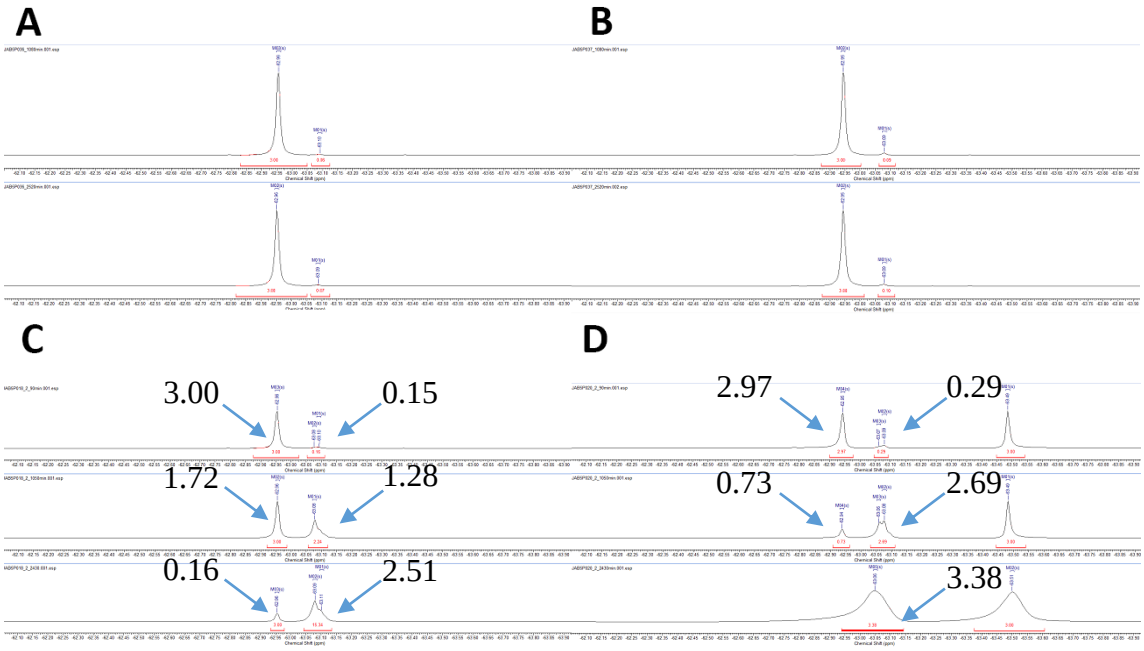

Figure 1.31. Evaluation of the Reactivity of **DPDS** with 4-(Trifluoromethyl)-Benzyl Alcohol at 23 and 80 °C. (A) The reaction at 23 °C for 0 h (top) and 42 h (bottom). (B) The reaction at 23 °C with *p*-nitrobenzoic acid for 0 h (top) and 42 h (bottom). (C) The reaction at 80 °C for 1.5 h (top), 17.5 h (middle), and 40.5 h (bottom). (D) The reaction with 3-(trifluoromethyl)-benzoic acid at 80 °C for 1.5 h (top), 17.5 h (middle), and 40.5 h (bottom). Large black numbers indicate the integrations of the peaks

1.10 DPDS in Catalytic-in-Phosphine Reactions

1.10.1 A Room Temperature Catalytic-in-Phosphine Mitsunobu

We chose to first explore the usage of **DPDS** in room temperature variants of catalytic-in-phosphine reactions. Naturally, we first turned towards the Mitsunobu reaction, as improving it was the original focus of this work. We thus set up a catalytic Mitsunobu reaction using extremely similar conditions as the work published by Buonomo and Aldrich,[112] with the only differences being a switch to room temperature and replacement of phenylsilane with **DPDS** (Scheme 1.16). Unfortunately, this did not furnish even trace amounts of the desired product. This was quite surprising, but additional attempts produced the same results. In every reaction, the alcohol and carboxylic acid were still present, the precatalyst was reduced, and no DIAD remained.

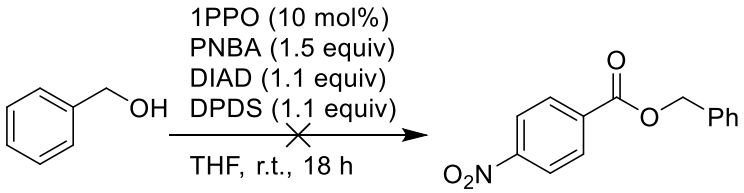

Scheme 1.16. Attempt at Developing an Ambient Catalytic-in-Phosphine Mitsunobu Reaction

As all of the DIAD disappeared by the end of the reaction, we investigated potential reactivities between **DPDS** and DIAD. To our surprise, **DPDS** did not react with DIAD when they were incubated together, even with the addition of heat, alcohol, and/or benzoic acid. However, we were able to ascertain what was going on through a clever experiment where we added benzoic acid, DIAD, and **DPDS** to a solution of THF and heated this for 2.5 h, monitoring with ^{1}H NMR. We then opened the tube and added **TMPPO**, which should quickly get reduced to the phosphine form, and again monitored this for 20 hours, this time at room temperature. As can be seen in Figure 1.32, both the methine and methyl protons on DIAD undergo a substantial

upfield shift during this time, indicating reduction of DIAD to form the hydrazine. The initial heating was performed to demonstrate that DIAD was present before the addition of **TMPPO**, that addition of the precatalyst initializes reduction to the hydrazine.

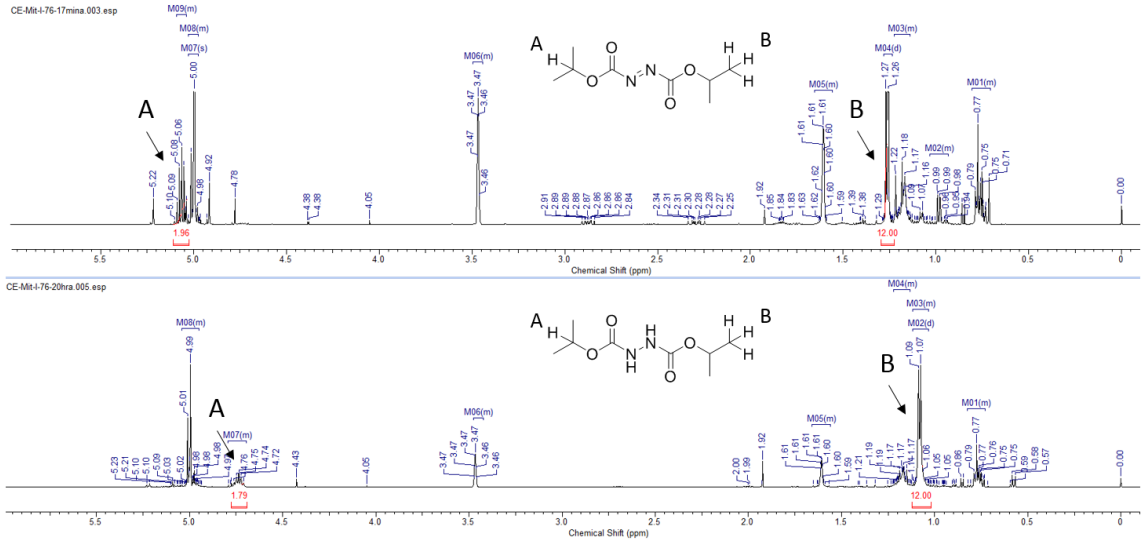

Figure 1.32. Evaluation of the Reactivity of **DPDS** with DIAD with Phosphine Present. Top: ^{1}H NMR spectra of a reaction mixture containing DIAD, **TMPPO**, **DPDS**, and 3-(trifluoromethyl)-benzoic acid 17 minutes after the addition of **TMPPO**. Bottom: ^{1}H NMR spectra of the same reaction mixture 20 hours post-addition. Note the upfield shift of both the methine (A) and methyl (B) protons.

This experiment expertly demonstrates that phosphine is key to the observed hydrazine formation. Phosphines are known to react with DIAD to form the Huisgen intermediate, as shown in Scheme 1.17, which we propose is the species that gets reduced by **DPDS**. The Huisgen intermediate has several similarities to a phosphine oxide or phosphine imine, including a tetravalent structure at the phosphorous center with an electron-deficient phosphorous atom. These similarities lend credence to the idea that this intermediate is the species that is reduced by **DPDS**. Potentially due to the formal positive charge present on the phosphorous, the Huisgen intermediate must be particularly rapidly reduced by **DPDS**, since zero product formation is observed under the conditions in Scheme 1.16 (Earlier scheme). This issue persisted regardless of

the choice of precatalyst, so we decided to move on to the development of other room temperature catalytic-in-phosphine reactions with **DPDS**.

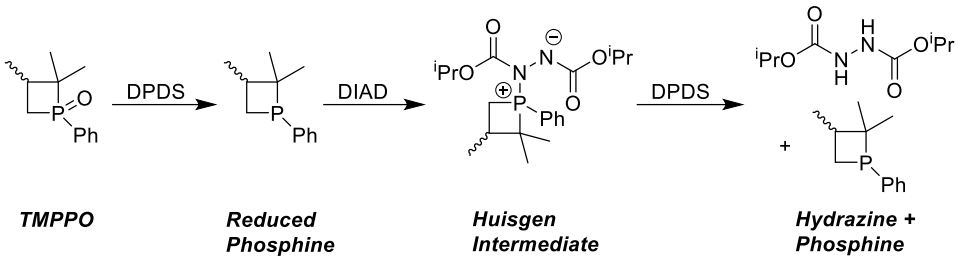

Scheme 1.17. Reduction of the Huisgen Intermediate by **DPDS** Prevents Development of a Room Temperature Catalytic Mitsunobu Reaction.

1.10.2 Room Temperature Catalytic-in-Phosphine Wittig Reactions with DPDS

In contrast to the catalytic Mitsunobu, we were successful in developing catalytic Wittig reactions, catalytic Appel reactions, and catalytic Staudinger reductions with **DPDS** that proceed under ambient conditions. Each of these reactions are run without any special considerations, such as the exclusion of air or water, and are thus truly "dump and stir" reactions. In every methodology, we ran multiple substrates to demonstrate the potential for ambient, additive-free phosphine recycling and to show the efficacy of **DPDS** in each one. However, we should note that we did not fully optimize these methodologies. This is why there is a limited number of substrates, and many of the yields could probably be improved by attempting a greater range of conditions.

For the catalytic Wittig, we determined the optimal number of equivalents of **DPDS** by testing the reaction of benzaldehyde with ethyl bromoacetate using DIPEA as the base and 10 mol% of **1PPO** for the precatalyst (Table 1.8). We found that using 1.0 equivalents of **DPDS** provided a 77% yield (99% based on recovered starting material (BRSM)) of the product with an excellent E:Z ratio. Using these conditions, we tested the efficacy of several other substrates, changing both the aldehyde and the ylide precursor, and found that the reactions proceeded with

yields in the 75% range for disubstituted alkenes (Table 1.9). With the trisubstituted alkene, our yield decreased to 54%, which is commensurate with a decreased yield observed by O'Brien and coworkers.[113] As little to no optimization was performed on the trisubstituted alkene, it is likely that the formation of such alkenes could be improved with additional time and effort.

Table 1.8. The Dependence of Yield on Equivalents of **DPDS** in Room Temperature Catalytic Wittig Reactions

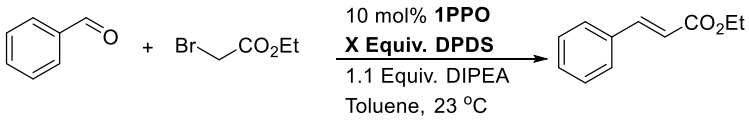

Entry	X Equiv. DPDS	Yield[a]	E/Z Ratio[b]
1	**1.0**	**77 (99[c])**	**>95:5**
2	0.8	44	86:14
3	0.5	20	Not Determined

[a]Isolated yield after 18 h; [b]Determined by ^{1}H NMR; [c]Yield based on recovered starting material.

Table 1.9. Catalytic Wittig Reactions Employing **DPDS** at Room Temperature

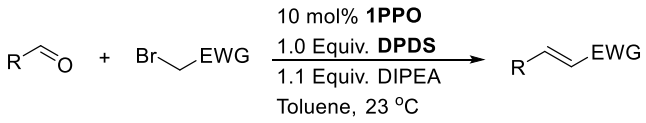

Entry	Aldehyde	Product	Yield[a]	E/Z Ratio[b]
1	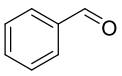	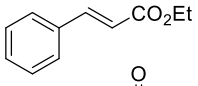	77	>95:5
2	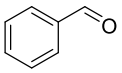	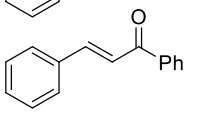	76[c]	>95:5
3	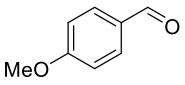	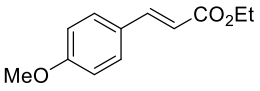	76	94:6
4	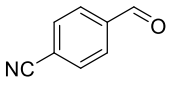	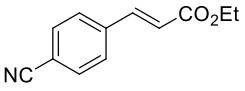	74	>95:5
5	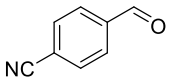	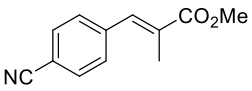	54	90:10

[a]Isolated yield after 18 h; [b]Determined by ^{1}H NMR.

1.10.3 Room Temperature Catalytic-in-Phosphine Staudinger Reductions with DPDS

The next reaction that we explored was the Staudinger reduction, seeking to develop the first catalytic-in-phosphine method under ambient conditions. **DPDS**-mediated catalytic Staudinger reductions proceeded smoothly, using 10 mol% **1PPO** and 1.0 equivalents of the silane to reduce multiple benzyl azides and an aliphatic azide to the corresponding amine in high yields over 18 hours at 23 °C (Table 1.10). It is again notable that the reducible nitro group remains completely untouched by this method. The stability of the primary alkyl chloride (entry 4) is also impressive.

Table 1.10. Catalytic Staudinger Reactions Employing **DPDS** at Room Temperature

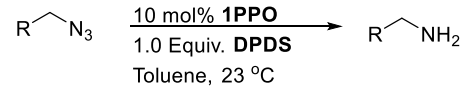

Entry	Azide	Product	Yield[a]
1	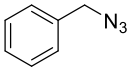	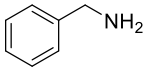	92
2	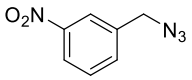	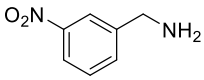	90
3	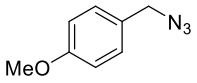	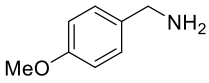	85
4	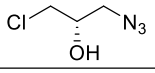	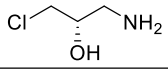	82

[a]Isolated yield after 18 h.

1.10.4 Room Temperature Catalytic-in-Phosphine Appel Reactions with DPDS

Finally, we performed catalytic Appel reactions using the bromonium donor originally identified by van Delft and coworkers.[114] Initially we used 10 mol% of the precatalyst **1PPO**, but van Delft and coworkers specifically noted that at high temperature **1PPO** is too nucleophilic and reacts with the bromine containing products.[115] Phosphetanes are known to have very low nucleophilicity,[116] so we decided to test the precatalyst **TMPPO** in place of **1PPO**. This switch

improved each of the yields by up to 15%, presumably due to better stability of the products when in the presence of the phosphine. Overall, our yields are increased compared to the original version at 80 °C developed by van Delft and coworkers.[117] We were unable to overcome the key limitation of their original methodology, the lack of product formation when the substrate is a secondary alcohol, meaning our methodology is improved compared to theirs, but would benefit from additional development.

Table 1.11. Catalytic Appel Reactions Employing **DPDS** at Room Temperature

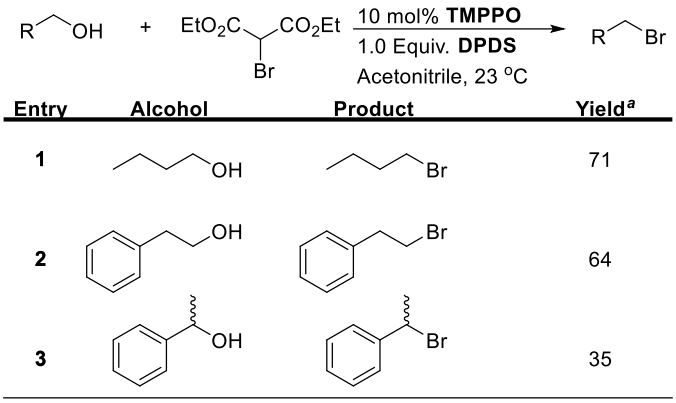

[a]Isolated yield after 18 h.

The development of these three ambient catalytic-in-phosphine reactions demonstrates the wide utility and chemoselectivity of **DPDS** in facilitating *in situ* phosphine recycling. We believe that **DPDS** will become the reagent of choice for phosphine recycling, due to its impressive bench-top stability, excellent chemoselectivity, remarkable potency, and broad applicability across reaction classes. Using it is also both simple, as it requires no additional additives, and cheap, as per our previously described large-scale synthesis.

1.11 Isolated Phosphine Oxide Reductions with DPDS

1.11.1 DPDS is a Superior Reducing Agent for TPPO

Having explored the phosphine recycling applications for **DPDS**, we next wanted to investigate its applicability in the broader area of general phosphine oxide reduction. New

phosphine ligands are continually being designed to tune the electronic and steric properties of transition metal complexes, facilitating access to novel transformations and the improvement of existing methods. As mentioned previously, the final step in the synthesis of many phosphine ligands is reduction of the corresponding phosphine oxide,[118] and the broad range of functional groups present in these ligands[119] necessitate agents and conditions that chemoselectively react with the P=O bond.

Currently, the state-of-the-art reduction conditions are overnight reactions utilizing a silane at temperatures upwards of 100 °C in combination with a catalytic additive. Lemaire and co-workers described the use of $Ti(O^iPr)_4$ and 1.25 equiv of **TMDSO**,[120] while Beller and co-workers disclosed that 15 mol% bis-(*p*-nitrophenyl)-phosphoric acid (**BNPA**) promotes reduction with diethoxymethylsilane (4 equiv).[121] Lemaire's method is more atom economical but lacks broad functional group tolerance, while the conditions reported by Beller have improved chemoselectivity but require a full 4 equiv of silane to be heated with the phosphine oxide for 48 h and can still require protecting groups for certain chemical moieties. Laboratory-scale syntheses of phosphines would be greatly enhanced with a rapid, chemoselective, and low-temperature method for reduction of phosphine oxides, eliminating protecting group usage and broadening the applicability of this process, while industrial-scale syntheses would benefit from a more atom-economical and additive-free method to reduce waste generation and improve the ease of purification.

In our initial foray with **TPPO**, we used 12.5 equivalents of silane in order to obtain pseudo-first order conditions with respect to the phosphine (Figure 1.17). This is far too many equivalents to by synthetically useful, so we started anew in attempting to develop an additive-free system in toluene using **TPPO** as our model substrate. To make our system as simple to implement as possible, we performed all reactions without the exculsion of air or water. Heating to 110 °C for 24 h sans additives, a substoichiometric amount of **DPDS** (0.75 equiv) provided an 80% yield of

triphenylphosphine (Table 1.12, Entry 1), which highlights the impressive activity of this new reagent. However, to complete reduction within 24 h, a slight excess of **DPDS** was required (Table 1.12, Entry 2). An investigation of "green" solvents indicated that toluene (PhMe) and *tert*-butyl acetate (TBAc) were optimal for this reduction. Switching the solvent to TBAc for better solubility, we consistently obtained a 99% yield of triphenylphosphine using 1.25 equivalents of **DPDS** in 24 h (Table 1, Entry 5).

Table 1.12. The Optimization of Additive-Free Phosphine Oxide Reductions with **DPDS**. Yields are the average from two reactions at 0.5 mmol scale after 24 h.

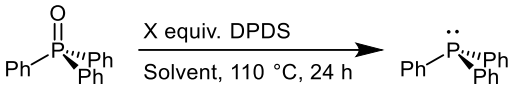

Entry	X Equiv.	Solvent	Yield (%)
1	0.75	PhMe	80
2	1.5	PhMe	99
3	1.0	TBAc	90
4	1.1	TBAc	97
5	1.25	TBAc	99

A real-time comparison of our optimized reaction to those reported by Beller and Lemaire revealed that our system, under "dump-and-stir" conditions as described above, is the fastest of the three (Figure 1). Notably, Lemaire's conditions struggled without the exclusion of air and water, while Beller's method undergoes a reaction trajectory that matches a single-exponential due the fact that a large excess of silane (4 equiv) was employed. Despite utilizing no additives and only a stoichiometric amount of silane, our system completes reduction in approximately half of the time of the current state-of-the-art conditions.

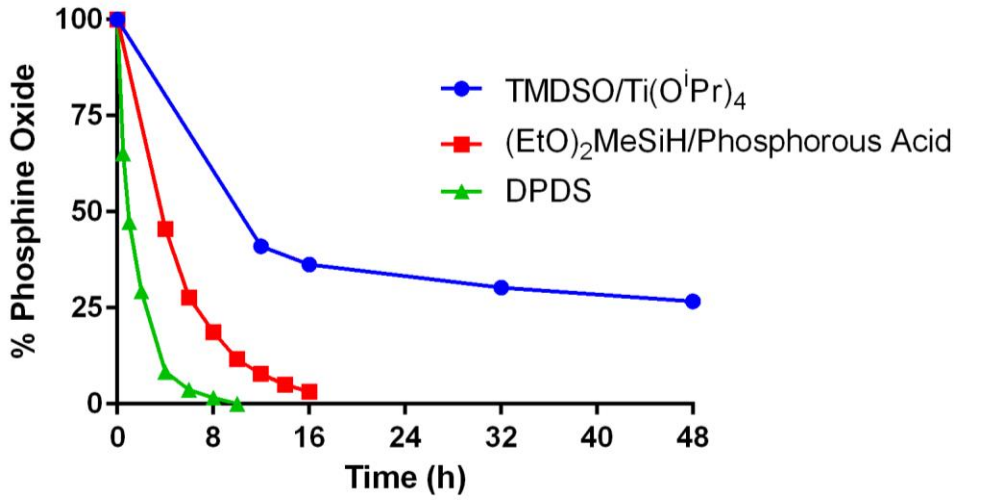

Figure 1.33. Comparison of the Reduction Rates of Our System, Lemaire's, and Beller's. All reductions were run under "dump and stir" conditions without the exclusion of air or water.

1.11.2 The Energy of Activation of Phosphine Oxide Reduction with DPDS

We next investigated the energies of activation with Arrhenius analysis, specifically to compare the activation energies we observe between acyclic and cyclic precatalysts, as well as to compare it with the relevant predicted transition state energies. The reduction of **TPPO** by **DPDS** was found to have an activation barrier of only 18.0 ± 1.1 kcal/mol (Figure 1.34). While ring strain is well-known to enhance the rate in which the P=O bond is reduced, only a modest decrease in the activation barrier is observed with **TMBPO** (ΔG^{++} = 14.2 ± 0.9 kcal/mol, Figure 1.35). Notably, these observed energies of activation are significantly lower than those calculated by Krenske (27.2 kcal/mol) for the 4-membered transition state resulting from a [2+2] reaction between hydridosilanes and phosphine oxides (TS-1). We credit this significant difference to the lower energy of the six-membered transition state (TS-2) achieved by the combination of hydrogen-bond donating silanols and phosphine oxides. These data are further evidence towards the assertion that hydridosilanes are incompetent reductants at temperatures below 120 °C.

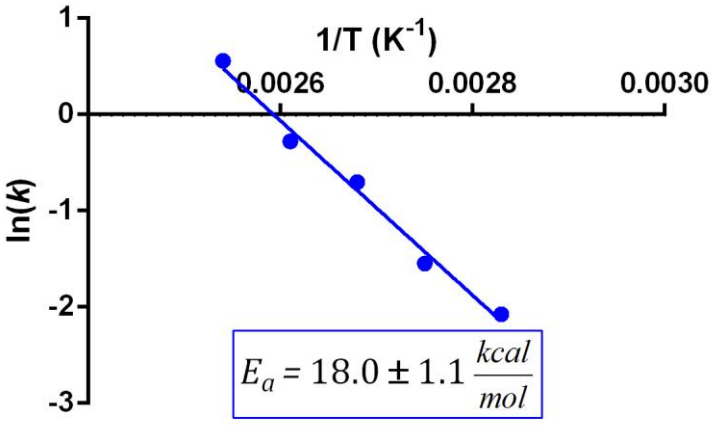

Figure 1.34. Arrhenius Analysis of the Reduction of **TPPO** by **DPDS**. Each data point is from obtained from reaction progress curves run in triplicate.

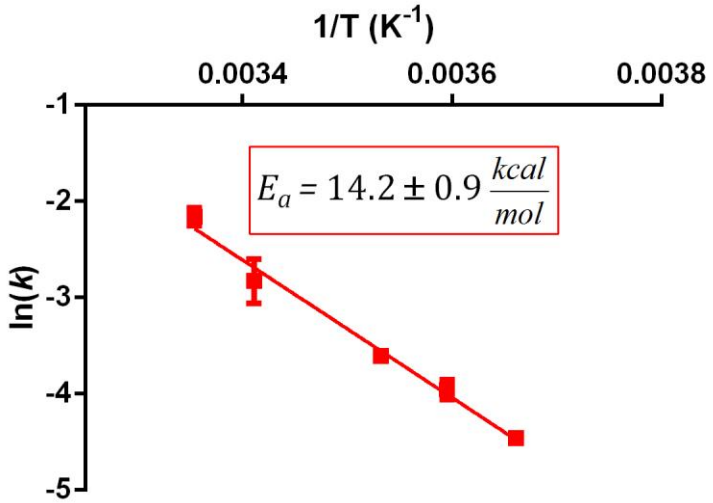

Figure 1.35. Arrhenius Analysis of the Reduction of **TMBPO** by **DPDS**. Each data point is from obtained from reaction progress curves run in triplicate.

1.11.3 The Substrate Scope of Additive-Free Reduction with DPDS

Returning to our optimized "dump and stir" conditions for the reduction of **TPPO** to triphenylphosphine, we examined the scope of **DPDS** reduction with a diverse panel of acyclic phosphine oxides (Table 1.13). Both electron-rich and electron-deficient tertiary phosphine oxides were cleanly reduced producing high yields of the corresponding phosphines with yields ranging from 80–99%. Somewhat surprisingly, trialkylphosphine oxides reduced more slowly

than phosphines bearing an aryl substituent. The reaction also worked well on 10 mmol scale, as the reduction of **TPPO** again occurred in quantitative yield. Bidentate phosphine oxides were also successfully reduced (Table 2, entries 5–9) with high fidelity in yields ranging from 75–94%. Reduction of chiral phosphine oxide to the corresponding phosphine occurred with retention of configuration, consistent with our proposed mechanism. Lastly, the secondary phosphine oxide diphenylphosphine oxide was by far the most rapidly reduced, with quantitative conversion in 10 minutes.

Table 1.13. The Substrate Scope of Additive-Free Reductions of Phosphine Oxides by **DPDS**. Yields are the isolated average from two reactions at 0.5 mmol scale.

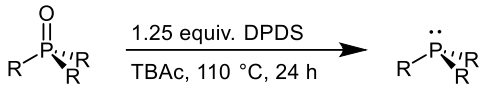

Entry	Phosphine	Yield (%)
1	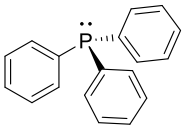	99
2	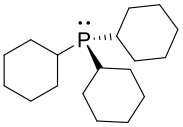	80
3	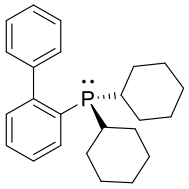	93
4	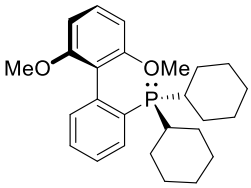	87
5	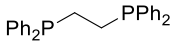	88
6	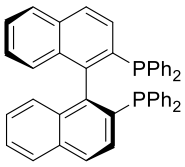	94
7	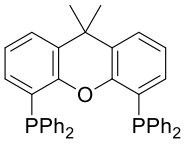	79
8	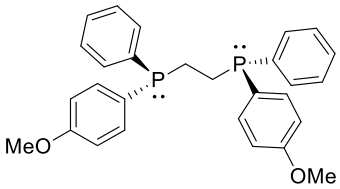	75
9	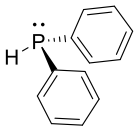	>99

1.11.4 Room Temperature Reduction of Acyclic Phosphine Oxides with DPDS in Combination with BNPA

Even though our reduction of phosphine oxides with **DPDS** represents the mildest conditions for this functional group transformation, we were interested in slashing promiscuous reactivity even further. We were encouraged to pursue reduction at ambient temperatures by the results of our Arrhenius analyses, as only a modest decrease in activation energy would be needed. To this effect, we investigated the combination of **DPDS** with Beller's phosphoric acid additive (**BNPA**), in an attempt to reduce the heat needed for these reductions. We noted that **BNPA** facilitated reduction with alkoxysilanes and hoped that this additive would bolster reactivity with our disiloxane. Our previous results also indicated compatibility between unprotected alcohols and **DPDS**, with or without an additive, as long as the temperature was maintained around ambient temperature (Table 1.7, Figure 1.32). We were delighted to find that addition of a combination of **BNPA** and **DPDS** to a solution of **TPPO** in EtOAc (used for solubility of **BNPA**) furnished the phosphine product in quantitative yield after 48 hours. Applying similar conditions (2.5 equiv **DPDS** per P=O bond, 20 mol% **BNPA** per P=O) to a range of acyclic phosphorous(V) oxides consistently afforded the product phosphines in both high yield and high specificity (Table 1.14). In parallel to our additive-free reductions, reducing electron-rich phosphine oxides with multiple alkyl substituents was slower, requiring a 70 hour reaction time. While these phosphine oxides were reduced rather slowly, the corresponding phosphines were produced in exquisite purity, oftentimes requiring simple filtration through a silica-gel plug. Similar to our methodology employing solely **DPDS**, a wide range of functional groups were tolerated, as mono- and bis-phosphine oxides were reduced efficiently, with high selectivity.

Table 1.14. The Substrate Scope of Room Temperature Reductions of Phosphine Oxides by **DPDS** and **BNPA**. Yields are the isolated average from two reactions at 0.5 mmol scale.

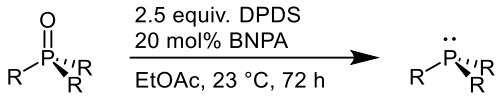

Entry	Phosphine	Yield (%)
1	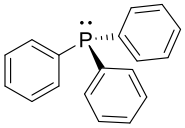	99
2	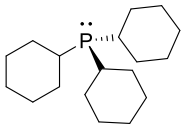	84
3	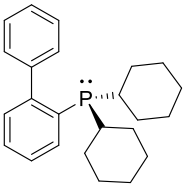	92
4	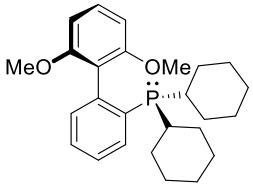	82
5	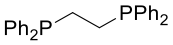	96
6	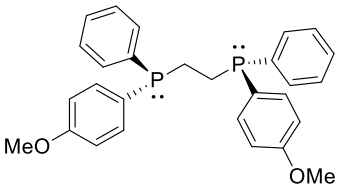	89
7	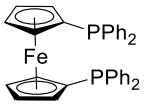	83
8	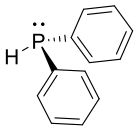	>99

1.12 Conclusion

Our initial interest in developing a room-temperature catalytic-in-phosphine reaction led us to design phosphetane precatalysts which were hypothesized to lower the energy barrier to silane-mediated reduction through increased ring strain and/or electron density on the oxygen of the P=O. These catalysts only provided a mild increase of the rate of reduction and displayed substantial stability concerns, but we observed that a conventional understanding of the reduction process could not account for a post-initiation rate increase. However, our data was of insufficient quality to definitively prove mechanistic theories, so we switched to VT-NMR and wrote a program that auto-integrated our NMR spectra. This new method of data collection facilitated a comprehensive kinetic and mechanistic investigation into silane-mediated phosphine oxide reduction. This led to several breakthroughs, with the most important likely the discovery that silane reduction of phosphine oxides at temperatures lower than 120 °C does not proceed through TS-1, but rather through the 6-membered transition state TS-2. Therefore, only hydrido-silanols, hydrido-disilazanes, or metallic hydrido-silyl-oxy species can reduce phosphine oxides at such temperatures, a theory that explains numerous reported reactivity trends among silane species.

We also thoroughly characterized the reductive process with phenylsilane, demonstrating that it requires a Lewis-basic catalyst to activate it to form phenylsilanol. In typical reduction systems with phenylsilane, the phosphine oxide serves as this catalyst. Synthesis of **DPDS**, which equilibrates with phenylsilanol in solution, allowed reduction to bypass that unproductive pre-activation step, and furnished by far the most potent silane reductant to date. **DPDS** was evaluated for its functional group tolerance, which was found to be exceptional, with the only blemish being a transient protection of alcohols when heated to 80 °C. Ironically, we could not accomplish our original goal of developing a room temperature catalytic Mitsunobu due to rapid reduction of the Huisgen intermediate by **DPDS** even under ambient conditions. However, **DPDS**

did facilitate the first additive-free ambient catalytic-in-phosphine Wittig reaction, and the first overall ambient catalytic-in-phosphine Appel and Staudinger reactions.

Next, we assessed the reductive potential of **DPDS** against acyclic phosphines for use in phosphine synthesis. Alone, it facilitated the fastest reduction of **TPPO** at 110 °C to date with only 1.25 equivalents of the reducing agent, far below the state-of-the-art conditions requiring 4 equivalents of diethoxymethylsilane and 15 mol% **BNPA**. Additionally, these reactions were extremely simple to set up, requiring the exclusion of neither air nor water. Mono- and bis-phosphines, both electron-deficient and electron-rich, were furnished from the corresponding oxides in 75-99% yield. We also developed a room temperature variant of this process where we used **BNPA** in combination with **DPDS** to reduce multiple acyclic phosphines in 82-99% yield. The potency of **DPDS** can thus either be used to render reduction additive-free or heat-free.

We anticipate that **DPDS** will become the reagent of choice for both *in situ* phosphine recycling and phosphine synthesis due to its excellent chemoselectivity and impressive potency. The development of multiple methods for the chemoselective room-temperature reduction of phosphine oxides should also enable the synthesis of functionally diverse phosphines from their corresponding oxides. Finally, and perhaps most importantly, we have dispelled many incorrect assumptions about the overall process. Scientists that attempt to improve the phosphine oxide reduction process now understand the requirements for reduction, an extremely key step to future development by either our group or any of the others that are working towards the same goals

1.13 Materials and Methods

All commercially available reagents were used without further purification. **1PPO** and **TMPPO** were synthesized as previously described. All synthesized phosphines were stored at -20 °C wrapped in foil to exclude light and all synthesized silanes were stored at ambient temperature in a desiccator with colored walls to exclude UV light. Molecular sieves were activated by

heating at 200 °C under reduced pressure. Tetrahydrofuran (THF), toluene, and dichloromethane (DCM) were dispensed from an Inert® solvent dispensing system. Deuterated THF was purchased from Sigma-Aldrich in dry 1 gram ampules and used without further drying. Deuterated chloroform, DCM, and toluene were purchased from Cambridge Isotopes and used without further drying from 10 gram bottles stored in a desiccator. Lithium chloride was stored in a desiccator and dried with a Bunsen burner immediately before use. Anhydrous magnesium chloride was dried and stored in a dessicator prior to use. Zinc chloride was purified in its molten form to remove water and hydrogen chloride from the salt immediately before use. Anhydrous sodium sulfate was purchased and used without further purification. Piperidine was distilled over calcium hydride under reduced pressure immediately before use. ^{1}H, ^{13}C, ^{19}F, and ^{31}P NMR spectra were recorded on a Varian 400 MHz spectrometer, Bruker Avance 500 MHz spectrometer, or Varian INOVA 600 MHz spectrometer with broadband probes. High resolution mass spectra were collected on a Bruker BioTOF II mass spectrometer using PEG or PPG internal standards. Silica gel column chromatography was performed with silica gel (Dynamic Absorbents, 60A) or using a Teledyne-Isco RF-200 Combi-Flash system. Kugelrohr distillations were performed with a Buchi glass oven B-585 instrument. Enantiomeric ratios (ERs) were determined using a Chiralcel OJ column on a Waters 2695 HPLC system with a Waters 2996 PDA for detection.

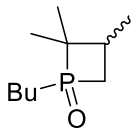

rac-1-*n*-butyl-2,2,3-Trimethylphosphetane-1-oxide (**TMBPO**). To a flame-dried two-neck round bottom flask equipped with a stir bar was added dried magnesium(0) powder (50 mesh, 0.43 g, 18 mmol), THF (2 mL), and one crystal of iodine. Stirring was initiated and a solution of bromobutane (1.6 mL, 15 mmol) in THF (13 mL) was added dropwise. When addition of the

bromide was complete, the reaction was refluxed for 2 h. The reaction was then cooled to 0 °C and a solution of **S1** (1.992 g, 12 mmol) in THF (10 mL) was added dropwise to the stirring solution of **S2**. The reaction was allowed to warm to 23 °C and stirred for 16 h. After 16 h, the reaction was quenched by the addition of H_2O (25 mL). The layers were separated and the aqueous layer was washed with DCM (3 × 25 mL). The organics were combined and dried ($MgSO_4$). The reaction was concentrated *in vacuo* to a yellow oil and loaded onto silica gel. Purification by flash column chromatography on silica gel (40 g SiO_2, 0–10% MeOH:DCM eluent, linear gradient) afforded the title compound (1.30 g, 57%) as off-white needles: R_f = 0.62 (5:95 MeOH:DCM) stained with iodine. ^{1}H NMR (500 MHz, $CDCl_3$) δ 2.46-2.40 (m, 1H), 2.10-2.04 (m, 1H), 1.86-1.82 (m, 1H), 1.73-1.70 (app. m, 2H), 1.68-1.65 (m, 2H), 1.49-1.45 (m, 2H), 1.26-1.16 (app. dd, 6H), 1.03-1.02 (d, 3H), 0.97-0.94 (t, 3H); ^{13}C NMR (125 MHz) δ 49.0, 37.3, 30.2, 25.9, 24.2, 23.7, 22.5, 1, 6.1, 14.4, 13.7; ^{31}P {^{1}H} NMR (202 MHz, $CDCl_3$) δ 49.68. HRMS for $C_{10}H_{21}NaOP$ [M + Na^+] calculated 211.122; found 211.1225.

Additional purification: Preparatory TLC (5:95 MeOH:DCM) was used to purify small amounts of **TMBPO** for some syntheses of this molecule. In order to visualize this molecule with iodine, heat iodine crystals and then drop into the TLC chamber. Top spot (stains yellow with iodine) is desired product.

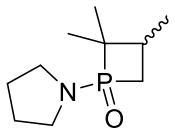

rac-2,2,3-Trimethyl-1-pyrrolidinylphosphetane-1-oxide (**TMPyrPO**). To a flame-dried round bottom flask equipped with a stir bar was added **S1** (2.16 g, 13 mmol), toluene (13 mL), trimethylamine (2.2 mL, 16 mmol), and pyrrolidine (1.2 mL, 14.6 mmol) sequentially. The reaction was sealed, purged with argon, and heated to 60 °C for 24 hours. After 24 hours, the reaction was cooled to 23 °C and filtered. The cake was washed with EtOAc (10 mL). The filtrate

was combined with the EtOAc wash, which were subsequently washed with 5% aqueous sodium bicarbonate (20 mL), dried ($MgSO_4$) and concentrated *in vacuo* to afford the title compound (1.96 g, 75%) as an orange oil and mixture of diastreomers: ^{1}H NMR (500 MHz, $CDCl_3$, Mixture of diastereomers) δ 3.33-3.23 (m, 4H), 2.65-2.60 (m, 1H), 2.14-2.06 (m, 1H), 1.91-1.88 (m, 4H), 1.58-1.53 (app. M, 1H), 1.23-1.17 (app. dd, 6H), 1.03-1.02 (d, 3H); ^{13}C NMR (125 MHz) δ 52.9, 52.3, 46.6,37.8, 37.3, 26.6, 23.2, 17.5, 14.5; ^{31}P {^{1}H} NMR (202 MHz, $CDCl_3$, Mixture of diastereomers) δ 48.83, 47.73. HRMS for $C_{10}H_{20}NNaOP$ [M + Na^+] calculated 224.1175; found 224.1199.

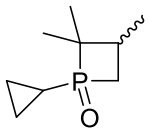

rac-1-cyclopropyl-2,2,3-Trimethylphosphetane-1-oxide (TMCypPO). To a flame-dried two-neck round bottom flask equipped with a stir bar was added dried magnesium(0) powder (50 mesh, 0.43 g, 18 mmol), THF (2 mL), and one crystal of iodine. Stirring was initiated and a solution of bromocyclopropane (1.3 mL, 15 mmol) in THF (13 mL) was added dropwise. When addition of the bromide was complete, the reaction was refluxed for 2 h. The reaction was then cooled to 0 °C and a solution of **S1** (2.0 g, 12 mmol) in THF (10 mL) was added dropwise to the stirring solution of **S3**. The reaction was allowed to warm to room temperature and was stirred for 16 h. After 16 h, the reaction was quenched by the addition of deionized water (25 mL). The layers were separated and the aqueous layer was washed with DCM (3 × 25 mL). The organic layers were combined and dried with $MgSO_4$, concentrated *in vacuo* to a yellow oil, and loaded onto silica gel. Purification by flash column chromatography on silica gel (40 g SiO_2, 0–10% MeOH:DCM eluent, linear gradient) afforded the title compound (730 mg, 32%) as a yellow oil and mixture of diastereomers: R_f = 0.60 (5:95 MeOH:DCM) stained with iodine. ^{1}H NMR (500 MHz, $CDCl_3$, Major diastereomer) δ 2.4-2.38 (m, 1H), 2.12-2.04 (m, 1H), 1.96-1.92 (m, 1H),

1.21-1.16 (app. dd, 6H), 0.99-0.98 (d, 3H), 0.87-0.74 (m, 4H); ^{13}C NMR (125 MHz, $CDCl_3$, Mixture of diasteromers) δ 49.0, 48.6, 46.6, 37.3, 36.9, 30.2, 25.9, 25.5, 24.3, 23.7, 22.6, 16.6, 16.1, 14.4, 14.2, 13.7, 12.1, 11.7; ^{31}P {^1H} NMR (202 MHz, $CDCl_3$, Mixture of Diastereomers) δ 48.08 (major), 55.97 (minor). HRMS for $C_9H_{18}OP$ [M + H^+] calculated 173.1090; found 173.1086.

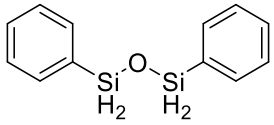

1,3-Diphenyl-disiloxane (**DPDS**).

Initial method from the chlorosilane – To a separatory funnel charged with 10 g of partially melted ice was added a solution of chlorophenylsilane (2 g, 14 mmol, 2.14 mL) in diethyl ether (8 mL). The reaction was allowed to warm and was swirled by hand every ten minutes for an hour. Then, more diethyl ether (15 mL) was added to the reaction and the aqueous layer was drained. The ether was washed with water (10 mL) and then dried with MgSO4. The reaction was filtered and the solvent was evacuated in-vacuo. The crude mixture was purified by Kugelrohr distillation to give 1.64 g (82%) of a colorless and clear oil. bp = 155 °C at 0.8 mmHg. NMR spectra and other physical data matched that of previous reports.[122]

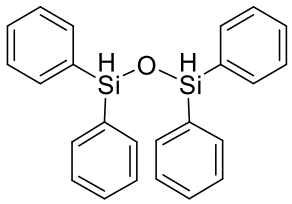

1,1,3,3-Tetraphenyl-disiloxane (**TPDS**). To a separatory funnel charged with 10 g of partially melted ice was added a solution of chlorodiphenylsilane (2.09 g, 9.6 mmol, 2.0

mL) in diethyl ether (8 mL). The reaction was allowed to warm and was swirled by hand every ten minutes for an hour. Then, more diethyl ether (15 mL) was added to the reaction and the aqueous layer was drained. The ether was washed with water (10 mL) and then dried with $MgSO_4$. The reaction was filtered and the solvent was evacuated *in-vacuo*. The crude mixture was purified by Kugelrohr distillation to give 1.65 g (90%) of a colorless solid (at 23 °C). bp = 290 °C at 0.6 mmHg. NMR spectra and other physical data matched that of previous reports.[123]

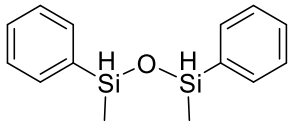

1,3-Dimethyl-1,3-diphenyl-disiloxane (**DMDPDS**). To a separatory funnel charged with 10 g of partially melted ice was added a solution of chloro(methyl)phenylsilane (2.19 g, 13.9 mmol, 2.1 mL) in diethyl ether (8 mL). The reaction was allowed to warm and was swirled by hand every ten minutes for an hour. Then, more diethyl ether (15 mL) was added to the reaction and the aqueous layer was drained. The ether was washed with water (10 mL) and then dried with $MgSO_4$. The reaction was filtered and the solvent was evacuated *in-vacuo*. The crude mixture was purified by Kugelrohr distillation to give 1.46 g (81%) of a colorless and clear oil. bp = 150 °C at 0.8 mmHg. NMR spectra and other physical data matched that of previous reports.[124]

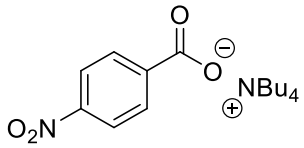

Tetra-*n*-butyl ammonium-*p*-nitrobenzoate. To a round bottom flask equipped a stir bar was added *p*-nitrobenzoic acid (500 mg, 3.0 mmol), tetrabutylammonium bromide (1.0 g,

3.0 mmol), and THF (10 mL). The reaction was fitted with a reflux condenser and heated to 80 °C for 28 h. The reaction was cooled to 23 °C and concentrated *in vacuo.* The residue was taken up in cold toluene (15 mL), filtered, and concentrated *in vacuo* to afford the title compound (1.00 g, 82%) as a yellow solid: NMR spectra and other physical data matched that of previous reports.[125]

Procedure for Phosphine Screen in the Catalytic Mitsunobu Reaction.

To a 2-dram vial equipped with a stir bar was added *p*-nitrobenzoic acid (125 mg, 1.5 equiv, 0.75 mmol) and **1PPO**, **TMPPO**, **TMBPO**, or **TMPyrPO** (0.1 equiv, 0.05 mmol). THF (2 mL) was added followed by benzyl alcohol (57 μL, 1.00 equiv, 0.50 mmol), DIAD (108 μL, 1.10 equiv, 0.55 mmol), and then phenylsilane (1.1 equiv, 0.55 mmol). Reactions were sealed with a PTFE septum in the screw cap and heated to 80 °C. After 18 hours, the reaction was cooled and concentrated directly onto silica gel. Benzyl 4-nitrobenzoate was purified with all spectra matching previously published spectra.

Procedure for Silane Screen in the Catalytic Mitsunobu Reaction.

To a 2-dram vial equipped with a stir bar was added *p*-nitrobenzoic acid (125 mg, 1.5 equiv, 0.75 mmol) and **1PPO**, **TMPPO**, or **TMBPO** (0.1 equiv, 0.05 mmol). THF (2 mL) was added followed by benzyl alcohol (57 μL, 1.00 equiv, 0.50 mmol), DIAD (108 μL, 1.10 equiv, 0.55 mmol), and then silane (1.1 equiv, 0.55 mmol). Reactions were sealed with a PTFE septum in the screw cap and heated to 80 °C. After 18 hours, the reaction was cooled and concentrated directly onto silica gel. Benzyl 4-nitrobenzoate was purified with all spectra matching previously published spectra.

Procedure for Reduction of Phosphine Precatalysts with Phenylsilane at Room Temperature.

To an NMR tube was added a phosphine oxide precatalyst (0.02 mmol, 0.04 M), d_8-toluene or d_8-THF (final volume of 500 μL), and phenylsilane (24.6 μL, 10 equiv., 0.2 mmol, 0.4 M). The tube was inverted three times to ensure proper mixing of the reagents and the interface between the tube and the cap was sealed with multiple layers of paraffin wax (parafilm®) to ensure no leaks. The reaction was heated to 25 °C and monitored by ^{31}P NMR.

Procedure for the Reduction of TPPO by DPDS for Figure 1.17.

To an NMR tube was added d_8-toluene (440 μL), **DPDS** (58 mg, 0.25 mmol, 0.5 M), and **TPPO** (5.6 mg, 0.02 mmol, 0.04 M). The tube was inverted three times to ensure proper mixing of the reagents and the interface between the tube and the cap was sealed with multiple layers of paraffin wax (parafilm®) to ensure no leaks. The reaction was heated to 110 °C and monitored with ^{31}P NMR.

Procedure for the reduction of 1PPO by TMDSA

To an NMR tube was added **1PPO** (3.7 mg, 1.0 equiv., 0.02 mmol, 0.04 M), d_2-DCM (458 μL), and **TMDSA** (42.0 μL, 15.0 equiv., 0.3 mmol, 0.6 M). The tube was inverted three times to ensure proper mixing of the reagents and the interface between the tube and the cap was sealed with multiple layers of paraffin wax (parafilm®) to ensure no leaks. The reaction was heated to 80 °C and monitored with ^{31}P NMR.

Procedure for the Reduction of 1PPO by TMDSO with Protic Acids.

To an NMR tube was added **1PPO** (3.7 mg, 1.0 equiv., 0.02 mmol, 0.04 M), d_8-THF (440 μL), **TMDSO** (53.0 μL, 15.0 equiv., 0.3 mmol, 0.6 M), and either TFA (7.6 μL, 5.0 equiv., 0.1 mmol, 0.2 M) or AcOH (6.0 μL, 5.0 equiv, 0.1 mmol, 0.2 M). The tube was inverted three times to ensure proper mixing of the reagents and the interface between the tube and the cap was sealed with multiple layers of paraffin wax (parafilm®) to ensure no leaks. The reaction was heated to 80 °C and monitored by ^{31}P NMR.

Procedure for the Reduction of 1PPO by TMDSO with Lewis Acids.

To an NMR tube was added **1PPO** (3.6 mg, 0.02 mmol, 0.04 M), d_8-THF (447 μL), **TMDSO** (53 μL, 0.3 mmol, 0.6 M), and LiCl, $MgCl_2$, or $ZnCl_2$ (0.1 mmol, 0.2 M). The tube was inverted three times to ensure proper mixing of the reagents and the interface between the tube and the cap was sealed with multiple layers of paraffin wax (parafilm®) to ensure no leaks. The reaction was heated to 80 °C and monitored by ^{31}P NMR for 7 h.

Procedure for the Reduction of 1PPO by $PhSiH_3$ with Lewis Acids.

To three separate NMR tubes was added **1PPO** (0.02 mmol, 0.04 M), d_8-THF (475 μL), and then $PhSiH_3$ (25 μL, 0.2 mmol, 0.4 M). To one of the tubes was added LiCl (4 mg, 0.1 mmol, 0.2 M) and to another was added $ZnCl_2$ (6.8 mg, 0.05 mmol, 0.1 M). All three tubes were inverted three times to ensure proper mixing of the reagents and the interface between the tubes and their respective caps were sealed with multiple layers of paraffin wax (parafilm®) to ensure no leaks. The reactions were heated to 80 °C and monitored by ^{31}P NMR.

General Procedure of Catalytic Staudinger Ligations (Ashfeld).

To a 2-dram vial equipped with a stir bar was added 4-nitrobenzoic acid (50a mg 0.3 mmol, 1.0 equiv.), **TPP** (13 mg, 0.05 mmol, 0.17 equiv.) or **TPPO** (13.8 mg, 0.05 mmol, 0.17 equiv.), toluene (1 mL), benzyl azide (45 □L, 0.36 mmol, 1.2 equiv.) followed by phenylsilane (36 µL, 0.3 mmol, 1.0 equiv.). The reaction was sealed and stirred at various temperatures. After 18 h, the reaction was diluted with acetone (5 mL) and loaded directly onto silica gel (200 mg). Purification by flash column chromatography (0–50% EtOAc:hexanes eluent, step-wise gradient, 10% EtOAc incremental increase every 6 column volumes) afforded the product.

General Procedure of Stoichiometric Staudinger Ligations (Ashfeld).

To a 2-dram vial equipped with a stir bar was added 4-nitrobenzoic acid (50.1 mg, 0.3 mmol, 1.0 equiv.), **TPP** (88mg, 0.33 mmol, 1.1 equiv.) toluene (1 mL), and then benzyl azide (45 µL, 0.36 mmol, 1.2 equiv.). The reaction was sealed and stirred at various temperatures. After 18 h, the reaction was diluted with acetone (5 mL) and loaded directly onto silica gel (200 mg). Purification by flash column chromatography (0–50% EtOAc:hexanes eluent, step-wise gradient, 10% EtOAc incremental increase every 6 column volumes) afforded the product.

Procedure for Analysis of the Reaction of TMCypPO with DPDS.

To an NMR tube was added **TMCypPO** (3.6 mg, 0.02 mmol, 0.04 M), d_8-toluene (450 µL), and **DPDS** (53 mg, 7.5 equiv., 0.15 mmol, 0.3 M). The tube was inverted three times to ensure proper mixing of the reagents and the interface between the tube and the cap was sealed with multiple layers of paraffin wax (parafilm®) to ensure no leaks. The reaction was heated to 25 °C and monitored by ^{31}P NMR and ^{1}H NMR. After 4 h, the

crude reaction mixture was poured from the NMR tube into a 1 dram vial. Aqueous hydrogen peroxide (30 %, 200 µL) was then added to the reaction mixture and the reaction was shaken on an orbital shaker for 10 minutes at 25 °C in which a color change to bright yellow was observed. The crude mixture was then diluted with DCM (3 mL) and samples were diluted another 1000-fold with acetonitrile. Samples were analyzed with an LC-MS using a C-18 column (Section 7.2.4) and an electrospray ionization source in positive mode. The ions corresponding to *m/z* = 173 and 175 were extracted from the total ion source to monitor the presence of the cyclopropyl and *n*-propyl compounds, respectively.

Procedure for Analysis of the Reaction of TMCypPO with TMDSO and Ti(^{i}OPr)$_4$.

To an NMR tube was added **TMCypPO** (3.6 mg, 0.02 mmol, 0.04 M), d_8-toluene (481.7 µL), **TMDSO** (17.7 µL, 5.0 equiv., 0.10 mmol, 0.2 M), and then Ti(^{i}OPr)$_4$ (0.6 µL, 0.1 equiv., 0.002 mmol, 0.004 M). The tube was inverted three times to ensure proper mixing of the reagents and the interface between the tube and the cap was sealed with multiple layers of paraffin wax (parafilm®) to ensure no leaks. The reaction was heated to 80 °C and monitored by ^{31}P NMR. After 4 h, the crude reaction mixture was poured from the NMR tube into a 1 dram vial. Aqueous hydrogen peroxide (30 %, 200 □L) was then added to the reaction mixture and the reaction was shaken on an orbital shaker for 10 minutes at 25 °C in which a color change to bright yellow was observed. The crude mixture was then diluted as in section 7.1 and monitored by LC-MS using a C-18 column (Section 7.2.4) and an electrospray ionization source in positive mode. The ions

corresponding to *m/z* = 173 and 175 were extracted from the total ion source to monitor the presence of the cyclopropyl and *n*-propyl compounds, respectively.

Procedure for Reduction of TMPPO by DMDPDS.

To an NMR tube was added a phosphine oxide precatalyst (0.02 mmol, 0.04 M), d_8-toluene, or d_8-THF (475 μL), and then silane (10 equiv., 0.15 mmol, 0.3 M). The tube was inverted three times to ensure proper mixing of the reagents and the interface between the tube and the cap was sealed with multiple layers of paraffin wax (parafilm®) to ensure no leaks. The reaction was heated to 80 °C and monitored with ^{31}P NMR.

Procedure for the Reduction of 1PPO by DHDS.

To an NMR tube was added **1PPO** (0.02 mmol, 0.04 M), d_8-THF (460 μL), and then **DHDS** (37 mg, 7.5 equiv., 0.15 mmol, 0.3 M). The tube was inverted three times to ensure proper mixing of the reagents and the interface between the tube and the cap was sealed with multiple layers of paraffin wax (parafilm®) to ensure no leaks. The reaction was monitored with a variable temperature ^{31}P NMR experiment at 80 °C.

Procedure for Testing the Reactivity of DPDS with Carboxylic Acids

To an NMR tube was added 3-(trifluoromethyl)-benzoic acid (19 mg, 0.1 mmol), d_8-THF or d_8-Toluene (0.5 mL), and then **DPDS** (53 mg, 0.22 mmol). The tube was sealed with a cap and inverted three times to ensure proper mixing of the reagents and the interface between the tube and the cap was sealed with multiple layers of paraffin wax (parafilm®) to ensure no leaks. The reaction was heated to 80 °C and monitored by ^{19}F NMR.

Procedure for Testing the Reactivity of DPDS with Alcohols

To an NMR tube was added d_8-THF (0.5 mL), 4-(trifluoromethyl)-benzyl alcohol (13.7 μL, 1.0 equiv, 0.10 mmol), hexafluorobenzene (11.5 μL, 1.0 equiv, 0.1 mmol) and **DPDS** (53 mg, 2.2 equiv, 0.22 mmol). The tube was inverted three times to ensure proper mixing of the reagents and the interface between the tube and the cap was sealed with multiple layers of paraffin wax (parafilm®) to ensure no leaks. The reactions were either heated to 80 °C or kept at 23 °C and monitored by ^{19}F NMR.

Procedure for Testing the Reactivity of DPDS with Alcohols in the Presence of Benzoic Acids

To an NMR tube was added 3-(trifluoromethyl)-benzoic acid (19 mg, 1.0 equiv, 0.10 mmol) or *p*-nitrobenzoic acid (16 mg, 1.0 equiv., 0.10 mmol), d_8-THF (0.5 mL), 4-(trifluoromethyl)-benzyl alcohol (13.7 μL, 1.0 equiv, 0.10 mmol), hexafluorobenzene (11.5 μL, 1.0 equiv, 0.1 mmol) and **DPDS** (53 mg, 2.2 equiv, 0.22 mmol). The tube was inverted three times to ensure proper mixing of the reagents and the interface between the tube and the cap was sealed with multiple layers of paraffin wax (parafilm®) to ensure no leaks. The reactions were either heated to 80 °C or kept at 23 °C and monitored with ^{19}F NMR.

Procedure for Testing the Reactivity of DPDS with Aldehydes

To an NMR tube was added 4-cyanobenzaldehyde (13.1 mg, 1.0 equiv, 0.10 mmol), d_8-THF (0.5 mL), and **DPDS** (53 mg, 2.2 equiv, 0.22 mmol). The tube was inverted three times to ensure proper mixing of the reagents and the interface between the tube and the cap was sealed with multiple layers of paraffin wax (parafilm®) to ensure no leaks. The reaction was heated to 80 °C and monitored with ^{1}H NMR.

Procedure for Testing the Reactivity of DPDS with DIAD

To an NMR tube was added DIAD (4.9 µL, 1.0 equiv, 0.025 mmol), d_8-THF (0.5 mL), 3-(trifluoromethyl)-benzoic acid (4.7 mg, 1.0 equiv, 0.025 mmol), and **DPDS** (13 mg, 2.3 equiv, 0.056 mmol). The tube was inverted three times to ensure proper mixing of the reagents and the interface between the tube and the cap was sealed with multiple layers of paraffin wax (parafilm®) to ensure no leaks. The reaction was heated to 80 °C and monitored by ^{1}H NMR through observation of a shift in ppm of the methine protons. After 2.5 h, the NMR tube was cooled to 23 °C, opened, and **TMPPO** (1 mg, 0.2 equiv, 0.005 mmol) was added. The tube was resealed, mixed, heated to 80 °C, and monitored by ^{1}H NMR.

1.14 Proof that a Phosphine Concentration Dependence Demonstrates Reduction does not Proceed by a Multi-Step Process

We first will represent the kinetic mechanism where reduction goes through a semi-stable intermediate and involves two steps through the figure below:

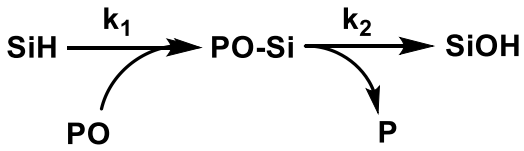

It is important to note that this is the kinetic mechanism being discussed. The real mechanism that would go through this kinetic mechanism includes phenylsilane, phenylsilanol, phenylsilanediol, and phenylsilanetriol. However, if, as was assumed prior to this paper, phenylsilane reduced phosphine oxides at a similar or greater rate than phenylsilanol and phenylsilanediol, then through reduction monitoring only k_1 and k_2 for

phenylsilane will be able to be extracted from the data, not whatever *k* values would exist for the same mechanism with phenylsilanol or phenylsilanediol. This is, again, due to the pseudo-first order nature of the experiment, so we can assume that the concentration of phenylsilane does not change throughout the course of the reaction. If a small amount of phenylsilanol is formed and it reduces at the same speed or slower, then its effect on the overall reduction progress will be negligible because of the >10x amount of phenylsilane present.

With that established, and remembering that we are making the assumption that phenylsilane is an equal or better reductant than phenylsilanol or phenylsilanediol, we can write the rate of formation of the intermediate species and phosphine formation:

$$Rate_{inter} = k_1[PO][SiH]$$

$$Rate_p = k_2[PO - SI]$$

We are using pseudo-first order conditions, so [SiH] is constant, and we can let $K_1 = k_1[SiH]$:

$$Rate_{inter} = K_1[PO]$$

$$Rate_p = k_2[PO - SI]$$

Using this combination of equations, we can solve for [P] and [PO-Si] as a function of time, k_1, k_2, and the initial concentration of [PO] (written as $[PO]_0$).

$$[PO - Si] = [PO]_0 * (\frac{K_1}{k_2 - K_1} e^{-K_1 t} + \frac{K_1}{K_1 - k_2} e^{-k_2 t})$$

$$[P] = [PO]_0 - [PO]_0 * (\frac{k_2}{k_2 - K_1} e^{-K_1 t} + \frac{K_1}{K_1 - k_2} e^{-k_2 t})$$

If we take [P] and divide it by the initial concentration of PO, we obtain:

$$\frac{[P]}{[PO]_0} = \frac{k_2}{k_2 - K_1} e^{-K_1 t} + \frac{K_1}{K_1 - k_2} e^{-k_2 t}$$

Therefore, the left side of the equation is equal to an expression that does not have $[PO]_0$ in it, an expression that is only dependent on the rate constants and the time. When we drew the graphs with %PO remaining on the y-axis, what we were basically doing is dividing the concentration of phosphine oxide present by $[PO]_0$. This quantity, then, should not change regardless of the value of $[PO]_0$. Since changing $[PO]_0$ does have an effect on the rate, the proposed multi-step mechanism with a semi-stable intermediate cannot be correct. It is also noteworthy that this data strongly supports the notion that phosphine oxide catalyzes the formation of phenylsilanol, as this provides a reason for the rate to increase when $[PO]_0$ increases.

1.15 LC-MS Traces for "Radical Clock" Experiment

TMCypPO Reduction with **TMDSO** & 10 mol% $Ti(^iPrO)_4$ (Lemaire's Conditions)

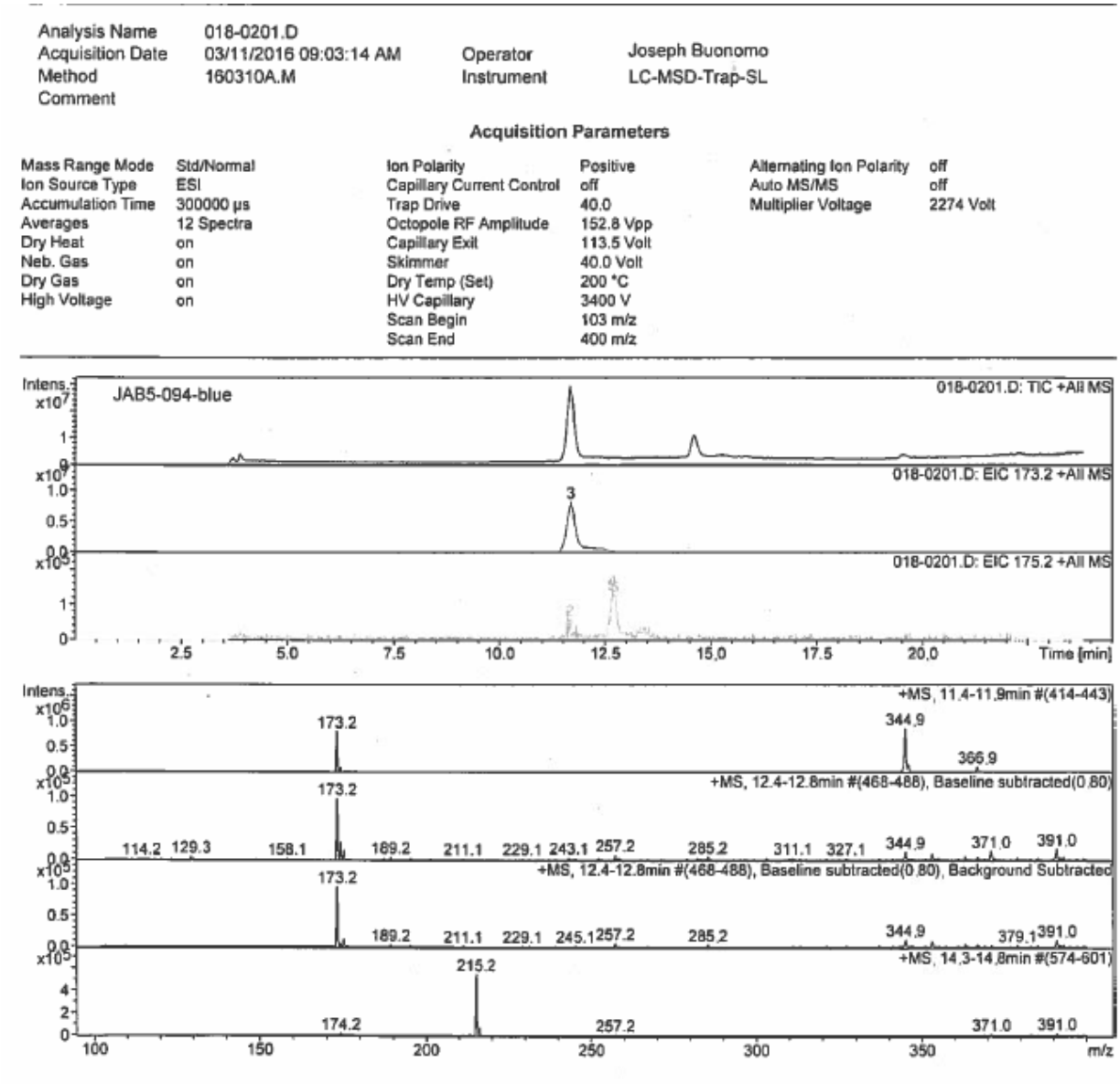

TMCypPO Reduction with **DPDS** (Standard Conditions)

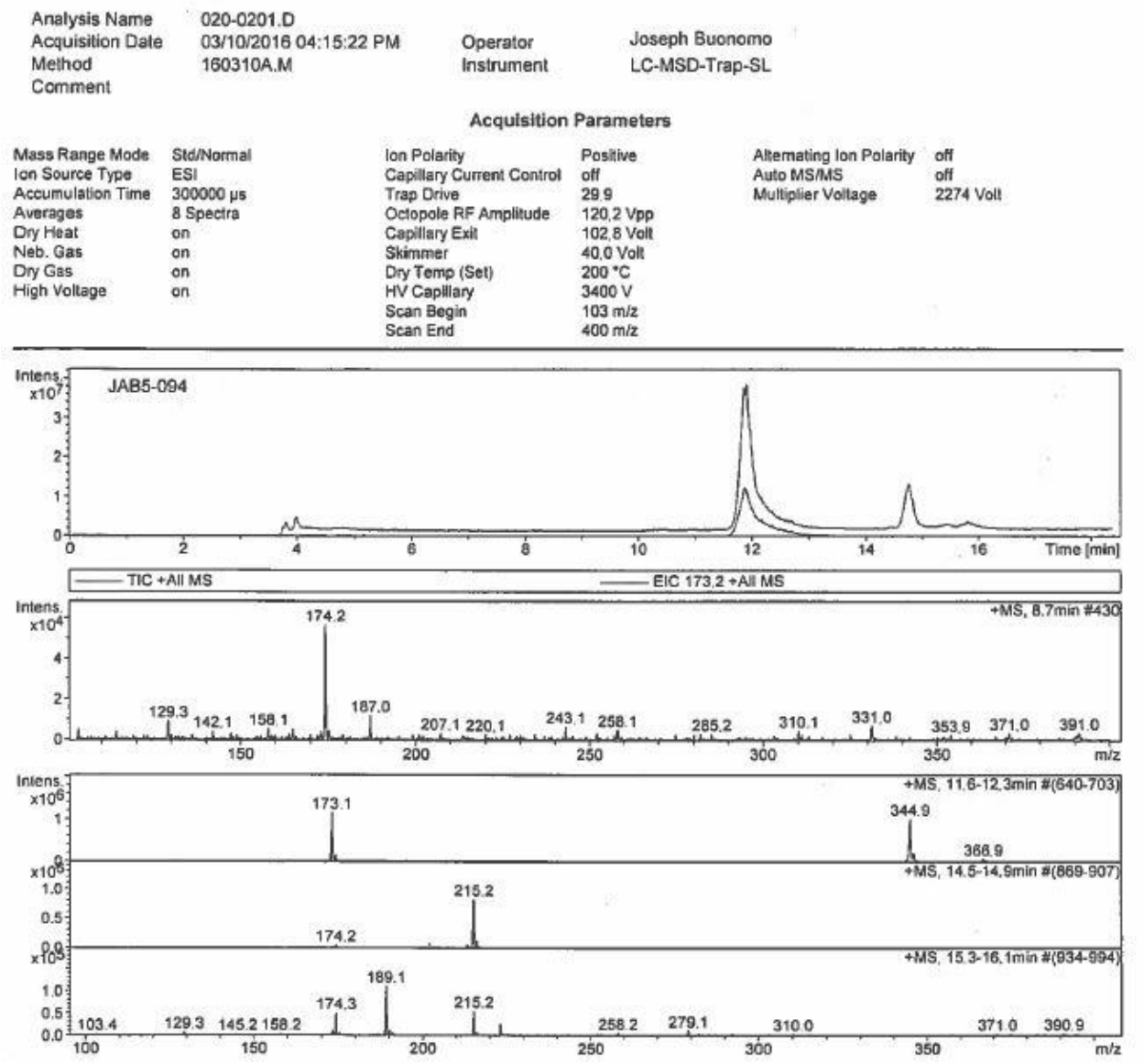

1.X16 ^{1}H, ^{31}P, and ^{13}C NMR Spectra

<u>TMBPO</u>:

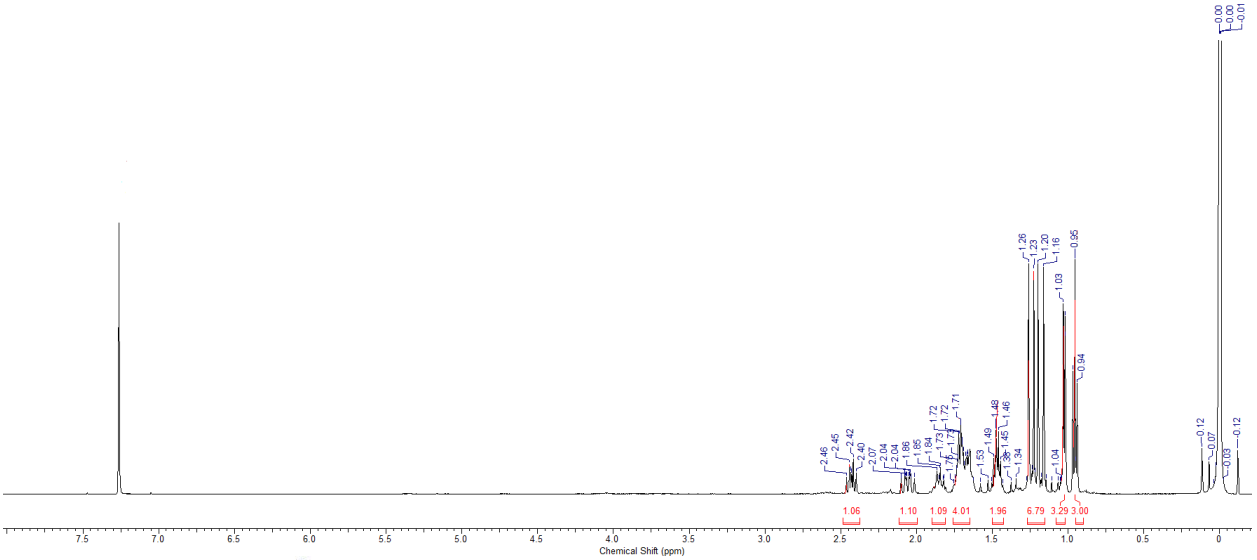
Chemical Shift (ppm)

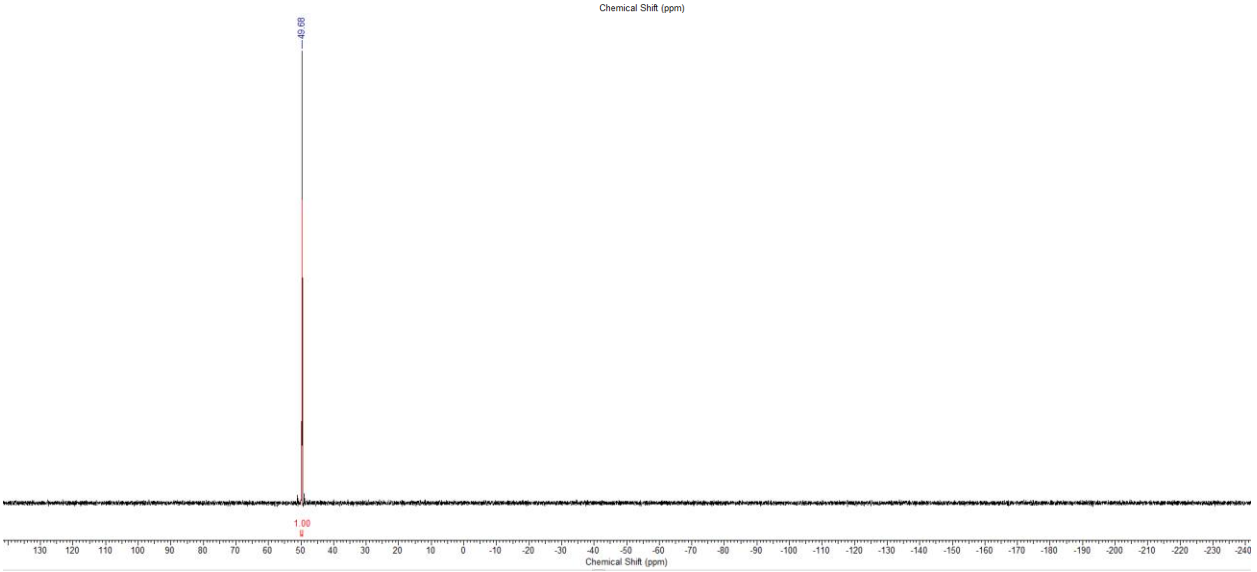
Chemical Shift (ppm)

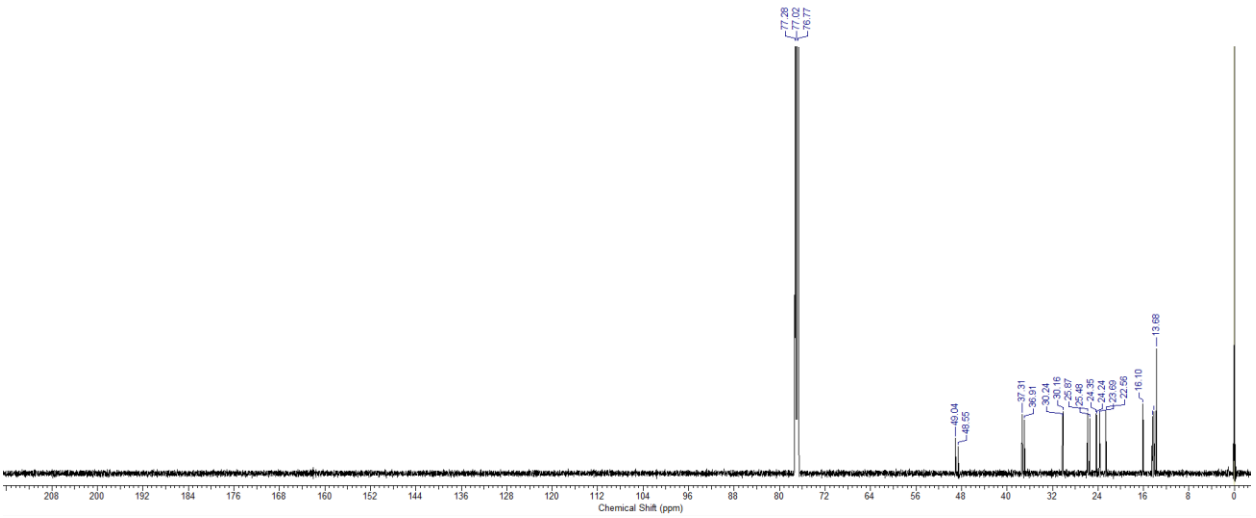
77.28
77.02
76.77
49.04
48.55
37.31
36.91
30.14
30.16
25.87
25.48
24.35
24.24
23.69
22.56
16.10
13.68
Chemical Shift (ppm)

TMPyrPO:

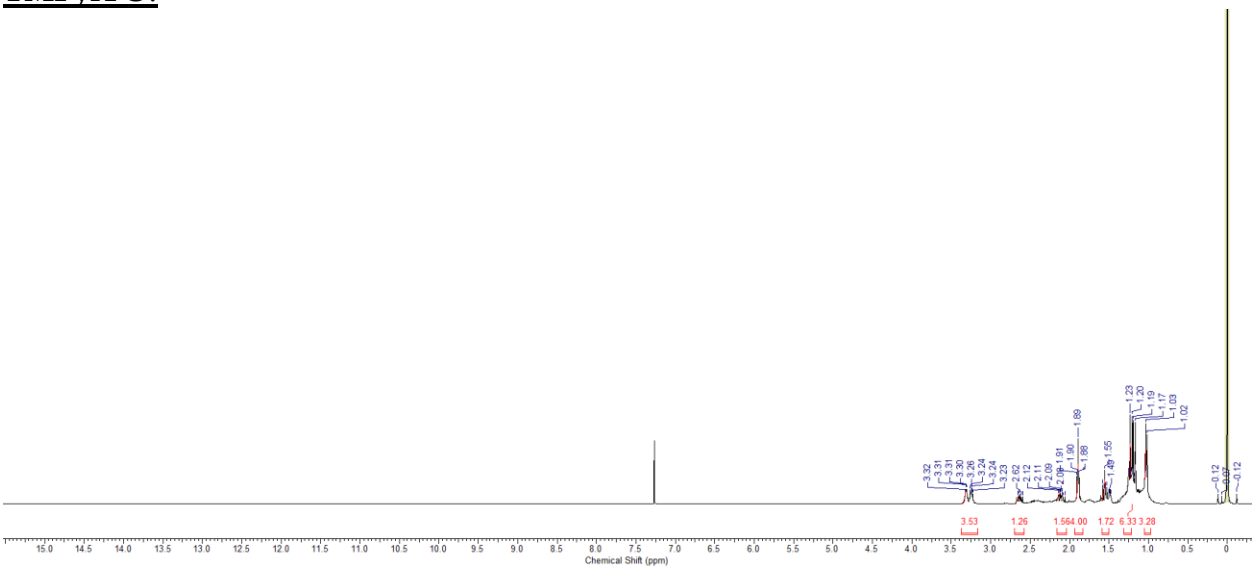
3.32
3.31
3.30
3.26
3.24
3.03
3.02
2.12
2.11
2.09
2.07
1.91
1.90
1.89
1.88
1.55
1.23
1.20
1.19
1.17
1.03
1.02
0.12
0.12
3.53
1.26
1.56
4.00
1.72
6.33
3.28
Chemical Shift (ppm)

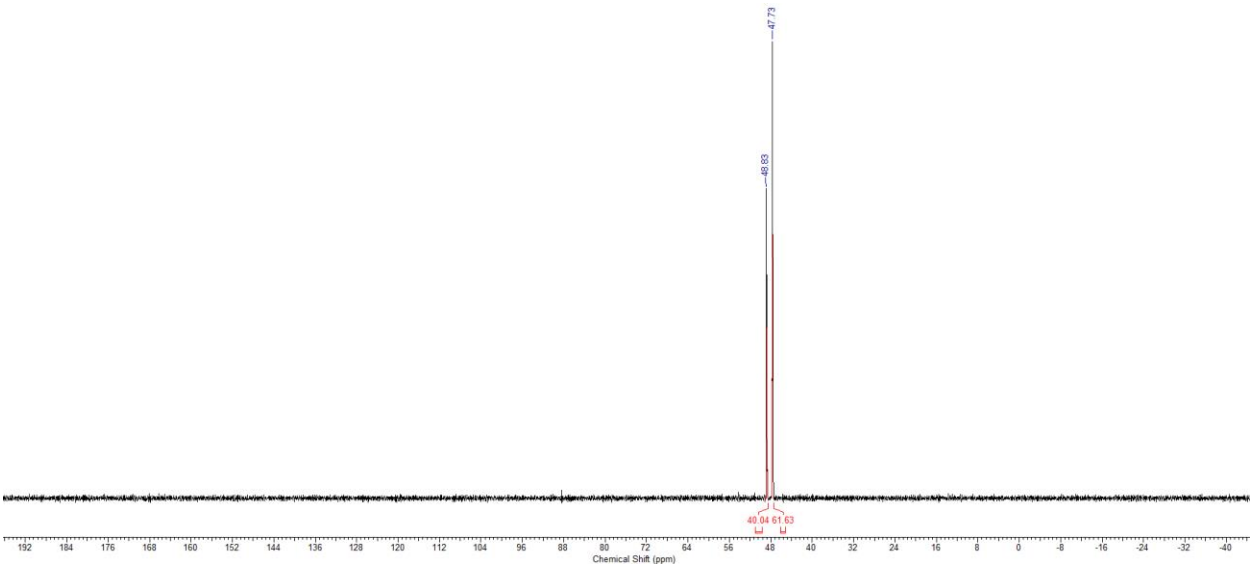
49.73
48.83
40.04
61.63
Chemical Shift (ppm)

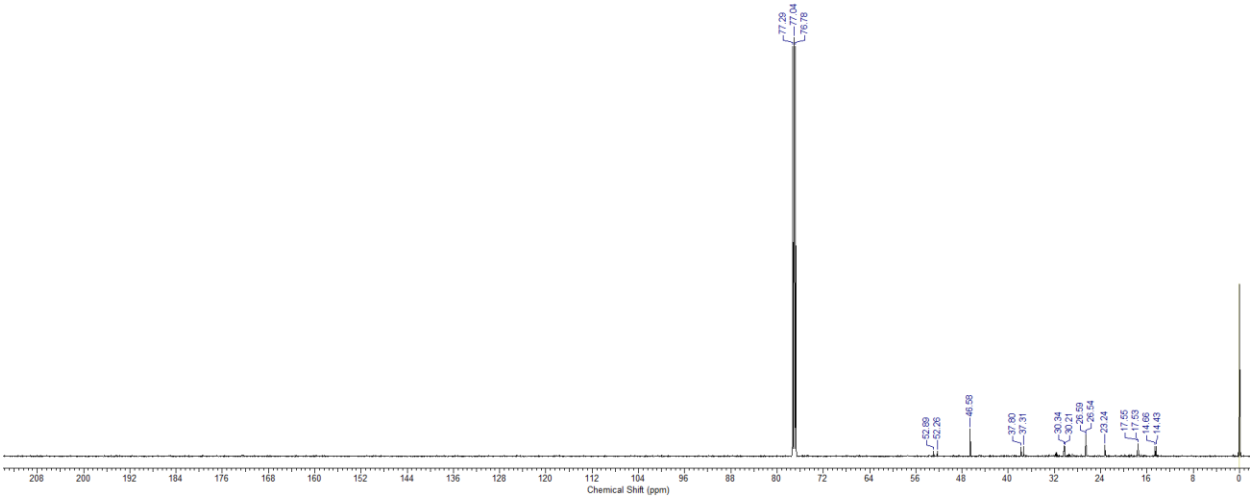
77.29
77.04
76.78
52.89
52.26
46.59
37.80
37.31
30.34
30.21
26.59
26.54
23.24
17.55
17.53
14.66
14.43
Chemical Shift (ppm)

TMCypPO:

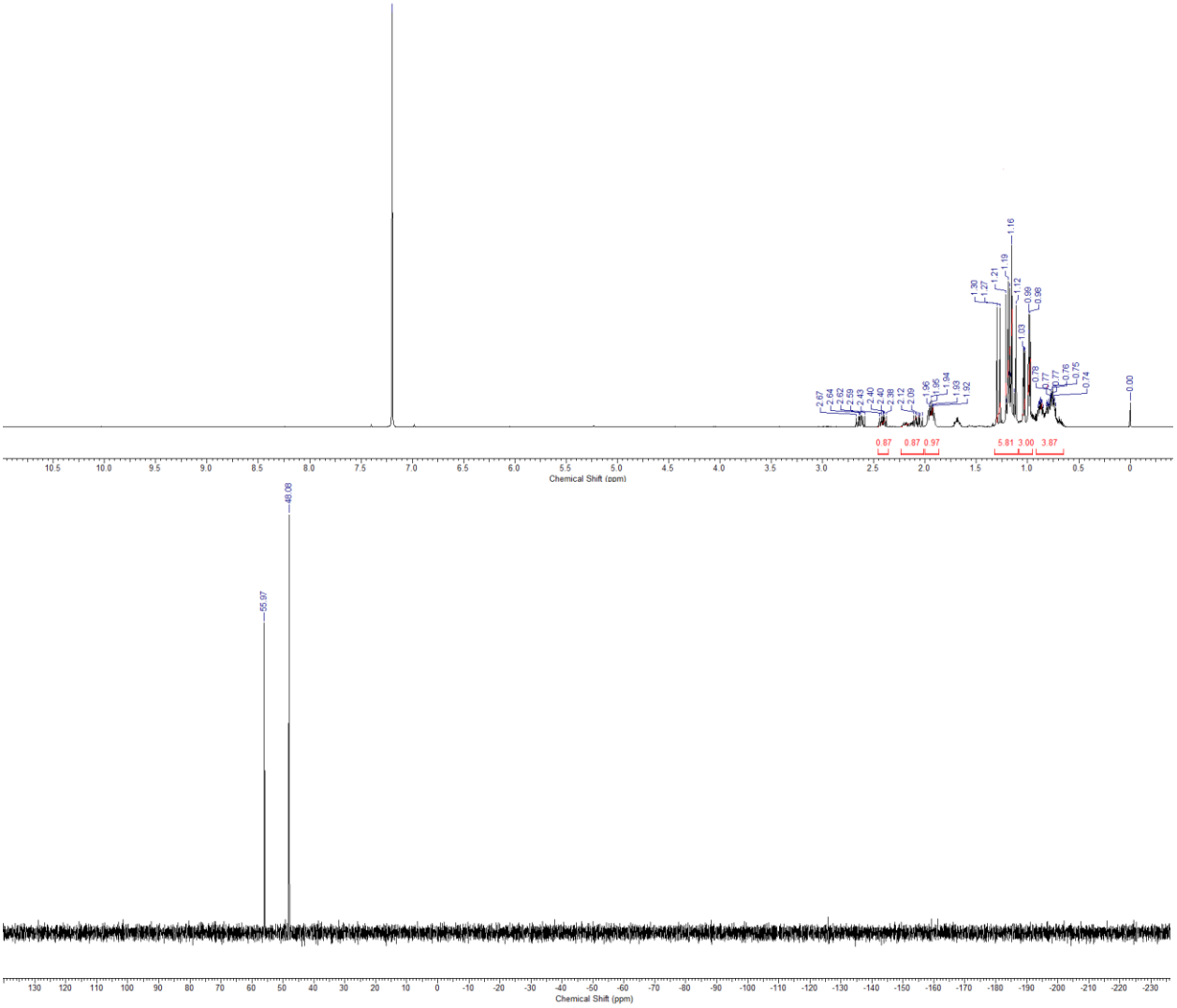
2.67
2.64
2.62
2.59
2.43
2.40
2.40
2.38
2.12
2.09
2.06
1.95
1.94
1.69
1.92
1.30
1.27
1.21
1.19
1.16
1.12
0.99
0.98
1.03
0.78
0.77
0.77
0.76
0.75
0.74
0.00
0.87
0.87
0.97
5.81
3.00
3.87
Chemical Shift (ppm)
55.97
49.08
Chemical Shift (ppm)

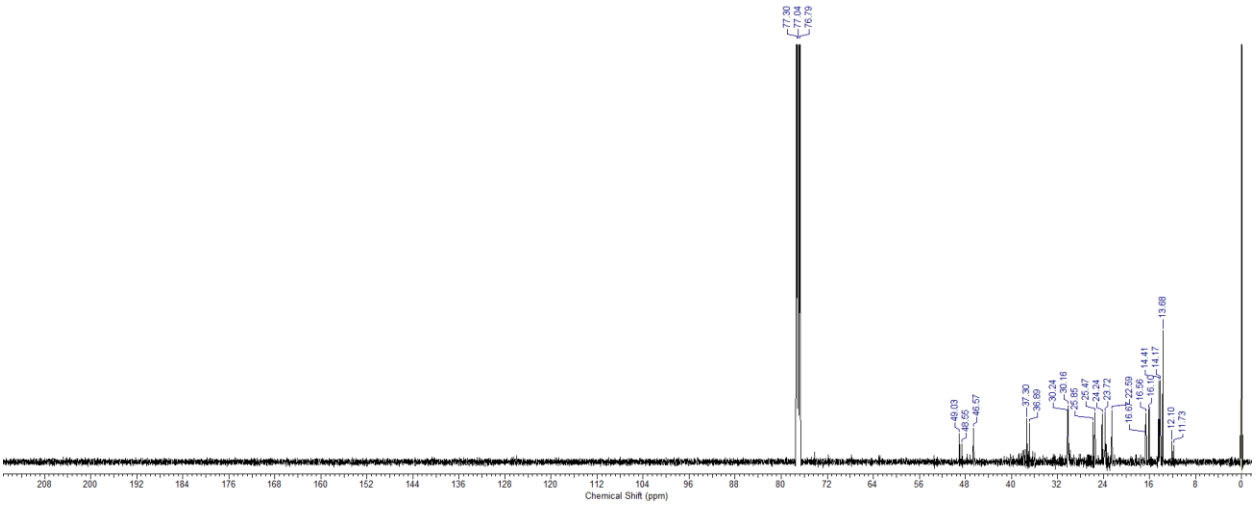
77.30
77.04
76.79
49.03
48.55
46.57
37.30
36.89
30.24
30.16
25.86
25.47
24.24
23.72
22.59
16.56
14.41
14.17
13.69
12.10
11.73
Chemical Shift (ppm)

DPDS:

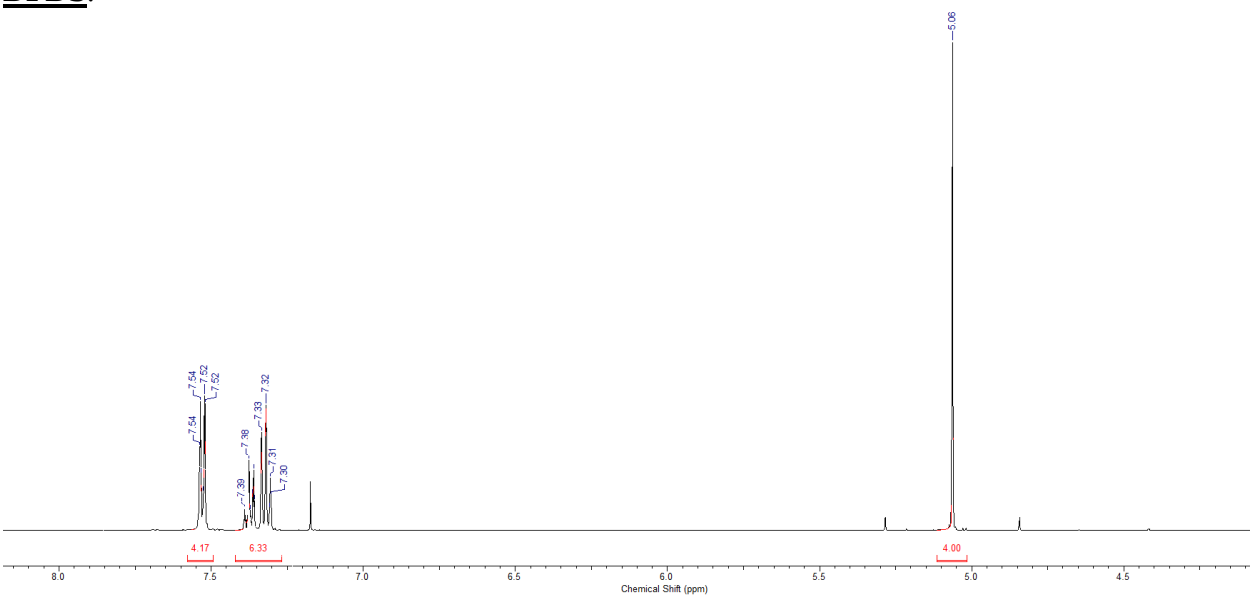
5.06
7.64
7.62
7.52
7.54
7.39
7.38
7.33
7.32
7.31
7.30
4.17
6.33
4.00
Chemical Shift (ppm)

TPDS:

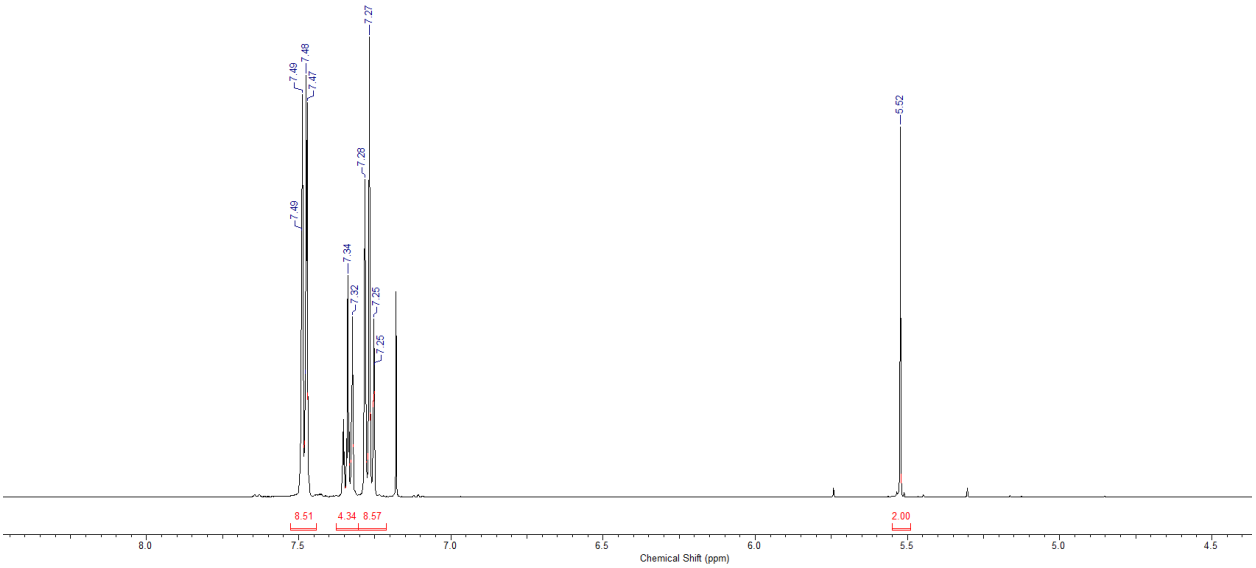

DMDPDS:

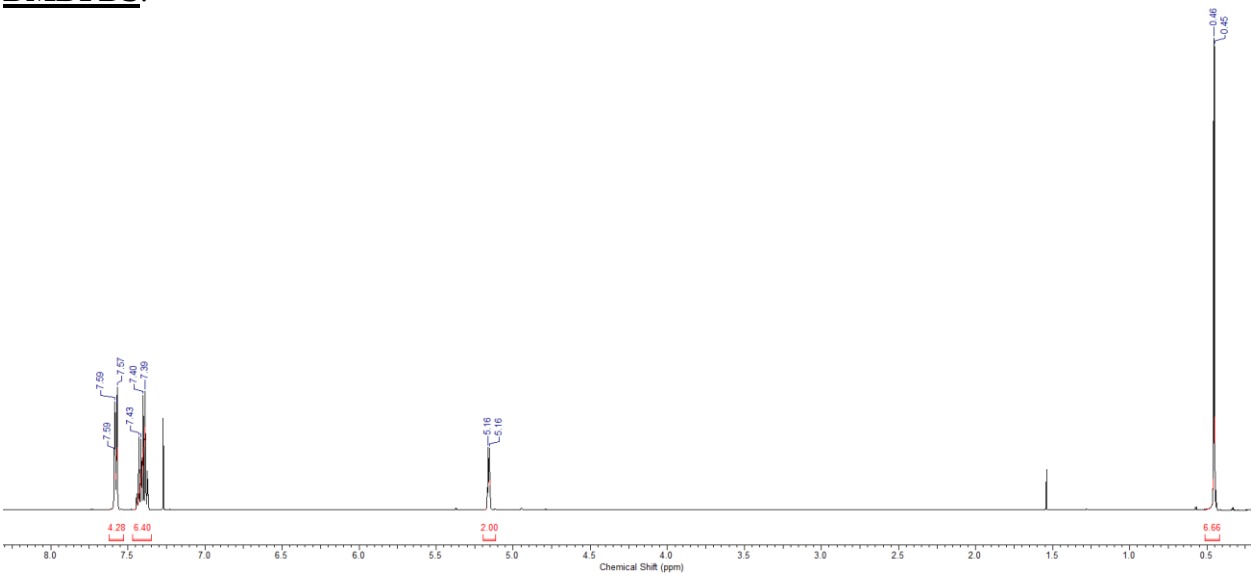

Ethyl (E)-cinnamate:

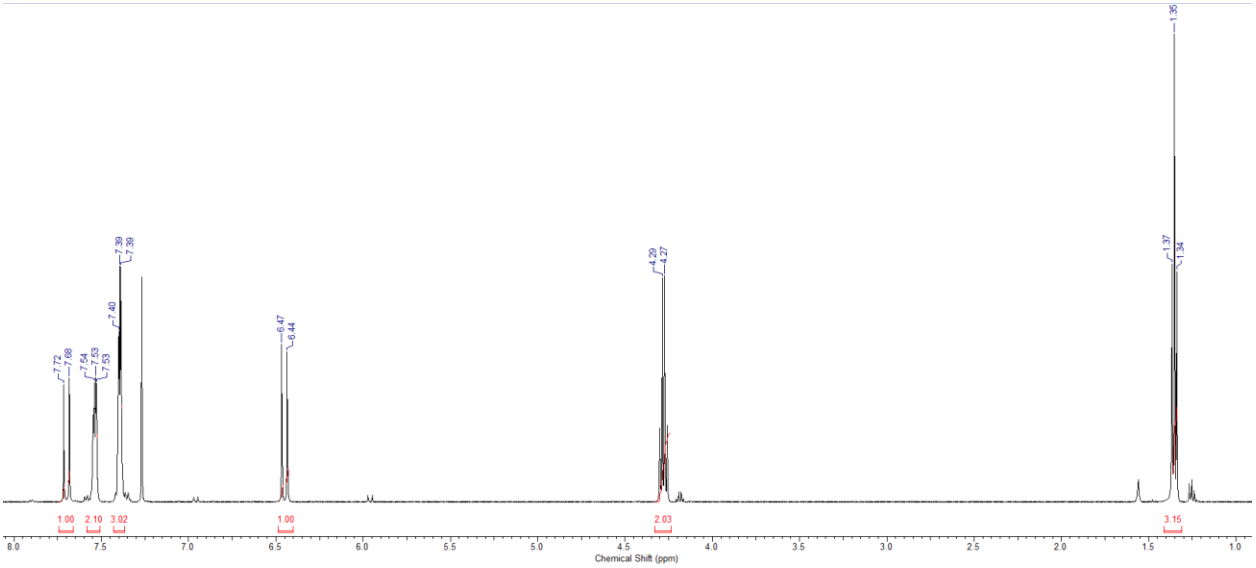

(E)-1,3-Diphenyl-propen-3-one:

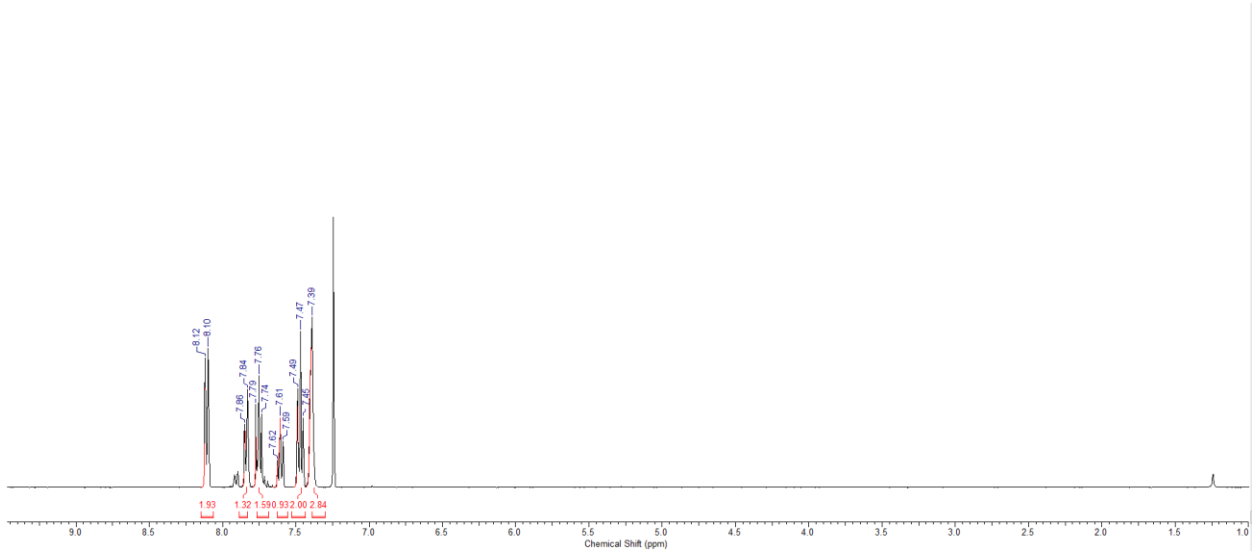

Ethyl (E)-*p*-methoxycinnamate:

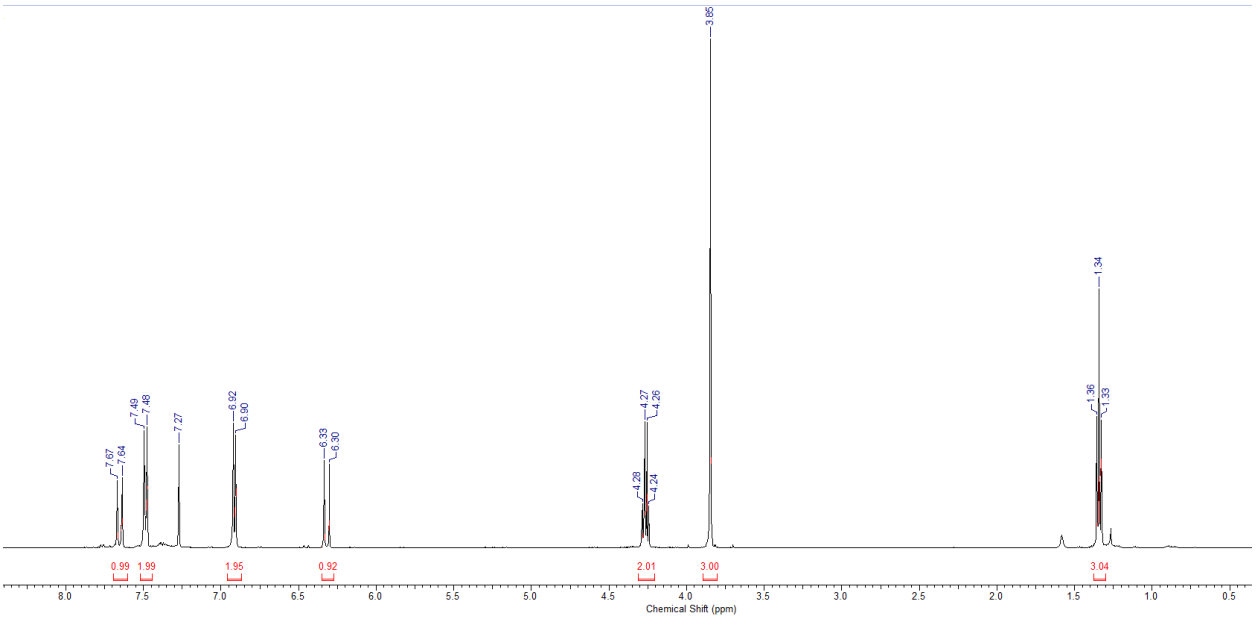

Ethyl (E)-*p*-cyanocinnamate:

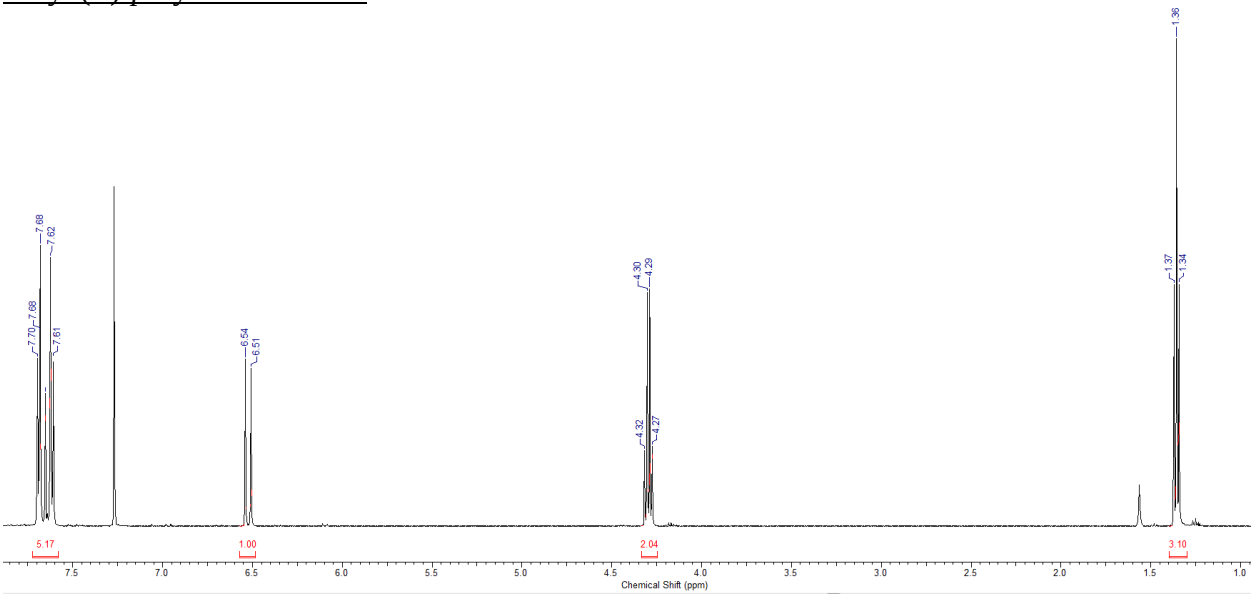

Methyl (E)-3-(*p*-cyanophenyl)-2-methylpropenoate:

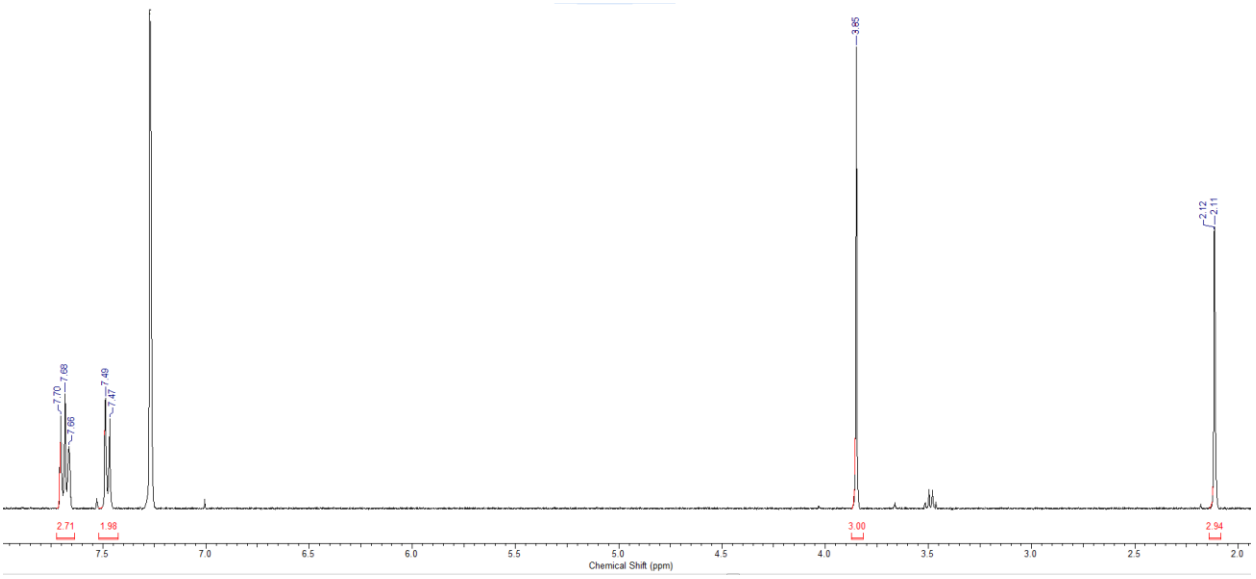

Benzylamine:

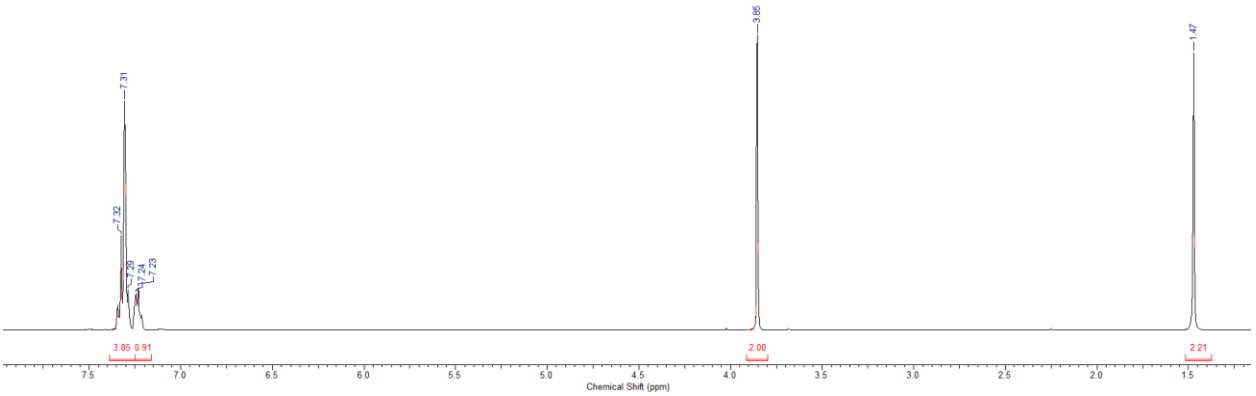

m-Nitrobenzylamine:

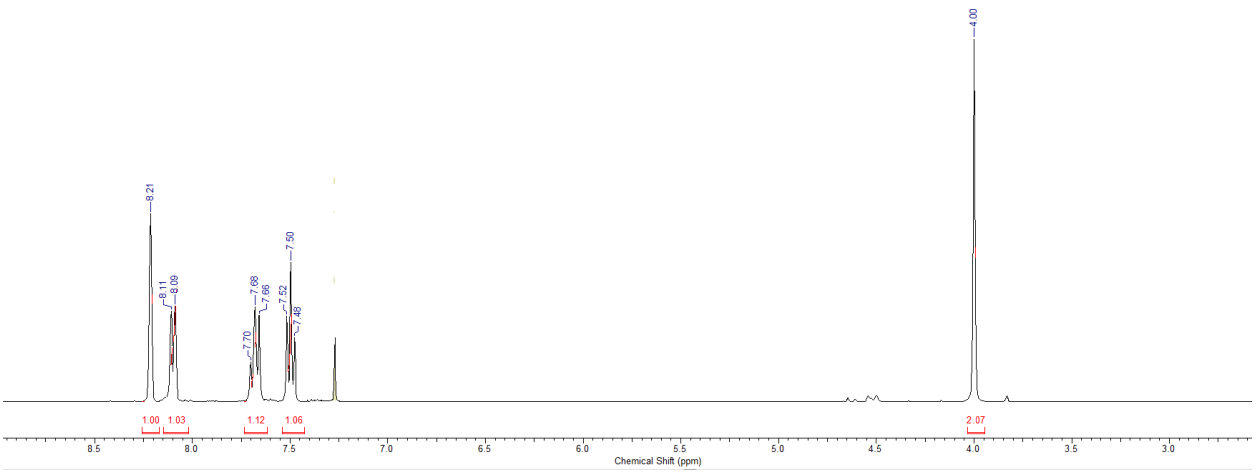

p-Methoxybenzylamine:

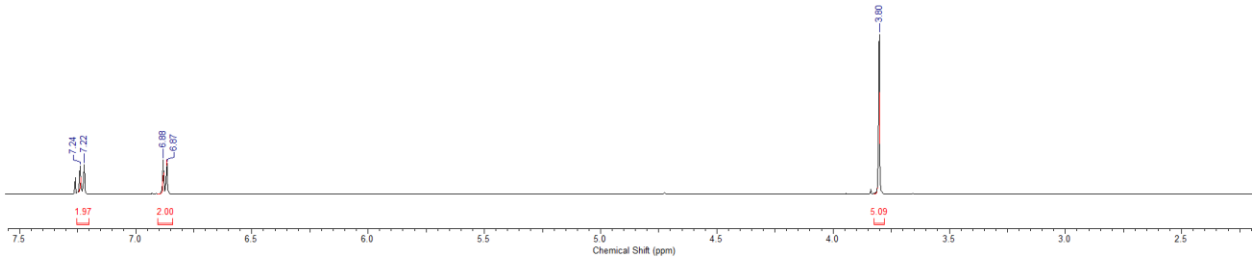

(2S)-1-Amino-3-chloro-2-propanol:

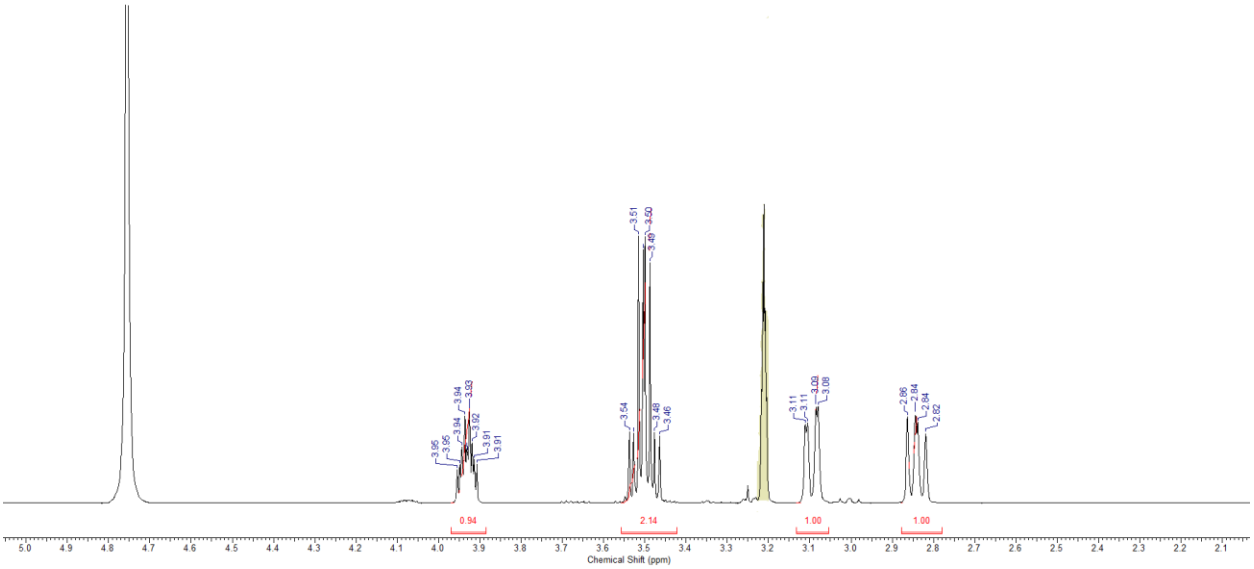

1-Bromobutane:

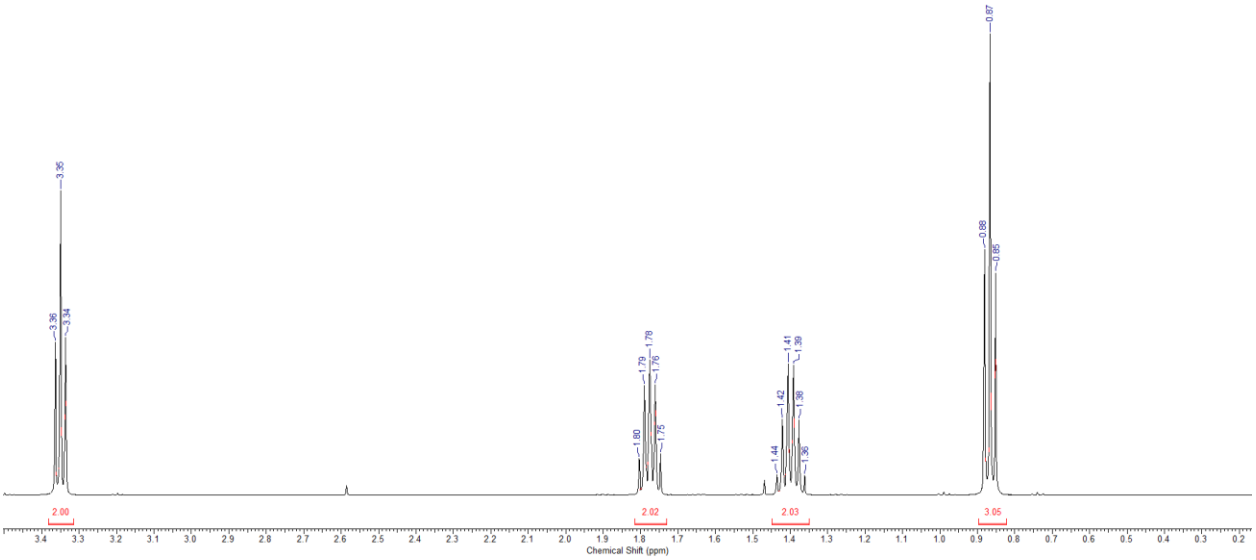

1-Bromo-2-phenylethane:

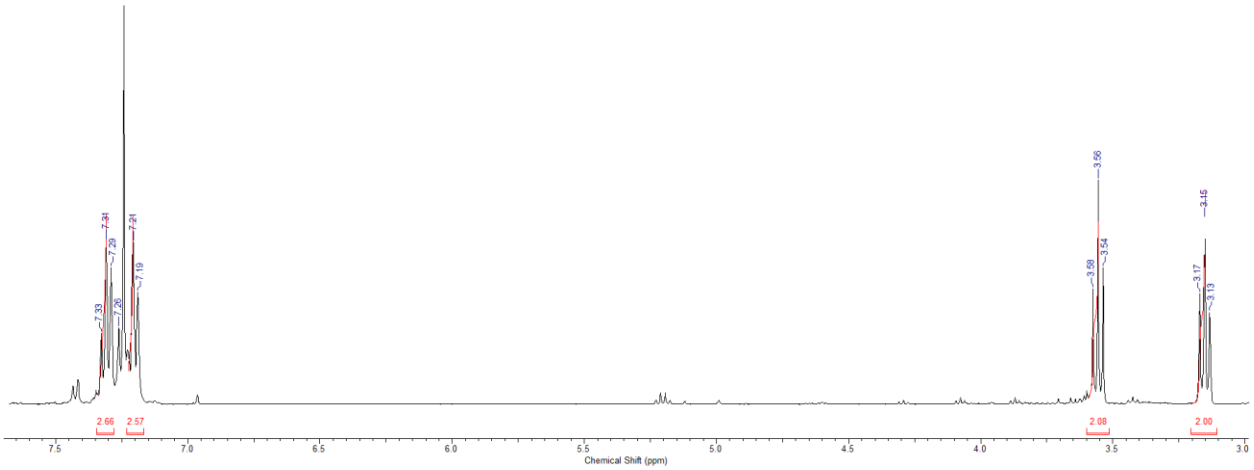

1-Bromo-1-phenylethane:

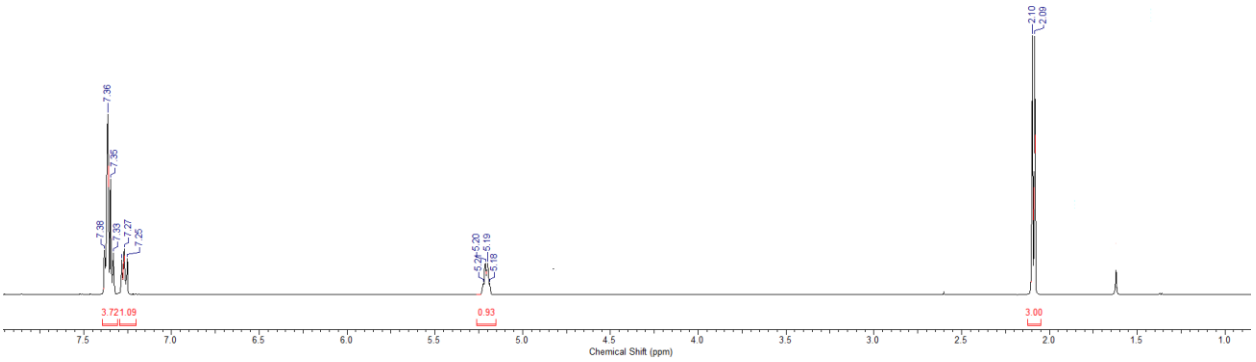

Chapter 2

The Development of Mechanism-Based Inhibitors of Tubercular BioA

Adapted with Permission from:

Eiden, C. G.; Maize, K. M.; Finzel, B. C.; Lipscomb, J. D.; Aldrich, C. C. Rational Optimization of Mechanism-Based Inhibitors through Determination of the Microscopic Rate Constants of Inactivation. *J. Am. Chem. Soc.* **2017**, *unknown*, PP

and

Eiden, C. G.; Aldrich, C. C. Synthesis of a 3-Amino-2,3-dihydropyrid-4-one and Related Heterocyclic Analogs as Mechanism-Based Inhibitors of BioA, a Pyridoxal-Phosphate (PLP) Dependent Enzyme. *J. Org. Chem.* **2017**, *unknown*, PP

This work was done in collaboration with Dr. John Lipscomb, Dr. Melanie Rogers, Dr. Brent Rivard, and Dr. Kimberly Maize. Dr. Maize obtained the crystal structure of inactivated BioA. Dr. Rogers and Dr. Rivard trained and assisted with the operation of the stopped-flow spectrophotometer and subsequent data processing. Dr. Lipscomb assisted with numerous aspects of the project, including the design of stopped-flow experiments, data presentation, and general guidance.

2.1 Introduction

Tuberculosis (TB) has plagued mankind for millennia and is currently the leading cause of infectious disease mortality and morbidity worldwide, being responsible for over 1.8 million deaths in 2015.[126] It is primarily caused by *Mycobacterium tuberculosis* (*Mtb*), an extremely slow-growing bacillus that requires extended periods of treatment and is impervious to most conventional anti-bacterials.[127] The introduction of antibiotics combined with public practices specifically aimed to prevent the transmission of TB led to a near-eradication of the disease from industrialized nations in the 20th century.[128] However, the last approved first-line drug for TB chemotherapy, Rifampin, was introduced in 1968. Combined with the necessary treatment time, the dearth of new antibiotics has led to the development of multiple drug-resistant TB strains.[129] In fact, reports over the last half century confirm the development of resistance to all first- and second-line antitubercular agents. It is thus imperative to develop new classes of anti-TB agents that are effective against drug-resistant TB and possess novel modes of action.

Cofactor biosynthesis is an excellent source of potential therapeutic targets as many of the pathways are essential and lack a corresponding mammalian counterpart.[130] Biotin (vitamin H) is the cofactor responsible for the activation of carbon dioxide in fatty acid biosynthesis and gluconeogenesis through attachment to acyl-CoA carboxylases (ACCs) and pyruvate coenzyme A carboxylase (PCC).[131,132] *Mycobacterium tuberculosis* is particularly sensitive to biotin deprivation, as though ACCs are required in numerous organisms, *Mtb* uniquely relies on three non-redundant ACCs to synthesize the unparagoned lipids found in the extraordinarily complex mycobacterial cell wall.[133134135] Additionally, gluconeogenesis is a vital process in *Mtb* to synthesize sugars needed for nucleotide and cell wall biosynthesis.[136]

Amiclenomycin (ACM, Figure 2.1A) is an antibiotic that was isolated in 1974 from a *Streptomyces lavendulae* strain.[137] It possesses selective antimicrobial activity against *Mtb* and

the fast-growing *Mycobacterium smegmatis* (*Msmeg*), and has been shown to exert its activity through inhibition of mycobacterial biotin biosynthesis.[138139] The aforementioned dependence of *Mtb* on several biotin-containing enzymes may explain the distinct vulnerability of mycobacteria to ACM.[140] The mechanism of action of ACM was elucidated by classic complementation studies employing biotin pathway intermediates.[141] In *Mtb* and *Msmeg*, biotin biosynthesis begins by hijacking of the fatty acid biosynthesis pathway to generate pimeloyl-ACP,[142] which is then elaborated to biotin over four enzymatic steps (Figure 2.1B).[143144145146147148] The first step is carried out by BioF, yielding 7-keto-8-aminopelargonic acid (KAPA) from the decarboxylative condensation of pimeloyl-ACP and L-alanine. BioA then effects the reductive amination of KAPA into 7,8-diaminopelargonic acid (DAPA), which is followed by the BioD-catalyzed carboxylation of DAPA to form dethiobiotin (DTB). The pathway concludes with insertion of the sulfur atom by the iron-sulfur cluster enzyme BioB, affording biotin. The addition of exogenous DAPA, DTB, or biotin to whole-cell *Msmeg* antagonized the activity of ACM, whereas KAPA did not.[149] Moreover, treatment of *Msmeg* with ACM led to an accumulation of KAPA.[150] Taken together, these data pinpointed the antepenultimate step performed by BioA as the likely target of ACM.

BioA is a pyridoxal-5′-phosphate (PLP) dependent aminotransferase that uses *S*-adenosylmethionine (SAM) as an amino donor when catalyzing the conversion of KAPA to DAPA.[151152] Through a combination of elegant kinetic and structural studies, the amino-1,4-cyclohexadienyl group on ACM was shown to bind the PLP of BioA.[153154] The resulting external aldimine then undergoes redox isomerization via a quinonoid intermediate to a ketimine (Figure 2.1C). However, rather than completing hydrolysis to generate the pyridoxamine-5′-phosphate (PMP) form of the cofactor, the ketimine intermediate tautomerizes to a stable aromatic adduct that covalently inactivates BioA.

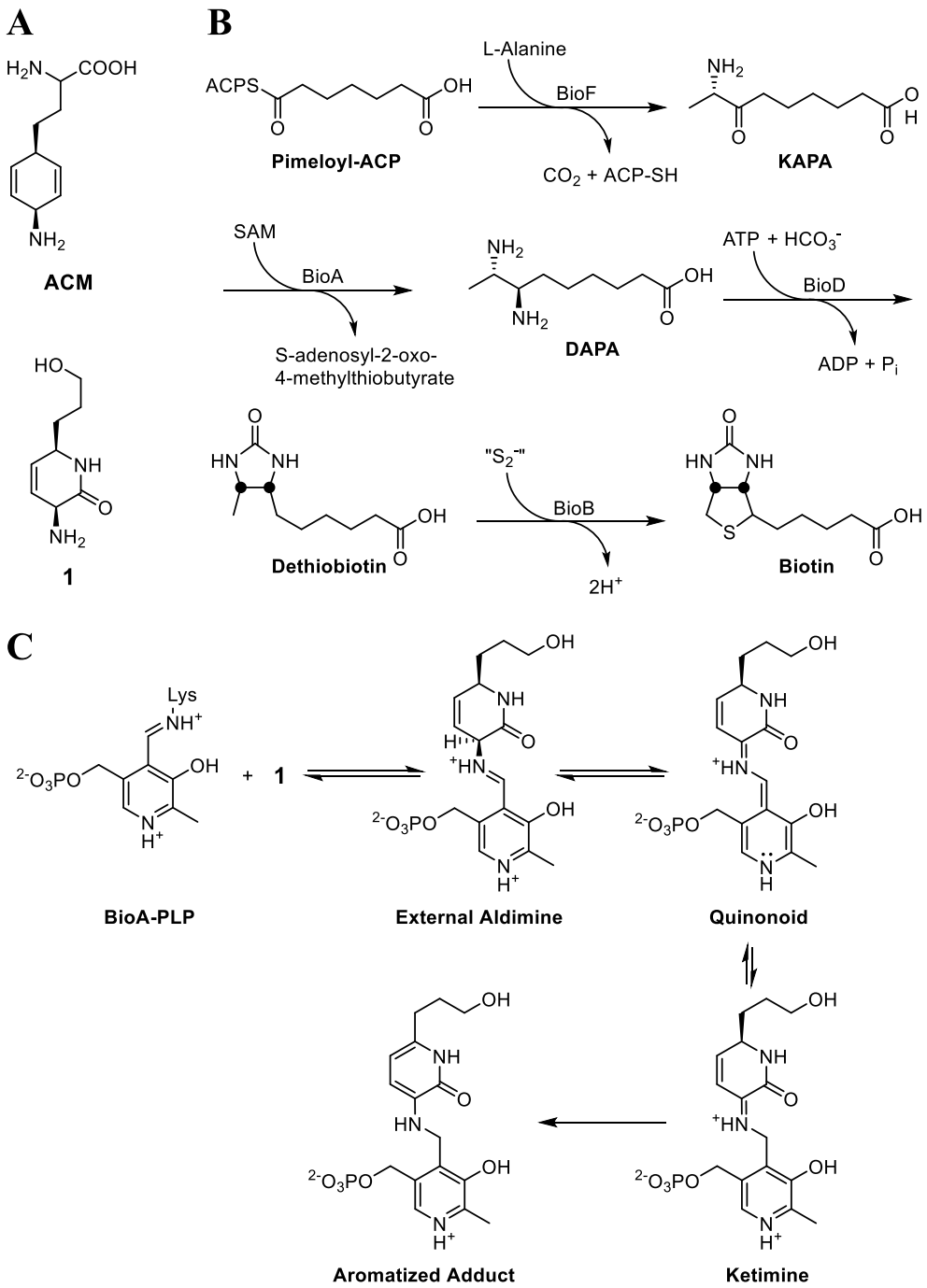

Figure 2.1. Biotin Biosynthesis, ACM, **1**, and the Inactivation of BioA by **1**. (A) Natural product ACM was the inspiration for **1**. (B) Biotin biosynthesis proceeds in four steps from pimeloyl-ACP. (C) Inactivation of BioA by **1** occurs via a 4-step process resulting in a stable, aromatized adduct bound to the PLP cofactor.

The discovery of the mechanism of inactivation explains both the reason for and the function of the rare 1,4-cyclohexadiene moiety in ACM. However, while the 1,4-cyclohexadiene is absolutely critical for ACM's activity, it is simultaneously the primary liability of ACM, as this moiety is chemically unstable and spontaneously aromatizes to an inactive benzene nucleus. Shi and Aldrich designed a series of chemically robust allylamine inhibitors (Table 2.1) with both acyclic (**2**) and cyclic warheads (**3A**-**C**) to replace the 1,4-cyclohexadiene of ACM.[155] Regrettably, the most effective of these compounds had minimal activity that was not time-dependent, and they were unable to draw any clear conclusions other than suggesting that an ideal warhead likely includes a flat ring. More fruitfully, Aldrich and coworkers have described the design of a simplified analogue **1** (Figure 2.1A) wherein the 1,3-cyclohexadiene warhead of ACM was replaced with a more stable 3,6-dihydropyrid-2-one moiety,[156] whose increased stability is derived from reduced aromatic stabilization energy of the corresponding 2-pyridone. Compound **1** was shown to inhibit BioA in a similar manner to ACM (Figure 2.1D), but further optimization of this scaffold has been hampered by the complex nature of the inactivation mechanism.

Table 2.1. Allylamine Inhibitors: Structures and Activity Against BioA.

Compound	Structure	IC_{50} (μM)
2	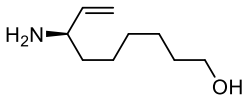	>100
3A	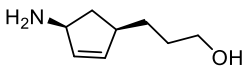	57.0 ± 1.9
3B	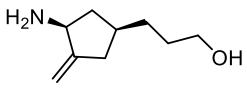	>100
3C	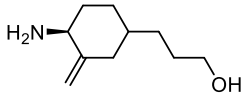	>100

Both **1** and ACM are mechanism-based inhibitors (MBIs) since they require transformation by the inhibited enzyme's machinery to form active inhibitory species. Unlike conventional rapidly reversible inhibitors, MBIs display time-dependent inhibition and cannot be characterized by IC_{50} or K_I values.[157] Rather, the rate constant of inactivation (k_{obs}) is typically measured as a function of inhibitor concentration to furnish the global kinetic parameters k_{inact} and K_I. k_{inact} and K_I are semi-analogous to Michaelis-Menten parameters and describe, respectively, the maximum possible value of k_{obs} at infinite inhibitor concentration and the concentration of inhibitor that produces a k_{obs} that is equal to one half of k_{inact}.[158]

In this study, we first designed direct analogues of **1**, changing the nature of the tail based on information from a fragment-based screen with BioA. The synthesis of the alternative tail structures proved exceptionally difficult to accomplish in combination with the already complex methods necessary for warhead construction, so we abandoned this approach. Seeking to change the compound scaffold, we thoroughly investigated MBI optimization techniques, and found both k_{inact} and K_I are complex conglomerates of the individual microscopic rate constants of inactivation, with neither of the parameters definitively assessing binding affinity nor the identity of the rate limiting step. The only certain way to optimize an MBI was through complete characterization, so we performed stopped-flow studies and elucidated each of the microscopic rate constants of inactivation. This revealed the identity of the rate determining step, and we designed alternative dihydropyrid-4-one, dihydropyran-4-one, and dihydrothiopyran-4-one scaffolds to increase the rate of inactivation while simultaneously improving compound accessibility. These compounds were constructed and tested for their inhibitory activity against BioA, and we found that the dihydropyrid-4-one scaffold had an increased k_{inact}, validating our design strategy. These findings substantially furthered the preclinical development of MBIs of BioA towards a novel anti-TB therapeutic

2.2 Adding an Electron Deficient Heterocycle

To improve Compound **1**, Finzel and coworkers investigated the structure of the binding pocket of BioA by co-crystallization with various fragments.[159] They sought to identify alternative tail structures to replace the hydroxypropyl tail, which was known to make few favorable contacts with the enzyme.[160] Unfortunately, they found that most fragments bound in the area occupied by the main pyridone ring of the PLP-adduct formed by **1**, but two fragments were determined to have 5-membered rings that rested several angstroms away. Each of these rings were highly electron deficient, and likely had moderate π-stacking interactions with a nearby phenylalanine residue. The 1,2,3-triazole ring can be formed efficiently and regioselectively using Cu(I)-catalyzed click chemistry, and we were unsure whether one or two methylene groups would allow for the triazole to occupy the correct space, so we designed compounds **4** and **5** (Figure 2.2) to capitalize on potential energetically favorable interactions with BioA.

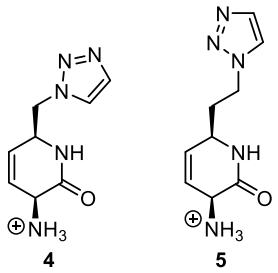

Figure 2.2. Dihydropyrid-2-one Analogues of **1**

The synthesis of **4** began with L-Boc-Serine **6** (Scheme 2.1), which was transformed into Weinreb Amide **7** utilizing EDC and NMM in CH_2Cl_2.[161] Performing this reaction in CH_2Cl_2 with NMM as the base was found to be superior to the more common aqueous system[162] in both yield and reproducibility. Isopropylidene protection followed by reduction with $LiAlH_4$ furnished Garner's Aldehyde **9** in excellent yield.[163,164] Wittig conditions afforded mono-substituted alkene

10 in a lower-than-desired yield, and the ensuing selective isopropylidene deprotection provided Boc-vinyl glycinol **11**.[165]

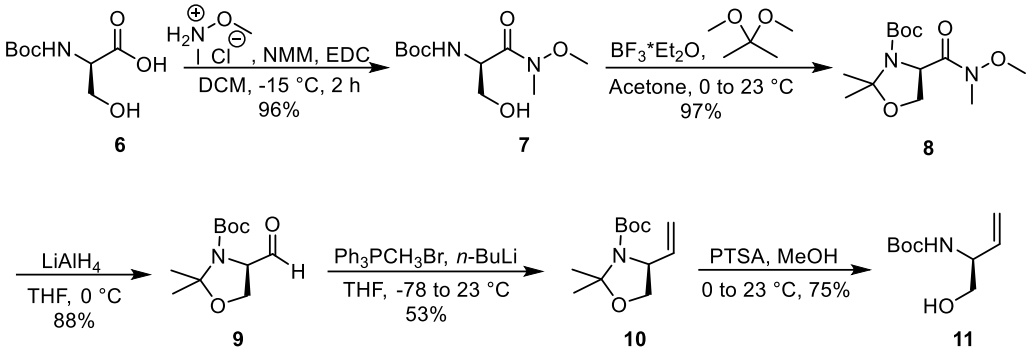

Scheme 2.1. Synthesis of Boc-Vinyl Glycinol **11**.

11 was utilized as the precursor to both the bottom and top halves of **4** (Scheme 2.2). In one path mesylation followed by azide displacement furnished **12** in reasonable yield, and subsequent Boc-deprotection using HCl in dioxane afforded amino-butene derivative **13**. **11** was also subjected to Jones' oxidation conditions to form Boc-vinyl glycine **14**.[166] The pKa of the α-proton of **14** is quite low by amino acid standards, so we used DEPBT, a coupling reagent developed specifically to avoid α-racemization,[167,168] to catalyze the amide coupling with **13**. Azido amide **15** was produced in good yield with no observed racemization of either stereocenter.

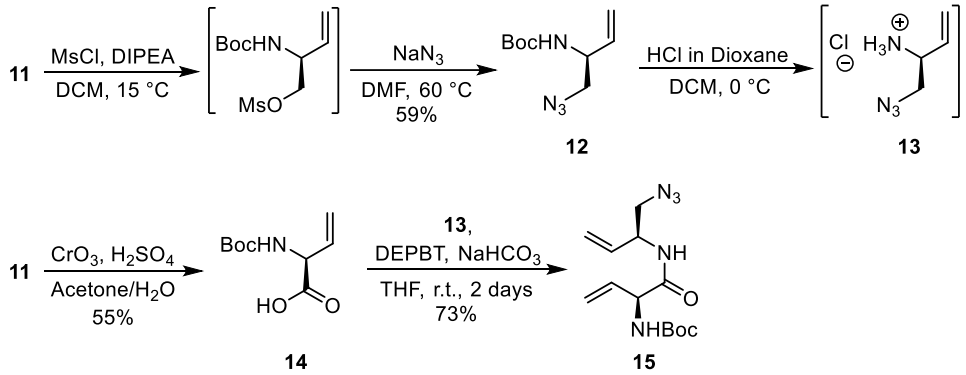

Scheme 2.2. Synthesis of Dihydropyrid-2-one Precursor Azido-amide **15**

At this point, the only steps that remained to synthesize **4** were the ring-closing metathesis (RCM) to form the dihydropyrid-2-one ring, a click reaction to construct the triazole, and removal

of the protecting group(s). To easily obtain analogues of **4** for further testing against BioA, it would be preferable to perform the click reaction as late in the synthetic scheme as possible. Therefore, we attempted an RCM reaction to form **16** using either the Grubbs II[169] or Hoveyda-Grubbs II[170,171] catalysts (Scheme 2.3), but neither provided anything besides starting material upon workup. Due to the lack of metathesis reactions performed on compounds containing azides, we suspect that the complete lack of reactivity is likely due to reduction of the ruthenium center of the catalysts. We then switched our focus to triazole formation. Using TMS-acetylene as a liquid substitute for acetylene, we attempted the click reaction using both Cu(I) iodide directly as well as *in situ* generation of Cu(I) by adding sodium ascorbate to Cu(II) sulfate.[172,173] Both reactions only provided 27% of desired TMS-triazole **17**, but isolation of the by-products revealed that the Cu(I) iodide system was causing homocoupling of the TMS-Acetylene,[174] while the Cu(II) conditions resulted in 51% of desilylated product **19**, resulting in a quite acceptable 78% overall yield. However, this reaction was extremely sluggish, completing only after a full week while requiring more than 20 equiv of TMS acetylene and nearly stoichiometric amounts of copper and ascorbate. Cu(I)-catalyzed click reactions are generally relatively rapid,[175] so we propose that steric hindrance substantially slows this reaction, as only a single methylene group separates the azide from a methine group with substituents of considerable size.

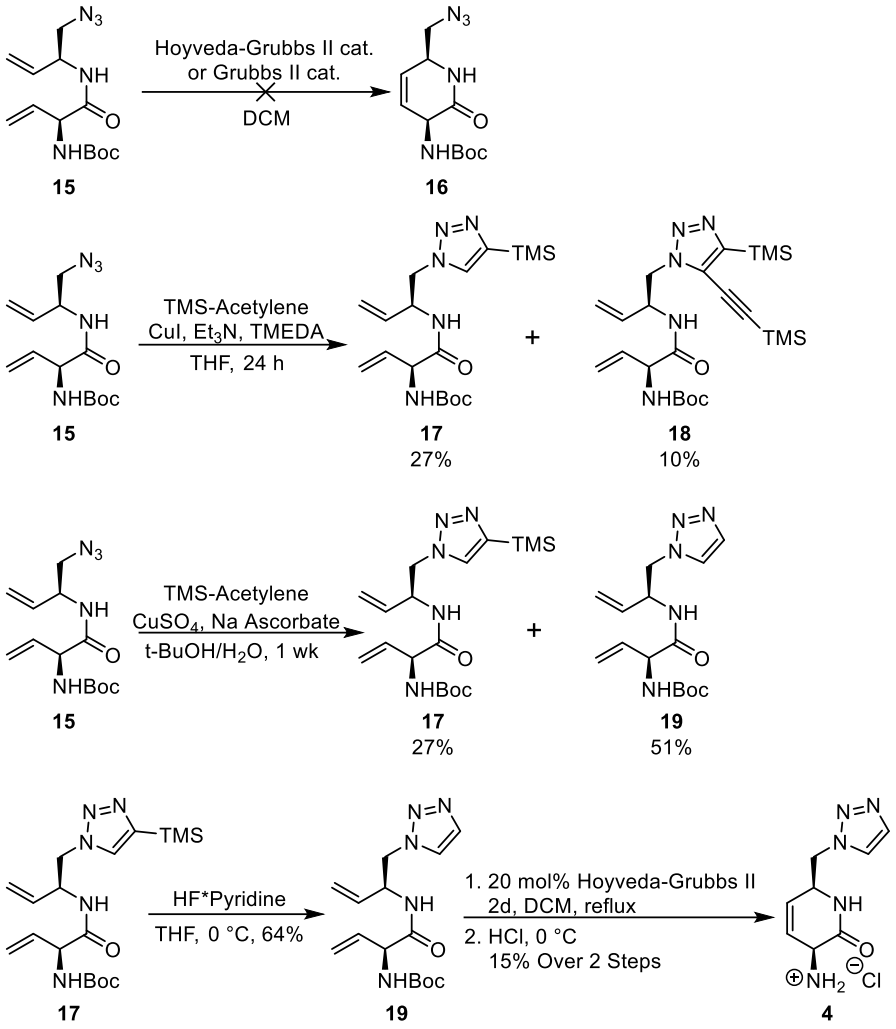

Scheme 2.3. Synthesis of Dihydropyrid-2-one Triazole **4**.

Deprotection of the TMS group of **17** to consolidate the click reaction products proceeded in reasonable yield. However, the RCM reaction proved quite difficult. We have previously discovered that the dihydropyrid-2-one core of **4** aromatizes when heated to 80 °C, so we maintained a temperature of 50 °C by refluxing CH_2Cl_2. Reacting **19** with 20 mol% of the Hoveyda-Grubbs II catalyst for two days under the exclusion of light provided the desired dihydropyrid-2-one, though it could not be separated from some of the catalyst decomposition products. Subsequent Boc deprotection and purification by trituration furnished amino-dihydropyrid-2-one **4** in poor yield from **19**.

4 was assayed for its activity against BioA and subjected to multiple co-crystallization conditions with the enzyme to attempt to observe an aromatized adduct. Unfortunately, **4** displayed no time-dependent inhibition of BioA, and failed to co-crystallize with BioA. Therefore, we began the synthesis of **5**, rationalizing the failure of **4** to the close proximity of the pyridone preventing the triazole from freely rotating to a configuration that would allow for the desired π-stacking interaction.

We wanted to structure the synthesis of **5** in such a way that would alleviate the difficulties we had with the RCM reaction and to form the triazoles at an even later stage for rapid derivatization. The original synthesis of **1** included a relatively high-yielding RCM reaction of a dihydropyrid-2-one precursor containing a TBS-protected hydroxypropyl tail.[176] Envisioning that alcohol **21** would be able to undergo the RCM far more readily than **15** or **19**, and could subsequently be modified to introduce an azide, we set out to synthesize amino-alcohol **20**.

The synthesis of **20** began with the conversion of D-methionine **22** to D-homoserine lactone hydrobromide **23** in good yield.[177] Boc protection then afforded D-Boc-homoserine lactone **24** in excellent yield. We then envisioned a two-step process of DIBAL reduction preceding a Wittig reaction on the resulting lactol would furnish **26**. DIBAL reduction proceeded smoothly, though **25** degraded upon purification with a silica gel column, so we instead directly took the product onto the Wittig reaction. This exact reaction has been reported once previously,[178] though with a curious procedure where following *in situ* generation of the phosphonium ylide, the product is added and refluxed in a mixture of CH_2Cl_2 and toluene. We tried this procedure several times, and were unable to obtain any product. In fact, the ylide appeared to degrade under such conditions, as we obtained considerable amounts of triphenylphosphine upon purification. Wittig reactions on 5-membered lactols with substituents at the α-position are known,[179] so we attempted standard Wittig conditions as well as a Horner-Wadsworth-Emmons reaction in attempts to produce **26**. These all failed.

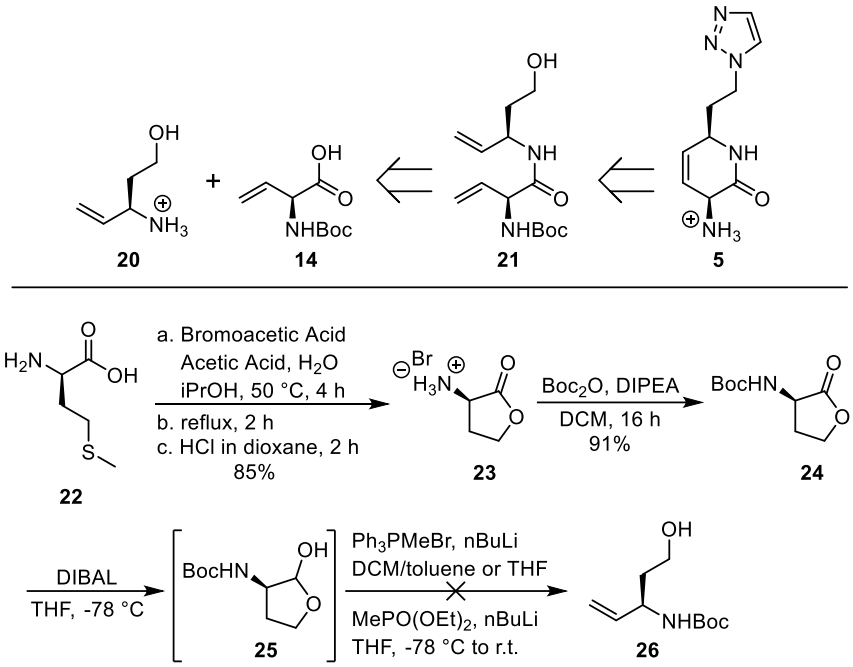

Scheme 2.4. Design of Amine Coupling Partner towards Dihydropyrid-2-one **5** and Initial Failed Route

Convinced that we would not be able to obtain **26** from **25**, both due to personal experience and by observing reported strategies aimed at bypassing that conversion, we changed our synthetic scheme. First, we endeavored to synthesize the bis-Boc protected version of **25**, as removing the acidic N-H proton could eliminate charge-charge interactions between the deprotonated amine and the ylide. Bis-Boc protection to construct **27** proceeded smoothly, but the increased reactivity and steric bulk of bis-Boc protection meant that bicyclo compound **28**[180] was the only product of the subsequent DIBAL reduction. We then chose to change our target molecule from mono-substituted alkene **20** to di-substituted alkene **30**, as the latter would allow for a Wittig reaction with a stabilized ylide that would not deprotonate the amine. The ethyl ester of **30** should be irrelevant as an RCM reaction to form the dihydropyrid-2-one would remove it.

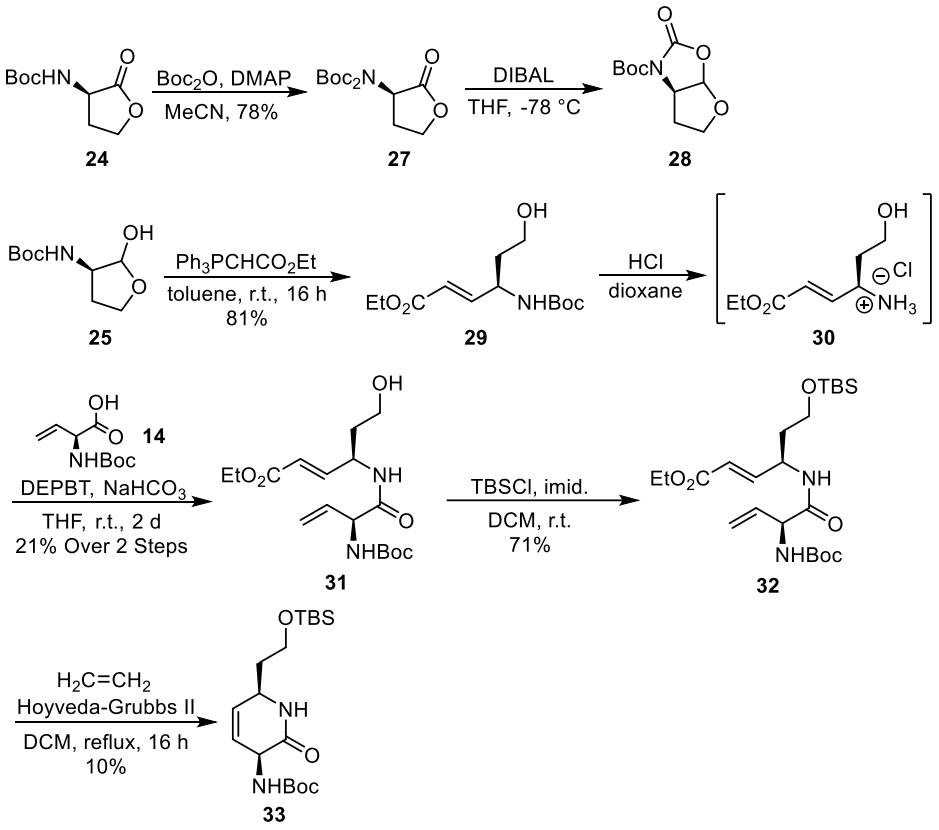

Scheme 2.5. Synthesis of Alternative Amine Coupling Partner **30** and Challenges to Obtain Dihydropyrid-2-one **33**

This plan initially tasted success, as addition of Ph_3PCHCO_2Et to **25** provided α,β-unsaturated ester **29** in quite good yield.[181] Subsequent deprotection of **29** afforded **30**[182], which was coupled with R-vinyl glycine **14** to form amide **31**. Unfortunately, this reaction worked very poorly when compared with the synthesis of **15**. The fact that we were starting with an ammonium salt as opposed to a free amine could have been the reason, though an alternative possibility was that the free alcohol was interfering in the reaction. The seminal publication on DEPBT suggests that alcohols do not require protection, but this was not extensively tested.[183] Regardless, we then attempted an RCM reaction using multiple conditions, but were unsuccessful in obtaining product. The alcohol of **31** was then protected with a TBS group in order to mirror the successful synthesis of **1**.[184] Unfortunately, subjecting **32** to RCM conditions resulted in an extremely

sluggish reaction. Utilizing upwards of 50 mol% of a RCM catalyst produced about 10% of product in 3-5 days, while the addition of ethylene gas, known to enhance the metathesis rate,[185] furnished about 10% product overnight. Neither set of conditions would result in a successful synthetic route to **5** and its analogues, as the yields were consistently too low, and at least four steps were required beyond this point. Therefore, we decided to take a step back and design an alternate route to **5** where both alkenes are mono-substituted and thus better disposed to take part in metathesis.

To avoid any potential side reactions during amide coupling with an unprotected alcohol and to potentially enhance the rate through using an amine and not an ammonium salt, we designed amine **34** and set it as our objective. The synthesis of **34** began with 4-penten-1-ol **36**, which was THP protected using standard methods. We then sought to add the amino group using conditions reported by Bao and Tambar for the stereoselective allylic amination of terminal olefins.[186] Addition of bis-benzenesulfonyl sulfurdiimide to **37** at 4 °C formed stable ene adduct **38** that can be purified by filtration. The rearrangement was then performed under Bao and Tambar's Pd-catalyzed conditions at low temperature, affording **39** in moderate yield and enantioselectivity, as ether-containing alkenes are reported to react less favorably. Aqueous base furnished mono-benzenesulfonyl **40** in excellent yield,[187] after which TBSOTf and dimethyl sulfide[188] were used to switch to a more desirable protecting group. Benzenesulfonylamines are extremely stable, and as such we had to resort to Birch conditions to obtain the desired deprotected amine **34**.

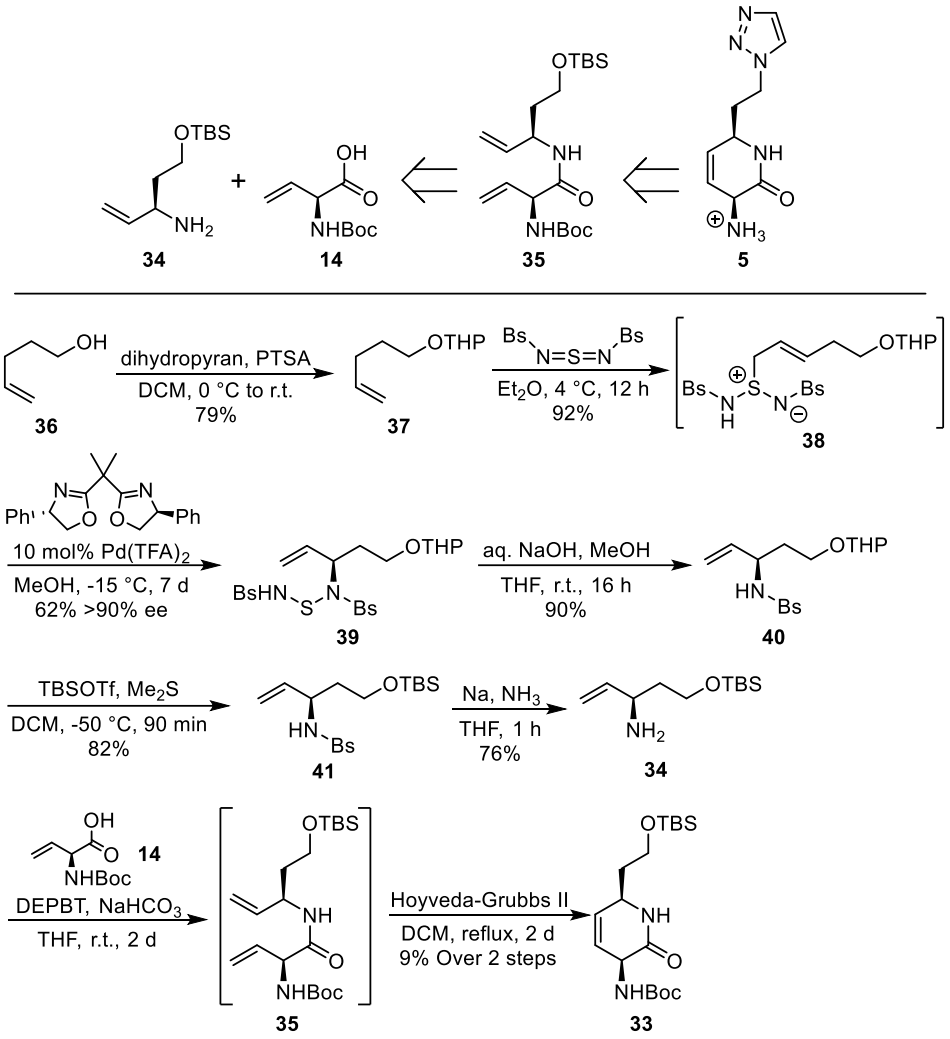

Scheme 2.6. Synthesis of Amine Precursor **34** via Enantioselective Allylic Amination and Challenges Towards the Dihydro-2-Pyridone Ring

34 was coupled with **14** to furnish amide **35**, which was then subjected to RCM conditions using either the Grubbs II or Hoyveda-Grubbs II catalyst. Unfortunately, the best yield that we obtained was 9% over both steps, and it was clear that the RCM was still not performing nearly to the degree that we desired. We were quite disappointed by this, and though there were certainly other methods that we could have attempted to synthesize **5**, we felt that the difficulty and length of the syntheses to this point rendered extensive derivatization improbable. Instead, we wanted to change scaffolds to facilitate more efficient syntheses. Rather than just pick a new scaffold that

made sense from an ease of synthesis standpoint, we decided to attempt the first fully-informed rational optimization of an MBI.

2.3 Optimization of MBIs

The failure of compound **4** compounded with the length of the synthesis of new dihydropyrid-2-one analogues prompted a re-evaluation of the goals of this project. If every dihydropyrid-2-one MBI worked wonderfully, then perhaps it would be worth the time and effort involved in designing and executing a personalized synthesis for each inhibitor. Since this was not the case, we sought to redesign the warhead of **1** to enable a more efficient synthetic route that included late-stage derivatization capabilities.

As previously discussed, early stage development of MBIs commonly revolves around improving the k_{inact}/K_I value of each inhibitor against the specified target. Usually, the warhead is left untouched, with optimization focused on gaining additional binding affinity through modification of the tail(s) of the MBI. The lack of direct optimization and development on MBI warheads means that few to no methods exist for rationalizing such processes. One can simply attempt to make molecules that can undergo the proposed mechanism of the MBI, but this level of rational design is far below what would be desired. In our case, this would involve following the suggestion of Shi and Aldrich that a flat ring is necessary, and then design flat rings that could form a stable adduct with the PLP of BioA. However, there are numerous compounds that fulfill those conditions, leaving us with far too many options.

In an attempt to develop a rational method that guides MBI warhead development, we undertook a detailed investigation into prior MBI optimization strategies, attempting to tease out clues as to what our next steps should be. As expected, we found a large number of reports that used K_I and k_{inact} to optimize their MBIs, with increasing the k_{inact}/K_I value as the ultimate goal.[189,190,191,192] The closest thing we observed to warhead optimization was a report that

synthesized a substantial number of warheads and then determined the k_{inact}/K_I values for each against the enzyme to establish which was optimal.[193] Notably, in almost all reports, K_I was being treated as the equilibrium constant of the initial binding event, and k_{inact} assumed to be the rate of the key activation step of the MBI. Copeland has previously discussed that for MBIs with a three-step mechanism of inactivation, the only time the K_I is equivalent to the K_D of the binding equilibrium is when the step immediately following binding is entirely rate limiting. As our presumed mechanism includes four steps (Figure 2.1), we decided to analyze generalized three and four-step kinetic mechanisms for MBI inactivation of an enzyme, specifically looking at the how K_I and k_{inact} change based on the individual microscopic rate constants of inactivation.

To begin, we derived the K_I and k_{inact} values for several potential MBI mechanisms in terms of the individual rate constants (Table 2.2). For our analysis, the k_{inact} of a MBI is defined as the maximum k_{obs} possible arising from infinite concentration of inhibitor, where k_{obs} is determined by fitting curves describing time-dependent formation of the final, inactivated complex, to exponentials of the type e^(-k_{obs}*t). The K_I is the concentration of inhibitor that produces a k_{obs} equal to half of k_{inact}. The values in Table 2.2 are derived assuming both a quasi-steady state for each intermediate Enzyme-Inhibitor complex and that the total enzyme concentration is constant. A sample derivation of the K_I and k_{inact} values of Mechanism 4 is included in the Methods section, showing the approach taken in deriving the values in Table 2.2.

Table 2.2. K_I and k_{inact} values for several mechanisms of MBIs as conglomerates of rate constants

#	Mechanism:	K_I (M)	k_{inact} (s^{-1})
1	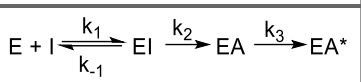	$\frac{(k_{-1}+k_2)k_2}{k_1(k_2+k_3)}$	$\frac{k_2k_3}{k_2+k_3}$
2	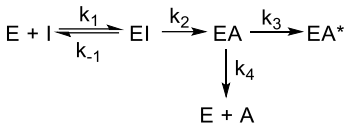	$\frac{(k_{-1}+k_2)(k_3+k_4)}{k_1(k_2+k_3+k_4)}$	$\frac{k_2k_3}{k_2+k_3+k_4}$
3	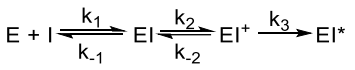	$\frac{k_{-1}(k_{-2}+k_3)+k_2k_3}{k_1(k_2+k_{-2}+k_3)}$	$\frac{k_2k_3}{k_2+k_{-2}+k_3}$
4	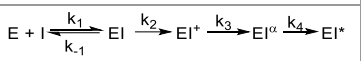	$\frac{(k_{-1}+k_2)k_3k_4}{k_1(k_2(k_3+k_4)+k_3k_4)}$	$\frac{k_2k_3k_4}{k_2(k_3+k_4)+k_3k_4}$
5	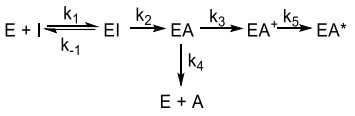	$\frac{(k_{-1}+k_2)k_3k_5+k_4k_5}{k_1(k_2(k_3+k_5)+k_5(k_3+k_4))}$	$\frac{k_2k_3k_5}{k_2(k_3+k_5)+k_5(k_3+k_4)}$
6	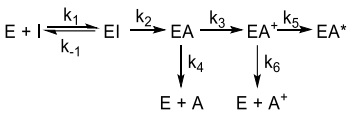	$\frac{(k_{-1}+k_2)(k_3+k_4)(k_5+k_6)}{k_1(k_2(k_3+k_5+k_6)+(k_3+k_4)(k_5+k_6))}$	$\frac{k_2k_3k_5}{k_2(k_3+k_5+k_6)+(k_3+k_4)(k_5+k_6)}$
7	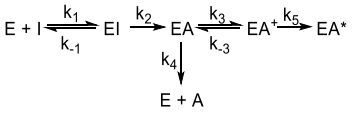	$\frac{(k_{-1}+k_2)(k_3k_5+k_{-3}k_4+k_4k_5)}{k_1(k_2(k_3+k_{-3}+k_5)+k_3k_5+k_4(k_{-3}+k_5))}$	$\frac{k_2k_3k_5}{k_2(k_3+k_{-3}+k_5)+k_3k_5+k_4(k_{-3}+k_5)}$
8	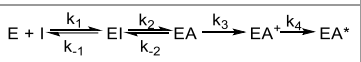	$\frac{(k_{-1}k_{-2}+k_{-1}k_3+k_2k_3)(k_4)}{k_1(k_2k_3+(k_3+k_{-2}+k_3)(k_4))}$	$\frac{k_2k_3k_4}{k_2k_3+(k_3+k_{-2}+k_3)(k_4)}$
9	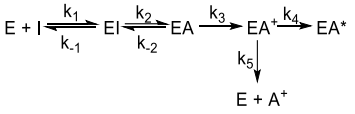	$\frac{(k_{-1}k_{-2}+k_{-1}k_3+k_2k_3)(k_4+k_5)}{k_1(k_2k_3+(k_3+k_{-2}+k_3)(k_4+k_5))}$	$\frac{k_2k_3k_4}{k_2k_3+(k_3+k_{-2}+k_3)(k_4+k_5)}$

The addition of more steps or reversibility causes K_I and k_{inact} to become significantly more complex congregates of the microscopic rate constants. Though Table 2.2 provides a wealth of valuable information, we wanted to explore exactly how the K_I and k_{inact} values depend on the individual rate constants in greater detail. K_I and k_{inact} were thus calculated from a wide range of

values for each of the individual rate constants for a few mechanisms. These results are shown in Table 2.3.

As mentioned previously, it is often naively assumed that a K_I value obtained experimentally for an MBI will estimate the K_D of the initial binding step with a high degree of fidelity. This is unequivocally shown to be untrue, as the K_I only accurately estimates the K_D of the initial binding event for both three- and four-step mechanisms when the step following binding is both irreversible and rate limiting. In every other case, the K_I underestimates the K_D, and often by a substantial margin (light blue, purple, green, and gray entries in Table 2.3). Since a significant number of MBIs will certainly inactivate enzymes through mechanisms where the second step is either reversible or non-rate limiting, it is unwise to assume without further information that K_I estimates K_D. The distinction between K_I and K_D is important because the K_D, not the K_I, determines how well an inhibitor will compete with the substrate for binding to the enzyme active site.

Table 2.3. The Effect of Changing the Rate Constants on K_I, k_{inact}, and K_D.

Mech#	k_1 ($M^{-1}s^{-1}$)	k_{-1} (s^{-1})	k_2 (s^{-1})	k_{-2} (s^{-1})	k_3 (s^{-1})	k_4 (s^{-1})	k_5 (s^{-1})	K_D (M)	K_I (M)	k_{inact} (s^{-1})	k_{inact}/K_I ($M^{-1}s^{-1}$)
2	5	50	5	N/A	0.2	0.05	N/A	10	0.52	0.19	0.37
2	5	50	5	N/A	2	0.05	N/A	10	3.20	1.42	0.44
2	80	80	5	N/A	0.2	0.05	N/A	1	0.05	0.19	3.8
2	20	100	1	N/A	1	1	N/A	5	3.37	0.33	0.097
2	20	100	1	N/A	10	1	N/A	5	4.63	0.83	0.18
2	20	100	10	N/A	1	1	N/A	5	0.92	0.83	0.90
2	20	100	1	N/A	1	0.1	N/A	5	2.65	0.95	0.36
2	80	40	1	N/A	1	1	N/A	1	0.34	0.33	0.97
2	5	50	0.03	N/A	1	0.2	N/A	10	9.76	0.024	0.0025
2	5	50	0.3	N/A	1	0.2	N/A	10	8.04	0.20	0.024
2	30	30	0.03	N/A	1	0.2	N/A	1	0.98	0.024	0.024
2	100	500	10	N/A	0.05	0.01	N/A	5	0.030	0.050	1.7
2	100	500	10	N/A	0.5	0.01	N/A	5	0.25	0.48	1.9
2	100	500	10	N/A	0.05	0.001	N/A	5	0.026	0.050	1.9
3	5	50	5	0.5	0.05	N/A	N/A	10, *0.91*	1.00	0.045	0.045
3	5	50	5	0.5	0.5	N/A	N/A	10, *0.91*	1.75	0.42	0.24
3	80	80	5	0.5	0.05	N/A	N/A	1, *0.091*	0.10	0.045	0.45
3	20	100	0.03	3	0.5	N/A	N/A	5, *4.95*	4.96	0.0042	0.00085
3	20	100	0.3	3	0.5	N/A	N/A	5, *4.5*	4.61	0.039	0.0085
3	20	100	0.3	0.3	5	N/A	N/A	5, *2.5*	4.75	0.27	0.057
3	20	100	3	3	0.5	N/A	N/A	5, *2.5*	2.70	0.23	0.085
3	20	100	30	3	0.5	N/A	N/A	5, *0.45*	0.54	0.45	0.83
5	5	50	1	N/A	1	0.3	1	10	4.01	0.30	0.075
5	5	50	10	N/A	1	0.3	1	10	0.73	0.88	1.2
5	5	50	1	N/A	10	0.3	1	10	4.93	0.88	0.18
5	5	50	1	N/A	1	3	1	10	6.80	0.17	0.025
5	5	50	1	N/A	1	0.3	10	10	4.01	0.30	0.075
5	5	50	1	N/A	1	0.3	0.02	10	0.25	0.019	0.076
5	5	50	1	N/A	1	0.3	0.2	10	1.82	0.14	0.077

The numbers in italics for results obtained for mechanism 3 arise from applying the rapid equilibrium assumption to the second step as well as the first step and obtaining a K_D that is more consistent with how the inhibitor would compete with substrate. This number is a fair estimate for the green entries, and the top and bottom dark blue ones.

The distinction between the two is further demonstrated by the observation that if the second step is irreversible and non-rate limiting, an increase in the speed of the rate limiting step will cause an increase in both the K_I and the k_{inact} values (light blue and purple entries in Table 2.3). Clearly, improving the rate of a step subsequent to an irreversible second step does not affect the K_D of the initial binding event whatsoever, but it does cause significant changes in the K_I value. This point calls into question k_{inact}/K_I as a consistently accurate measure of inactivation efficiency. An MBI with the rate constants in the second purple entry of Table 2.3 is clearly a better inhibitor than an MBI with the rate constants in the first purple entry. It would compete with substrate

substantially better, but its k_{inact}/K_I value is only about 10% improved. This point is not to say that k_{inact}/K_I is a useless constant (it is certainly not), but rather to illustrate that it has pitfalls if treated as a complete descriptor of inactivation efficiency.

A final point that is demonstrated from the results in Table 2.3 is that, if the second step is reversible, improving the equilibrium of this step increases the k_{inact} and lowers the K_I at the same time. This is not unexpected, as the extended reversibility would affect the apparent K_D of binding, if not the K_D of the initial binding event itself. Still, this result is one of the reasons that extensive kinetic analysis of an MBI could prove valuable; it reveals which steps are reversible/irreversible and even which steps are kinetically important. If the second step is reversible, a 5-fold improvement of its equilibrium results in around a 25-fold improvement in inhibitory potency (Note: this does assume a rapid equilibrium for the second step).

All of this analysis clearly demonstrates that kinact/KI is not an accurate global measure of enzymatic activity unless additional information is known about the system. Instead, it suggested that complete characterization of the mechanism of inactivation of a MBI would be necessary to allow for rational optimization. This would accurately describe the KD of binding and reveal the identity of the rate determining step for optimization of the kinact. Researchers would then be able to direct their efforts to effect the desired improvements.

Complete characterization of the mechanism of inactivation requires obtaining each of the microscopic rate constants of this process. This likely requires some sort of detectable spectroscopic change to occur in the enzyme during the process of inactivation. Fortunately, most of the classes of enzymes that MBIs are commonly used to target contain such spectroscopic changes, including flavin-containing enzymes,[194] heme-dependent oxidases,[195,196] quinone-dependent oxidases,[197] and PLP-dependent enzymes such as BioA. There are also cases where the inhibitor itself undergoes detectable changes in a spectroscopic property.[198] With so many systems containing such spectroscopic signatures, we propose that complete characterization of

MBIs is a widely applicable method. We also choose to optimize MBIs of BioA using this method, beginning with complete characterization of the process of inactivation of BioA by **1**.

2.4 Stopped Flow Evaluation of Inhibitor 1 Against BioA

PLP-dependent enzymes undergo a series of states with distinguishable absorbance signatures, ideal for study with stopped-flow spectrophotometry. Incubation of **1** with BioA under stopped-flow conditions utilizing a diode-array detector showed three distinct absorbance regions with large, time-dependent changes (Figure 2.3B). An absorbance peak with a λ_{max} of 410 nm decreases over time, while a corresponding increase is observed at 318 nm (Figure 2.4). These changes are likely caused by disappearance of the external aldimine and subsequent formation of the final, aromatized adduct (Figure 2.3). Finding a peak with a λ_{max} of 540 nm, which increases and then decreases in magnitude (Figure 2.5), can be surmised to be due to the presence of a quinonoid.[199] Previous examination of quinonoid intermediates in PLP-dependent mechanisms generally place the λ_{max} between 490 and 520 nm, though observation of such species is quite rare.[200,201,202] We propose that the additional double bond on **1** that is in resonance with the quinonoid (Figure 2.3A) causes the observed red shift of the peak.

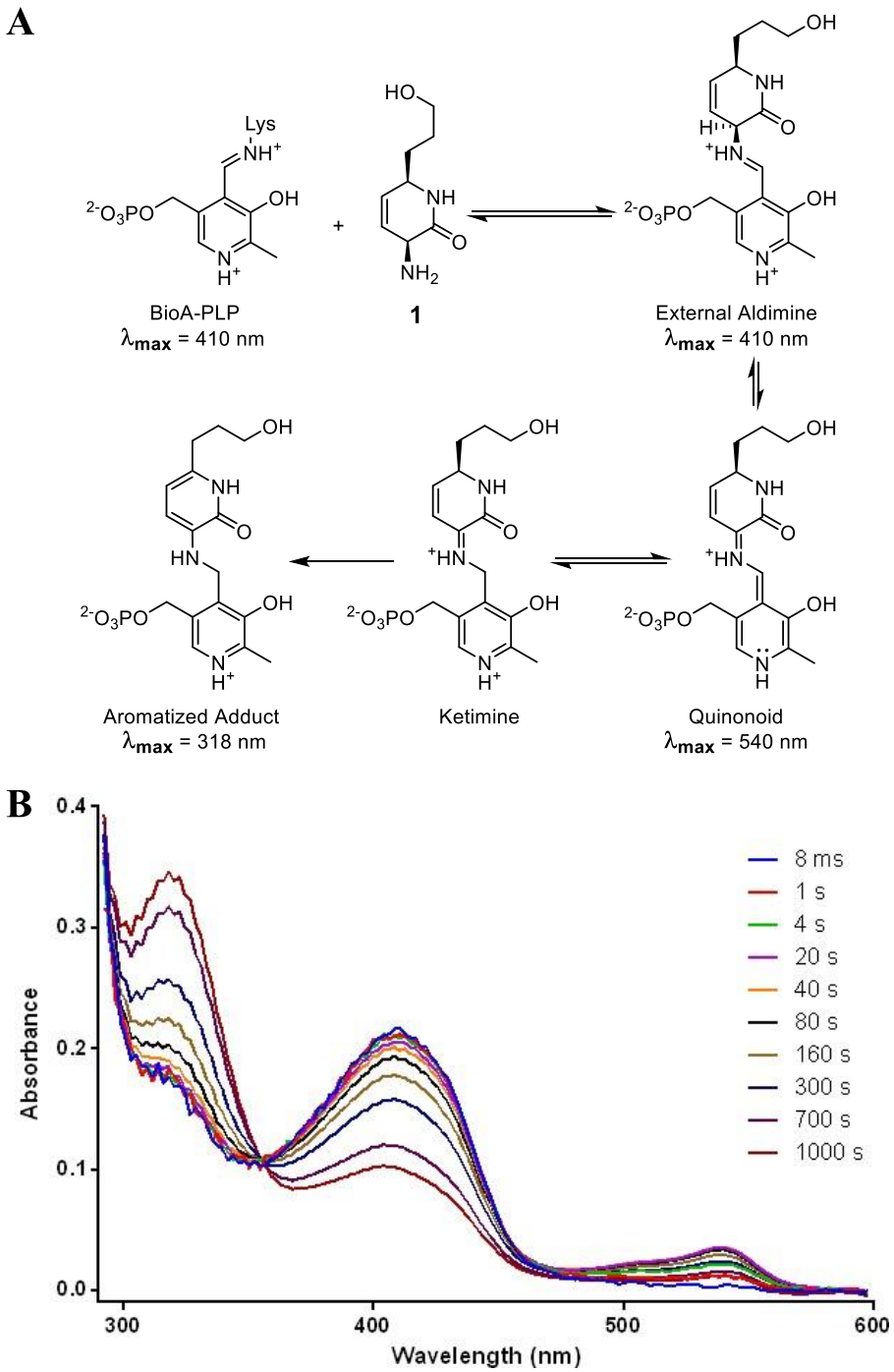

Figure 2.3. BioA Mechanism and Observed Inactivation by **1**. (A) Postulated mechanism of inactivation of BioA by compound **1** with observed absorbance maxima. (B) Absorbance traces from incubation of 12.5 µM BioA with 250 µM **1** in BICINE pH 8.6 at 23 °C

Fitting the reaction time course observed at 540, 410, or 318 nm to summed exponential expressions revealed two fast and one slow reciprocal relaxation times (RRTs) (Figure 2.4, 2.5). The slow RRT had a value significantly less that the k_{inact}, indicating that it arises a minor side reaction. Therefore, kinetic evidence for only two of the four postulated steps was initially obtained. However, close inspection of the earliest time points in the 540 nm time course showed a very short (<2 s) burst in absorbance that was previously unaccounted for (Figure 2.5B). Refitting the 540 nm time course to include another exponential with a very fast RRT allowed the early time domain to be accurately modeled. The observation of three kinetically competent RRTs shows that the reaction must have at least 3 steps.

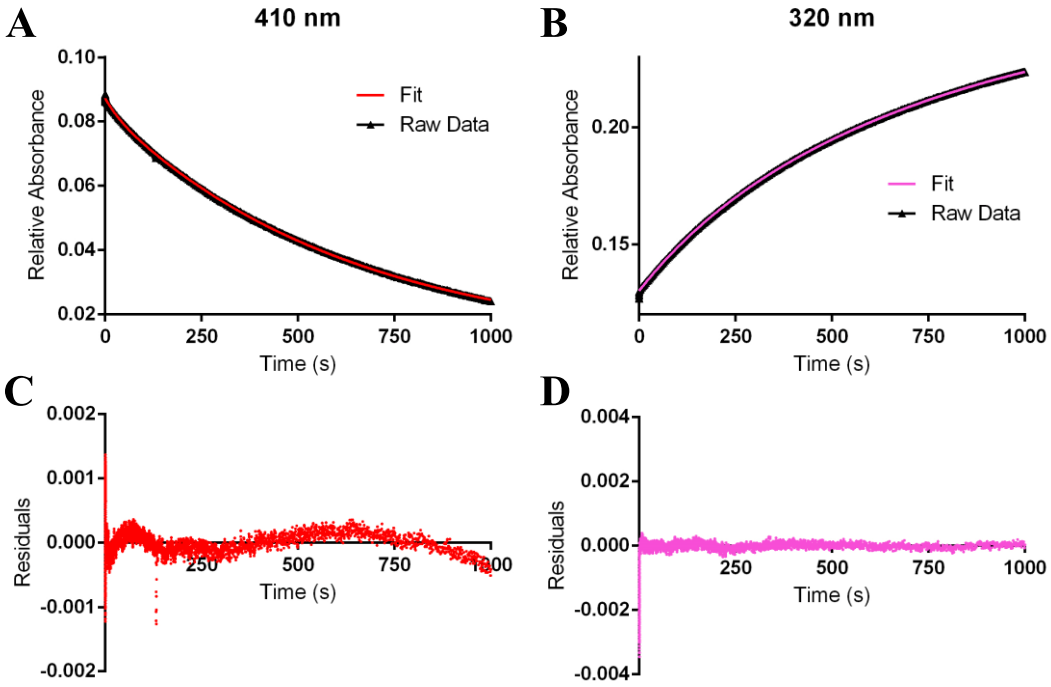

Figure 2.4. Traces Obtained from Spectrophotometrically Monitoring the Incubation of BioA with **1**. All traces use 12.5 µM BioA with 200 µM **1** in BICINE pH 8.6 at 23 °C. (A) Trace obtained from monitoring at 410 nm for 1000 s with fitting. (B) Trace obtained from monitoring at 320 nm for 1000 s with fitting. (C) Residuals from fitting of part (A). (D) Residuals from fitting of part (B).

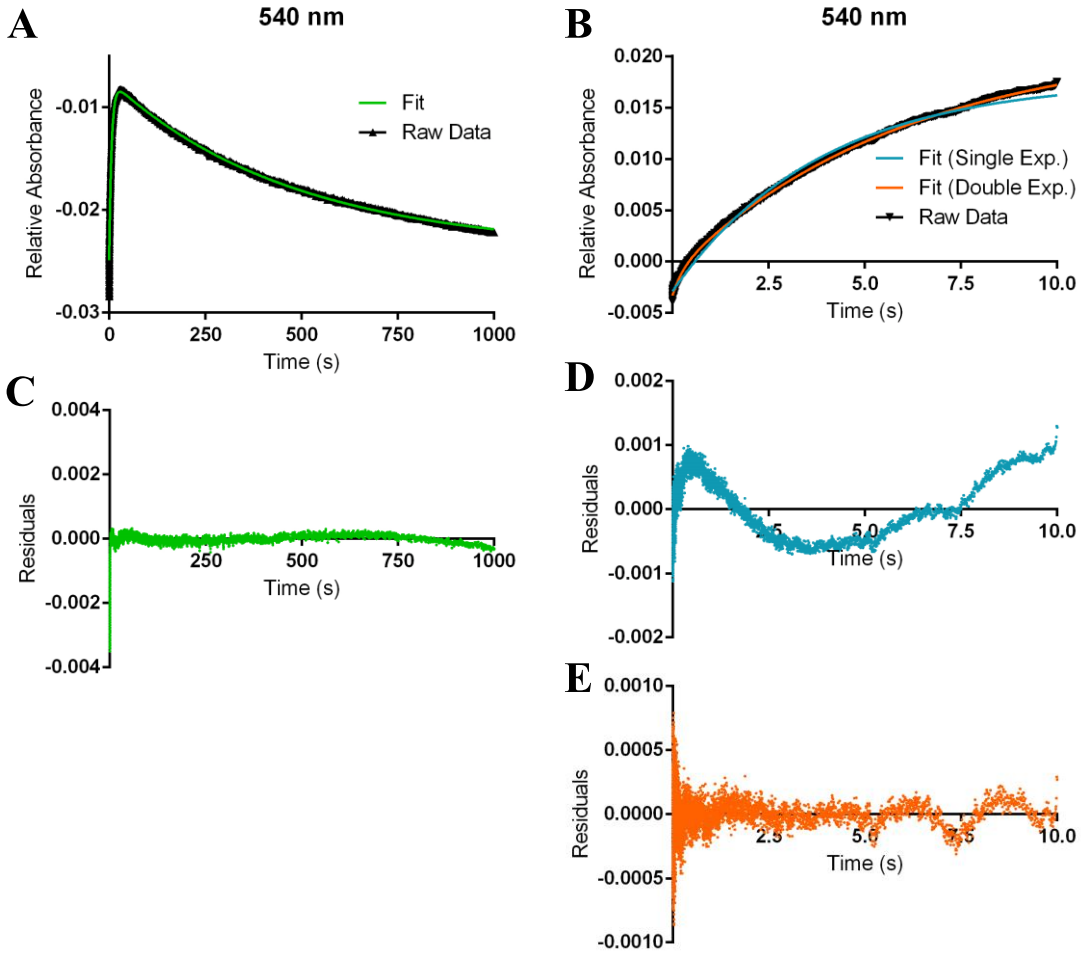

Figure 2.5. Traces from Spectrophotometric Monitoring of the Incubation of BioA with **1** at 540 nm. All traces use 12.5 μM BioA with 200 μM **1** in BICINE pH 8.6 at 23 °C. (A) 1000 s trace with fitting. (B) 10 s trace with fitting using one (blue) or two (orange) exponentials. (C) Residuals from fitting of part (A). (D) Residuals from single exponential fitting of part (B). (E) Residuals from double exponential fitting of part (B).

An examination of the concentration dependence on **1** for each of the kinetically competent RRTs reveals distinctive patterns. The fastest RRT displays a linear correlation with the concentration of **1**, while the second fastest RRT shows no dependence and the slowest RRT has a hyperbolic dependence (Figure 2.6). The magnitudes of the RRTs are separated by ~30-fold, facilitating the data analysis. The linear relationship for the fastest RRT means that it reflects primarily binding of **1**, probably through rapid formation of the external aldimine. The very slight absorbance increase at 540 nm is unexpected for the aldimine, but feasible.[203,204] The intercept

and slope of the plot give the reverse and forward rate constants for binding, respectively, while the ratio gives the binding K_D. Because the reaction is reversible and the RRT is large, it is likely that this binding reaction reaches near equilibrium prior to the downstream reactions. If this is the case, then one would expect the plot of at least one of the other RRTs to exhibit a hyperbolic concentration dependence on **1**, as seen for the slowest RRT (Figure 2.6C). The forward and reverse rate constants for the step following initial complex formation, as well as the K_D for the immediately preceding binding reaction can be computed from the hyperbolic curve. Accordingly, the K_D computed in this way is in good agreement with the K_D computed from the plot in Figure 2.6A (180 vs 240 μM). The intercept at zero of the hyperbolic curve means that the remaining RRT should not exhibit a concentration dependence on **1** and gives information about only the rate constants for downstream steps. Thus, the lack of concentration dependence on **1** of the second fastest RRT (Figure 2.6B) indicates that it correlates with the rate constant(s) for a step or steps that follow the irreversible second step of the sequence. This analysis suggests that the slowest step in the sequence is the formation of the quinonoid, and the second fastest step corresponds to its disappearance.

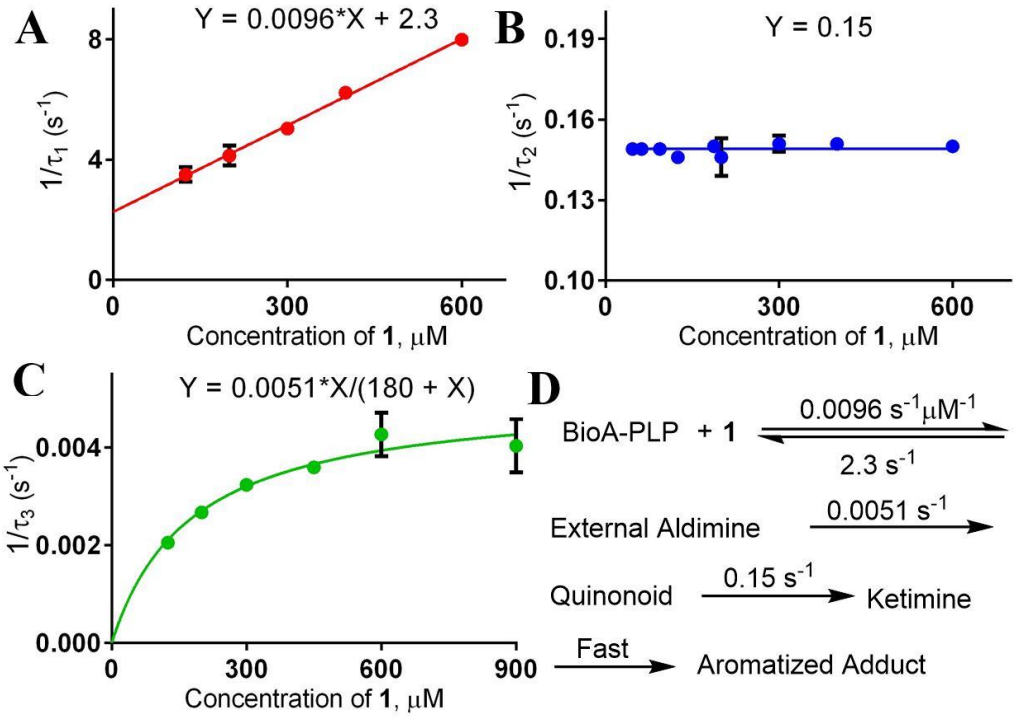

Figure 2.6. Dependence of the Reciprocal Relaxation Times on the Concentration of **1** and the Final Rate Constants Determined. (A-C) Dependence of the observed RRTs on the concentration of 1. (D) Rate constants determined from analysis of graphs A-C. First step forward rate constant is the slope in part (A); reverse rate constant is the intercept in part (A). Second step rate constant is the asymptote of the hyperbola in part (C) minus the y-intercept. Third step rate constant is the y-value in part (B).

The microscopic rate constants of inactivation are displayed in Figure 2.6D. Using the formula from Table 2.2, entry 2, K_I and k_{inact} were calculated from the determined rate constants and are within 2-fold of the experimentally determined values under steady-state conditions. This assignment of rate constants to specific steps was also confirmed by multiple checks using simulation and estimation of the maximum amount of quinonoid formation. It is notable that the tautomerization step to form the aromatized adduct is not observed by this analysis, and thus must be significantly (>30×) faster than ketimine formation, which is plausible as its rate would only be limited by the access of the bound inhibitor to proton donors and acceptors.

The kinetic analysis reveals that there are no detectable reversible steps post-binding and that the second step is almost entirely rate-limiting, which means K_I approximates the K_D of the

Michaelis complex [BioA•**1**] and k_{inact} approximates the rate of formation of the quinonoid. This provides all the information necessary for rational optimization of the scaffold of **1**. We now know that only the first step is reversible, so improving the initial binding equilibrium provides a corresponding increase to the overall K_D. However, the key discovery is that k_{inact} equals the rate of quinonoid formation. This is essential for the scaffold-hopping that we are going to attempt to do. Ideally, the new scaffold would be much easier to synthesize, have similar structural features to the dihydropyrid-2-one of **1**, and facilitate more rapid quinonoid formation.

2.5 Design, Synthesis, and Evaluation of Modified Warheads

Since the quinonoid is formed following the deprotonation of the α-proton on **1** by Lys283 of BioA (Figure 2.3A), we hypothesized lowering the pK_a of this proton would enhance k_{inact}. 2,3-Dihydro-4-pyranone (**42**) and 2,3-dihydro-4-pyridone (**43**) scaffolds (Figure 2.7) were initially designed based on the computationally predicted pK_a values of their α-protons: 15.1 for **42** and 14.3 for **43**, which are nearly six pK_a units less than the predicted value for **1** (pK_a ~ 21.1). The greater acidity is due to conversion of the amide in **1** to a more electron withdrawing vinylogous ester and amide in **42** and **43**, respectively. We were also attracted to the scaffolds of **42** and **43** because they remove the second stereocenter (at C6 in **1**) by shifting the position of the olefin, a change that we expected would simplify analogue synthesis. Synthesizing **42** and **43** would allow for direct comparison of the dihydropyrid-2-one ring of **1** to its dihydropyran-4-one and dihydropyrid-4-one counterparts.

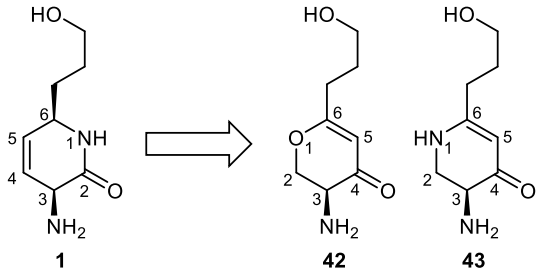

Figure 2.7. Dihydropyran-4-one and Dihydropyrid-4-one Scaffolds for MBI Development

Both ring systems have previously been reported, with 2,3-dihydro-4-pyranones commonly synthesized through hetero-Diels-Alder (HDA) reactions between Danishefsky's diene and aldehydes.[205] Unfortunately, the HDA method is generally limited to variation at C2 and C6, and modification of Danishefsky's diene to introduce an amino group appeared quite challenging. Georg and co-workers recently reported a versatile synthesis of 2,3-dihydro-4-pyridones through 6-*endo-dig* cyclization of an ynone derived from β-amino acids; however, the introduction of amino substituents at C3 was not disclosed.[206207208] Modifying this strategy, we envisioned that using ynones derived from either serine or 1,2-diaminopropionic acid could be cyclized to efficiently construct the desired ring systems with an amino group at C3 (Scheme 2.7). The ynones could be synthesized from the addition of an alkynyllithium reagent to an amino acid derived Weinreb amide.

First Generation Syntheses of 42 and 43. To begin the synthesis of **42**, commercially available Boc-serine was again transformed into Weinreb amide **7** by employing EDC and NMM in CH_2Cl_2 (Scheme 2.7).[209] Addition of three equivalents of alkynyllithium **44** to **7** furnished α-amino ynone **45** upon quench.[210] Unfortunately, all of the standard conditions (AgOTf[211], AuCl[212], $Pd(MeCN)_4(BF_4)_2$[213]) that promote 6-*endo-dig* cyclizations of alcohols into ynones instead provided the 5-*endo-dig* product. It was difficult to confirm this cyclization, as 5-membered cyclic enaminones and 2,3-dihydro-4-pyranones have very similar 1D NMR resonances,[214215] and the isolated product was unstable and polymerized readily. Thankfully, an HMBC correlation between the α-proton and the fully substituted olefinic carbon combined with a lack of correlation between the protons on the hydroxymethyl chain and that same carbon confirmed the identity of the cyclic enaminone. It is worth noting that this synthesis was also attempted unsuccessfully with a trityl group replacing the Boc, imagining that significant increases in steric hindrance towards cyclization could be helpful. While these results were

disappointing, we remained undismayed towards pursuing an analogous synthesis of **43**, since we surmised the enhanced nucleophilicity of the β-amino group of **47** over the β-hydroxy group in **45** would override the unproductive competitive cyclization of the α-Boc-amine.

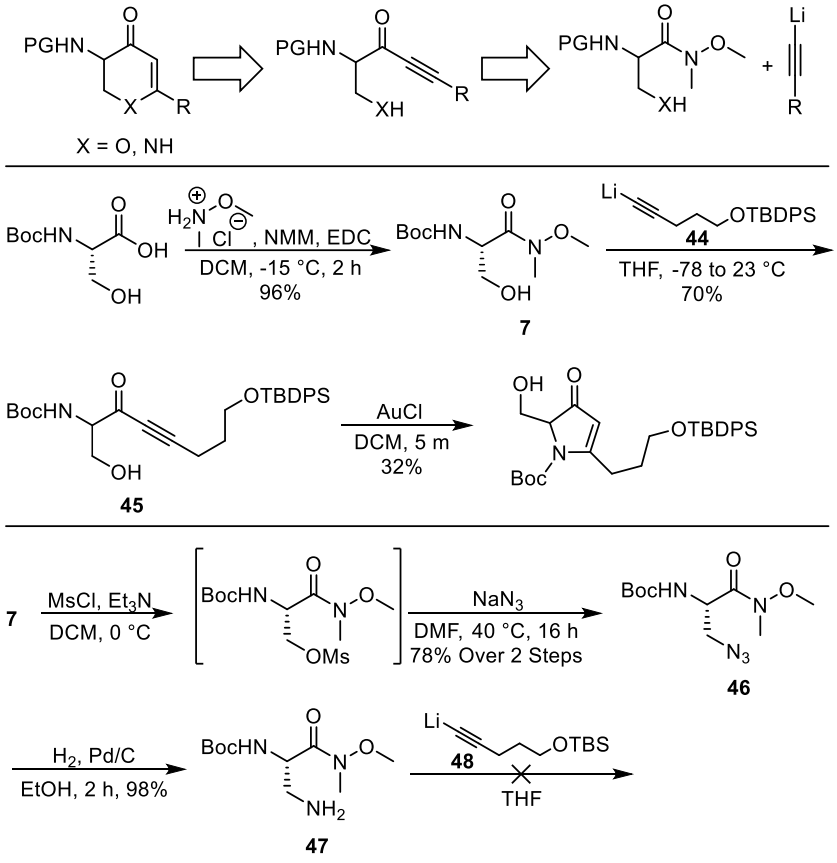

Scheme 2.7. Retrosynthetic Analysis & First Generation Syntheses Towards **42** and **43**

A congruent route for the synthesis of **43** necessitates the conversion of the alcohol in **7** to an amine. To begin, **46** was synthesized through mesylation of **7** followed by azide displacement. Notably, the yield of the azide displacement increased by 20% when a longer reaction time was used concomitant with reduced heat (from 60 °C to 40 °C). Using MeOH as the solvent for the subsequent hydrogenation gave widely variable yields,[216] but switching to EtOH afforded **47**, the desired diaminopropionic acid derivative, in excellent yield. However, addition of lithium

acetylide **48** to **47** only furnished the product in trace quantities, instead producing many uncharacterizable highly polar products in addition to a low yield (<10%) of the enynone that would result from addition of the alkyne and elimination of the β-amino.[217]

As the synthesis of **45** from **7** and **44** was quite facile, further investigation seemed warranted to understand the failure of **48** to add into **47**. An obvious difference in reactivity between **7** and **47** is that the alcohol of **7** gets deprotonated by alkynyllithium species, whereas the unprotected amino group of **47** does not. **7** and **47** also have highly contrasting solubility in THF: **7** is highly soluble (>0.5 M), whereas the maximum solubility of **47** is ~0.02 M. The lack of solubility of **47** appeared more likely to be causing the undesired reactivity, so we hypothesized that **47**, following mono- or di-lithiation (di-lithiation through reaction of the acetylide with the Weinreb amide of **47**), was forming insoluble aggregates that had perplexing reactivity.[218] Polar additives, both organic (HMPA, DMPU, TMEDA, LiHMDS), and inorganic (LiCl) were added to the reaction to break up the potential aggregates,[219] with none producing a desired effect. The use of alkynylmagensium reagents was also unproductive. Having no remaining alternatives, we chose to protect the β-amino group of **47** to enhance solubility. Common amino protecting groups orthogonal to Boc, such as Fmoc or Cbz, could not be used for this synthesis, so bis-PMB and trityl protecting groups were chosen (Scheme 2.8). Compounds **49** and **50** were synthesized using standard conditions in moderate yield. When **49** and **50** were subjugated to the problematic ynone-formation reaction, isolation of the products revealed large (>40%) yields of tritylamine and bis-PMB-amine indicating competitive β-elimination was a major side-reaction. Given the extremely poor nature of these leaving groups, this is unexpected, but must be facilitated by lithium coordination. These results also shed light on the failure of combining β-amino **47** and lithium acetylide **48**, suggesting a similar elimination mechanism occurs with ejection of lithium amide, formally an endergonic process. Notably, elimination was not observed with **7** since the

β-hydroxy group is deprotonated under the reaction conditions and elimination would formally lead to release of the dianion lithium oxide, an even more endergonic process.

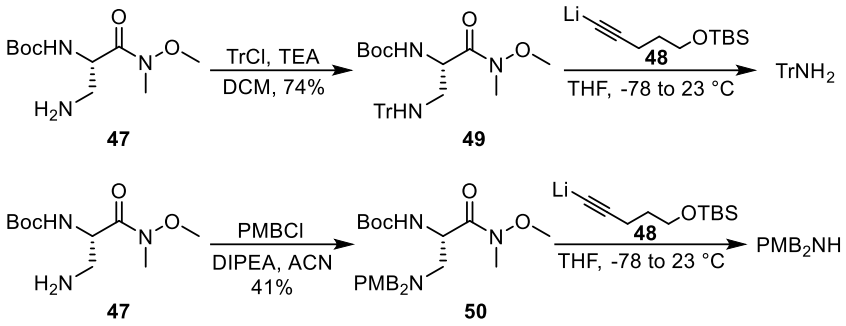

Scheme 2.8. Amine Protection Reveals **48** causes Beta-Elimination of **47**.

Design and Synthesis of Dihydrothiopyranone 51. Having now uncovered the reasons for the failure of the original syntheses of both **42** and **43**, a shrewd solution came to bear. We hypothesized replacing the ethereal oxygen in **42** with a sulfur atom, thus changing the heterocyclic core, should solve the problems with the originally designed synthesis while maintaining the molecule's ability to inactivate BioA. Thiols are more acidic than alcohols and should therefore remain deprotonated during the key Weinreb amide coupling reaction with an alkynyllithium, preventing β-elimination. Thiols are also substantially more nucleophilic; consequently, the resulting ynone should favor the desired 6-*endo-dig* cyclization pathway over the undesired 5-*endo-dig* pathway observed with **7**.[220] We thus began the synthesis of **51**, the 2,3-dihydro-4-thiopyranone analogue of **42** and **43** (Scheme 2.9).

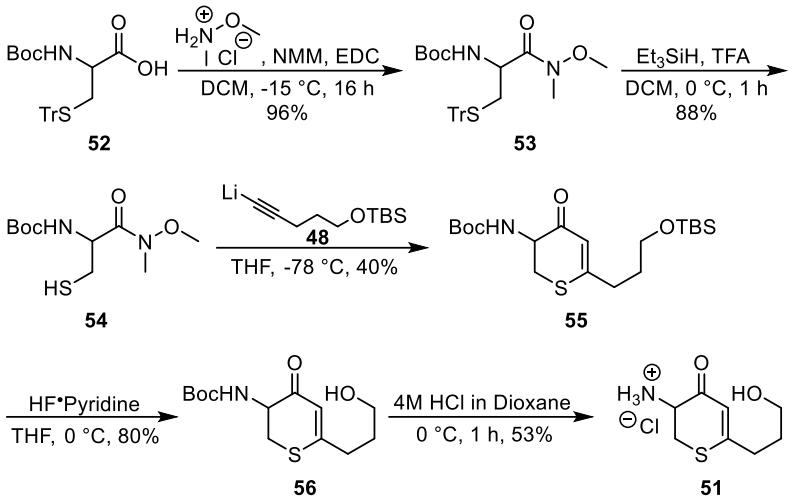

Scheme 2.9. Synthesis of Dihydrothiopyran-4-one **51** from Cysteine Precursors

Compound **15** was synthesized from (±)-**14** using our optimized conditions for Weinreb amide formation in excellent yield. *S*-Trityl deprotection proceeded smoothly with the addition of Et_3SiH and a drop of TFA to afford **16**.[221] Addition of **10** to **16** while maintaining a temperature of -78 °C provided the desired 2,3-dihydro-4-thiopyranone ring through spontaneous cyclization of the intermediate ynone, validating our synthetic plan. The TBS group was deprotected to produce **18**, after which Boc-deprotection was attempted. The use of TFA in CH_2Cl_2 furnished a mixture of desired product **13** and its TFA ester,[222] a virtually unprecedented esterification under these conditions. However, switching to HCl in dioxane provided **13** in a convenient, 5-step synthesis from commercially available *N*-Boc-*S*-trityl cysteine **14**.

Second Generation Syntheses of 2 and 3. Bolstered by the successful synthesis of dihydrothiopyranone **51**, we envisioned two alternate approaches to tackle the synthesis of **42** and **43**. In the first of these, we recognized that bis-protection of the α-amino group of **45** would be necessary for the synthesis of **42** to prevent competitive 5-*endo-dig* cyclization while for target **43** protection of the β-amino group of **47** with a suitable protecting group would be required to prevent undesired β-elimination. Both of these strategies appeared challenging. For example, bis-

Boc-α-amino protection would certainly react with the adjacent alkoxide generated *in situ* from the addition of a lithium acetylide,[223] while the protecting group requirements for the β-amino group are overly restrictive due the necessity for orthogonality with the α-amino Boc and compatibility under the strongly basic reaction conditions of the alkynyllithium addition. The second approach, that we ultimately elected to perform, involved installation of the troublesome α-amino group post-cyclization, which would considerably simplify the synthesis and avoid both of the aforementioned challenges. The feasibility of the new synthetic plan was supported by a report by Collet and coworkers,[224] who demonstrated the reagent *N*-Boc-3-(4-cyanophenyl)oxaziridine could electrophilically transfer a –NHBoc group to the carbon of an enolate. Moreover, a report by Gouault and coworkers confirmed that the required enolate could be regioselectively generated in an analogous C6-substituted N-Boc protected 2,3-dihydro-4-pyridone derivative and react successfully in an aldol-type reaction.[225]

As stated above, the retrosynthetic plan calls for cyclization of an ynone followed by electrophilic amination at the C3 carbon. (Scheme 2.10) The second-generation synthesis of **42** begins with the mono-PMB-protection of 1,3-propanediol **57** to form **58**.[226] Subsequent Jones oxidation and Weinreb amide formation[227] afforded ynone precursor **59**. Addition of alkynyllithium **60** furnished **61** in excellent yield, which was then deprotected with DDQ to provide β-hydroxy ynone **62**. The ensuing cyclization using AgOTf afforded dihydro-4-pyranone **63** without incident, ready for the electrophilic amination. To our surprise, addition of LiHMDS to a solution of **63** resulted in a rearrangement of the heterocycle to form **64**, which was rigorously characterized. The simplest route to formation of **64** is α-enolate formation leading to β-elimination of the endocyclic ether oxygen, rupturing the dihydropyranone core and forming an alkoxy-dienone, furnishing **64** upon quench, similar to the mechanism previously been

postulated by Boring and Sindelar.[228] The facility of this base-catalyzed degradation pathway completely nullified this synthetic route.

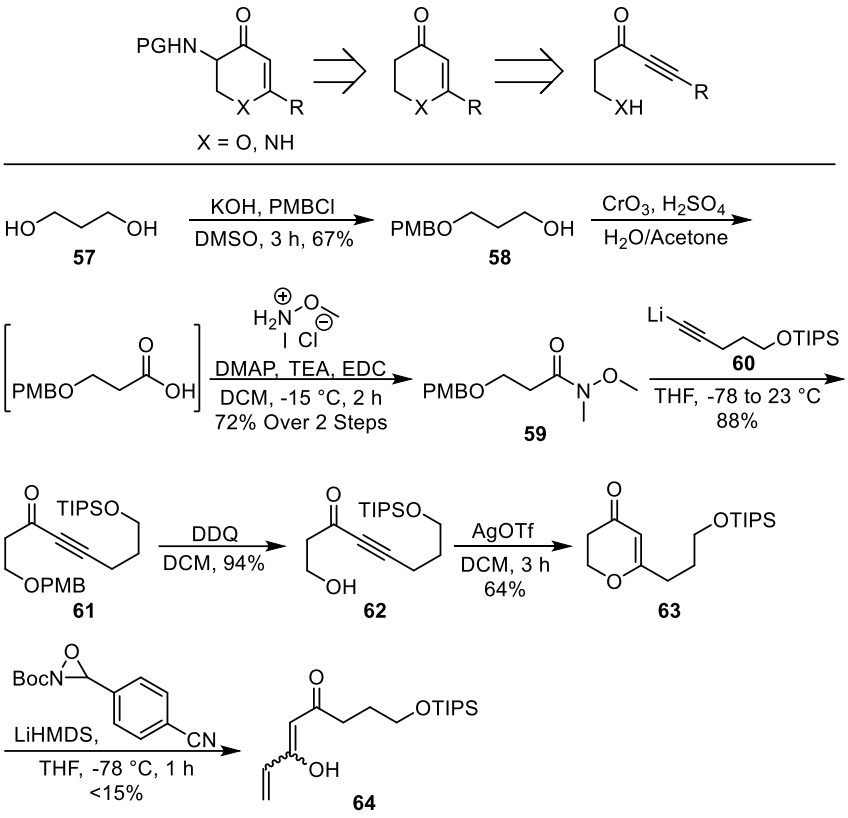

Scheme 2.10. Synthesis of 2-Amino-Dihydropyran-4-ones by Electrophilic Amination Leads to Ring Cleavage via Beta-Elimination

As mentioned previously, Gouault and coworkers had demonstrated that replacing the ethereal oxygen with a Boc-protected amino, as an analogous second generation synthesis of **43** would necessitate, would result in stable and nucleophilic enolates for the desired electrophilic amination,[229] so we chose to proceed with this synthesis. Boc-β-alanine **65** was first transformed into Weinreb amide **66** using standard conditions (Scheme 2.11). Subsequent addition of **48** furnished Boc-protected β-amino ynone **67**, primed for cyclization. Ynone **67** was added to PPh_3AuOTf generated *in situ* from the combination of AgOTf and PPh_3AuCl, producing dihydropyridone **68**.[230] Enolate formation employing LiHMDS followed by addition of *N*-Boc-3-

(4-cyanophenyl)oxaziridine afforded the desired electrophilic amination product **69**. In this reaction, the byproduct *p*-cyanobenzaldehyde undergoes rapid aldol addition with the enolate, limiting the theoretical yield to approximately 50%.[34] Deprotection of the TBS group using HF·pyridine proceeded smoothly; however, the final bis-Boc deprotection of **70** proved unconquerable. Boc groups on the N1 position of dihydro-4-pyridones are much more challenging to remove than standard alkyl-amino Boc groups, requiring up to 24 hours using TFA in CH_2Cl_2.[231] Several conditions were attempted (TFA in CH_2Cl_2, HCl in dioxane/EtOAc, phenol and TMSCl in CH_2Cl_2)[232] that provided only trace amounts of product. The Boc-amino group on C3 was cleanly deprotected within an hour applying any of these conditions, but longer reaction times to remove the second Boc group resulted in extensive decomposition. We speculate that dimerization of the resulting α-aminoketones to a tricyclic pyrazine derivative is occurring based on the well-known propensity of α-aminoketones to furnish dihydropyrazines, which can spontaneously oxidize.[233]

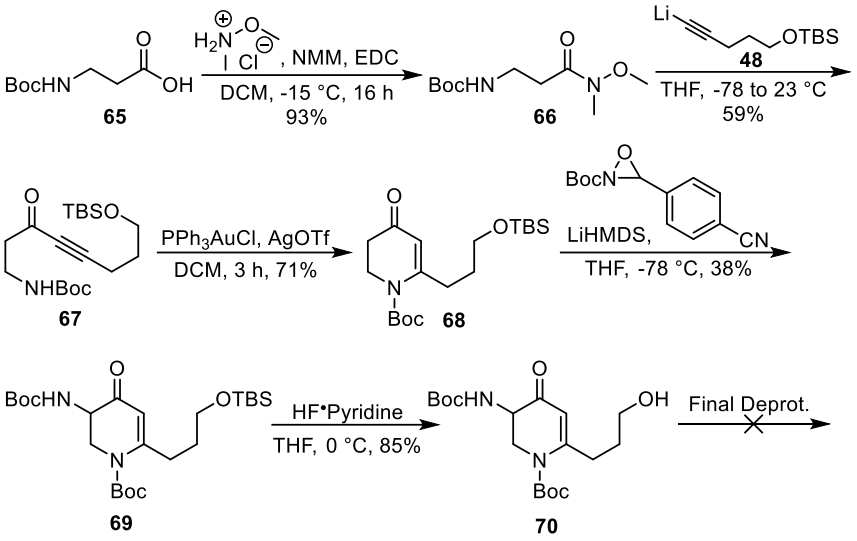

Scheme 2.11. Synthesis of **43** by Electrophilic Amination Fails During the Final Deprotection

Third Generation Syntheses of 42 and 43. Frustrated by the repeated failures, it was decided to return to the original retrosynthetic plans and modify them to accommodate necessary changes. As mentioned above, in the synthesis of **43**, the β-amino group on **47** needs to be protected with either an amide or carbamate group so that the addition of the lithium acetylide removes the amino proton. Most conventional amide and carbamate protecting groups are either not stable to lithiates or appeared impossible to remove without side-reactivity. One that appeared adequate for our purposes is (2-Trimethylsilyl)ethoxycarbonyl (Teoc), which is quite robust to lithiation and can be removed in the presence of a Boc group with TBAF.[234]

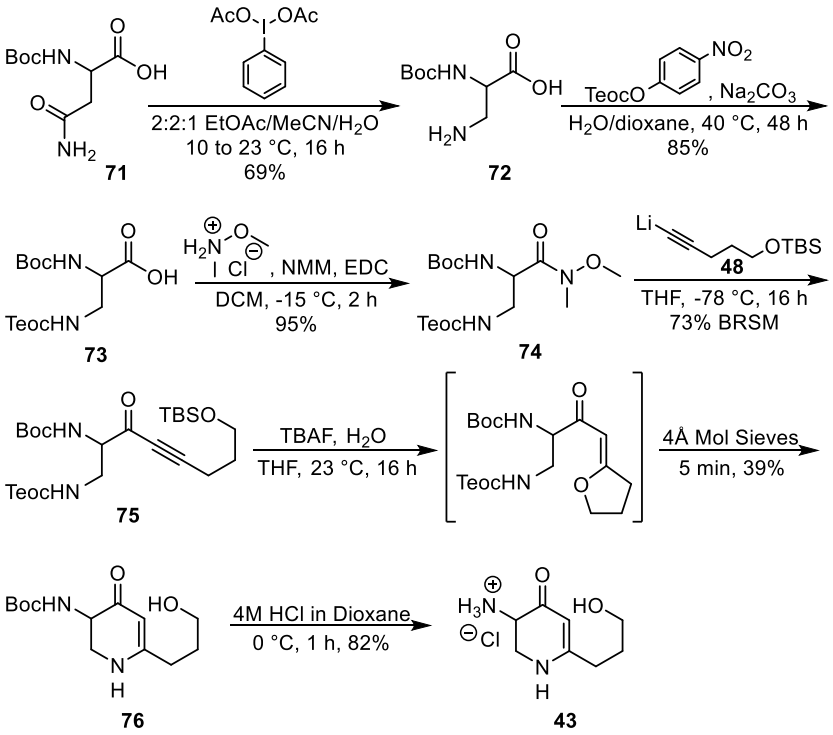

Scheme 2.12. Synthesis of **43** using Teoc Protection of the Beta-Amino Group

The synthesis of **43** using this revised route began with (±)-Boc-asparagine **71** (Scheme 2.12). A modified Hoffman rearrangement provided mono-Boc protected **72** with only a filtration necessary for purification.[235] Subsequent addition of 4-nitrophenyl 2-(trimethylsilyl)ethyl carbonate, in a modified procedure from the one developed by Rosowski and Wright,[236] afforded differentially protected diaminopropionic acid derivative **73** following purification by simple aqueous extraction. The only previous synthesis of **73**, published by Boger and coworkers in 2000, required four steps from *N*-Boc-serine methyl ester.[237] Formation of the Weinreb amide furnished **74**, which reacted with alkynyllithium **48** to provide ynone **75**. Compared to the previous conversion of **66** to **67**, formation of **75** was quite sluggish, likely due to increased steric hindrance from the Teoc group. The most challenging point of the synthesis proved the next step, concomitant removal of the Teoc and TBS groups.

Attempted deprotection of **75** using TBAF rapidly consumed the starting material, yet only yielded **76** in a 12% yield with numerous highly polar side-products. We hypothesized this was due to the strong basicity of TBAF. AcOH and water are known to attenuate both the basicity and reactivity of TBAF,[238] and as such they were each added to TBAF deprotections of **75**, attempting to remove the Teoc and TBS groups while leaving the rest of the molecule intact. To our dismay their inclusion either abolished activity (AcOH, >10 equiv H_2O) or slowed the reaction without improvement of the yield (<10 equiv H_2O). Careful monitoring by TLC showed a faint intermediate spot with an R_f value slightly below the staring material that rapidly appeared following the addition of TBAF and slowly disappeared during the course of the reaction. Isolation of this spot revealed that the TBS group had been removed and liberated alcohol cyclized into the ynone, forming a substituted tetrahydrofuran (Scheme 2.12). This was the sole product when >10 equivalents of H_2O was added to the TBAF reaction, though it appeared to degrade during chromatography, as we were never able to isolate it in yields above 50%. Realizing that the formation of the vinylogous ester in the tetrahydrofuran intermediate would tame the acidity of the α or γ protons as compared to **75**, which were believed to be the source of the low yield, a two-step process was developed for this dual deprotection. First, TBAF and water (60 equiv) were stirred with **75** for 16 h, after which it had been entirely converted to the tetrahydrofuran intermediate. Then 4 Å molecular sieves were added, sequestering much of the water and causing deprotection of the Teoc group within 5 minutes. This procedure more than tripled the yield to 39%, a feasible yield for continuing. The speed of the second Teoc deprotection surprised us, but commercially available 1 M TBAF in THF contains 5% (w/w) H_2O significantly dampening its activity.[239] Very little water remains -following addition of the sieves, so the TBAF is extremely reactive and can remove even a robust group like Teoc in under 5 min. We also tried replacing the TBS group in **76** with several common protecting groups (Bn, THP, MOM) to test whether mono-Teoc deprotection could improve the cyclization yield.

Unfortunately, in all attempted cyclizations lacking the TBS group, the yield never approached 20%, further demonstrating the importance of the vinylogous ester intermediate. Finally, deprotection of **76** employing 4 M HCl in dioxane completed the synthesis of dihydropyridone **43**.

Turning our attention towards the synthesis of **42**, *N*,*N*-diprotection of the serine-derived Weinreb amide was deemed essential prior to ynone formation. The most common ways to protect both protons of an amine group are using either phthalimide or bis-Boc, both of which were eliminated from consideration for this system. Phthalimide deprotection requires relatively harsh conditions that would be incompatible with the remaining heterocycle, while the bis-Boc derivative is extremely bulky and would be highly susceptible to intramolecular cyclization with the β-alkoxy generated from alkynyllithium addition to form a stable oxazolidinone. Instead, we decided to adopt the approach reported by Devlin & Du Bois[240] which utilized dual Boc and MOM protecting groups to protect an amine. This appeared ideal for our system, as MOM and Boc share similar stability profiles as well as deprotection conditions, and a MOM group is both less electron withdrawing and smaller than a Boc group, making intramolecular cyclization to form an oxazolidinone much slower.

Beginning with **7**, standard TBS protection conditions afforded **77** in excellent yield. MOM protection using KHMDS as the base furnished the desired tri-protected serine derivative,[241] whose R_f was coincident with **77**. This intermediate was not isolated, but directly deprotected with HF·Pyridine to furnish Weinreb amide **78**. Surprisingly, when **78** was left in $CDCl_3$ overnight for ^{13}C NMR characterization, the molecule cyclized to 1,3-oxazolidine due to residual acid (Scheme 2.13), an undesirable reaction that foreshadowed complications with the future Lewis acid catalyzed 6-*endo-dig* cyclization. The use of non-acidic solvents such as acetone or CH_2Cl_2 was necessary for successful characterization. Addition of **44** to **78** at -78 °C furnished

the desired dual Boc-MOM protected ynone **79** in satisfactory yield. Maintaining a temperature of -78 °C proved essential to prevent the aforementioned intramolecular cyclization of the β-alkoxide into the Boc group.

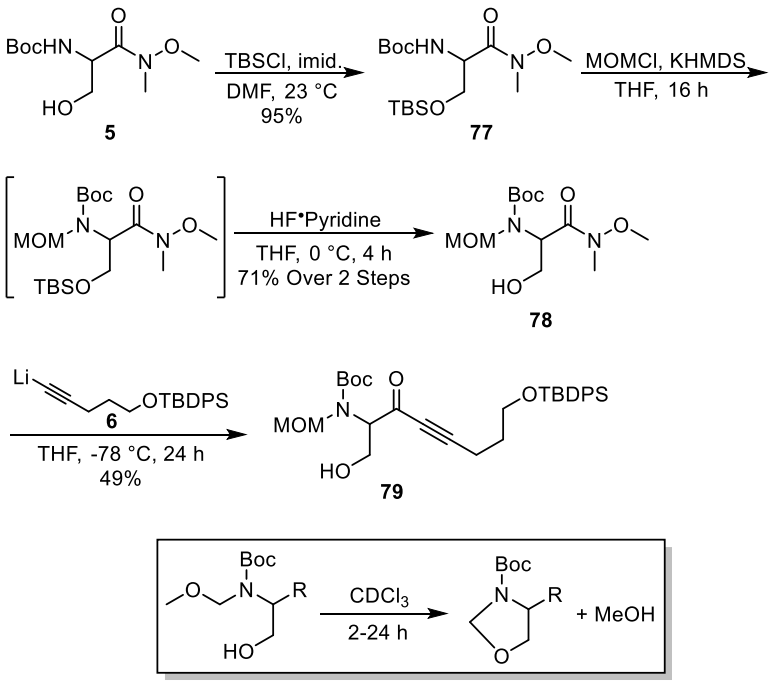

Scheme 2.13. Synthesis of Dual Boc-MOM Protected Amino Ynone **79** and Side Reactivity from the Beta-Hydroxyl

To our consternation, the cyclization of **79** to dihydropyranone **80** proved problematic, as standard conditions (AgOTf, AuCl) rapidly produced **80** along with a bevy of side-products (Table 2.4, entries 1-2). The reactivity of the MOM group in the presence of Ag(I) salts has been previously exploited in several synthetic transformations,[242] so the observed side-reactivity was not surprising. The rapidity of these reactions suggested that dampening the activity of the Lewis acid would be necessary to improve the reaction. Lowering the temperature, while successful in completely stopping the reaction (Table 2.4, entry 3), did not alleviate the undesired reactivity at temperatures where the reaction proceeded (Table 2.4, entry 4). Pursuing alternative alkynophillic Lewis acids lead to the discovery that PPh_3AuCl did not promote any reaction

(Table 2.4, entry 5), in contrast to AuCl. Surmising that the substantially increased electron density from the phosphine ligand dampened the reactivity of the gold catalyst, we attempted to see if a "sweet spot" in electron density on the gold could be attained, where cyclization would occur without the undesired side-reactivity. A well-known way to modify the properties of gold catalysts is to induce ion exchange through the addition of silver salts.[243] Switching to bistriflimide (Table 2.4, entry 6) provided a very similar product profile to the original conditions, but the substitution of hexafluoroantimonate (Table 2.4, entry 7) afforded **80** in substantially increased yield, validating this approach. The use of triflate (Table 2.4, entry 8) proved the most successful, producing the highest yield with a modest reaction time of 3 h. The undesired side products were still present with this modification, but in greatly lessened amounts.

Table 2.4. Metal-Catalyzed Cyclization of Hydroxy-Ynone **79** to Dihydropyran-4-one **80**

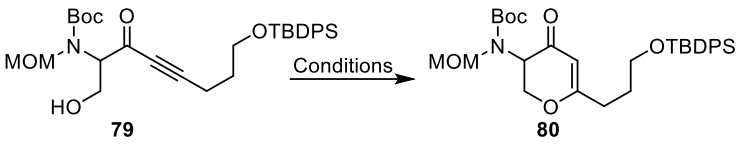

79 **80**

Entry	Conditions	Yield
1	AgOTf (1.0 equiv), 5 min, 23 °C	15%
2	AuCl (0.1 equiv), 5 min, 23 °C	10%
3	AgOTf (1.0 equiv), 3 h, -40 °C	N.R.
4	AgOTf (1.0 equiv), 20 min, -15 °C	~10%
5	PPh_3AuCl (0.1 equiv), 3 h, 23 °C	N.R.
6	PPh_3AuCl (0.1 equiv), $AgNTf_2$ (0.05 equiv), 10 min, -78 to 0 °C	7%
7	PPh_3AuCl (0.1 equiv), $AgSbF_6$ (0.07 equiv), 16 h, -78 to 0 °C	43%
8	PPh_3AuCl (0.2 equiv), AgOTf (0.1 equiv), 3 h, -78 to 0 °C	52%

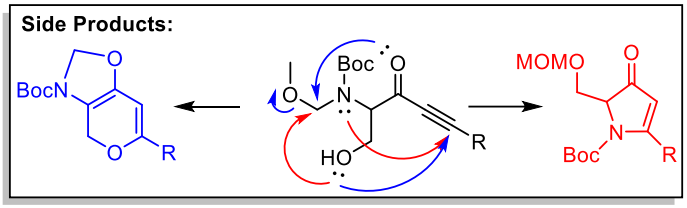

TBDPS deprotection of **80** using HF·Pyridine swiftly afforded penultimate intermediate **81** (Scheme 2.14). However, standard Boc deprotection conditions were unsuccessful in forming the final product **42**, instead leading to degradation. Fearing that aprotic conditions were leading to attack of the ketone onto the MOM group as seen previously (Table 2.4), both aqueous acid and a switch of the solvent to MeOH were attempted, with neither providing more than trace amounts of product. Employing a Lewis acid in anhydrous conditions was also fruitless, as $SnCl_4$[244] failed to produce **42**. A report by Hu and coworkers[245] using $BiCl_3$ as a Lewis acid in a partially

aqueous environment appeared perfect for our system. Indeed, slight modifications to their procedure furnished **42**, completing the trio of desired scaffolds.

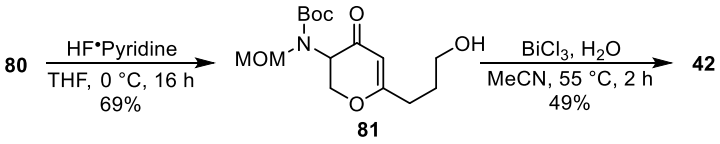

Scheme 2.14. Final Deprotections to Furnish Dihydropyran-4-one **42**.

Biochemical Results. Compounds **42**, **43**, and **51** were then evaluated for their ability to irreversibly inhibit BioA. We developed a LC-MS/MS method for the detection of dethiobiotin with biotin as an internal standard and used it with the conditions previously established by Aldrich and coworkers for assaying BioA by coupling it with tubercular BioD.[246] 0.5 μM BioA was preincubated with 0.05-1 mM of inhibitor in the absence of substrates, and aliquots were removed at times between 2 and 40 minutes. Each of these aliquots were assayed for their remaining enzymatic activity by measuring the production of DTB following the addition of substrates and BioD. Neither dihydro-4-pyranone **42** nor dihydro-4-thiopyranone **51** had any inhibitory activity; however, dihydro-4-pyridone **43** displayed time-dependent inhibition of BioA, consistent with what one would expect from a MBI. The lack of activity of **42** and **51** was found to due to their instability in the basic aqueous conditions of the assay. The k_{obs} values were obtained through plotting the observed rates of DTB formation versus preincubation time at each inhibitor concentration. Next, the k_{obs} values were plotted against the concentration of inhibitor, and fitting this data to a hyperbola produced the K_I and k_{inact} values displayed in Table 2.5 (See experimental section). Dihydropyrid-4-one **43** possesses a nearly 3-fold increase in k_{inact} relative to **1**, and the rate limiting step cannot be slower than the k_{inact}, so we successfully increased the rate of quinonoid formation by at least 3-fold. This validates our hypothesis that lowering the pK_a of the α-proton would lead to more rapid deprotonation by BioA, though this improvement was

less than we anticipated based on the predicted difference in pK_a between **43** and **1**. Unfortunately, this did come with a concomitant increase in the K_I value when compared to **1**, likely due to a loss of binding affinity in the initial equilibrium.

Table 2.5. K_I and k_{inact} Values for the Inhibition of BioA by **1**, **42**, **43**, and **51**

Compound	Structure	k_{inact} (min^{-1})	K_I (mM)
1	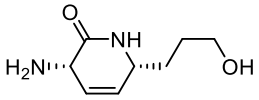	0.18 ± 0.01	0.52 ± 0.07
42	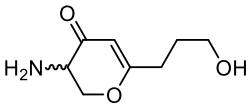	<0.01	>5
43	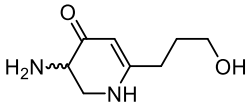	0.48 ± 0.12	3.9 ± 1.2
51	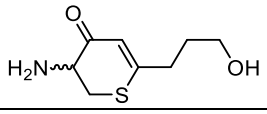	<0.01	>5

Based on the crystal structures available, the higher K_I could not have been predicted, so we consider it an unfortunate happenstance. The increased k_{inact} value means that the dihydro-4-pyridone scaffold has greater potential for development, as it has a higher theoretical limit for mechanism-based inhibition for BioA. It is also extremely likely that binding affinity could be regained through replacement of the 3-hydroxypropyl chain, and the fact **43** can be constructed in 7 steps from commercially available starting materials would greatly expedite such syntheses. However, based on the stringent requirements for Teoc deprotection and the reactions sequence required for moderate yield formation of **75**, all analogues of **43** would have to be synthesized directly from **76**. This certainly makes a reasonable number of analogues feasible, but it does limit the available pool without development of another synthetic route that could integrate alternative tail structures.

On the other hand, the increased k_{inact} of **43** provides strong support for our method of MBI optimization. Rational optimization of an MBI's rate limiting step, to our knowledge, has not been previously performed. Our stopped-flow analyses directed us to improving the rate of quinonoid formation, which we successfully accomplished through the synthesis of **43**, an inhibitor with a decreased pK_a value of the α-proton. When viewed through the lens of being the first attempt rational optimization of an MBI and providing a roadmap for others to do the same, this work is a resounding triumph.

2.6 Conclusion.

This work highlights the continued preclinical development of MBIs of BioA, including switching scaffolds and the development of a novel approach to MBI optimization. We initially attempted to develop analogues of **1** through replacement of its hydroxypropyl tail by either a methylene or di-methylene linkage to electron-deficient triazoles. We successfully synthesized

compound **4**, but it had no activity against BioA and the difficulty of analogue development convinced us that an alternative scaffold was necessary. An extensive investigation into K_I and k_{inact} for various mechanisms by which mechanism-based inhibition can occur revealed that these parameters are commonly interpreted incorrectly. It also demonstrated that complete knowledge of the microscopic rate constants of inhibition is necessary for rational optimization of MBIs. To advance the development of MBIs of BioA while also providing an example of the novel approach of complete MBI characterization, we analyzed the inhibition of BioA by **1** using stopped-flow spectrophotometry. This revealed that **1** inactivated BioA by a rapid reversible binding step followed by two irreversible steps that were significantly slower. The rate of quinonoid formation was found to be the kinetic bottleneck, which was vital information towards the design of new scaffolds for BioA inhibition. We designed dihydropyran-4-one **42**, dihydropyrid-4-one **43**, and dihydrothiopyran-4-one **51** as potential inhibitors of BioA with reduced pK_a values of the α-proton. Envisioning congruent synthetic pathways of cyclization following generation of an α-amino ynone intermediate, we easily constructed **51** but were forced to amend our strategies for **42** and **43**, as competitive 5-*exo*-*dig* cyclization, β-elimination of the ynone, and dimerization of the resultant α-amino carbonyls all complicated the syntheses of the scaffolds. We were able to overcome these challenges utilizing specialized protecting groups, including Teoc protection of the β-amino group in the assembly of **43** and Boc-MOM protection of the α-amino group in the synthesis of **42**. Dihydropyran-4-one **42** and dihydrothiopyran-4-one **51** were found to be unstable in the assay conditions, but dihydropyrid-4-one **43** possessed an improved k_{inact} against BioA, validating our pK_a-based design strategy. The synthesis of **43** facilitates construction of many analogues, but an alternative synthetic route would be necessary for compounds that contain a shorter carbon chain for the tail of the MBI. The increased k_{inact} also demonstrates the value of our rational approach to optimization, and this work should provide a clear blueprint for its usage in future rational MBI development.

2.7 Experimental Procedures.

General Methods. All reactions were performed under an inert atmosphere of dry Ar in oven-dried (150 °C) or flame-dried glassware. ^{1}H and ^{13}C NMR spectra were recorded on a 400, 500, or 600 MHz spectrometer. Proton chemical shifts are reported in ppm from an internal standard of residual chloroform (7.26), methanol (3.31), or acetone (2.05), and carbon chemical shifts are reported in ppm from an internal standard of residual chloroform (77.16), methanol (49.00), or acetone (29.84). Proton chemical data are reported as follows: chemical shift, multiplicity (s = singlet, d = doublet, t = triplet, q = quartet, pent = pentet, m = multiplet, br = broad), coupling constant(s), integration. High resolution mass spectra were obtained on a TOF II TOF/MS instrument equipped with an ESI interface. TLC analysis were performed on TLC silica gel plates and were visualized with UV light, ninhydrin, 10% PMA, or $KMnO_4$ solution. Purifications were performed by flash chromatography on silica gel or with a medium-pressure flash chromatography system equipped with flash column silica cartridges.

Materials. An anhydrous solvent dispensing system using two packed columns of neutral alumina was used for drying THF and CH_2Cl_2, while two packed columns of molecular sieves were used to dry DMF, and the solvents were dispensed under Argon. **7**[247], **8-10**[248], **11**[249], **12-13**[250], **14**[251], **23**[252], **24-25**[253], **27**[254], **37**[255], **44**[256], **48**[257], **58**[258], and **60**[259] were prepared as previously described.

Enzymatic Assay to Determine the Global Kinetic Parameters of of BioA.

A. Assay Procedure. 50× DMSO solutions of inhibitor (final concentrations 0, 200 µM, 400 µM, 700 µM, and 1 mM) were added to 1× buffer solutions of 100 mM Bicine, 50 mM $NaHCO_3$, 1 mM $MgCl_2$, 5 mM ATP, pH 8.6. BioA (0.5 µM) was then added to each to well (total volume 50 µL) to initiate BioA inactivation.

In order to measure residual BioA activity, a coupled assay with BioD was used, which together with BioA converts 7-keto-8-aminopelargonic acid (KAPA) to dethiobiotin. This was accomplished by removing 5 µL aliquot of the initial solution at various incubation time points (2.5, 5, 10, 20, and 40 min) and adding to 95 µL of a reaction solution, containing saturating concentrations of all substrates and diluting the initial inhibitor 20-fold, ensuring no further inhibition. The final concentrations present in the reaction solution are 100 mM Bicine (pH 8.6), 50 mM $NaHCO_3$, 1 mM $MgCl_2$, 5 mM ATP, 5 mM SAM, 25 nM BioA, 2 µM BioD, 1 mM TCEP, and 25 µM KAPA.[57] The reaction solutions were run for 60 min (which remained under initial velocity conditions), then quenched with a solution of 500 nM biotin in 10% trichloroacetic acid. The dethiobiotin concentration was quantified by LC-MS/MS analysis with a gradient from 0-100% MeCN–H_2O containing 0.1% Formic Acid. Biotin was monitored through the *m*/*z* 243→200 transition and dethiobiotin was monitored through the *m*/*z* 213→170 transition. Assays were run in duplicate on multiple days. The negative control contained no inhibitor (DMSO only), and the positive control contained no BioA.

B. Data Analysis. The LC-MS/MS traces were analyzed by MultiQuant 2.0.2 to obtain the area under the curve (AUC) for both dethiobiotin (analyte) and biotin (internal standard). Then, the dethiobiotin AUC was divided by the biotin AUC, and this number was converted into a concentration using the standard curve. A plot was generated of preincubation time vs. percentage of BioA activity remaining, and curves for each concentration of inhibitor were fit to equation 3 with Graphpad Prism to obtain values for k_{obs} at each inhibitor concentration:

$$y = Ae^{-k_{obs}t} \quad (1)$$

In equation 1, y is the concentration of dethiobiotin, and A is the activity observed with no inhibitor. The concentration of inhibitor was then plotted against the generated k_{obs} values, and this was fit to equation 2 with Graphpad Prism to determine the K_I and k_{inact} values.

$$k_{obs} = k_{inact}\frac{[I]}{K_I+[I]} \quad (2)$$

Sample Derivation of the K_I and k_{iaact} Values for Mechanism 4 in Table 2.2

This is written for the following mechanism:

$$E + I \underset{k_{-1}}{\overset{k_1}{\rightleftharpoons}} EI \xrightarrow{k_2} EA \xrightarrow{k_3} EB \xrightarrow{k_4} EP$$

The labels for the intermediate and final complexes are changed to allow for simple writing with Word's equation editor. K_I and k_{inact} are defined as they are in **Table S1**, and the assumptions necessary are the quasi-steady state assumption for each intermediate Enzyme-Inhibitor complex and that the total enzyme concentration stays constant.

$$\frac{d[EP]}{dt} = k_4[EB]$$

$$\frac{d[EB]}{dt} = k_3[EA] - k_4[EB] = 0$$

$$\frac{d[EA]}{dt} = k_2[EI] - k_3[EA] = 0$$

$$\frac{d[EI]}{dt} = k_1[E][I] - (k_2 + k_{-1})[EI] = 0$$

$$[E]_0 = [E] + [EI] + [EA] + [EB] + [EP] = constant$$

We express [EI] in terms of the other variables:

$$k_1([E]_0 - [EI] - [EA] - [EB] - [EP])[I] - (k_2 + k_{-1})[EI] = 0$$

$$k_1([E]_0 - [EA] - [EB] - [EP])[I] = (k_2 + k_{-1})[EI] + k_1[EI][I]$$

$$([E]_0 - [EA] - [EB] - [EP])[I] = \frac{(k_2 + k_{-1})[EI]}{k_1} + [EI][I]$$

Letting $K_M = (k_2 + k_{-1})/k_1$:

$$([E]_0 - [EA] - [EB] - [EP])[I] = [EI](K_M + [I])$$

$$\frac{([E]_0 - [EA] - [EB] - [EP])[I]}{(K_M + [I])} = [EI]$$

Solving for [EA]:

$$k_2[EI] - k_3[EA] = 0$$

$$k_2\frac{([E]_0 - [EA] - [EB] - [EP])[I]}{(K_M + [I])} - k_3[EA] = 0$$

$$k_2\frac{([E]_0 - [EB] - [EP])[I]}{(K_M + [I])} = k_2\frac{[EA][I]}{(K_M + [I])} + k_3[EA]$$

$$k_2\frac{([E]_0 - [EB] - [EP])[I]}{(K_M + [I])} = (k_2\frac{[I]}{(K_M + [I])} + k_3)[EA]$$

$$k_2\frac{([E]_0 - [EB] - [EP])[I]}{(K_M + [I])(k_2\frac{[I]}{(K_M + [I])} + k_3)} = [EA]$$

$$k_2\frac{([E]_0 - [EB] - [EP])[I]}{k_2[I] + k_3(K_M + [I])} = [EA]$$

Now, we solve for [EB]:

$$k_3[EA] - k_4[EB] = 0$$

$$k_2k_3\frac{([E]_0 - [EB] - [EP])[I]}{k_2[I] + k_3(K_M + [I])} - k_4[EB] = 0$$

$$k_2k_3\frac{([E]_0 - [EP])[I]}{k_2[I] + k_3(K_M + [I])} = k_2k_3\frac{[EB][I]}{k_2[I] + k_3(K_M + [I])} + k_4[EB]$$

$$k_2k_3\frac{([E]_0 - [EP])[I]}{k_2[I] + k_3(K_M + [I])} = (k_2k_3\frac{[I]}{k_2[I] + k_3(K_M + [I])} + k_4)[EB]$$

$$k_2k_3\frac{([E]_0 - [EP])[I]}{(k_2[I] + k_3(K_M + [I]))(k_2k_3\frac{[I]}{k_2[I] + k_3(K_M + [I])} + k_4)} = [EB]$$

$$k_2k_3\frac{([E]_0 - [EP])[I]}{k_2k_4[I] + k_3k_4(K_M + [I]) + k_2k_3[I]} = [EB]$$

Now, solving for [EP]:

$$\frac{d[EP]}{dt} = k_4[EB]$$

$$\frac{d[EP]}{dt} = k_2k_3k_4\frac{([E]_0 - [EP])[I]}{k_2k_4[I] + k_3k_4(K_M + [I]) + k_2k_3[I]}$$

Let us define X:

$$X = k_2k_3k_4\frac{[I]}{k_2k_4[I] + k_3k_4(K_M + [I]) + k_2k_3[I]}$$

$$\frac{d[EP]}{dt} = ([E]_0 - [EP]) * X$$

$$\frac{d[EP]}{([E]_0 - [EP])} = X * dt$$

$$\frac{d[EP]}{[EP] - [E]_0} = -X * dt$$

$$\int \frac{d[EP]}{[EP] - [E]_0} = \int -X * dt$$

With D as the constant that arises from evaluation of an indefinite integral:

$$ln([EP] - [E]_0) = -Xt + D$$

$$e^{ln([EP]-[E]_0)} = e^{-Xt+D}$$

$$[EP] - [E]_0 = e^{-Xt+D}$$

$$[EP] = [E]_0 + e^{-Xt+D}$$

$$[EP] = [E]_0 + e^{-Xt} * e^D$$

Since D is just a random, unknown constant, let us set e^D = F:

$$[EP] = [E]_0 + F * e^{-Xt}$$

Now, we know that at time t= 0, [EP] = 0:

$$0 = [E]_0 + F * e^0$$

$$-[E]_0 = F$$

$$[EP] = [E]_0 - [E]_0 e^{-Xt}$$

This means that when evaluating an inactivation time course and fitting it to an exponential, the k_{obs} is equal to X.

$$k_{obs} = k_2 k_3 k_4 \frac{[I]}{k_2 k_4 [I] + k_3 k_4 (K_M + [I])) + k_2 k_3 [I]}$$

$$k_{obs} = k_2 k_3 k_4 \frac{[I]}{(k_2 k_3 + k_2 k_4 + k_3 k_4)[I] + k_3 k_4 K_M}$$

$$k_{obs} = \frac{k_2 k_3 k_4}{k_2 k_3 + k_2 k_4 + k_3 k_4} * \frac{[I]}{[I] + \frac{k_3 k_4 K_M}{(k_2 k_3 + k_2 k_4 + k_3 k_4)}}$$

k_{inact} is the left fraction in the equation directly above, as at infinite concentration of I, the right fraction will become 1, and k_{obs} will be equal to the left fraction. K_I is equal to the bottom right of the right fraction, as when the concentration of inhibitor equals this constant, the k_{obs} will be half of the k_{inact}.

Stopped-Flow Analysis of the Inhibition of BioA by 1.

A. Experimental Notes. Water used in all experiments was purified with a Millipore Super-Q system. Stopped flow experiments were performed using an Applied Photophysics stopped-flow instrument (model SX.18MV with the SX Pro-Data upgrade) at 25 °C. One syringe was filled with the stated concentration of BioA in 100 mM BICINE pH 8.6. The other syringe was filled with a solution derived from diluting a 20 mM solution of **1** in DMSO with 100 mM BICINE pH 8.6 to the specified concentration of **1**. All buffers were degassed prior to use. BioA was expressed as previously described[260] and **1** was synthesized as previously described.[261] Experiments were either monitored with a diode-array or a single wavelength detector. The concentration of BioA was kept below one-fifth of the concentration of **1**, establishing pseudo-first order conditions. The kinetic data was analyzed to extract reciprocal relaxation times with

Applied Photophysics Pro-Data Viewer through fitting reaction time courses to summed exponential expressions. Simulations of the system with the obtained rate constants were performed with Tenua.

B. Data Analysis. The reaction time course for a series of first order or pseudo first order reactions can be fit by a sum of exponential expressions where the number of exponential terms is equal to the number of steps.[262,263] The time course is fit using nonlinear regression analysis to yield reciprocal relaxation times (RRTs) and amplitudes of the exponential terms. The RRT values are only equal to rate constants for individual steps in the reaction series if each step is irreversible. The order of magnitude of the RRTs in this case do not necessarily correlate with the order of steps in the reaction series. The presence of an irreversible step in the reaction series uncouples RRTs so that some of the RRTs may correlate with the rate constants for specific steps in the reaction series that occur after the irreversible step. For the reaction considered in this study, the second step is functionally irreversible, so one of the RRTs directly gives the rate constant for the final step in the reaction series. The presence of an irreversible step can often be detected by the lack of substrate concentration dependence on some of the RRT values. This is true because reversible steps couple RRT values such that a given RRT reflects more than one rate constant. In the general case, it is necessary to extract the rate constants from experimental RRT values using expressions derived by integrating the series of differential rate equations that pertain to the proposed reaction steps. This leads to complex equations relating RRTs and rate constants. For example, for a two-step reversible binding reaction, the two RRTs are equal to the plus and minus roots of a quadratic equation containing all of the forward and reverse rate constants for the steps. Thus, neither of the RRTs correlates directly to one step of the series, but both will contain the second order rate constant for substrate binding and exhibit substrate concentration dependence. A useful simplification is possible if the substrate (or inhibitor) binding reaction initiates the reaction series and is fast compared with downstream reactions.[264,265]

This allows it to reach an approximate equilibrium before the succeeding reactions occur. The specific criterion is that the reverse rate constant for binding reaction exceed the forward rate constant for the following reaction by >3 fold. If this is the case, then a plot of the fast RRT vs substrate concentration will be linear (which is what we observe) with the slope and intercept equal to the forward and reverse binding rate constants, respectively (equation 3). The plot of the slower RRT vs substrate concentration will be hyperbolic with the y-intercept equal to the reverse rate constant of the step following binding. The extrapolated maximum value of the hyperbola will be the sum of the forward and reverse rate constants for this reaction and the apparent K_D for the curve will be the K_D of the preceding binding reaction (equation 4, where A is the substrate or inhibitor).

$$RRT_{fast} \approx k_1[\mathrm{A}] + k_{-1} \quad (3)$$

$$RRT_{slow} \approx \frac{k_2[A]}{K_{D1}+[A]} + k_{-2} \quad (4)$$

If the K_D values determined from the two plots agree, then it suggests that the criteria for utilization of this simplification have been met and that one reaction directly follows the other. For the data analyzed in this study, the fastest and slowest RRTs give linear and hyperbolic plots vs **1**, respectively, and these plots yield similar values for the binding K_D (240 µM from equation 3, 180 µM from equation 4). The concentration dependencies of all three observed RRTs allowed the reactions to be put in the correct sequence and the rate constants and K_D values to be extracted.

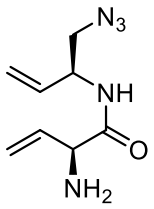

(S)-2-[(*tert*-Butoxycarbonyl)amino]-N-((S)-1-azidobut-3-en-2-yl)but-3-enamide (15). To a solution of **14** (280 mg, 1.4 mmol, 1.0 equiv) in THF (15 mL) at 0 °C was added **13** (180 mg, 1.6 mmol, 1.2 equiv), $NaHCO_3$ (590 mg, 7.0 mmol, 5.0 equiv) and DEPBT (1.5 g, 4.9 mmol, 3.5 equiv). The reaction was stirred for 1 h, then allowed to warm up to 23 °C. After 48 h, the reaction mixture was partitioned between EtOAc (75 mL) and saturated aqueous NH_4Cl (50 mL). The layers were separated and the aqueous layer was extracted with EtOAc (3 × 20 mL). The organic layers were then combined and washed with water (1 × 30 mL) and brine (1 × 30 mL), dried ($MgSO_4$), and concentrated. Purification by flash chromatography (5% EtOAc–hexane to 25% EtOAc–hexane, linear gradient) afforded the title compound (302 mg, 73%) as a white powder: R_f = 0.15 (20% EtOAc–hexane); ^{1}H NMR (600 MHz, $CDCl_3$) δ 6.46 (br. s., 1H), 5.93 (ddd, J = 6.5, 10.6, 17.0 Hz, 1H), 5.81 (ddd, J = 5.3, 10.4, 17.2 Hz, 1H), 5.22–5.46 (m, 5H), 4.61–4.77 (m, 2H), 3.41–3.54 (m, 2H), 1.45 (s, 9H); ^{13}C NMR (150 MHz, $CDCl_3$) δ 169.7, 155.4, 134.3, 133.7, 118.4, 117.7, 80.3, 57.1, 54.3, 51.0, 28.3;

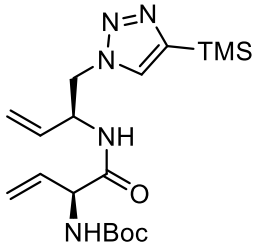

(S)-2-[(*tert*-Butoxycarbonyl)amino]-N-((S)-1-(4-(trimethylsilyl)-1H-1,2,3-triazol-1-yl)but-3-en-2-yl)but-3-enamide (17). To a solution of **15** (150 mg, .50 mmol, 1.0 equiv) and TMS acetylene (250 mg, 2.5 mmol, 5.0 equiv) in *t*-BuOH (2 mL) was added a solution of $CuSO_4$*5 H_2O (13 mg, .05 mmol, 0.1 equiv) and sodium ascorbate (31 mg, .15 mmol, 0.3 equiv) in water (2 mL). The reaction mixture was stirred vigorously. After 24 h, 0.1 equiv of $CuSO_4$*5 H_2O, 0.3 equiv of sodium ascorbate, and 3.0 equiv of TMS acetylene were added. After an additional 48 h, 0.1 equiv of $CuSO_4$*5 H_2O, 0.3 equiv of sodium ascorbate, 3.0 equiv of TMS acetylene, and

water (0.2 mmol) were added. Following another 48 h, 0.3 equiv of sodium ascorbate and 3.0 equiv of TMS acetylene were added. 48 h after the final addition of reagents, the reaction was partitioned between EtOAc (80 mL) and 1 M NH_4OH (40 mL). The layers were separated and the organic layer was washed with 1 M NH_4OH (1 × 40 mL). The combined aqueous layers were extracted with EtOAc (2 × 30 mL). The combined organic extracts were washed with brine (1 × 30 mL), dried ($MgSO_4$), and concentrated. Purification by flash chromatography (20% EtOAc–hexane to 80% EtOAc–hexane, linear gradient) afforded both the title compound (54 mg, 27%) and its desilylated analog **19** (82 mg, 51%), both as white powders: R_f = 0.2 (50% EtOAc–hexane); ^{1}H NMR (600 MHz, $CDCl_3$) δ 7.53 (s, 1H), 6.72 (d, J = 7.6 Hz, 2H), 5.71–5.89 (m, 3H), 5.15–5.42 (m, 5H), 4.84–4.96 (m, 1H), 4.45–4.70 (m, 3H), 1.44 (s, 9H), 0.32 (s, 9H); ^{13}C NMR (150 MHz, $CDCl_3$) δ 169.8, 155.1, 146.6, 133.6, 133.3, 130.1, 118.30, 118.27, 80.1, 57.1, 52.1, 52.0, 28.3, -1.2; MS (ESI+) calcd for $C_{18}H_{32}N_5O_3Si$ $[M + H]^+$ 394.2269, found 394.2.

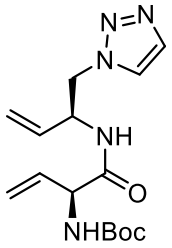

(S)-N-((S)-1-(1H-1,2,3-Triazol-1-yl)but-3-en-2-yl)-2-[(*tert*-Butoxycarbonyl)amino]-but-3-enamide (19). To a solution of **17** (54 mg, .14 mmol, 1.0 equiv) in anhydrous THF (2 mL) at 0 °C was added HF·Pyridine (1 mL) dropwise. After 2 h the reaction was partitioned between EtOAc (60 mL) and saturated $NaHCO_3$ (20 mL). The layers were separated and the aqueous layer was extracted with EtOAc (2 x 20 mL). The combined organic layers were dried ($MgSO_4$) and concentrated. Purification by flash chromatography (30% EtOAc–hexane to 80% EtOAc–hexane, linear gradient) afforded the title compound (28 mg, 64%) as a white powder: R_f = 0.2 (80% EtOAc–hexane); ^{1}H NMR (600 MHz, $CDCl_3$) δ 7.68 (s, 1H), 7.60 (s, 1H), 6.79–6.96 (m, 1H),

5.76–5.88 (m, 2H), 5.21–5.36 (m, 5H), 4.90 (pen, J = 6.2 Hz, 1H), 4.54–4.70 (m, 3H), 1.44 (s, 9H); ^{13}C NMR (150 MHz, $CDCl_3$) δ 170.0, 155.3, 133.7, 133.4, 133.1, 124.6, 118.5, 118.4, 80.3, 57.2, 52.6, 51.8, 28.3;

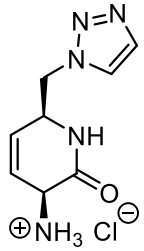

(3S,6S)-6-((1H-1,2,3-Triazol-1-yl)methyl)-3-amino-3,6-dihydropyridin-2(1H)-one Hydrochloride Salt (4). To a solution of **19** (60 mg, .19 mmol, 1.0 equiv) in CH_2Cl_2 (20 mL) was added Hoveyda-Grubbs II Catalyst (12 mg, .019 mmol, 0.1 equiv). The reaction was refluxed under the exclusion of light for 24 h followed by the addition of Hoveyda-Grubbs II Catalyst (12 mg). After a total of 48 h at reflux, the reaction mixture was concentrated. Purification by flash chromatography (0% MeOH–CH_2Cl_2 to 10% MeOH–CH_2Cl_2, linear gradient) afforded the Boc-protected analog of the title compound (11 mg, R_f = 0.40 (10% CH_2Cl_2–hexane)) and **19** (23 mg). This analog (11 mg, 0.38 mmol, 1.0 equiv) was then dissolved in 4 M HCl in dioxane (2 mL). After 1 h, the reaction mixture was concentrated. Purification by trituration (dissolve in MeOH, crash out with Et_2O) afforded the title compound (6.4 mg, 15%) as a white solid: ^{1}H NMR (600 MHz, CD_3OD) δ 7.99 (s, 1H), 7.75 (s, 1H), 6.16–6.22 (m, 1H), 5.90–5.96 (m, 1H), 4.59–4.75 (m, 3H), 4.40–4.46 (m, 1H).

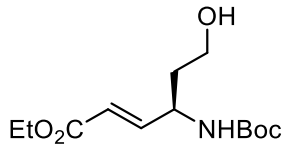

Ethyl (R,E)-4-[(*tert*-butoxycarbonyl)amino]-6-hydroxyhex-2-enoate (29). To a solution of **25** (202 mg, 1.0 mmol, 1.0 equiv) in toluene (25 mL) at 23 °C was added Ph_3PCHCO_2Et (523 mg,

1.5 mmol, 1.5 equiv). After 6 h, the reaction was partitioned between EtOAc (120 mL) and water (50 mL). The layers were separated and the organic layer was washed with brine (1 × 50 mL), dried ($MgSO_4$), and concentrated. Purification by flash chromatography (300 mL 10% EtOAc–hexane, 800 mL 40% EtOAc–hexane), afforded the title compound (221 mg, 81%) as a clear oil: R_f = 0.35 (50% EtOAc–hexane); ^{1}H NMR, ^{13}C NMR, and MS data matched reported values.[266]

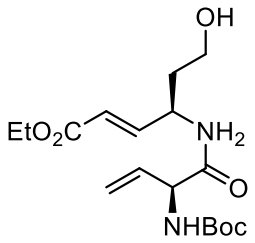

Ethyl (R,E)-4-((S)-2-[(*tert*-butoxycarbonyl)amino]but-3-enamido)-6-hydroxyhex-2-enoate (31). To a solution of **29** (273 mg, 1.0 mmol, 1.0 equiv) in CH_2Cl_2 (5 mL) at 0 °C was added 4 M HCl in dioxane (2.5 mL) After 15 min, the ice bath was removed and the reaction was allowed to warm to 23 °C, and after 1 h the reaction mixture was concentrated to give a white solid. This was added to a solution of **14** (200 mg, 1.0 mmol, 1.0 equiv) in THF (15 mL) at 0 °C, followed by $NaHCO_3$ (420 mg, 5.0 mmol, 5.0 equiv) and DEPBT (1.05 g, 3.5 mmol, 3.5 equiv). The reaction was stirred for 1 h, then allowed to warm up to 23 °C. After 48 h, the reaction mixture was partitioned between EtOAc (100 mL) and saturated aqueous NH_4Cl (10 mL). Water (70 mL) was added and the layers were separated. The aqueous layer was extracted with EtOAc (2 × 100 mL). The organic layers were then combined and washed with water (1 × 30 mL) and brine (1 × 30 mL), dried ($MgSO_4$), and concentrated. Purification by flash chromatography (25% EtOAc–hexane to 70% EtOAc–hexane, linear gradient) afforded the title compound (75 mg, 21%) as a pale yellow powder: R_f = 0.35 (50% EtOAc–hexane); ^{1}H NMR (400 MHz, $CDCl_3$) δ 6.90 (dd, J = 5.1, 15.7 Hz, 1H), 6.84 (br. s., 1H), 5.84–6.02 (m, 2H), 5.40 (d, J = 16.8 Hz, 1H), 5.25–5.36 (m, 2H), 4.86 (br. s, 1H), 4.66 (br. s., 1H), 4.20 (q, J = 7.0 Hz, 2H), 3.58–3.81 (m, 2H), 2.68 (br. s,

1H), 1.93–2.08 (m, 1H), 1.58–1.69 (m, 1H), 1.46 (s, 9H), 1.29 (t, J = 7.2 Hz, 3H); ^{13}C NMR (100 MHz, $CDCl_3$) δ 170.4, 166.1, 155.4, 146.6, 133.6, 121.6, 118.5, 80.5, 60.6, 58.8, 57.3, 48.1, 36.2, 28.3, 14.2;

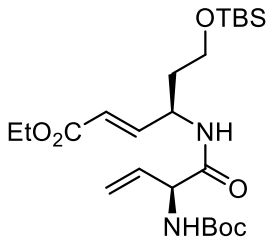

Ethyl (R,E)-4-((S)-2-[(*tert*-butoxycarbonyl)amino]but-3-enamido)-6-((tert-butyldimethylsilyl)oxy)hex-2-enoate (32). To a solution of **31** (128 mg, 0.27 mmol, 1.0 equiv) in CH_2Cl_2 (20 mL) at 0 °C was added imidazole (53 mg, 0.81 mmol, 3.0 equiv) and TBSCl (45 mg, 0.32 mmol, 1.2 equiv). The reaction mixture was allowed to warm to 23 °C after an hour, and after 16 h it was partitioned between CH_2Cl_2 (60 mL) and water (20 mL). The layers were separated and the organic layer was washed with saturated aqueous NH_4Cl (1 × 20 mL) and brine (1 × 20 mL), dried ($MgSO_4$), and concentrated. Purification by flash chromatography (10% EtOAc–hexane to 30% EtOAc–hexane, linear gradient) afforded the title compound (91 mg, 71%) as a pale yellow oil: R_f = 0.25 (20% EtOAc–hexane); ^{1}H NMR (400 MHz, $CDCl_3$) δ 6.92 (d, J = 7.8 Hz, 1H), 6.86 (dd, J = 5.1, 15.7 Hz, 1H), 5.79–5.96 (m, 2H), 5.46 (br. s, 1H), 5.35 (d, J = 17.2 Hz, 1H), 5.25 (d, J = 10.2 Hz, 1H), 4.72–4.82 (m, 1H), 4.61 (br. s, 1H), 4.15 (q, J = 7.0 Hz, 2H), 3.68 (dd, J = 4.3, 6.7 Hz, 2H), 1.86–1.97 (m, 1H), 1.70–1.80 (m, 1H), 1.43 (s, 9H), 1.25 (t, J = 7.2 Hz, 3H), 0.88 (s, 9H), 0.04 (s, 6H); ^{13}C NMR (100 MHz, $CDCl_3$) δ 169.3, 166.1, 155.1, 146.8, 133.9, 121.3, 118.0, 80.0, 60.3, 59.9, 57.1, 48.8, 35.6, 28.2, 25.9, 18.2, 14.1, -5.5;

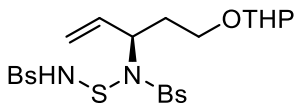

4-Bromo-N-(((4-bromophenyl)sulfonamido)thio)-N-((3R)-5-((tetrahydro-2H-pyran-2-yl)oxy)pent-1-en-3-yl)benzenesulfonamide (39). To a solution of bis-benzenesulfonylsulfur diimide (2.0 g, 5.8 mmol, 1.0 equiv) in Et_2O at 3 °C was added **37** (4.34 g, 25.4 mmol, 4.3 equiv). After 24 h, the reaction mixture was filtered, and cold Et_2O (80 mL) was used to wash the cake. Collecting the precipitate afforded the titular compound (2.73 g, 92%: R_f = 0.25 (10% MeOH–CH_2Cl_2)), which spontaneously undergoes an ene-type reaction at 23 °C, so were unable to characterize this product by NMR (^{1}H NMR was always a mixture of **38** and *rac*-**39**).

To a solution of **38** (3.33 g, 6.5 mmol, 1.0 equiv) in MeOH (20 mL) at -78 °C was added a pre-mixed solution of $Pd(TFA)_2$ (216 mg, 0.65 mmol, 0.1 equiv) and the bis-oxazoline chiral ligand (260 mg, 0.78 mmol, 0.12 equiv) in 36 mL MeOH dropwise. The reaction mixture was maintained at -78 °C for the duration of the addition, then stirred at -15 °C. After 7 days, the reaction mixture was concentrated down and purified by flash chromatography (10% EtOAc–hexane to 30% EtOAc–hexane, linear gradient) to afford the title compound (2.05 g, 62%, >90% ee): R_f = 0.65 (50% EtOAc–hexane); Proper characterization of **39** by ^{1}H NMR was extremely difficult due to the presence of multiple stereocenters in addition to rotamers from the benzenesulfonyl groups. Therefore, after verifying that the product was at least quite similar to the desired product, we carried it forward to the synthesis of **40**, where we were able to obtain accurate characterization.

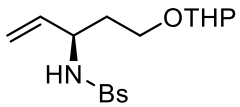

4-Bromo-N-((3R)-5-((tetrahydro-2H-pyran-2-yl)oxy)pent-1-en-3-yl)benzenesulfonamide (40). To a solution of **39** (2.05 g, 4.0 mmol, 1.0 equiv) in MeOH (40 mL) and THF (10 mL) was added 1 N NaOH (10 mL). After 48 h, the organic solvent was removed by rotary evaporation. Water (40 mL) was added and the aqueous layer was extracted with EtOAc (3 × 100 mL). The

combined organic layers were dried ($MgSO_4$) and concentrated. Purification by flash chromatography (10% EtOAc–hexane to 30% EtOAc–hexane, linear gradient) afforded the title compound (1.19 g, 90%) as a clear oil: R_f = 0.65 (50% EtOAc–hexane); ^{1}H NMR (400 MHz, $CDCl_3$) δ 7.88 (dd, J = 3.7, 6.8 Hz, 2H), 7.44–7.60 (m, 3H), 5.56–5.72 (m, 1.5H), 5.44 (br. s., 0.5H), 5.10–5.23 (m, 1H), 5.05 (t, J = 9.2 Hz, 1H), 4.50 (d, J = 17.6 Hz, 1H), 3.94–4.08 (m, 1H), 3.72–3.93 (m, 2H), 3.41–3.58 (m, 1.5H), 3.30–3.41 (m, 0.5H), 1.68–1.87 (m, 4H), 1.57 (br. s., 4H);

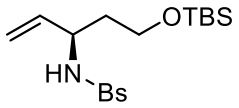

(R)-4-bromo-N-(5-((tert-butyldimethylsilyl)oxy)pent-1-en-3-yl)benzenesulfonamide (41). To a solution of **40** (1.19 g, 3.6 mmol, 1.0 equiv) in CH_2Cl_2 (20 mL) at -50 °C was added TBSOTf (1.24 g, 4.7 mmol, 1.3 equiv). After 50 min, Me_2S (670 mg, 10.8 mmol, 3.0 equiv) was also added to the reaction mixture. After 2 h of stirring, the reaction was quenched with the addition of 1:1 Et_3N/MeOH (10 mL). CH_2Cl_2 (100 mL) was then added and the reaction mixture was washed with saturated aqueous $NaHCO_3$ (1 × 25 mL) and brine (1 × 25 mL). The organic layer was then dried ($MgSO_4$) and concentrated. Purification by flash chromatography (5% EtOAc–hexane to 20% EtOAc–hexane, linear gradient) afforded the title compound (1.04 g, 82%) as a lear oil: R_f = 0.8 (50% EtOAc–hexane); ^{1}H NMR (400 MHz, $CDCl_3$) δ 7.83–7.91 (m, 2H), 7.52–7.58 (m, 1H), 7.45–7.52 (m, 2H), 5.79 (d, J = 6.3 Hz, 1H), 5.65 (ddd, J = 6.1, 10.5, 16.9 Hz, 1H), 5.17 (td, J = 1.3, 17.1 Hz, 1H), 5.06 (td, J = 1.1, 10.4 Hz, 1H), 4.00 (dq, J = 5.0, 6.3 Hz, 1H), 3.73 (ddd, J = 4.0, 8.1, 10.5 Hz, 1H), 3.59 (ddd, J = 4.3, 6.0, 10.4 Hz, 1H), 1.54–1.76 (m, 2H), 0.92 (s, 9H), 0.06 (s, 6H); ^{13}C NMR (100 MHz, $CDCl_3$) δ 141.1, 137.3, 132.3, 128.8, 127.2, 116.2, 60.3, 55.3, 36.4, 25.8, 18.1, -5.6;

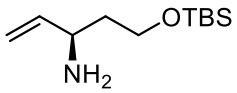

(R)-5-((*tert*-butyldimethylsilyl)oxy)pent-1-en-3-amine (34). A 3-necked flask was charged with a coldfinger (attached to a bubbler) in the middle, an ammonia source on one side, and a septum on the other. The flask was cooled to -78 °C and ammonia flowed through the apparatus until 10-15 mL had liquefied. Excess sodium metal was then added. To this ammonia/sodium solution was added a solution of **41** (209 mg, 0.59 mmol, 1.0 equiv) in dry THF (10 mL) dropwise. After 1 h, the reaction was quenched with the addition of EtOH, and the mixture was allowed to warm to 23 °C. The reaction mixture was then partitioned between EtOAc (50 mL) and 10% aqueous Na_2CO_3 (20 mL). The organic layer was then dried ($MgSO_4$) and concentrated. Purification by flash chromatography (5% MeOH–$CH_2Cl_2$to 30% MeOH–CH_2Cl_2, linear gradient) afforded the title compound (97 mg, 76%) as a white powder: R_f = 0.35 (50% MeOH–CH_2Cl_2); ^{1}H NMR (400 MHz, $CDCl_3$) δ 5.76 (ddd, J = 6.7, 10.3, 17.1 Hz, 1H), 5.07 (d, J = 17.2 Hz, 1H), 4.96 (d, J = 10.6 Hz, 1H), 3.58–3.73 (m, 2H), 3.43 (q, J = 6.7 Hz, 1H), 1.55–1.66 (m, 2H), 1.52 (br. s., 2H), 0.84 (s, 9H), 0.00 (s, 6H); ^{13}C NMR (100 MHz, $CDCl_3$) δ 143.1, 113.2, 60.4, 51.7, 40.0, 25.8, 18.1, -5.5;

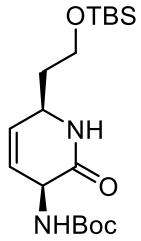

(3S,6R)-3-[(*tert*-butoxycarbonyl)amino]-6-(2-((tert-butyldimethylsilyl)oxy)ethyl)-3,6-dihydropyridin-2(1H)-one (33). To a solution of **14** (600 mg, 3.0 mmol, 1.8 equiv) in dry THF (40 mL) at 0 °C was added $NaHCO_3$ (1.12 g, 13.3 mmol, 7.8 equiv) and DEPBT (2.39 g, 8.0 mmol, 4.7 equiv) sequentially. After 1 h, a solution of **34** (368 mg, 1.7 mmol, 1.0 equiv) in dry THF (15 mL) was added dropwise. After 3 d, the reaction was quenched with the addition of

saturated aqueous NH_4Cl (5 mL) and subsequent water (50 mL). The reaction mixture was extracted with EtOAc (2 × 100 mL). The combined organic layers were washed with brine (1 × 30 mL), dried ($MgSO_4$), and concentrated. Purification by flash chromatography (5% MeOH–CH_2Cl_2 to 30% MeOH–CH_2Cl_2, linear gradient) afforded **35** in modest purity.

To the resulting solution of **35** in dry DCM was added Hoveyda-Grubbs II catalyst (29 mg, 0.46 mmol). The reaction mixture was heated to reflux for 2 d, then cooled and concentrated. Purification by flash chromatography (5% EtOAc–hexane to 25% EtOAc–hexane, linear gradient) afforded the title compound (28 mg, 9%) as a pale yellow oil: R_f = 0.2 (20% EtOAc–hexane); ^{1}H NMR 400 MHz, $CDCl_3$) δ 7.03 (br. s., 1H), 5.94 (d, J = 9.8 Hz, 1H), 5.71 (d, J = 10.2 Hz, 1H), 5.26–5.43 (m, 1H), 4.56 (br. s., 1H), 4.12–4.25 (m, 1H), 3.69–3.91 (m, 2H), 1.75–1.83 (m, 1H), 1.45 (s, 9H), 0.92 (s, 9H), 0.09 (s, 6H); ^{13}C NMR (100 MHz, $CDCl_3$) δ 166.0, 155.9, 127.2, 127.0, 79.8, 61.7, 60.0, 53.1, 37.8, 28.3, 25.8, 18.1, -5.6;

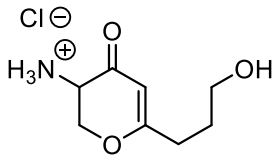

3-Amino-6-(3-hydroxypropyl)-2,3-dihydro-4*H*-pyran-4-one (42). To a solution of **81** (9.0 mg, 0.029 mmol, 1.0 equiv) in MeCN (0.5 mL) was added $BiCl_3$ (17 mg, 0.054 mmol, 1.9 equiv). The reaction was then sealed and heated at 55 °C for 2 h. MeOH (5 mL) was then added and the reaction mixture was filtered, then concentrated to 3 mL. H_2O (10 mL) was added and the mixture was filtered again. Removal of the solvent afforded the title compound (2.9 mg, 49%) as a white solid: ^{1}H NMR (400 MHz, CD_3OD) δ 5.49 (s, 1H), 4.75 (dd, J = 10.0, 5.0 Hz, 1H), 4.18–-4.32 (m, 2H), 3.56 (t, J = 6.1 Hz, 2H), 2.41 (t, J = 7.6 Hz, 2H), 1.77 (pent, J = 7.0 Hz, 2H); ^{13}C NMR (100 MHz, CD_3OD) δ 187.9, 181.9, 103.1, 69.2, 61.9, 50.8, 32.4, 30.4; HRMS (ESI+) calcd for $C_8H_{14}NO_3$ $[M + H]^+$ 172.0968, found 172.0967 (error 0.4 ppm).

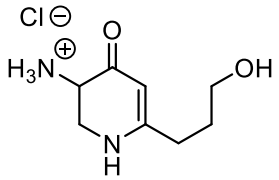

(±)-3-Amino-6-(3-hydroxypropyl)-2,3-dihydro-1*H*-pyridin-4-one hydrochloride (43). To a pre-chilled flask containing **76** (12 mg, 0.044 mmol, 1.0 equiv) was added cold 4 M HCl in dioxane (2 mL). After 45 min at 0 °C, the reaction mixture was concentrated. The residue was taken up in a minimal amount of methanol and precipitated with ether to afford the title compound (7.5 mg, 82%) as a white powder in equilibrium with a dimer (4:1 monomer:dimer): ^{1}H NMR (400 MHz, CD_3OD) δ 4.52 (t, J = 6.9 Hz, 1H dimer), 4.18 (dd, J = 16.2, 7.2 Hz, 1H dimer), 3.98-4.08 (m, 1H dimer, 1H monomer), 3.88 (dd, J = 12.9, 6.7 Hz, 1H monomer), 3.66 (t, J = 5.7 Hz, 2H, dimer), 3.58 (t, J = 6.2 Hz, 2H monomer), 3.51 (t, J = 13.7 Hz, 1H monomer), 2.84 (t, J = 7.2 Hz, 2H, dimer), 2.41 (td, J = 7.6, 2.5 Hz, 2H monomer), 1.97 (pent, J = 6.6 Hz, 2H, dimer), 1.79 (pent, J = 7.0 Hz, 2H monomer); ^{13}C NMR (100 MHz, DMSO-d_6) δ 183.9, 169.0, 93.6, 59.8, 49.4, 42.8, 30.63, 30.61; HRMS (ESI+) calcd for $C_8H_{15}N_2O_2$ $[M + H]^+$ 171.1128, found: 171.1133 (error 2.9 ppm).

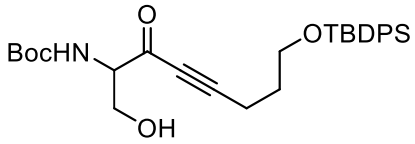

2-[(*tert*-Butoxycarbonyl)amino]-8-(*tert*-butyldiphenylsilyloxy)-1-hydroxy-oct-4-yn-3-one (45). To a solution of 5-(*tert*-butyldiphenylsilyloxy)-1-pentyne[267] (11.2 g, 34.9 mmol, 3.4 equiv) in THF (110 mL) at -78 °C was added *n*-BuLi (15.7 mL of a 2.5 M solution in hexanes, 39.1 mmol 3.8 equiv). The reaction was stirred for 2 h, then a solution of **7** (2.56 g, 10.3 mmol, 1.0 equiv) in THF (50 mL) was added slowly. The reaction was allowed to warm to 23 °C over 2 h. After 16 h, the reaction was quenched by the dropwise addition of glacial AcOH (20 mL). The reaction mixture was partitioned between saturated aqueous $NaHCO_3$ (150 mL) and EtOAc (300

mL). The layers were separated and the organic layer was washed with saturated aqueous $NaHCO_3$ (1 × 150 mL) and saturated aqueous NaCl (1 × 100 mL), dried ($MgSO_4$), and concentrated. Purification by flash chromatography (500 mL 10% EtOAc–hexane, 1 L 15% EtOAc–hexane, 500 mL 20% EtOAc–hexane, 1.5 L 25% EtOAc–hexane), afforded the title compound (3.37 g, 64%) as a yellow oil: R_f = 0.1 (20% EtOAc–hexane); ^{1}H NMR (400 MHz, $CDCl_3$) δ 7.67 (d, J = 7.0 Hz, 4H), 7.33–7.50 (m, 6H), 5.67 (d, J = 7.0 Hz, 1H), 4.41 (br s, 1H), 3.94–4.15 (m, 2H), 3.75 (t, J = 5.7 Hz, 2H), 2.59 (t, J = 7.0 Hz, 2H), 1.85 (pent, J = 6.3 Hz, 2H), 1.47 (s, 9H), 1.08 (s, 9H); ^{13}C NMR (100 MHz, $CDCl_3$) δ 184.3, 155.7, 135.4, 133.4, 129.6, 127.6, 98.4, 80.2, 78.9, 63.4, 62.8, 61.9, 30.4, 28.2, 26.8, 19.1, 15.7; HRMS (ESI+) calcd for $C_{29}H_{39}NNaO_5Si$ $[M + Na]^+$ 532.2490, found 532.2498 (error 1.5 ppm).

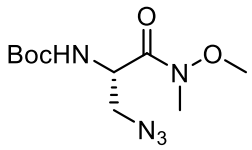

(*S*)-3-Azido-2-[(*tert*-butoxycarbonyl)amino]-*N*-methoxy-*N*-methylpropanamide (46). To a solution of **7** (9.5 g, 38.2 mmol, 1.0 equiv), Et_3N (6.4 ml, 45.8 mmol, 1.2 equiv) in CH_2Cl_2 (150 mL) at 0 °C was added $MeSO_2Cl$ (3.2 mL, 42.0 mmol, 1.1 equiv) dropwise. The mixture was stirred for 1 h at 0 °C, then the reaction mixture was washed with water (1 × 70 mL), saturated aqueous $NaHCO_3$ (1 × 70 mL), 10% aqueous $KHSO_4$ (1 × 70 mL), and saturated aqueous NaCl (1 × 70 mL). The organic layer was dried ($MgSO_4$), concentrated, and placed under high vacuum for 30 min. It was then redissolved in DMF (175 mL), to which NaN_3 (7.5 g, 115 mmol, 3.5 equiv) was added. The reaction was heated at 40 °C for 18 h, then partitioned between ice (200 g) and EtOAc (250 mL). Following melting of the ice, the layers were separated and the aqueous layer was extracted with EtOAc (2 × 250 mL). The combined organic extracts were then dried ($MgSO_4$) and concentrated. Purification by flash chromatography (5% EtOAc–hexane to 30%

EtOAc–hexane, linear gradient) afforded the title compound (8.10 g, 78%) as a clear oil: R_f = 0.55 (50% EtOAc–hexane); ^{1}H NMR, ^{13}C NMR, and HRMS data matched reported values.[268]

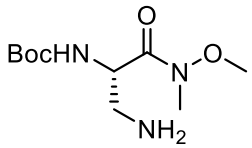

(*S*)-3-Amino-2-[(*tert*-butoxycarbonyl)amino]-*N*-methoxy-*N*-methylpropanamide (47). To a solution of **46** (219 mg, 0.80 mmol, 1.0 equiv) in EtOH (11 mL) was added 10% Pd/C (85 mg). The reaction vessel was then sealed and flushed 3 times with H_2. After 4 h, the reaction mixture was filtered over EtOH-wetted Celite and concentrated to afford the title compound (193 mg, 98%) as a white solid: ^{1}H NMR (400 MHz, $CDCl_3$) δ 5.45 (d, J = 7.04 Hz, 1H), 4.70 (br s., 1H), 3.78 (s, 3H), 3.23 (s, 3H), 3.01 (dd, J = 13.3, 4.7 Hz, 1H), 2.86 (dd, J = 13.3, 5.8 Hz, 1H), 1.45 (s, 9H); ^{13}C NMR (100 MHz, $CDCl_3$) δ 171.3, 155.7, 79.7, 61.5, 52.8, 44.0, 32.0, 28.3; HRMS (ESI+) calcd for $C_{10}H_{22}N_3O_4$ $[M + H]^+$ 246.1605, found 246.1615 (error 4.1 ppm).

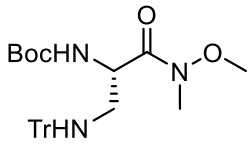

(*S*)-2-[(*tert*-Butoxycarbonyl)amino]-*N*-methoxy-*N*-methyl-3-(tritylamino)propanamide (49). To a solution of **47** (1.02 g, 4.10 mmol, 1.0 equiv) and Et_3N (1.27 mL, 9.03 mmol, 2.2 equiv) in CH_2Cl_2 (50 mL) at 23 °C was added trityl chloride (1.42 g, 4.93 mmol, 1.2 equiv). After 12 h, the reaction mixture was concentrated. Purification by flash chromatography (5% EtOAc–hexane to 30% EtOAc–hexane, linear gradient) afforded the title compound (1.15 g, 74%) as a clear oil: R_f = 0.65 (50% EtOAc–hexane); ^{1}H NMR (400 MHz, $CDCl_3$) δ 7.44 (d, J = 7.8 Hz, 6H), 7.21–7.32 (m, 6H), 7.10–7.21 (m, 3H), 5.40 (d, J = 8.6 Hz, 1H), 4.86 (br s, 1H), 3.67 (s, 3H), 3.19 (s, 3H), 2.55 (dt, J = 10.8, 4.5 Hz, 1H), 2.27 (td, J = 11.6, 5.7 Hz, 1H), 1.96 (br s, 1H), 1.45 (s, 9H); ^{13}C NMR (100 MHz, $CDCl_3$) δ 172.2, 155.6, 145.7, 128.5, 127.8, 126.3, 79.7,

70.5, 61.5, 50.9, 45.6, 32.2, 28.4; HRMS (ESI+) calcd for $C_{29}H_{35}N_3NaO_4$ $[M + Na]^+$ 512.2520, found 512.2503 (error 3.3 ppm).

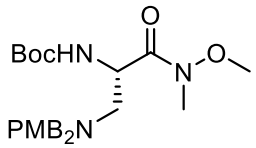

(*S*)-2-[(*tert*-Butoxycarbonyl)amino]-3-[*bis*(4-methoxybenzyl)amino]-*N*-methoxy-*N*-methylpropanamide (50). To a solution of **47** (0.732 g, 2.96 mmol, 1.0 equiv) and DIPEA (1.56 mL, 8.9 mmol, 3.0 equiv) in MeCN (11 mL) at 23 °C was added PMBCl (1.0 mL, 7.4 mmol, 2.5 equiv). After 24 h, Et_3N (5 mL) was added and the reaction was partitioned between saturated aqueous NaCl (70 mL) and EtOAc (80 mL). The layers were separated and the aqueous layer was extracted with EtOAc (2 × 80 mL). The combined organic extracts were dried ($MgSO_4$) and concentrated. Purification by flash chromatography (5% EtOAc–hexane to 60% EtOAc–hexane, linear gradient) afforded the title compound (596 mg, 41%) as a clear oil: R_f = 0.45 (50% EtOAc–hexane); ^{1}H NMR (400 MHz, $CDCl_3$) δ 7.25 (d, J = 8.6 Hz, 4H), 6.84 (d, J = 8.6 Hz, 4H), 5.01 (d, J = 8.6 Hz, 1H), 4.90 (br s, 1H), 3.61–3.84 (m, 11H), 3.41 (d, J = 13.3 Hz, 2H), 3.17 (s, 3H), 2.55–2.74 (m, 2H), 1.48 (s, 9H); ^{13}C NMR (100 MHz, $CDCl_3$) δ 172.0, 158.6, 155.4, 131.1, 130.1, 113.6, 79.3, 61.5, 57.5, 55.2, 54.9, 49.3, 32.0, 28.4; HRMS (ESI+) calcd for $C_{26}H_{38}N_3O_6$ $[M + H]^+$ 488.2755, found 488.2769 (error 3.1 ppm).

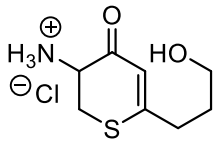

(±)-3-Amino-6-(3-hydroxypropyl)-2,3-dihydro-4*H*-thiopyran-4-one hydrochloride (51). To a pre-chilled flask containing **56** (51 mg, 0.177 mmol, 1.0 equiv) was added cold 4 M HCl in dioxane (10 mL). After 1 h at 0 °C, the reaction mixture was concentrated in vacuo. The residue was dissolved in a minimal amount of MeOH and precipitated with ether, which afforded the title

compound (21 mg, 53%) as a white solid: ^{1}H NMR (400 MHz, CD_3OD) δ 6.23 (s, 1H), 4.30 (dd, J = 14.9, 4.7 Hz, 1H), 3.60 (t, J = 6.1 Hz, 2H), 3.45 (dd, J = 14.6, 13.0 Hz, 1H), 3.34 (dd, J = 12.7, 4.7 Hz, 1H), 2.56 (dt, J = 7.6, 2.4 Hz, 2H), 1.84 (pent, J = 7.0 Hz, 2H); ^{13}C NMR (100 MHz, CD_3OD) δ 188.0, 167.5, 119.1, 60.1, 52.7, 34.1, 31.4, 28.7; HRMS (ESI+) calcd for $C_8H_{14}NO_2S$ $[M + H]^+$ 188.0740, found 188.0740 (error 0 ppm).

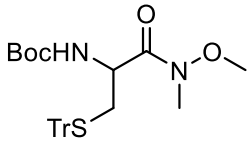

(±)-*N*-(*tert*-Butoxycarbonyl)-*S*-trityl-cysteine *N*′-methoxy-*N*′-methylamide (53). To a solution of (±)-**52** (2.5 g, 5.4 mmol, 1.0 equiv), *N*-methylmorpholine (0.66 ml, 5.9 mmol, 1.1 equiv), and *N*,*O*-dimethylhydroxylamine·HCl (0.60 g, 5.9 mmol, 1.1 equiv) in CH_2Cl_2 (15 mL) at -15 °C was added EDC (1.13 g, 5.9 mmol, 1.1 equiv) in four equal portions over 15 min. The mixture was stirred for 16 h at -15 °C, then partitioned between 1 N aqueous HCl (25 mL) and CH_2Cl_2 (40 mL). The organic layer was separated and washed with 1 N aqueous HCl (1 × 25 mL), after which the aqueous layers were combined and extracted with CH_2Cl_2 (1 × 50 mL) The combined organic extracts were washed with saturated aqueous $NaHCO_3$ (2 × 30 mL), saturated aqueous NaCl (1 × 30 mL), dried ($MgSO_4$), and concentrated to afford the title compound (2.62 g, 96%) as a white solid: R_f = 0.45 (50% EtOAc–hexane); ^{1}H NMR, ^{13}C NMR, and HRMS data matched reported values.[269]

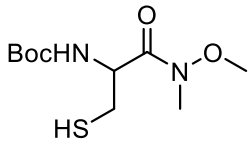

(±)-*N*-(*tert*-Butoxycarbonyl)-cysteine *N*′-methoxy-*N*′-methylamide (54). To a solution of **53** (2.60 g, 5.13 mmol, 1.0 equiv) and Et_3SiH (0.98 mL, 6.16 mmol, 1.2 equiv) in CH_2Cl_2 (60 mL) at 0 °C was added TFA (2.4 mL, 31.3 mmol, 6.1 equiv), causing the solution to turn bright

yellow due to the presence of the triphenylmethyl cation. The reaction was stirred for 1 h at 0 °C until the solution had again become clear, then quenched with saturated aqueous $NaHCO_3$ (50 mL). The layers were separated and the aqueous layer was extracted with CH_2Cl_2 (3 × 50 mL). The combined organic extracts were dried ($MgSO_4$) and concentrated under reduced pressure. Purification by flash chromatography (10% EtOAc–hexane to 40% EtOAc–hexane, linear gradient) afforded the title compound (1.19 g, 88%) as a clear oil: R_f = 0.45 (50% EtOAc–hexane); ^{1}H NMR (400 MHz, $CDCl_3$) δ 5.44 (d, J = 6.7 Hz, 1H), 4.88 (br s, 1H), 3.78 (s, 3H), 3.24 (s, 3H), 2.74–2.97 (m, 2H), 1.39–1.55 (m, 10H, $C(C\underline{H}_3)_3$ and $S\underline{H}$); ^{13}C NMR (101 MHz, $CDCl_3$) δ 170.6, 155.3, 80.0, 61.7, 51.9, 32.1, 28.3, 27.1; HRMS (ESI+) calcd for $C_{10}H_{20}N_2NaO_4S$ $[M + Na]^+$ 287.1036, found 287.1023 (error 4.5 ppm).

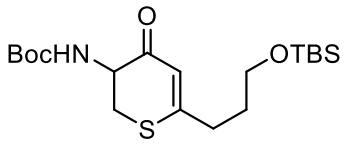

(±)-3-*N*-[(*tert*-Butoxycarbonyl)amino]-6-[3-(*tert*-butyldimethylsilyloxy)propyl]-2,3-dihydro-4*H*-thiopyran-4-one (55). To a solution of 5-(*tert*-butyldimethylsilyloxy)-1-pentyne[270] (282 mg, 1.42 mmol, 3.2 equiv) in THF (10 mL) at -78 °C was added *n*-BuLi (0.58 mL of a 2.5 M solution in hexanes, 1.45 mmol 3.3 equiv). The reaction was stirred for 1 h, then a solution of **54** (117 mg, .44 mmol, 1.0 equiv) in THF (5 mL) was added dropwise. After 5 h at -78 °C, the reaction was quenched by the dropwise addition of saturated aqueous NH_4Cl (5 mL). The reaction mixture was allowed to warm to 23 °C and partitioned between saturated aqueous NH_4Cl (20 mL) and EtOAc (50 mL). The layers were separated and the aqueous layer was extracted with EtOAc (2 × 40 mL). The combined organic extracts were dried ($MgSO_4$) and concentrated. Purification by flash chromatography (0% EtOAc–hexane to 15% EtOAc–hexane, linear gradient) afforded the title compound (71 mg, 40%) as a pale yellow oil: R_f = 0.2 (10% EtOAc–hexane); ^{1}H NMR (400 MHz, $CDCl_3$) δ 6.08 (s, 1H), 5.79 (br s, 1H), 4.34 (d, J = 14.1 Hz, 1H),

3.61 (t, J = 6.1 Hz, 2H), 3.50 (d, J = 9.4 Hz, 1H), 3.01 (t, J = 13.5 Hz, 1H), 2.45 (t, J = 7.6 Hz, 2H), 1.71–1.83 (pent, J = 6.8 Hz, 2H), 1.44 (s, 9H), 0.87 (s, 9H), 0.03 (s, 6H); ^{13}C NMR (101 MHz, $CDCl_3$) δ 191.1, 166.2, 155.5, 119.8, 80.1, 61.5, 54.5, 34.6, 31.73, 31.67, 28.3, 25.9, 18.2, -5.4 (2C); HRMS (ESI+) calcd for $C_{19}H_{35}NNaO_4SSi$ [M + Na]$^+$ 424.1948, found 424.1960 (error 2.8 ppm).

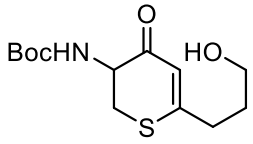

(±)-3-*N*-[(*tert*-Butoxycarbonyl)amino]-6-(3-hydroxypropyl)-2,3-dihydro-4*H*-thiopyran-4-one (56). To a solution of **55** (70 mg, 0.174 mmol, 1.0 equiv) in THF (7 mL) at 0 °C was added HF·Pyridine (0.7 mL) dropwise over 30 min. The reaction was stirred at 0 °C for 3 h, then quenched with saturated aqueous $NaHCO_3$ (25 mL). The aqueous layer was extracted with EtOAc (4 × 35 mL). The combined organic extracts were dried ($MgSO_4$), concentrated, and purified by flash chromatography (15% EtOAc–hexane to 65% EtOAc–hexane, linear gradient) affording the title compound (40 mg, 80%) as a white powder: R_f = 0.45 (80% EtOAc–hexane); ^{1}H NMR (400 MHz, $CDCl_3$) δ 6.12 (s, 1H), 5.81 (br s, 1H), 4.37–4.40 (m, 1H), 3.69 (t, J = 6.3 Hz, 2H), 3.50–3.54 (m, 1H), 3.04 (t, J = 13.5 Hz, 1H), 2.51 (t, J = 7.8 Hz, 2H), 2.06 (br s, 1H, O<u>H</u>), 1.86 (pent, J = 7.0 Hz, 2H), 1.46 (s, 9H); ^{13}C NMR (101 MHz, $CDCl_3$) δ 191.1, 165.8, 155.5, 119.8, 80.1, 61.3, 54.5, 34.4, 31.6, 31.4, 28.3; HRMS (ESI+) calcd for $C_{13}H_{21}NNaO_4S$ [M + Na]$^+$ 310.1083, found 310.1088 (error 1.6 ppm).

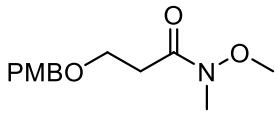

3-(4-Methoxybenzyloxy)-*N*-methoxy-*N*-methylpropanamide (59). To a solution of **58** (3.78 g, 19.3 mmol, 1.0 equiv) in acetone (11 mL) at 0 °C was added 2 M Jones' Reagent (23.2

mL). The mixture immediately turned green and some precipitation was observed. After 90 min, iPrOH was added until the reaction turned deep blue, signifying a complete quench. The reaction mixture was filtered over Celite and concentrated to remove all of the acetone. The crude product was dissolved in water (30 mL) and extracted with EtOAc (3 × 100 mL). The combined organic extracts were dried ($MgSO_4$), concentrated, then redissolved in CH_2Cl_2 (130 mL). To this solution was sequentially added *N*,*O*-dimethylhydroxylamine hydrochloride (2.52 g, 25.1 mmol, 1.3 equiv), EDC (4.8 g, 25.1 mmol, 1.3 equiv), Et_3N (3.5 mL, 25.1 mmol, 1.3 equiv), and DMAP (3.1 g, 25.1 mmol, 1.3 equiv). After 16 h at 23 °C, the reaction mixture was washed with 1 M aqueous HCl (1 × 50 mL), saturated aqueous NaCl (1 × 50 mL), saturated aqueous $NaHCO_3$ (1 × 50 mL), and saturated aqueous NaCl (1 × 50 mL). The organic layer was then dried ($MgSO_4$), and concentrated. Purification by flash chromatography (20% EtOAc–hexane to 60% EtOAc–hexane, linear gradient) afforded the title compound (2.34 g, 72%) as a clear viscous liquid: ^{1}H NMR (400 MHz, $CDCl_3$) δ 7.26 (d, J = 8.5 Hz, 2H), 6.87 (d, J = 8.6 Hz, 2H), 4.47 (s, 2H), 3.72–3.85 (m, 5H), 3.67 (s, 3H), 3.18 (s, 3H), 2.74 (t, J = 6.5 Hz, 2H); ^{13}C NMR (100 MHz, $CDCl_3$) δ 172.3, 159.2, 130.4, 129.3, 113.7, 72.9, 65.6, 61.3, 55.2, 32.5, 32.0; HRMS (ESI+) calcd for $C_{13}H_{19}NNaO_4$ $[M + Na]^+$ 276.1206, found 276.1206 (error 0 ppm).

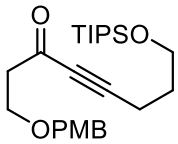

1-(4-Methoxybenzyloxy)-8-(triisopropylsilyloxy)oct-4-yn-3-one (61). To a solution of 5-(triisopropylsilyloxy)-1-pentyne[271] (2.9 g, 12.0 mmol, 1.3 equiv) in THF (40 mL) at -78 °C was added *n*-BuLi (4.4 mL of a 2.5 M solution in hexanes, 11.0 mmol 1.2 equiv). The reaction was stirred for 1.5 h, then a solution of **59** (2.34 g, 12.0 mmol, 1.0 equiv) in THF (50 mL) was added dropwise. The reaction was allowed to warm to 23 °C over 2 h, and after 16 h was quenched with AcOH (2 mL). EtOAc (300 mL) was then added and the reaction mixture was washed with

saturated aqueous $NaHCO_3$ (2 × 100 mL) and saturated aqueous NaCl (1 × 50 mL), dried ($MgSO_4$), and concentrated. Purification by flash chromatography (0% EtOAc–hexane to 15% EtOAc–hexane, linear gradient) afforded the title compound (3.51 g, 88%) as a pale yellow liquid: R_f = 0.7 (20% EtOAc–hexane); ^{1}H NMR (400 MHz, $CDCl_3$) δ 7.26 (d, J = 8.5 Hz, 2H), 6.88 (d, J = 8.6 Hz, 2H), 4.46 (s, 2H), 3.81 (s, 3H), 3.72–3.80 (m, 4H), 2.82 (t, J = 6.3 Hz, 2H), 2.50 (t, J = 7.2 Hz, 2H), 1.79 (pent, J = 6.5 Hz, 2H), 0.97–1.16 (m, 21H); ^{13}C NMR (100 MHz, $CDCl_3$) δ 185.8, 159.2, 130.1, 129.3, 113.8, 94.7, 80.8, 72.8, 64.6, 61.5, 55.3, 45.7, 31.0, 18.0, 15.5, 11.9; HRMS (ESI+) calcd for $C_{25}H_{40}NaO_4Si$ $[M + Na]^+$ 455.2588, found 455.2594 (error 1.1 ppm).

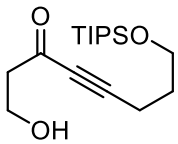

1-Hydroxy-8-(triisopropylsilyloxy)oct-4-yn-3-one (62). To a solution of **61** (3.45 g, 7.97 mmol, 1.0 equiv) in CH_2Cl_2 (60 mL) at 23 °C was added DDQ (2.17 g, 9.56 mmol 1.2 equiv) and H_2O (6 mL). After 1.5 h, the reaction mixture was partitioned between CH_2Cl_2 (50 mL) and saturated aqueous $NaHCO_3$ (50 mL). The layers were separated and the aqueous layer was extracted with CH_2Cl_2 (3 × 100 mL). The combined organic extracts were dried ($MgSO_4$) and concentrated. Purification by flash chromatography (5% EtOAc–hexane to 20% EtOAc–hexane, linear gradient) afforded the title compound (2.34 g, 94%) as a pale yellow liquid: R_f = 0.15 (20% EtOAc–hexane); ^{1}H NMR (400 MHz, $CDCl_3$) δ 3.91 (q, J = 5.6 Hz, 2H), 3.78 (t, J = 5.9 Hz, 2H), 2.82 (t, J = 5.5 Hz, 2H), 2.53 (t, J = 7.0 Hz, 2H), 2.19 (t, J = 6.5 Hz, 1H, O<u>H</u>), 1.81 (pent, J = 6.5 Hz, 2H), 1.00–1.16 (m, 21H); ^{13}C NMR (101 MHz, $CDCl_3$) δ 187.3, 95.4, 80.8, 61.4, 57.7, 47.6, 30.9, 18.0, 15.5, 11.9; HRMS (ESI+) calcd for $C_{17}H_{32}NaO_3Si$ $[M + Na]^+$ 335.2013, found 335.2022 (error 2.7 ppm).

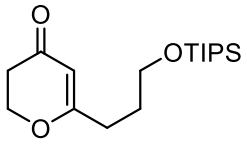

6-[3-((Triisopropylsilyl)oxy)propyl]-2,3-dihydro-4*H*-pyran-4-one (63). To a solution of **62** (2.36 g, 7.55 mmol, 1.0 equiv) in CH_2Cl_2 (150 mL) was added AgOTf (1.94 g, 7.55 mmol, 1.0 equiv). After 2 h, the reaction mixture was filtered over Celite, concentrated, and purified by flash chromatography (5% EtOAc–hexane to 20% EtOAc–hexane, linear gradient) affording the title compound (1.46 g, 62%) as a clear oil: R_f = 0.15 (20% EtOAc–hexane); ^{1}H NMR (400 MHz, $CDCl_3$) δ 5.36 (s, 1H), 4.46 (t, J = 6.9 Hz, 2H), 3.72 (t, J = 6.1 Hz, 2H), 2.52 (t, J = 6.9 Hz, 2H), 2.37 (t, J = 7.6 Hz, 2H), 1.79 (pent, J = 6.9 Hz, 2H), 1.02–1.13 (m, 21H); ^{13}C NMR (100 MHz, $CDCl_3$) δ 192.2, 177.9, 104.6, 67.9, 62.1, 35.7, 31.3, 29.6, 18.0, 11.9; HRMS (ESI+) calcd for $C_{17}H_{32}NaO_3Si$ $[M + Na]^+$ 335.2013, found 335.2021 (error 2.4 ppm).

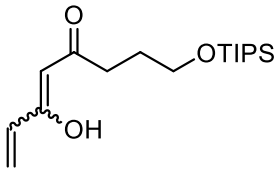

6-Hydroxy-1-[(triisopropylsilyl)oxy]octa-5,7-dien-4-one (64). To a solution of **63** (1.39 g, 4.0 mmol, 1.0 equiv) in THF (40 mL) at -78 °C was added LiHMDS (4.9 mL of a 1M solution in THF, 4.9 mmol, 1.1 equiv). After 30 min at -78 °C, N-Boc-cyanophenyl oxaziridine (0.60 g, 2.45 mmol, 0.55 equiv) was added over 10 min as a solution in THF (10 mL). After 50 min, saturated aqueous NH_4Cl (5 mL) was added, and the reaction was warmed to 23 °C. The reaction mixture was then partitioned between saturated aqueous NH_4Cl (50 mL) and EtOAc (100 mL). The layers were separated and the aqueous layer was extracted with EtOAc (2 x 100 mL). The combined organic extracts were dried ($MgSO_4$) and concentrated. Purification by flash chromatography (5% EtOAc–hexane → 30% EtOAc–hexane, linear gradient) afforded the title compound (157 mg, 11%) as a clear liquid, along with several other products that were unable to

be fully characterized: R_f = 0.8 (20% EtOAc–hexane); ^{1}H NMR (400 MHz, $CDCl_3$) δ 6.26 (dd, J = 17.1, 1.5 Hz, 1H), 6.13 (dd, J = 17.1, 10.6 Hz, 1H), 5.67 (dd, J = 10.4, 1.4 Hz, 1H), 5.58 (s, 1H), 3.73 (t, J = 6.1 Hz, 2H), 2.52 (t, J = 7.6 Hz, 2H), 1.87 (pent, J = 6.8 Hz, 2H), 0.99–1.15 (m, 21H); ^{13}C NMR (101 MHz, $CDCl_3$) δ 202.1, 175.4, 132.4, 125.1, 100.3, 62.4, 37.0, 28.4, 18.0, 12.0; HRMS (ESI+) calcd for $C_{17}H_{32}NaO_3Si$ $[M + Na]^+$ 335.2013, found 335.2005 (error 2.4 ppm).

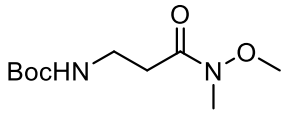

3-[(*tert*-Butoxycarbonyl)amino]-*N*-methoxy-*N*-methylpropanamide (66). To a solution of *N*-Boc-*β*-alanine (8.5 g, 45.0 mmol, 1.0 equiv), *N*-methylmorpholine (5.5 ml, 49.5 mmol, 1.1 equiv), and *N*,*O*-dimethylhydroxylamine·HCl (4.98 g, 49.5 mmol, 1.1 equiv) in CH_2Cl_2 (100 mL) at -15 °C was added EDC (9.49 g, 49.5 mmol, 1.1 equiv) in four equal portions over 15 min. The mixture was stirred for 16 h at -15 °C, then washed with 1 N aqueous HCl (2 × 25 mL), saturated aqueous $NaHCO_3$ (2 × 25 mL), and saturated aqueous NaCl (1 × 25 mL). The organic layer was then dried ($MgSO_4$), and concentrated to afford the title compound (9.69 g, 93%) as a white solid: R_f = 0.1 (50% EtOAc–hexane); ^{1}H NMR, ^{13}C NMR, and HRMS data matched reported values.[272]

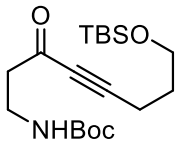

1-[(*tert*-Butoxycarbonyl)amino]-8-(*tert*-butyldimethylsilyloxy)oct-4-yn-3-one (67). To a solution of 5-(*tert*-butyldimethylsilyloxy)-1-pentyne[273] (4.25 g, 21.4 mmol, 2.2 equiv) in THF (35 mL) at -78 °C was added *n*-BuLi (8.6 mL of a 2.5 M solution in hexanes, 21.4 mmol 2.2 equiv). The reaction was stirred for 1.25 h, then a solution of **66** (2.25 g, 9.7 mmol, 1.0 equiv) in THF (15 mL) was added dropwise. The reaction was allowed to warm to 23 °C after 2 h. After 16 h, the reaction was quenched by the dropwise addition of AcOH (5 mL), then partitioned between

saturated aqueous $NaHCO_3$ (50 mL) and EtOAc (150 mL). The layers were separated and the organic layer was washed with saturated aqueous $NaHCO_3$ (1 × 50 mL) and saturated aqueous NaCl (1 × 50 mL), dried ($MgSO_4$), and concentrated. Purification by flash chromatography (5% EtOAc–hexane to 25% EtOAc–hexane, linear gradient) afforded the title compound (2.13 g, 59%) as a clear oil: R_f = 0.3 (20% EtOAc–hexane); ^{1}H NMR (400 MHz, $CDCl_3$) δ 4.94 (br s, 1H), 3.69 (t, J = 5.7 Hz, 2H), 3.41 (q, J = 5.6 Hz, 2H), 2.78 (t, J = 5.5 Hz, 2H), 2.48 (t, J = 7.0 Hz, 2H), 1.78 (pent, J = 6.5 Hz, 2H), 1.44 (s, 9H), 0.90 (s, 9H), 0.06 (s, 6H); ^{13}C NMR (100 MHz, $CDCl_3$) δ 186.7, 155.7, 95.0, 80.7, 79.3, 61.1, 45.5, 35.1, 30.7, 28.4, 25.9, 18.3, 15.5, -5.4; HRMS (ESI+) calcd for $C_{19}H_{35}NNaO_4Si$ $[M + Na]^+$ 392.2228, found 392.2220 (error 2.0 ppm).

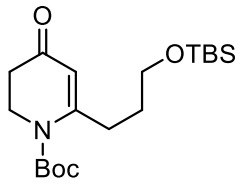

1-*tert*-Butoxycarbonyl-6-[3-(*tert*-butyldimethylsilyloxy)propyl]-2,3-dihydro-4*H*-pyridin-4-one (68). To a solution of **67** (2.127 g, 5.8 mmol, 1.0 equiv) and PPh_3AuCl (143 mg, 0.29 mmol, 0.05 equiv) in CH_2Cl_2 (35 mL) at 23 C was added AgOTf (200 mg, 0.58 mmol, 0.1 equiv). After 2 h, the reaction mixture was filtered over Celite and concentrated. Purification by flash chromatography (0% EtOAc–hexane to 25% EtOAc–hexane, linear gradient) afforded the title compound (1.501 g, 71%) as a clear oil: R_f = 0.35 (20% EtOAc–hexane); ^{1}H NMR (400 MHz, $CDCl_3$) δ 5.41 (s, 1H), 4.01 (t, J = 6.7 Hz, 2H), 3.62 (t, J = 6.1 Hz, 2H), 2.76 (t, J = 7.6 Hz, 2H), 2.48 (t, J = 6.7 Hz, 2H), 1.72 (pent, J = 6.9 Hz, 2H), 1.54 (s, 9H), 0.90 (s, 9H), 0.05 (s, 6H); ^{13}C NMR (100 MHz, $CDCl_3$) δ 194.7, 161.3, 152.0, 112.3, 83.0, 62.2, 46.6, 37.3, 32.3, 31.1, 28.1, 25.9, 18.3, -5.3; HRMS (ESI+) calcd for $C_{19}H_{35}NNaO_4Si$ $[M + Na]^+$ 392.2228, found 392.2222 (error 1.5 ppm).

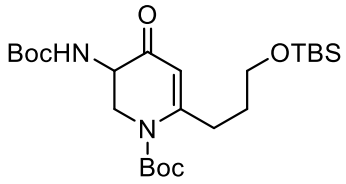

(±)-1-(*tert*-Butoxycarbonyl)-3-[(*tert*-butoxycarbonyl)amino]-6-[3-(*tert*-butyldimethylsilyloxy)propyl]-2,3-dihydro-4*H*-pyridin-4-one (69). To a solution of **68** (1.48 g, 4.0 mmol, 1.0 equiv) in THF (50 mL) at -78 °C was added LiHMDS (4.4 mL of a 1 M solution in THF, 4.4 mmol, 1.1 equiv). After 30 min at -78 °C, *N*-Boc-cyanophenyloxaziridine (0.54 g, 2.2 mmol, 0.55 equiv) was added over 10 min as a solution in THF (10 mL). After 50 min, saturated aqueous NH_4Cl (5 mL) was added, and the reaction was warmed to 23 °C. The reaction mixture was then partitioned between saturated aqueous NH_4Cl (50 mL) and EtOAc (100 mL). The layers were separated and the aqueous layer was extracted with EtOAc (2 × 100 mL). The combined organic extracts were dried ($MgSO_4$) and concentrated. Purification by flash chromatography (0% EtOAc–hexane to 25% EtOAc–hexane, linear gradient) afforded the title compound (744 mg, 38%) as a clear oil: R_f = 0.55 (20% EtOAc–hexane); ^{1}H NMR (400 MHz, $CDCl_3$) δ 5.37 (s, 1H), 5.31 (br s, 1H), 4.78 (dd, J = 12.3, 5.3 Hz, 1H), 4.22 (d, J = 12.5 Hz, 1H), 3.62 (dt, J = 6.1, 3.1 Hz, 2H), 3.24 (t, J = 13.2 Hz, 1H), 2.99 (td, J = 14.7, 7.5 Hz, 1H), 2.58 (td, J = 15.0, 7.6 Hz, 1H), 1.72 (pent, J = 6.9 Hz, 2H), 1.52–1.64 (m, 9H), 1.46 (s, 9H), 0.90 (s, 9H), 0.05 (s, 6H); ^{13}C NMR (100 MHz, $CDCl_3$) δ 191.7, 162.9, 155.5, 151.8, 108.7, 83.6, 80.0, 62.0, 53.7, 51.3, 32.1, 31.2, 28.3, 28.0, 25.9, 18.3, -5.3 (2C); HRMS (ESI+) calcd for $C_{24}H_{44}N_2NaO_6Si$ $[M + Na]^+$ 507.2861, found 507.2876 (error 3.0 ppm).

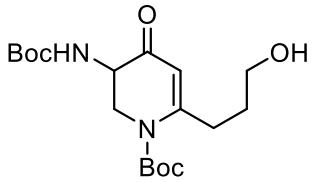

(±)-1-(*tert*-Butoxycarbonyl)-3-[(*tert*-butoxycarbonyl)amino]-6-(3-hydroxypropyl)-2,3-dihydro-4*H*-pyridin-4-one (70). To a solution of **69** (734 mg, 1.51 mmol, 1.0 equiv) in THF (50 mL) at 0 °C was added HF·Pyridine (5 mL) over a 30 min period. After 4 h at 0 °C, the reaction mixture was partitioned between saturated aqueous $NaHCO_3$ (50 mL) and EtOAc (100 mL). The layers were separated and the aqueous layer was extracted with EtOAc (4 × 60 mL). The combined organic extracts were dried ($MgSO_4$) and concentrated. Purification by flash chromatography (20% EtOAc–hexane to 70% EtOAc–hexane, linear gradient) afforded the title compound (478 mg, 85%) as a clear oil: R_f = 0.55 (80% EtOAc–hexane); ^{1}H NMR (400 MHz, $CDCl_3$) δ 5.38 (s, 1H), 5.29 (br s, 1H), 4.76 (dd, J = 12.5, 5.5 Hz, 1H), 4.21 (d, J = 12.1 Hz, 1H), 3.67 (t, J = 6.0 Hz, 2H), 3.25 (t, J = 13.1 Hz, 1H), 3.01 (dt, J = 14.5, 7.2 Hz, 1H), 2.64 (dt, J = 15.1, 7.7 Hz, 1H), 1.73–1.85 (m, 2H), 1.54 (s, 9H), 1.45 (s, 9H); ^{13}C NMR (101 MHz, $CDCl_3$) δ 191.7, 162.7, 155.5, 151.8, 108.8, 83.8, 80.1, 61.7, 53.7, 51.2, 31.7, 31.1, 28.3, 28.0; HRMS (ESI+) calcd for $C_{18}H_{30}N_2NaO_6$ $[M + Na]^+$ 393.1996, found 393.2012 (error 4.1 ppm).

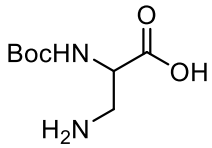

(±)-3-Amino-2-[(*tert*-butoxycarbonyl)amino]propionic acid (72). To a slurry of **(±)-***N*-Boc-asparagine (10.0 g, 43.1 mmol, 1.0 equiv) in 2:2:1 EtOAc–MeCN–H_2O (120 mL) at 10 °C was added iodosobenzene diacetate (16.6 g, 51.5 mmol, 1.2 equiv). The reaction was allowed to warm to 23 °C over 2 h. After 16 h, the reaction mixture was filtered, and the filter cake was washed with EtOAc (150 mL), then dried *in vacuo* to afford the title compound (6.06 g, 69%) as a white solid. ^{1}H NMR, ^{13}C NMR, and HRMS data matched reported values.[274]

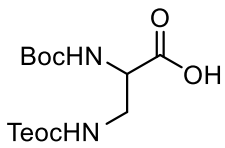

(±)-2-(*tert*-Butoxycarbonyl)amino-3-[2-(trimethylsilyl)ethyloxycarbonyl]propionic acid (73). To a solution of **72** (0.41 g, 2.01 mmol, 1.0 equiv) in 1.5 M aqueous Na_2CO_3 (10 mL) at 23 °C was added 4-nitrophenyl 2-(trimethylsilyl)ethyl carbonate (Teoc-ONp) (0.68 g, 2.41 mmol, 1.2 equiv) in dioxane (5 mL) dropwise. The reaction was heated to 40 °C for 48 h, after which it was a bright yellow solution. $Na_2S_2O_4$ was then added to the reaction mixture until the solution turned white, which signifies when the *p*-nitrophenol has been reduced to the aniline. H_2O (30 mL) was added and the reaction mixture was extracted with Et_2O (1 × 20 mL). The layers were separated and the organic layer was extracted with 1 N Na_2CO_3 (3 × 15 mL). The combined aqueous extracts were acidified to a pH of 2 with 2 N HCl and extracted with CH_2Cl_2 (3 × 100 mL). The combined organic extracts were dried ($MgSO_4$) and concentrated to afford the title compound (0.593 g, 85%) as a clear oil: R_f = 0.1 (10% MeOH– CH_2Cl_2); ^{1}H NMR, ^{13}C NMR, and HRMS data matched reported values.[275]

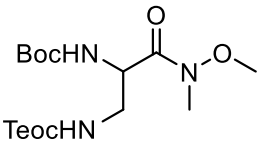

(±)-2-*N*-(*tert*-Butoxycarbonyl)-3-*N*-[2-(trimethylsilyl)ethyloxycarbonyl]-2,3-diamino-*N*-methoxy-*N*-methylpropanamide (74). To a solution of **73** (0.58 g, 1.66 mmol, 1.0 equiv), *N*-methylmorpholine (0.20 ml, 1.83 mmol, 1.1 equiv), and *N*,*O*-dimethylhydroxylamine·HCl (0.18 g, 1.83 mmol, 1.1 equiv) in CH_2Cl_2 (13 mL) at -15 °C was added EDC (1.13 g, 5.9 mmol, 1.1 equiv) in four equal portions over 15 min. The mixture was stirred for 2 h at -15 °C, then partitioned between saturated aqueous 1 N HCl (35 mL) and CH_2Cl_2 (35 mL). The layers were separated and the aqueous layer was extracted with CH_2Cl_2 (1 × 50 mL), after which the organic layers were combined and washed with saturated aqueous $NaHCO_3$ (1 × 30 mL), dried ($MgSO_4$), and concentrated, affording the title compound (0.62 g, 95%) as a white solid: R_f = 0.45 (50% EtOAc–hexane); ^{1}H NMR (400 MHz, $CDCl_3$) δ 5.54 (br s, 1H), 5.11 (br s, 1H), 4.75 (br s, 1H),

4.11 (t, J = 8.4 Hz, 2H), 3.76 (s, 3H), 3.48 (br s, 2H), 3.19 (s, 3H), 1.42 (s, 9H), 0.94 (t, J = 8.40 Hz, 2H), 0.01 (s, 9H); ^{13}C NMR (101 MHz, $CDCl_3$) δ 170.6, 156.8, 155.5, 79.8, 63.1, 61.6, 50.9, 42.7, 32.3, 28.2, 17.6, -1.6; HRMS (ESI+) calcd for $C_{16}H_{33}N_3NaO_6Si$ $[M + Na]^+$ 414.2031, found: 414.2032 (error 0.2 ppm).

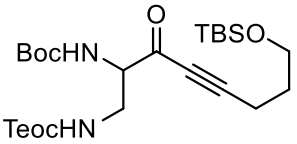

(±)-2-[(*tert*-Butoxycarbonyl)amino]-8-(*tert*-butyldimethylsilyloxy)-1-[2-(trimethylsilyl)ethoxycarbonyl]-oct-4-yn-3-one (75). To a solution of 5-(*tert*-butyldimethylsilyloxy)-1-pentyne[276] (0.96 g, 4.82 mmol, 3.2 equiv) in THF (15 mL) at -78 °C was added *n*-BuLi (1.99 mL of a 2.5 M solution in hexanes, 4.97 mmol 3.3 equiv). After 2 h, a solution of **74** (0.59 g, 1.51 mmol, 1.0 equiv) in THF (15 mL) was added dropwise. After 16 h at -78 C, AcOH (3 mL) was added dropwise to quench. The reaction mixture was partitioned between EtOAc (80 mL) and saturated aqueous $NaHCO_3$ (40 mL). The aqueous layer was extracted with EtOAc (1 × 80 mL), and the combined organic extracts were dried ($MgSO_4$) and concentrated. Purification by flash chromatography (5% EtOAc–hexane to 30% EtOAc–hexane, linear gradient) afforded the title compound (317 mg, 40%, 73% BRSM) as a pale yellow oil: R_f = 0.3 (20% EtOAc–hexane); ^{1}H NMR (400 MHz, $CDCl_3$) δ 5.62 (br s, 1H), 5.08 (br s, 1H), 4.40 (br s, 1H), 4.12 (t, J = 8.4 Hz, 2H), 3.47–3.78 (m, 4H), 2.49 (t, J = 7.0 Hz, 2H), 1.78 (pent, J = 6.5 Hz, 2H), 1.43 (s, 9H), 0.94 (t, J = 8.4 Hz, 2H), 0.87 (s, 9H), 0.04 (s, 6H), 0.01 (s, 9H); ^{13}C NMR (101 MHz, $CDCl_3$) δ 184.5, 157.0, 155.5, 98.9, 80.1, 78.9, 63.4, 61.7, 61.1, 42.0, 30.6, 28.2, 25.8, 18.2, 17.6, 15.7, -1.6, -5.5; HRMS (ESI+) calcd for $C_{25}H_{48}N_2NaO_6Si_2$ $[M + Na]^+$ 551.2943, found: 551.2955 (error 2.2 ppm).

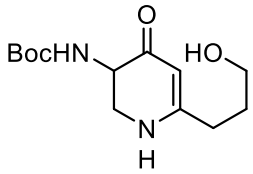

(±)-3-[(*tert*-Butoxycarbonyl)amino]-6-(3-hydroxypropyl)-2,3-dihydro-1*H*-pyridin-4-one (76). To a solution of 1 M TBAF in THF (2.72 mL, 2.72 mmol, 4.0 equiv) at 0 °C was added H_2O (0.74 mL, 40.8 mmol, 60 equiv), THF (10 mL), and a solution of **75** (0.36 g, 0.68 mmol, 1.0 equiv) in THF (10 mL), respectively. The reaction was allowed to warm to 23 °C over 2 h. After 16 h, 4 Å molecular sieves (6 g) were added, and 5 min after saturated aqueous $NaHCO_3$ (30 mL) was added to quench. The reaction mixture was filtered through a thin pad of Celite and extracted with EtOAc (3 × 25 mL). The combined organic extracts were dried ($MgSO_4$) and concentrated. Purification by flash chromatography (0% MeOH–CH_2Cl_2 to 10% MeOH–CH_2Cl_2, linear gradient) afforded the title compound (72 mg, 39%) as a pale yellow oil: R_f = 0.3 (10% MeOH–CH_2Cl_2); ^{1}H NMR (400 MHz, $CDCl_3$) δ 6.40 (br s, 1H), 5.63 (br s, 1H), 4.99 (s, 1H), 3.93–4.18 (m, 2H), 3.68 (t, J = 5.9 Hz, 2H), 3.16 (t, J = 13.1 Hz, 1H), 2.37 (t, J = 7.0 Hz, 2H), 1.81 (pent, J = 6.5 Hz, 2H), 1.44 (s, 9H); ^{13}C NMR (101 MHz, $CDCl_3$) δ 188.6, 167.7, 156.2, 95.6, 79.9, 61.2, 52.0, 46.4, 31.5, 30.2, 28.3; HRMS (ESI+) calcd for $C_{13}H_{22}N_2NaO_4$ $[M + Na]^+$ 293.1472, found: 293.1469 (error 0.2 ppm).

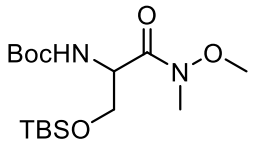

***N*-(*tert*-Butoxycarbonyl)-*O*-(*tert*-butoxydimethylsilyl)-serine-*N*′-methoxy-*N*′-methylamide (77).** To a solution of **5** (3.0 g, 12.1 mmol, 1.0 equiv) in DMF (35 mL) at 23 °C was added imidazole (2.49 g, 36.2 mmol, 3.0 equiv) and *tert*-butyldimethylchlorosilane (2.25 g, 14.5 mmol, 1.2 equiv) sequentially. After 16 h, the reaction was partitioned between 10% $KHSO_4$

(60 mL) and EtOAc (250 mL). The layers were separated and the organic layer was washed with 10% $KHSO_4$ (1 × 60 mL) and saturated aqueous $NaHCO_3$ (1 × 50 mL). The combined organic extracts were dried ($MgSO_4$) and concentrated. Purification by flash chromatography (5% EtOAc–hexane to 25% EtOAc–hexane, linear gradient) afforded the title compound (4.16 g, 95%) as a clear oil. ^{1}H NMR, ^{13}C NMR, and HRMS data matched reported values.[277]

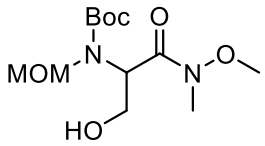

***N*-(*tert*-Butoxycarbonyl)(methoxymethyl)serine-*N'*-methoxy-*N'*-methylamide (78).** To a solution of **77** (12.6 g, 34.8 mmol, 1.0 equiv) in THF (100 mL) at -78 °C was added solid KHMDS (13.2 g, 66.2 mmol, 1.9 equiv). After 1 h, MOMCl (8.0 g, 99.3 mmol, 2.9 equiv) was added dropwise, and the reaction was allowed to warm to 23 °C over 2 h. After 16 h, the reaction mixture was partitioned between saturated aqueous NH_4Cl (200 mL) and EtOAc (250 mL). The layers were separated and the aqueous layer was extracted with EtOAc (1 × 250 mL). The combined organic extracts were dried ($MgSO_4$) and concentrated. To a solution of the resulting mixture in THF (130 mL) at 0 °C was added HF·Pyridine (14 mL). Saturated aqueous $NaHCO_3$ (400 mL) was added after 4.5 h to quench. The product was extracted with EtOAc (2 × 300 mL), and the combined organic extracts were dried ($MgSO_4$) and concentrated. Purification by flash chromatography (25% EtOAc–hexane to 55% EtOAc–hexane, linear gradient) afforded the title compound (7.2 g, 71%) as a colorless oil: R_f = 0.15 (50% EtOAc–hexane); ^{1}H NMR (400 MHz, acetone-d_6) δ 5.12 (br s, 0.5H), 4.76–4.95 (m, 2.5H), 3.91 (br s, 1H), 3.77 (s, 3H), 3.67–3.75 (m, 1H), 3.58–3.66 (m, 1H), 3.32 (br s, 3H), 3.14 (br s, 3H), 1.47 (s, 9H); ^{13}C NMR (100 MHz, acetone-d_6) δ 171.5, 156.0, 81.1, 77.5, 61.9, (61.2, 61.1), (59.3, 57.7), 56.0, 32.6, 28.5; HRMS (ESI+) calcd for $C_{12}H_{24}N_2NaO_6$ $[M + Na]^+$ 315.1527, found 315.1538 (error 3.5 ppm).

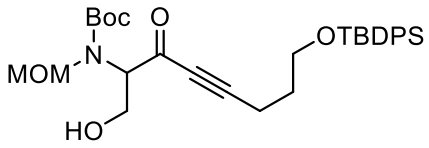

2-[(*tert*-Butoxycarbonyl)(methoxymethyl)amino]-8-(*tert*-butyldiphenylsilyloxy)-1-hydroxy-oct-4-yn-3-one (79). To a solution of 5-(*tert*-butyldiphenylsilyloxy)-1-pentyne[278] (0.507 g, 1.57 mmol, 2.3 equiv) in THF (8 mL) at -78 °C was added *n*-BuLi (0.66 mL of a 2.5 M solution in hexanes, 1.64 mmol 2.4 equiv). The reaction was stirred for 1.5 h, then a solution of **78** (200 mg, 0.68 mmol, 1.0 equiv) in THF (10 mL) was added dropwise. After 16 h at -78 °C, the reaction was quenched by the dropwise addition of AcOH (3 mL). The reaction mixture was allowed to warm to 23 °C and partitioned between saturated aqueous NH_4Cl (20 mL) and EtOAc (50 mL). The layers were separated and the aqueous layer was extracted with EtOAc (2 × 40 mL). The combined organic extracts were dried ($MgSO_4$) and concentrated. Purification by flash chromatography (5% EtOAc–hexane to 40% EtOAc–hexane, linear gradient), afforded the title compound (185 mg, 49%) as a pale yellow oil: R_f = 0.55 (50% EtOAc-hexane); ^{1}H NMR (400 MHz, acetone-d_6, ratio of rotamers 1:1) δ 7.63–7.78 (m, 4H), 7.38–7.53 (m, 6H), 4.89 (dd, J = 10.8, 6.0 Hz, 1H), 4.75 (dd, J = 10.8, 6.0 Hz, 1H), 4.07–4.30 (m, 1.5H), 3.75–4.00 (m, 3.5H), 3.38 (s, 1.5 H), 3.36 (s, 1.5H), 2.57–2.67 (m, 2H), 1.80–1.91 (m, 2H), 1.48 (s, 4.5 H), 1.40 (s, 4.5H), 1.05 (s, 9H); ^{13}C NMR (100 MHz, acetone-d_6) δ (185.2, 184.9), (155.6, 155.3), 136.1, 134.4, 130.7, 128.8, (95.3, 94.9), (81.8, 81.5), (80.48, 80.41), (80.33, 80.14), (69.7, 69.4), 63.0, (61.4, 60.9), (56.4, 56.3), (31.58, 31.53), (28.6, 28.4), 27.3, 19.8, 16.0; HRMS (ESI+) calcd for $C_{31}H_{43}NNaO_6Si$ $[M + Na]^+$ 576.2752, found 576.2744 (error 1.4 ppm).

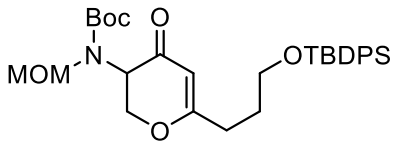

3-[(*tert*-Butoxycarbonyl)(methoxymethyl)amino]-6-[3-(*tert*-butyldiphenylsilyloxy)propyl]-2,3-dihydro-4*H*-pyran-4-one (80). To a solution of **79** (23 mg, 0.042 mmol, 1.0 equiv), and PPh_3AuCl (2 mg, 0.004 mmol, 0.1 equiv) in CH_2Cl_2 (15 mL) at -78 °C was added AgOTf (750 µg, 0.003 mmol, 0.075 equiv). The reaction was stirred for 40 min at -78 °C, then placed in an ice bath to warm to 0 °C. After 30 min, the reaction mixture was partitioned between saturated aqueous NaCl (5 mL) and CH_2Cl_2 (10 mL). The layers were separated and the aqueous layer was extracted with CH_2Cl_2 (1 × 10 mL). The combined organic extracts were dried ($MgSO_4$) and concentrated. Purification by flash chromatography (100 mL hexane, 150 mL 10% EtOAc-hexane, 75 mL 15% EtOAc-hexane, 100 mL 20% EtOAc-hexane) afforded the title compound (12 mg, 52%) as a pale yellow oil: R_f = 0.3 (20% EtOAc–hexane); ^{1}H NMR (400 MHz, acetone-d_6, ~1.4:1 mixture of rotamers) δ 7.62–7.77 (m, 4H), 7.35–7.54 (m, 6H), 5.30 (s, 1H), 4.39–4.82 (m, 4.3H), 4.21 (dd, J = 13.7, 6.3 Hz, 0.7H), 3.75 (t, J = 6.3 Hz, 2H), 3.30 (s, 3H), 2.45 (t, J = 7.4 Hz, 2H), 1.87 (pent, J = 6.9 Hz, 3H), 1.47 (s, 3.7H), 1.37 (s, 5.3H), 1.05 (s, 9H); ^{13}C NMR (100 MHz, acetone-d_6) δ (189.6, 189.5), (177.54, 177.47), (155.4, 155.1), 136.4, 134.5, 130.7, 128.8, (104.4, 104.1), 81.5, (79.9, 79.7), (70.4, 70.3), 63.6, (58.9, 58.2), (55.7, 55.6), 31.5, 30.2, (28.4, 28.3), 27.3, 19.8; HRMS (ESI+) calcd for $C_{31}H_{43}NNaO_6Si$ [M + Na]$^+$ 576.2752, found 576.2750 (error 0.3 ppm).

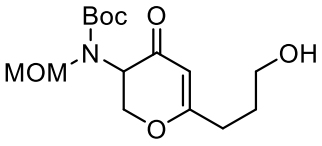

3-[(*tert*-Butoxycarbonyl)(methoxymethyl)amino]-6-(3-hydroxypropyl)-2,3-dihydro-4*H*-pyran-4-one (81). To a solution of **80** (0.48 g, 0.87 mmol, 1.0 equiv) in THF (45 mL) at 0 °C was added HF·Pyridine (4.5 mL) dropwise. The reaction was stirred for 16 h at 0 °C, then quenched with saturated aqueous $NaHCO_3$ (100 mL) over 5 min. The aqueous layer was extracted with EtOAc (3 × 80 mL), and the combined organic extracts were dried ($MgSO_4$) and

concentrated. Purification by flash chromatography (15% EtOAc–hexane to 80% EtOAc–hexane, linear gradient) afforded the title compound (0.189 g, 69%) as a pale yellow oil: R_f = 0.55 (EtOAc); ^{1}H NMR ($CDCl_3$, 500 MHz, 1:1 mixture of rotamers) δ 5.40 (s, 0.5 H), 5.37 (s, 0.5H), 4.80 (dd, J = 11.2, 5.9 Hz, 1H), 4.53–4.72 (m, 2.5H), 4.44–4.50 (m, 1H), 4.24 (dd, *J* = 13.9, 6.0 Hz, 0.5H), 3.70 (br s, 2H), 3.36 (s, 1.5H), 3.32 (s, 1.5H), 2.29–2.44 (m, 2H), 1.76–1.89 (m, 2H), 1.49 (s, 4.5H), 1.44 (s, 4.5H); ^{13}C NMR (100 MHz, $CDCl_3$) δ (189.7, 189.4), (177.2, 176.9), (154.6, 154.5), (103.9, 103.5), (81.8, 81.5), (79.3, 79.1), (69.7, 69.6), 61.7, (57.9, 57.2), (55.7, 55.5), 31.0, 29.2, (28.2, 28.1); HRMS (ESI+) calcd for $C_{15}H_{25}NNaO_6$ $[M + Na]^+$ 338.1574, found 338.1579 (error 1.5 ppm).

Section 2.8. Spectra of Synthesized Compounds

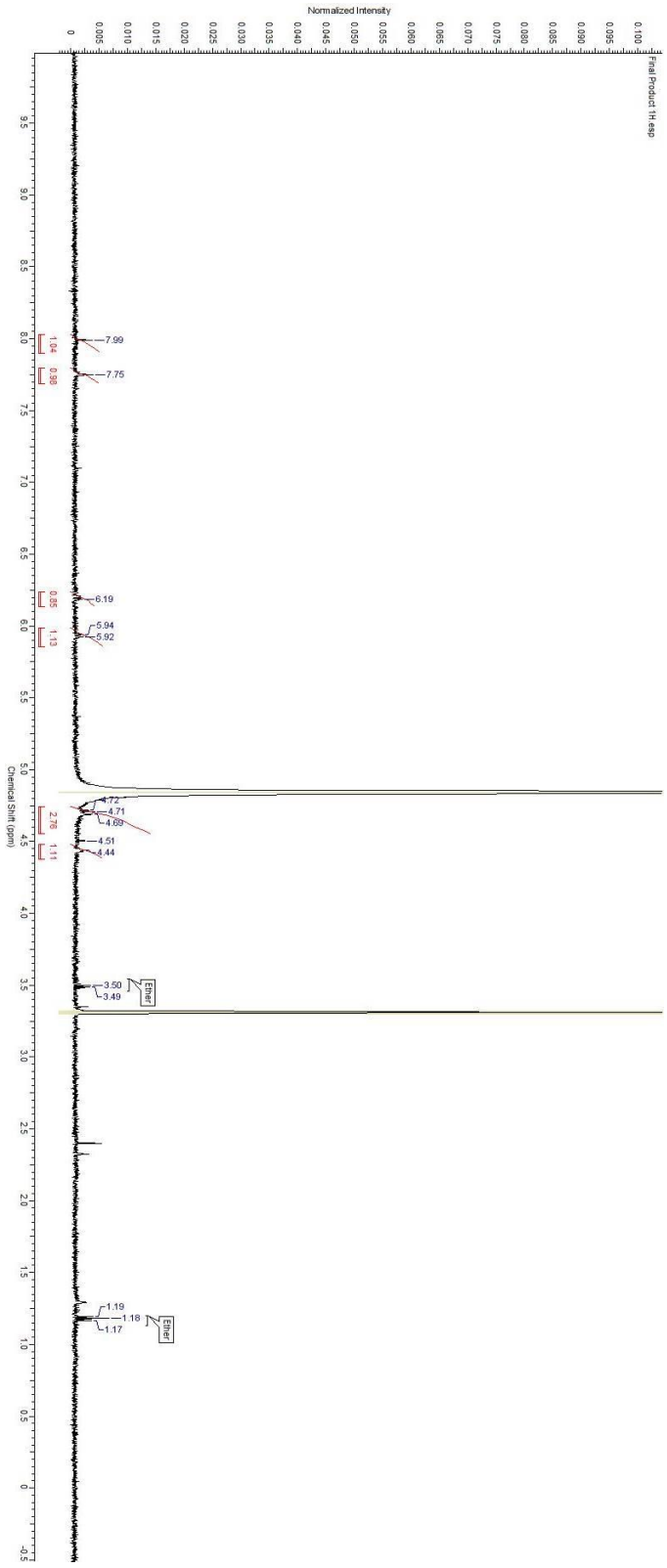

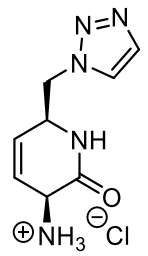

4

600 MHz, CD_3OD

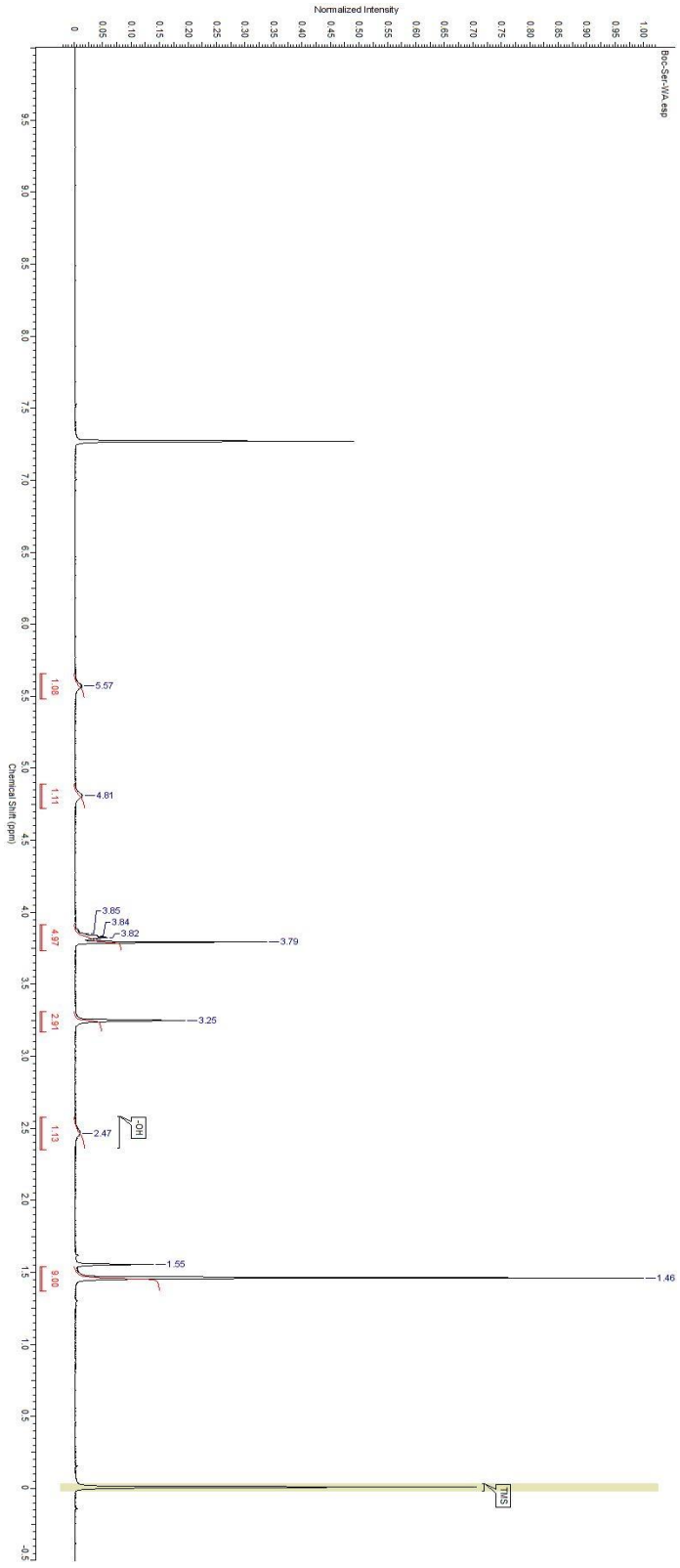

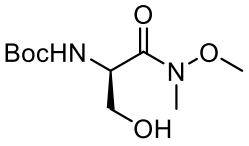

7

400 MHz, $CDCl_3$

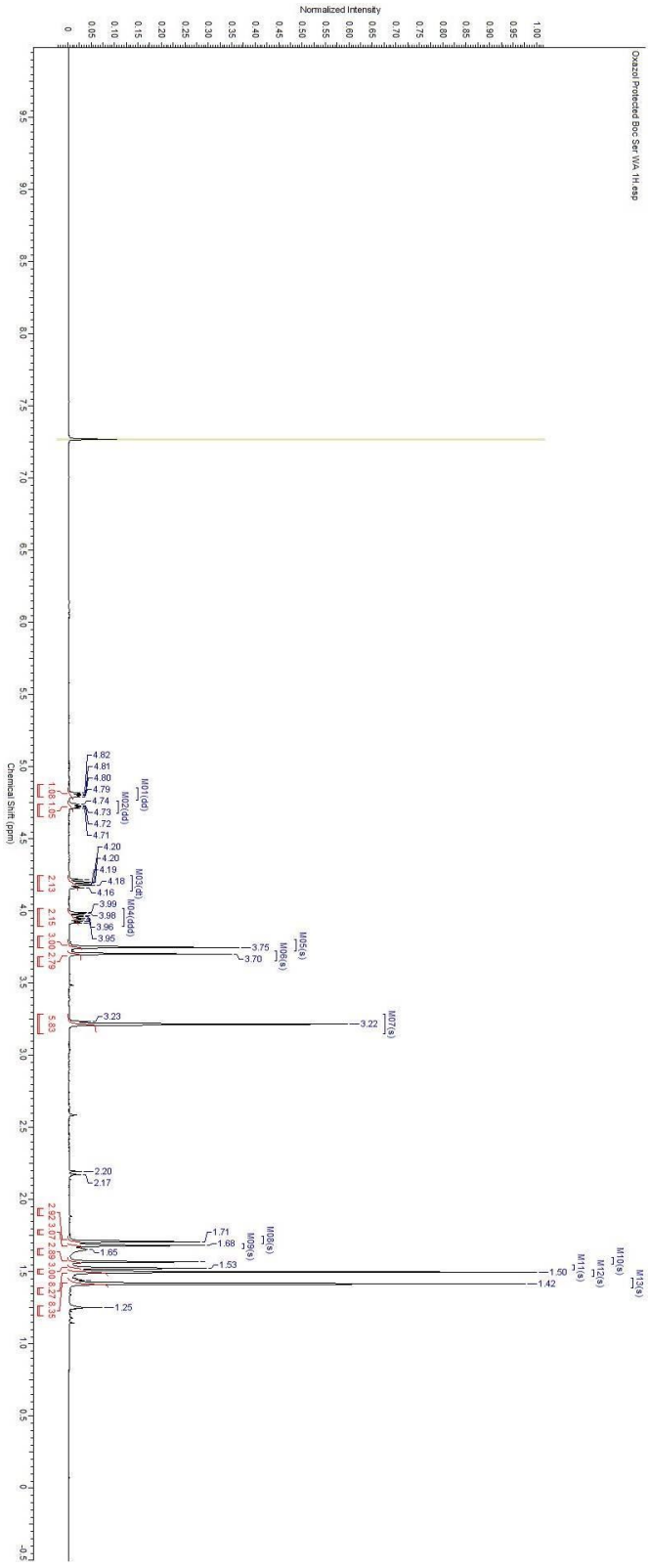

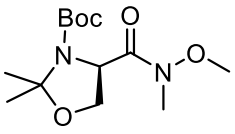

8

400 MHz, $CDCl_3$

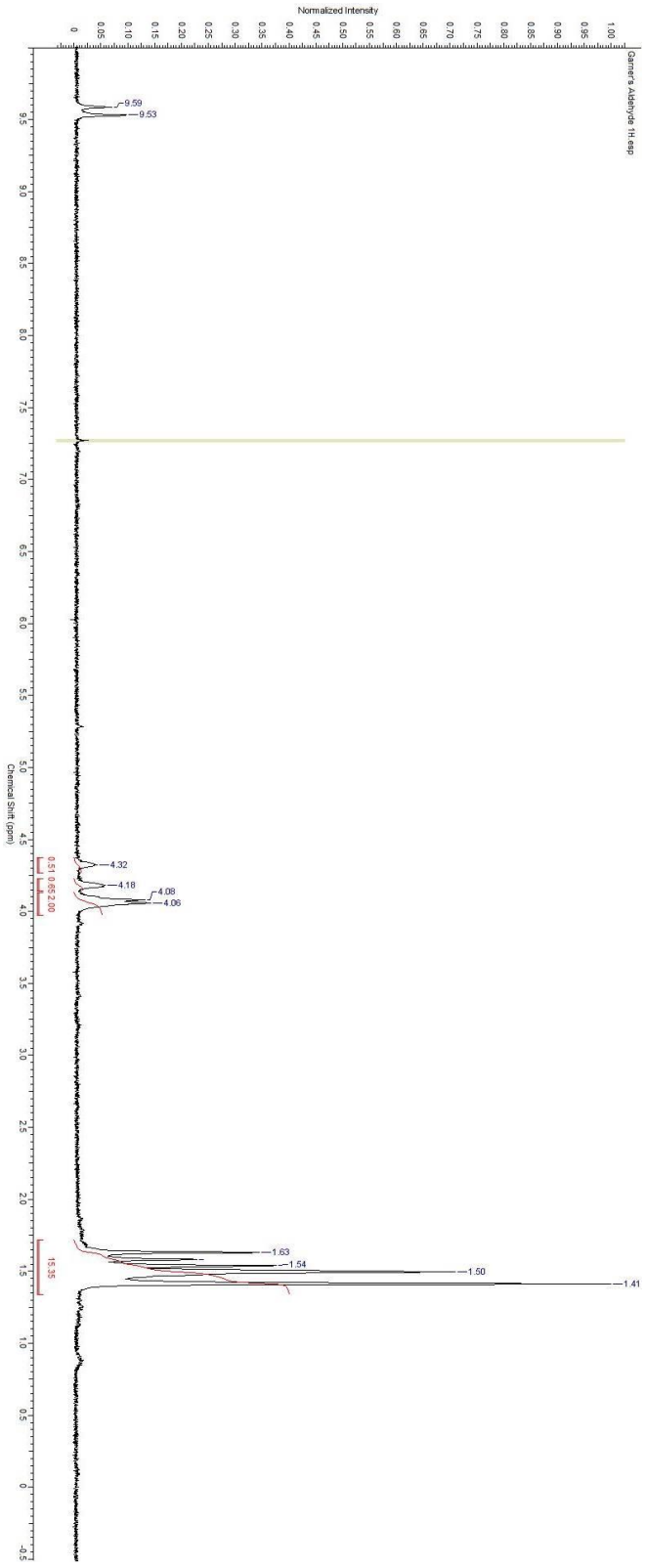

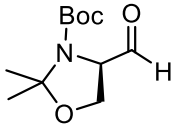

9

600 MHz, $CDCl_3$

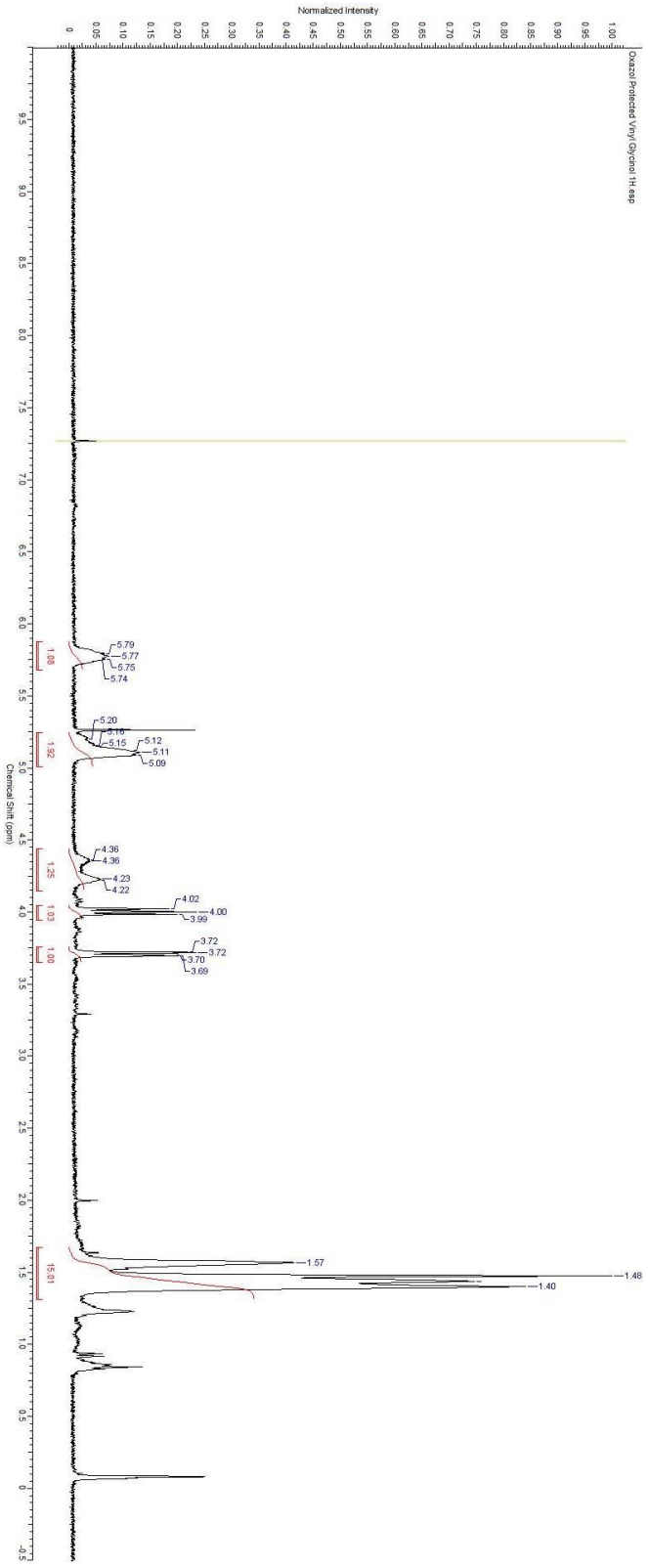

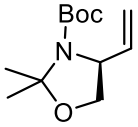

10

600 MHz, $CDCl_3$

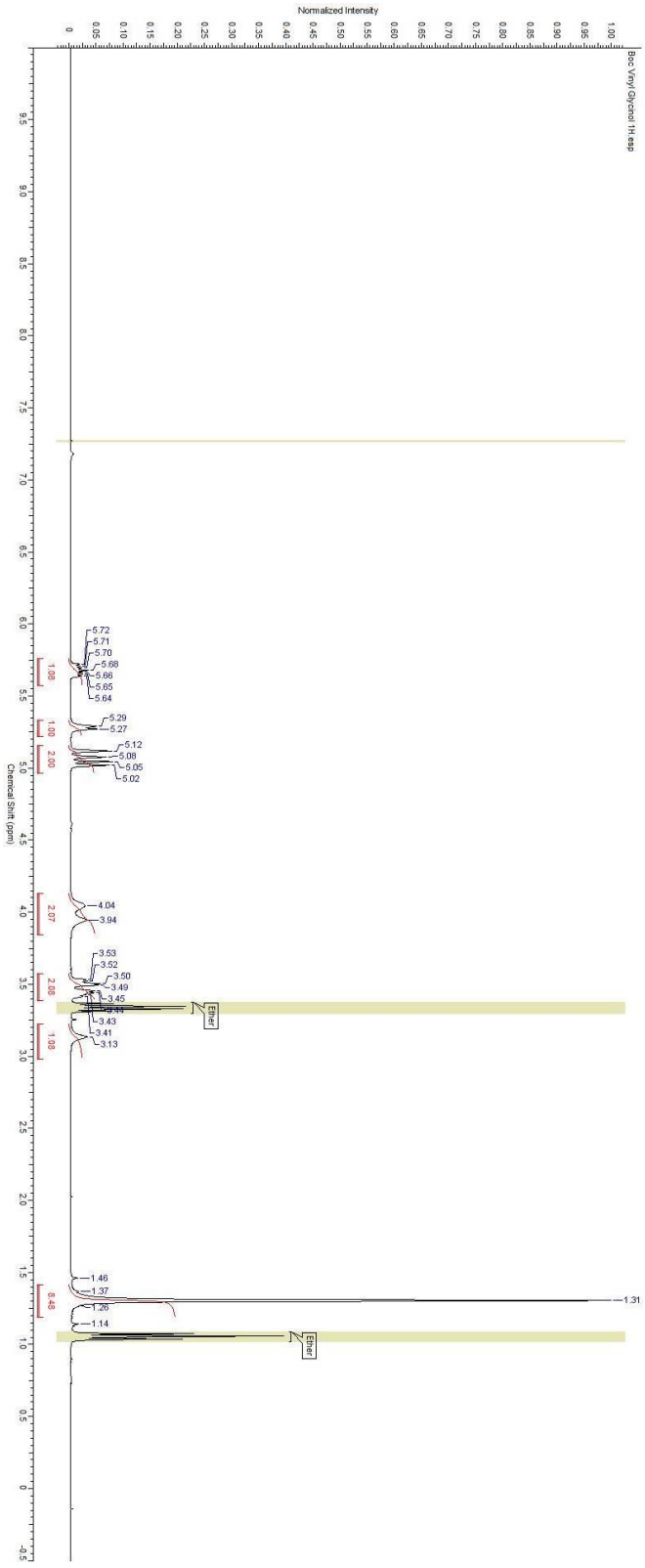

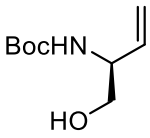

11

600 MHz, $CDCl_3$

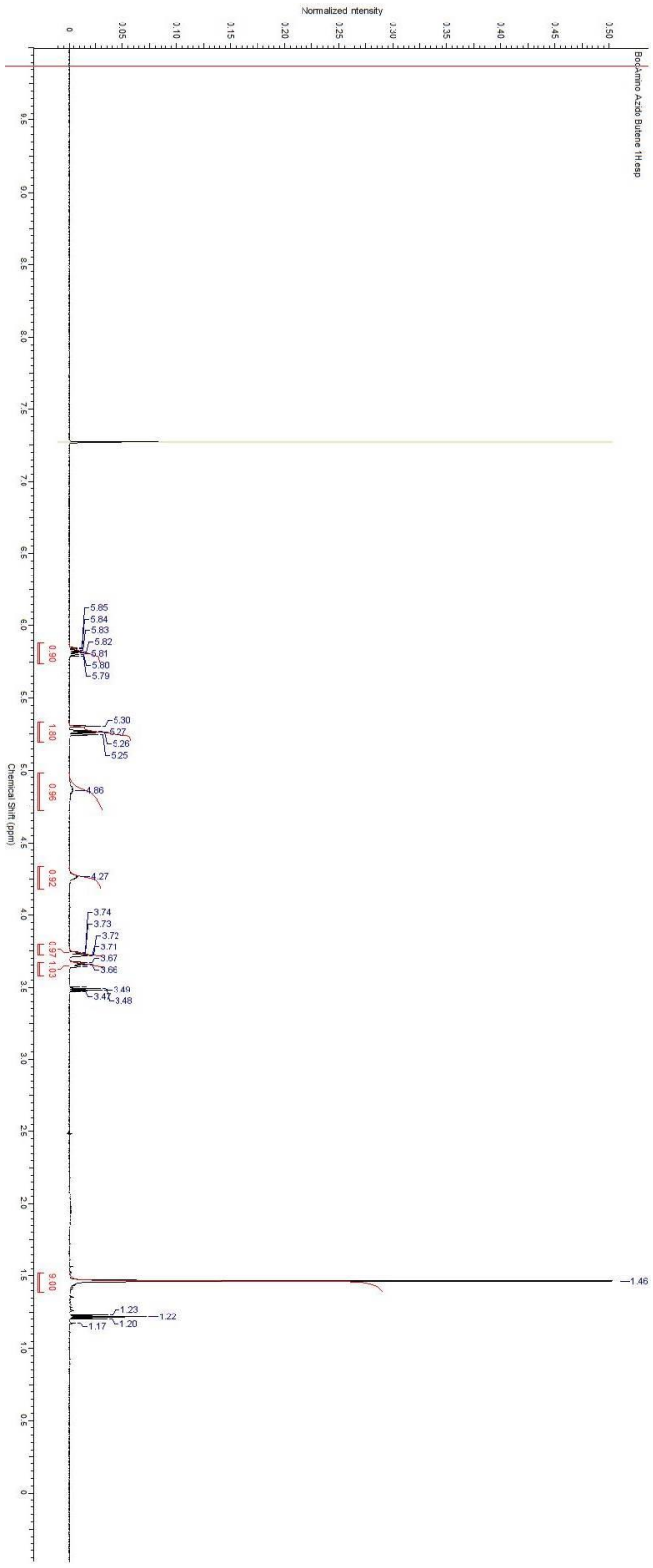

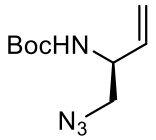

12

600 MHz, $CDCl_3$

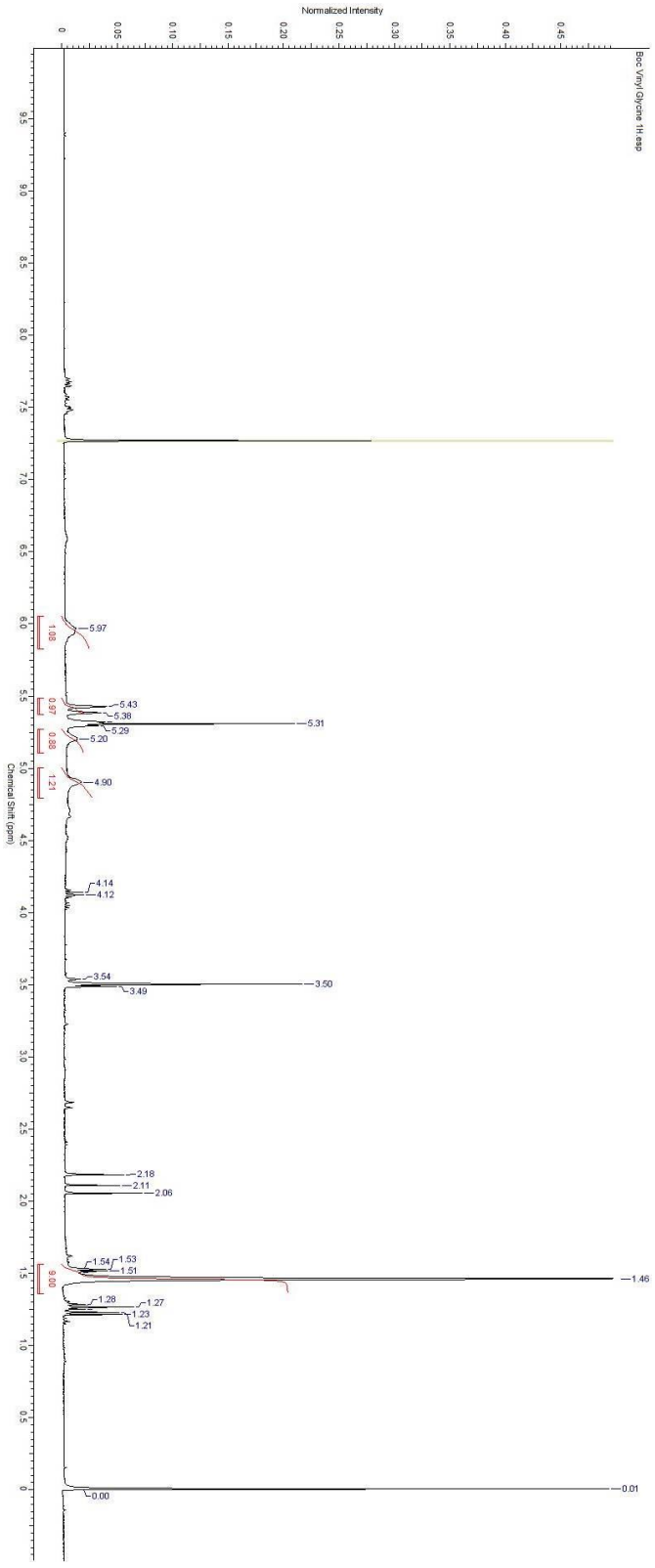

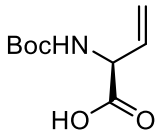

14

600 MHz, $CDCl_3$

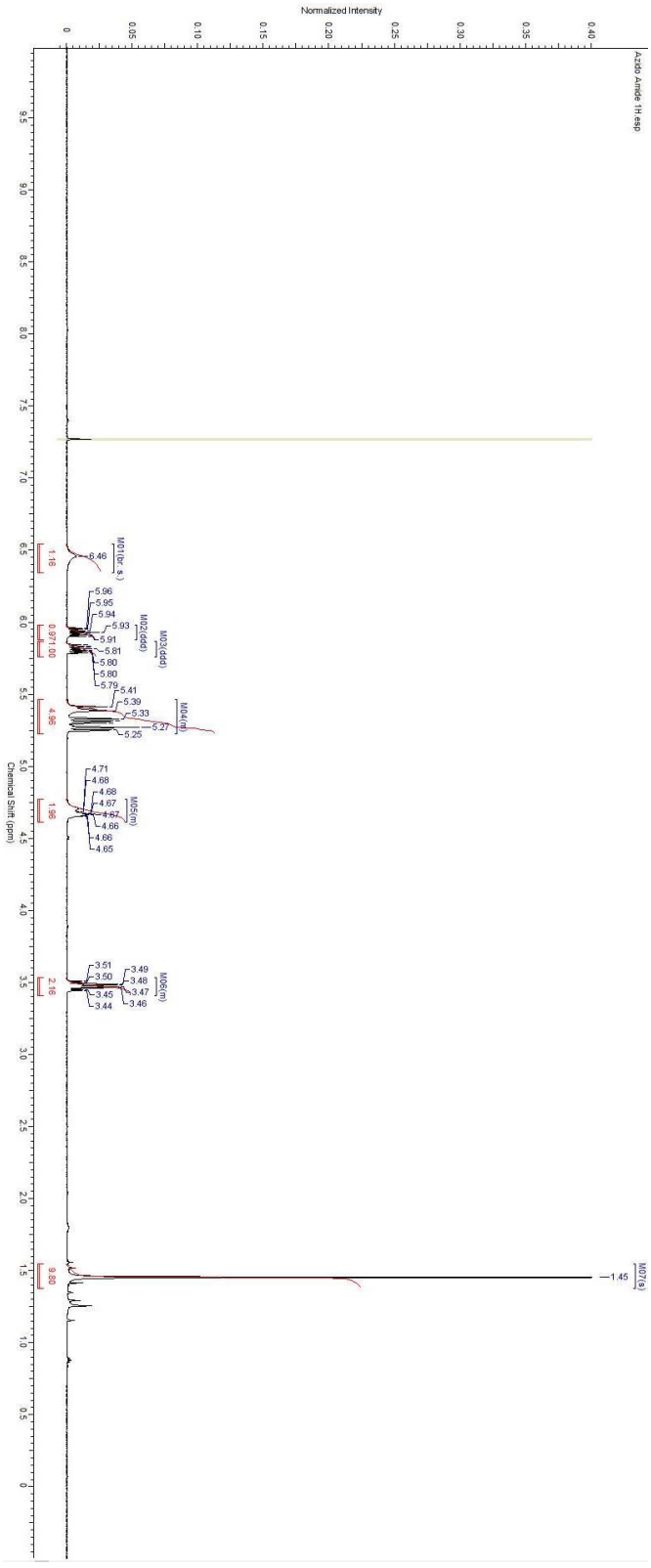

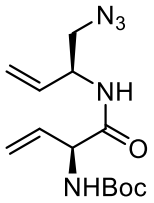

15

600 MHz, $CDCl_3$

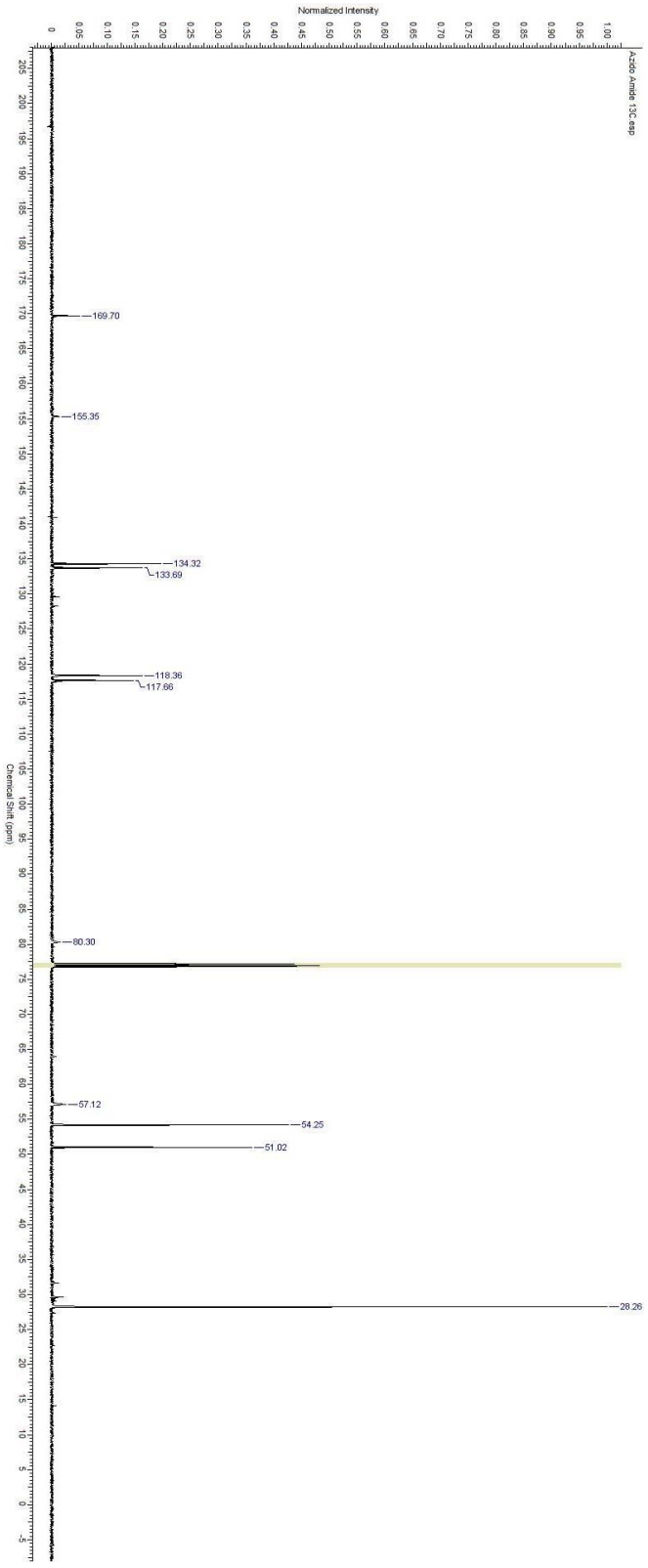

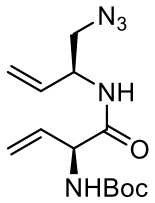

15

150 MHz, $CDCl_3$

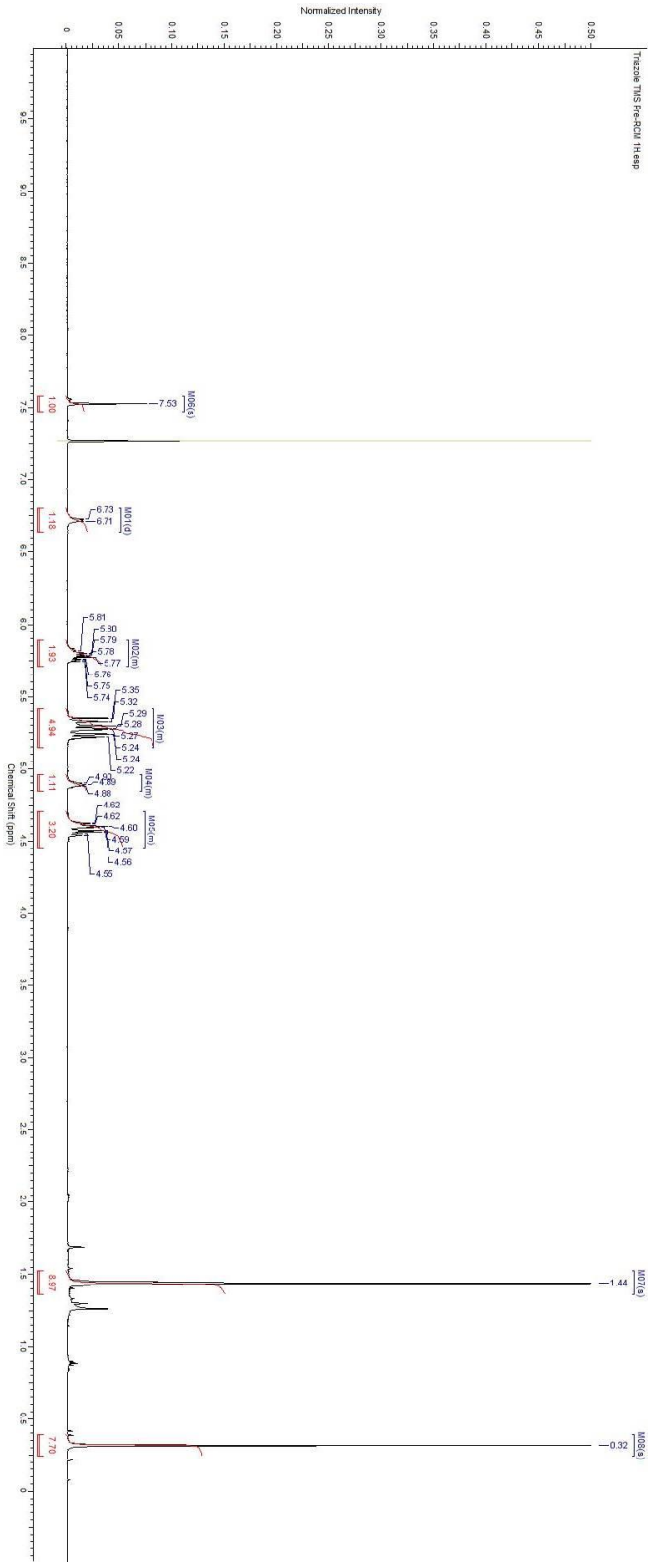

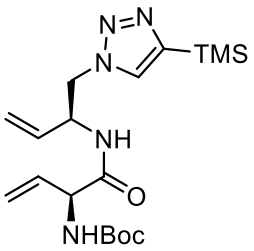

17

600 MHz, $CDCl_3$

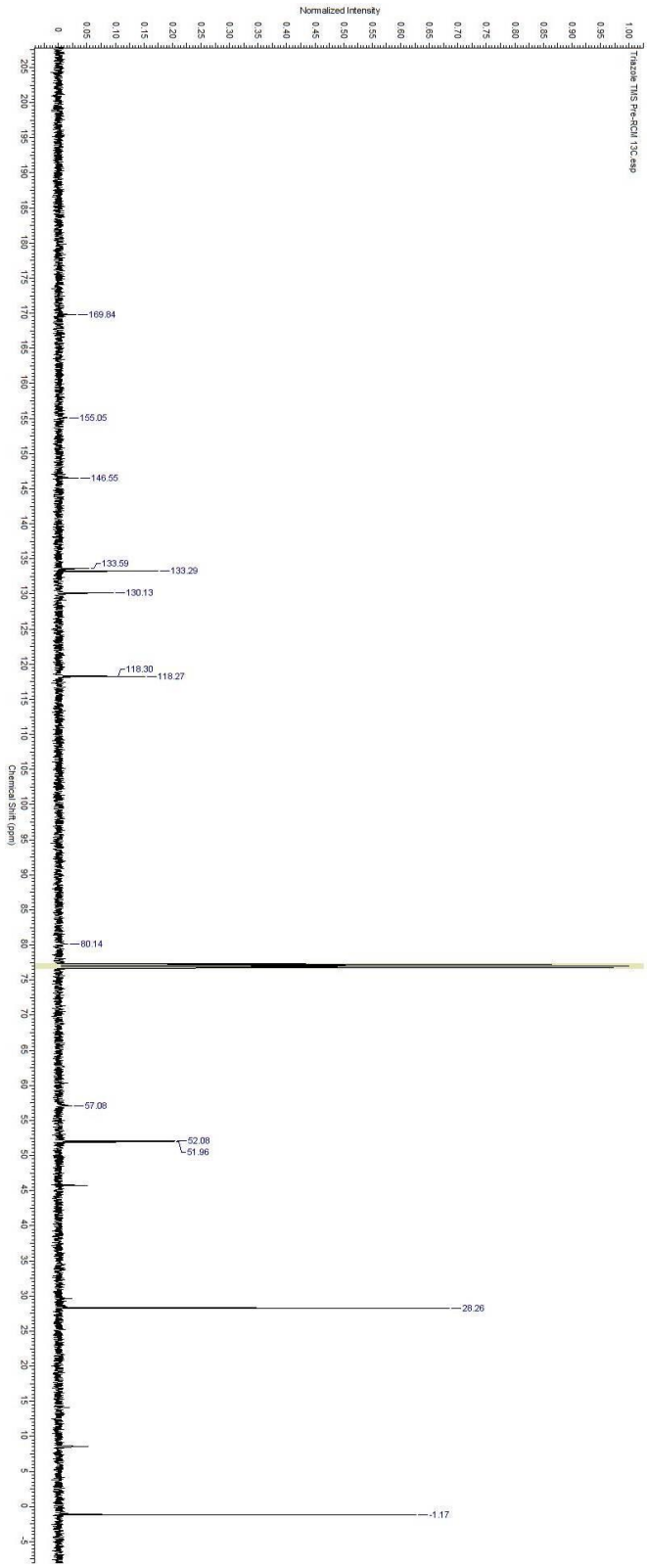

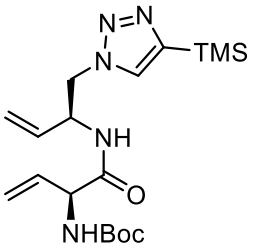

17

150 MHz, $CDCl_3$

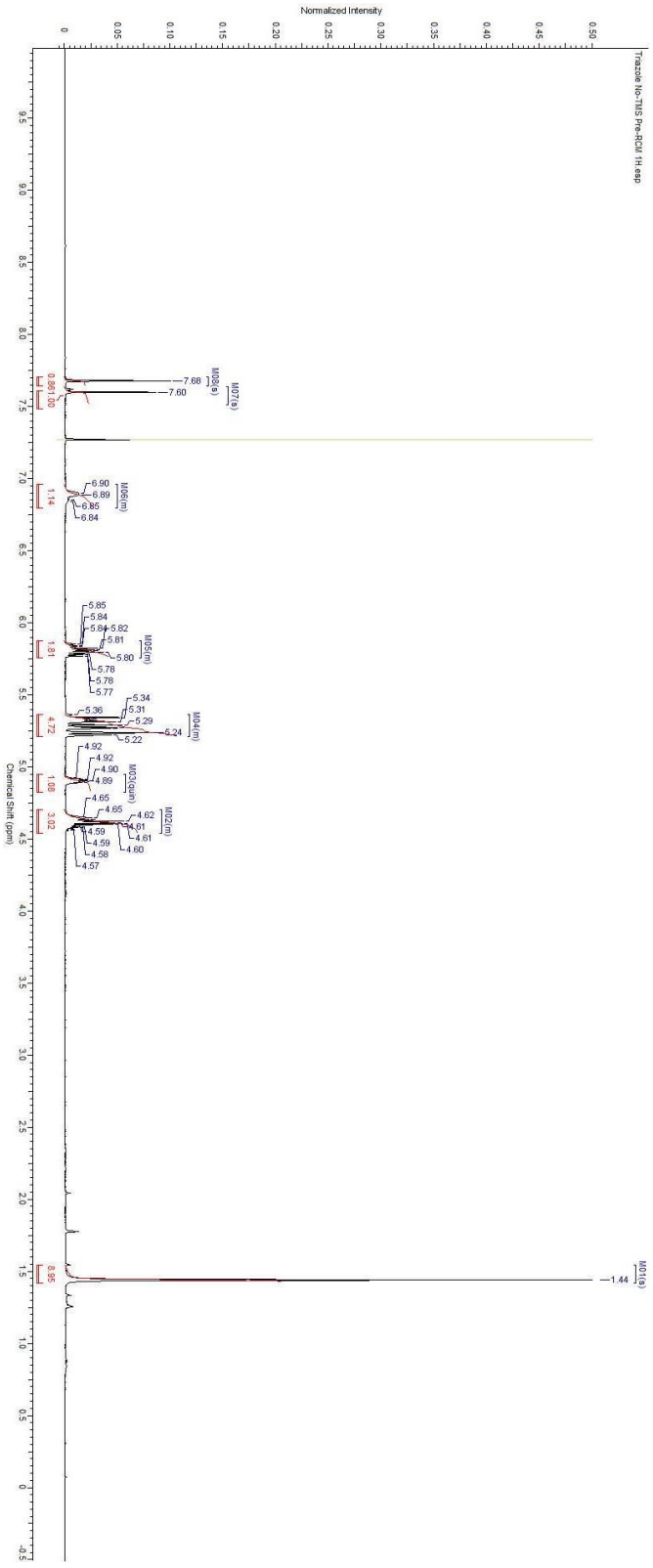

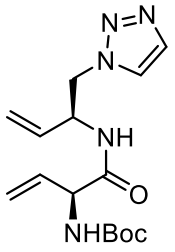

19

600 MHz, $CDCl_3$

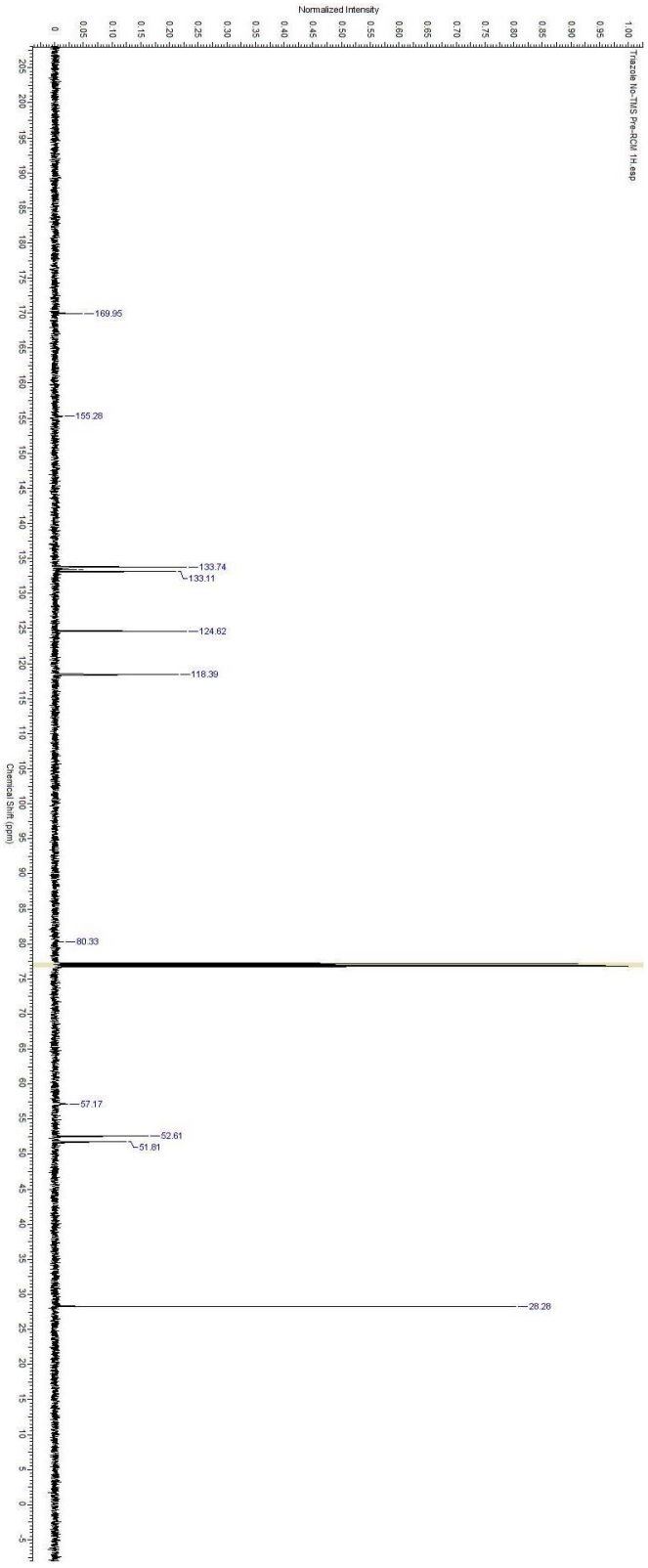

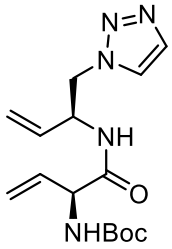

19

600 MHz, $CDCl_3$

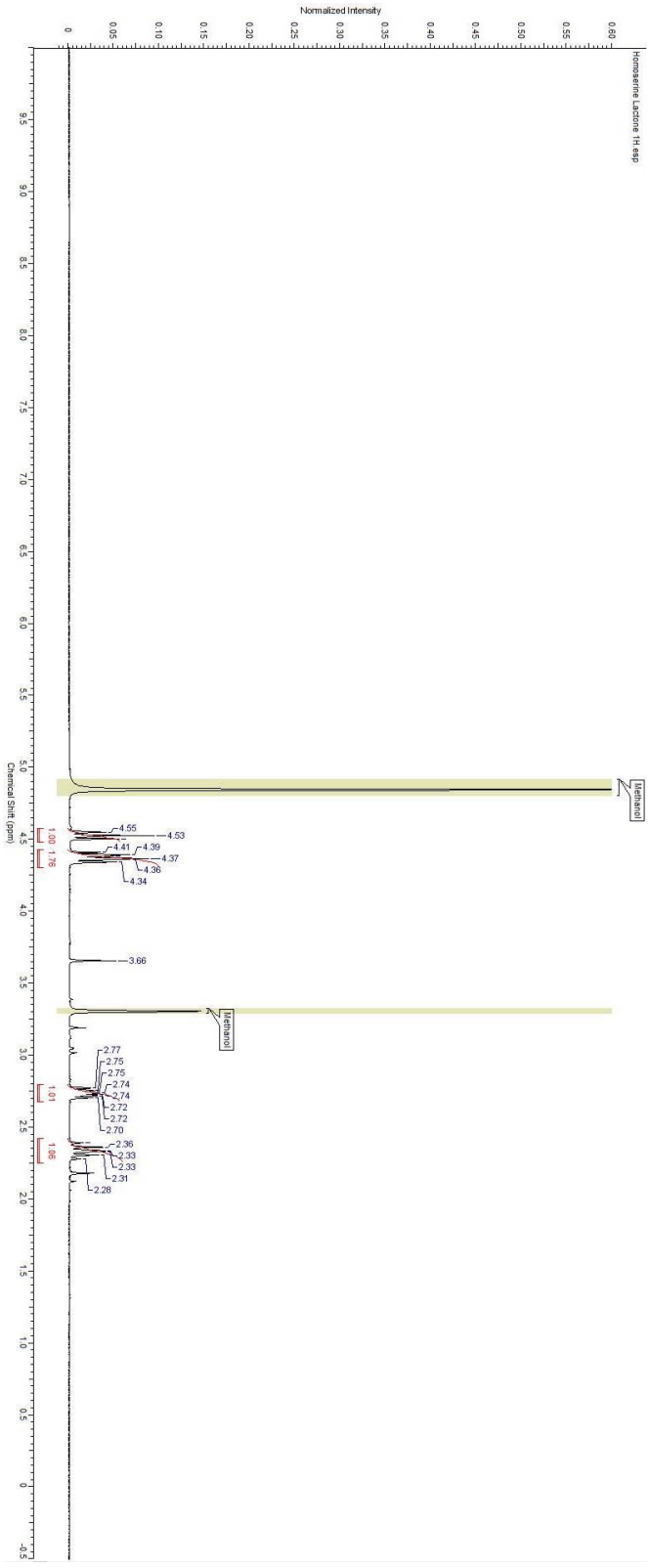

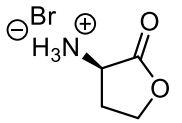

23

400 MHz, CD_3OD

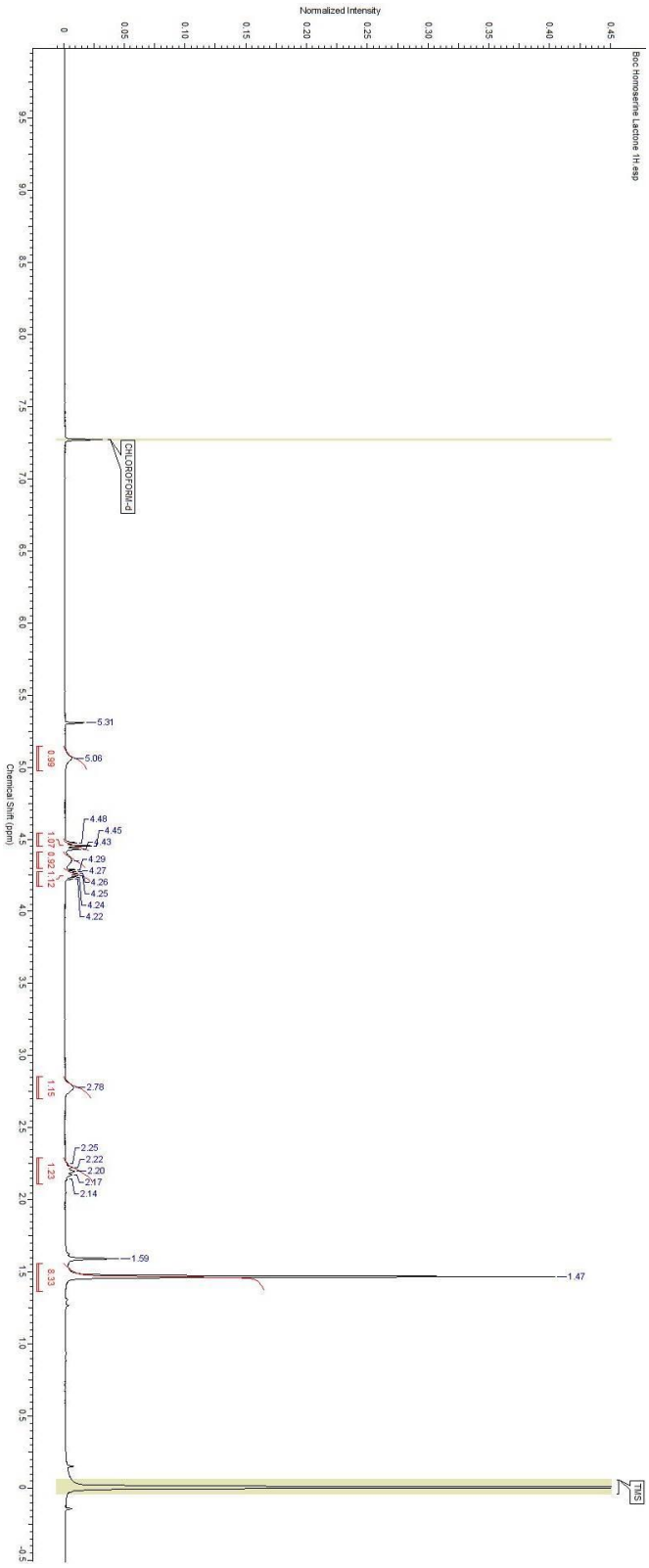

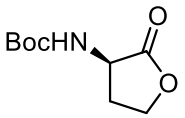

24

400 MHz, $CDCl_3$

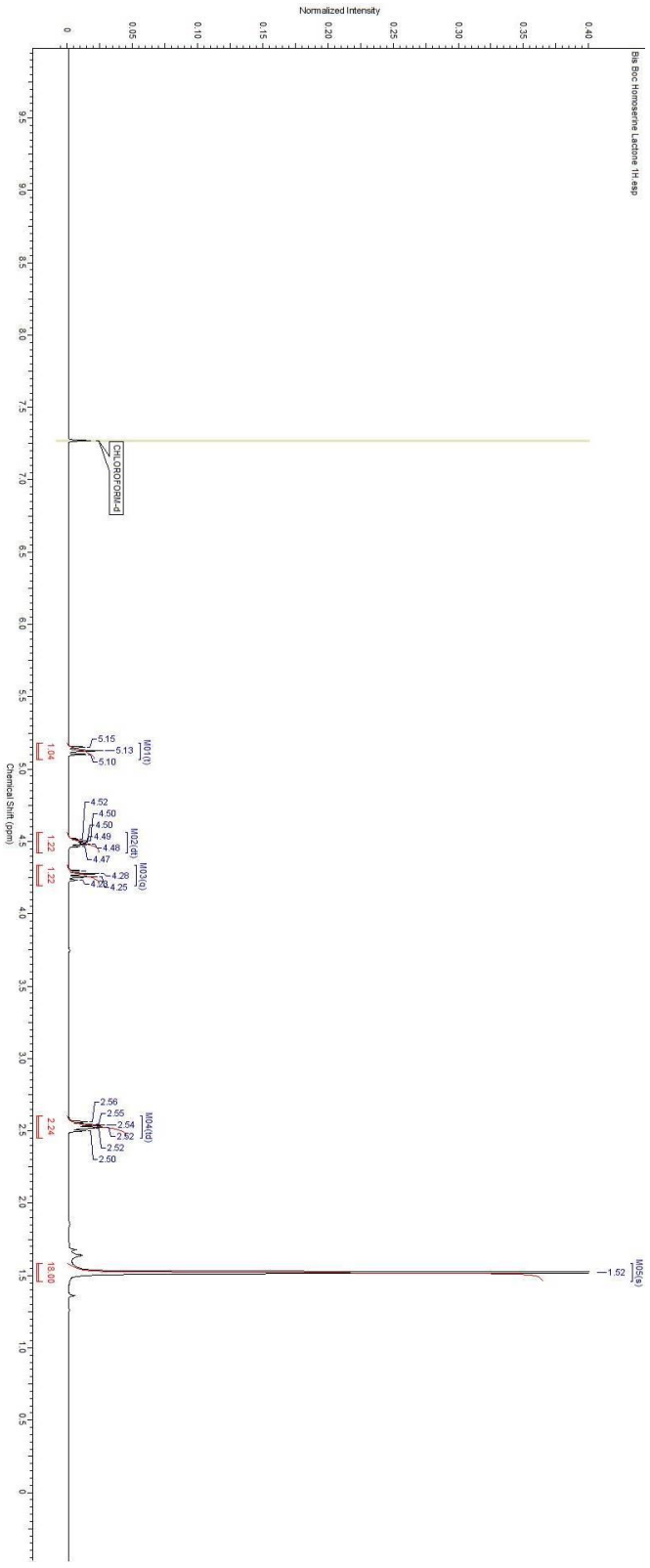

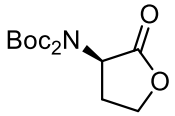

27

400 MHz, $CDCl_3$

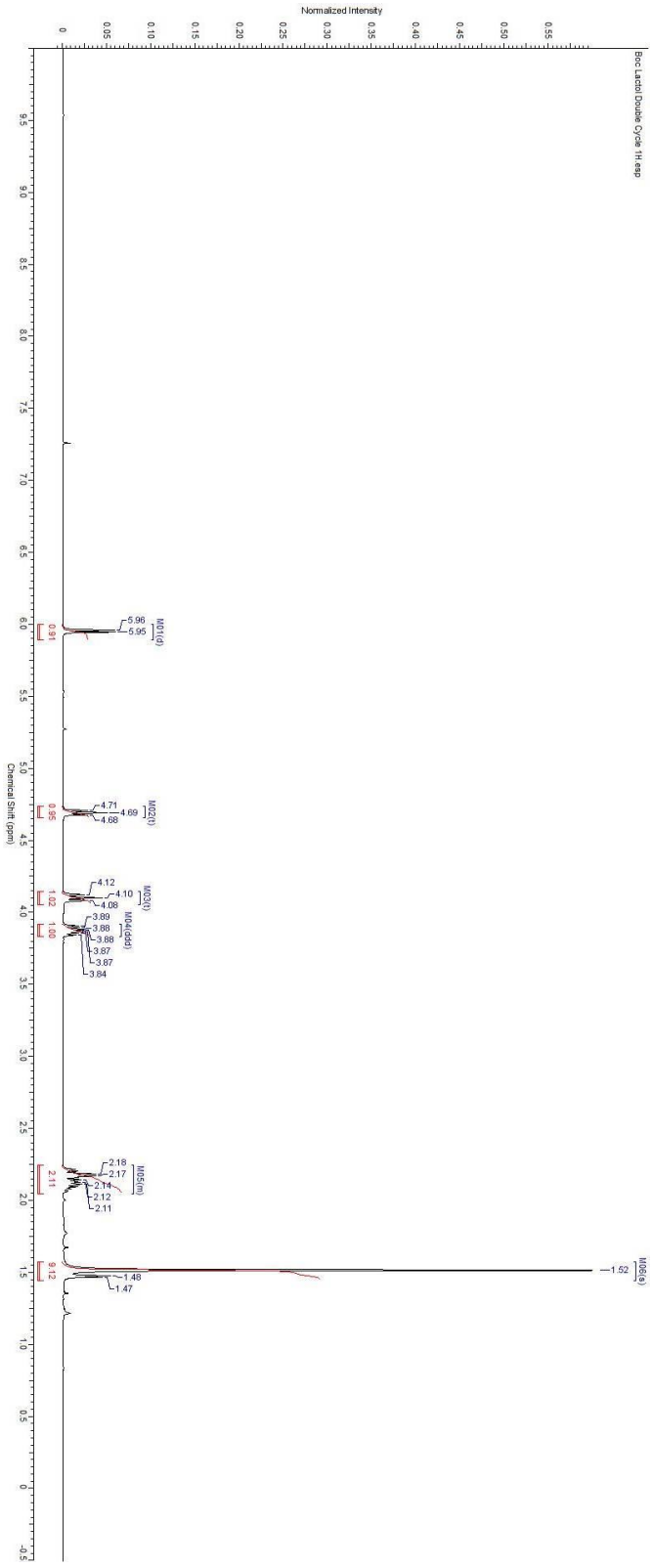

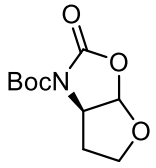

28

400 MHz, $CDCl_3$

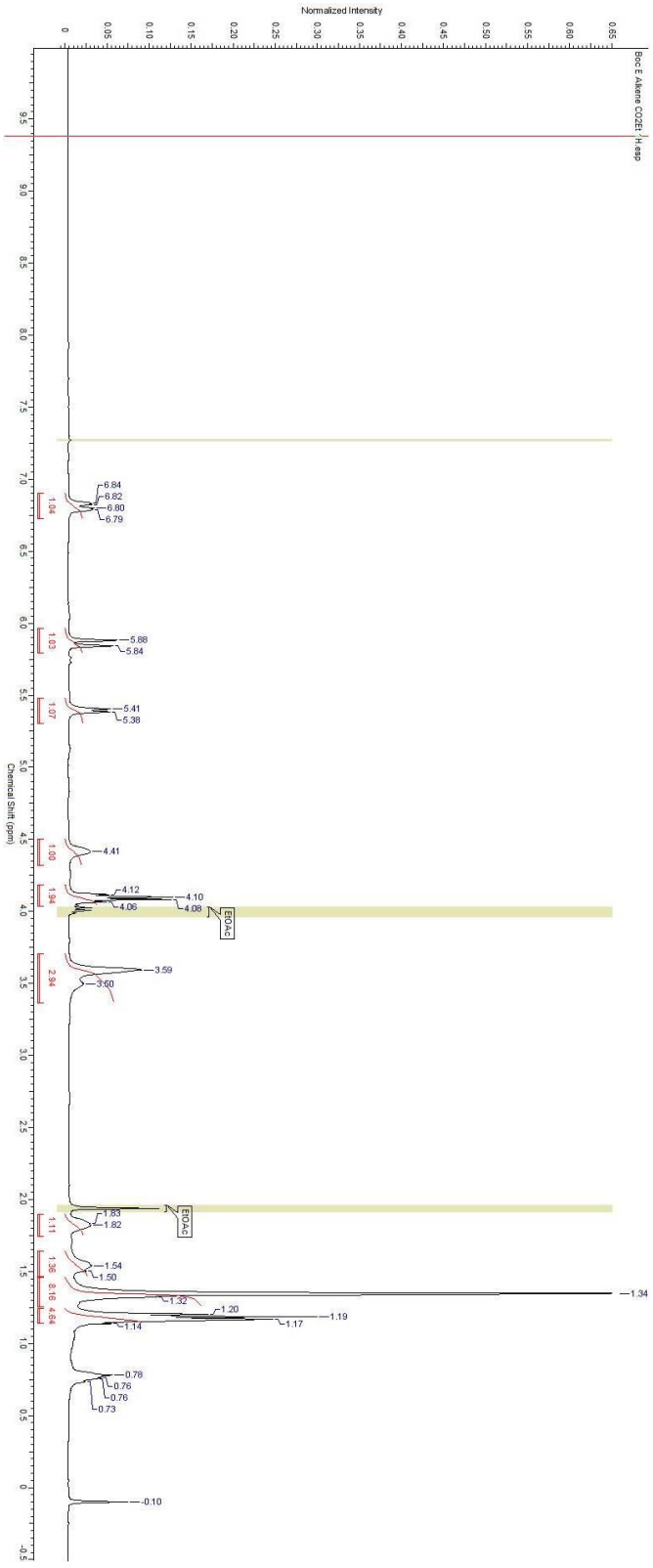

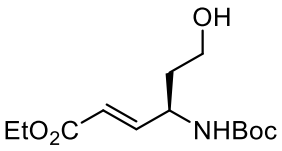

29

400 MHz, $CDCl_3$

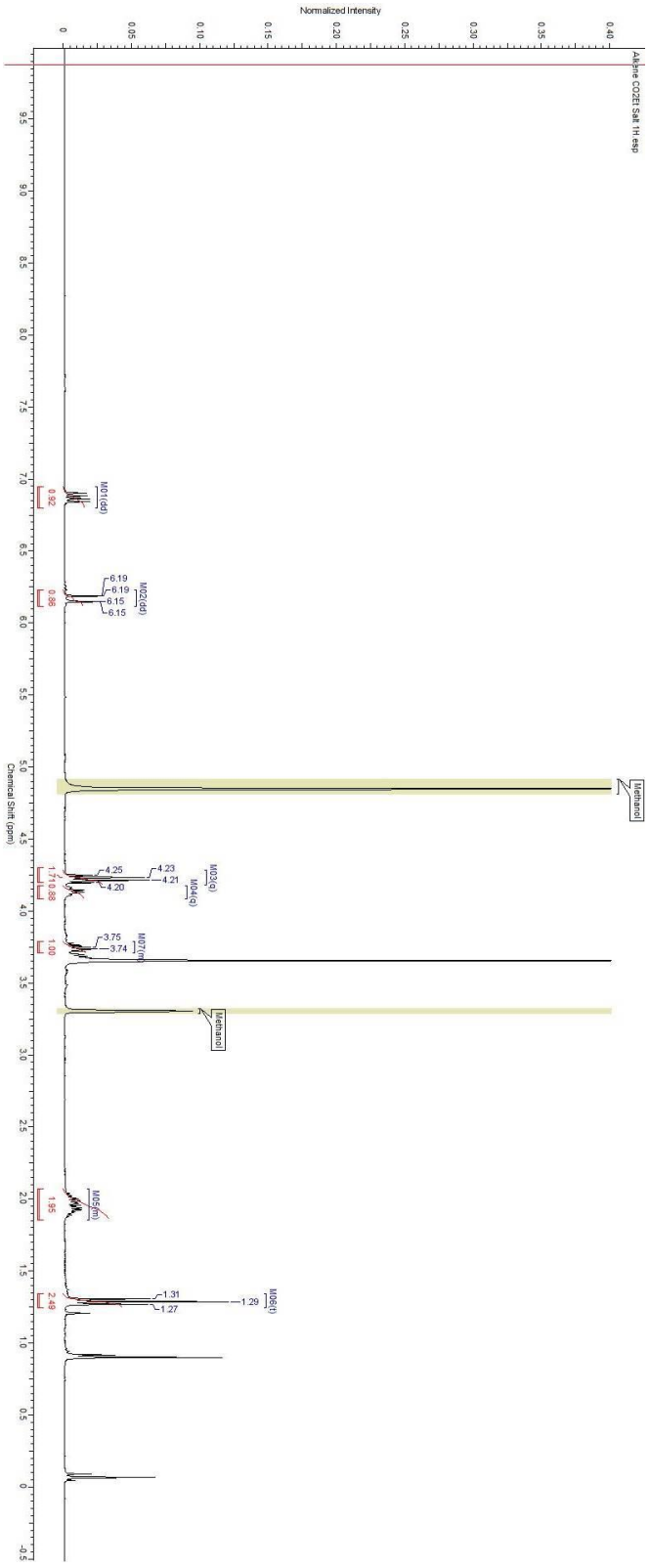

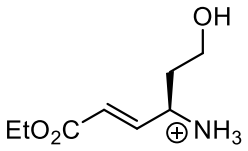

30

400 MHz, CD_3OD

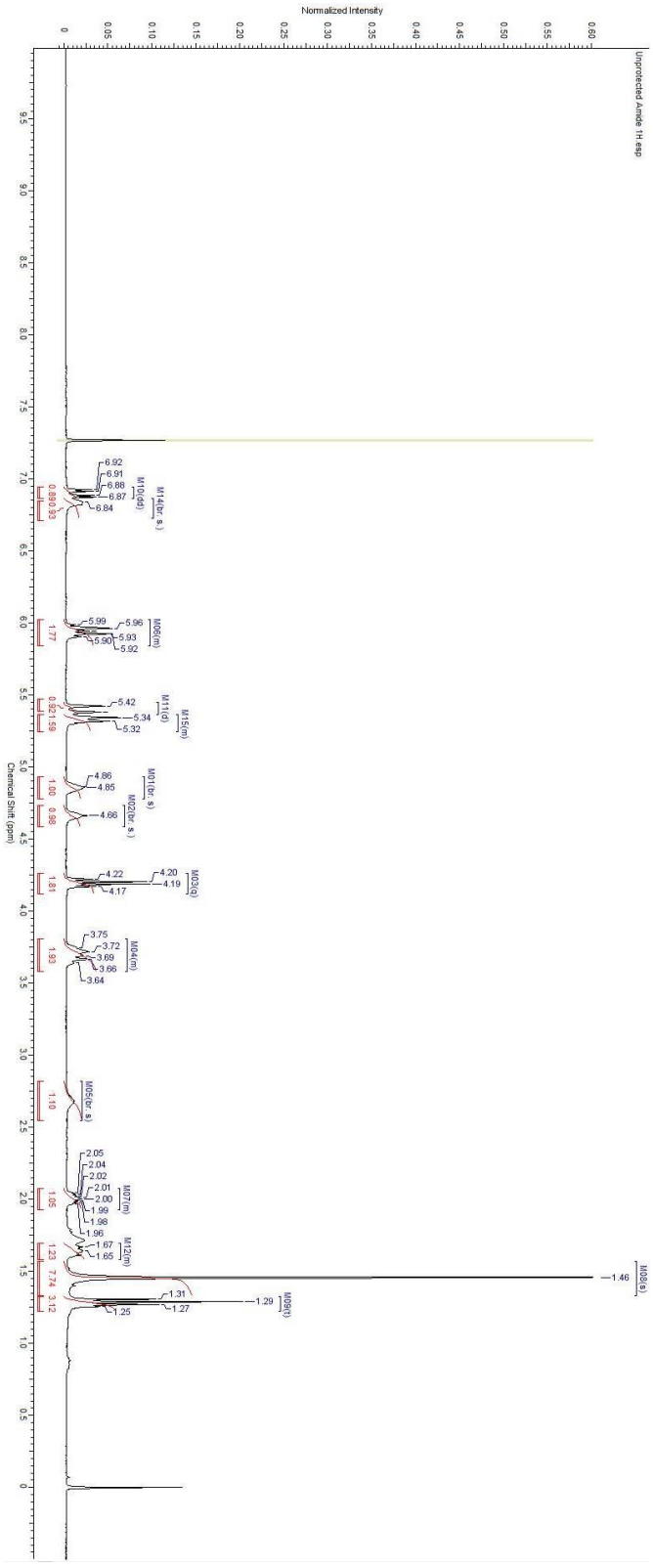

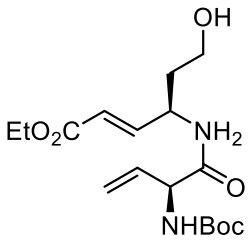

31

400 MHz, $CDCl_3$

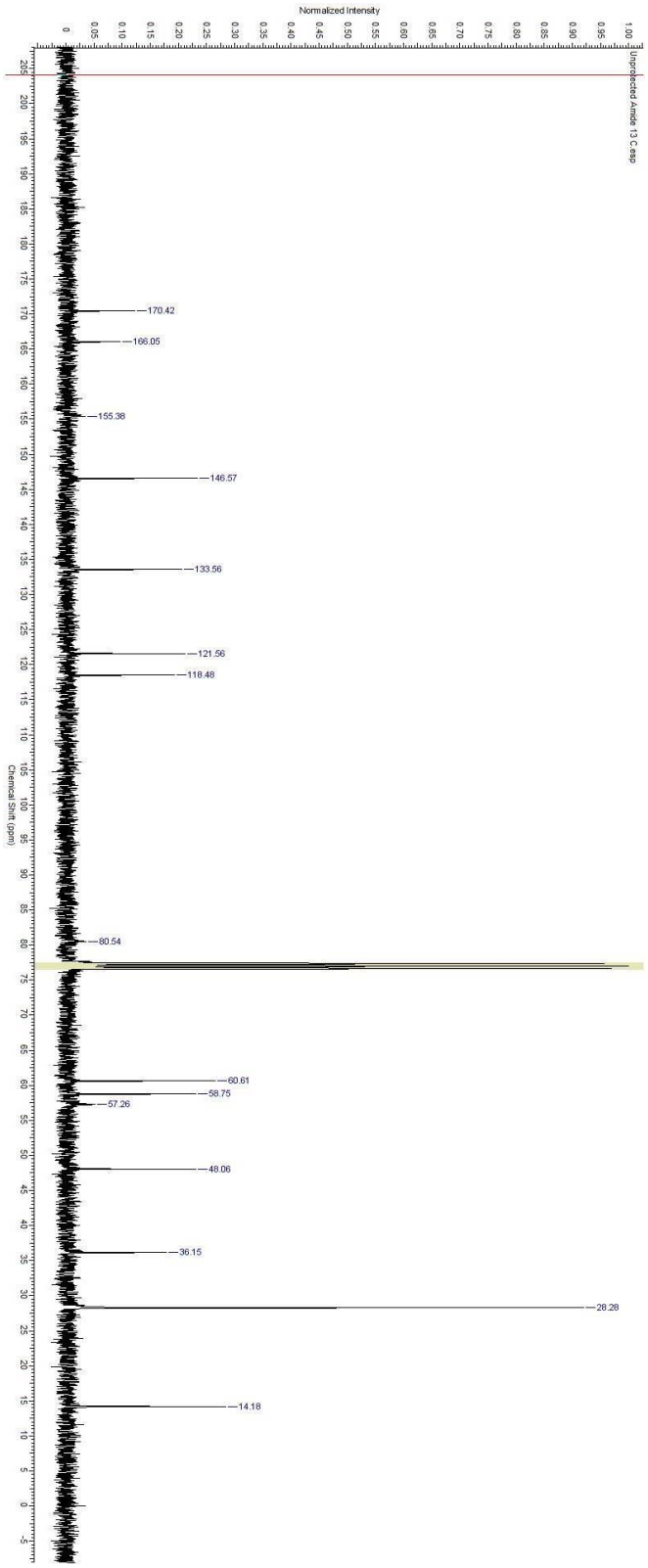

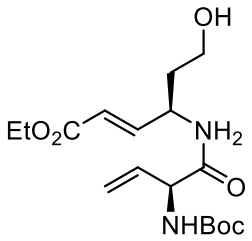

31

100 MHz, $CDCl_3$

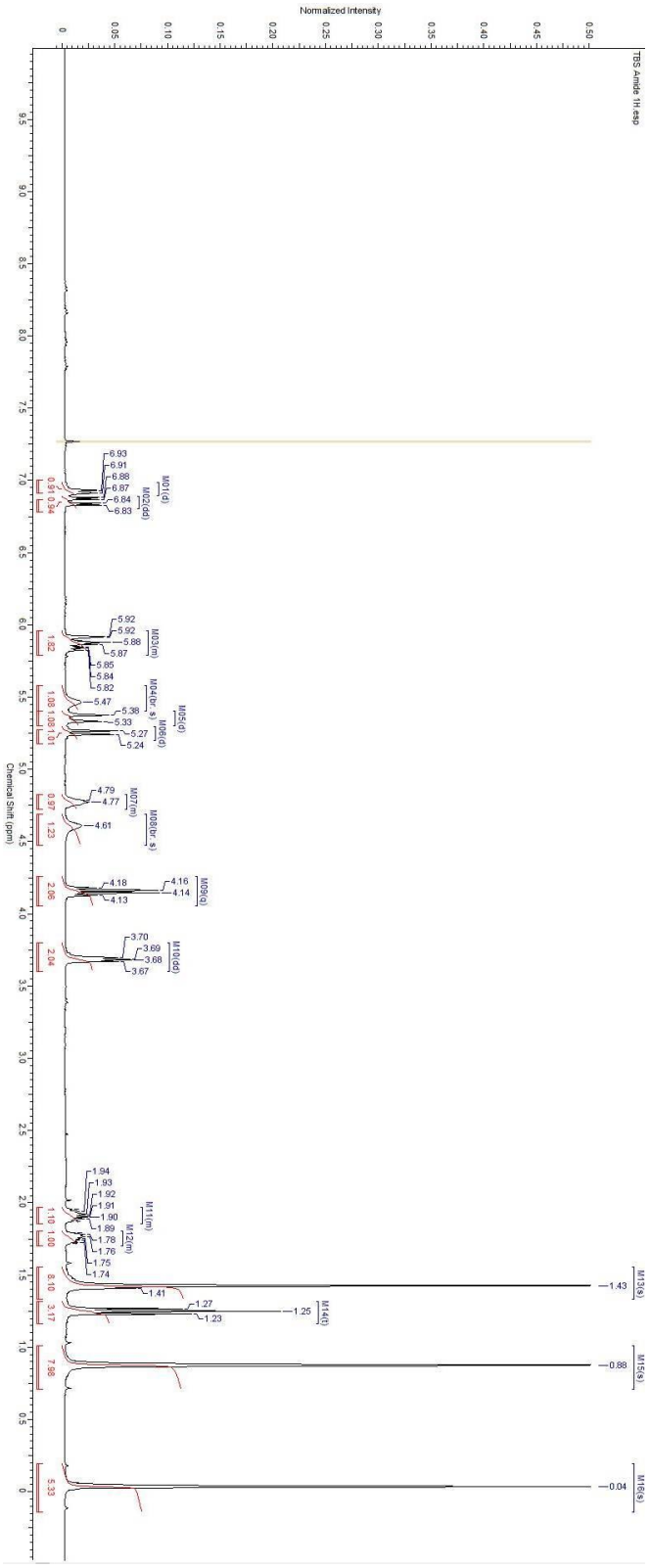

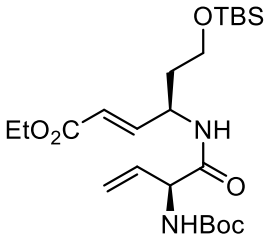

32

400 MHz, $CDCl_3$

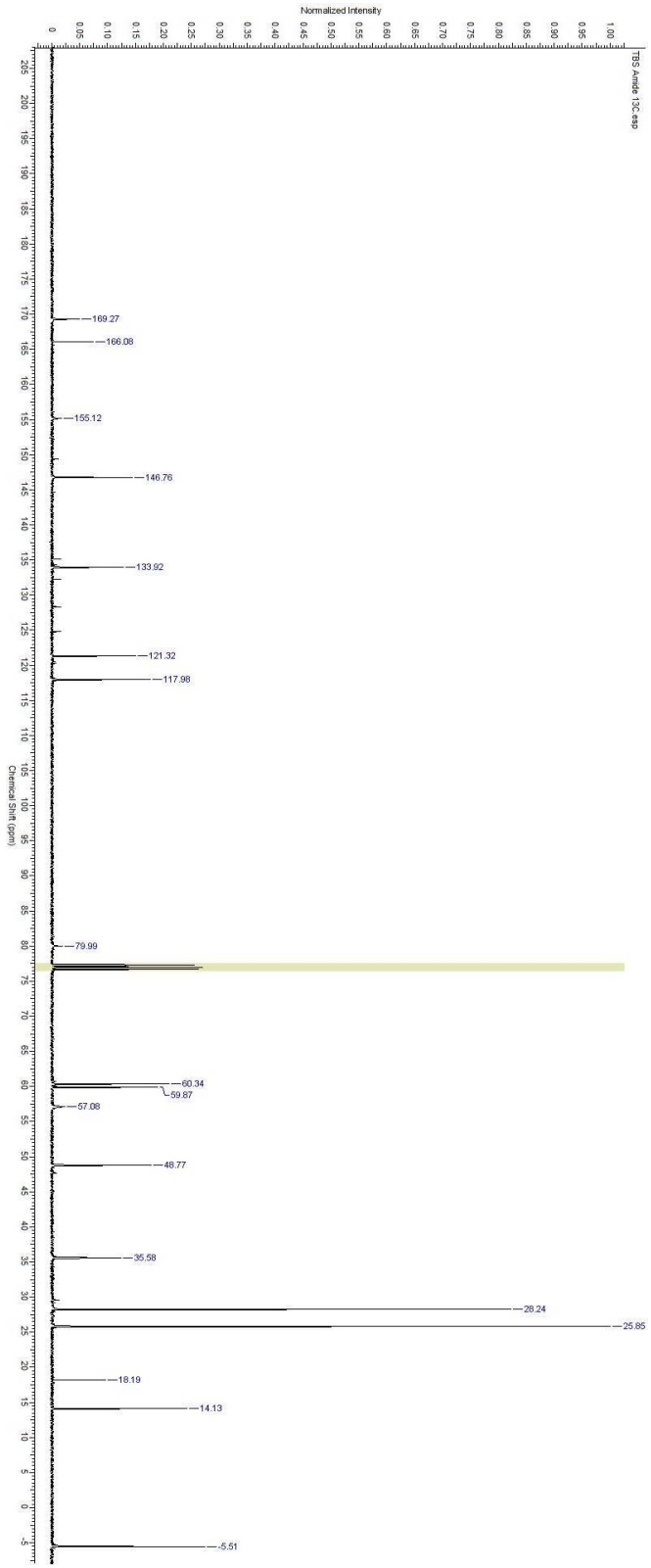

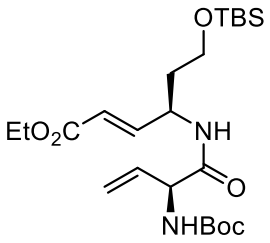

32

100 MHz, $CDCl_3$

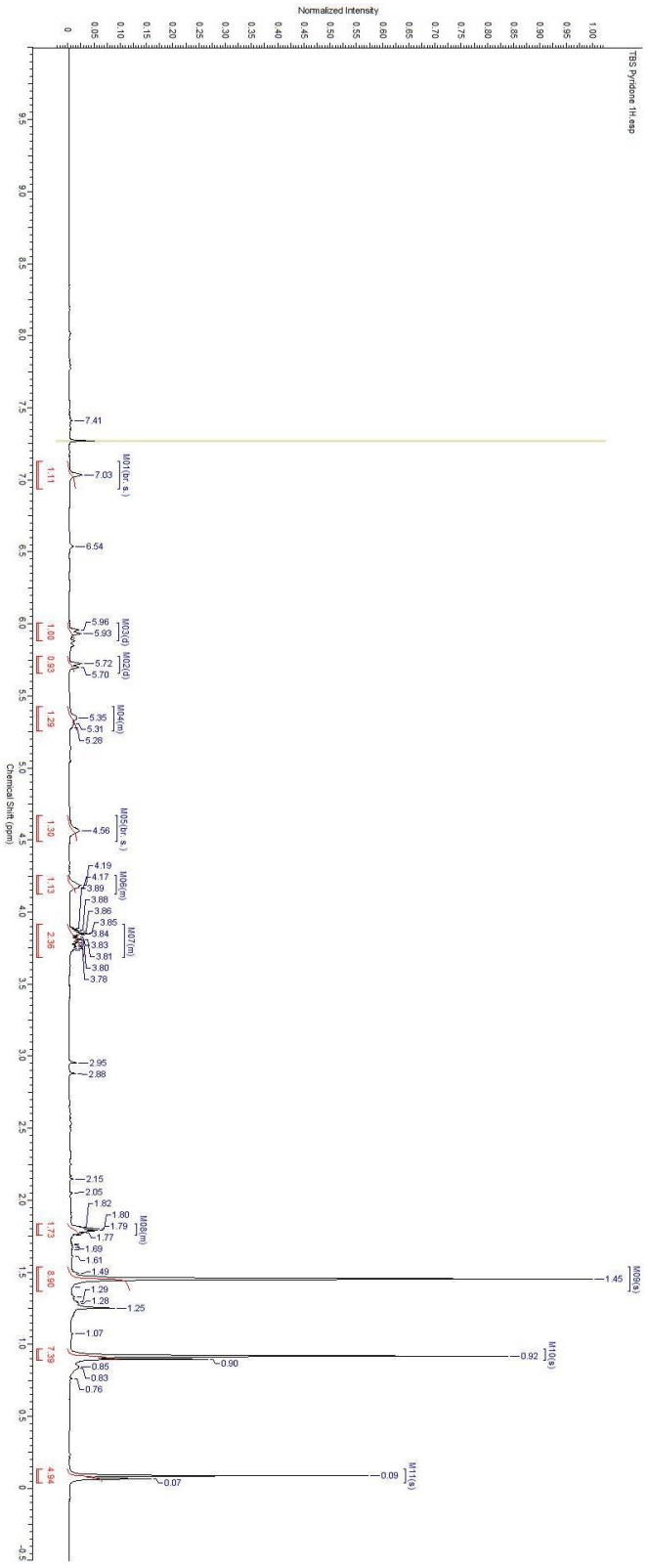

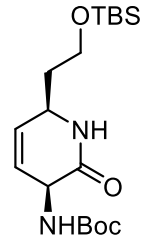

33

400 MHz, $CDCl_3$

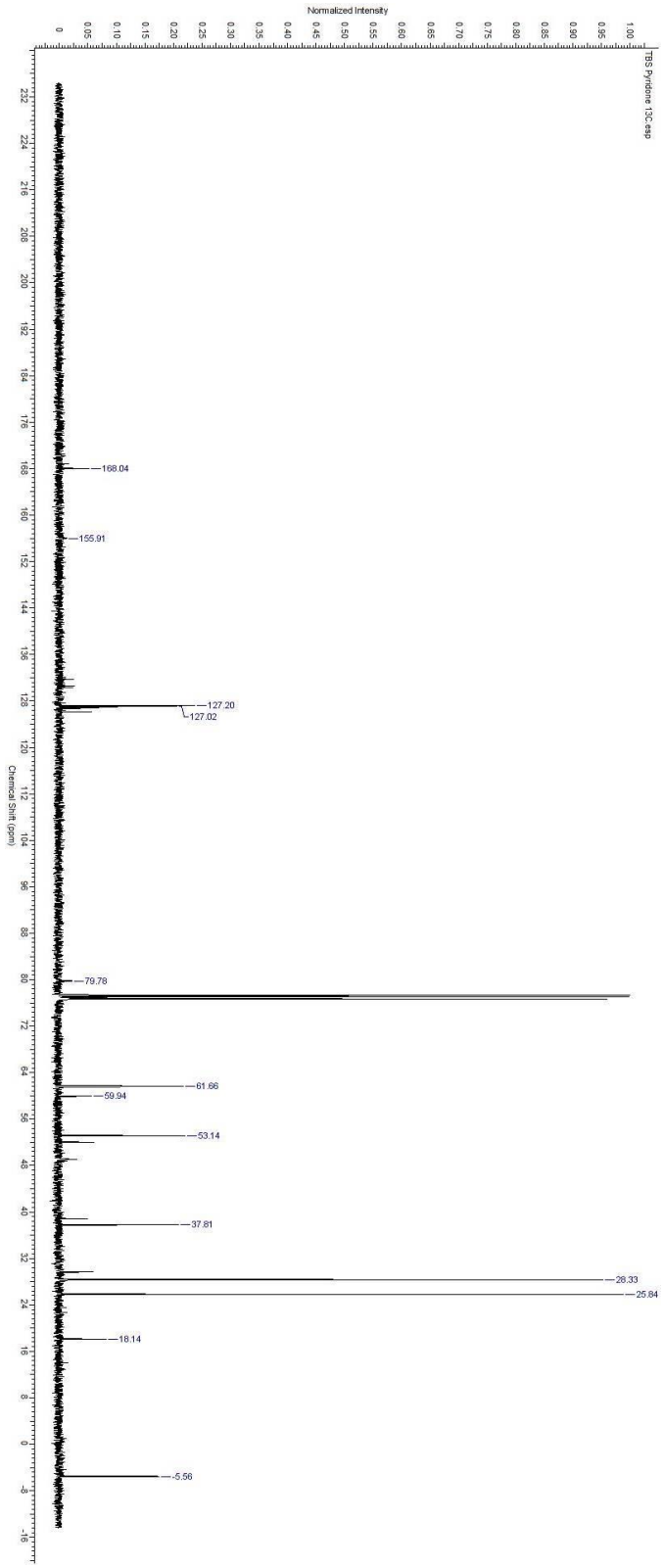

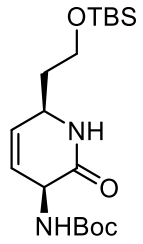

33

100 MHz, $CDCl_3$

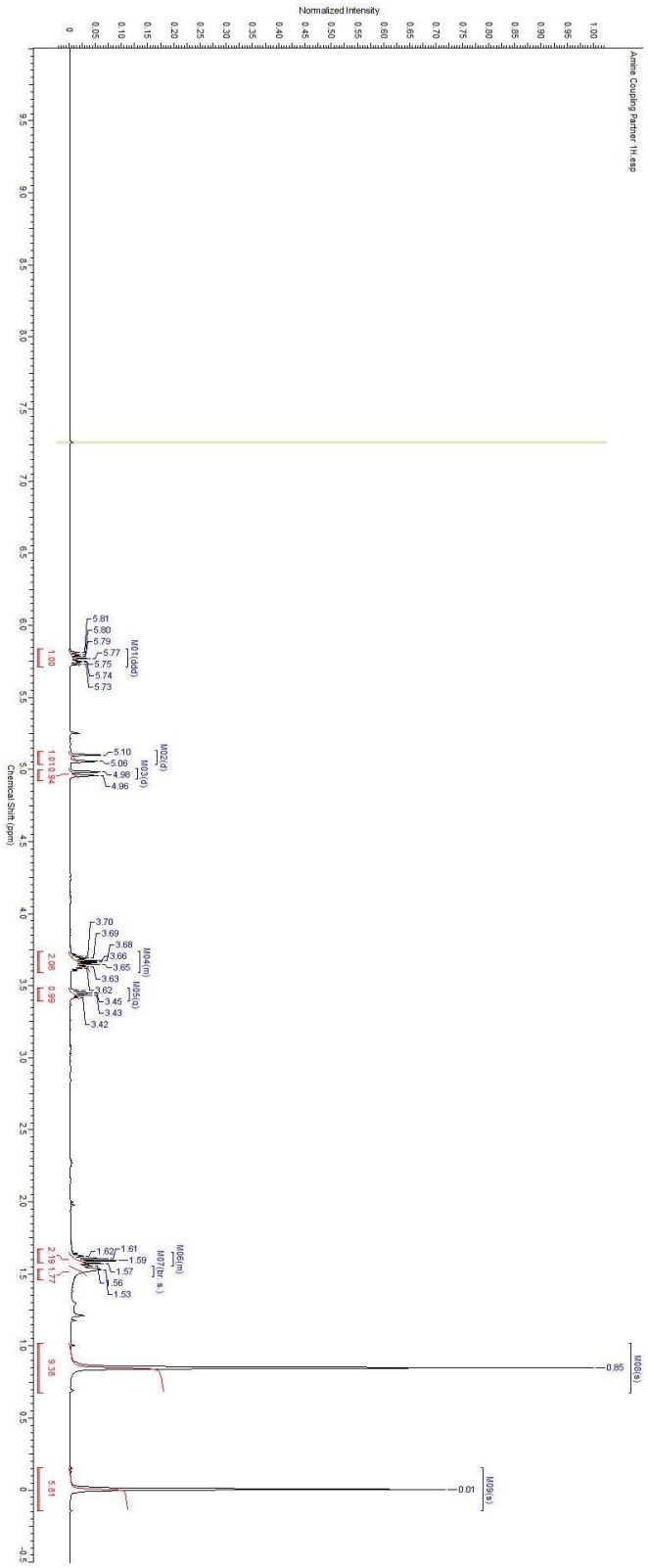

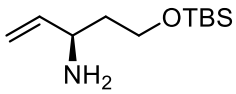

34

400 MHz, $CDCl_3$

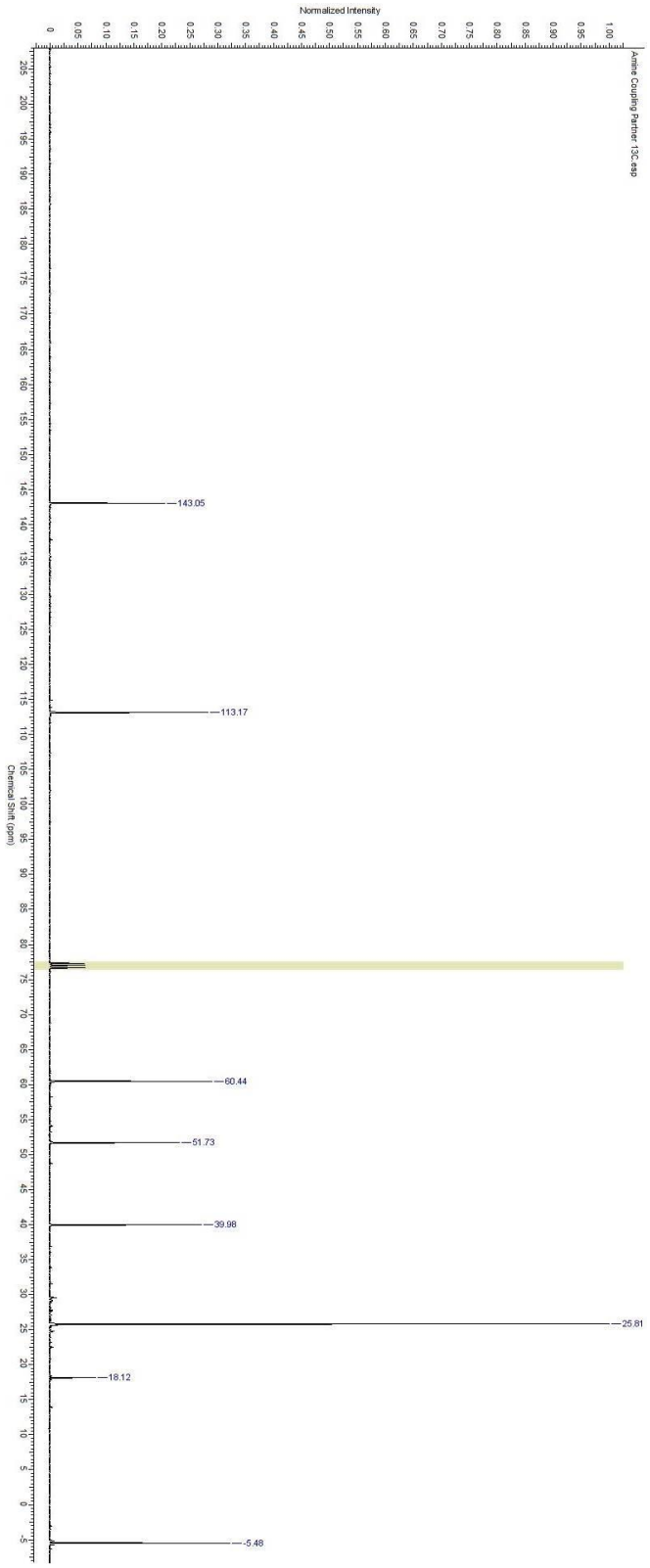

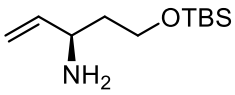

34

100 MHz, $CDCl_3$

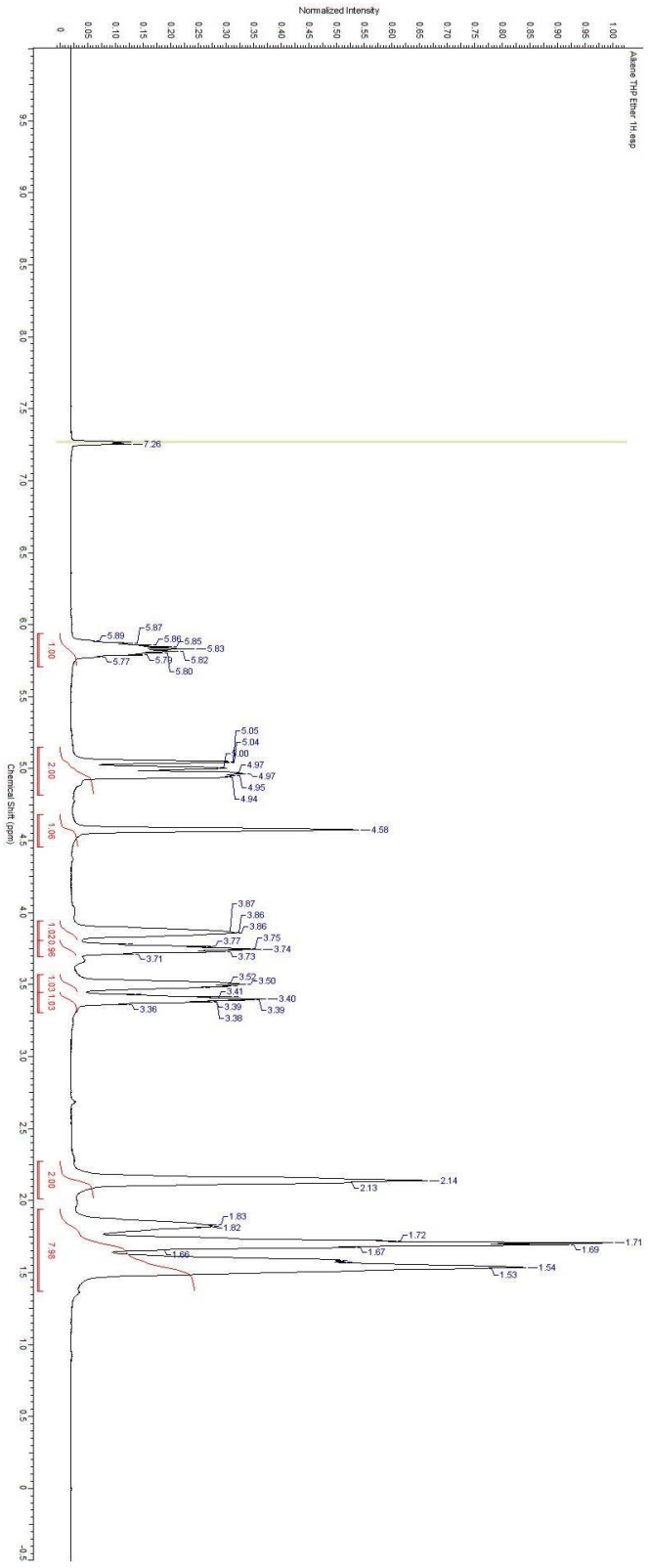

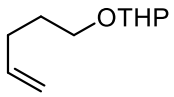

37

400 MHz, $CDCl_3$

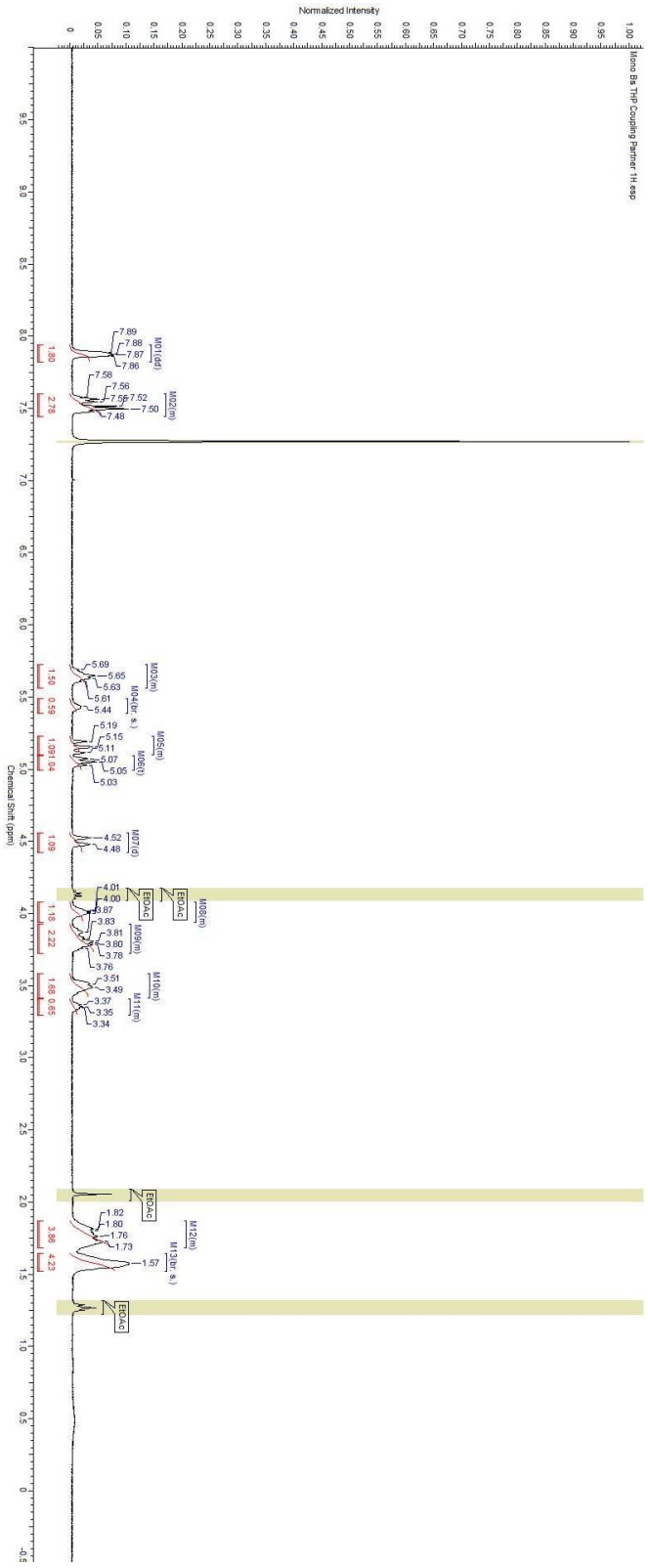

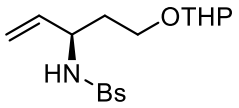

40

400 MHz, $CDCl_3$

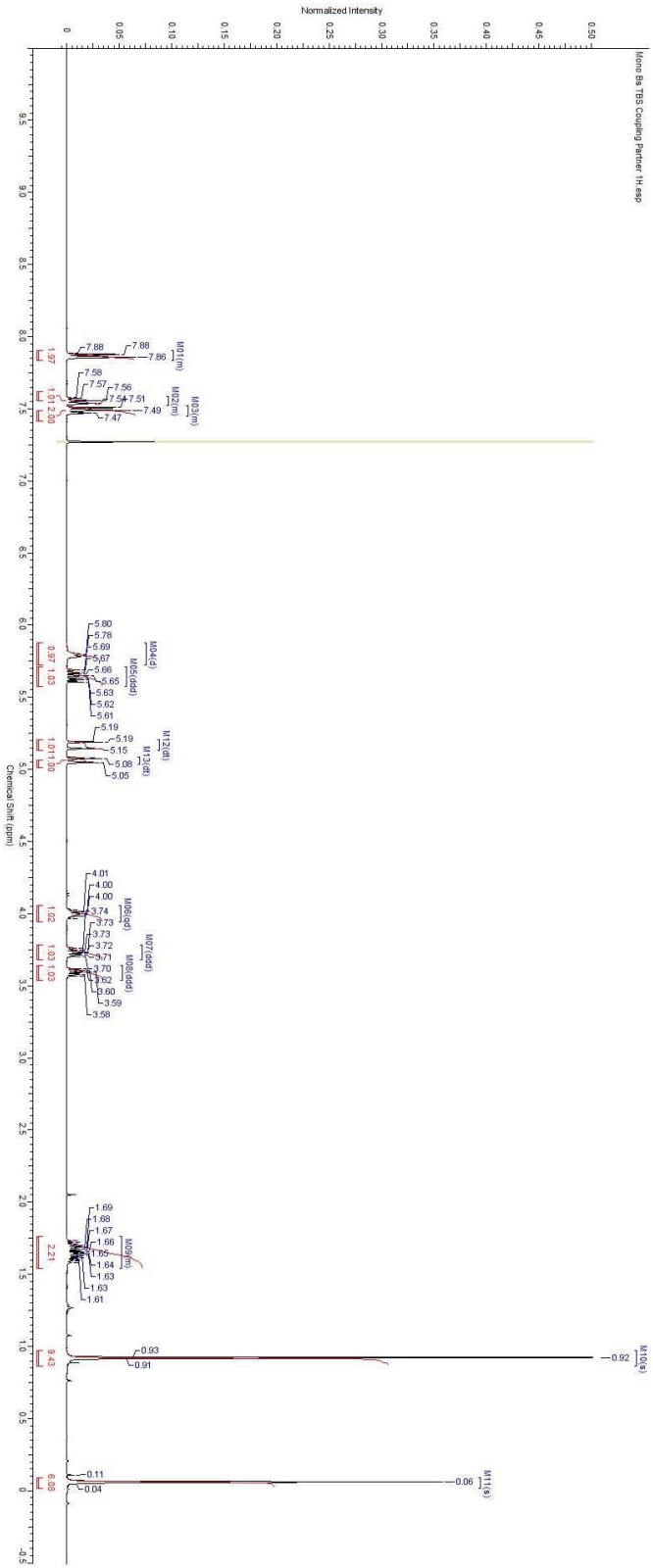

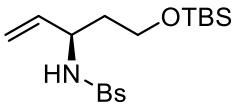

41

400 MHz, $CDCl_3$

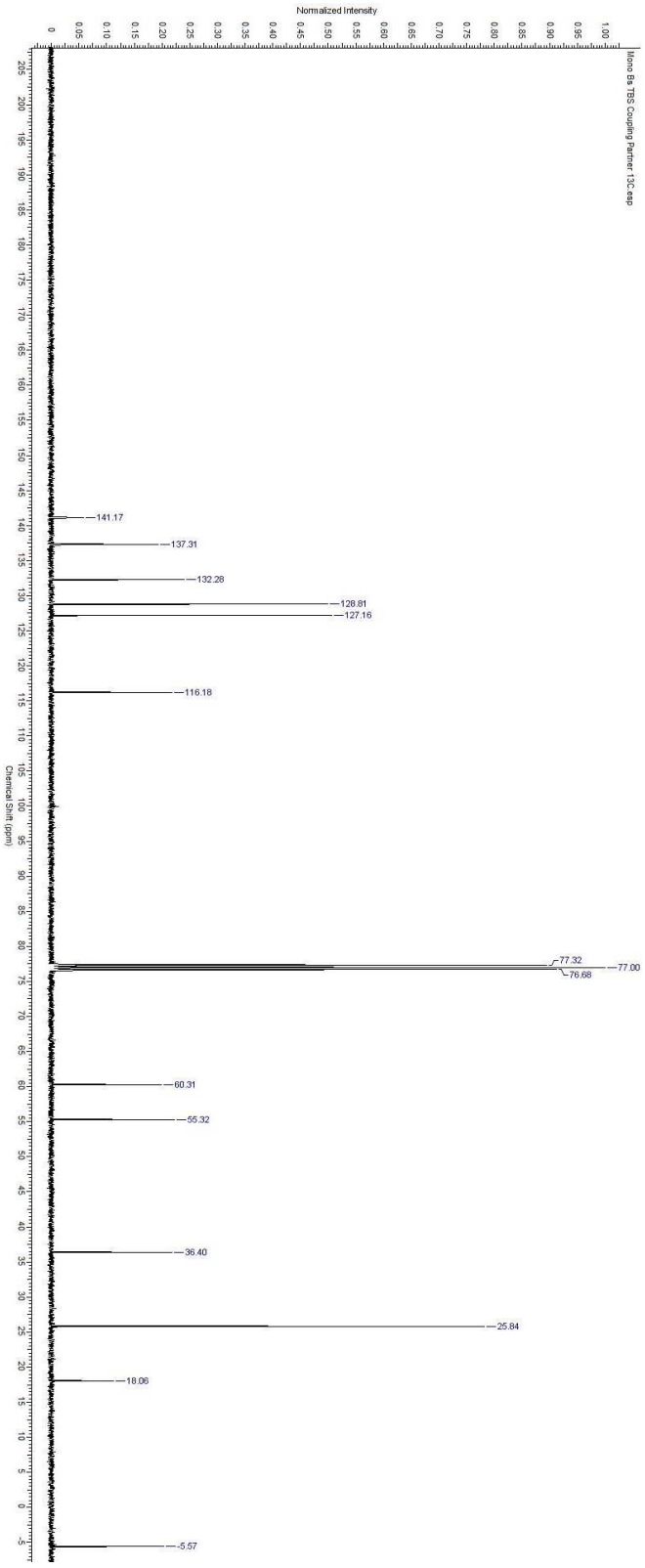

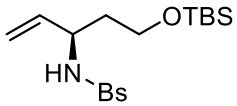

41

100 MHz, $CDCl_3$

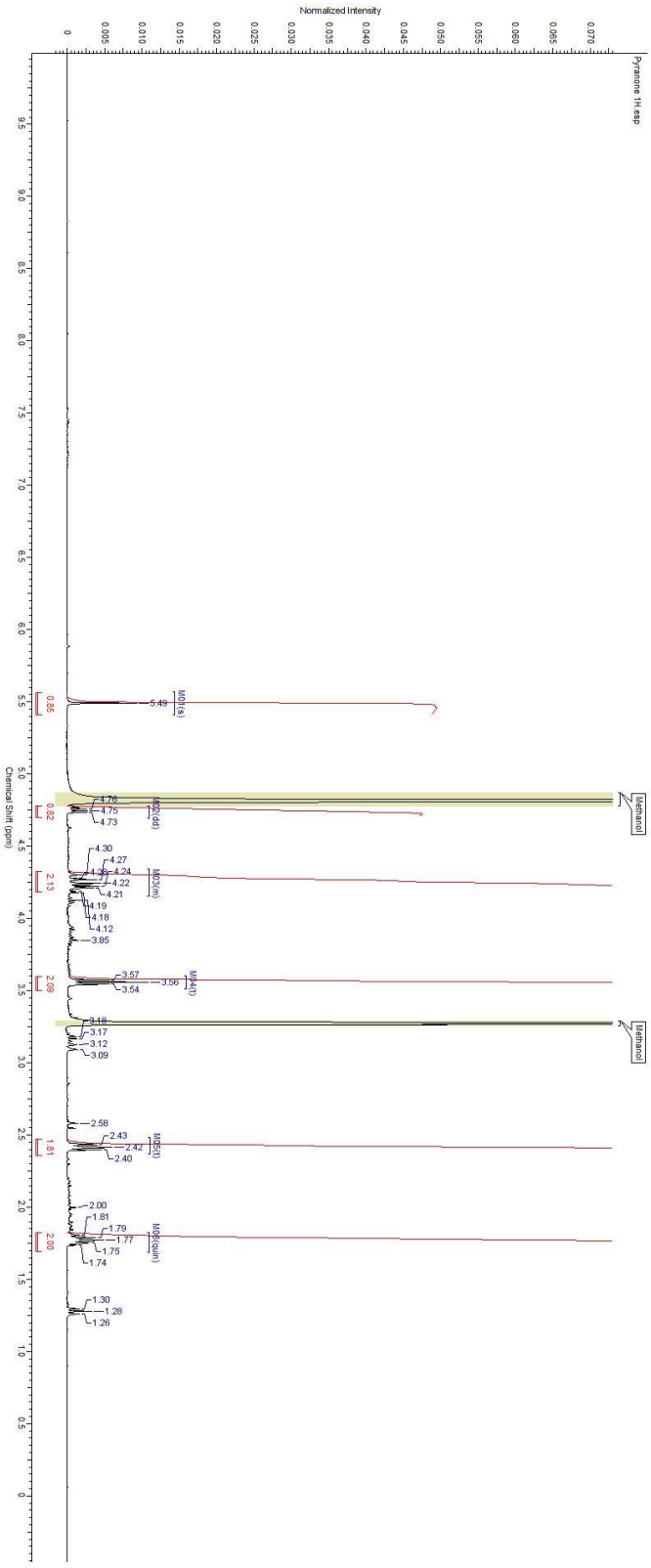

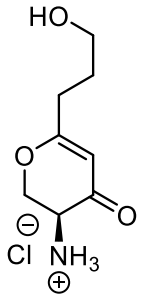

42

400 MHz, CD_3OD

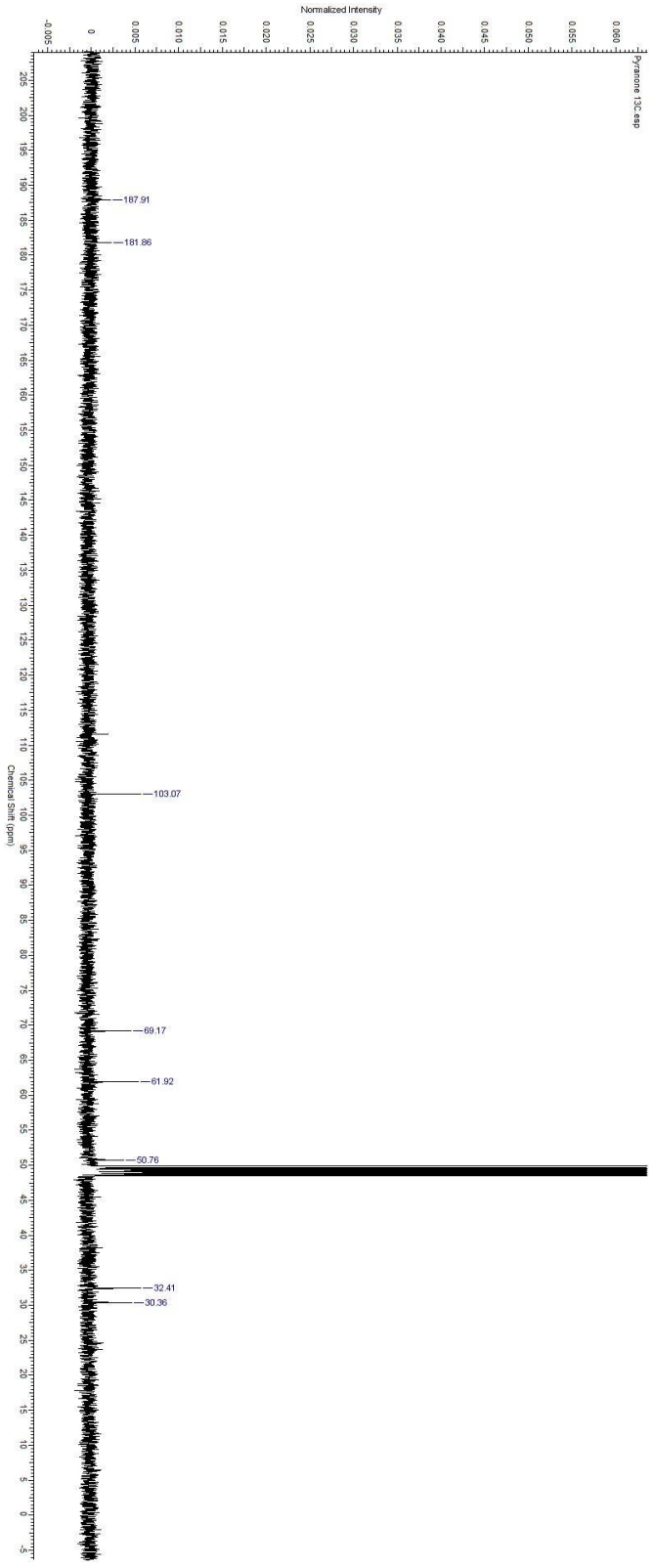

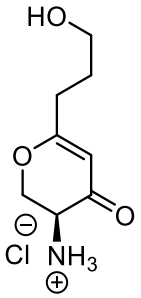

42

100 MHz, CD_3OD

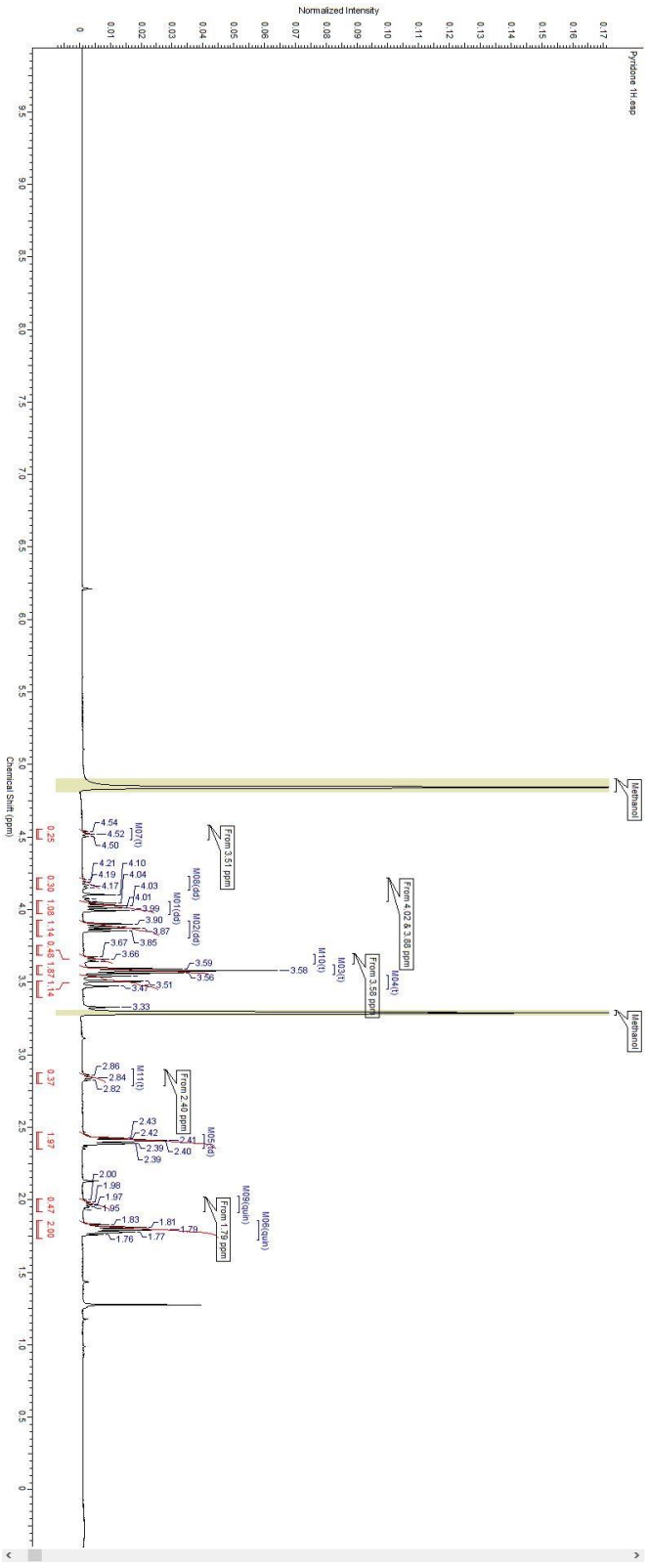

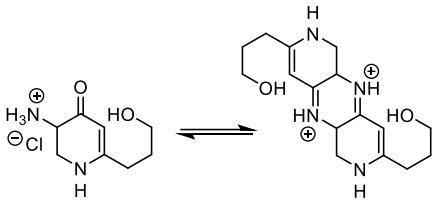

Also notable is that the alkenyl proton is not observed, this is assumed to be due to exchange with solvent

43

400 MHz, CD_3OD

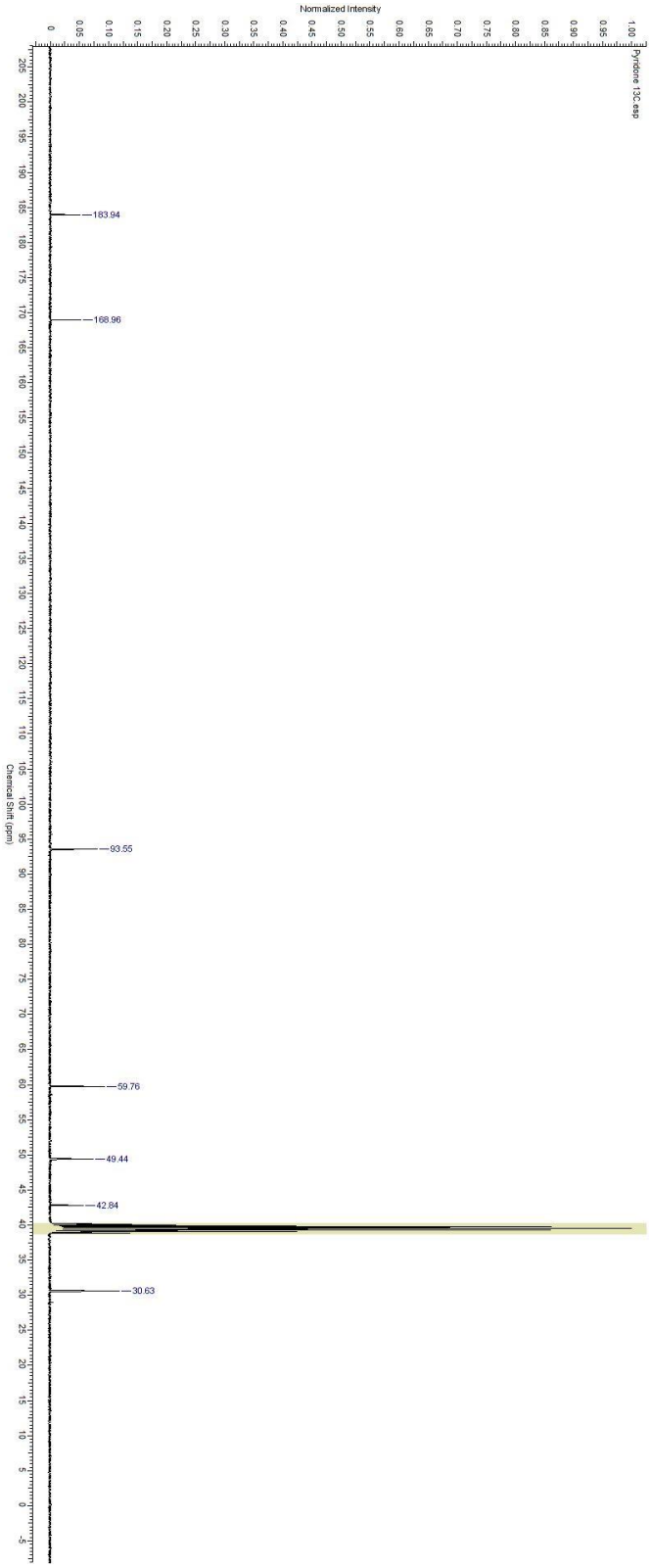

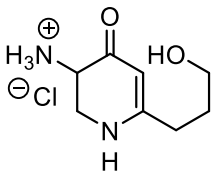

43

100 MHz, CD_3OD

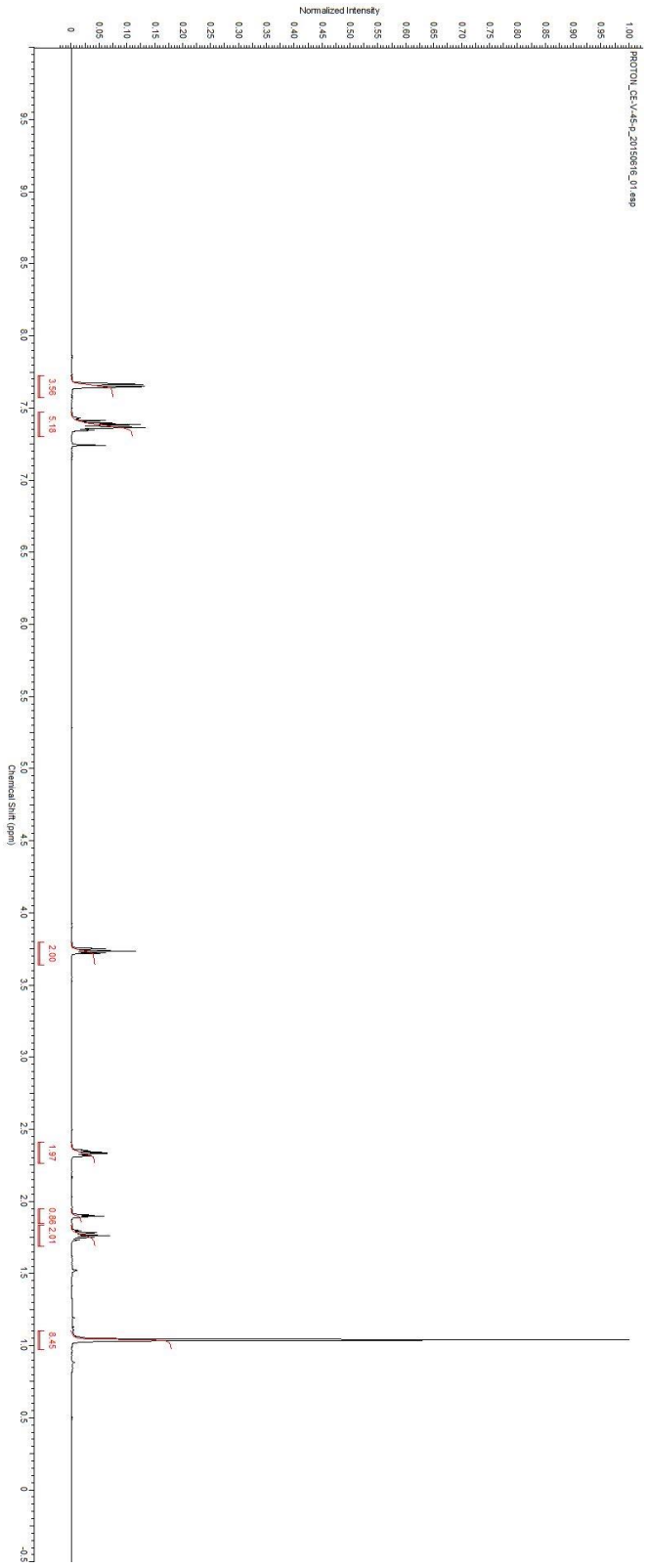

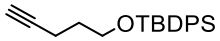

400 MHz, $CDCl_3$

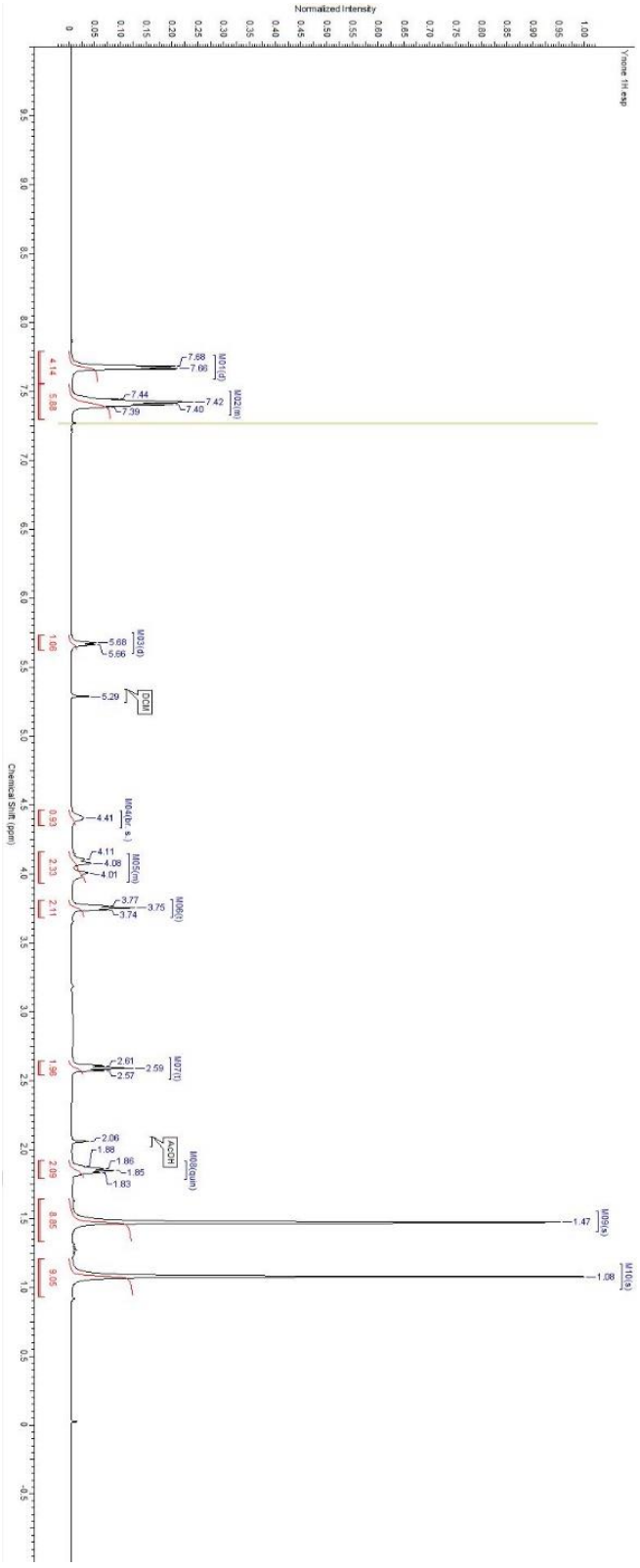

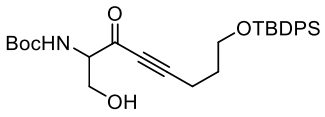

45

400 MHz, $CDCl_3$

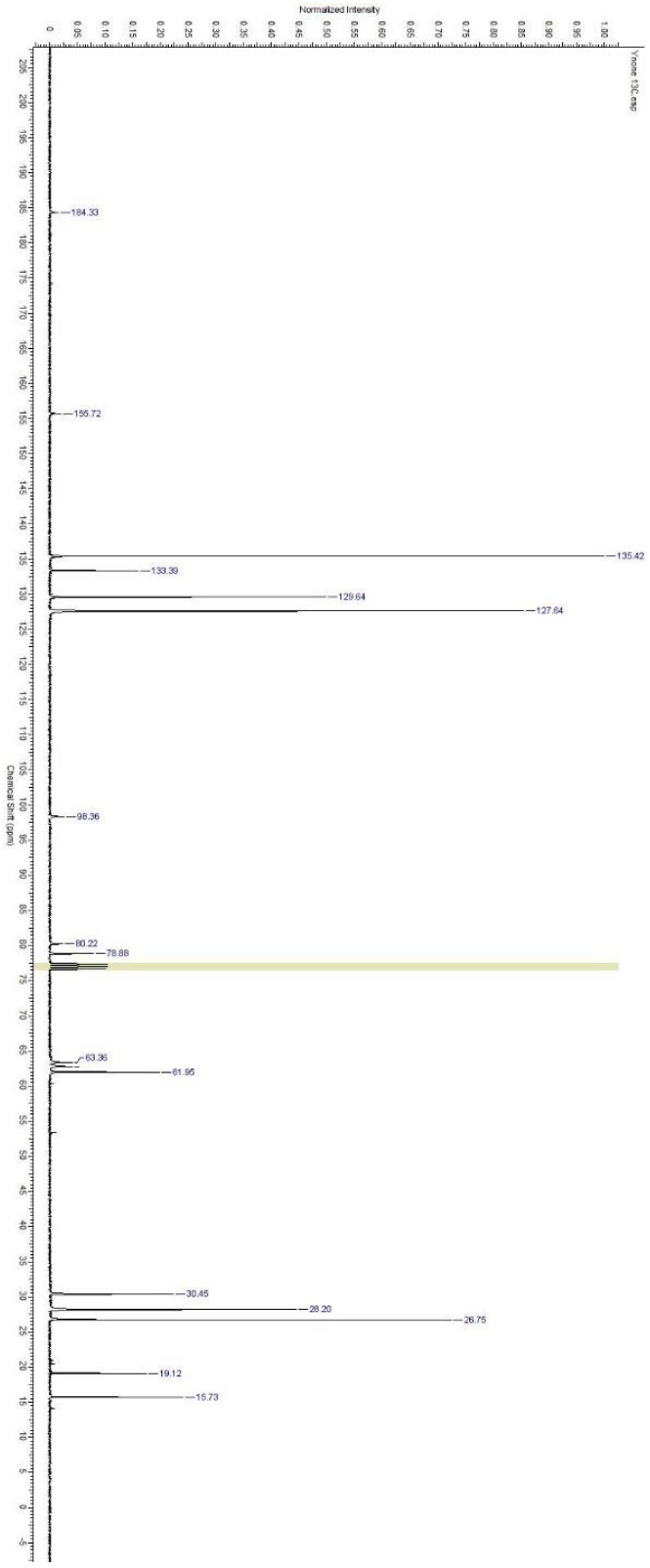

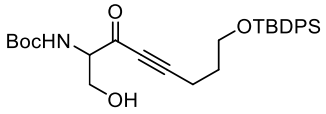

45

100 MHz, $CDCl_3$

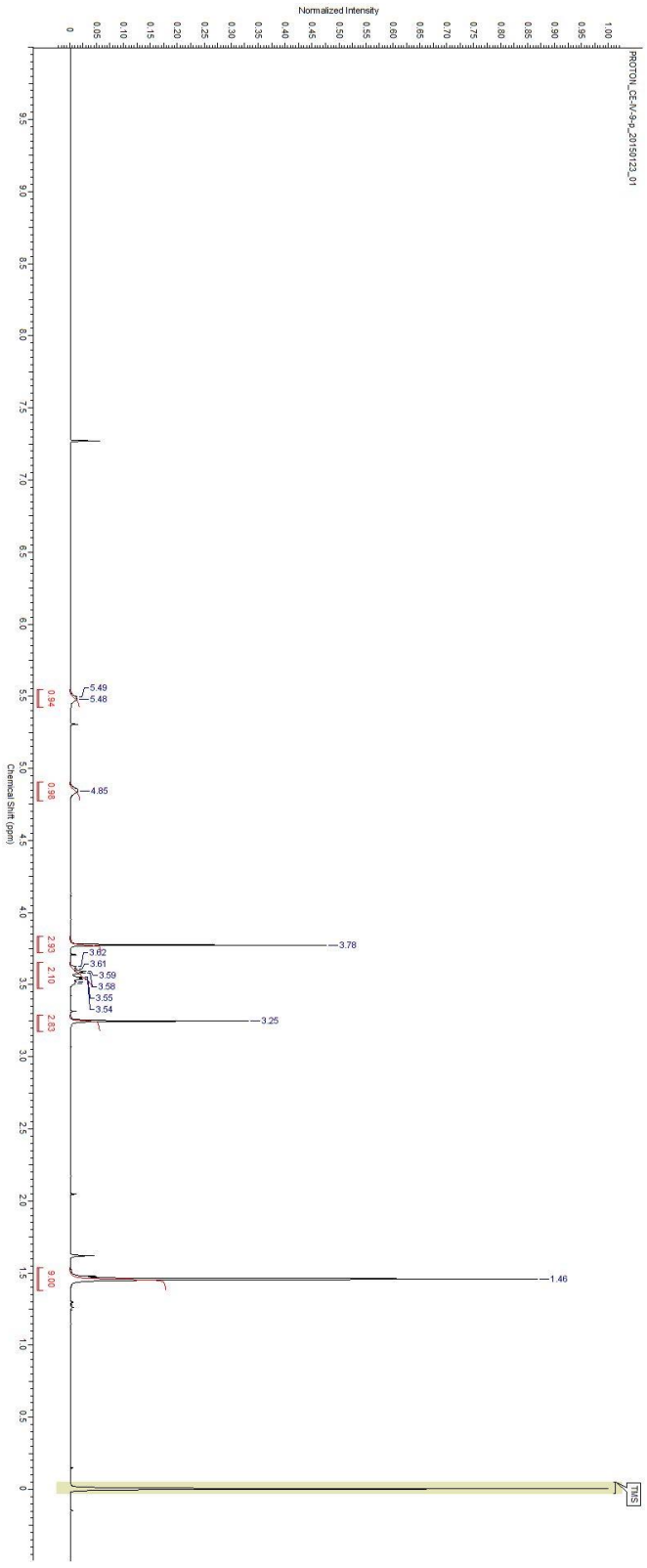

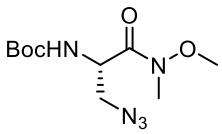

46

400 MHz, $CDCl_3$

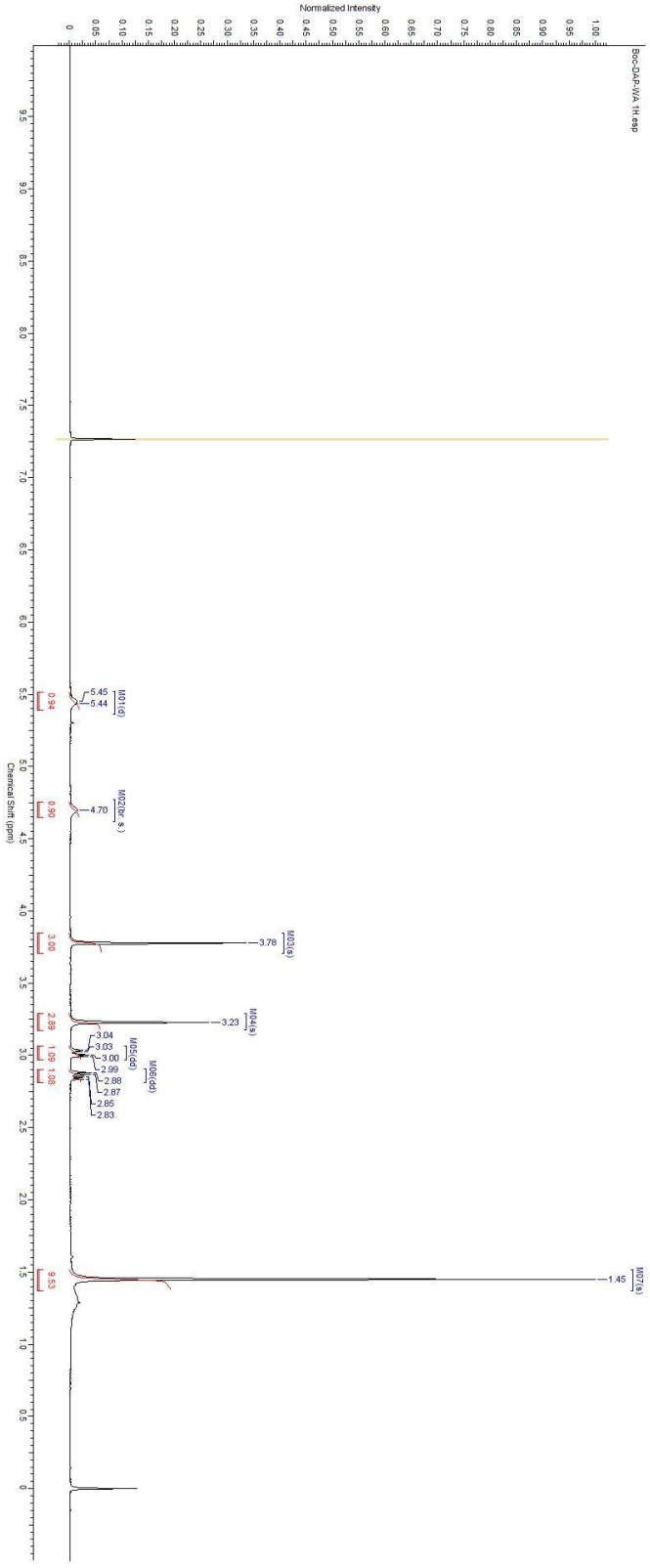

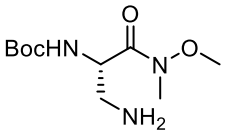

47

400 MHz, $CDCl_3$

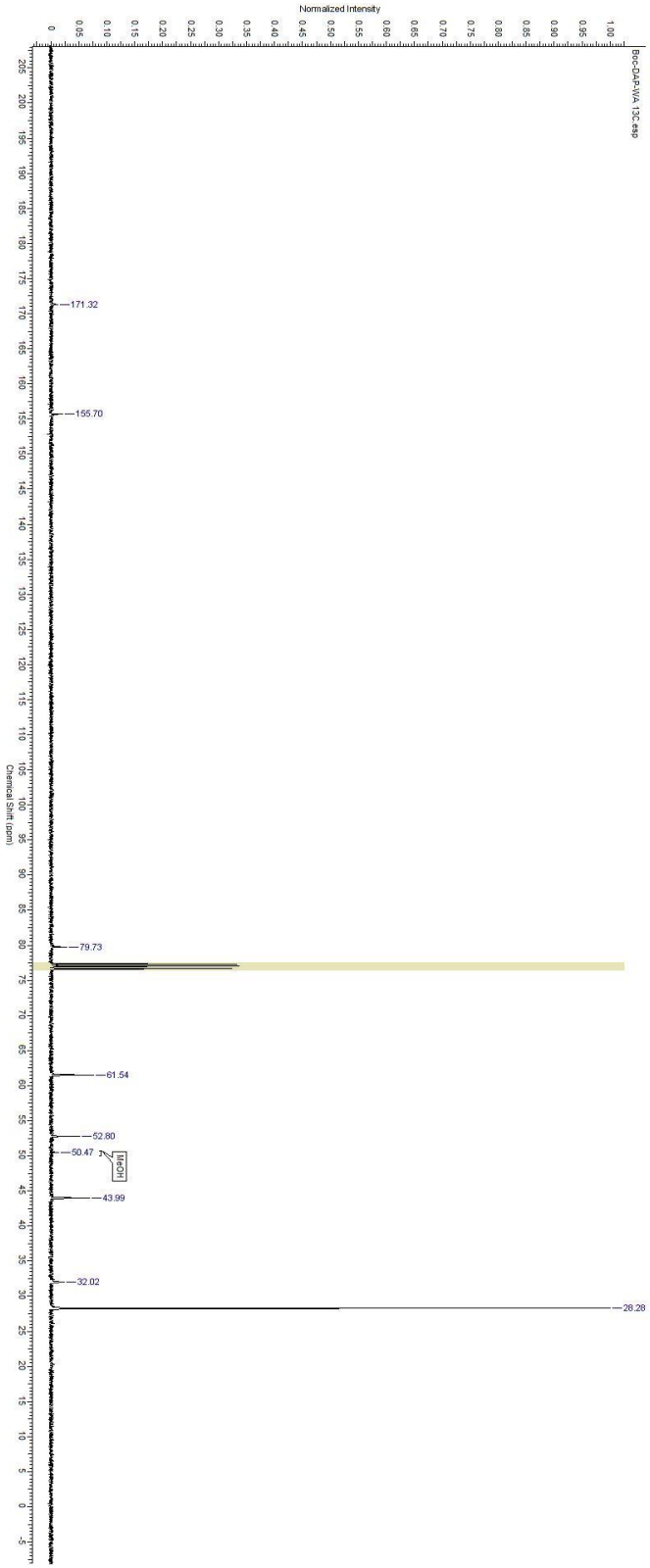

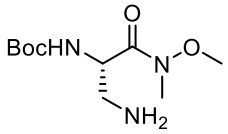

47

100 MHz, $CDCl_3$

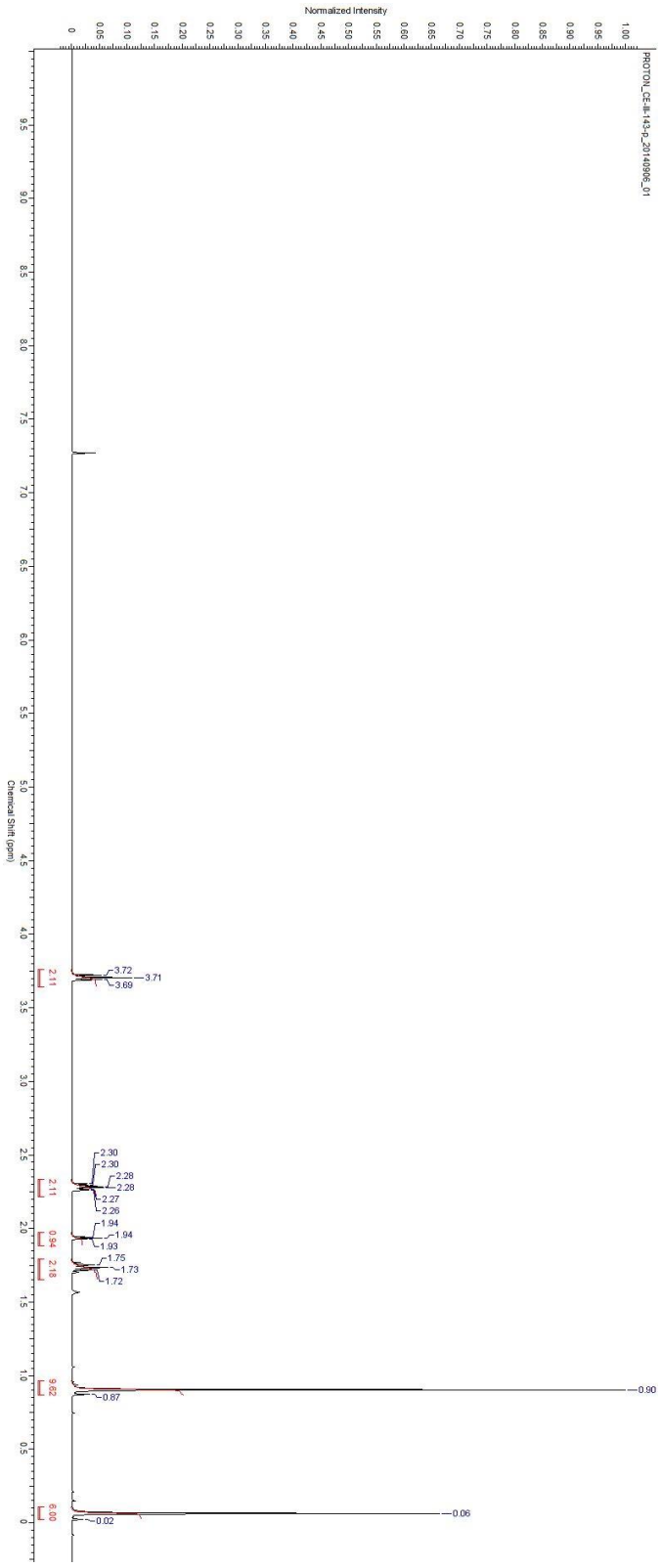

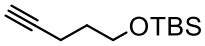

400 MHz, $CDCl_3$

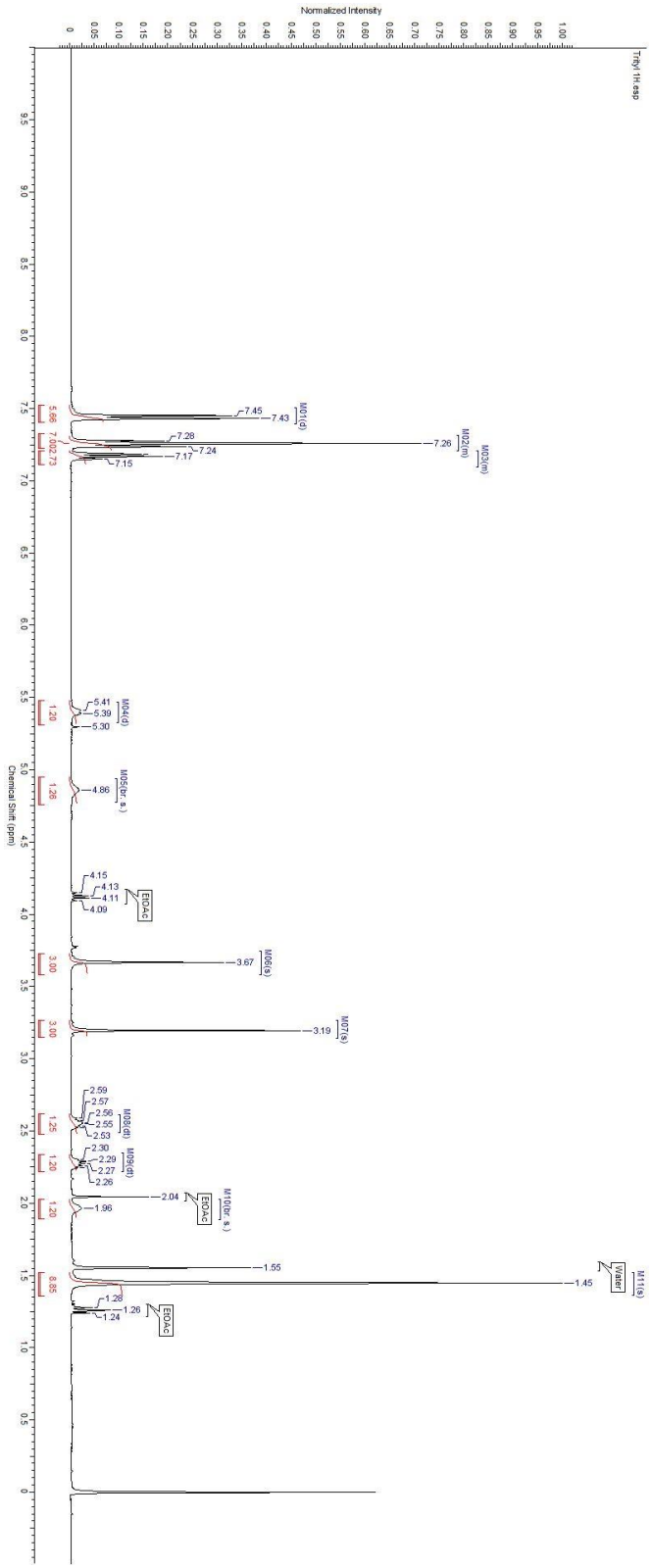

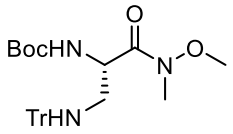

49

400 MHz, $CDCl_3$

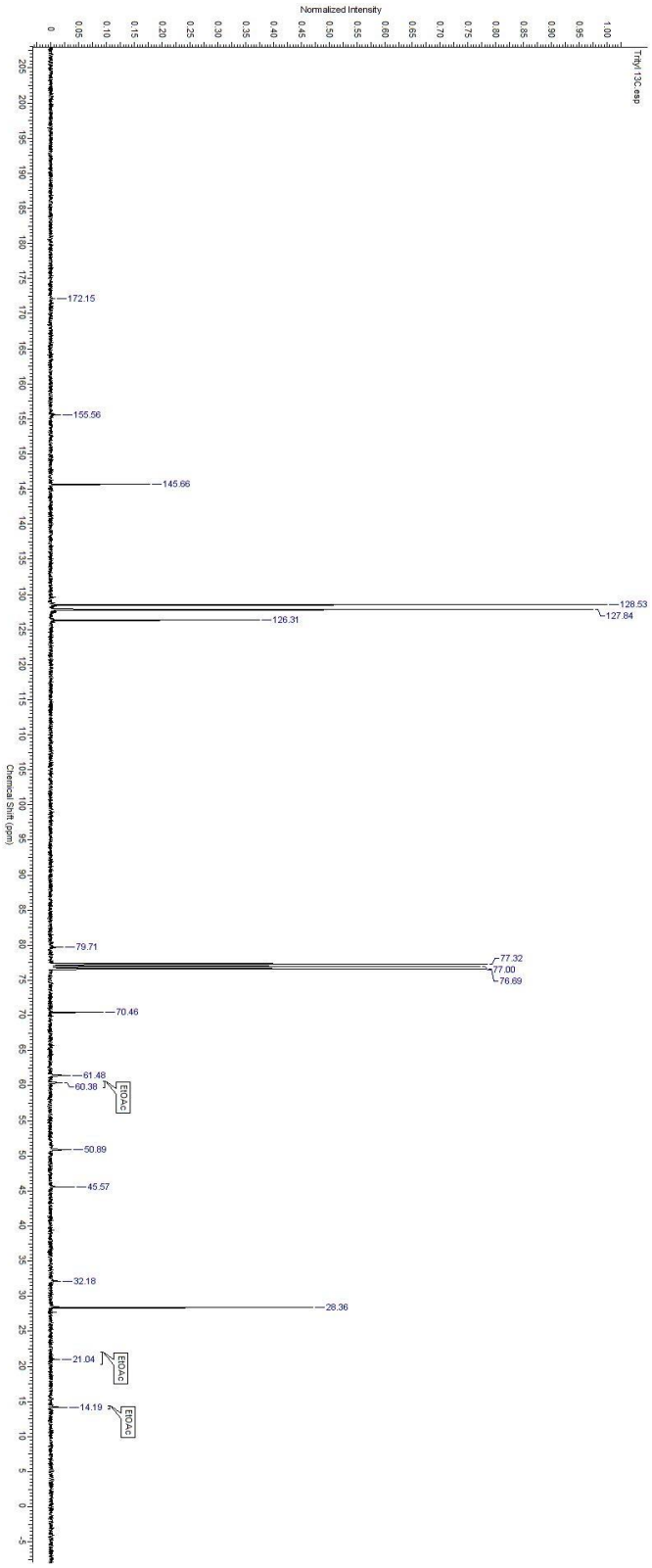

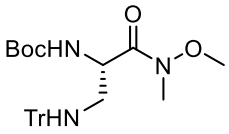

49

100 MHz, $CDCl_3$

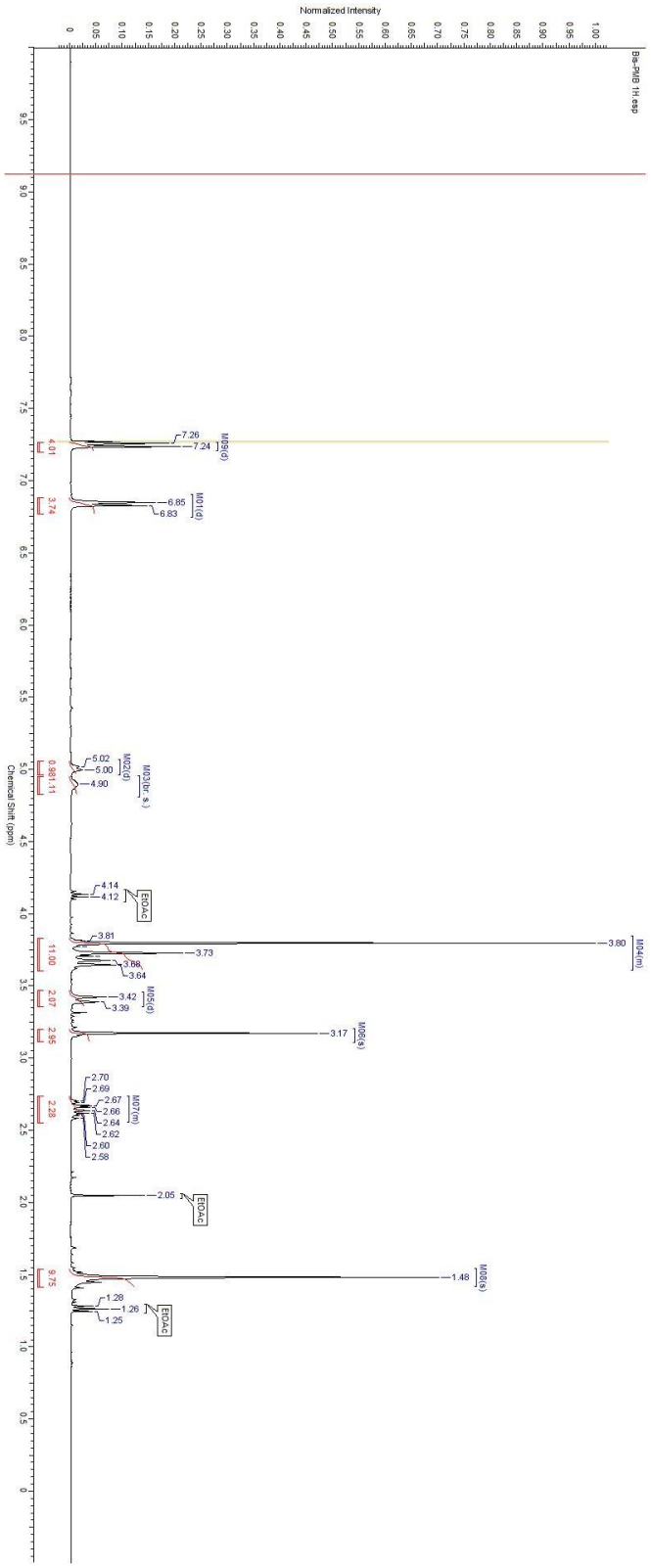

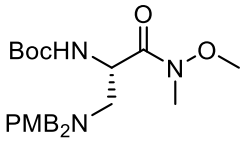

50

400 MHz, $CDCl_3$

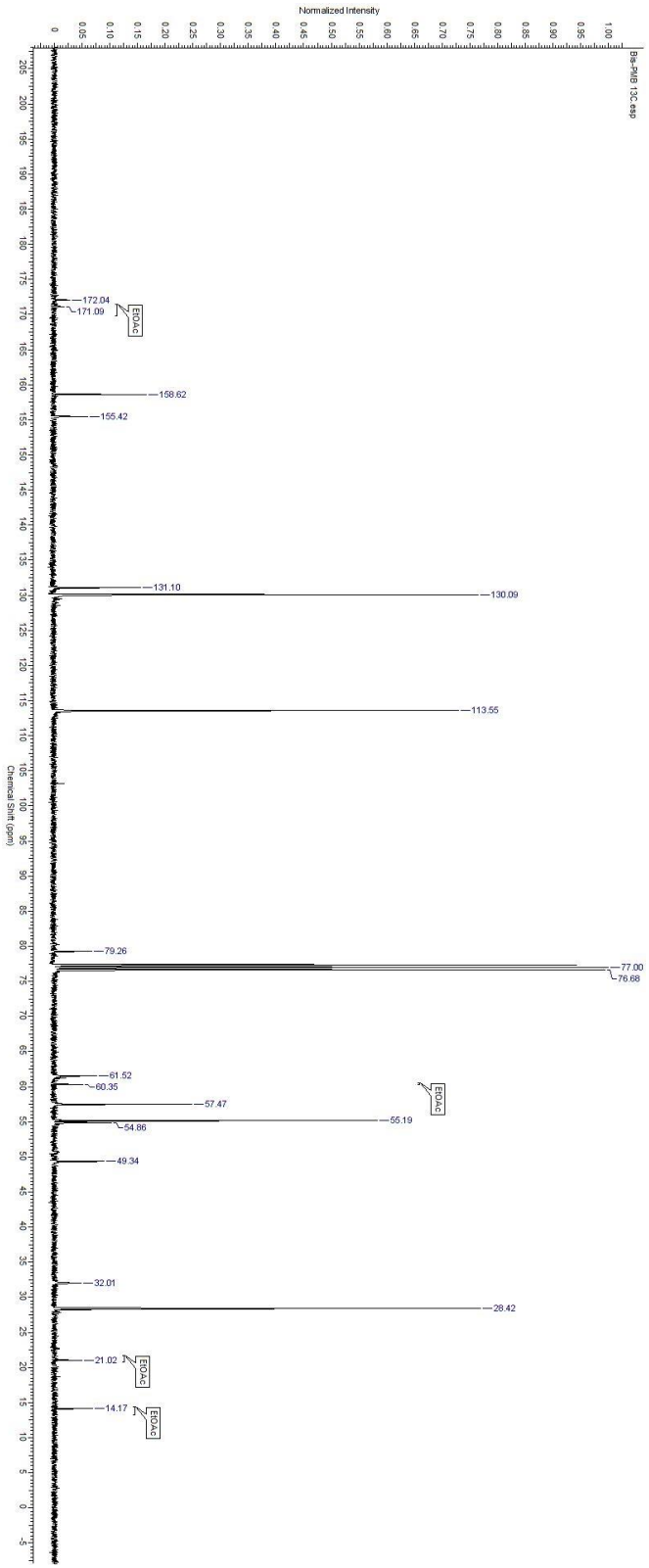

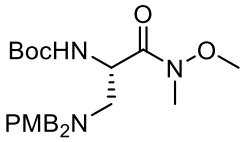

50

100 MHz, $CDCl_3$

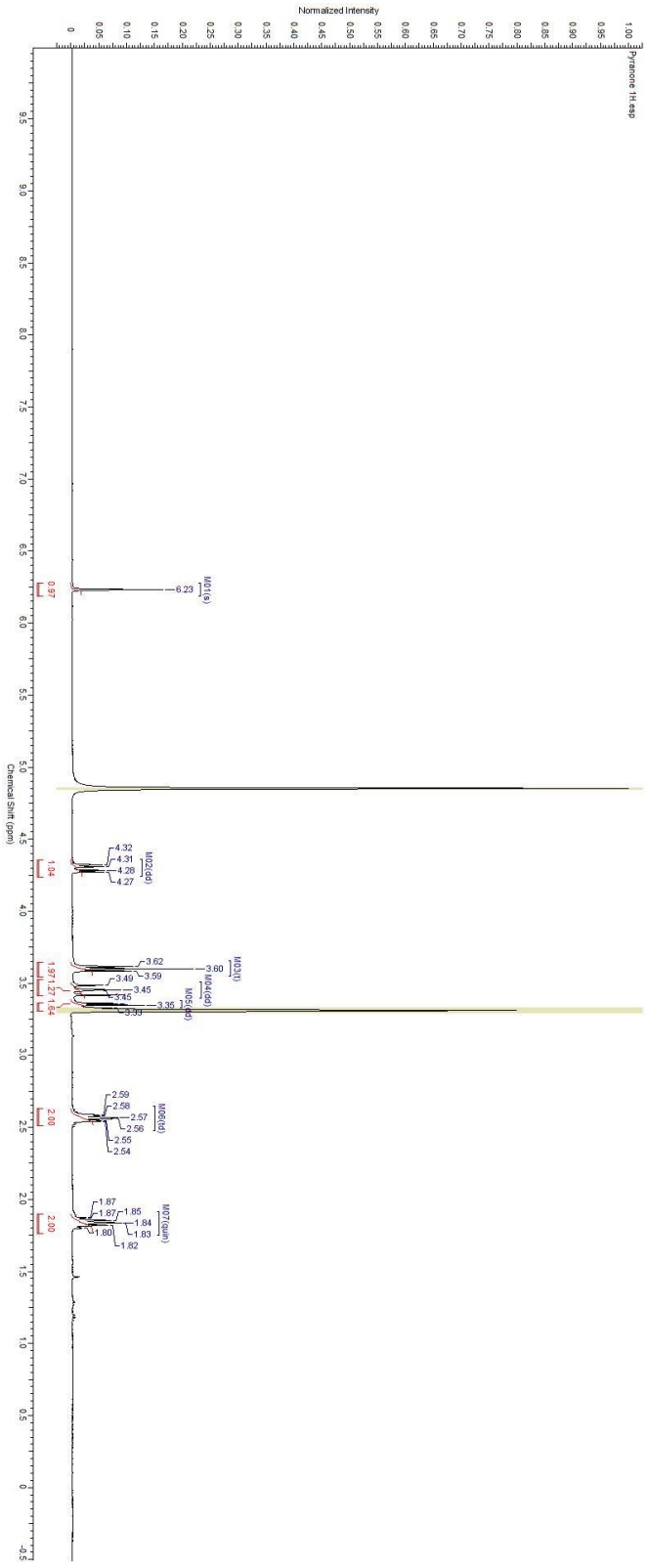

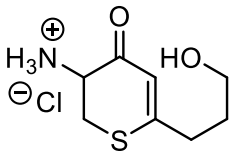

51

400 MHz, CD_3OD

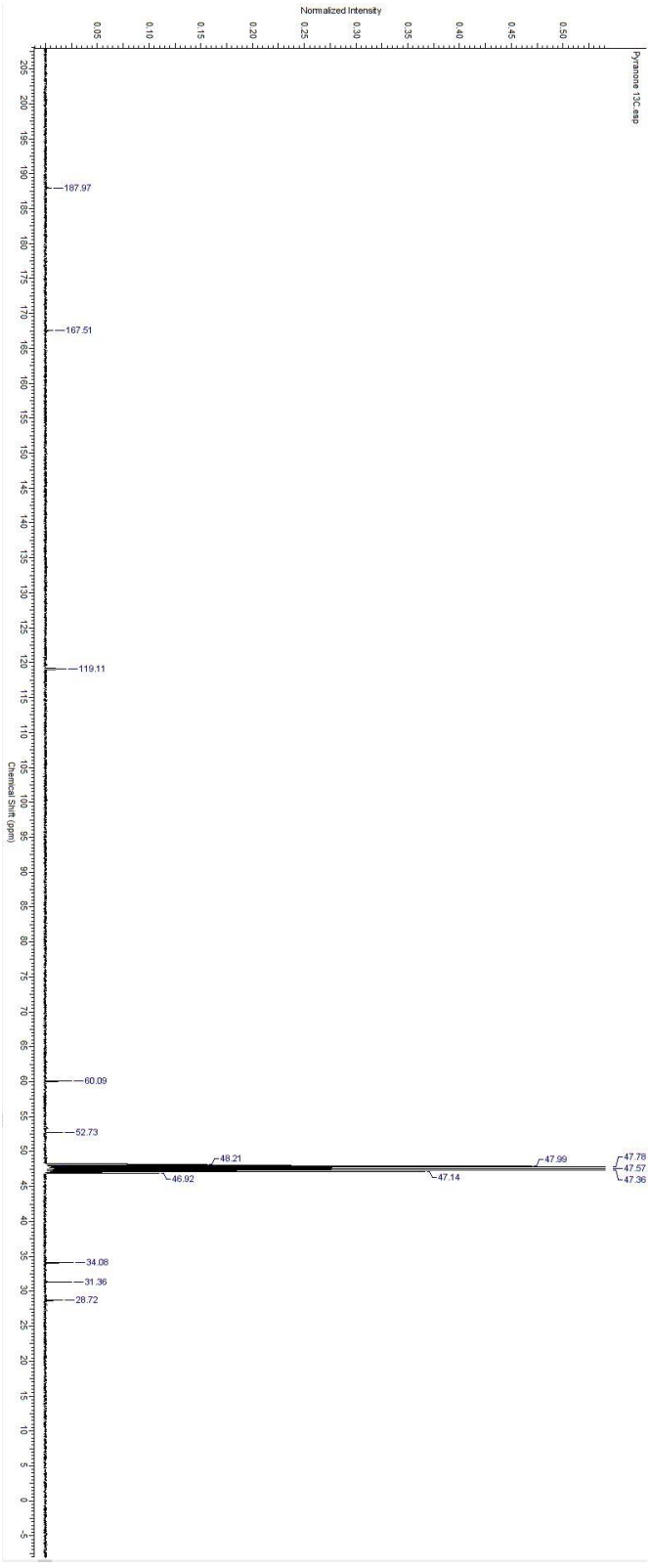

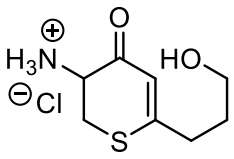

51

100 MHz, CD_3OD

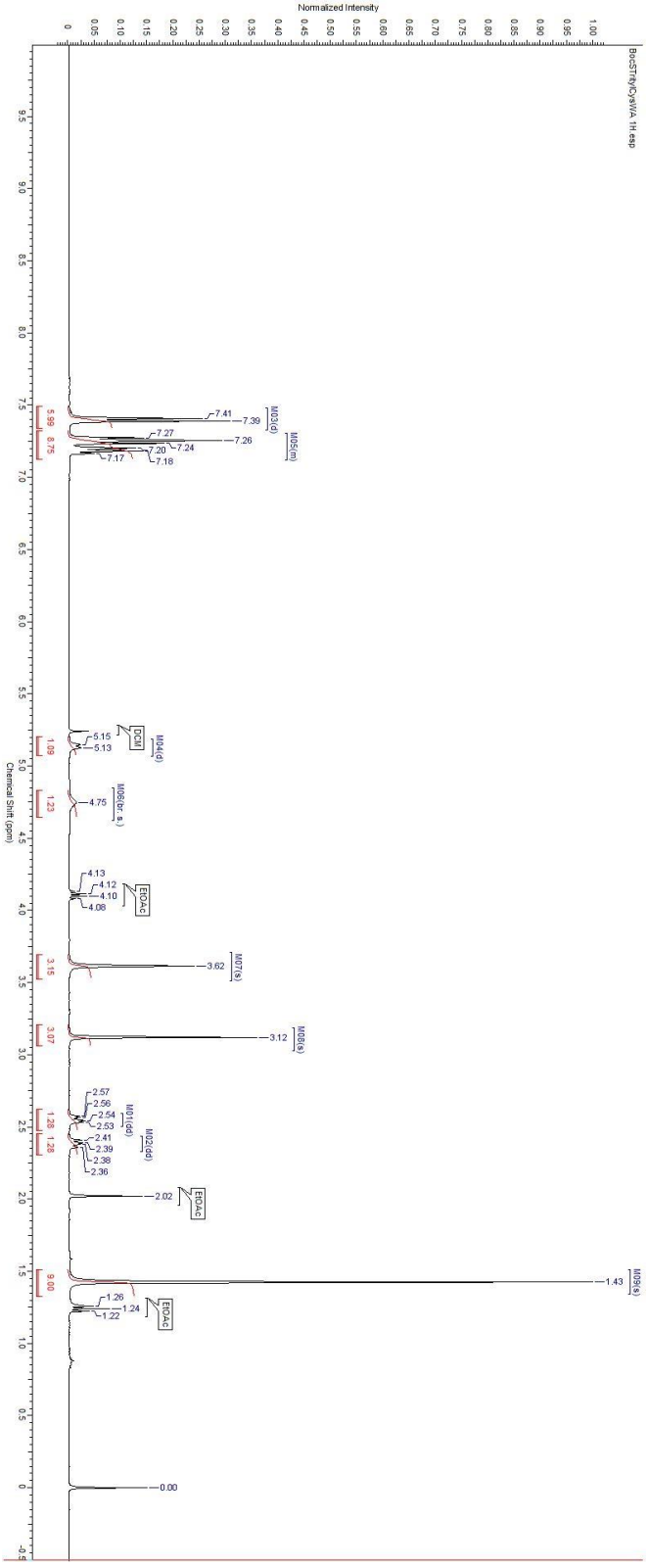

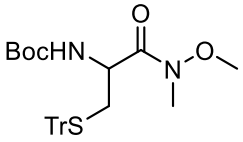

53

400 MHz, $CDCl_3$

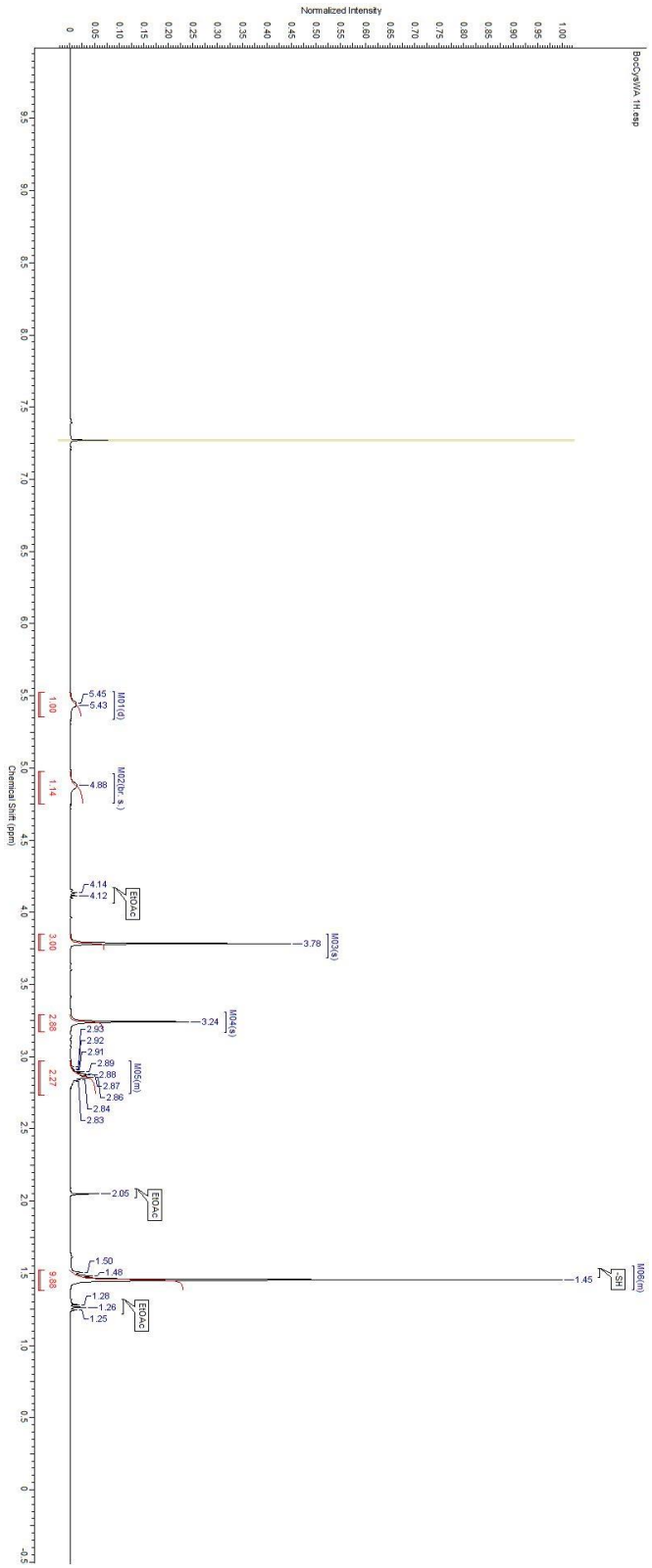

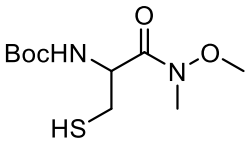

54

400 MHz, $CDCl_3$

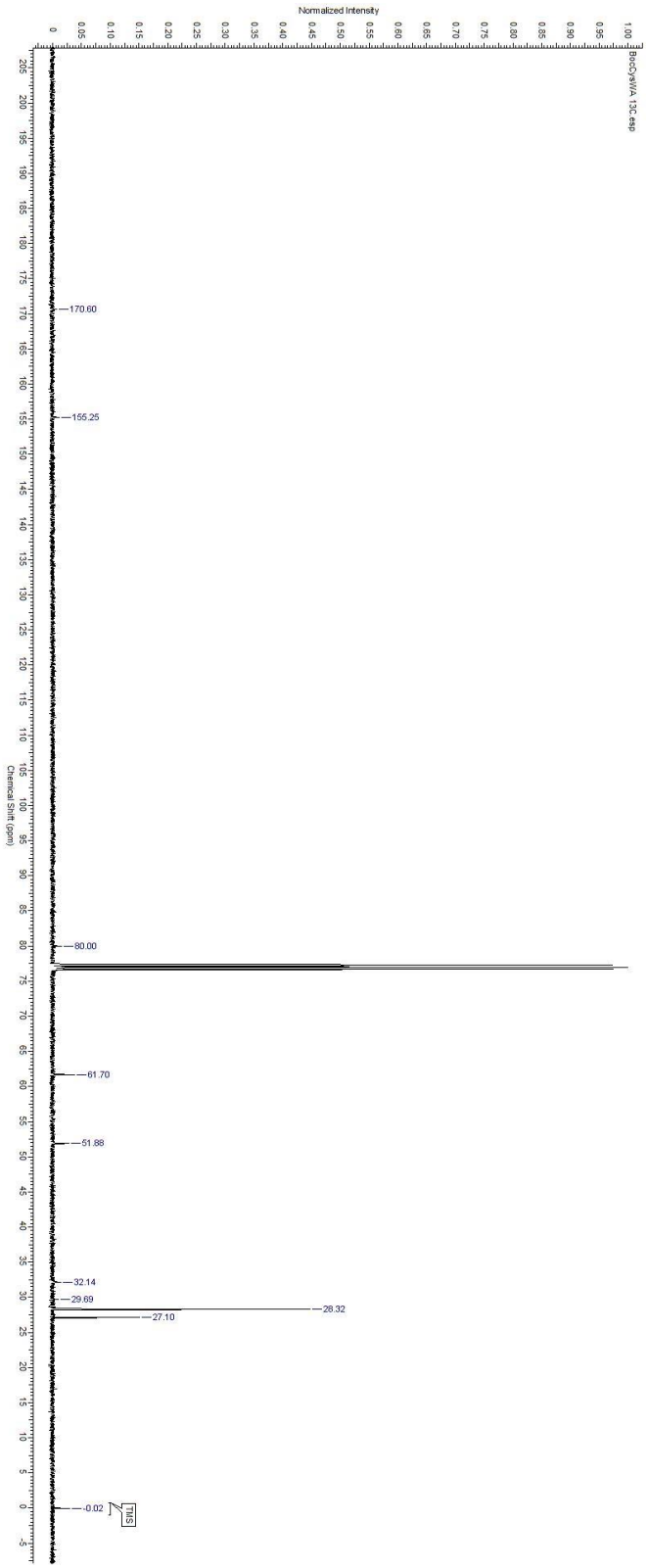

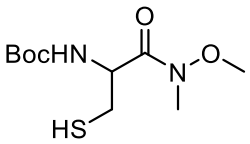

54

100 MHz, $CDCl_3$

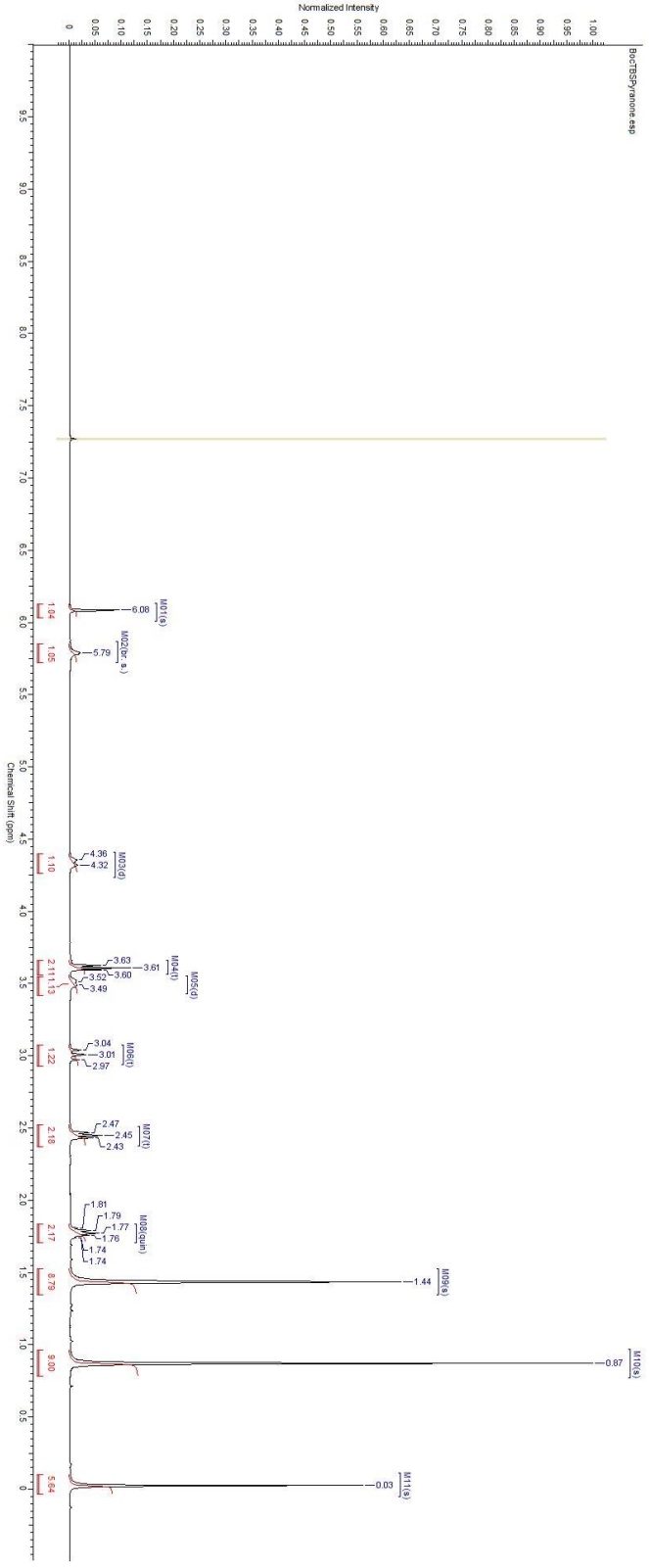

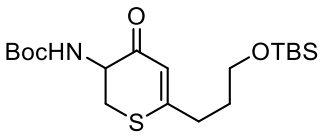

55

400 MHz, $CDCl_3$

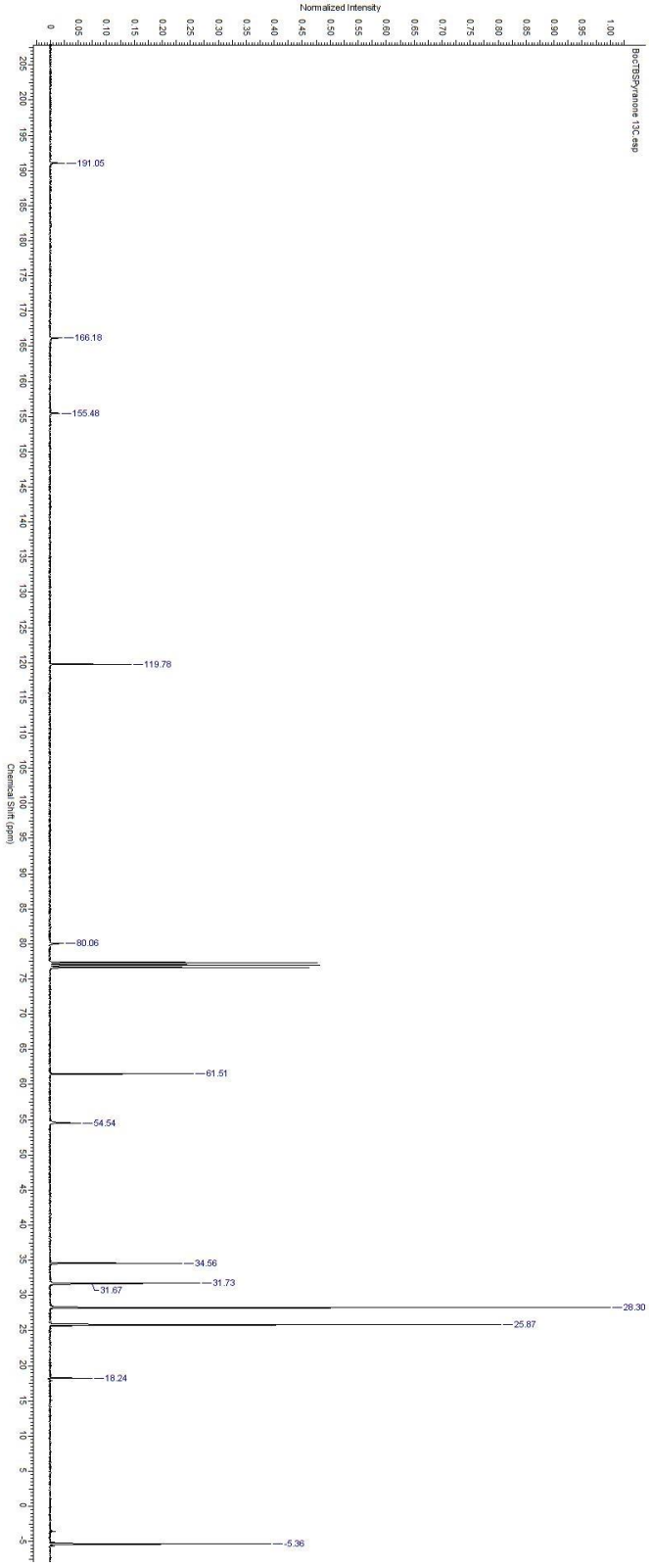

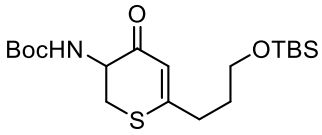

55

100 MHz, $CDCl_3$

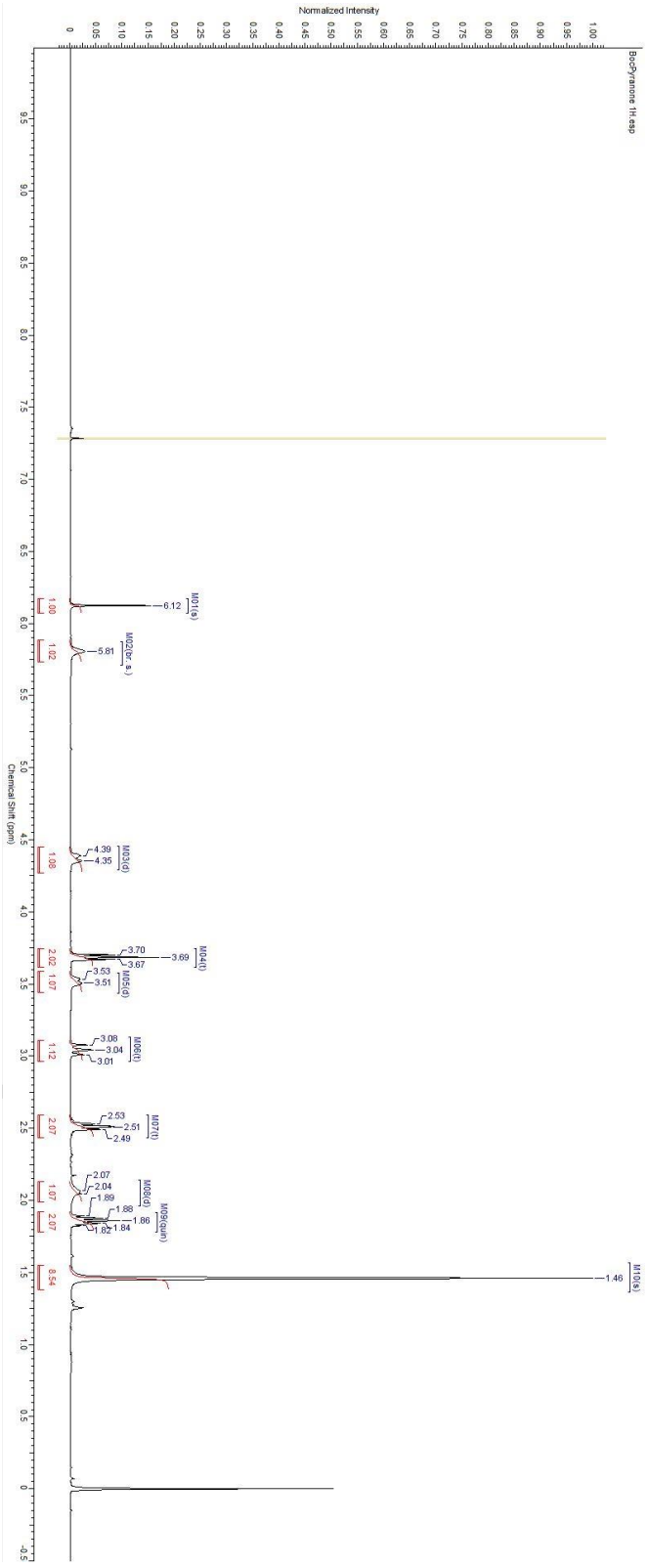

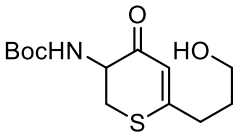

56

400 MHz, $CDCl_3$

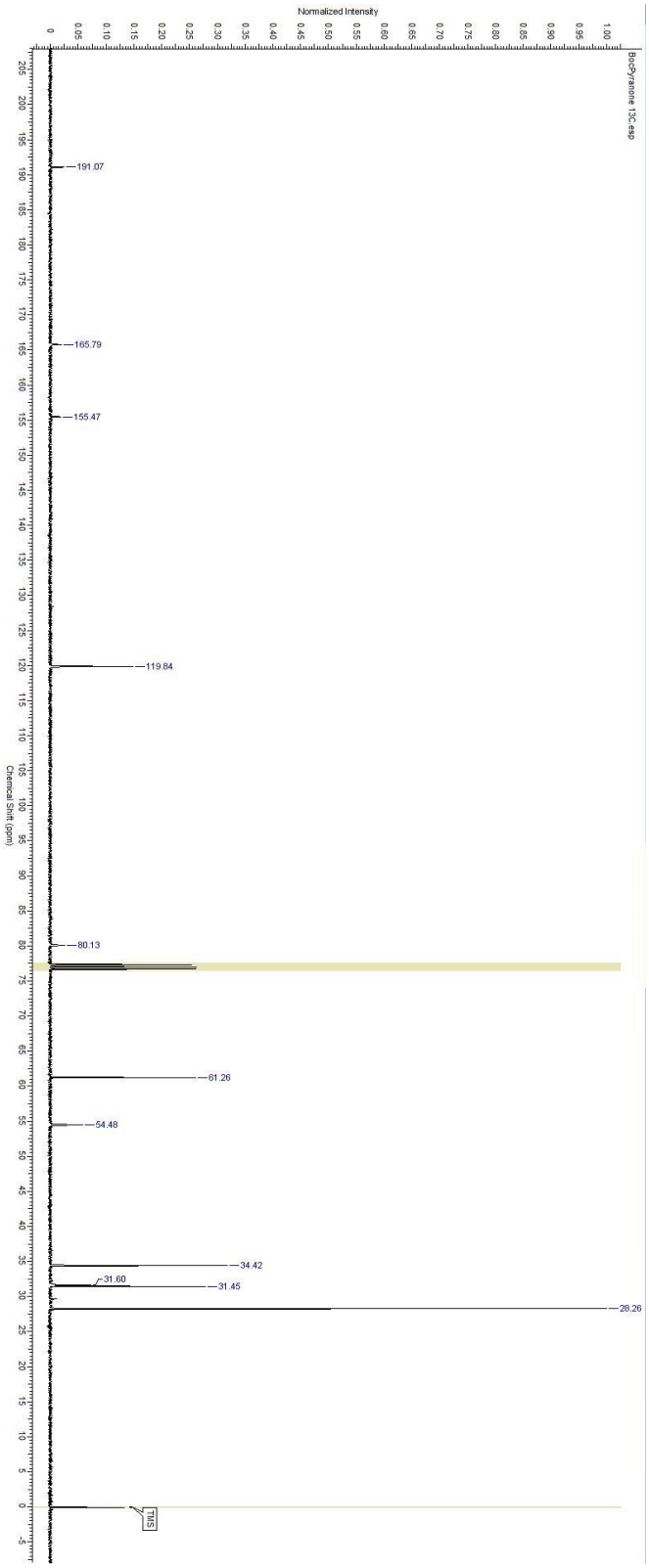

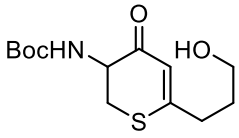

56

100 MHz, $CDCl_3$

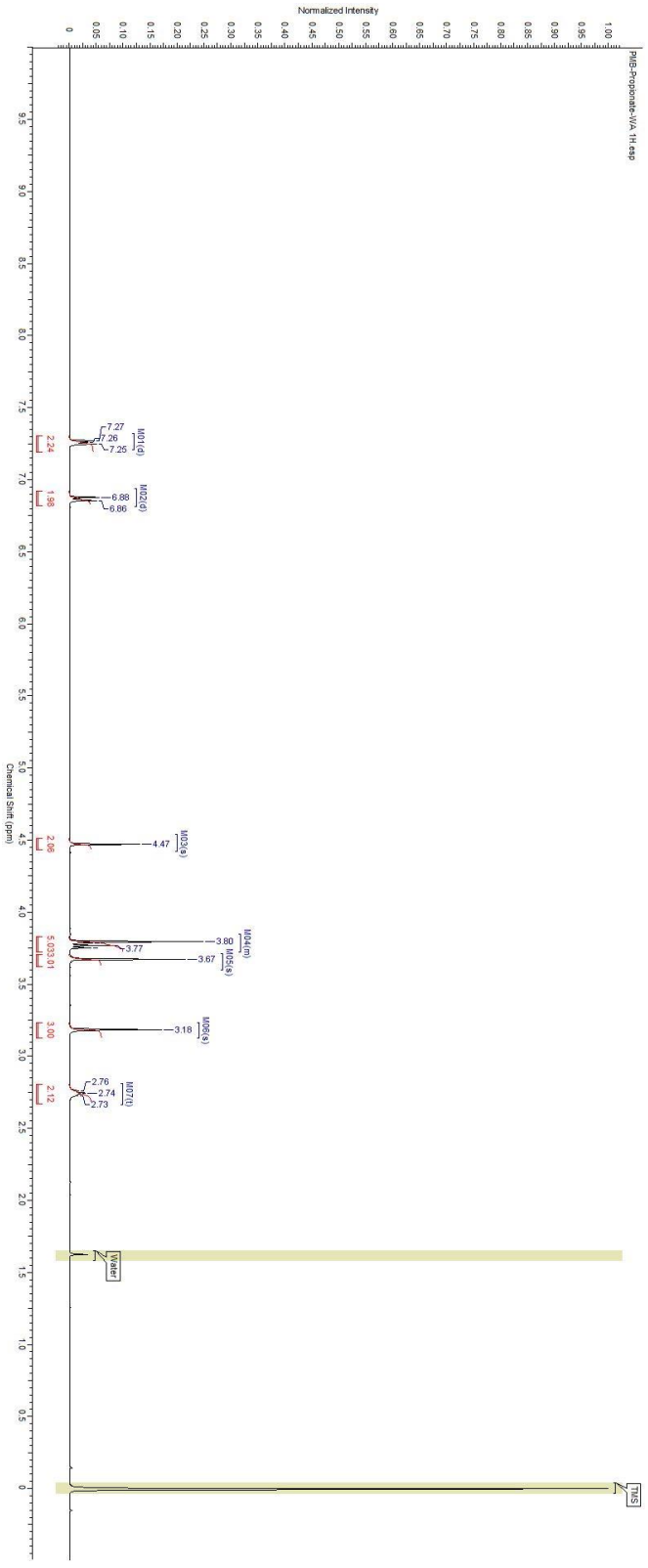

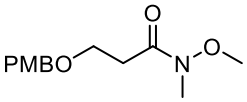

59

400 MHz, $CDCl_3$

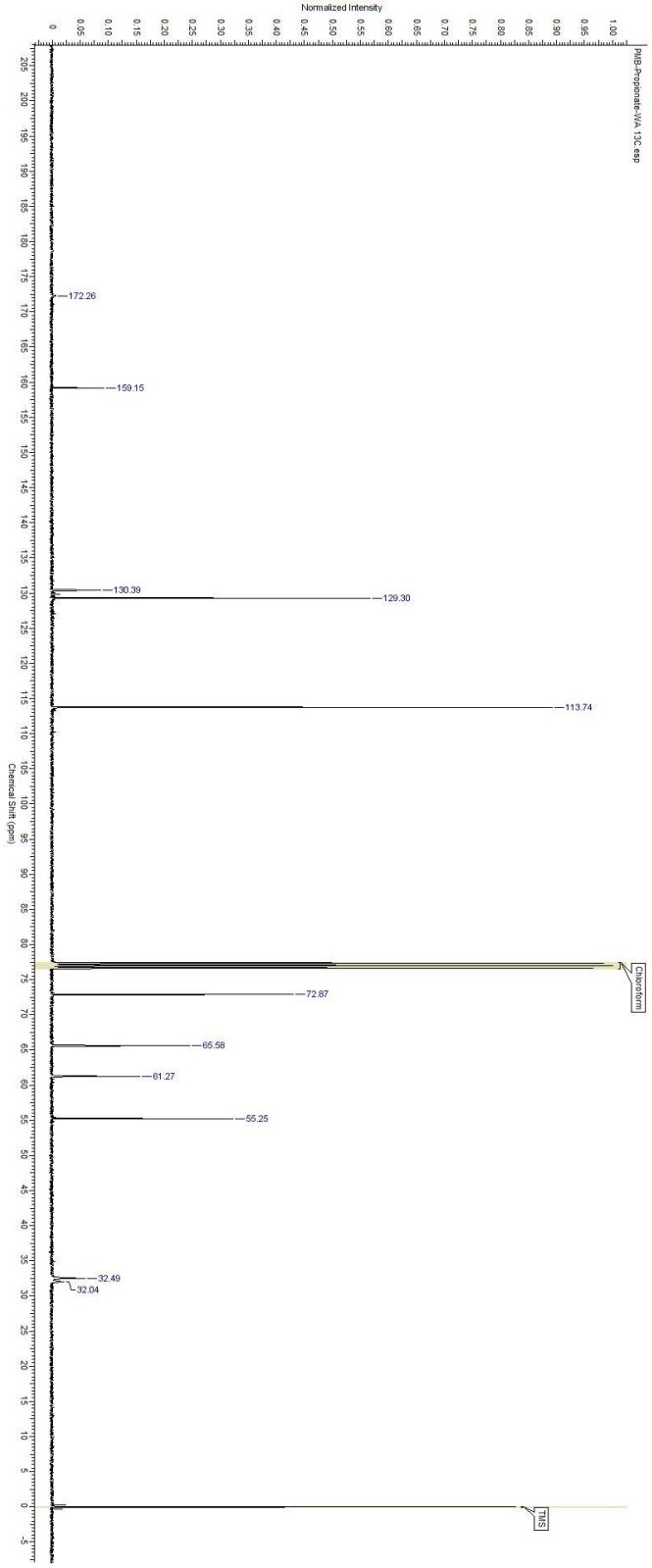

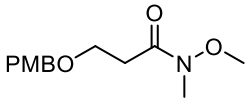

59

100 MHz, $CDCl_3$

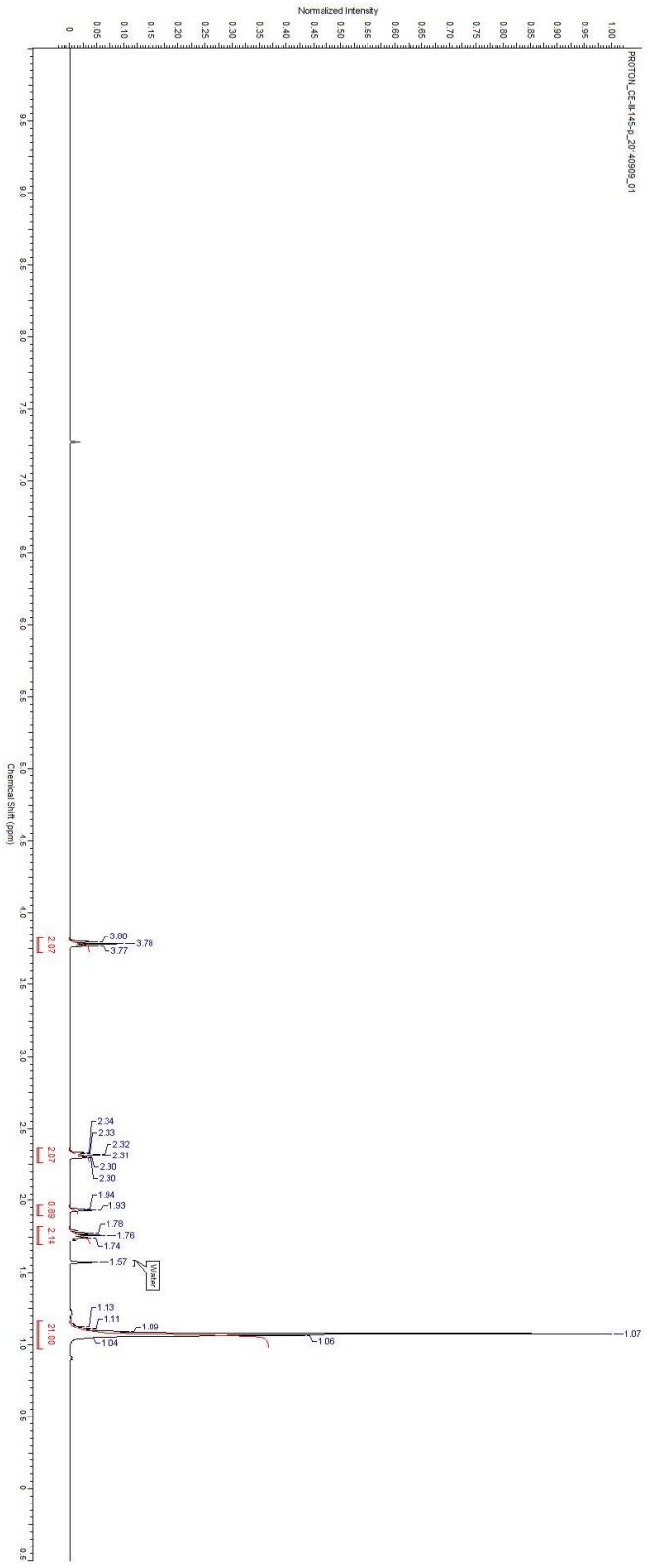

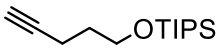

400 MHz, $CDCl_3$

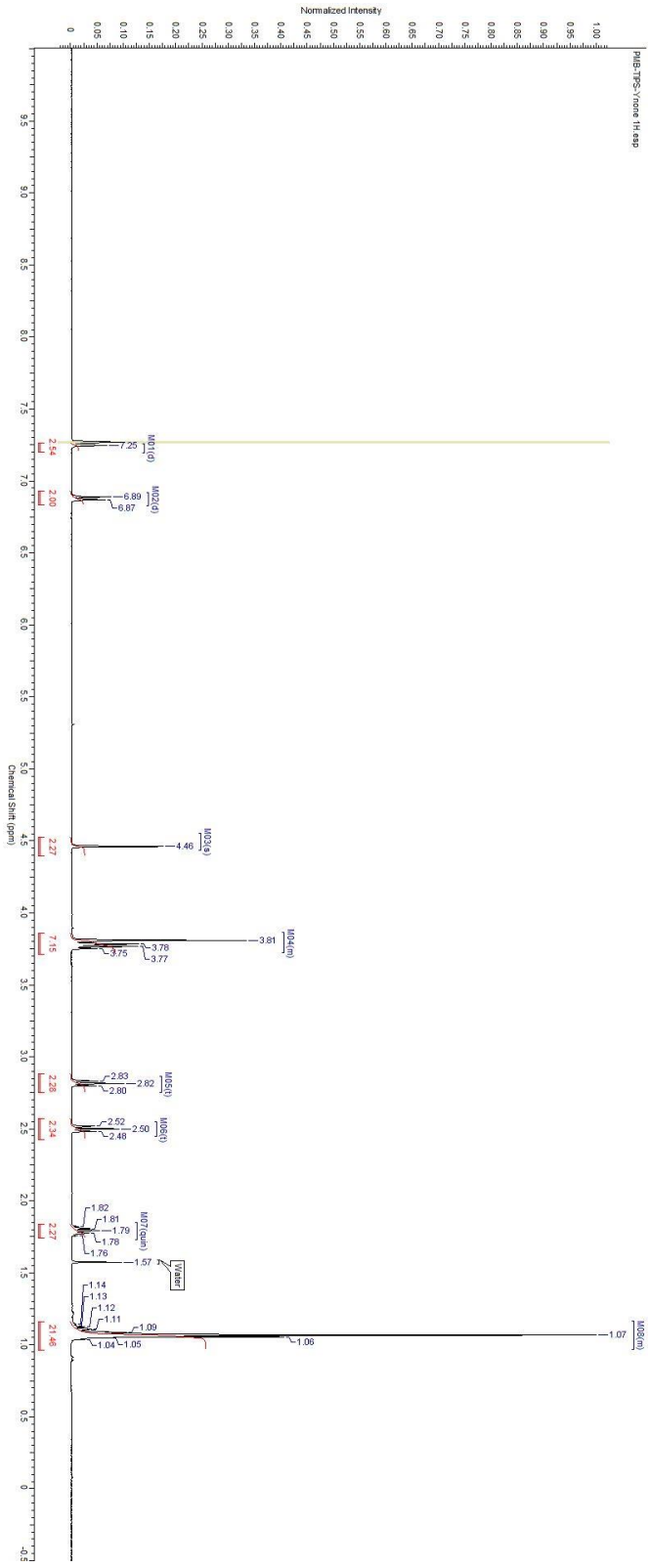

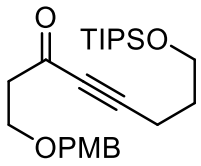

61

400 MHz, $CDCl_3$

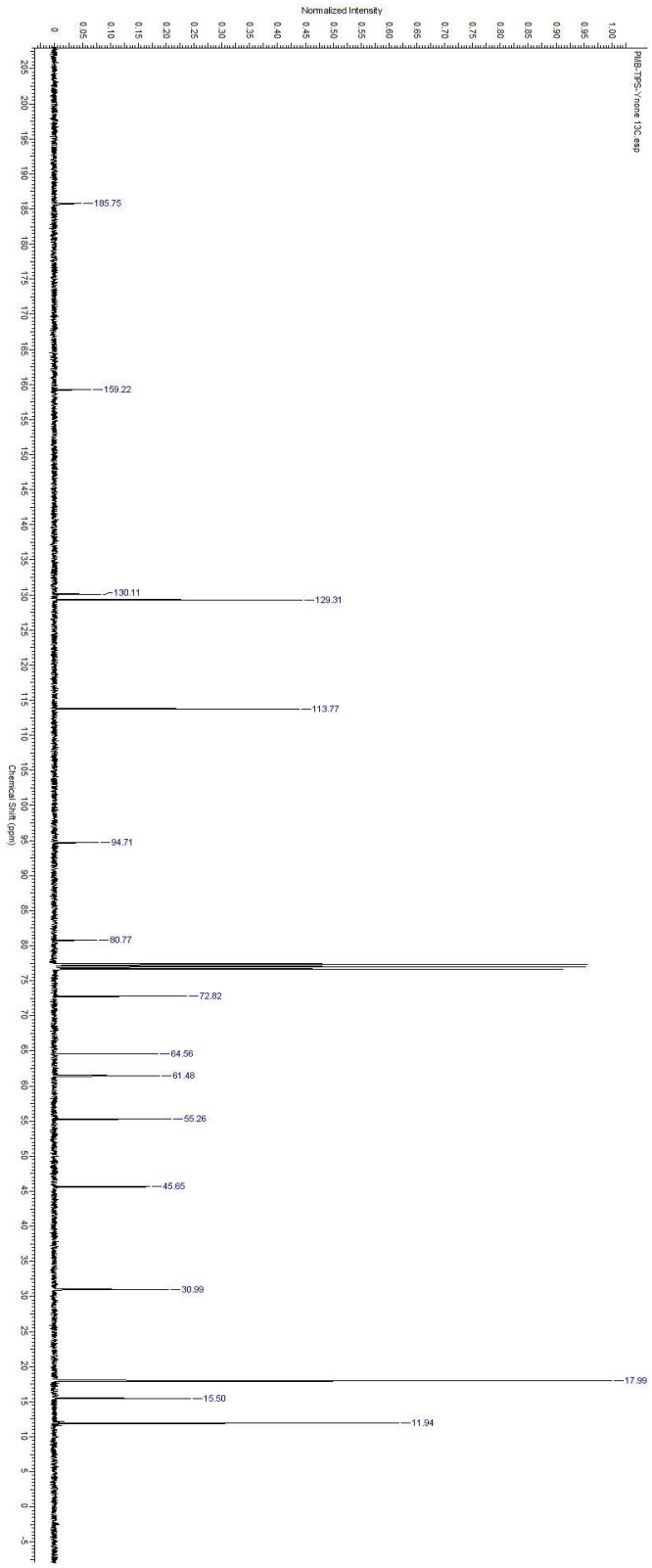

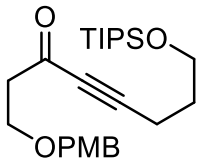

61

100 MHz, $CDCl_3$

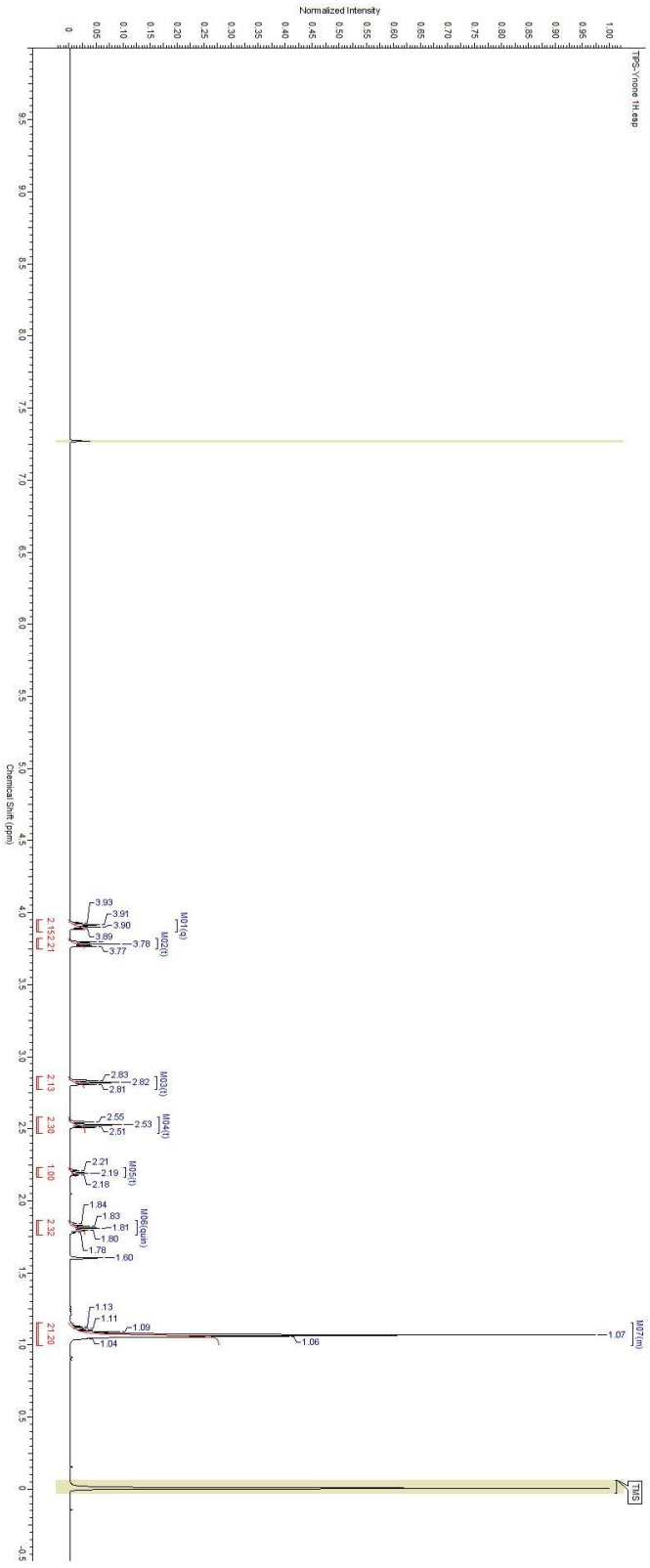

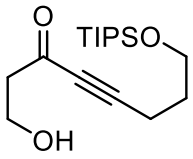

62

400 MHz, $CDCl_3$

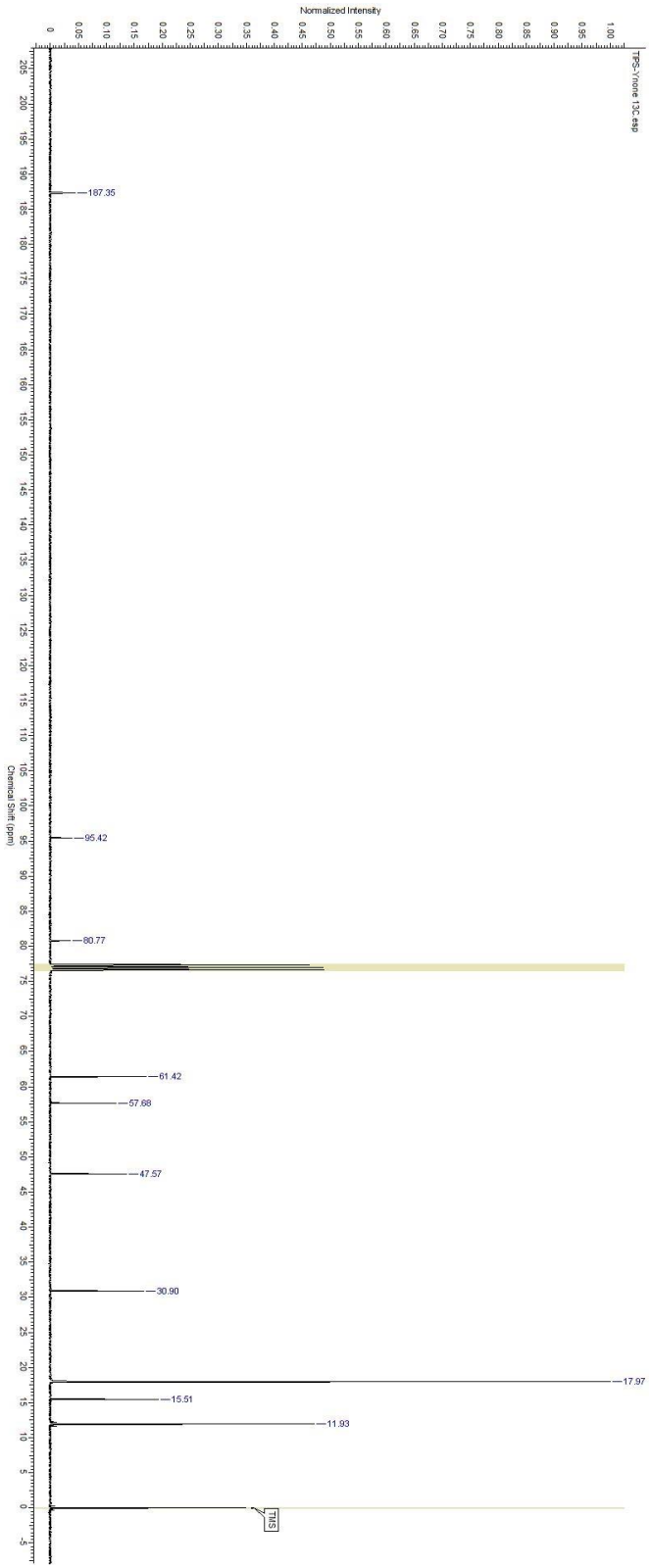

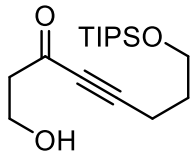

62

100 MHz, $CDCl_3$

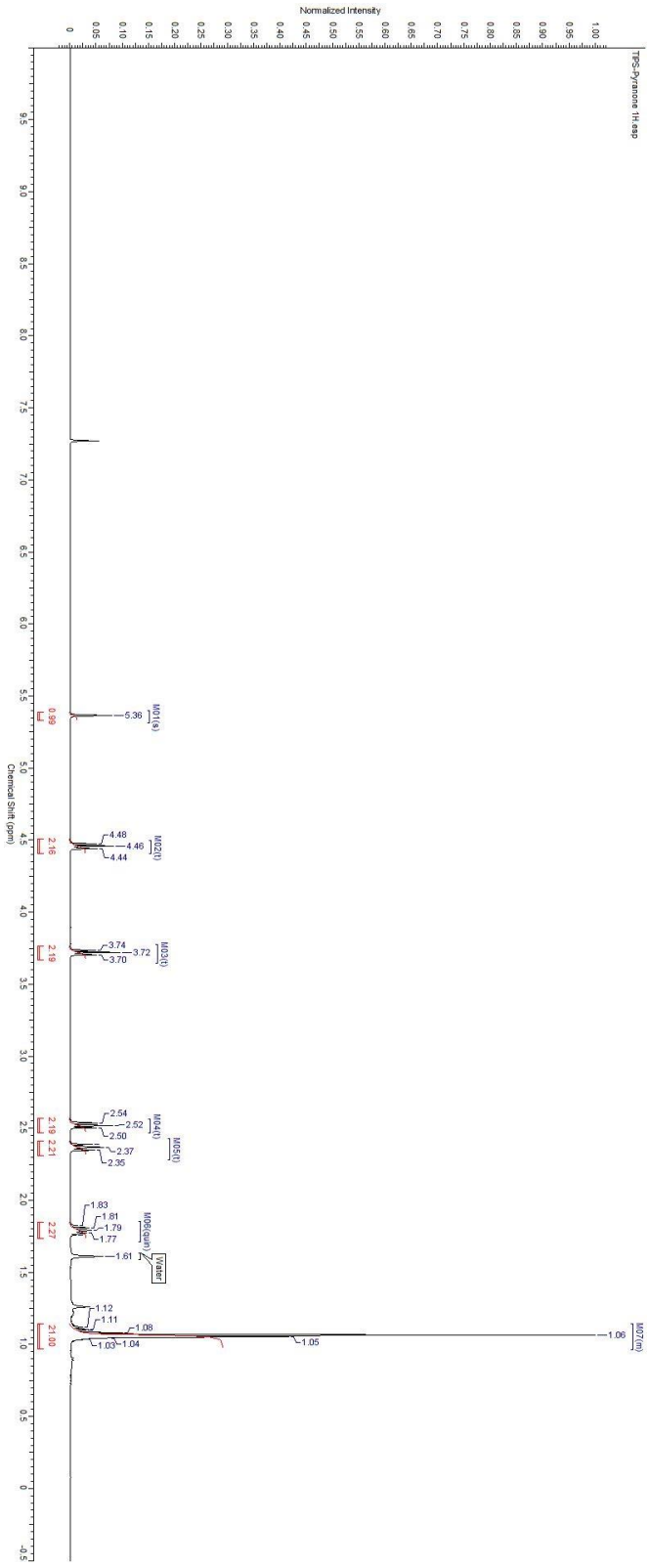

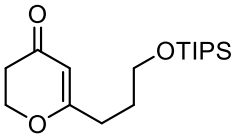

63

400 MHz, $CDCl_3$

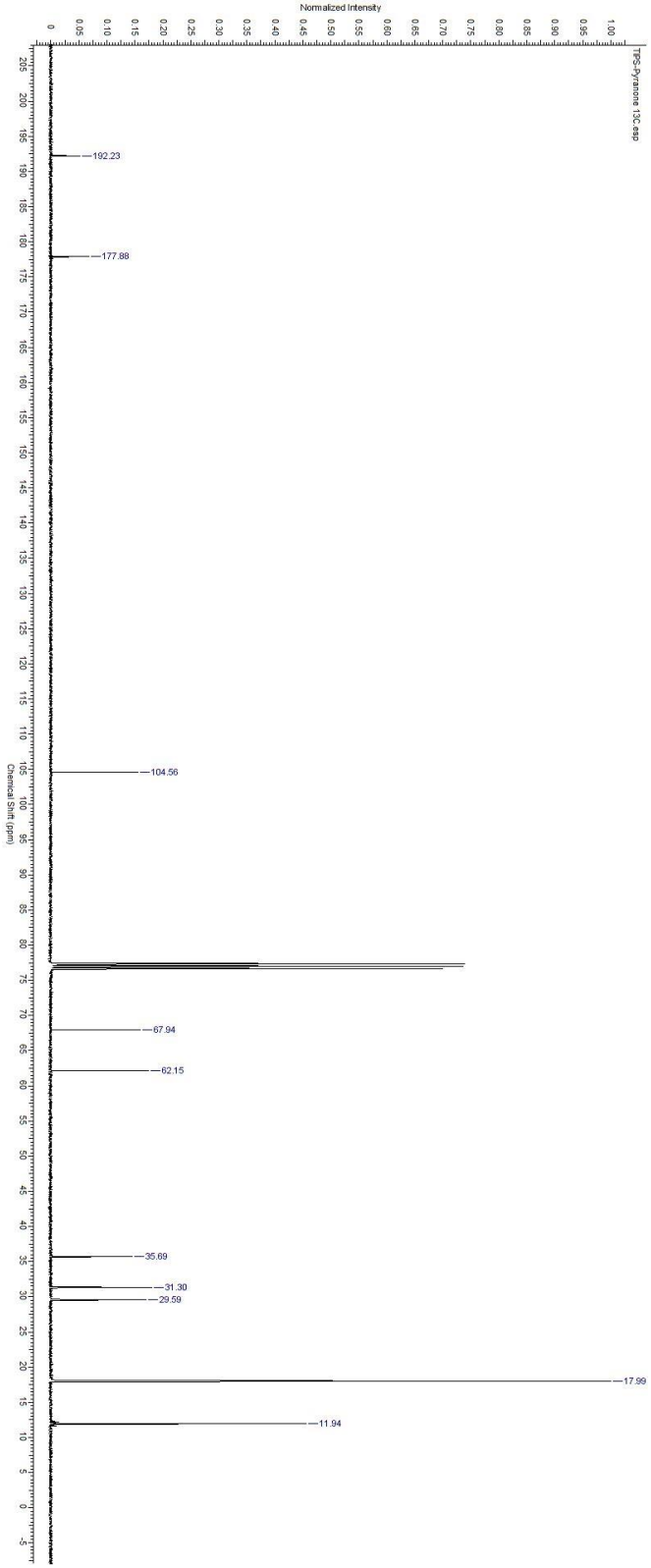

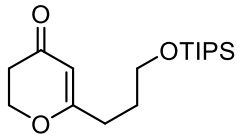

63

100 MHz, $CDCl_3$

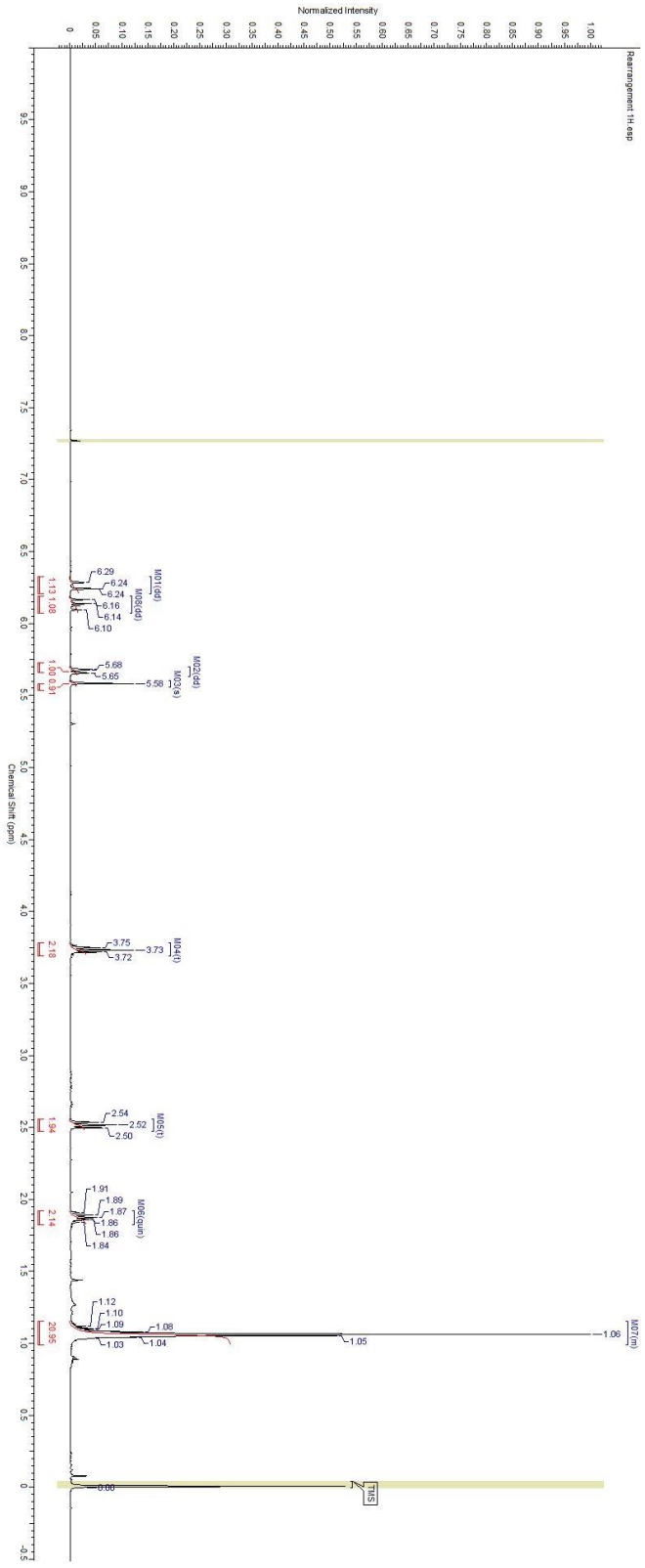

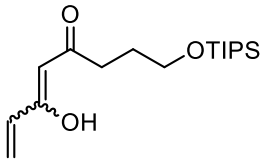

64

400 MHz, $CDCl_3$

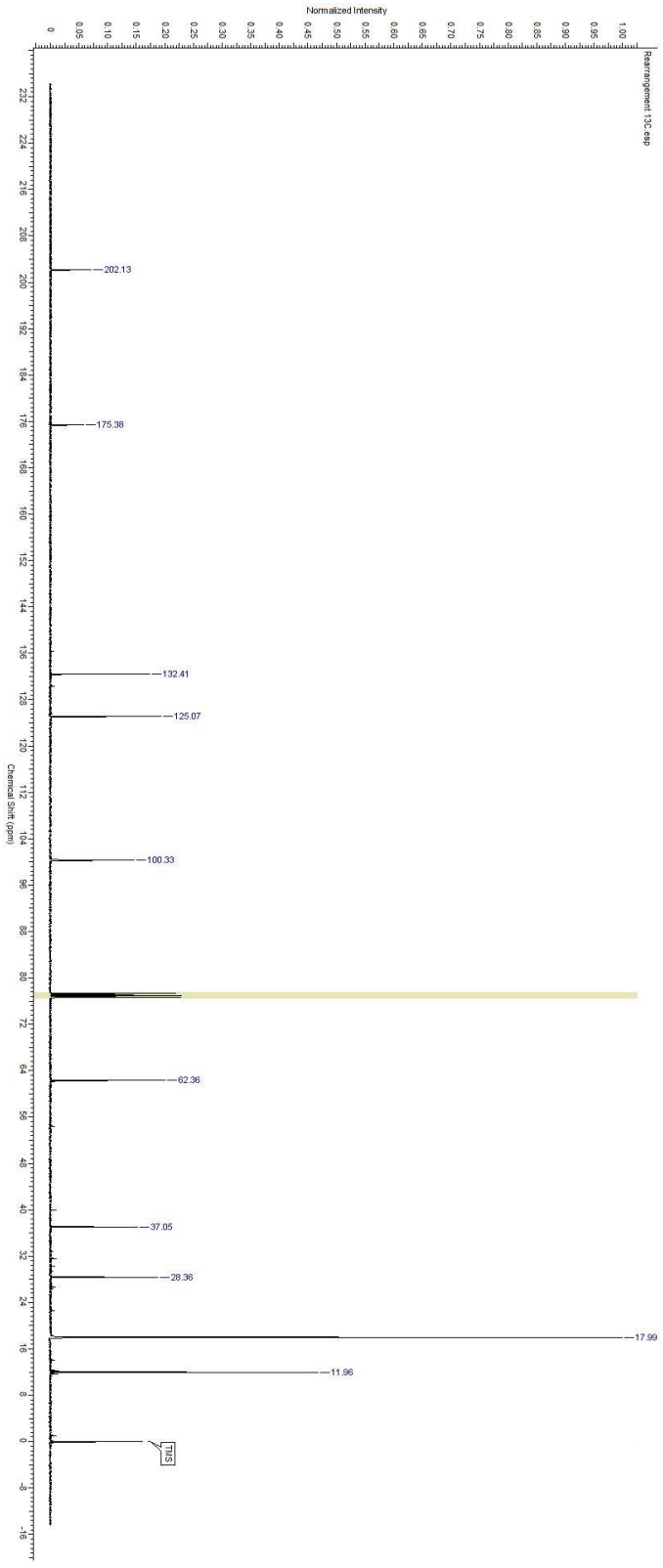

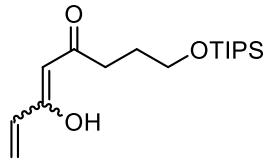

64

100 MHz, $CDCl_3$

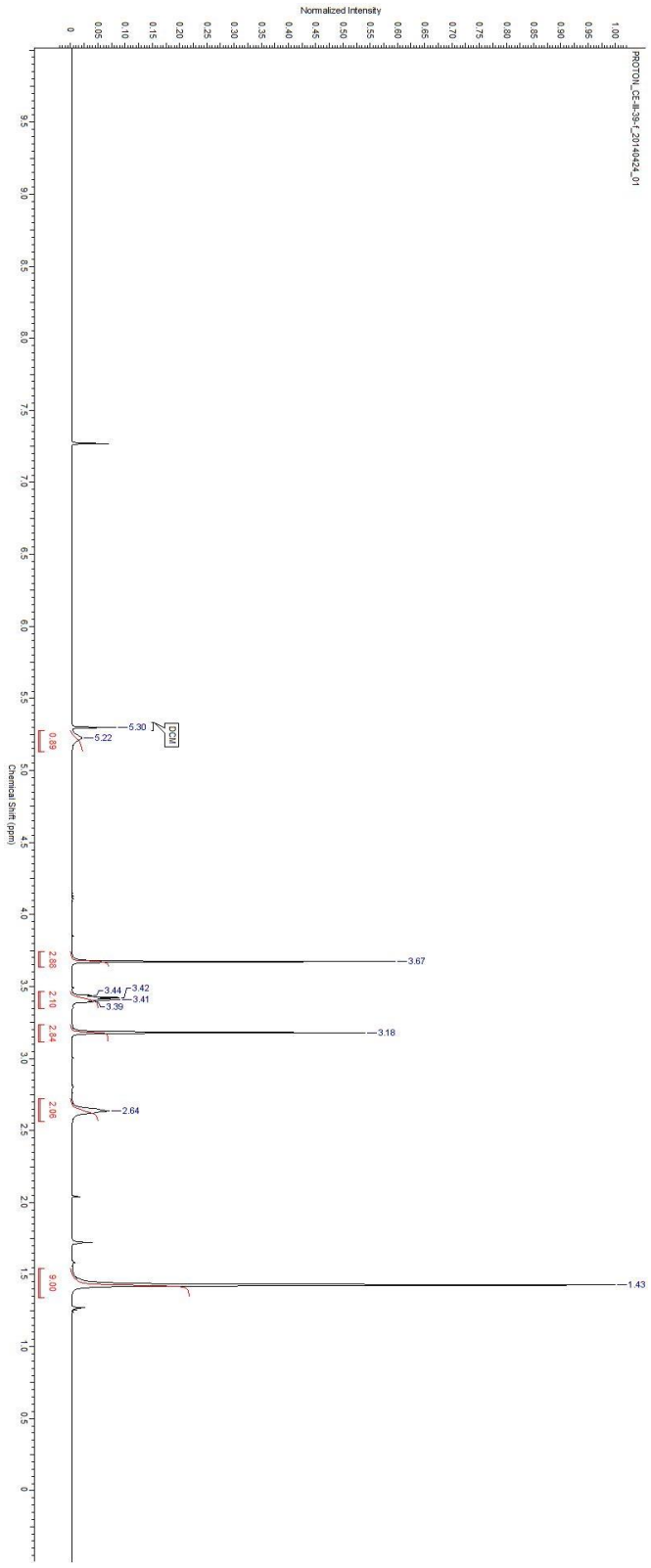

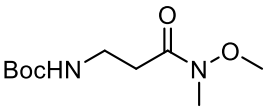

66

400 MHz, $CDCl_3$

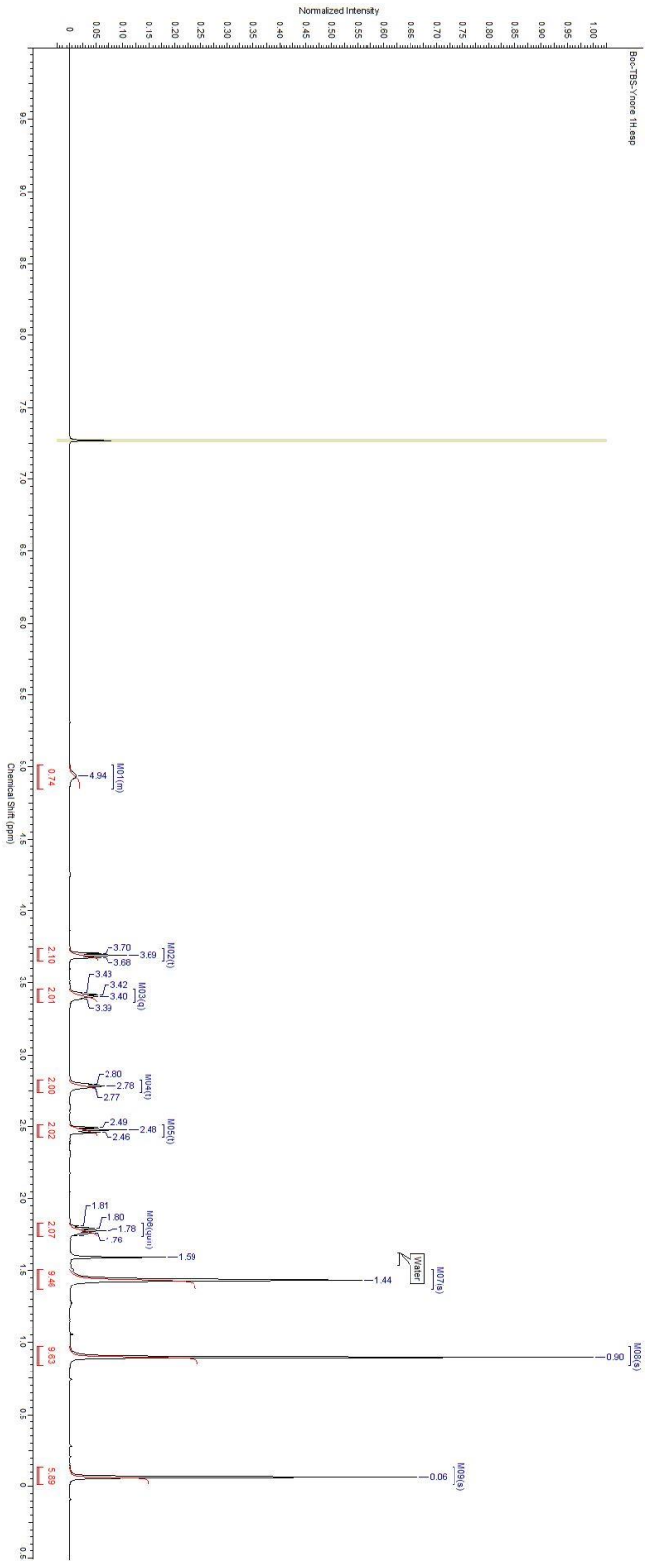

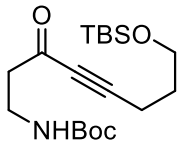

67

400 MHz, $CDCl_3$

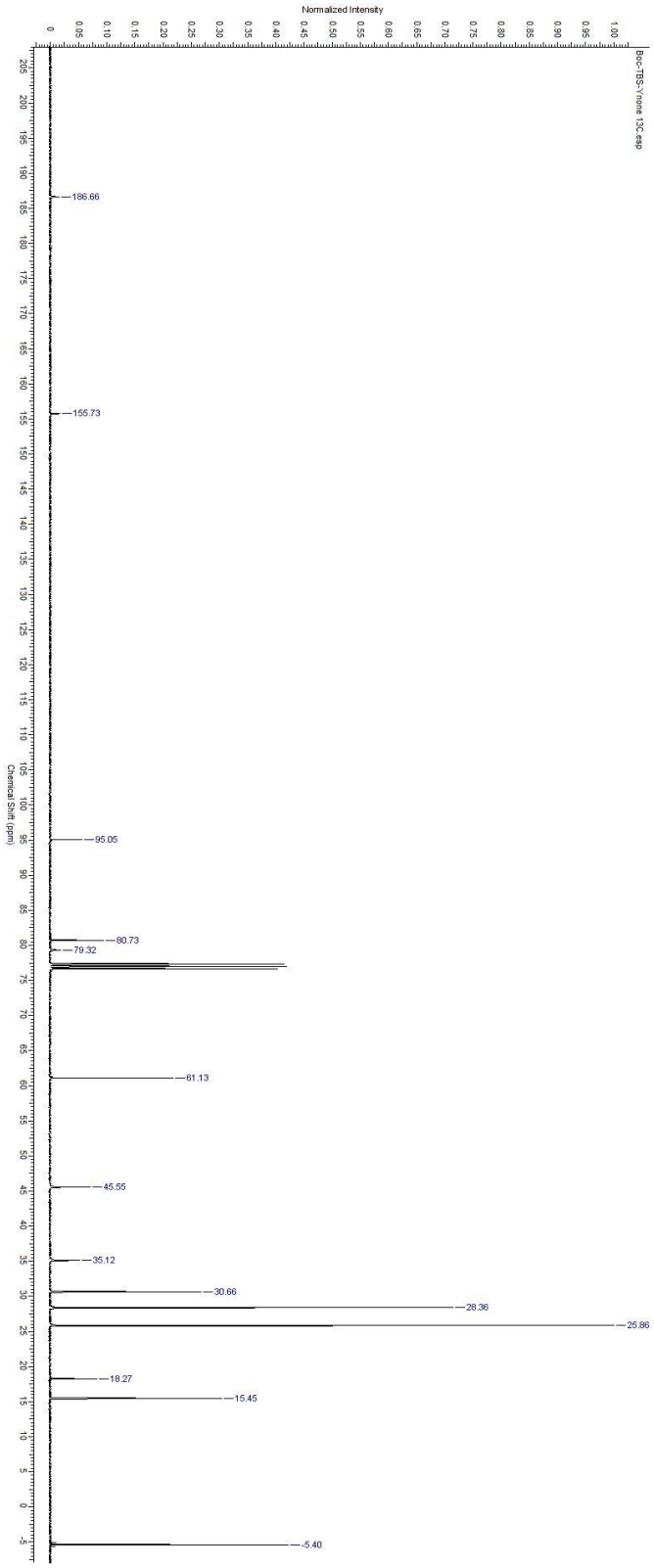

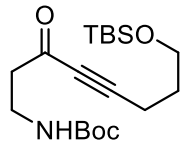

67

400 MHz, $CDCl_3$

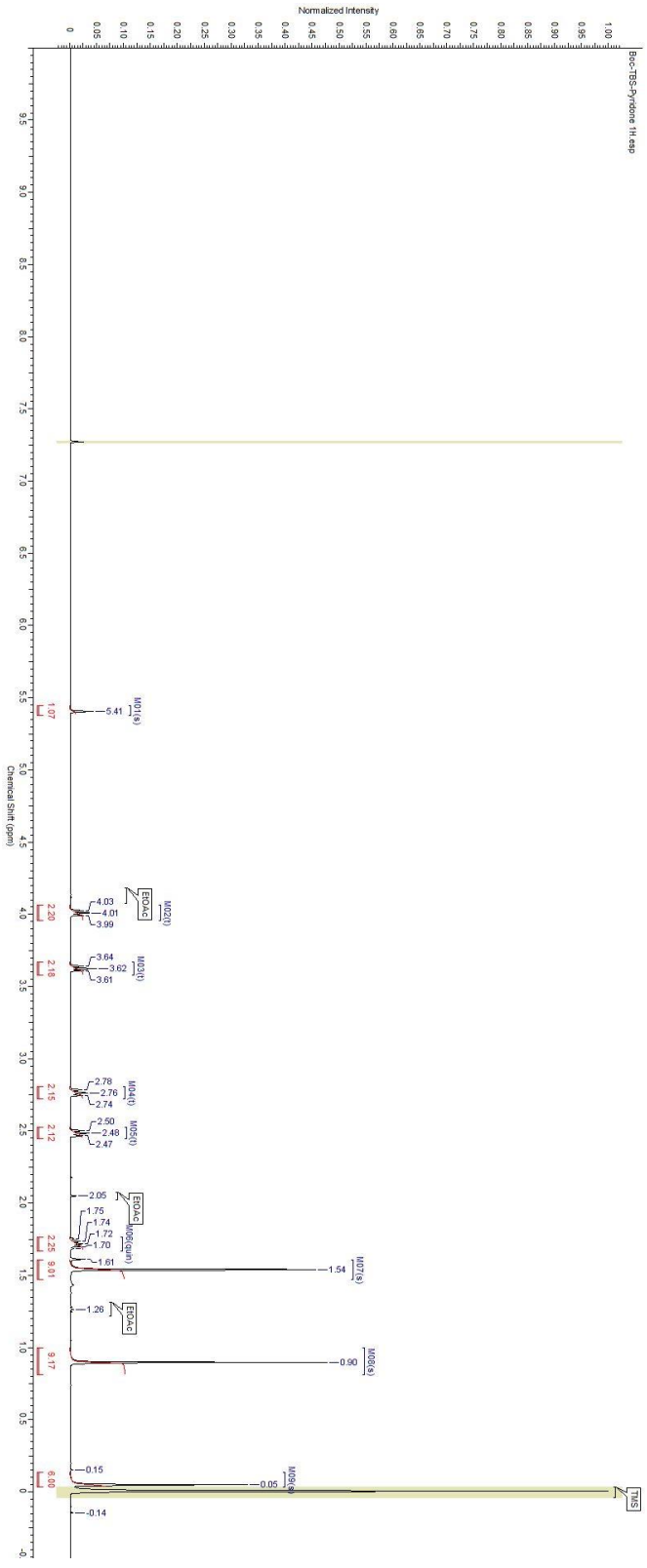

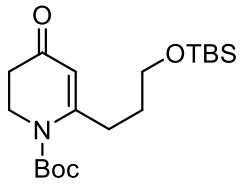

68

400 MHz, $CDCl_3$

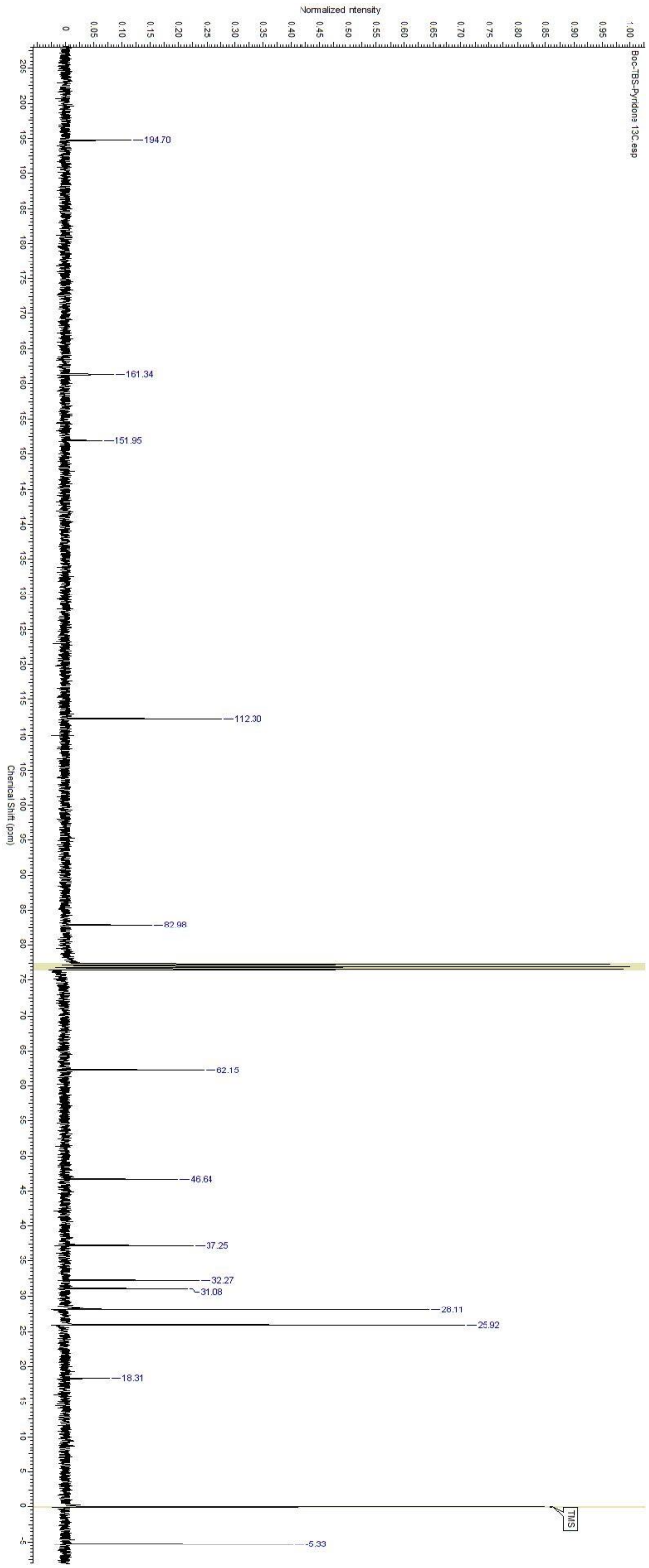

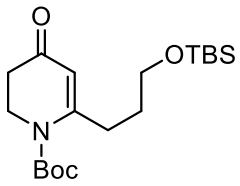

68

100 MHz, $CDCl_3$

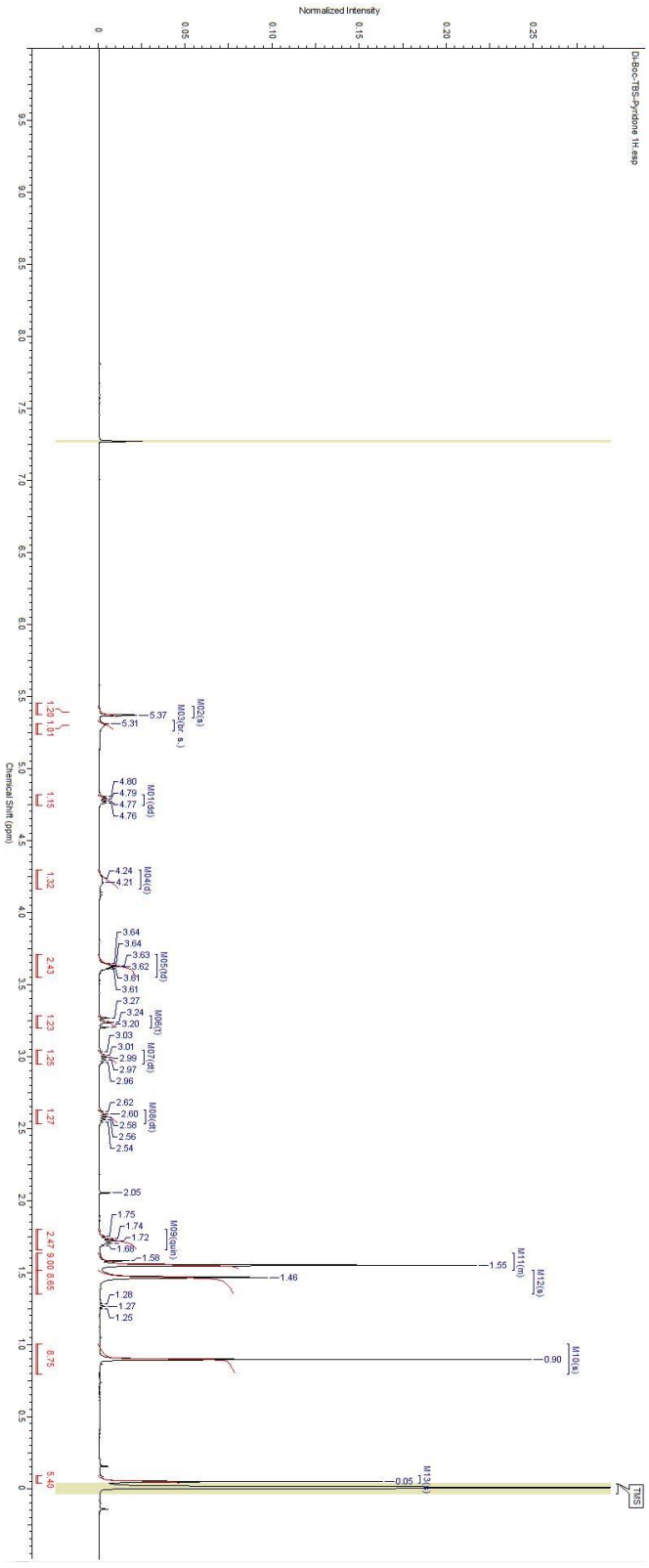

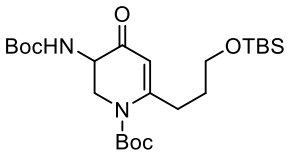

69

400 MHz, $CDCl_3$

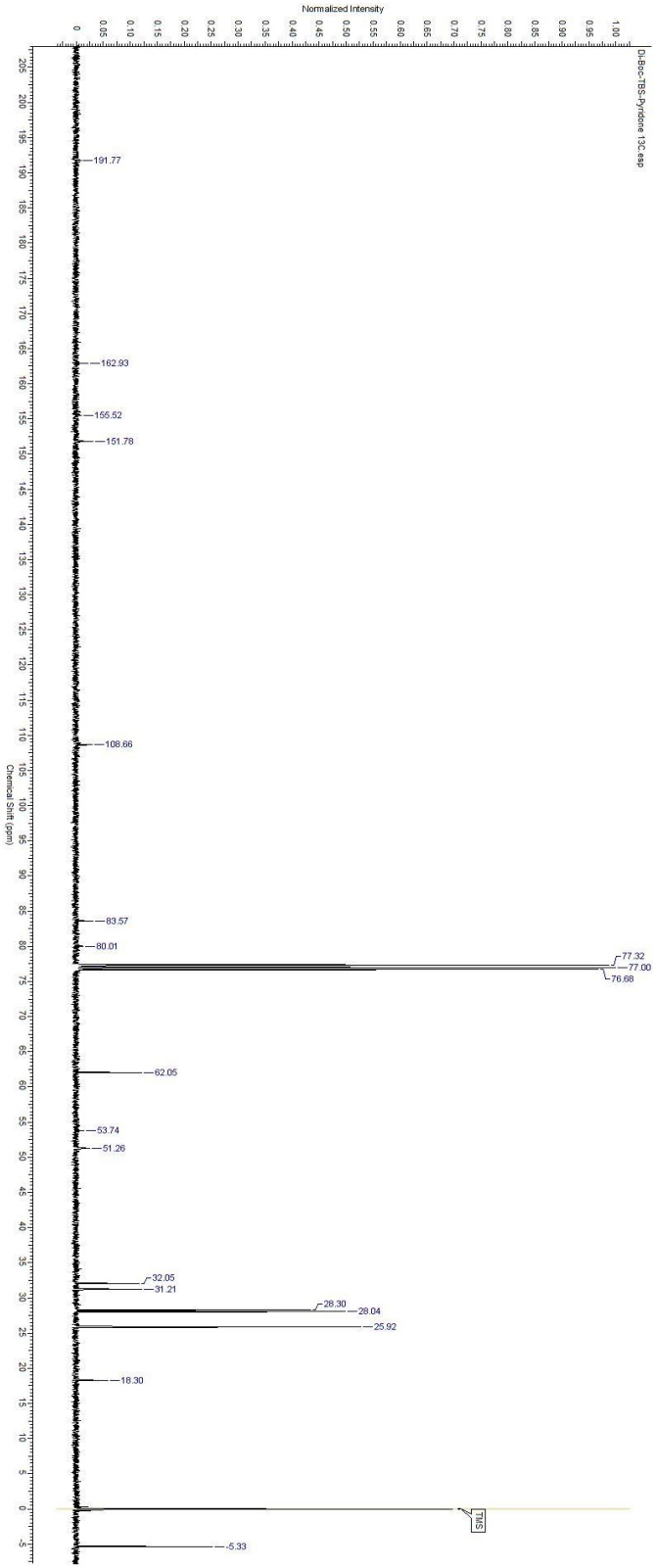

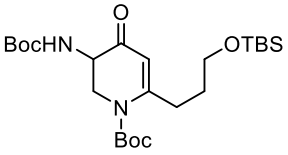

69

100 MHz, $CDCl_3$

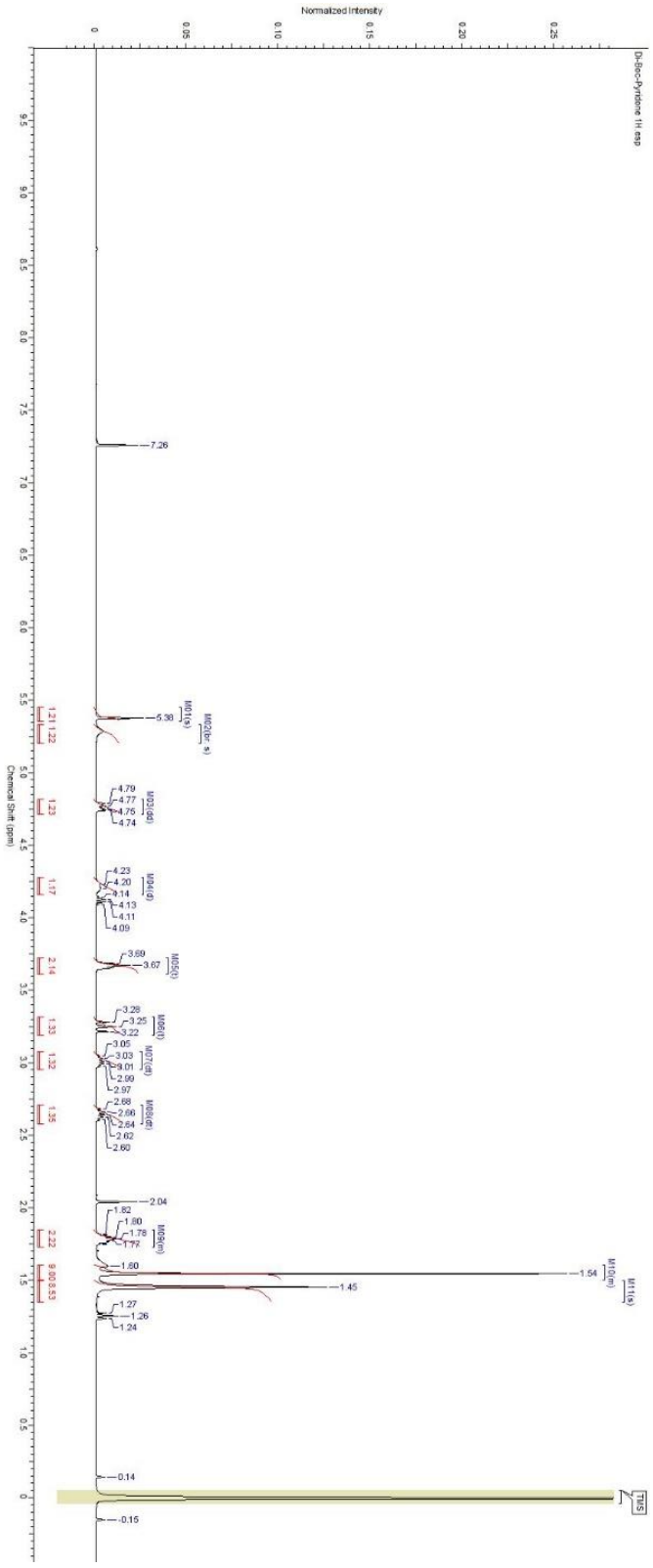

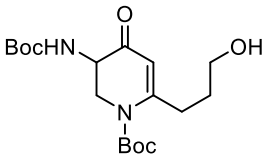

70

400 MHz, $CDCl_3$

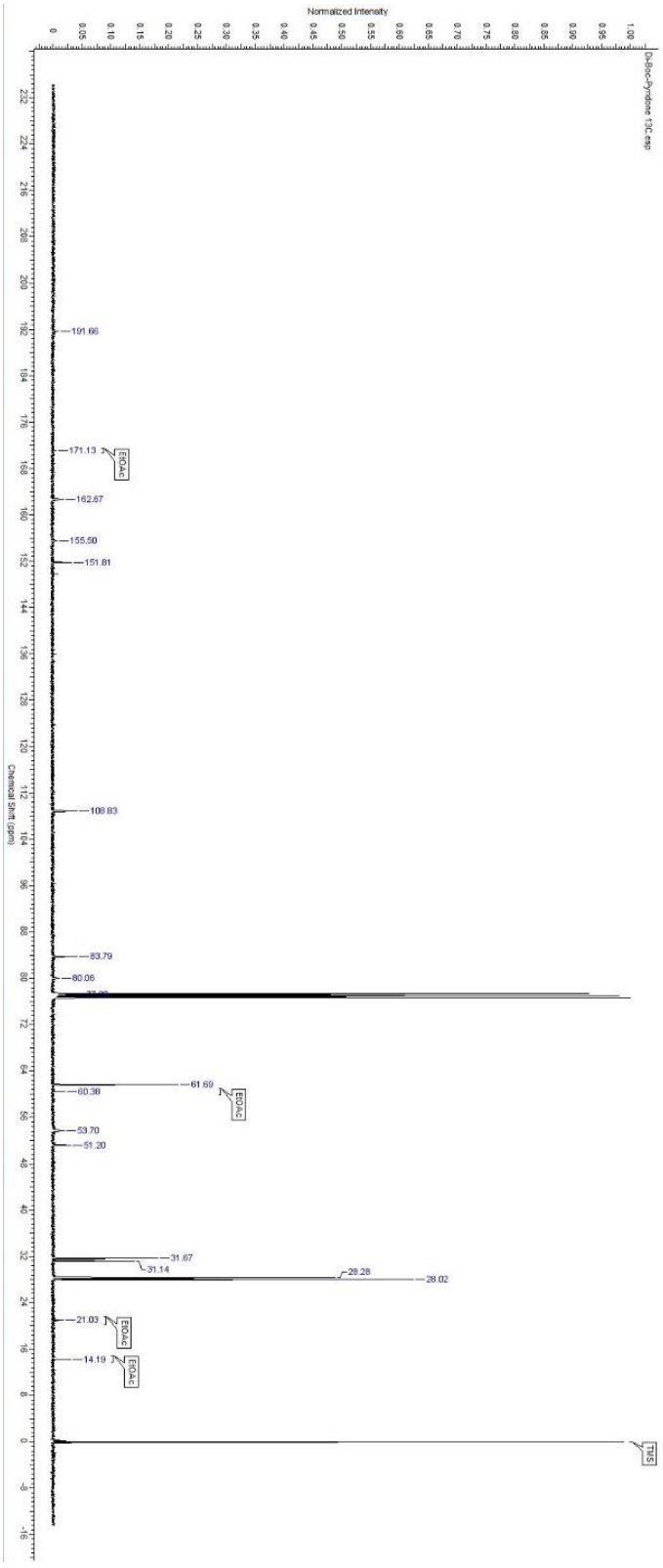

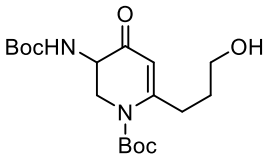

70

100 MHz, $CDCl_3$

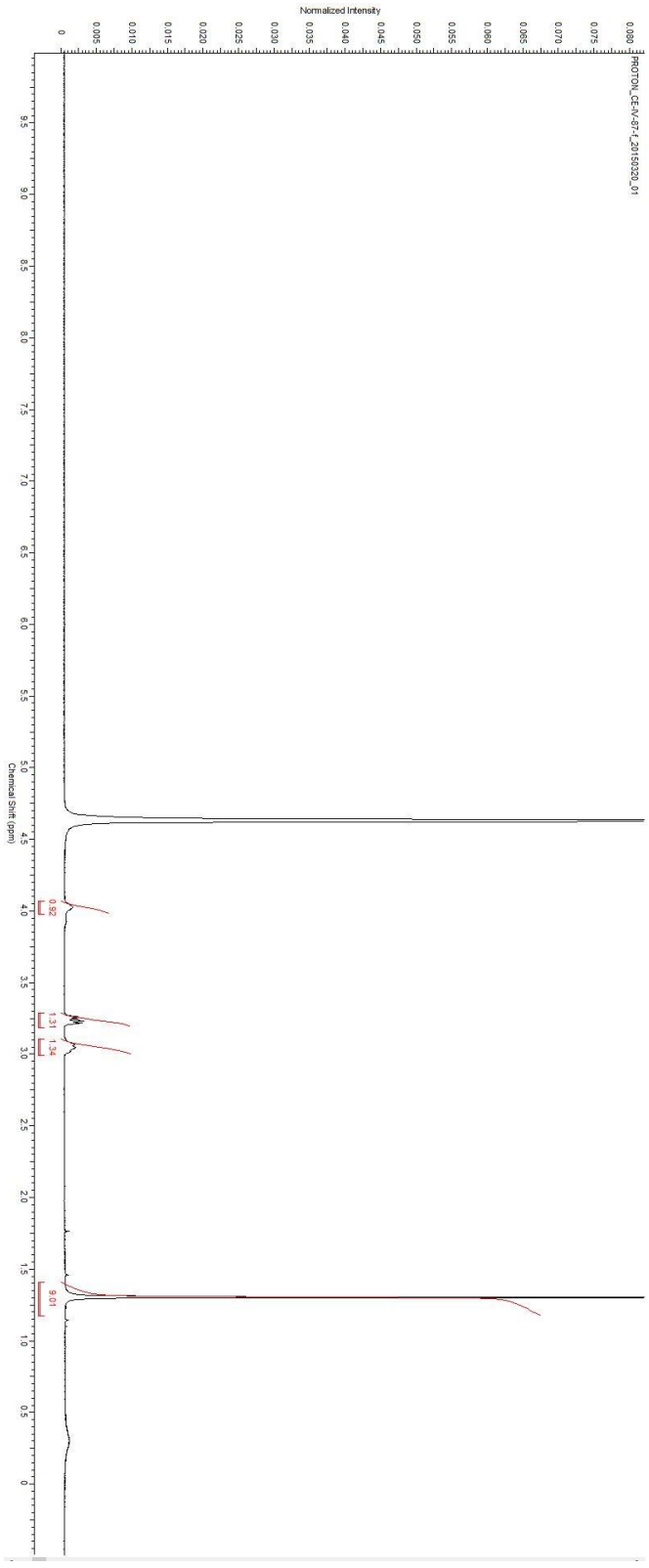

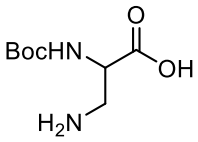

72

400 MHz, D_2O

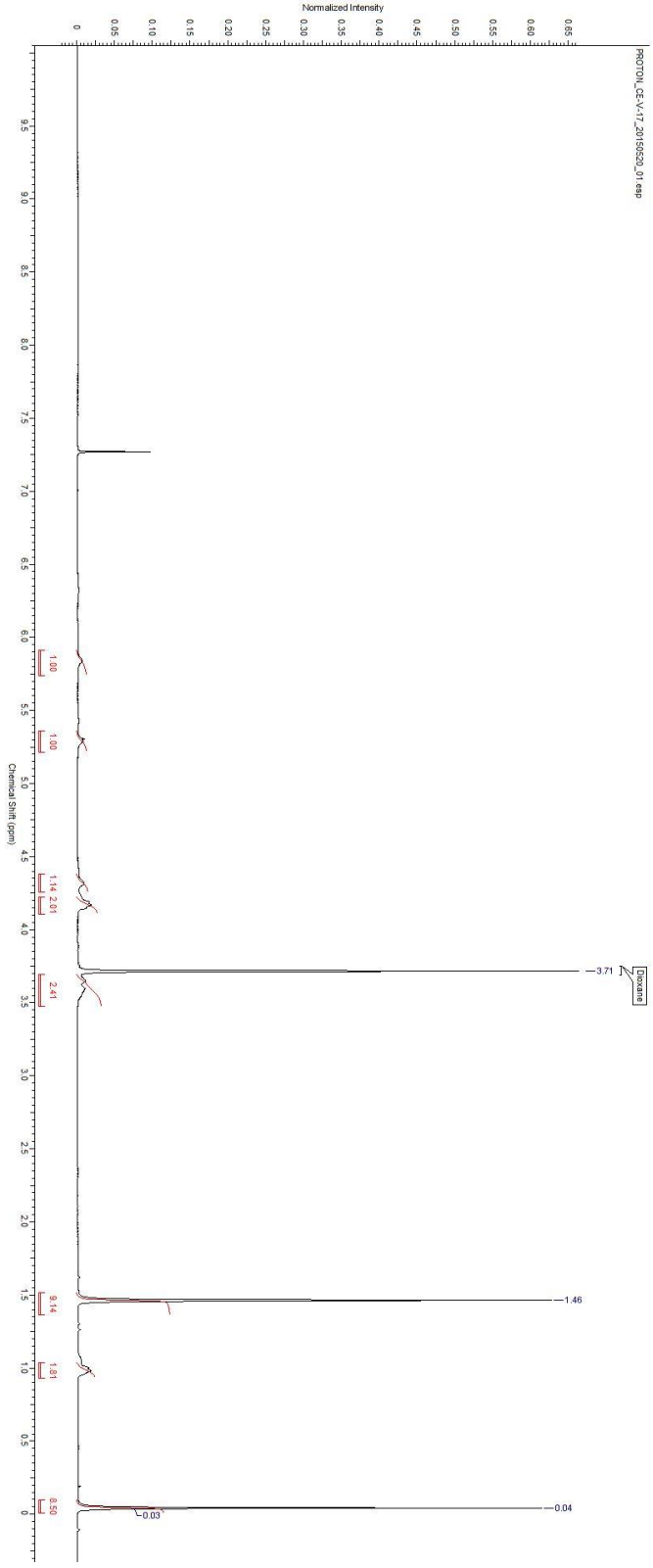

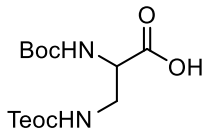

73

400 MHz, $CDCl_3$

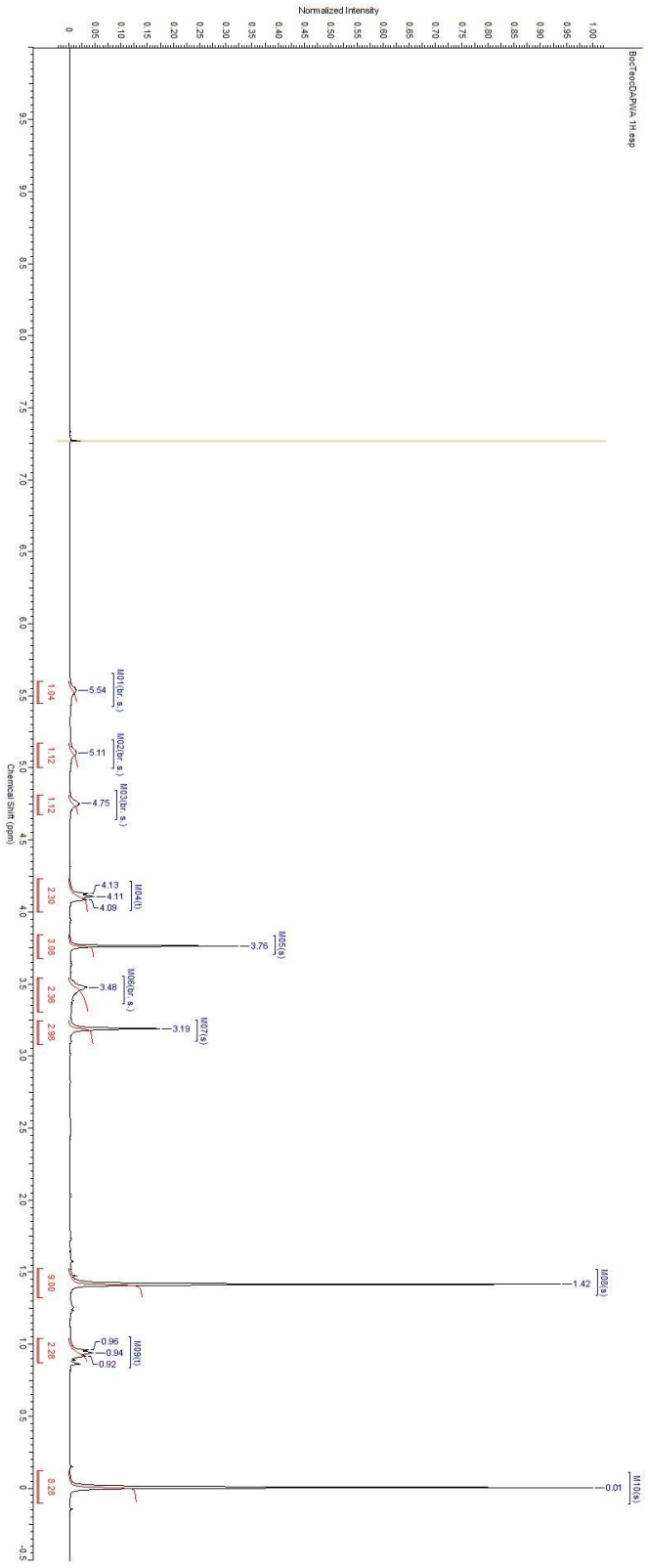

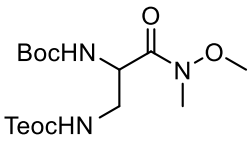

74

400 MHz, $CDCl_3$

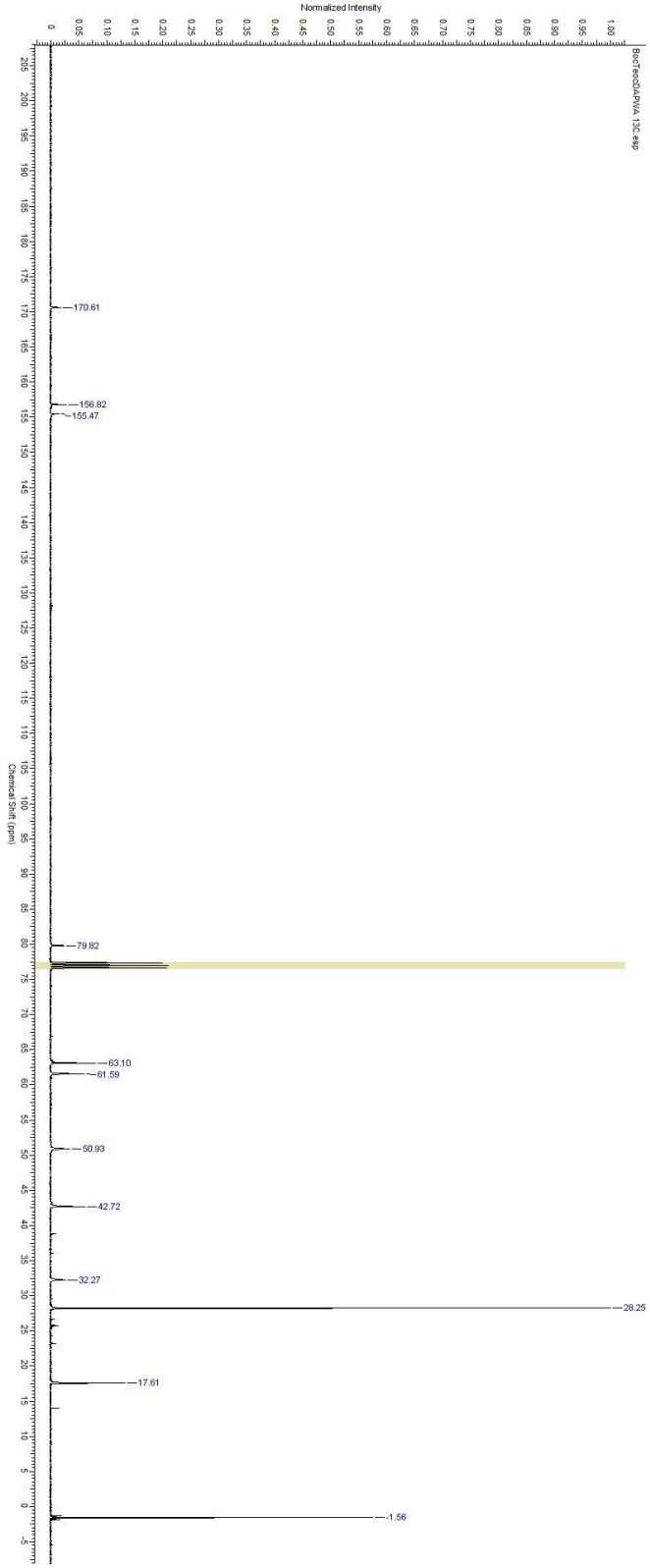

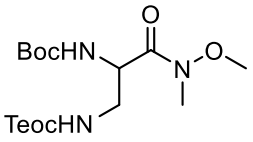

74

400 MHz, $CDCl_3$

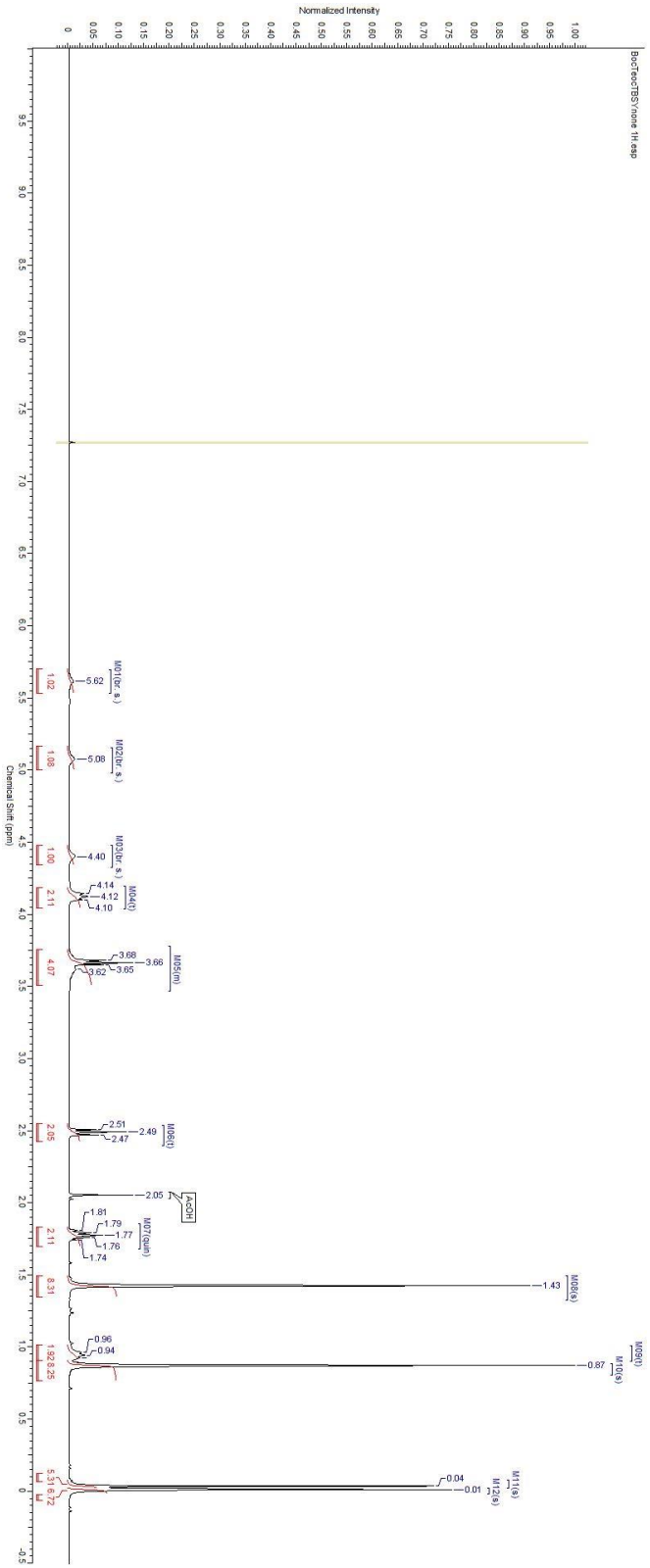

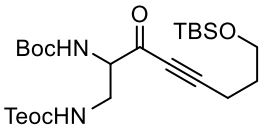

75

400 MHz, $CDCl_3$

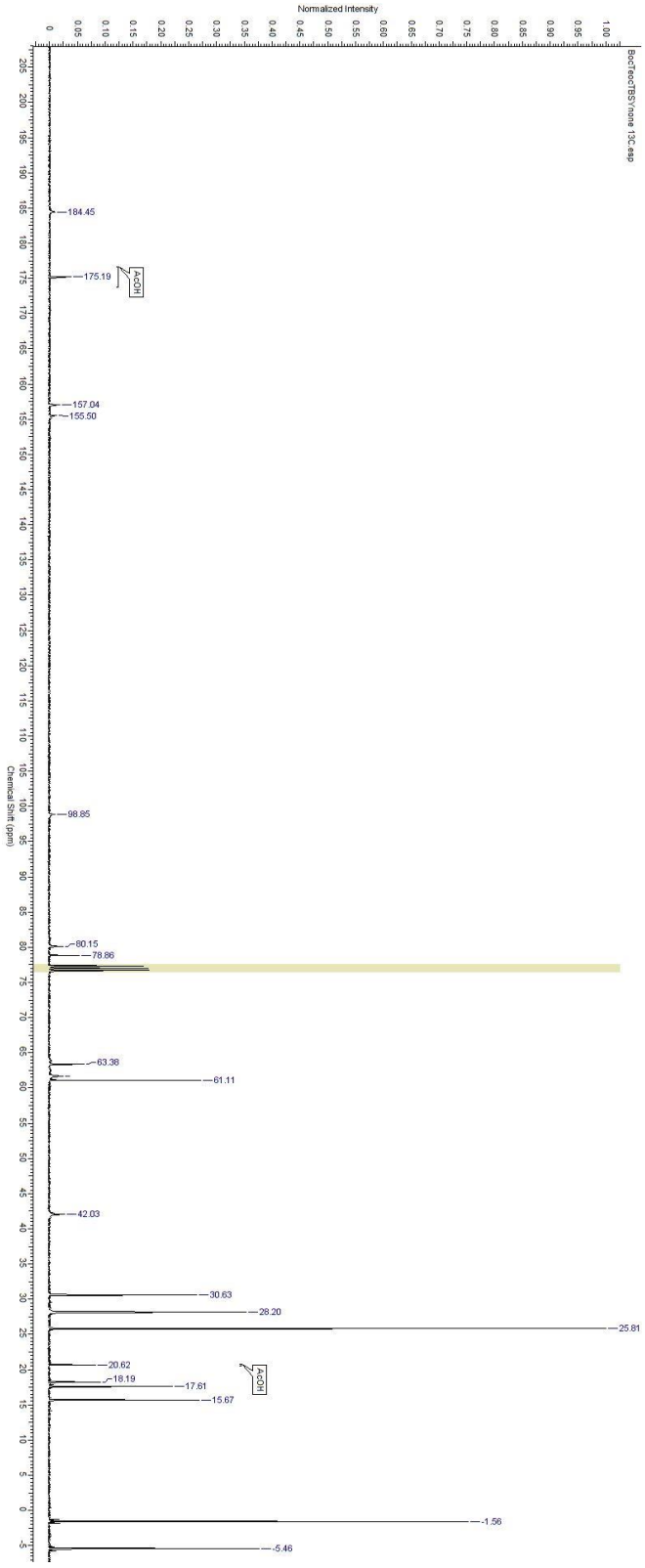

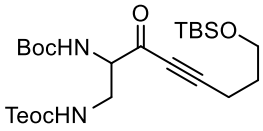

75

100 MHz, $CDCl_3$

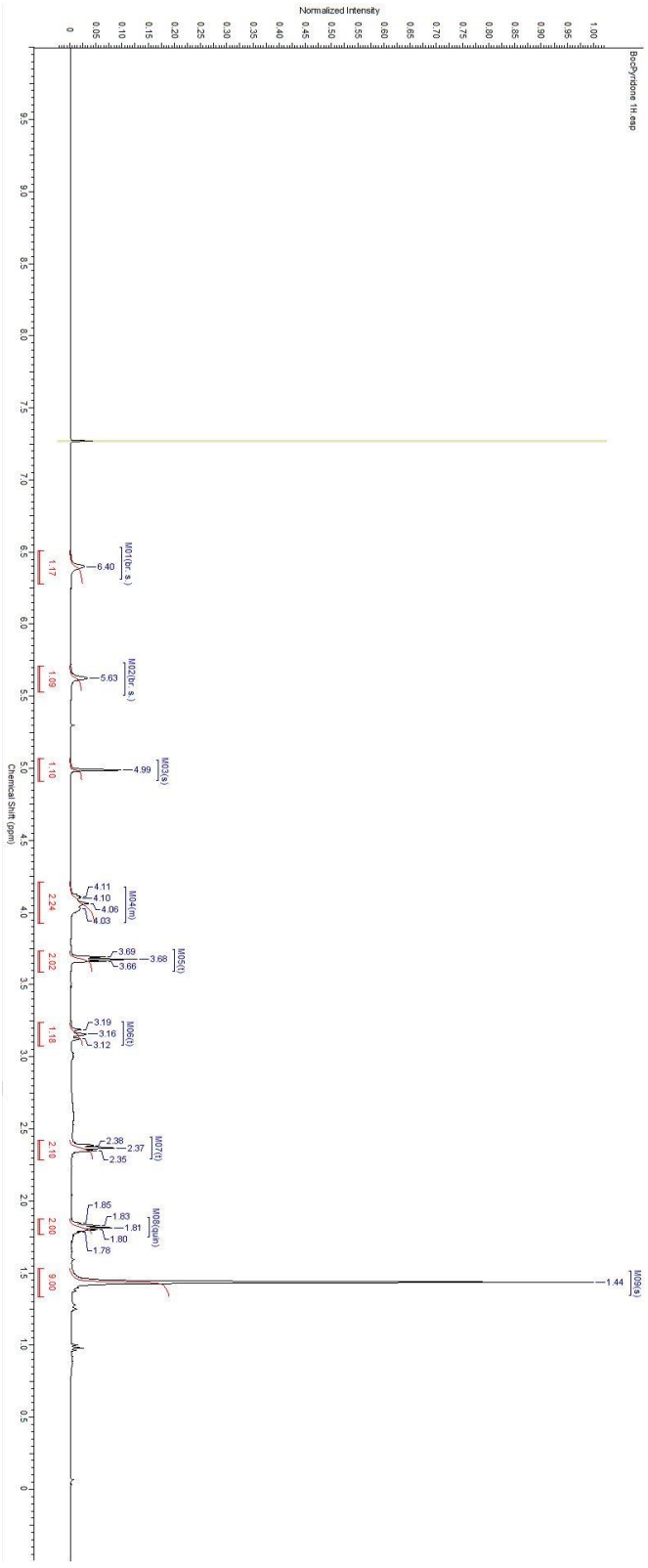

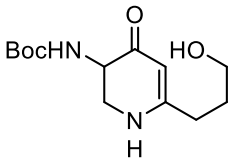

76

400 MHz, $CDCl_3$

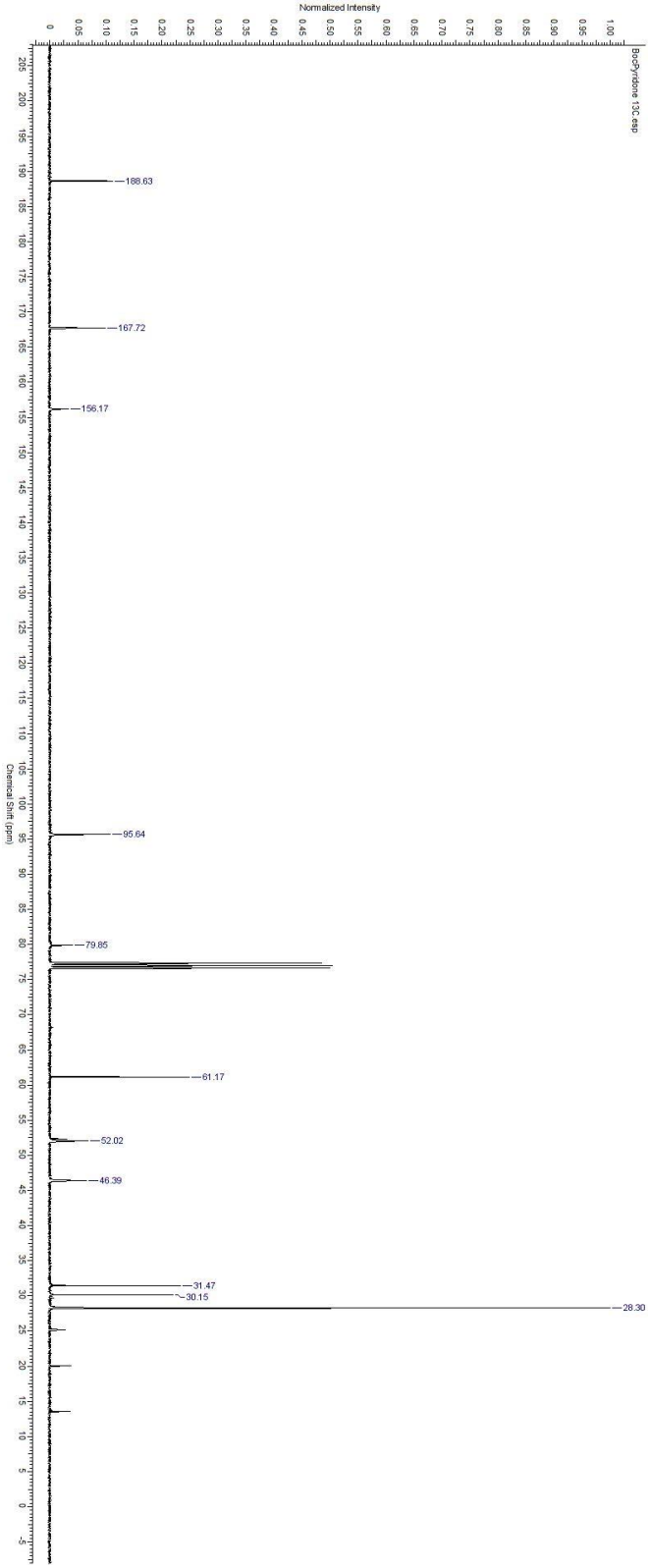

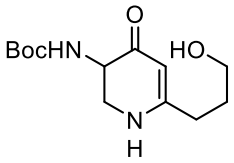

76

100 MHz, $CDCl_3$

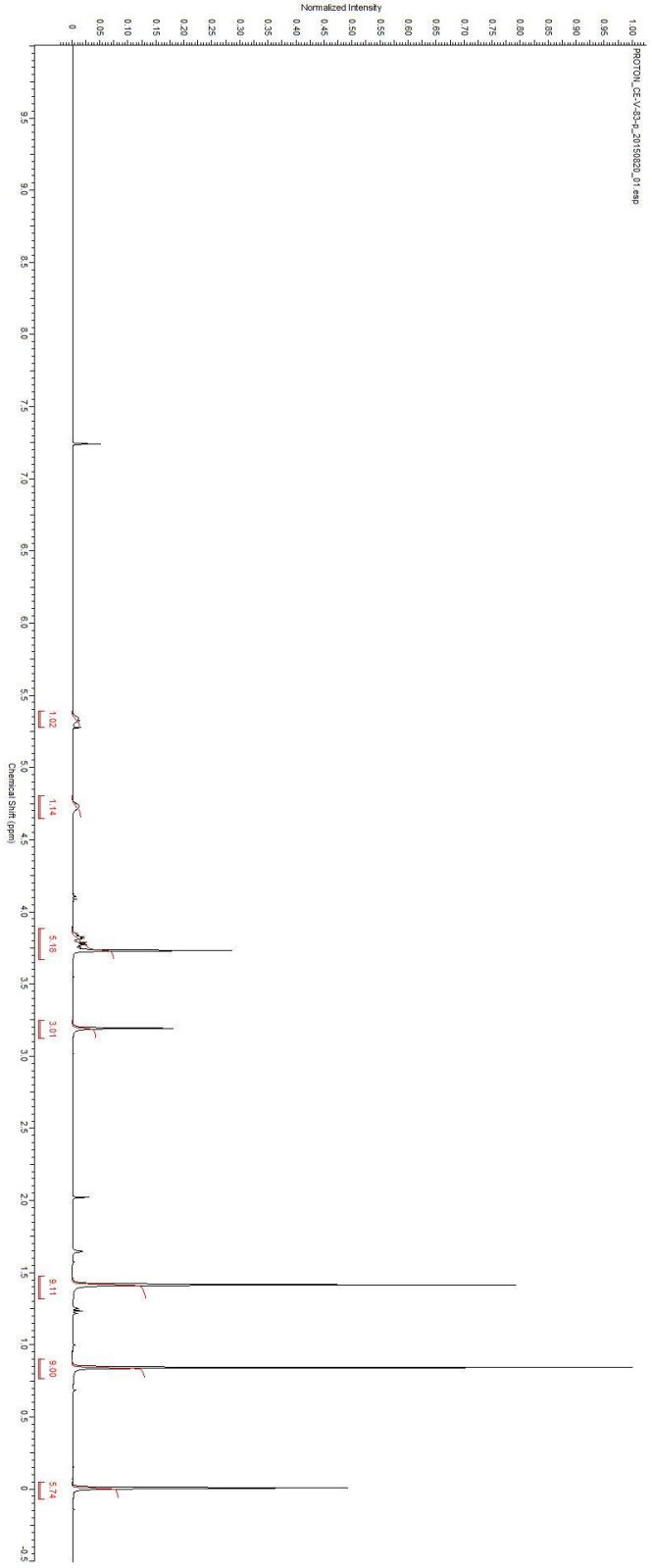

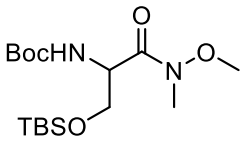

77

400 MHz, $CDCl_3$

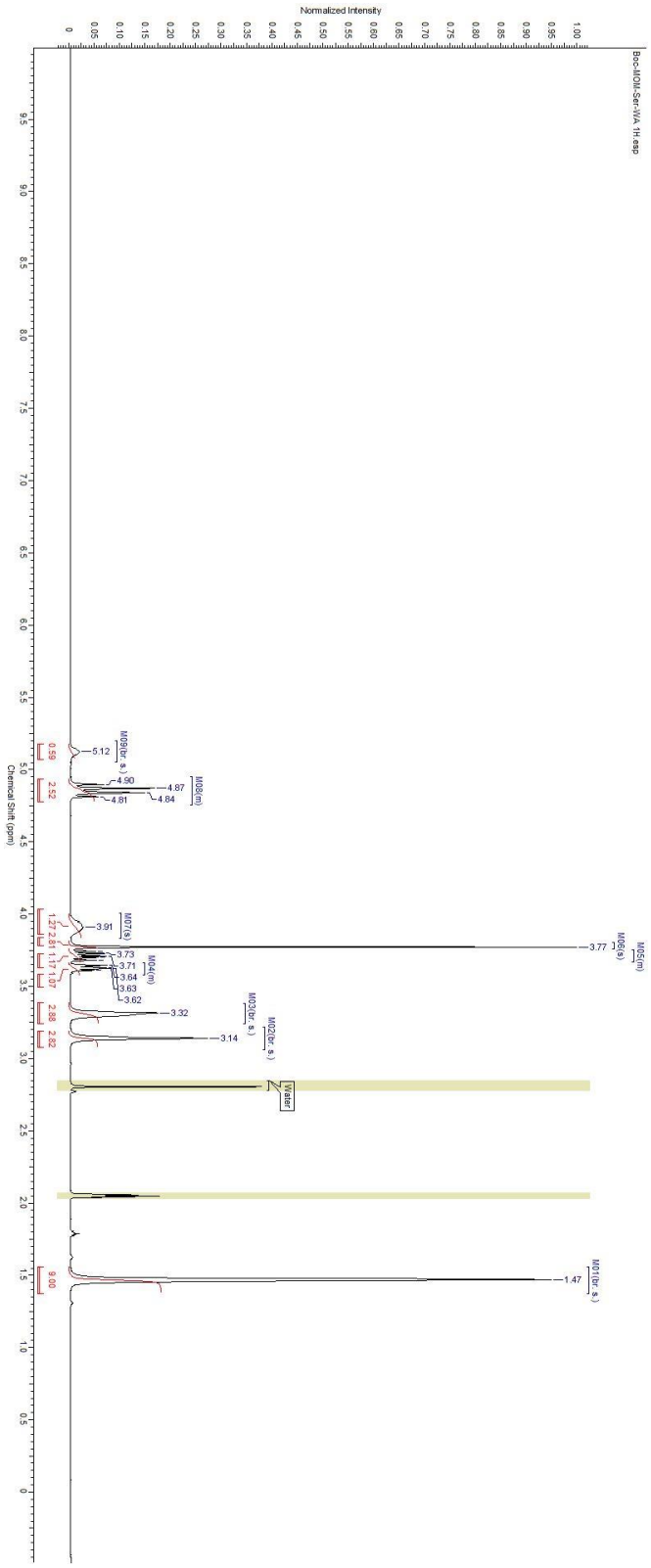

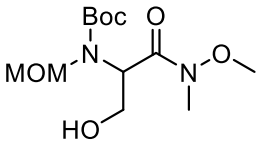

78

400 MHz, $(CD_3)_2CO$

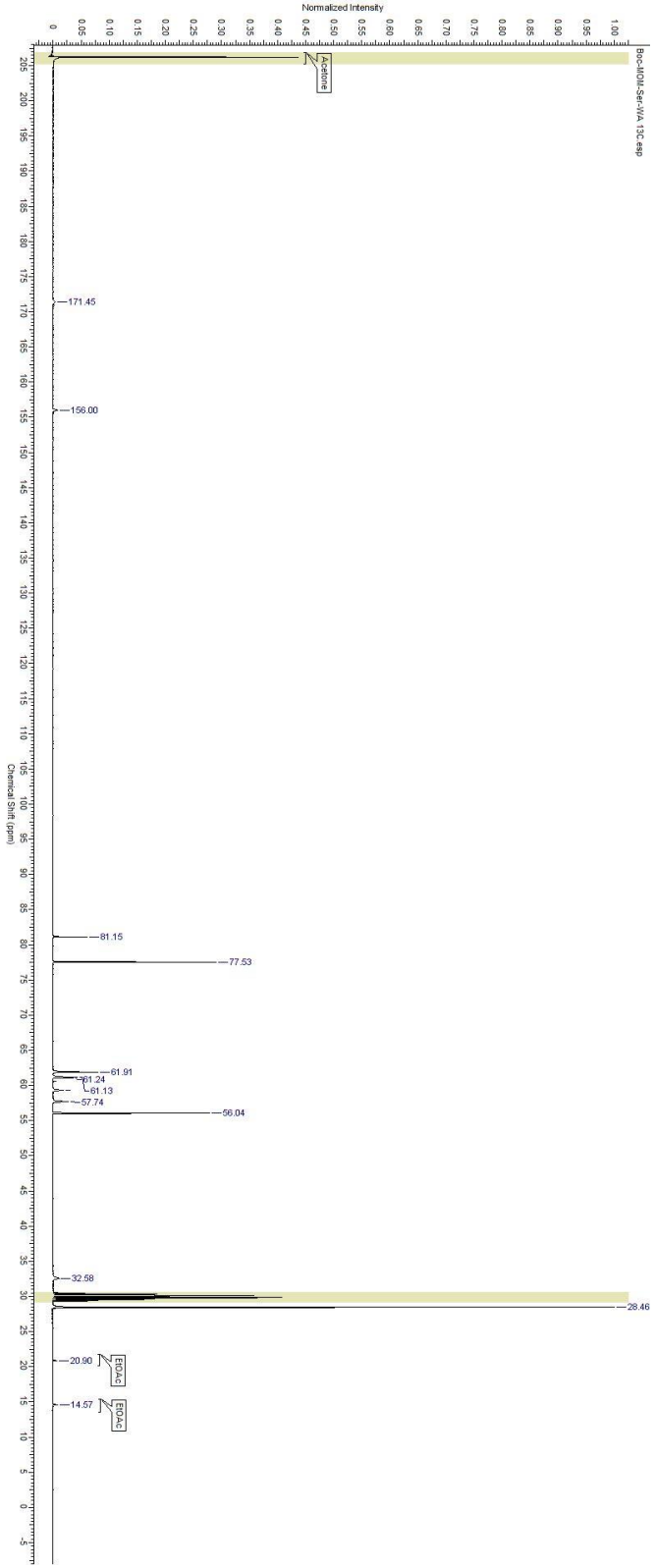

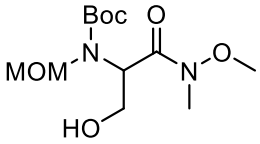

78

100 MHz, $(CD_3)_2CO$

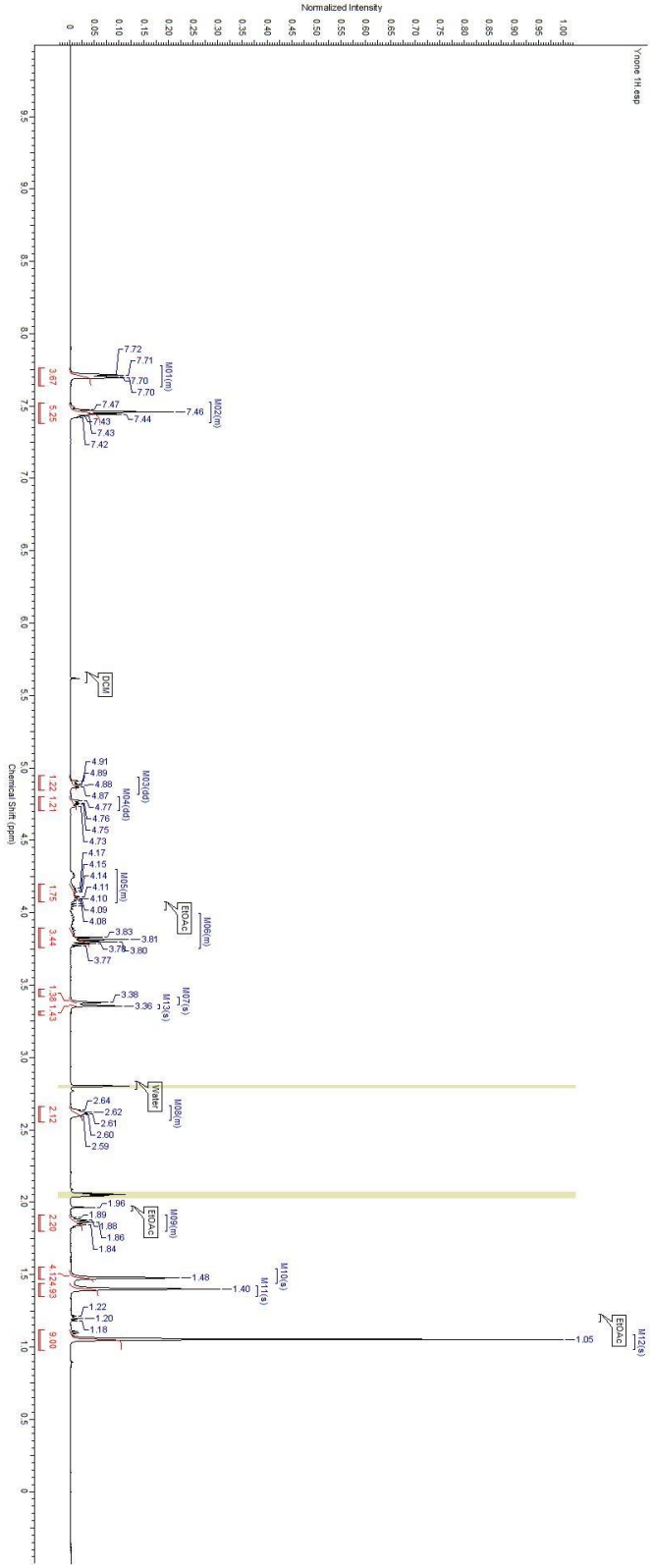

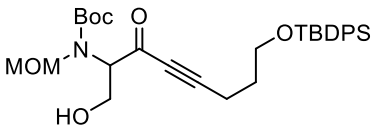

79

400 MHz, $(CD_3)_2CO$

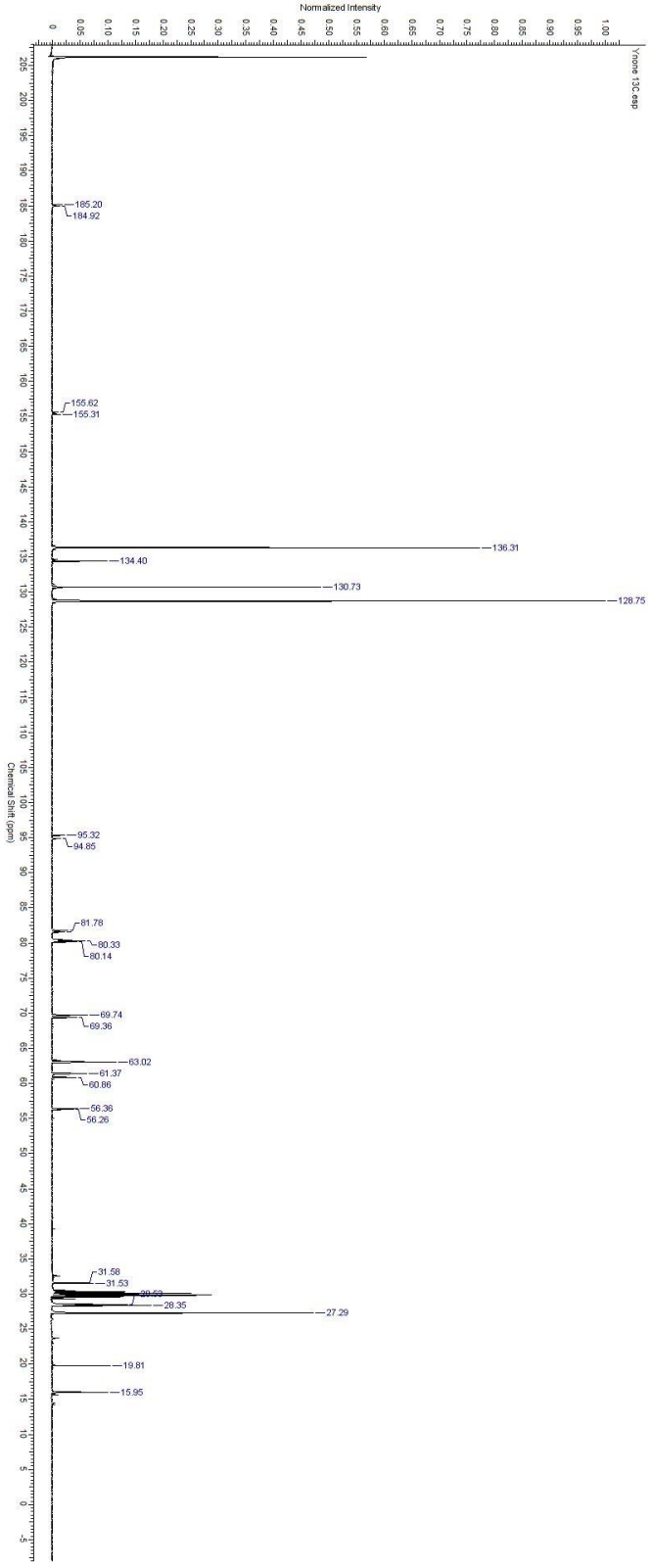

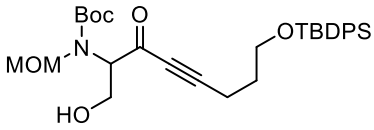

79

100 MHz, $(CD_3)_2CO$

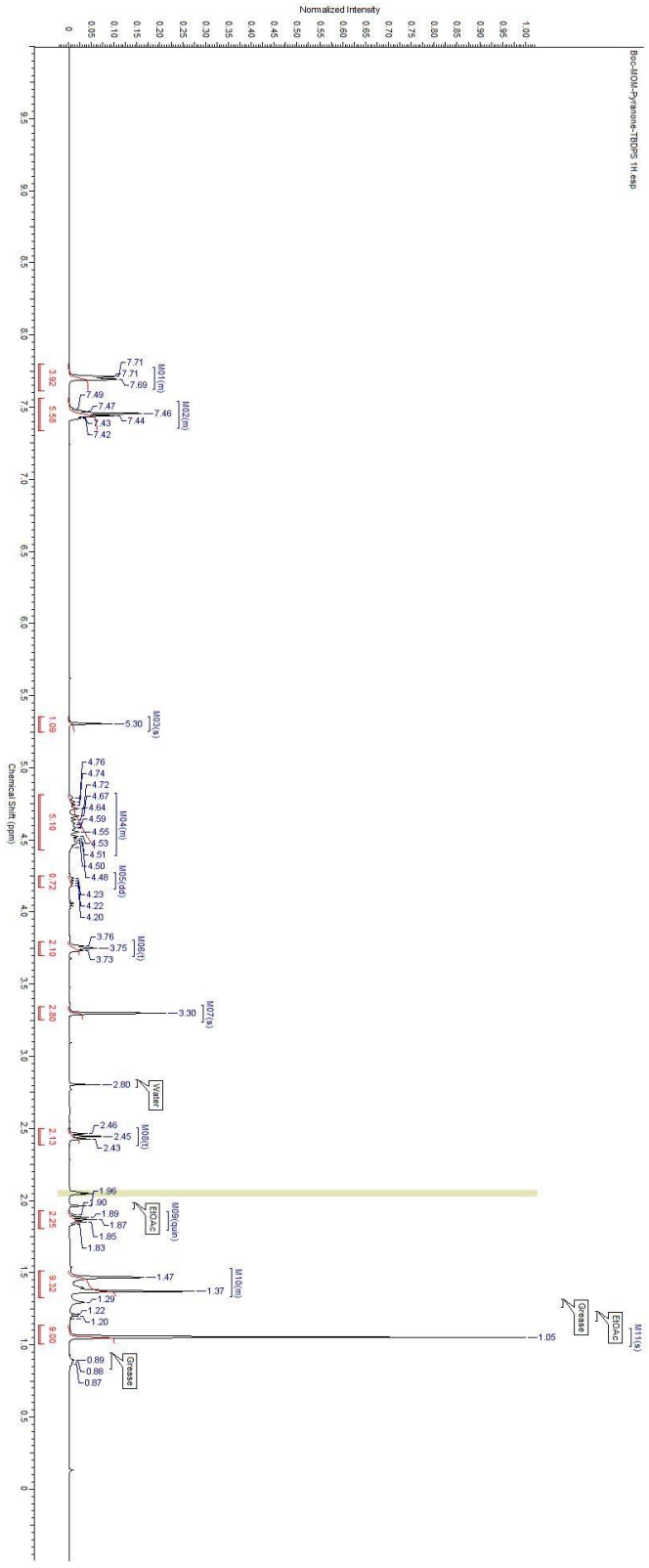

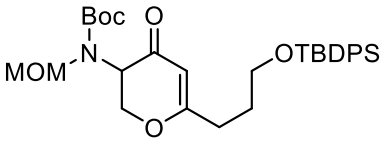

80

400 MHz, $(CD_3)_2CO$

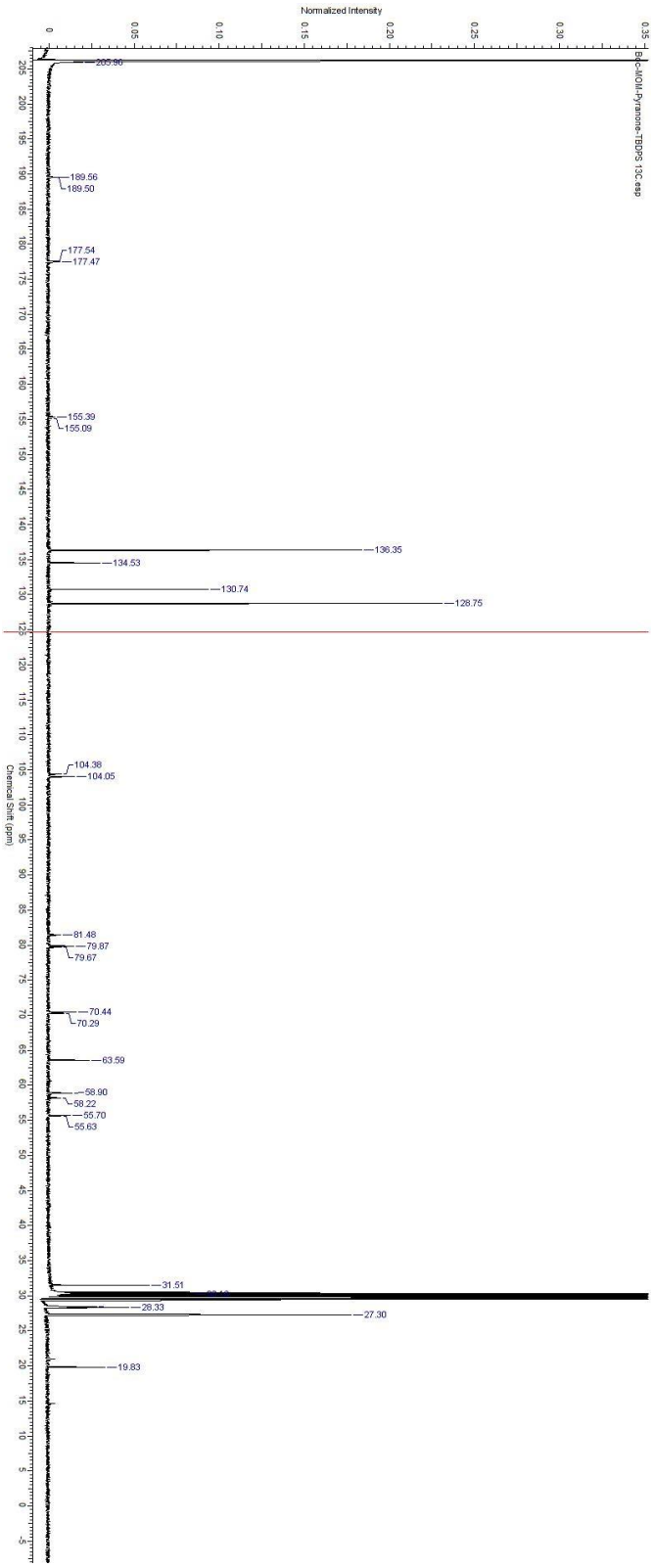

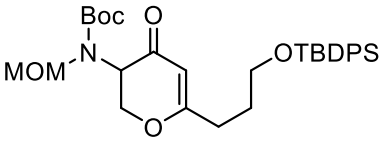

80

100 MHz, $(CD_3)_2CO$

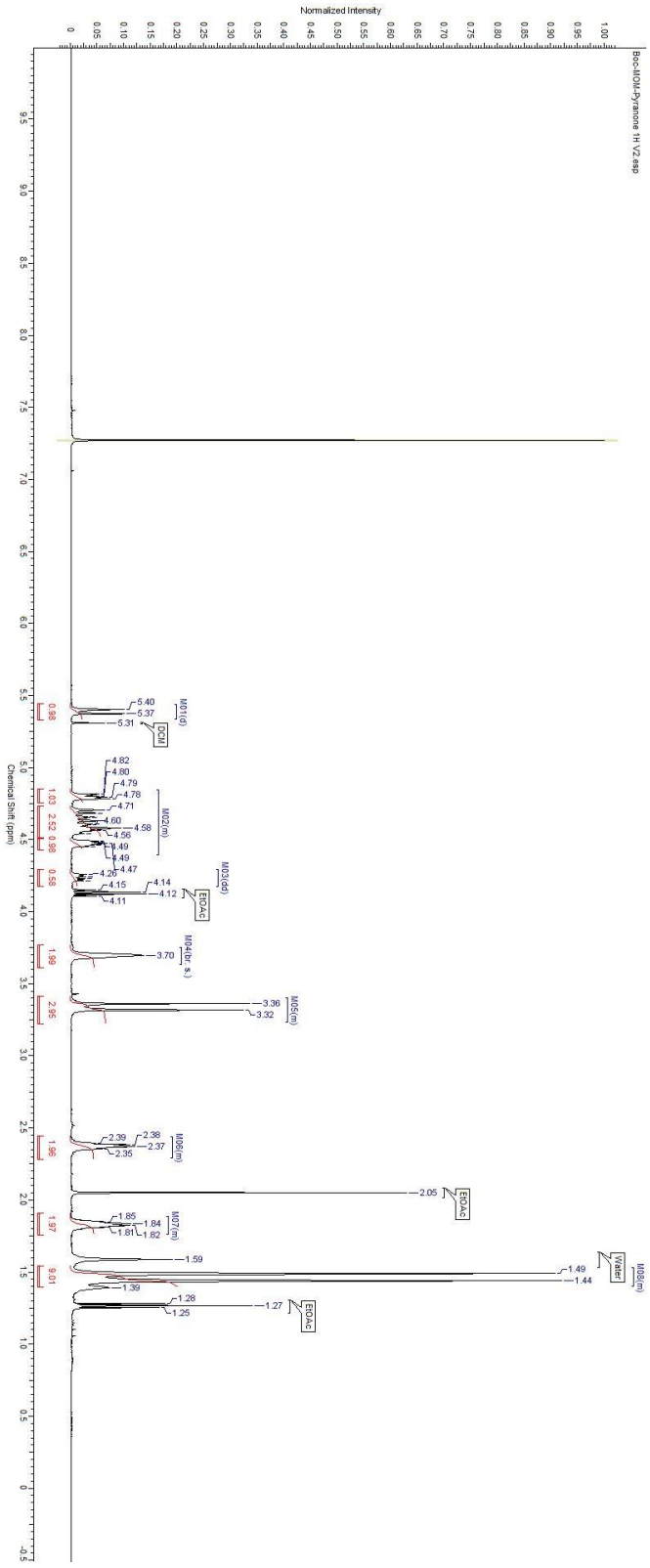

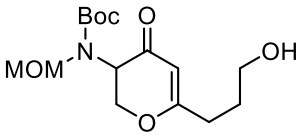

81

500 MHz, $CDCl_3$

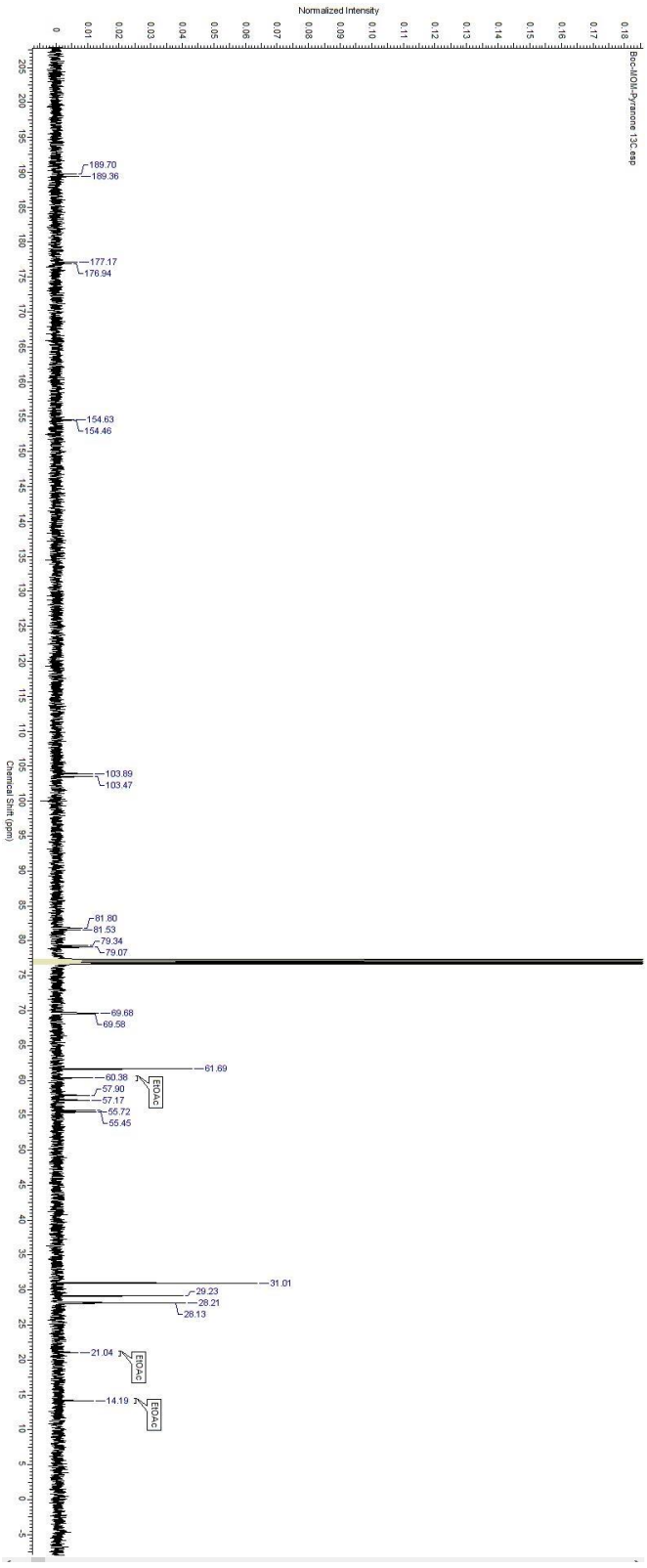

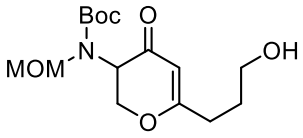

81

125 MHz, $CDCl_3$

[1] (a) Wittig, G. & Schollkopf, U. Uber Triphenyl-phosphin-methylene als olefinbildende Reagenzien (I. Mitteil.) *Chem. Ber.* **1954**, *87*, 1318-1330. (b) Maryanoff, B. E. & Reitz, A. B. The Wittig Olefination Reaction and Modifications Involving Phosphoryl-Stabilized Carbanions. Stereochemistry, Mechanism, and Selected Synthetic Aspects. *Chem. Rev.* **1989**, *89*, 863-927. (c) Byrne, P. A. & Gilheany, D. G. The modern interpretation of the Wittig reaction mechanism *Chem. Soc. Rev.* **2013**, *42*, 6670-6696

[2] (a) Mitsunobu, O.; Yamada, M.; Mukaiyama, T. *Bull. Chem. Soc. Jpn.* **1967**, *40*, 935-939. (b) Mitsunobu, O. & Yamada, M. T. *Bull. Chem. Soc. Jpn.* **1967**, *40*, 2380-2382 (c) But, T. Y. S. & Toy, P. H. The Mitsunobu Reaction: Origin, Mechanism, Improvements, and Applications *Chem. Asian J.* **2007**, *2*, 1340-1355 (d) Hughes, D. Progress in the Mitsunobu Reaction. A Review *Org. Prep. Proc. Int.* **1996**, *28*, 127-164.

[3] Staudinger, J. & Meyer, J. Uber neue organishche Phosphorverbindungen III. Phosphinmethylenderivate und Phosphinimine. *Helv. Chim. Acta* **1919**, *2*, 635-646.

[4] (a) Appel, R. Tertiary Phosphane/Tetrachloromethane, a Versatile Reagent for Chlorination, Dehydration, and P-N Linkage *Angew. Chem. Int. Ed.* **1975**, *14*, 801-811 (b) de Andrade, V. & de Mattos, M. New Reagents and Synthetic Approaches to the Appel Reaction. *Curr. Org. Syn.* **2015**, *12*, 309-327.

[5] (a) Allen, D. W. Phosphines and related C-P bonded compounds *Organophosphorous Chem.* **2016**, *45*, 1-50. (b) Nell, B. P. & Tyler, D. R. Synthesis, reactivity, and coordination chemistry of secondary phosphines *Coord. Chem. Rev.* **2014**, *279*, 23-42

[6] Denton, R. M.; An, J.; Adeniran, B. Phosphine Oxide-Catalysed Chlorination Reactions of Alcohols Under Appel Conditions. *Chem. Commun.* **2010**, *46*, 3025-3027.

[7] For an extremely non-generalizable method, see Marsden, S. P.; McGonalgle, A. E.; McKeever-Abbas, B. Catalytic aza-Wittig Cyclizations for Heteroaromatic Synthesis *Org. Lett.* **2008**, *10*, 2589-2591.

[8] Denton, R. M.; An, J.; Adeniran, B. Phosphine Oxide-Catalysed Chlorination Reactions of Alcohols Under Appel Conditions. *Chem. Commun.* **2010**, *46*, 3025-3027.

[9] Denton, R. M.; Tang, X.; Przeslak, A. Catalysis of Phosphorus(V)-Mediated Transformations: Dichlorination Reactions of Epoxides Under Appel Conditions *Org. Lett.* **2010**, *12*, 4678-4681

[10] Lao, Z. & Toy, P. H. Catalytic Wittig and aza-Wittig reactions *Beilstein J. Org. Chem.* **2019**, *12*, 2577 2587

[11] Hein, F.; Issleib, K.; Rabold, H. Uber die Reduktion von tertiaren Phosphinoxyden bzw. –sulfiden mit Lithium- bzw. Calciumalanat zu den entsprechenden Phosphinen *Z. Anorg. Allg. Chem.* **1956**, *287*, 208-213

[12] Hein, F.; Issleib, K.; Rabold, H. Uber die Reduktion von tertiaren Phosphinoxyden bzw. –sulfiden mit Lithium- bzw. Calciumalanat zu den entsprechenden Phosphinen *Z. Anorg. Allg. Chem.* **1956**, *287*, 208-213

[13] Issleib, K. & Grams, G. *Z. Anorg. Allg. Chem.* **1959**, *299*, 58-68

[14] Campbell, I. G. M. & Way, J. K. Synthesis and Stereochemistry of Heterocyclic Phosphorous Compounds. Part II.* Loss of Optical Activity in the Reduction of (+)-2-Carboxy-9-phenyl-9-phosphafluorene 9-Oxide. *J. Chem. Soc.* **1961**, 2133-2141.

[15] van Kalkeren, H. A.; van Delft, F. L.; Rutjes, F. P. J. T. Organophosphorus Catalysis to Bypass Phosphine Oxide Waste *ChemSusChem* **2013**, *6*, 1615-1624

[16] Hagemeyer, A.; Rieker, C. W.; Lautensack, T.; Hermeling, D. US Patent 5,689,005, **1995**

[17] (a) Yano, T.; Kuroboshi, M.; Tanaka, H. *Tetrahedron Lett.* **2010**, *51*, 698–701. (b) Kuroboshi, M.; Yano, T.; Kamenoue, S.; Kawakubo, H.; Tanaka, H. *Tetrahedron* **2011**, *67*, 5825– 5831. (c) Tanaka, H.; Yano, T.; Kobayashi, K.; Kamenoue, S.; Kuroboshi, M.; Kawakubo, H. *Synlett* **2011**, 582-584. (d) Kawakubo, H.; Kuroboshi, M.; Yano, T.; Kobayashi, K.; Kamenoue, S.; Akagi, T.; Tanaka, H.; *Synthesis* **2011**, 4091-4098

[18] Koster, R. & Morita, Y. *Angew. Chem.* **1965**, *77*, 589-590

[19] Fritzsche, H.; Hasserodt, U.; Korte, F.; Friese, G.; Adrian, K.; Arenz, H. J.; *Chem. Ber.* **1964**, *97*, 1988-1993

[20] Fritzsche, H.; Hasserodt, U.; Korte, F.; Friese, G.; Adrian, K. *Chem. Ber.* **1965**, *98*, 171-174

[21] Fritzsche, H.; Hasserodt, U.; Korte, F.; Friese, G.; Adrian, K.; Arenz, H. J.; *Chem. Ber.* **1964**, *97*, 1988-1993

[22] Fritzsche, H.; Hasserodt, U.; Korte, F.; Friese, G.; Adrian, K. *Chem. Ber.* **1965**, *98*, 171-174
[23] O'Brien, C. J.; Tellez, J. L.; Nixon, Z. S.; Kang, L. J.; Carter, A. L.; Kunkel, S. R.; Przeworski, K. C.; Chass, G. A. *Angew. Chem. Int. Ed.* **2009**, *48*, 6836-6839
[24] Fritzsche, H.; Hasserodt, U.; Korte, F.; Friese, G.; Adrian, K.; Arenz, H. J.; *Chem. Ber.* **1964**, *97*, 1988-1993
[25] O'Brien, C. J.; Tellez, J. L.; Nixon, Z. S.; Kang, L. J.; Carter, A. L.; Kunkel, S. R.; Przeworski, K. C.; Chass, G. A. *Angew. Chem. Int. Ed.* **2009**, *48*, 6836-6839
[26] van Kalkeren, H. A.; Leenders, S. H. A. M.; Hommersom, C. R. A.; Rutjes, F. P. J. T.; van Delft, F. L. In Situ Phosphine Oxide Reduction: A Catalytic Appel Reaction *Chem. Eur. J.* **2011**, *17*, 11290-11295
[27] van Kalkeren, H. A.; Leenders, S. H. A. M.; Hommersom, C. R. A.; Rutjes, F. P. J. T.; van Delft, F. L. In Situ Phosphine Oxide Reduction: A Catalytic Appel Reaction *Chem. Eur. J.* **2011**, *17*, 11290-11295
[28] Li, Y.; Lu, L.-Q. Das, S.; Pisiewicz, S.; Junge, K.; Beller, M. Highly Chemoselective Metal-Free Reduction of Phosphine Oxides to Phosphines *J. Am. Chem. Soc.* **2012**, *134*, 18325-18329
[29] Lenstra, D. C.; Rutjes, F. P. J. T.; Mecinovic, J. Triphenylphosphine-catalysed amide bond formation between carboxylic acids and amines *Chem. Commun.* **2014**, *50*, 5763-5766
[30] Fourmy, K. & Voituriez, A. Catalytic Cyclization Reactions of Huisgen Zwitterion with α-Ketoesters by in Situ Chemoselective Phosphine Oxide Reduction *Org. Lett.* **2015**, *17*, 1537-1540
[31] Berthod, M.; Favre-Reguillon, A.; Mohamad, J.; Mignani, G.; Docherty, G.; Lemaire, M. *Synlett* **2007**, *2007*, 1545-1548
[32] (a) Berk, S. C. & Buchwald, S. L. *J. Org. Chem.* **1993**, *58*, 3221 (b) Petit, C.; Favre-Reguillon, A.; Albela, B. L.; Bonneviot, L; Mignani, G.; Lemaire, M. *Organometallics* **2009**, *28*, 6379-6382
[33] Li, Y.; Das, S.; Zhou, S.; Junge, K.; Beller, M. General and Selective Copper-Catalyzed Reduction of Tertiary and Secondary Phosphine Oxides: Convenient Synthesis of Phosphines *J. Am. Chem. Soc.* **2012**, *134*, 9727-9732
[34] O'Brien, C. J.; Lavigne, F.; Coyle, E. E.; Holohan, A. J.; Doonan, B. J.; *Chem. Eur. J.* **2013**, *19*, 5854-5858
[35] O'Brien, C. J.; Lavigne, F.; Coyle, E. E.; Holohan, A. J.; Doonan, B. J.; *Chem. Eur. J.* **2013**, *19*, 5854-5858
[36] O'Brien, C. J.; Lavigne, F.; Coyle, E. E.; Holohan, A. J.; Doonan, B. J.; *Chem. Eur. J.* **2013**, *19*, 5854-5858
[37] Coyle, E. E.; Doonan, B. J.; Holohan, A. J.; Walsh, K. A.; Lavigne, F.; Krenske, E. H.; O'Brien, C. J. Catalytic Wittig Reactions of Semi- and Nonstabilized Ylides Enabled by Ylide Tuning. *Angew. Chem. Int. Ed.* **2014**, *53*, 12907-12911
[38] Kosal, A. D.; Wilson, E. E.; Ashfeld, B. L. Phosphine-Based Redox Catalysis in the Direct Traceless Staudinger Ligation of Carboxylic Acids and Azides *Angew. Chem. Int. Ed.* **2012**, *51*, 12036-12040
[39] van Kalkeren, H. A.; te Grotenhuis, C.; Haasjes, F. S.; Hommersom, C. A.; Rutjes, F. P. J. T.; van Delft, F. L. *Eur. J. Org. Chem.* **2013**, 7059-7066
[40] Buonomo, J. A. & Aldrich, C. C. Mitsunobu Reactions Catalytic in Phosphine and a Fully Catalytic System *Angew. Chem. Int. Ed.* **2015**, *54*, 13041-13044
[41] Schirmer, M.-L.; Adomeit, S.; Werner, T. First Base-Free Catalytic Wittig Reaction *Org. Lett.* **2015**, *17*, 3078-3081
[42] Zhao, W.; Yan, P. K.; Radosevich, A. T. A Phosphetane Catalyzes Deoxygenative Condensation of α-Keto Esters and Carboxylic Acids via P^{III}/P^{V}=O Redox Cycling *J. Am. Chem. Soc.* **2015**, *137*, 616-619
[43] Reichl, K. D.; Dunn, N. L.; Fastuca, N. J.; Radosevich, A. T. Biphilic Organophosphorus Catalysis: Regioselective Reductive Transposition of Allylic Bromides via P^{III}/P^{V} Redox Cycling *J. Am. Chem. Soc.* **2015**, *137*, 5292-5295
[44] Lee, C.-J.; Chang, T.-H.; Yu, J.-K.; Reddy, G. M.; Hsiao, M.-Y.; Lin, W. Synthesis of Functionalized Furans via Chemoselective Reduction/Wittig Reaction Using Catalytic Triethylamine and Phosphine *Org. Lett.* **2016**, *18*, 3758-3761
[45] Wang, L; Sun, M.; Ding, M.-W. Catalytic Intramolecular Wittig Reaction Based on a Phosphine/Phosphine Oxide Catalytic Cycle for the Synthesis of Heterocycles *Eur. J. Org. Chem.* **2017** 2568-2578.
[46] Fritzsche, H.; Hasserodt, U.; Korte, F.; Friese, G.; Adrian, K. *Chem. Ber.* **1965**, *98*, 171-174

[47] Horner, L. & Balzer, W. D. *Tetrahedron Lett.* **1965**, *6*, 1157-1162
[48] Byrne, P. A. *Chem. Soc. Rev.* **2013**, *42*, 6670-6696
[49] Marsi, K. L. *J. Org. Chem.* **1974**, *39*, 265-267
[50] Krenske, E. H. *J. Org. Chem.* **2012**, *77*, 3969-3977
[51] Demchuk, O. M., Jasinski, R. & Pietrusiewicz, K. M. New Insights into the Mechanism of Reduction of Tertiary Phosphine Oxides by Means of Phenylsilane. *Heteroat. Chem.* **2015**, *26*, 441-448.
[52] Petit, C.; Poli, E.; Favre-Réuillon, A.; Khrouz, L.; Denis-Quanquin, S.; Bonneviot, L.; Mignani, G.; Lemaire, M. Unraveling the Catalytic Cycle of Tertiary Phosphine Oxides Reduction with Hydrosiloxane and $Ti(OiPr)_4$ through EPR and ^{29}Si NMR Spectroscopy. *ACS Catal.* **2013**, *3*, 1431-1438.
[53] O'Brien, C. J.; Lavigne, F.; Coyle, E. E.; Holohan, A. J.; Doonan, B. J.; *Chem. Eur. J.* **2013**, *19*, 5854-5858
[54] Van Kalkeren, H. A.; Leenders, S. H. A. M.; Hommersom, C. A.; Rutjes, F. P. J. T.; van Delft, F. L. *Chem. Eur. J.* **2011**, *17*, 11290-11295
[55] O'Brien, C. J.; Tellez, J. L.; Nixon, Z. S.; Kang, L. J.; Carter, A. L.; Kunkel, S. R.; Przeworski, K. C.; Chass, G. A. *Angew. Chem. Int. Ed.* **2009**, *48*, 6836-6839
[56] Li, Y.; Lu, L.-Q. Das, S.; Pisiewicz, S.; Junge, K.; Beller, M. Highly Chemoselective Metal-Free Reduction of Phosphine Oxides to Phosphines *J. Am. Chem. Soc.* **2012**, *134*, 18325-18329
[57] O'Brien, C. J.; Lavigne, F.; Coyle, E. E.; Holohan, A. J.; Doonan, B. J.; *Chem. Eur. J.* **2013**, *19*, 5854-5858
[58] Buonomo, J. A. & Aldrich, C. C. Mitsunobu Reactions Catalytic in Phosphine and a Fully Catalytic System *Angew. Chem. Int. Ed.* **2015**, *54*, 13041-13044
[59] But, T. Y. S. & Toy, P. H. The Mitsunobu Reaction: Origin, Mechanism, Improvements, and Applications *Chem. Asian J.* **2007**, *2*, 1340-1355
[60] Buonomo, J. A. & Aldrich, C. C. Mitsunobu Reactions Catalytic in Phosphine and a Fully Catalytic System *Angew. Chem. Int. Ed.* **2015**, *54*, 13041-13044
[61] O'Brien, C. J.; Tellez, J. L.; Nixon, Z. S.; Kang, L. J.; Carter, A. L.; Kunkel, S. R.; Przeworski, K. C.; Chass, G. A. *Angew. Chem. Int. Ed.* **2009**, *48*, 6836-6839
[62] van Kalkeren, H. A.; Leenders, S. H. A. M.; Hommersom, C. R. A.; Rutjes, F. P. J. T.; van Delft, F. L. In Situ Phosphine Oxide Reduction: A Catalytic Appel Reaction *Chem. Eur. J.* **2011**, *17*, 11290-11295
[63] O'Brien, C. J.; Lavigne, F.; Coyle, E. E.; Holohan, A. J.; Doonan, B. J.; *Chem. Eur. J.* **2013**, *19*, 5854-5858
[64] van Kalkeren, H. A.; Leenders, S. H. A. M.; Hommersom, C. R. A.; Rutjes, F. P. J. T.; van Delft, F. L. In Situ Phosphine Oxide Reduction: A Catalytic Appel Reaction *Chem. Eur. J.* **2011**, *17*, 11290-11295
[65] Cremer, S. E. & Chorvat, R. J. *J. Org. Chem.* **1967**, *32*, 4066-4070
[66] (a) Jungermann, E.; McBride, J. J.; Clutter, R.; Mais, A. A New Phosphorylation Reaction of Olefins. I. Scope of the Reaction *J. Org. Chem.* **1962**, *27*, 606 (b) McBride, J. J.; Jungermann, E.; Killheffer, J. V.; Clutter, R. J. A New Phosphorylation Reaction of Olefins. II. A Novel Synthesis of a Four-Membered Phosphorous-Containing Ring Compound[1,2] *J. Org. Chem.* **1962**, *27*, 1833-1836
[67] Zhao, W.; Yan, P. K.; Radosevich, A. T. A Phosphetane Catalyzes Deoxygenative Condensation of α-Keto Esters and Carboxylic Acids via P^{III}/P^{V}=O Redox Cycling *J. Am. Chem. Soc.* **2015**, *137*, 616-619
[68] O'Brien, C. J.; Lavigne, F.; Coyle, E. E.; Holohan, A. J.; Doonan, B. J.; *Chem. Eur. J.* **2013**, *19*, 5854-5858
[69] Marsi, K. L. *J. Org. Chem.* **1974**, *39*, 265-267
[70] Reichl, K. D.; Dunn, N. L.; Fastuca, N. J.; Radosevich, A. T. Biphilic Organophosphorus Catalysis: Regioselective Reductive Transposition of Allylic Bromides via P^{III}/P^{V} Redox Cycling *J. Am. Chem. Soc.* **2015**, *137*, 5292-5295
[71] Emsley, J.; Middleton, T. B.; Williams, J. K. Investigations into the Reaction of Phosphorus Trihalides and Alkenes and the Formation of the Phosphetan Ring *J. Chem. Soc., Dalton Trans.* **1976**, 979-984
[72] Buonomo, J. A. & Aldrich, C. C. Mitsunobu Reactions Catalytic in Phosphine and a Fully Catalytic System *Angew. Chem. Int. Ed.* **2015**, *54*, 13041-13044
[73] O'Brien, C. J.; Tellez, J. L.; Nixon, Z. S.; Kang, L. J.; Carter, A. L.; Kunkel, S. R.; Przeworski, K. C.; Chass, G. A. *Angew. Chem. Int. Ed.* **2009**, *48*, 6836-6839

[74] Buonomo, J. A. & Aldrich, C. C. Mitsunobu Reactions Catalytic in Phosphine and a Fully Catalytic System *Angew. Chem. Int. Ed.* **2015**, *54*, 13041-13044
[75] Buonomo, J. A. & Aldrich, C. C. Mitsunobu Reactions Catalytic in Phosphine and a Fully Catalytic System *Angew. Chem. Int. Ed.* **2015**, *54*, 13041-13044
[76] Zhao, W.; Yan, P. K.; Radosevich, A. T. A Phosphetane Catalyzes Deoxygenative Condensation of α-Keto Esters and Carboxylic Acids via P^{III}/P^{V}=O Redox Cycling *J. Am. Chem. Soc.* **2015**, *137*, 616-619
[77] Buonomo, J. A. & Aldrich, C. C. Mitsunobu Reactions Catalytic in Phosphine and a Fully Catalytic System *Angew. Chem. Int. Ed.* **2015**, *54*, 13041-13044
[78] Brouwer, H. Evaluation of Algorithms for Automated Phase Correction of NMR Spectra *J. Magn. Res.* **2009**, *201*, 230-238
[79] Cobas, C. Why aren't Bruker FIDs time corrected? http://nmr-analysis.blogspot.com/2008/02/why-arent-bruker-fids-time-corrected.html (last accessed 5-10-17)
[80] Cobas, C. Bruker Smiles http://nmr-analysis.blogspot.com/2010/05/bruker-smiles.html (last accessed 5-10-17)
[81] Bao, Q.; Feng, J.; Chen. L.; Chen, F.; Liu, Z.; Jiang, B.; Liu, C. A robust automatic phase correction method for signal dense spectra *J. Magn. Res.* **2013**, *234*, 82-89
[82] O'Brien, C. J.; Lavigne, F.; Coyle, E. E.; Holohan, A. J.; Doonan, B. J.; *Chem. Eur. J.* **2013**, *19*, 5854-5858
[83] Li, Y.; Lu, L.-Q. Das, S.; Pisiewicz, S.; Junge, K.; Beller, M. Highly Chemoselective Metal-Free Reduction of Phosphine Oxides to Phosphines *J. Am. Chem. Soc.* **2012**, *134*, 18325-18329
[84] Berthod, M.; Favre-Reguillon, A.; Mohamad, J.; Mignani, G.; Docherty, G.; Lemaire, M. *Synlett* **2007**, *2007*, 1545-1548
[85] Xiao, M. & Hochberg, A. K. US Patent 2009/0069588, **2009**
[86] O'Brien, C. J.; Lavigne, F.; Coyle, E. E.; Holohan, A. J.; Doonan, B. J.; *Chem. Eur. J.* **2013**, *19*, 5854-5858
[87] Marsi, K. L. *J. Org. Chem.* **1974**, *39*, 265-267
[88] Demchuk, O. M., Jasinski, R. & Pietrusiewicz, K. M. New Insights into the Mechanism of Reduction of Tertiary Phosphine Oxides by Means of Phenylsilane. *Heteroat. Chem.* **2015**, *26*, 441-448.
[89] Kupareva, A.; Maki-Arvela, P.; Grenman, H.; Eranen, K.; Murzin, D. Y. The base-catalyzed transformation of tetramethyldisiloxane: influence of reaction media *J. Chem. Technol. Biotechnol.* **2015**, *90*, 34-43
[90] Fritzsche, H.; Hasserodt, U.; Korte, F.; Friese, G.; Adrian, K.; Arenz, H. J.; *Chem. Ber.* **1964**, *97*, 1988-1993
[91] Fritzsche, H.; Hasserodt, U.; Korte, F.; Friese, G.; Adrian, K.; Arenz, H. J.; *Chem. Ber.* **1964**, *97*, 1988-1993
[92] Marsi, K. L. *J. Org. Chem.* **1974**, *39*, 265-267
[93] Van Kalkeren, H. A.; Leenders, S. H. A. M.; Hommersom, C. A.; Rutjes, F. P. J. T.; van Delft, F. L. *Chem. Eur. J.* **2011**, *17*, 11290-11295
[94] O'Brien, C. J.; Tellez, J. L.; Nixon, Z. S.; Kang, L. J.; Carter, A. L.; Kunkel, S. R.; Przeworski, K. C.; Chass, G. A. *Angew. Chem. Int. Ed.* **2009**, *48*, 6836-6839
[95] Marsi, K. L. *J. Org. Chem.* **1974**, *39*, 265-267
[96] Prabusankar, G.; Murugavel, R.; Butcher, R. J. Stabilization of Organosilanetriols in Amine Matrices: Trapping Intermediates between $RSi(OH)_3$ and $(RSiO_3)^{3-}$ Anions *Organometallics* **2004**, *23*, 2305-2314
[97] Marsi, K. L. *J. Org. Chem.* **1974**, *39*, 265-267
[98] O'Brien, C. J.; Lavigne, F.; Coyle, E. E.; Holohan, A. J.; Doonan, B. J.; *Chem. Eur. J.* **2013**, *19*, 5854-5858
[99] Kosal, A. D.; Wilson, E. E.; Ashfeld, B. L. Phosphine-Based Redox Catalysis in the Direct Traceless Staudinger Ligation of Carboxylic Acids and Azides *Angew. Chem. Int. Ed.* **2012**, *51*, 12036-12040
[100] Ruan, Z.; Lawrence, R. M.; Cooper, C. B. Phenylsilane as an active amidation reagent for the preparation of carboxamides and peptides. *Tetrahedron Lett.* **2006**, *47*, 7649-7651
[101] Andrews, K. G.; Summers, D. M.; Donnelly, L. J.; Denton, R. M. Catalytic Reductive *N*-alkylation of Amines using Carboxylic Acids *Chem. Commun.* **2016**, *52*, 1855-1858
[102] Berthod, M.; Favre-Reguillon, A.; Mohamad, J.; Mignani, G.; Docherty, G.; Lemaire, M. *Synlett* **2007**, *2007*, 1545-1548

[103] Petit, C.; Favre-Reguillon, A.; Albela, B. L.; Bonneviot, L; Mignani, G.; Lemaire, M. *Organometallics* **2009**, *28*, 6379-6382
[104] Petit, C.; Poli, E.; Favre-Réuillon, A.; Khrouz, L.; Denis-Quanquin, S.; Bonneviot, L.; Mignani, G.; Lemaire, M. Unraveling the Catalytic Cycle of Tertiary Phosphine Oxides Reduction with Hydrosiloxane and $Ti(OiPr)_4$ through EPR and ^{29}Si NMR Spectroscopy. *ACS Catal.* **2013**, *3*, 1431-1438.
[105] Petit, C.; Poli, E.; Favre-Réuillon, A.; Khrouz, L.; Denis-Quanquin, S.; Bonneviot, L.; Mignani, G.; Lemaire, M. Unraveling the Catalytic Cycle of Tertiary Phosphine Oxides Reduction with Hydrosiloxane and $Ti(OiPr)_4$ through EPR and ^{29}Si NMR Spectroscopy. *ACS Catal.* **2013**, *3*, 1431-1438.
[106] B. Osmialowski, K. Mroczynska, E. Kolehmainen, M. Kowalska, A. Valkonen, M. Pietrzak, K. Rissanen, *J. Org. Chem.* **2013**, *78*, 7582-7593
[107] Petit, C.; Poli, E.; Favre-Réuillon, A.; Khrouz, L.; Denis-Quanquin, S.; Bonneviot, L.; Mignani, G.; Lemaire, M. Unraveling the Catalytic Cycle of Tertiary Phosphine Oxides Reduction with Hydrosiloxane and $Ti(OiPr)_4$ through EPR and ^{29}Si NMR Spectroscopy. *ACS Catal.* **2013**, *3*, 1431-1438.
[108] Xin, S.; Aitken, C.; Harrod, J. F.; Mu, Y.; Samuel, E. Redistribution Reactions of alkoxy- and siloxysilanes, catalyzed by dimethyltitanocene *Can. J. Chem.* **1990**, *68*, 471-476
[109] Petit, C.; Poli, E.; Favre-Réuillon, A.; Khrouz, L.; Denis-Quanquin, S.; Bonneviot, L.; Mignani, G.; Lemaire, M. Unraveling the Catalytic Cycle of Tertiary Phosphine Oxides Reduction with Hydrosiloxane and $Ti(OiPr)_4$ through EPR and ^{29}Si NMR Spectroscopy. *ACS Catal.* **2013**, *3*, 1431-1438.
[110] Xin, S.; Aitken, C.; Harrod, J. F.; Mu, Y.; Samuel, E. Redistribution Reactions of alkoxy- and siloxysilanes, catalyzed by dimethyltitanocene *Can. J. Chem.* **1990**, *68*, 471-476
[111] Kupareva, A.; Maki-Arvela, P.; Grenman, H.; Eranen, K.; Murzin, D. Y. The base-catalyzed transformation of tetramethyldisiloxane: influence of reaction media *J. Chem. Technol. Biotechnol.* **2015**, *90*, 34-43
[112] Buonomo, J. A. & Aldrich, C. C. Mitsunobu Reactions Catalytic in Phosphine and a Fully Catalytic System *Angew. Chem. Int. Ed.* **2015**, *54*, 13041-13044
[113] O'Brien, C. J.; Lavigne, F.; Coyle, E. E.; Holohan, A. J.; Doonan, B. J.; *Chem. Eur. J.* **2013**, *19*, 5854-5858
[114] van Kalkeren, H. A.; Leenders, S. H. A. M.; Hommersom, C. A.; Rutjes, F. P. J. T.; van Delft, F. L. *Chem. Eur. J.* **2011**, *17*, 11290-11295
[115] van Kalkeren, H. A.; Leenders, S. H. A. M.; Hommersom, C. A.; Rutjes, F. P. J. T.; van Delft, F. L. *Chem. Eur. J.* **2011**, *17*, 11290-11295
[116] Marinetti, A. & Carmichael, D. *Chem. Rev.* **2002**, *102*, 201.
[117] van Kalkeren, H. A.; Leenders, S. H. A. M.; Hommersom, C. A.; Rutjes, F. P. J. T.; van Delft, F. L. *Chem. Eur. J.* **2011**, *17*, 11290-11295
[118] (a) Allen, D. W. Phosphines and related C-P bonded compounds *Organophosphorous Chem.* **2016**, *45*, 1-50. (b) Nell, B. P. & Tyler, D. R. Synthesis, reactivity, and coordination chemistry of secondary phosphines *Coord. Chem. Rev.* **2014**, *279*, 23-42
[119] (a) Ogasawara, M.; Tseng, Y.-Y.; Arae, S.; Morita, T.; Nakaya, T.; Wu, W.-Y.; Takahashi T.; Kamikawa, K. Phosphine-Olefin Ligands Based on a Planar-Chiral (π-Arene)chromium Scaffold: Design, Synthesis, and Application in Asymmetric Catalysis. *J. Am. Chem. Soc.* **2014,** *136*, 9377-9384 (b) Li, W. & Zhang, J. Recent developments in the synthesis and utilization of chiral β-aminophosphine derivatives as catalysts or ligands *Chem. Soc. Rev.* **2016**, *45*, 1657 (c) Wang, D.; Cao, P.; Wang, B.; Jia, T.; Lou, Y.; Wang, M.; Liao, J. Copper(I)-Catalyzed Asymmetric Pinacolboryl Addition of *N*-Boc-imines Using a Chiral Sulfoxide-Phosphine Ligand *Org. Lett.* **2015**, *17*, 2420-2423
[120] Berthod, M.; Favre-Reguillon, A.; Mohamad, J.; Mignani, G.; Docherty, G.; Lemaire, M. *Synlett* **2007**, *2007*, 1545-1548
[121] Li, Y.; Lu, L.-Q. Das, S.; Pisiewicz, S.; Junge, K.; Beller, M. Highly Chemoselective Metal-Free Reduction of Phosphine Oxides to Phosphines *J. Am. Chem. Soc.* **2012**, *134*, 18325-18329
[122] N. W. Mitzel, A. Schier, H. Beruda, H. Schmidbaur, *Chem. Ber.* **1992**, *125*, 1053-1059
[123] V. M. Uvarov, D. A. de Vekki, V. P. Reshetilovskii, N. K. Skvortsov, *Russ. J. Gen. Chem.* **2010**, *80*, 35-46

[124] A. Benouargha, D. Boulahia, B. Boutevin, G. Caporiccio, F. Guida-Pietrasanta, A. Ratsimihety, *Phosphorous Sulfur Silicon Relat. Elem.* **1996**, *113*, 79-87
[125] B. Osmialowski, K. Mroczynska, E. Kolehmainen, M. Kowalska, A. Valkonen, M. Pietrzak, K. Rissanen, *J. Org. Chem.* **2013**, *78*, 7582-7593
[126] World Health Organization. Global Tuberculosis Report 2016. http://www.who.int/tb/publications/global_report/en/ (last accessed 5-8-17)
[127] World Health Organization. Treatment of Tuberculosis Guidelines, 4th ed. http://www.who.int/tb/publications/2010/9789241547833/en/ (last accessed 5-8-17)
[128] Centers for Disease Control and Prevention (CDC) (1999). Control of infectious diseases. MMWR Morb. Mortal. Wkly. Rep. 48, 621–629.
[129] World Health Organization. Global Tuberculosis Report 2016. http://www.who.int/tb/publications/global_report/en/ (last accessed 5-8-17)
[130] Gerdes, S. Y.; Scholle, M. D.; D'Souza, M.; Bernal, A.; Baev, M. V.; Farrell, M.; Kurnasov, O. V.; Daugherty, M. D.; Mseeh, F.; Polanuyer, B. M.; Campbell, J. W.; Anantha, S.; Shatalin, K. Y.; Showdhury, S. A. K.; Fonstein, M. Y.; Osterman, A. L. From Genetic Footprinting to Antimicrobial Drug Targets: Examples in Cofactor Biosynthetic Pathways *J. Bacteriol.* **2002**, *184*, 4555-4572
[131] Jitrapakdee, S.; St Maurice, M.; Rayment, I.; Cleland, W. W.; Wallace, J. C.; Attwood, P. V.; *Biochem. J.* **2008**, *413*, 369-387
[132] Marquet, A.; Tse Sum Bui, B.; Florentin, D. *Vitamins & Hormones* **2001***, 61*, 51-101
[133] Bansal-Mutalik, R. & Nikaido, H. *Proc. Nat. Acad. Sci.* **2014***, 111*, 4958-4963.
[134] Barry III, C. E.; Lee, R. E.; Mdluli, K.; Sampson, A. E.; Schroeder, B. G.; Slayden, R. A.; Yuan, Y. *Prog. Lipid Res.* **1998***, 37*, 143-179.
[135] Brennan, P. J.; Nikaido, H. *Annu. Rev. Biochem.* **1995***, 64*, 29-63
[136] Marrero, J.; Rhee, K. Y.; Schnappinger, D.; Pethe, K.; Ehrt, S.; *Proc. Nat. Acad. Sci.* **2010**, *107*, 9819-9824
[137] Okami, Y.; Kitahara, T.; Hamada, M.; Naganawa, H.; Kondo, S.; Maeda, K.; Takeuchi, T.; Umezawa, H.; *J. Antibiot.* **1974**, *27*, 656-664
[138] Kitahara, T.; Hotta, K.; Yoshida, M.; Okami, Y.; *J. Antibiot.* **1975**, *28*, 215.
[139] Hotta, K.; Kitahara, T.; Okami, Y; *J. Anitbiot.* **1975**, *28*, 222.
[140] Woong Park, S.; Klotzsche, M.; Wilson, D. J.; Boshoff, H. I.; Eoh, H.; Manjunatha, U.; Blumenthal, A.; Rhee, K.; Barry III, C. E.; Aldrich, C. C.; Ehrt, S.; Schnappinger, D. *PLoS Pathog* **2011***, 7*, e1002264
[141] Hotta, K.; Kitahara, T.; Okami, Y; *J. Anitbiot.* **1975**, *28*, 222.
[142] Lin. S.; Hanson, R. E.; Cronan, J. E.; *Nat. Chem. Biol.* **2010**, *6*, 682-688
[143] Bhor, V. M.; Dev, S.; Vasanthakumar, G. R.; Kumar, P.; Sinha, S.; Surolia, A. *J. Biol. Chem.* **2006**, *281*, 25076.
[144] Mann, S.; Ploux, O. *Biochim. Biophys. Acta* **2011**, *1814*, 1459
[145] Mann, S.; Ploux, O. *FEBS J.* **2006**, *273*, 4778
[146] Mann, S.; Colliandre, L.; Lebesse, G.; Ploux, O. *Biochimie* **2009**, *91*, 826
[147] Escalettes, F.; Florentin, D.; Bui, B. T. S.; Lesage, D.; Marquet, A. *J. Am. Chem. Soc.* **1999**, *121*, 3571
[148] Farrar, C. E.; Siu, K. K. W.; Howell, P. L.; Jarrett, J. T. *Biochemistry* **2010**, *49*, 9985
[149] Kitahara, T.; Hotta, K.; Yoshida, M.; Okami, Y.; *J. Antibiot.* **1975**, *28*, 215.
[150] Kitahara, T.; Hotta, K.; Yoshida, M.; Okami, Y.; *J. Antibiot.* **1975**, *28*, 215.
[151] Mann, S.; Ploux, O. *Biochim. Biophys. Acta* **2011**, *1814*, 1459. (c) Mann, S.; Ploux, O. *FEBS J.* **2006**, *273*, 4778
[152] Mann, S.; Colliandre, L.; Lebesse, G.; Ploux, O. *Biochimie* **2009**, *91*, 826
[153] Mann, S.; Lesage, D.; Tabet, J.-C.; Marquet, A.; *Tetrahedron* **2003**, *59*, 5209-5214
[154] Mann, S.; Florentin, D.; Lesage, D.; Drujon, T.; Ploux, O.; Marquet, A.; *Helv. Chim. Acta* **2003**, *86*, 3836-3850
[155] Shi, C. & Aldrich, C. C.; Design and Synthesis of Potential Mechanism-Based Inhibitors of the Aminotransferase BioA Involved in Biotin Biosynthesis *J. Org. Chem.* **2012**, *77*, 6051-6058

[156] Shi, C.; Geders, T. W.; Park, S. W.; Wilson, D. J.; Boshoff, H. I.; Abayomi, O.; Barry, C. E.; Schnappinger, D.; Finzel, B. C.; Aldrich, C. C. *J. Am. Chem. Soc.* **2011***, 133*, 18194-18201

[157] Copeland, R. A. *Evaluation of Enzyme Inhibitors in Drug Discovery: a Guide for Medicinal Chemists and Pharmacologists*; John Wiley & Sons: Hoboken, NJ, 2006

[158] Copeland, R. A. *Evaluation of Enzyme Inhibitors in Drug Discovery: a Guide for Medicinal Chemists and Pharmacologists*; John Wiley & Sons: Hoboken, NJ, 2006

[159] Dai, R.; Geders, T. W.; Liu, F.; Park, S. W.; Schnappinger, D.; Aldrich, C. C.; Finzel, B. C.; Fragment-Based Exploration of Binding Site Flexibility in *Mycobacterium tuberculosis* BioA. *J. Med. Chem.* **2015**, *58*, 5208-5217

[160] Shi, C.; Geders, T. W.; Park, S. W.; Wilson, D. J.; Boshoff, H. I.; Abayomi, O.; Barry, C. E.; Schnappinger, D.; Finzel, B. C.; Aldrich, C. C. *J. Am. Chem. Soc.* **2011***, 133*, 18194-18201

[161] Campbell, A. D.; Raynham, T. M.; Taylor, R. J. K. *Synthesis* **1998**, *12*, 1707-1709

[162] Ageno, G.; Banfi, L.; Cascio, G.; Guanti, G.; Manghisi, E.; Riva, R.; Rocca, V. *Tetrahedron* **1995**, *51*, 8121-8134

[163] Garner, P.; Park, J. M.; Malecki, E. *J. Org. Chem.* **1988**, *53*, 4395;

[164] Campbell, A. D.; Raynham, T. M.; Taylor, R. J. K.; A Simplified Route to the *(R)*-Garner Aldehyde and (*S*)-Vinyl Glycinol. *Synthesis.* **1998**, 1707

[165] Banba, Y.; Abe, C.; Nemoto, H.; Kato, A.; Adachi, I.; Takahata, H.; Asymmetric synthesis of fagomine and its congeners. *Tetrahetron: Asymmetry* **2001**, *12*, 817-819

[166] Berkowitz, D. & Maiti, G.; Following an ISES Lead: The First Examples of Asymmetric Ni(0)-Mediated Allylic Amination. *Org. Lett.* **2004**, *6*, 2661-2664.

[167] Li, H.; Jiang, X.; Ye, Y.; Fan, C.; Romo, T.; Goodman, M. *Org. Lett.* **1999**, *1*, 91

[168] Jiang, W.; Wanner, J.; Lee, R. J.; Bounaud, P.-Y.; Boger, D. L. *J. Am. Chem. Soc.* **2002**, *124*, 5288

[169] Scholl, M.; Ding, S.; Lee, C. W.; Grubbs, R. H. Synthesis and Activity of a New Generation of Ruthenium-Based Olefin Metathesis Catalysts Coordinated with 1,3-Dimesityl-4,5-dihydroimidazol-2-ylidene Ligands *Org. Lett.* **1999**, *1*, 953–956.

[170] Gessler, S.; Randl, S.; Blechert, S. Synthesis and metathesis reactions of phosphine-free dihydroimidazole carbene ruthenium complex. *Tetrahedron Lett.* **2000**, *41*, 9973–9976.

[171] Garber, S. B.; Kingsbury, J. S.; Gray, B. L.; Hoveyda, A. H. Efficient and Recyclable Monomeric and Dendritic Ru-Based Metathesis Catalysts *J. Am. Chem. Soc.* **2000**, *122*, 8168–8179.

[172] Tornøe, C. W.; Christensen, C.; Meldal, M. Peptidotriazoles on Solid Phase: [1,2,3]-Triazoles by Regiospecific Copper(I)-Catalyzed 1,3-Dipolar Cycloadditions of Terminal Alkynes to Azides *J. Org. Chem*. **2002**, *67*, 3057–3064.

[173] Rostovtsev, V. V.; Green, L. G.; Fokin, V. V.; Sharpless, K. B. A Stepwise Huisgen Cycloaddition Process: Copper(I)-Catalyzed Regioselective Ligation of Azides and Terminal Alkynes *Angew. Chem. Int. Ed.* **2002**, *41*, 2596-2599

[174] Suarez, J. R.; Collado-Sanz, D.; Cardenas, D. J.; Chiara, J. L. Nonafluorobutanesulfonyl Azide as a Shelf-Stable Highly Reactive Oxidant for the Copper-Catalyzed Synthesis of 1,3-Diynes from Terminal Alkynes *J. Org. Chem.* **2015**, *80*, 1098-1106

[175] Rostovtsev, V. V.; Green, L. G.; Fokin, V. V.; Sharpless, K. B. A Stepwise Huisgen Cycloaddition Process: Copper(I)-Catalyzed Regioselective Ligation of Azides and Terminal Alkynes *Angew. Chem. Int. Ed.* **2002**, *41*, 2596-2599

[176] Shi, C.; Geders, T. W.; Park, S. W.; Wilson, D. J.; Boshoff, H. I.; Abayomi, O.; Barry, C. E.; Schnappinger, D.; Finzel, B. C.; Aldrich, C. C. *J. Am. Chem. Soc.* **2011***, 133*, 18194-18201

[177] Natelson, S. & Natelson, E. A. Preparation of D-, DL-, and L-Homoserine Lactone from Methionine *Microchem. J.* **1989**, *40*, 226-232

[178] Wright, D. L.; Schulte II, J. P.; Page, M. A.; *Org. Lett.* **2000**, *2*, 1847

[179] White, J. D. & Hrnciar, P. *J. Org. Chem.* **2000**, *65*, 9129

[180] The identity of **28** was determined through ^{1}H NMR (spectrum included) ^{1}H NMR (400 MHz, $CDCl_3$) δ 5.95 (d, *J* = 5.5 Hz, 1H), 4.69 (t, *J* = 6.1 Hz, 1H), 4.10 (t, *J* = 8.4 Hz, 1H), 3.87 (ddd, *J* = 5.5, 9.3, 11.4 Hz, 1H), 2.05-2.24 (m, 2H), 1.52 (s, 9H)

[181] Kim, S. J.; Chang, M.; Kim, H.-D. Asymmetric Transformation of L-Homoserine Lactone to an Optically Active 2-Substituted Pyrrolidine for Clemastine *Tetrahedron: Asymmetry* **2011**, *22*, 1901-1905

[182] The structure of **30** was confirmed through ^{1}H NMR (spectrum included) ^{1}H NMR (400 MHz, CD_3OD) δ 6.87 (dd, *J* = 7.5, 15.8 Hz, 1H), 6.17 (dd, *J* = 1.0, 15.8 Hz, 1H), 4.22 (q, *J* = 7.0 Hz, 2H), 4.14 (q, *J* = 7.0 Hz, 1H), 3.71–3.79 (m, 1H), 3.66–3.71 (m, 1H), 1.86–2.07 (m, 2H), 1.29 (t, *J* = 7.2 Hz, 3H) but it was not fully characterized and a yield was not determined.

[183] Li, H.; Jiang, X.; Ye, Y.; Fan, C.; Romo, T.; Goodman, M. *Org. Lett.* **1999**, *1*, 91

[184] Shi, C.; Geders, T. W.; Park, S. W.; Wilson, D. J.; Boshoff, H. I.; Abayomi, O.; Barry, C. E.; Schnappinger, D.; Finzel, B. C.; Aldrich, C. C. *J. Am. Chem. Soc.* **2011***, 133*, 18194-18201

[185] Mori, M.; Sakakibara, N.; Kinoshita, A.; Remarkable Effect of Ethylene Gas in the Intramolecular Enyne Metathesis of Terminal Alkynes *J. Org. Chem.* **1998**, *63*, 6082

[186] Bao, H. & Tambar, U. K.; Catalytic Enantioselective Allylic Amination of Unactivated Terminal Olefins via an Ene Reaction/[2,3]-Rearrangement *J. Am. Chem. Soc.* **2012**, *134*, 18495-18498

[187] Bao, H. & Tambar, U. K.; Catalytic Enantioselective Allylic Amination of Unactivated Terminal Olefins via an Ene Reaction/[2,3]-Rearrangement *J. Am. Chem. Soc.* **2012**, *134*, 18495-18498

[188] Kim, S. & Kee, I. S. *Tetrahedron Lett.* **1990**, *31*, 2899

[189] Tuttle, J. B.; Anderson, M.; Bechle, B. M.; Campbell, B. M.; Chang, C.; Dounay, A. B.; Evrard, E.; Fonseca, K. R.; Gan, X.; Ghosh, S.; Horner, W.; James, L. C.; Kim, J.-Y.; McAllister, L. A.; Pandit, J.; Parikh, V. D.; Rago, B. J.; Salafia, M. A.; Strick, C. A.; Zawadzke, L. E.; Verhoest, P. R. Structure-Based Design of Irreversible Human KAT II Inhibitors: Discovery of New Potency-Enhancing Interactions *ACS Med. Chem. Lett.* **2013**, *4*, 37-40

[190] Pattanalk, P.; Bethel, C. R.; Huger, A. M.; Huger, K. M.; Distler, A. M.; Taracila, M.; Anderson, V. E.; Fritsche, T. R.; Jones, R. N.; Pagadala, S. R. R.; van den Akker, F.; Buynak, J. D.; Bonomo, R. A.; Strategic Design of an Effective β-Lactamase Inhibitor *J. Biol. Chem.* **2009**, *284*, 945-953

[191] Harling, J. D.; Deakin, A. M.; Campos, S.; Grimley, R.; Chaudry, L.; Nye, C.; Polyakova, O.; Bessant, C. M.; Barton, N.; Somers, D.; Barrett, J.; Graves, R. H.; Hanns, L.; Kerr, W. J.; Solari, R. Discovery of Novel Irreversible Inhibitors of Interleukin(IL)-2-inducible Tyrosine Kinase (Itk) by Targeting Cysteine 442 in the ATP Pocket *J. Biol. Chem.* **2013**, *288*, 28195-28206

[192] Ruggeri, R. B.; Buckbinder, L.; Bagley, S. W.; Carpino, P. A.; Conn, E. L.; Dowling, M. S.; Fernando, D. P.; Jiao, W.; Kung, D. W.; Orr, S. T. M.; Qi, Y.; Rocke, B. N.; Smith, A.; Warmus, J. S.; Zhang, Y.; Bowles, D.; Widlicka, D. W.; Eng, H.; Ryder, T.; Sharma, R.; Wolford, A.; Okerberg, C.; Walters, K.; Maurer, T. S.; Zhang, Y.; Bonin, P. D.; Spath, S. N.; Xing, G.; Hepworth, D.; Ahn, K.; Salgutkar, A. S. *J. Med. Chem.* **2015**, *58*, 8513-8528

[193] Kopecny, D.; Sebela, M.; Briozzo, P.; Spichal, L.; Houba-Herin, N.; Masek, V.; Joly, N.; Madzak, C.; Anzenbacher, P.; Laloue, M. Mechanism-Based Inhibitors of Cytokinin Oxidase/Dehydrogenase Attack FAD Cofactor *J. Mol. Biol.* **2008**, *380*, 886-899

[194] Kopecny, D.; Sebela, M.; Briozzo, P.; Spichal, L.; Houba-Herin, N.; Masek, V.; Joly, N.; Madzak, C.; Anzenbacher, P.; Laloue, M. Mechanism-Based Inhibitors of Cytokinin Oxidase/Dehydrogenase Attack FAD Cofactor *J. Mol. Biol.* **2008**, *380*, 886-899

[195] Malachowski, W. P.; Winters, M.; DuHadaway, J. B.; Lewis-Ballester, A.; Badir, S.; Wai, J.; Rahman, M.; Sheik, E.; LaLonde, J. M.; Yeh, S.; Prendergast, G. C.; Muller, A. J.; *Eur. J. Med. Chem.* **2016**, *108*, 564.

[196] Angelastro, M. R.; Laughlin, M. E.; Schatzman, G. L.; Bey, P.; Blohm, T. R.; *Biochem. Biophys. Res. Commun.* **1989**, *162*, 1571.

[197] Lee, Y.; Ling, K.; Lu, X.; Silverman, R. B.; Shepard, E. M.; Dooley, D. M; Sayre, L. M.; *J. Am. Chem. Soc.* **2002**, *124*, 12135.

[198] Pattanalk, P.; Bethel, C. R.; Huger, A. M.; Huger, K. M.; Distler, A. M.; Taracila, M.; Anderson, V. E.; Fritsche, T. R.; Jones, R. N.; Pagadala, S. R. R.; van den Akker, F.; Buynak, J. D.; Bonomo, R. A.; Strategic Design of an Effective β-Lactamase Inhibitor *J. Biol. Chem.* **2009**, *284*, 945-953
[199] Phillips, R. S. *Biochim. Biophys. Acta* **2015**, *1854*, 1167
[200] Karsten, W. E.; Ohshiro, T.; Izumi, Y.; Cook, P. F.; Biochemistry **2005**, *44*, 15930.
[201] Karsten, W. E. & Cook, P. F.; Biochim. Biophys. Acta **2009**, *1790*, 575.
[202] Zakomirdina, L. N.; Kulikova, V. V.; Gogoleva, O. I.; Dementieva, I. S.; Faleev, N. G.; Demidkina, T. V.; *Biochemistry (Moscow)* **2002**, *10*, 1189.
[203] Phillips, R. S. *Biochim. Biophys. Acta* **2015**, *1854*, 1167
[204] Karsten, W. E.; Ohshiro, T.; Izumi, Y.; Cook, P. F.; Biochemistry **2005**, *44*, 15930.
[205] Danishefsky, S.; Kato, N.; Askin, D.; Kerwin, J. F. *J. Am. Chem. Soc.* **1982***, 104*, 360-362
[206] Turunen, B. J. & Georg, G. I. *J. Am. Chem. Soc.* **2006**, *128*, 8702-8703
[207] Niphakis, M. J.; Turunen, B. J.; Georg, G. I. *J. Org. Chem.* **2010**, *75*, 6793-6805
[208] Gouault, N.; Le Roch, M.; Cheignon, A.; Uriac, P.; David, M. *Org. Lett.* **2011***, 13*, 4371-4373
[209] Campbell, A. D.; Raynham, T. M.; Taylor, R. J. K. *Synthesis* **1998**, *12*, 1707-1709
[210] So, R. C.; Ndonye, R.; Izmirian, D. P.; Richardson, S. K.; Guerrera, R. L.; Howell, A. R. *J. Org. Chem.* **2004***, 69*, 3233-3235
[211] Fuwa, H.; Matsukida, S.; Sasaki, M. *Synlett* **2010***, 2010*, 1239-1242
[212] Schuler, M.; Silva, F.; Bobbio, C.; Tessier, A.; Gouverneur, V. *Angew. Chem. Int. Ed.* **2008***, 47*, 7927-7930
[213] Reiter, M.; Turner, H.; Gouverneur, V. *Chem. Eur. J.* **2006***, 12*, 7190-7203
[214] Li, P.; Evans, C. D.; Wu, Y.; Cao, B.; Hamel, E.; Joullie, M. M. *J. Am. Chem. Soc.* **2008***, 130*, 2351-2364
[215] Spina, R.; Colacino, E.; Gabriele, B.; Salerno, G.; Martinez, J.; Lamaty, F. *J. Org. Chem.* **2013***, 78*, 2698-2702
[216] Mazaleyrat, J.-P.; Xie, J.; Wakselman, M. *Tetrahedron Lett.* **1992**, *33*, 4301-4302
[217] The enynone was highly unstable even at low temperature, but we were able to determine its identity through ^{1}H NMR and a COSY. ^{1}H NMR (400 MHz, $CDCl_3$) δ = 7.65 (d, J = 6.7 Hz, 4H), 7.50-7.31 (m, 6H), 7.28 (s, 1H), 6.52 (s, 1H), 5.96 (s, 1H), 3.76 (t, J = 5.7 Hz, 2H), 2.61 (t, J = 7.0 Hz, 2H), 1.86 (pent, J = 6.5 Hz, 2H), 1.49 (s, 9H), 1.06 (s, 9H).
[218] Seebach, D.; Bossler, H.; Gründler, H.; Shoda, S.; Wenger, R. *Helv. Chim. Acta* **1991***, 74*, 197-224
[219] Seebach, D.; Bossler, H.; Gründler, H.; Shoda, S.; Wenger, R. *Helv. Chim. Acta* **1991***, 74*, 197-224
[220] Rosiak, A. & Christoffers, J. *Tetrahedron Lett.* **2006***, 47*, 5095-5097
[221] Crich, D.; Krishnamurthy, V.; Brebion, F.; Karatholuvhu, M.; Subramanian, V.; Hutton, T. K. *J. Am. Chem. Soc.* **2007***, 129*, 10282-10294
[222] The TFA ester was isolated as part of a mixture with the desired product. ^{1}H NMR (400 MHz, $CDCl_3$) δ = 6.22 (s, 1H), 4.42 (t, J = 6.3 Hz, 2H), 4.25-4.31 (m, 1H), 3.42-3.49 (m, 1H), 3.31-3.35 (m, 1H), 2.59 (t, J = 7.6 Hz, 2H), 2.08 (pent, J = 7.0 Hz, 2H). HMBC correlation between the protons at 4.42 ppm (on the side chain) and a carbon at 156 ppm confirmed the structure
[223] Ito, M.; Yamanaka, M.; Kutsumura, N.; Nishiyama, S. *Tetrahedron Lett.* **2003***, 44*, 7949-7952
[224] Vidal, J.; Guy, L.; Sterin, S.; Collet, A. *J. Org. Chem.* **1993***, 58*, 4791-4793
[225] Gouault, N.; Le Roch, M.; Cheignon, A.; Uriac, P.; David, M. *Org. Lett.* **2011***, 13*, 4371-4373
[226] Shibahara, S.; Fujino, M.; Tashiro, Y.; Okamoto, N.; Esumi, T.; Takahashi, K.; Ishihara, J.; Hatakeyama, S. *Synthesis* **2009***, 2009*, 2935-2953
[227] Rej, R. K. & Nanda, S. *Eur. J. Org. Chem.* **2014***, 2014*, 860-871
[228] Boring, D. L. & Sindelar, R. D. *J. Org. Chem.* **1988**, *53*, 3617-3621
[229] Gouault, N.; Le Roch, M.; Cheignon, A.; Uriac, P.; David, M. *Org. Lett.* **2011***, 13*, 4371-4373
[230] Gouault, N.; Le Roch, M.; Cheignon, A.; Uriac, P.; David, M. *Org. Lett.* **2011***, 13*, 4371-4373
[231] Leflemme, N.; Dallemagne, P.; Rault, S. *Tetrahedron* **2004***, 60*, 4861-4865
[232] Kaiser, E.; Picart, F.; Kubiak, T.; Tam, J. P.; Merrifield, R. B. *J. Org. Chem.* **1993***, 58*, 5167-5175
[233] Badrinarayanan, S. & Sperry, J. *Org. Biomol. Chem.* **2012**, *10*, 2126-2132

[234] Wuts, P. G. M. & Greene, T. W. *Greene's Protective Groups in Organic Synthesis*, 4th ed.; Wiley-Interscience: Hoboken, NJ, 2006;
[235] Mitra, R.; Ganesh, K. N. *Chem. Commun.* **2011***, 47*, 1198-1200
[236] Rosowsky, A.; Wright, J. E. *J. Org. Chem.* **1983***, 48*, 1539-1541
[237] Boger, D. L.; Lee, J. K. *J. Org. Chem.* **2000***, 65*, 5996-6000
[238] Hogrefe, R. I.; McCaffrey, A. P.; Borozdina, L. U.; McCampbell, E. S.; Vaghefi, M. M. *Nucleic Acids Res.* **1993***, 21*, 4739-4741
[239] Hogrefe, R. I.; McCaffrey, A. P.; Borozdina, L. U.; McCampbell, E. S.; Vaghefi, M. M. *Nucleic Acids Res.* **1993***, 21*, 4739-4741
[240] Sloan Devlin, A.; Du Bois, J. *Chem. Sci.* **2013***, 4*, 1059-1063
[241] Kawabata, T.; Chen, J.; Suzuki, H.; Fuji, K. *Synthesis* **2005***, 2005*, 1368-1377
[242] Lee, J. H.; Jeong, W.; Rhee, Y. H. *Synthesis* **2014***, 46*, 2155-2160
[243] Gouault, N.; Le Roch, M.; Cheignon, A.; Uriac, P.; David, M. *Org. Lett.* **2011***, 13*, 4371-4373
[244] Freeman, N. S. & Gilon, C. *Synlett* **2009***, 2009*, 2097-2100
[245] Navath, R. S.; Pabbisetty, K. B.; Hu, L. *Tetrahedron Lett.* **2006***, 47*, 389-393
[246] Wilson, D. J.; Shi, C.; Duckworth, B. P.; Muretta, J. M.; Manjunatha, U.; Sham, Y. Y.; Thomas, D. D.; Aldrich, C. C.; *Anal. Biochem.* **2011**, *416* (1), 27–38.
[247] Li, P.; Evans, C. D.; Wu, Y.; Cao, B.; Hamel, E.; Joullie, M. M. *J. Am. Chem. Soc.* **2008***, 130*, 2351-2364
[248] Campbell, A. D.; Raynham, T. M.; Taylor, R. J. K.; A Simplified Route to the *(R)*-Garner Aldehyde and (*S*)-Vinyl Glycinol. *Synthesis.* **1998**, 1707
[249] Banba, Y.; Abe, C.; Nemoto, H.; Kato, A.; Adachi, I.; Takahata, H.; Asymmetric synthesis of fagomine and its congeners. *Tetrahetron: Asymmetry* **2001**, *12*, 817-819
[250] Keyes, R. F.; Carter, J. J.; Zhang, X.; Ma, Z.; Short and Efficient Synthesis of a Vinyl-Substituted Tricyclic Erythromycin Derivative. *Org. Lett.* **2005**, *7*, 847-849.
[251] Berkowitz, D. & Maiti, G.; Following an ISES Lead: The First Examples of Asymmetric Ni(0)-Mediated Allylic Amination. *Org. Lett.* **2004**, *6*, 2661-2664.
[252] *Microchemical Journal Reference – get from old comp.*
[253] Pattenden, G. & Reynolds, S. J.; *J. Chem. Soc. Perkin Trans. 1* **1994**, *4*, 379
[254] Biel, M.; Deck, P.; Giannis, A.; Waldmann, H.; *Chem. Eur. J.* **2006**, *12*, 4121-4143
[255] Yadav, J. S.; Thrimurtulu, N.; Venkatesh, M.; Raghavendra Rao, K. V.; Prasad, A. R.; Subba Reddy, B. V.; *Synthesis* **2010**, *1*, 73-78.
[256] Clausen, D. J.; Wan, S.; Floreancig, P. E. *Angew. Chem. Int. Ed.* **2011***, 50*, 5178-5181
[257] Shi, C.; Geders, T. W.; Park, S. W.; Wilson, D. J.; Boshoff, H. I.; Abayomi, O.; Barry, C. E.; Schnappinger, D.; Finzel, B. C.; Aldrich, C. C. *J. Am. Chem. Soc.* **2011***, 133*, 18194-18201
[258] Dussault, P. H.; Eary, C. T.; Woller, K. R. *J. Org. Chem.* **1999***, 64*, 1789-1797
[259] Shibahara, S.; Fujino, M.; Tashiro, Y.; Okamoto, N.; Esumi, T.; Takahashi, K.; Ishihara, J.; Hatakeyama, S. *Synthesis* **2009***, 2009*, 2935-2953
[260] Geders, T. W.; Gustafson, K.; Finzel, B. C.; *Acta Crystallogr. Sect. F Struct. Biol. Cryst. Commun.* **2012**, *68*, 596.
[261] Shi, C.; Geders, T. W.; Park, S. W.; Wilson, D. J.; Boshoff, H. I.; Abayomi, O.; Barry, C. E.; Schnappinger, D.; Finzel, B. C.; Aldrich, C. C.; *J. Am. Chem. Soc.* **2011**, *133*, 18194-18201.
[262] Verge, D. & Arrio-Dupont, M.; *Biochemistry* **1981**, *20*, 1210-1216.
[263] Groce, S. L.; Miller-Rodeberg, M. A.; Lipscomb, J. D.; *Biochemistry* **2004**, *43*, 15141-15153.
[264] Groce, S. L.; Miller-Rodeberg, M. A.; Lipscomb, J. D.; *Biochemistry* **2004**, *43*, 15141-15153.
[265] Whittaker, J. W. & Lipscomb, J. D.; *J. Biol. Chem.* **1984**, *259*, 4476-4486.
[266] Alberico, D.; Paquin, J.-F.; Lautens, M.; *Tetrahedron* **2005**, *61*, 6283-6297
[267] Clausen, D. J.; Wan, S.; Floreancig, P. E. *Angew. Chem. Int. Ed.* **2011***, 50*, 5178-5181
[268] Zhang, X.; Krishnamurthy, R. *Angew. Chem. Int. Ed.* **2009***, 48*, 8124-8128
[269] Doi, T.; Numajiri, Y.; Munakata, A.; Takahashi, T. *Org. Lett.* **2006***, 8*, 531-534

[270] Shi, C.; Geders, T. W.; Park, S. W.; Wilson, D. J.; Boshoff, H. I.; Abayomi, O.; Barry, C. E.; Schnappinger, D.; Finzel, B. C.; Aldrich, C. C. *J. Am. Chem. Soc.* **2011***, 133*, 18194-18201

[271] Shibahara, S.; Fujino, M.; Tashiro, Y.; Okamoto, N.; Esumi, T.; Takahashi, K.; Ishihara, J.; Hatakeyama, S. *Synthesis* **2009***, 2009*, 2935-2953

[272] Blaney, P.; Grigg, R.; Rankovic, Z.; Thornton-Pett, M.; Xu, J. *Tetrahedron* **2002***, 58*, 1719-1737

[273] Shi, C.; Geders, T. W.; Park, S. W.; Wilson, D. J.; Boshoff, H. I.; Abayomi, O.; Barry, C. E.; Schnappinger, D.; Finzel, B. C.; Aldrich, C. C. *J. Am. Chem. Soc.* **2011***, 133*, 18194-18201

[274] Mitra, R.; Ganesh, K. N. *Chem. Commun.* **2011***, 47*, 1198-1200

[275] Boger, D. L.; Lee, J. K. *J. Org. Chem.* **2000***, 65*, 5996-6000

[276] Shi, C.; Geders, T. W.; Park, S. W.; Wilson, D. J.; Boshoff, H. I.; Abayomi, O.; Barry, C. E.; Schnappinger, D.; Finzel, B. C.; Aldrich, C. C. *J. Am. Chem. Soc.* **2011***, 133*, 18194-18201

[277] So, R. C.; Ndonya, R.; Izmirian, D. P.; Richardson, S. K.; Guerrera, R. L.; Howell, A. R.; *J. Org. Chem.* **2004**, *69*, 3233-3235

[278] Clausen, D. J.; Wan, S.; Floreancig, P. E. *Angew. Chem. Int. Ed.* **2011***, 50*, 5178-5181